THE UNIVERSITY OF MICHIGAN

COLLEGE OF ENGINEERING

DEPARTMENT OF ELECTRICAL AND COMPUTER ENGINEERING

Radiation Laboratory

MICROWAVE DIELECTRIC BEHAVIOR OF VEGETATION MATERIAL

Mohamed A. El-Rayes
Fawwaz T. Ulaby

Radiation Laboratory
Department of Electrical Engineering
and Computer Science
The University of Michigan
Ann Arbor, MI 48109-2122

NASA/Goddard Space Flight Center
Earth Survey Applications Division
Earth Resources Branch
Greenbelt, MD 20771

Contract NAG 5-480

January, 1987

Ann Arbor, Michigan

ERRATA

page	line	error	correction
xxv	6	potatos	potatoes
xxv	6	tomatos	tomatoes
9	12	later	latter
9	15	aquired	acquired
21	19	meaningfull	meaningful
23	15	approachs	approaches
37	17	branchs	branches
40	1	trsnsmission	transmission
64	13	straight forward	straightforward
68	11	successfull	successful
73	13	inspection	iteration
106,107,108	3	PLEXYGLASS	PLEXIGLASS
109	8	PLEXYGLASS	PLEXIGLASS
112	1	$Y_3^{(1)}$	$Y_3^{(2)}$
112	1	$Y_{in}^{(1)}$	$Y_{in}^{(2)}$
153	17	1985	1984
A.42	4	REAL	Imaginary

022132-4-T

MICROWAVE DIELECTRIC BEHAVIOR OF VEGETATION MATERIAL

Mohamed A. El-Rayes
Fawwaz T. Ulaby

Radiation Laboratory
Department of Electrical Engineering
and Computer Science
The University of Michigan
Ann Arbor, MI 48109-2122

January, 1987

Supported by:

NASA/Goddard Space Flight Center
Earth Survey Applications Division
Earth Resources Branch
Greenbelt, MD 20771

Contract NAG 5-480

ABSTRACT

The microwave dielectric behavior of vegetation was examined through the development of theoretical models involving dielectric dispersion by both "bound" and "free" water and supported by extensive dielectric measurements conducted over a wide range of conditions. The experimental data were acquired using an open-ended coaxial probe that was developed for sensing the dielectric constant of thin layers of materials, such as leaves, from measurements of the complex reflection coefficient using a network analyzer. The probe system was successfully used to record the spectral variation of the dielectric constant over a wide frequency range extending from 0.5 GHz to 20.4 GHz at numerous temperatures between -40^0C and $+40^0C$. The vegetation samples – which included corn leaves and stalks, tree trunks, branches and needles, and other plant material – were measured over a wide range of moisture conditions (where possible). To model the dielectric spectrum of the bound water component of the water included in vegetation, dielectric measurements were made for several sucrose-water solutions as analogs for the situation in vegetation. The results were used in conjunction with the experimental data for leaves to determine some of the constant coefficients in the theoretical models. Two models, both of which provide good fit to the data, are proposed. The first model treats the water in vegetation as two independent components, a bound water component with a relaxation frequency of 0.178 GHz and a free water component with a relaxation frequency of 18 GHz at 22^0C. The second model treats all the water as a single mixture with a relaxation frequency that increases with moisture content from about 0 for dry vegetation to 18 GHz for vegetation with very high moisture contents.

ACKNOWLEDGEMENTS

This report documents the results of research conducted from 1982-1986. The first phase covered the period 1982-1984 and was conducted at the University of Kansas, and the latter phase was conducted at the University of Michigan.

Table of Contents

LIST OF FIGURES

LIST OF TABLES

Chapter 1

Introduction

Over the past two decades, spaceborne microwave sensors have been playing an increasingly important role in the study of the earth's surface and atmosphere. They can provide near-global coverage of the earth's surface unhampered by cloud cover and with independence of sun angle. Furthermore, the ability of microwave energy to penetrate through dry media has proved useful for studying subsurface terrain features (Carver et al, 1985). In recent years, the field of microwave remote sensing has made significant advances along several fronts. A prime example of a major technological development is the recent realization of digital techniques that can provide real-time processing of SAR images. Also, improved scattering and emission models are now available to relate the backscattering coefficient σ^0 and emissivity e of a distributed target to its dielectric and geometric properties.

Since 1962, numerous microwave radiometers have been flown on earth-orbiting satellites; some examples of these space missions are given in Table 1.1(Ulaby et

al, 1982):

Year	1962	1972	1973	1978
Spacecaft Instrument acronym	Mariner 2	Nimbus 5	Skylab S193	Nimbus 7 SMMR
Frequency(GHz)	15.8,22.2	19.3	13.9	6.6,10.7,18,21,37
Type Of Scanning	Mechanical	Electrical	Mechanical	Mechanical
Swath-Width (Km)	Planetary	3000	180	800
Resolution (Km)	1300	25	16	18×27

Table 1.1 Examples of space missions.

Also, several SAR systems have been flown in space including Seasat(1978), SIR-A (1981), and SIR-B (1984).Many experiments have been conducted to relate σ^0 and e to target characteristics at various frequencies and polarizations. Some of these experiments have utilized truck-mounted radar systems to observe the backscattering and emission from natural targets as a function of frequency, look angle, and polarization (Ulaby et al, 1982).

The dielectric properties of natural targets play a key role in remote sensing. Its importance stems from the fact that it determines, besides the sensor parameters and the target geometrical features, the backscattering and natural emission from a distributed target. Also, the dielectric properties of a target relate its physical properties (e.g. its water content or temperature) to its σ^0 and e. This feature is very important in remote sensing science because it is a

critical ingredient of the inverse scattering process. Yet, understanding of the dielectric behavior of natural materials remains superficial at the present time and this is particularly true in the case of vegetation. Only a few experiments have been conducted to date to examine the dielectric properties of vegetation material. Reviewing the literature requires a minor effort because only a few measurements and modelling attempts (Carlson, 1967; Broadhurst, 1971; Tan, 1981; Ulaby and Jedlicka, 1984) have been conducted so far. Moreover, these attempts were limited to narrow ranges of the major parameters of interest, namely plant type and parts, frequency band, moisture content, effective salinity, and temperature. The following table provides a comparison between the range of parameters already tested and those desired from the standpoint of natural variability -as far as the physical parameters are concerned- and in terms of the frequency range of interest to the remote sensing community:

Measured Parameter	Available Data	Desired Range
Frequency (GHz)	1-2,3.5-6.5,7.5-8.5	.1-20
Moisture Content (percent gravimetric)	0-60	0-90
Temperature (^{0}C)	20 to 25	-40 to +40
Effective NaCl (Parts Per Thousands)	11	4 to 40

Table 1.2 Available and desired ranges of parameters.

Another shortcoming of the studies already conducted on this subject is the lack of a comprehensive model that relates different plant physical parameters to the dielectric properties using as a few free parameters as possible. This lack of knowledge motivated the current research to study these missing pieces and to try to develop a universal model for vegetation materials. The parameters of interest are frequency (.1 to 20 GHz), temperature (-40 to +40 ^{0} C), water content (0 to 90 % gravimetric), vegetation density (by testing different plants and parts), and salinity (4 to 40 parts per thousand). An additional major goal is to establish the role of bound water in the dielectric process.

The goals of this study can be summed up as follows:

1. To develop a dielectric measurement system suitable for dielectric measurements of plant parts. The system should be fast, reliable, accurate, operate over a broad frequency range, and suitable for temperature measurements.

2. To generate a dielectric constant database for a variety of plant types and parts as a function of:

   (a) moisture level,

   (b) electromagnetic frequency,

(c) vegetation bulk density,

(d) effective NaCl salinity of included liquids,

(e) temperature, and

(f) part location relative to root system.

3. To develop an understanding of the different mechanisms that contribute to the overall dielectric behavior of vegetation materials, and to establish, if possible, the roles of salinity and bound water.

4. To develop a general physical mixing model for plant materials that incorporates all of the previously mentioned parameters. Empirical and semi-empirical models will be developed as well.

Chapter 2

Background

A vegetation material, such as a leaf, can be considered a heterogeneous vegetation-water mixture consisting of four components: (1) free water, (2) bound water, (3) bulk vegetation matter, and (4)air. Since plants are, in general, found in nature with a very high water content, their dielectric properties are mainly determined by the properties of included water. It was found (Ulaby and Jedlicka, 1984) however, that these fluids have a finite salinity equivalent to an NaCl salinity of about 10 ppt [1]. Therefore, the first section of this chapter will provide the background material for the dielectric properties of liquid water as a function of various physical parameters. It is of great importance to note the similarity between the general dielectric behavior of liquid water and that of wet plants. Any deviation however, should be studied and properly attributed to other causes. Some of these causes may include the effects of bound water which differs substantially from free water. Another important cause may be the various structural differences within a plant part which may affect the de-

[1] Parts Per Thousand

polarization shape factors (DeLoor, 1968;DeLoor, 1982), which , in turn, may have a significant influence upon the dielectric constant of the vegetation-water mixture. This topic is examined in section 2.2. Next, in section 2.3, a short review is presented of the general principles of plant physiology as they relate to the study of the dielectric properties of vegetation material. Finally, in section 2.4, a brief discussion of previous studies is presented.

2.1 Dielectric Properties Of Liquid Water

The dielectric properties of water have been extensively studied, and are quite well understood with regard to the dependence on salinity, frequency, and temperature. A complete analysis is presented in Hasted (Hasted, 1973). Also, a comprehensive summary of the dielectric properties of natural targets, including water, is provided by Ulaby et al (Ulaby et al, 1986). Since the dielectric properties of liquid water are based on the well known Debye equation (Debye, 1912), it will prove useful to provide a brief background of the Debye equation and the associated relaxation process.

2.1.1 What Is A Relaxation Process

This section is intended to present a brief description of the mechanism by which water molecules exhibit a spectral absorption line at microwave frequencies. For a complete analysis the reader is referred to the classical book of Debye (Debye, 1912), or those by Hasted (Hasted, 1973) and Pethig (Pethig, 1979).

Polar Molecules

The permittivity of a material may be regarded as the proportionality factor between electric charge and electric field intensity. Also, it reflects the extent to which a localized charge distribution can be distorted through polarization by an external electric field. The polarizability, α, is defined as the dipole moment induced by a unit electric field and is given by

$$\alpha_t = \alpha_e + \alpha_a + \alpha_0 \tag{2.1}$$

where α_t is the total polarizability, α_e is the electric polarizability (due to displacement of the electron cloud relative to the nuclei), α_a is the atomic polarizability (due to displacement of the atomic nuclei relative to one another), and α_o is the orientational polarizability (due to a permanent electric dipole moment). Thus, α_0 only exists in polar materials, e.g. water, and the higher the polarizability of a material, the higher its static dielectric constant. For non-polar materials, the polarizability arises from two effects, namely electronic and atomic polarization. Since the dispersion due to the fall-off of the atomic polarization, α_a, occurs at frequencies comparable with the natural frequencies of vibrations of the atoms in a molecule (i.e. in the infrared spectrum around 10^{14} Hz), and that for electronic polarization, α_e, occurs at still higher frequencies corresponding to electronic transitions between different energy levels in the atom (visible, UV, and X-ray frequencies), the dielectric properties of non-polar materials are constant in the microwave band and do not show any temperature dependence either.

Polar molecules, although electrically neutral, have a charge distribution such that the centers of positive and negative charge are not coincidental. These molecules are termed polar, and were found to have a high static dielectric constant (e.g., ϵ_s of water is about 80.). The slowest polarization mechanism is often that of dipolar reorientation. The dipole moments are just not able to orient fast enough to keep in alignment with the applied electric field and the total polarizability falls from α_t to $(\alpha_t - \alpha_o)$. This fall in polarizability, with its related reduction in dielectric constant (e.g., ϵ_s drops roughly from 80 to 4.5 for water), and the occurence of energy absorption is referred to as dielectric relaxation or dispersion. It is worth noting here that the dispertion due to α_o is completely different from that due to α_a or α_e. The former is a relaxation dispersion while the later is a resonance dispersion [2].

Debye's Equation

The total dipole moment of molecules in a polar material represents the degree of polarization aquired after the application of an external electric field

$$\bar{m} = \alpha_t \bar{E}_1 \tag{2.2}$$

where $\bar{m}$ is the dipole momont and $\bar{E}_1$ is the local electric field. This equation may be written in the form

$$\bar{m} = \bar{\mu} + \alpha \bar{E}_1 \tag{2.3}$$

[2] e.g. relaxation dispersion has the broadest spectrum known in physics which is approximately 1.4 decades wide.

where $\bar{\mu}$ is the permanent dipole moment and $\alpha = \alpha_a + \alpha_e$.

Since $\bar{\mu}$ is a permanent moment, the application of an electric field will generate a torque $\bar{\mu} \times \bar{E}$ tending to align the molecules with the field. Obviously, this orienting tendency is opposed by thermal agitation. The potential energy of a dipole moment $\bar{\mu}$ in a field $\bar{E}_1$ is given by

$$U = -\bar{\mu}\bar{E}_1 = -\mu E_1 \cos\theta \tag{2.4}$$

where θ is the angle between $\bar{\mu}$ and $\bar{E}_1$. According to the Boltzmann distribution law, the relative probability of finding a dipole oriented in an element of solid angle $d\theta$ is proportional to $\exp(-U/KT)$ and the thermal average of $\cos\theta$ can be shown to be (Pethig, 1979)

$$< \cos\theta >= \coth x - \frac{1}{x} \tag{2.5}$$

where $x = \frac{\mu E_1}{KT}$. It was shown, for $\bar{E}_1 < 10^5 v/m$, that

$$< \cos\theta > \simeq \frac{\mu E_1}{3KT} \tag{2.6}$$

and that the average moment per dipole in the direction of the applied field, $\bar{\mu_d}$, is given by

$$\bar{\mu_d} = \mu < \cos\theta >= \frac{\mu^2 \bar{E}_1}{3KT}. \tag{2.7}$$

Hence, the total polarizability is

$$\alpha_t = \frac{\mu^2}{3KT} + \alpha_e + \alpha_a. \tag{2.8}$$

We must keep in mind, however, that equation (2.8) is only valid for small values of electric field ($E_1 \leq 10^5 v/m$); if the fields are higher than that, a more complicated expression is required (Hasted, 1973).

One of the most difficult problems in dielectric theory is to relate the local field (acting on a molecular dipole), to the externally applied field (macroscopic field). Many researchers have tried to relate $\bar{E}_1$ to $\bar{E}$ and their results were not generally satisfactory (e.g. the Mossotti-Clausius-Lorentz formulation). To derive a mathematical model for the orientational relaxation process, we shall assume that the polarization, P is given by

$$P = P_1 + P_2 = X_1 E + P_2 \tag{2.9}$$

where P_1 is the polarization due to atomic and molecular displacements (it responds instantly to $\bar{E}$, at least at microwave frequencies), P_2 is the polarization due to dipolar reorientation (it lags behind $\bar{E}$ at microwave frequencies), and X_1 is the dielectric susceptibility. It can be shown that (Pethig, 1979)

$$\frac{dP_2}{dt} = \frac{1}{\tau}(X_2 E - P_2) \tag{2.10}$$

where $X_2 E$ is the final value of P_2, and τ is the relaxation time constant. Solving equation (2.10) for E as a step function at $t = 0$ when $P_2 = 0$ yields

$$P = P_1 + P_2 = (X_1 + X_2(1 - \exp\frac{-t}{\tau}))E, \tag{2.11}$$

which shows that the polarization reaches its final value exponentially with a time constant τ. A solution for (2.11) of an alternating field, $\bar{E} = \bar{E}_0 \exp(j\omega t)$, can be shown to be (Pethig, 1979)

$$P = P_1 + P_2 = (X_1 + \frac{X_2}{1 + j\omega\tau})E \tag{2.12}$$

which corresponds to a complex dielectric constant of the form

$$\epsilon = \epsilon_\infty + \frac{\epsilon_s - \epsilon_\infty}{1 + j\omega\tau} \tag{2.13}$$

where ϵ is the macroscopic complex dielectric constant, ϵ_∞ is its high frequency (or optical) limit, ϵ_s is its low frequency (or static) limit, and τ is the relaxation characteristic time. The complex dielectric constant can be expressed in real numbers as

$$\epsilon = \epsilon' - \epsilon'' \tag{2.14}$$

and the real and imaginary parts can be expressed as

$$\epsilon' = \epsilon_\infty + \frac{\epsilon_s - \epsilon_\infty}{1 + \omega^2\tau^2} \tag{2.15}$$

and

$$\epsilon'' = \frac{(\epsilon_s - \epsilon_\infty)\omega\tau}{1 + \omega^2\tau^2}. \tag{2.16}$$

Equations (2.13) to (2.16) are commonly known as the Debye dispersion formulas.

Some of the interesting features of the Debye relaxation process are:

1. Its transition extends roughly over four decades in frequency.

2. The width of the ϵ'' peak at the half-height value is roughly 1.4 decades in frequency (very broad !).

3. It is possible to represent a relaxation graphically in two different ways:

(a) *Two straight lines:* If we plot the following relations $\epsilon''\omega = (\epsilon_s - \epsilon')/\tau$ and $\epsilon''/\omega = (\epsilon' - \epsilon_\infty)\tau$, we will have two straight lines whereby τ can be estimated from their slopes (Pethig, 1979). This is a useful technique if the measurement data are not enough to describe the relaxation behavior (e.g. measurement frequency band is either lower or higher than resonance frequency).

(b) *Cole-Cole plot:* In order to check for single or multiple relaxation times, this plot can prove very useful. Using equations (2.15) and (2.16), and by eliminating $\omega\tau$, we can show that

$$(\epsilon' - \frac{\epsilon_s - \epsilon_\infty}{2})^2 + (\epsilon'')^2 = (\frac{\epsilon_s - \epsilon_\infty}{4})^2 \qquad (2.17)$$

Equation (2.17) is an equation of a circle. A Cole-Cole plot can be easily constructed by plotting ϵ'' versus ϵ' with frequency as a variable parameter.

4. Since relaxation time τ represents a molecular process that usually follows an Arrhenius temperature law, we can write

$$\tau = A \exp(\frac{\Delta H}{RT}) \qquad (2.18)$$

where ΔH is the Arrhenius activation enthalpy per mole, and A is a constant. From equation (2.18)

$$\frac{\partial(\ln \tau)}{\partial(\frac{1}{T})} = \frac{\Delta H}{R} \qquad (2.19)$$

so that a plot of $\ln \tau$ against $\frac{1}{T}$ gives a straight line of slope $\frac{\Delta H}{R}$. A more complete expression for (2.18) can be given as (Pethig, 1979).

$$\tau = \frac{h}{KT} \exp(\frac{-\Delta S}{R}) \exp(\frac{\Delta H}{RT}) \tag{2.20}$$

where h is Planck's constant and ΔS is the molar entropy of activation. A plot of $\ln(\tau T)$ or $\ln(\frac{\omega_s}{T})$ against $\frac{1}{T}$ should be a straight line of negative slope, from which ΔH can be calculated. It is generally the practice to plot simply $\ln(\omega_s)$ against $\frac{1}{T}$ and compare with other activation energy graphs (because of the approximate nature of this treatment).

5. Deviation from an ideal Debye-type single relaxation could occur for many molecular systems. This effect tends to *smear* the relaxation pattern (ϵ'' curve becomes broader). Examples of this phenomena and their respective representation can be given as follows:

   (a) *Cole-Cole equation*

   $$\epsilon = \epsilon_\infty + \frac{\epsilon_s - \epsilon_\infty}{1 + (j\omega\tau)^\alpha} \tag{2.21}$$

   where α represents the width of the symmetrical distribution of relaxation times. A graphical technique (using chords) was designed (Hasted, 1973) to analyze data that has a symmetrical distribution of relaxation times.

   (b) *Modified Cole-Cole equation*

   $$\epsilon = \epsilon_\infty + \frac{\epsilon_s - \epsilon_\infty}{1 + j^{1-\alpha}(\omega\tau)^{1-\beta}} \tag{2.22}$$

where β is a constant less than unity.

(c) *Cole-Davidson equation*

$$\epsilon = \epsilon_\infty + \frac{\epsilon_s - \epsilon_\infty}{(1 + j\omega\tau)^\alpha}. \tag{2.23}$$

This equation corresponds to an asymmetrical distribution of relaxation times and gives rise to a skewed arc in $\epsilon'(\epsilon'')$ diagram.

(d) *In general*, we can write

$$\epsilon = \epsilon_\infty + (\epsilon_s - \epsilon_\infty) \int_0^\infty \frac{G(\tau)d\tau}{1 + j\omega\tau} \tag{2.24}$$

where $G(\tau)$ represents a general distribution of relaxation times.

2.1.2 Pure Water

For pure water, it is assumed that the ionic conductivity is zero, which means that there are no free ions to contribute to the total loss (especially at low frequencies). The frequency dependence is given by the Debye equations (2.13)-(2.16):

$$\epsilon_w = \epsilon_{w\infty} + \frac{\epsilon_{ws} - \epsilon_{w\infty}}{1 + j\omega\tau_w} \tag{2.25}$$

It was found experimentally that $\epsilon_{w\infty}$, ϵ_{ws}, and f_w $(=1/2\pi\tau_w)$ are functions of temperature, especially ϵ_{ws} and f_w. Complete analysis and polynomial expressions can be found in (Hasted, 1973; Stogryn, 1971; Klein & Swift, 1977; and Ulaby et al, 1986).

The importance of liquid water at microwave frequencies stems from the fact that its relaxation frequency lies within this band. For example,

$$f_w(0^0C) = 9\text{GHz} \tag{2.26}$$

and

$$f_w(20^0C) = 17\text{GHz} \tag{2.27}$$

It was found that $\epsilon_{w\infty} \simeq 4.9$ by Lane and Saxton (1952). Figure 2.1 illustrates the frequency behavior of ϵ'_w and ϵ''_w for water at 20^0C Curves for sea water (s $\simeq$ 30 ppt)are shown also for comparison purposes.

2.1.3 Saline Water

A saline solution is defined as a solution that contains free ions whether these ions are of organic or non-organic nature. The salinity, s, of a solution is defined as the total mass of dissolved solid salts in grams in one kilogram of solution. An equivalent Debye-like equation could be used to represent saline solutions in the following modified form

$$\epsilon'_{sw} = \epsilon_{sw\infty} + \frac{\epsilon_{sws} - \epsilon_{sw\infty}}{1 + (\frac{f}{f_{sw}})^2} \tag{2.28}$$

and

$$\epsilon''_{sw} = \frac{(\epsilon_{sws} - \epsilon_{sw\infty})(\frac{f}{f_{sw}})}{1 + (\frac{f}{f_{sw}})^2} + \frac{\sigma_i}{2\pi\epsilon_0 f} \tag{2.29}$$

where the subscript sw refers to saline water, σ_i is the ionic conductivity in $Siemens/m$, and ϵ_0 is the free space dielectric constant ($\epsilon_0 = 8.854 \times 10^{-12} f/m$).

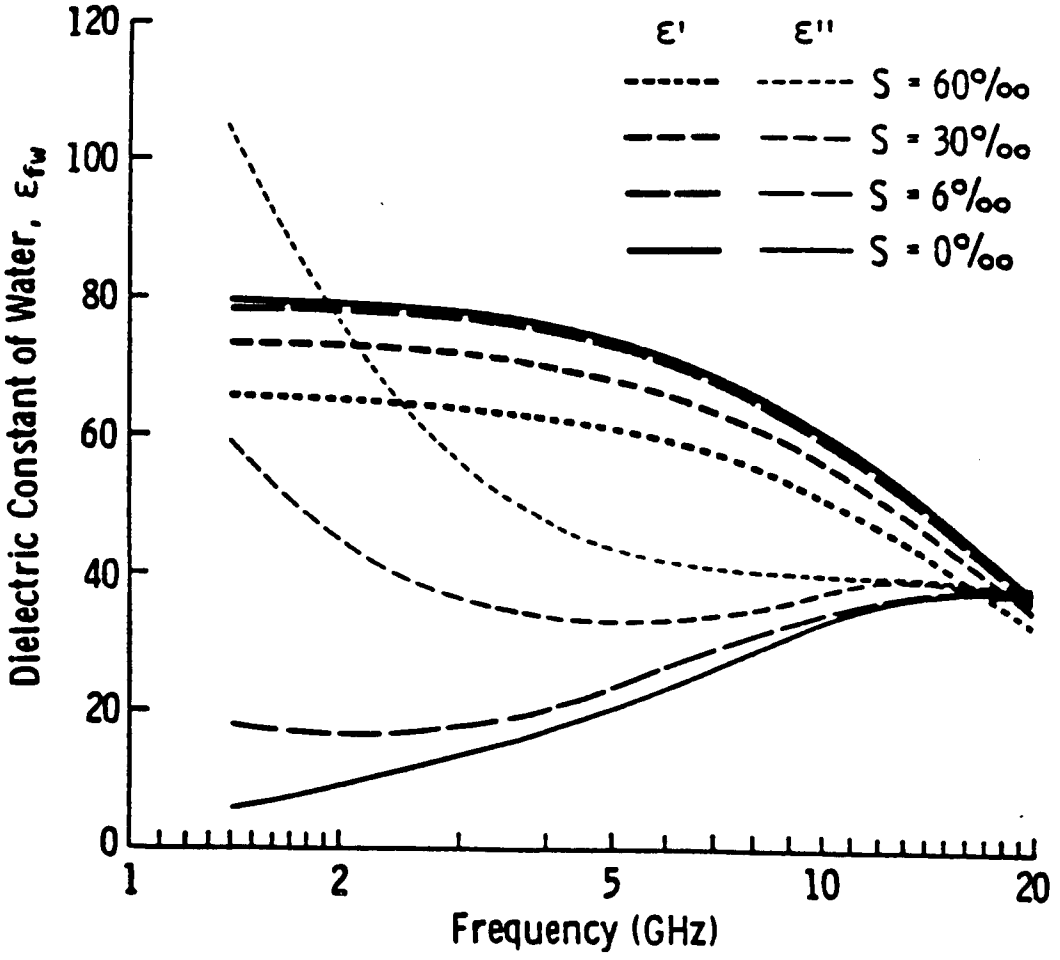

Figure 2.1. Dielectric constant spectra for liquid water with salinity (in ppt) as parameter at room temperature ($20^{0}C$). Calculated from [Stogryn, 1971].

Again, σ_i, ϵ_{sw0}, and f_{sw0} were found to be functions of salinity (in addition to their temperature dependence). Complete expressions are given in (Stogryn, 1971)and (Klein and Swift, 1977) in the form of polynomial fits. The equations are repeated here because they will be used in future chapters:

$$\epsilon_{sw\infty} = 4.9, \tag{2.30}$$

$$\epsilon_{sws}(T,0) = 87.74 - 4.0008T + 9.398 \times 10^{-4}T^2 + 1.410 \times 10^{-6}T^3, \tag{2.31}$$

$$2\pi\tau(T,0) = 1.1109 \times 10^{-10} - 3.824 \times 10^{-12}T + 6.938 \times 10^{-14}T^2 - 5.096 \times 10^{-16}T^3, \tag{2.32}$$

$$\sigma_{sea\ water}(T,S) = \sigma_{sea\ water}(25,S)exp(-\Delta\alpha), \tag{2.33}$$

where $\Delta = 25 - T$ and α is a function of T and S,

$$\alpha = 2.033\times10^{-2}+1.266\times10^{-4}\Delta+2.464\times10^{-6}\Delta^2-S[1.849\times10^{-5}-2.551\times10^{-7}\Delta+2.551\times10^{-} \tag{2.34}$$

and

$$\sigma_{sea\ water}(25,S) = S[0.182521-1.46192\times10^{-3}S+2.09324\times10^{-5}S^2-1.28205\times10^{-7}S^3], \tag{2.35}$$

in the range $0 \leq S \leq 40$.

2.1.4 Bound Water

The term *bound water* is always encountered in the literature of plant physiology, especially that dealing with cold and drought resistance (Kramer, 1955). The concept of bound water is founded on the observation that a part of the water in both living and nonliving materials behaves in a different manner from free water. While free water freezes at 0^0C, acts as a solvent, and is usually available for physiological processes, bound water does not. It remains unfrozen at some low temperature, usually -20^0C or -25^0C, it is also known not to function as a solvent, and in general it seems to be unavailable for physiological processes. It should be understood here that there is no sharp distinction between unbound and bound water ; rather, there exists a gradual transition between free water and completely bound water. Bound water was found to resist oven drying even at 100^0C for a long period of time. Obviously, water bound that firmly plays an important role as a cell constituent in the tolerance of drying of some seeds, spores, microorganisms, and a few higher plants (Kramer, 1983).

Much of the bound water is held on the surfaces of hydrophilic colloids [3], but some is associated with hydrated ions and molecules. Kramer (Kramer, 1955) wrote a thorough review on bound water and described 14 different methods for measuring it:

[3] A colloid is a phase dispersed to such a degree that the surface forces become an important factor in determining its properties

1. *The Cryoscopic Method,* based on the assumption that bound water does not act as a solvent.

2. *The Dilatometric Method,* using the fact that ice occupies more volume than water and that bound water does not freeze at normal freezing temperatures.

3. *The Calorimetric Method,* since one gram of free water ice absorbs about 79.75 calories when it thaws, it is possible to estimate the amount of total free water in plant tissues using a calorimeter.

4. *The Direct Pressure Method,* differences in the amount of water expressed from various materials under a given pressure can indicate differences in bound water contents.

5. *Refractometric Method,* using a refractometer (Dumanskii, 1933; and Siminova, 1939).

6. *Polarimetric Method,* (Koets, 1931)

7. *The X-ray Method,* the presence of shells of oriented water molecules should give X-ray patterns similar to those produced by ice, this method is useful qualitatively and not quantitatively.

8. *Infrared Absorption,* Infrared transmission curve for bound water was found to be different from that of free water.

9. *Heat Of Welting,* it is known that when colloids imbibe water, heat is released because water molecules loose part of their kinetic energy when they are adsorbed on the interfaces.

10. *Specific Heat Method,* it was observed that bound water has an abnormally low specific heat.

11. *Drying Method,* since bound water is so tightly held by colloids, it remains in samples dried at temperatures as high as 200^0C.

12. *Osmotic Pressure Method* (Levitt and Scarth, 1936).

13. *Dielectric Constant Method,* since, in general, the dielectric constant of free water is much higher than that of bound water (Marinsco 1931), it is possible to estimate bound water content using dielectric measurements (as will be discussed in Chapter 5).

14. *Vapor-pressure Method,* adding a nonelectrolyte to free water lowers its vapor pressure. If adding sucrose, e.g., results in an abnormally large decrease in vapor pressure, this indicates that a certain amount of the water is bound.

Although there are many methods to measure the amount of bound water in plant tissues, only a few of them proved to be accurate enough to produce meaningfull results. The calorimetric, dilatometric, and cryoscopic methods are used most frequently. According to Kramer (Kramer, 1955), the amount of bound

water found in plant tissues varies with the species tested, the environment in which the plants are grown, and the method used to measure it. There is more bound water in woody plants than there is in herbacious plants. Also some research (Levitt, 1980) indicates that plants have more bound water in the winter than in the summer and more in plants from dry habitats than in those from moist habitats. As a final remark, bound water exists in general in cell walls where it can scarcely affect the protoplasm, and it is held so firmly that it can not act as a solvent or take part in physiological processes. Hence, bound water may have some importance in seeds, spores, and other air-dry plant structure, but it probably is of little significance in growing plants.

The last remark underscores the bound water importance in physiological processes; however, its importance in determining the dielectric properties of vegetation materials is significant, especially at microwave frequencies. Many researchers claimed to observe a relaxation frequency for bound water similar to that of free water, except it takes place at frequencies well below that of free water (e.g. Hoekstra and Doyle, 1971). A possible peak of power absorption takes place around $500 - 1500\ MHz$ and was attributed to bound-water relaxation. There are two factors, however, that hold back a proper characterization of this relaxation:

1. *Ionic Conductivity* dominates losses at and below 1 GHz and tends to mask the effect of bound water. It would be useful to test a plant tissue that has very low values of salinity, if such a plant really exists.

2. *Small Volume Fractions* of bound water pose another serious problem, especially for fresh plants, where the free water volume is the largest component. If we attempt to examine a dried plant part that has a low moisture level, the increase in salinity would tend to counteract the relative increase in the volume ratio of bound water to free water and hence ionic conductivity would still be dominant.

In Chapter 5, an attempt was made to isolate an appreciable amount of bound water that has no free ions and hence, no conductivity losses. This water was bound on the surfaces of sugar molecules (e.g., sucrose and dextrose) and was tested over the frequency range from .2-20 GHz. The observed relaxation frequency was found to be in agreement with previous reports which place it at around 1 GHz. A complete description and analysis of the experiment will be given in Chapter 5.

In Chapter 6, however, a conclusion was reached that the nature of bound water is subjective and it depends entirely on how we look at it. Two approachs were used: (i) the dual relaxation spectrum (refer to Sec. 6.3.1 to 6.3.4) and (ii) the single relaxation spectrum (refer to Sec. 6.3.5).

2.1.5 Temperature Dependence

As mentioned in Section 2.1.1 and 2.1.2, the dielectric behavior of liquid water has a strong dependence on temperature above freezing. The dependence is even more drastic below freezing, which is called the *freezing point discontinuity* ,

where the magnitudes of the real and imaginary parts drop rather sharply[4]. One way to detect a relaxation behavior is to measure the dielectric constant of a material as a function of temperature and observe the gradient of the imaginary part. Three cases would arise:

1. If $\frac{\partial \epsilon''}{\partial T}$ is *negative*, the dominant loss mechanism is relaxation and the measurement frequency is below the relaxation frequency ($f < f_0$).

2. If $\frac{\partial \epsilon''}{\partial T}$ is *positive*, then either:

   (a) losses are completely or partially caused by a relaxation process and in this case $f > f_0$,

   (b) losses are completely or partially caused by conductivity, or

   (c) both relaxation ($f > f_0$) and conductivity losses exist.

3. If $\frac{\partial \epsilon''}{\partial T}$ is $\simeq 0$ then either:

   (a) the material is lossless (e.g. dry),

   (b) there are two different mechanisms affecting the losses, relaxation (with $f < f_0$) and conductivity, and they are comparable in magnitude, or

   (c) a relaxation peak ($f = f_0$) exists at that particular temperature.

As mentioned above, at the freezing point discontinuity the dielectric properties of a sample drastically change because liquid water (with, e.g., $\epsilon \simeq 80 - j4$

[4]free water freezes at 0^0C while bound water freezes around (or even below) -25^0C

at 1 GHZ) changes into ice (whose $\epsilon \simeq 3.15 - j0$ at 1 GHz) which represents big steps in both the real and imaginary parts. Bound water, however, freezes at temperatures well below free water; it was reported in several papers (e.g., Hoekstra and Doyle, 1971) to have a freezing point between -20^0C and -30^0C. This last observation could prove useful in studying the bound water in plant tissues by extending the temperature measurements down to -50^0C. A complete report of these measurements will be given in Chapter 5.

2.2 Dielectric Mixing Models

A vegetation part, such as a leaf, is considered to be a heterogeneous mixture of free water, bound water, bulk vegetation material, and air. An average dielectric constant can be measured for a particular heterogeneous mixture consisting of two or more substances. This average quantity depends on the volume fractions, the dielectric constants, the shape factors, and the orientation (relative to the applied electric field) of each and every constituent in the mixture. The continuous medium (or the host material) is usually taken to be the substance with the largest volume fraction in the mixture. For a more complete review, the reader is referred to (Ulaby et al, 1986). For the purpose of this study, only randomly oriented and randomly distributed inclusions will be considered. In the general development of most dielectric mixing models, it is assumed that the inclusions are much smaller in size than the applied wavelength in order for the equations to hold. These conditions are suitable assumptions for vegetation

materials in most cases. However, a study of the effect of inclusions' orientations could be useful in future research, especially for parts that have an obvious orientation pattern (e.g., a tree trunck). In the following three sections, a brief discussion of the mixing models used in the course of this study is given. They include theoretical models (DeLoor, 1968), semi-emperical models (Birchak et al, 1974), and emperical models (Dobson et al, 1985).

2.2.1 DeLoor's Mixing Model

The mixing formula as proposed by Polder and Van Santan (Polder and Van Santan, 1946) and DeLoor (DeLoor, 1956) for a host medium with dispersed randomly-oriented and randomly-distributed inclusions is given by:

$$\epsilon_m = \epsilon_h + \sum_{i=1}^{n} \frac{v_i(\epsilon_i - \epsilon_h)}{3} \sum_{j=1}^{3} \frac{1}{1 + (\frac{\epsilon_i}{\epsilon^*} - 1)A_j} \tag{2.36}$$

where ϵ_m is the macroscopic dielectric constant of the mixture, ϵ_h is the host or continuum dielectric constant, v_i and ϵ_i are the volume filling factor and the dielectric constant of the i_{th} dispersed inclusion, respectively, ϵ^* is the effective relative dielectric constant near an inclusion-host boundary, A_j are the depolarization factors along the main axes of the ellipsoidal inclusions, and n is the number of different inclusions in the mixture. The sum of the depolarization factors is equal to

$$\sum_{j=1}^{3} A_j = 1 \tag{2.37}$$

These factors, known also as shape factors, are determined by the inclusion shapes. Three special cases are considered as follows:

1. *Circular discs* ; $A_j = (0, 0, 1)$ Equation (2.36) will reduce to the following form

$$\epsilon_m = \epsilon_h + \sum_{i=1}^{n} \frac{v_i}{3}(\epsilon_i - \epsilon_h)(2 + \frac{\epsilon^*}{\epsilon_i}) \tag{2.38}$$

2. *Spheres* ; $A_j = (\frac{1}{3}, \frac{1}{3}, \frac{1}{3})$

$$\epsilon_m = \epsilon_h + \sum_{i=1}^{n} v_i(\epsilon_i - \epsilon_h)\frac{3\epsilon^*}{2\epsilon^* + \epsilon_i} \tag{2.39}$$

3. *Needles* ; $A_j = (\frac{1}{2}, \frac{1}{2}, 0)$

$$\epsilon_m = \epsilon_h + \sum_{i=1}^{n} \frac{v_i}{3}(\epsilon_i - \epsilon_h)\frac{5\epsilon^* + \epsilon_i}{\epsilon^* + \epsilon_i}. \tag{2.40}$$

Equation 2.36 can not be used in its present form, since no information is available on ϵ^*. However, after a thorough investigation of the available data, it was found (DeLoor, 1956; DeLoor, 1968) that ϵ^*, in general, lies between ϵ_m and ϵ_h. An upper and a lower limit for ϵ_m can be established by setting $\epsilon^* = \epsilon_m$ and $\epsilon^* = \epsilon_h$ in (2.36), respectively. Moreover, when the depolarization factors are not known, which is generally the case, it is still possible to estimate the limits of ϵ_m. The limits in this latter case lie further apart than when the shape factors are known. These limits are given by (DeLoor, 1968):

1. *Upper Limit* (circular discs; $\epsilon^* = \epsilon_m$)

$$\epsilon_m = \frac{\epsilon_h + \frac{2}{3}\sum_{i=1}^{n} v_i(\epsilon_i - \epsilon_h)}{1 - \frac{1}{3}\sum_{i=1}^{n} v_i(1 - \frac{\epsilon_h}{\epsilon_i})} \tag{2.41}$$

2. *Lower Limit* (spheres ; $\epsilon^* = \epsilon_h$)

$$\epsilon_m = \epsilon_h + 3\sum_{i=1}^{n} v_i \frac{\epsilon_h(\epsilon_i - \epsilon_h)}{(2\epsilon_h + \epsilon_i)} \tag{2.42}$$

where the variables used in (2.38)-(2.42) are as defined in connection with (2.36). These limits are of great help in studying the unknown shape factors for any system by plotting the measured data along with the expected limits.

2.2.2 Semi-empirical Models

There are two semi-empirical models that have proved to be useful for modeling vegetation material, namely, Birchak and the Debye-like models.

1. *Birchack Model*

$$\epsilon = (\sum_{i=1}^{n} \epsilon_i^{\alpha} v_i)^{1/\alpha} \tag{2.43}$$

where α is the only free parameter. When α is equal to .5, the Birchak model is called *the refractive model.*

2. *Debye-like Model* Since the dielectric properties of biological materials are dominated by the dielectric properties of liquid water, a Debye-like model would, in general, be the obvious choice for semi-empirical modeling. Of course, a slight modification is necessary to this formulation in order to include conductivity losses and a spread of relaxation times. The proposed form of Debye's equation is as follows

$$\epsilon_m = \epsilon_{m\infty} + \frac{\epsilon_{ms} - \epsilon_{m\infty}}{1 + j\frac{f}{f_m}} - j\frac{\sigma_m}{\omega\epsilon_0} \tag{2.44}$$

where the variables are as defined earlier and the subscript m indicates the vegetation mixture. $\epsilon_{m\infty}$ and ϵ_{ms} could be evaluated for a particular

mixture provided that we know the following:

(a) the volume fractions, v_i, of all the constituents,

(b) $\epsilon_{\infty i}$ and ϵ_{si} of all the constituents, and

(c) the proper mixing formulas relating ϵ_{ms} to ϵ_{si} of the constituents, and similarly for ϵ_{∞}.

Since volume fractions can be determined from vegetation physical parameters, [5], and $\epsilon_{\infty i}$ and ϵ_{si} are known, the only unknown is the proper mixing formulas. It is possible, for convenience, to use Birchack model, which gives

$$\epsilon_{m\infty}^{\alpha} = \sum_{i=1}^{N} v_i \epsilon_{\infty i}^{\alpha}, \tag{2.45}$$

and

$$\epsilon_{ms}^{\alpha} = \sum_{i=1}^{N} v_i \epsilon_{si}^{\alpha}. \tag{2.46}$$

The problem now is to determine a suitable value (or values) for α to best fit the measured data. Similarly, f_m can be selected by optimizing the model to fit the data points, and the relaxation frequency of liquid water can be used as an initial condition. The form of σ_m is not known, since the effective $NaCl$ salinity changes as a function of moisture content. Hence, in general,

$$\sigma_m = f(M_v) \tag{2.47}$$

where M_v is the volumetric moisture of the material. Two possible representations for σ_m may be proposed

[5] As will be discussed in chapter 6

1. $\sigma_m = A - BM_v$, and

2. $\sigma_m = \frac{A}{M_v}$

Obviously, the first form is more suitable since σ_m remains finite even at $M_v = 0$. For a vegetation mixture, the number of constituents can be two, three, or four depending on the model used. Since the bulk vegetation material and air are *non-polar* materials, they do not have any temperature sensitivity. The only temperature-dependent constituents are the free and bound water.

2.2.3 Empirical Models

The most suitable and most commonly used empirical model for the dielectric constant of vegetation materials is simply a polynomial function. Linear regression can be used to determine the unknown coefficients and an evaluation of the fit is performed in terms of correlation and mean-squared errors. Individual polynomials are generated for ϵ' and ϵ'' as a function of M_v (volumetric moisture) for a particular plant type, part, and at a given frequency and temperature. The disadvantages of this approach are

1. there is no physical significance for the coefficients, and

2. the model is not easily extendable to other moisture, temperature, and/or frequency conditions.

On the other hand, the major advantages are

- Simplicity, and

- The ability to achieve almost a perfect fit to the data by properly choosing the order of the polynomial.

2.3 Water in Plant Materials

Water is one of the most common and most important substances on the earth's surface. It is the most significant single environmental factor that determines the kinds and amounts of vegetation cover on various parts of the globe.

2.3.1 Ecological and Physiological Importance of Water

It is almost a general rule that wherever water is abundant, vegetation cover is lushy, and deserts are where water is scarce. The ecological importance of water stems from its physiological importance. Every plant process is affected directly or indirectly by the water supply. If the water supply is decreased, plants will suffer loss of turgor and wilting, cessation of cell enlargement, closure of stomata, reduction in photosynthesis, interference with many basic metabolic processes, and continued dehydration will, eventually, cause death of most organisms (Kramer, 1983).

2.3.2 Uses of Water in Plants

According to Kramer, the function of water in plant materials may be listed as follows:

1. *Constituent:* Fresh weight of most herbaceous plant parts is 80-90% water, and water constitutes over 50% of the fresh weight of woody plants. Some

plant parts, e.g. seeds, can be dehydrated to the air-dry condition, or even to the oven-dry condition without loss of viability, but a marked decrease in physiological activity accompanies the loss of water.

2. *Solvent:* Gases, minerals, and other solutes can enter plant cells and move from cell to cell and organ to organ through the continuous liquid phase throughout the plant.

3. *Reactant:* Water is essential to many processes such as photosynthesis and hydrolytic processes.

4. *Maintenance of Turgidity:* This is important for cell enlargement and growth and for maintaining the form of herbaceous plants. It is also important for various plant structures (Kramer, 1983).

2.4 Previous Studies

Very few studies have been conducted to date with the goal of measuring and modeling the microwave dielectric properties of green vegetation. Extensive dielectric measurements have been conducted and reported for grains (Nelson, 1978) however. This short section reviews some of the reported data for green vegetation, and provides brief discussions of the measurement systems used and their reliability.

2.4.1 Carlson (1967)

A cavity perturbation technique was employed to measure the relative dielectric constant of green vegetation samples (grass, corn, spruce, and taxus) at room temperature and at a single frequency of 8.5 GHz. The measurements were made as a function of water content from freshly-cut samples to perfectly dry ones. The relative dielectric constant was found to be roughly proportional to the moisture content and can be modeled as

$$(\epsilon' - j\epsilon'') = 1.5 + (\frac{\epsilon'_w}{2} - j\frac{\epsilon''_w}{3})f \tag{2.48}$$

for the samples of corn, grass, and taxus, where $\epsilon' - j\epsilon''$ is the relative dielectric constant of vegetation samples, $\epsilon'_w - j\epsilon''_w$ is the relative dielectric constant of water, and f is the fractional amount of water in the sample. The major source of errors in this experiment was due to the measurement uncertainty of the sample size.

2.4.2 Broadhurst (1970)

Broadhurst (1970) used a TEM coaxial waveguide with a specimen of the material under test occupying some of the space between the coaxial conductors. His measurements were conducted at room temperature (23^0C) on living foliage, plant materials, and clay soil over a wide frequency band extending from 100 KHz to 4.2 GHz. In order to calibrate the system for accuracy, distilled water was measured and compared to reported data. The results were within 10% accuracy for the real part, while sizeable errors were observed for the imaginary part. Also, a check on the precision of the leaf measurements was made

by taking six separate samples from a leaf type and by measuring each sample three different times (after each measurement the sample was removed from the chamber and then repacked and measured). An analysis of variance was then conducted on the data to ascertain the components of variance for instrumental error and for variability between leaves. The scatter in the data due to the leaf was, generally, greater than that due to instrumental errors. The scatter due to the leaf was primarily due to measurement errors of leaf thickness, and secondarily due to variations in leaf biological structure. The uncertainty in the thickness measurements amounts to $5-10\%$ and the overall uncertainty was below 20%. Excessive scatter in the data above 1 GHz was caused by higher-order mode propagation in the line.

2.4.3 Tan (1981)

Similar to Carlson's set-up, Tan used a cavity waveguide resonator at 9.5 GHz to measure tropical vegetation samples (grass, casuarina, rubber leaf, rubber wood) at room temperature. Measurements were made as a function of sample water content. The overall accuracy of the system is estimated to be $10-15\%$ for both the real and imaginary parts of ϵ. Extending Carlson's modeling approach, Tan used six different mixing formulas to model his data. He concluded that the best model that fits his data was the Polder and Van Santen model (1946) with parameters $\epsilon^* = \epsilon_m$ and $A_j = (0,0,1)$. In other words the water inclusions have a circular disc shape within the vegetation host. Again, the main source of error is due to thickness measurements of the plant samples.

2.4.4 Ulaby and Jedlicka (1984)

These measurements (Ulaby and Jedlicka, 1984) were conducted using a waveguide transmission technique in three different bands, namely, L-band (1.1 – 1.9 GHz), C-band (3.5 – 6.5 GHz), and X-band (7.6 – 8.4 GHz). Vegetation types investigated included wheat, corn, and soybeans. Leaves, stalks, and corn heads were measured as a function of their water content. Also, extracted fluids from these parts were measured and compared to saline solutions. An accurate systematic procedure (McKinley, 1983) was developed to measure vegetation densities as they change with volumetric moisture.

Uncertainties in the data were due to sample preparation and data-reduction techniques rather than to variations in measurement system stability. In the modeling efforts conducted, the vegetation medium was considered to be a four-component mixture with the vegetation bulk material as the host and free water, bound water, and air as the inclusions. Also, a three-phase mixture model was attempted with dry vegetation as the host (bulk vegetation material and air) and free water, and bound water as inclusions. The volume of bound water and its dielectric properties were chosen arbitrarily to be 5% and $(3.15 - j0)$, respectively. The reason behind the latter assumption is the view of bound water as a state where water molecules are so strongly bound to colloidal surfaces that they assume the dielectric properties of ice. Another modeling approach was adopted using a two-phase mixture model, in which the host was taken to be the dry vegetation part (bulk vegetation and air) and the inclusions were taken to

be liquid water with effective (or depressed) dielectric properties.

2.4.5 summary

Table 2.1 shows a summary of the previous studies:

Parameter	Carlson,1967	Broadhurst,1970	Tan,1981	Ulaby and Jedlicka,1984
System	Partially-filled cavity	TEM Coaxial Cell	Partially-filled Cavity	Waveguides, Transmission
Frequency	8.5 GHz	100 KHz-4.2 GHz	9.5 GHz	1.1-1.9 GHz 3.5-6.5 GHz 7.6-8.4 GHz
Moisture %	65	80	60	80
Temperature	23^0C	23^0C	21^0C	23^0C
Accuracy ϵ'%	10-20	10	10-20	5
Accuracy ϵ''%	10-20	10-100	10-20	5-37
Plants	grass corn taxus blue spruce	bampoo Tulip tree	grass casuarina rubber	corn wheat soybeans
Parts	leaves	leaves branchs	leaves wood	leaves stalks fluids

Table 2.1: Comparison between previous microwave dielectric measurements on vegetation material.

From the brief discussion in the previous subsections, we can conclude the following:

1. Only a few attempts have been made to date to study the microwave dielectric properties of plants.

2. The available measurements were made in limited microwave frequency bands.

3. None of these measurements covered temperature ranges beyond room temperatures $(20 - 25^0C)$.

4. Attempts to model the dielectric behavior of vegetation-water mixtures have been only marginally successful, at best.

These shortcomings motivated the development and use of a measurement technique that would operate over a wide frequency range, that is suitable for dielectric measurements as a function of temperature, and that can measure the dielectric constant accurately, rapidly, and non-destructively. This technique is the subject of Chapter 4.

Chapter 3

Dielectric Measurement Systems-General

Many studies have been conducted in the past (Von Hippel,1954) to examine the dielectric properties of natural and artificial materials. However, very few of these were concerned with vegetation materials. In the past three decades, great improvements have been realized in terms of microwave measurement techniques. The development of automatic network analyzers and sweep frequency measurements has led to the development of better and faster dielectric measurement techniques. This chapter will provide a review of microwave dielectric measurement techniques and systems, with particular emphasis placed on those that may be suitable for vegetation materials.

3.1 Transmission Techniques

The measured quantity in this case is the transmission coefficient (both amplitude and phase, T_m and ϕ_m). The problem is to measure it accurately and then use it to infer the dielectric constant of the unknown material. The most com-

monly used trsnsmission systems are the waveguide and the free space systems and these will be the subject of the next two sections.

3.1.1 Waveguide System

The block diagram shown in Fig. 3.1 represents a standard system used for measuring the amplitude and phase of the TE_{10} mode transmission coefficient. The main part of the system is a network analyzer capable of comparing the phase and amplitude of both arms, when the sample holder is empty, and again when the sample holder is filled with the unknown material. If we assume that the sample holder is of length L, we can write (Hallikainen et al, 1985).

$$T_m = |T_m|e^{j\phi_m} = \frac{(1-R^2)e^{-\gamma L}}{1-R^2e^{-2\gamma L}} \tag{3.1}$$

where $\gamma \equiv$ propagation constant of the dielectric-filled waveguide and $\gamma = \alpha + j\beta$.

$R \equiv$ the field reflection coefficient $= \frac{Z-Z_0}{Z+Z_0}$ where $Z_0 \equiv$ the characteristic impedance of the waveguides connected to the sample holder. Z and Z_0 are given by

$$Z = \frac{jw\mu_0}{\gamma} = \frac{2\pi\eta_0}{\lambda_0}\frac{\beta(1+j\alpha/\beta)}{\alpha^2+\beta^2}, \tag{3.2}$$

and

$$Z_0 = \frac{jw\mu_0}{\gamma_0} = \frac{2\pi\eta_0}{\lambda_0\beta_0} \tag{3.3}$$

where $w = 2\pi f$,

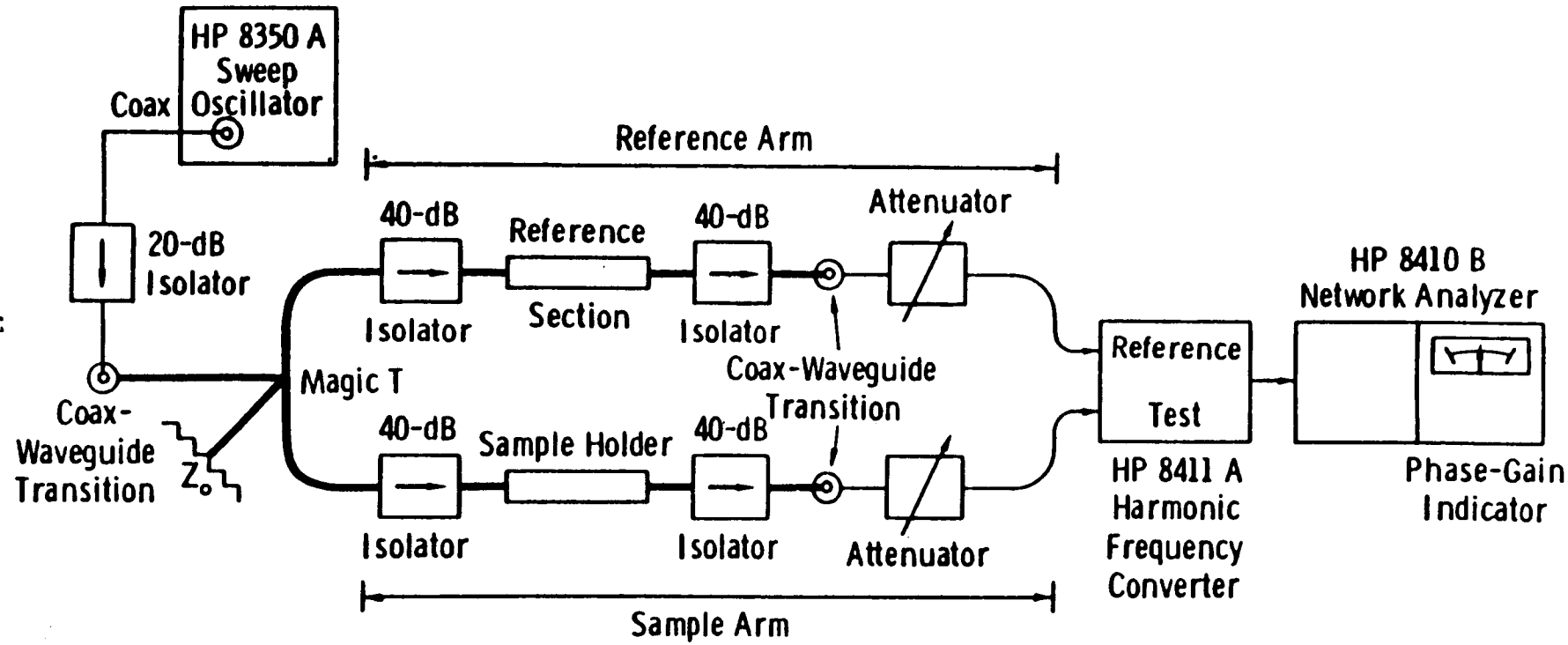

Figure 3.1. Waveguide transmission measurement system.

$\mu_0 \equiv$permeability of free space,

$\lambda_0 \equiv$ free space wavelength,

$\eta_0 = (\mu_0/\epsilon_0)^{1/2}$, $\equiv$ the intrinsic impedance of free space,

$\gamma_0 = j\beta_0 \equiv$ the propagation constant in the air-filled waveguide connected to the sample holder.

β_0 and γ are given by

$$\beta_0 = \frac{2\pi}{\lambda_0}[1 - (\frac{\lambda_0}{\lambda_c})^2]^{1/2} \tag{3.4}$$

$$\gamma = \alpha + j\beta = \frac{2\pi}{\lambda_0}[(\frac{\lambda_0}{\lambda_c})^2 - \epsilon]^{1/2} \tag{3.5}$$

where $\lambda_c = a/2$ is the cutoff wavelength of the guide of width a (for TE_{10} mode). From measurements of $/T_m/$ and ϕ_m, it is possible to determine α and β, from which the real and imaginary parts of ϵ may be determined:

$$\epsilon' = (\frac{\lambda_0}{2\pi})^2[(\frac{2\pi}{\lambda c})^2 - (\alpha^2 - \beta^2)], \tag{3.6}$$

$$\epsilon'' = (\frac{\lambda_0}{2\pi})^2(2\alpha\beta), \tag{3.7}$$

In practice, because of the nonlinear relationships between the measured quantities $/T_m/$ and ϕ_m and the quantities α and β, an iterative procedure is used to solve for α and β. The details of the procedure are given in Hallikainen et al (1985).

3.1.2 Free-Space System

As shown in Fig. 3.2, the free-space transmission system is basically similar to the waveguide system. The only difference is the utilization of two antennas and a sample holder, in the form of a dielectric slab, instead of waveguide sections. Consequently, the analysis is the same if we set $1/\lambda_c = 0$ in (3.4), (3.5), and (3.6). Again, an iterative procedure is used to determine ϵ.

3.2 Reflection Techniques

The problem here is to measure the reflection coefficient at the end of a transmission line (both amplitude, $|\rho_m|$ and phase, ϕ_m) and to try to relate it to ϵ of an unknown medium. Reflection techniques have, in general, two major problems: first, since the reflection coefficients for most natural materials are very close to unity, great care has to be taken in measuring $|\rho_m|$, and second, the mathematical expressions relating ρ_m to ϵ are usually derived for an infinite sample, a condition that can not be satisfied in practice. In the next two subsections a brief description will be given for two measurement systems based on the reflection technique.

3.2.1 Slotted Line System

This system was used by Broadhurst, as discussed earlier in Section 2.5, and it is shown schematically in Fig.3.3 (Broadhurst, 1970). The measurement of dielectric constant can be related to the measurement of the admittance of a

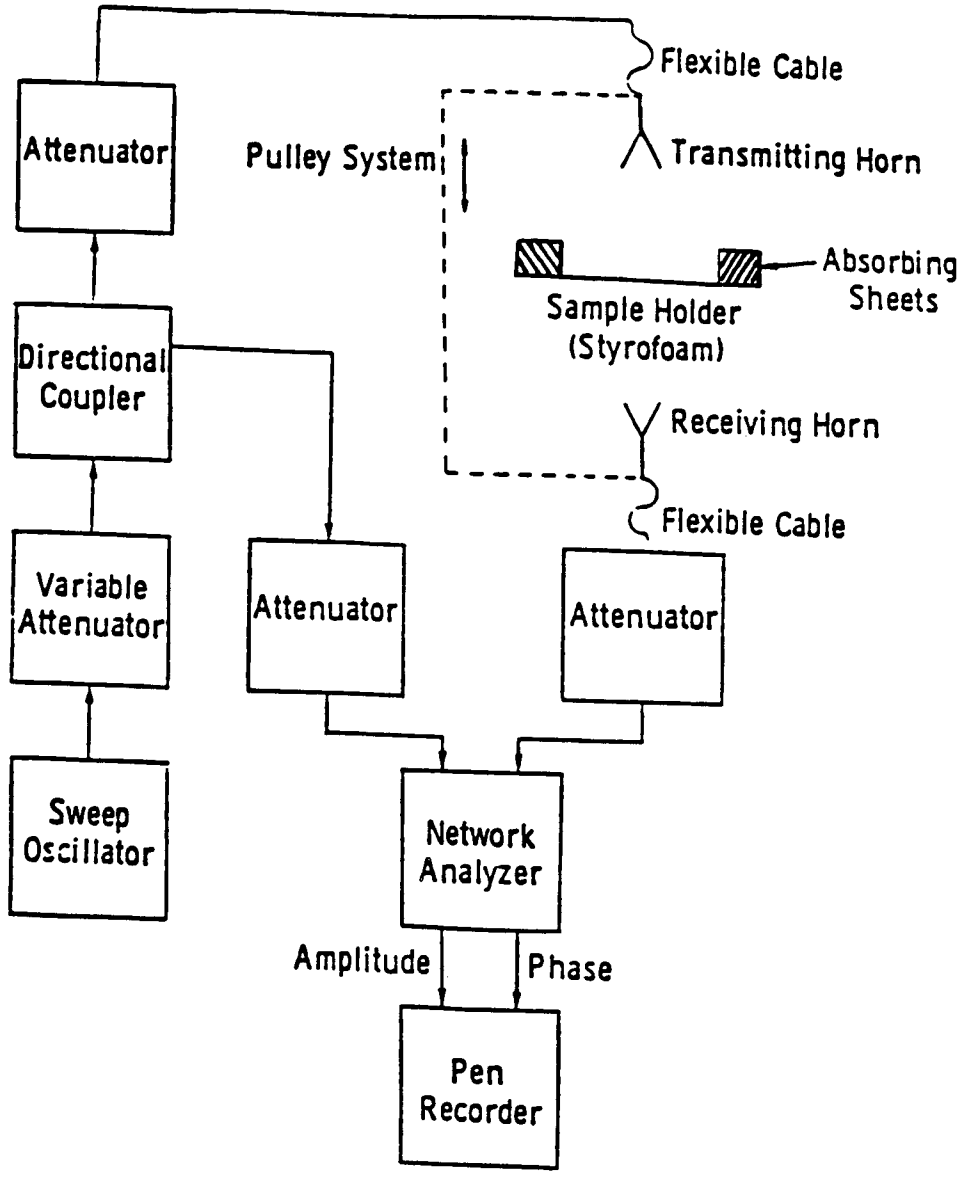

Figure 3.2. 3-18 GHz free-space transmission measurement system.

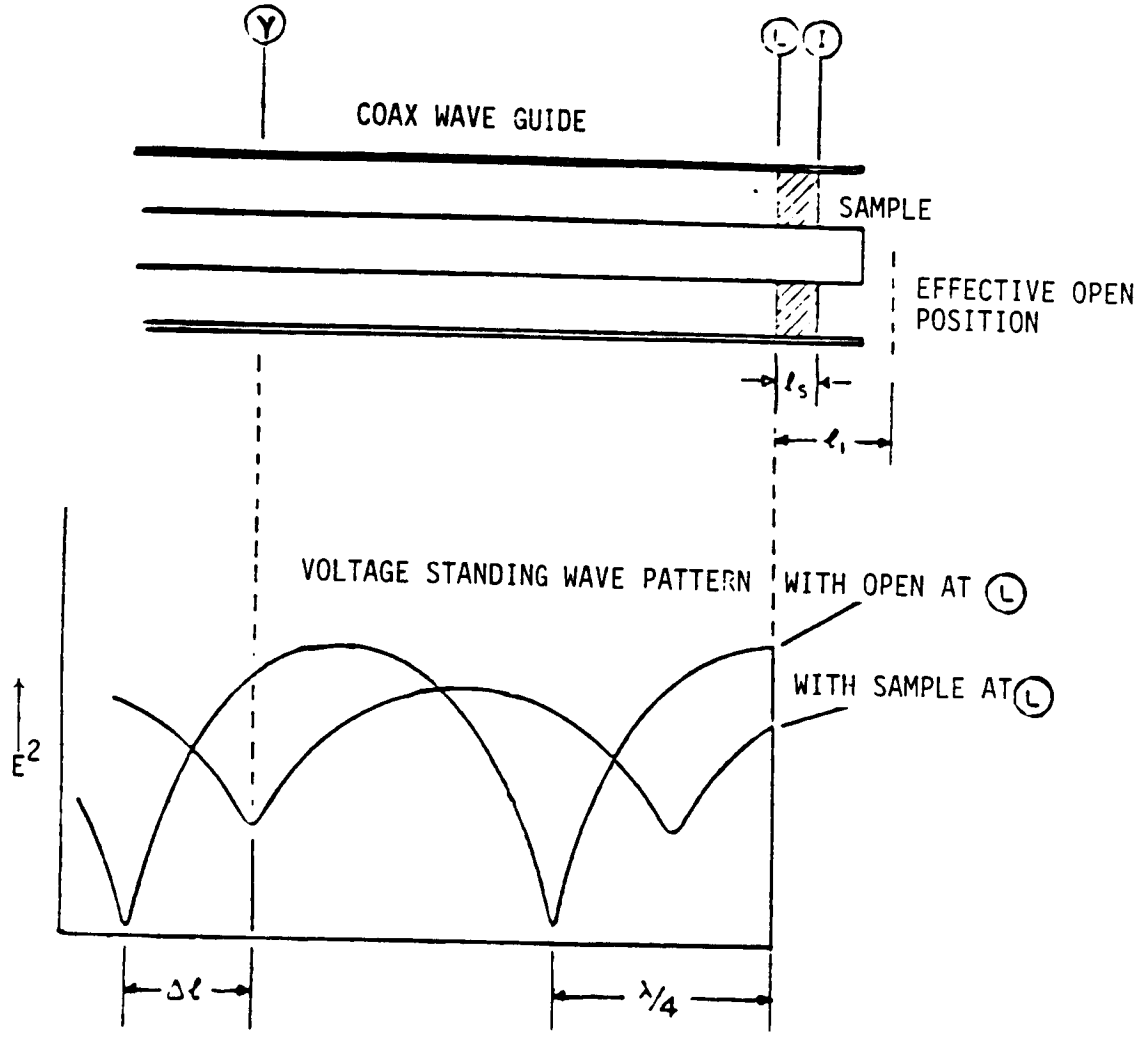

Figure 3.3. A schematic diagram of the coaxial wave guide used for the leaf measurements and the corresponding standing wave patterns assumed in the derivation of the working equations [Broadhurst, 1971].

coaxial transmission line with a specimen of the material occupying some of the space between the coaxial conductors (Broadhurst, 1970). The measurement of the admittance of a coaxial line is equivalent to the measurement of reflection coefficient at the same plane of reference.

The characteristic admittance Y_ϵ of a section of the line filled with an unknown material of permittivity $\epsilon = \epsilon' - j\epsilon''$ is given by (Kraus and Carver, 1973)

$$Y_\epsilon = \frac{\sqrt{\epsilon}}{60\ ln(a/b)} \tag{3.8}$$

where a and b are the outer and inner radii of the line. Similarly, for an air-filled coaxial line, the characteristic admittance and propagation factor are given by

$$Y_0 = \frac{1}{60\ ln(a/b)}, \tag{3.9}$$

And the propagation constants γ_ϵ and γ_0 are given by

$$\gamma_\epsilon = j\frac{w}{c}\sqrt{\epsilon}, \tag{3.10}$$

and

$$\gamma_0 = j\frac{w}{c} \tag{3.11}$$

where $c \equiv$speed of light $= \frac{1}{\sqrt{\mu_0\epsilon_0}}$.

In the following mathematical treatment, it will be assumed that the operating frequency is low enough for the line to propagate in the TEM mode only.

The admittance Y_M at point M, refer to Fig. 3.3, can be expressed in terms of the admittence Y_L at point L, Y_0, and γ_0 as follows:

$$Y_M = Y_0 \frac{Y_L + Y_0 tanh(\gamma_0 l)}{Y_0 + Y_L tanh(\gamma_0 l)}, \tag{3.12}$$

where l is the length of line between M & L.

Since it is impossible to achieve an open circuit at the end of the line, an extra length, l_1, is determined where the actual open circuit is located. Using equation (3.12) to transform the effective open circuit to point I,

$$Y_I = Y_0 tanh\gamma_0(l_1 - l_s) \tag{3.13}$$

If we transform this admittance from point I to point L (through the sample), we can show that

$$Y_L = Y_\epsilon \frac{Y_I + Y_\epsilon tanh(\gamma_\epsilon l_s)}{Y_I + Y_\epsilon tanh(\gamma_\epsilon l_s)}, \tag{3.14}$$

or

$$Y_L = Y_\epsilon \frac{Y_0 tanh\gamma_0(l_1 - l_s) + Y_\epsilon tanh(\gamma_\epsilon l_s)}{Y_\epsilon + Y_0 tanh\gamma_0(l_1 - l_s) tanh(\gamma_\epsilon l_s)} \tag{3.15}$$

Substituting $Y_\epsilon = Y_0\sqrt{\epsilon}$ and $\gamma_\epsilon = \gamma_0\sqrt{\epsilon}$ and simplifying we obtain

$$Y_L = Y_0 \frac{tanh[\gamma_0(l1 - l_s)] + \sqrt{\epsilon} tanh(\sqrt{\epsilon}\gamma_0 l_s)}{1 + \frac{1}{\sqrt{\epsilon}} tanh[\gamma_0(l_1 - l_s)] tanh(\sqrt{\epsilon}\gamma_0 l_s)} \tag{3.16}$$

Equation (3.16) relates a measureable quantity, the admittance Y_L, to the unknown dielectric constant of the sample ϵ. The relationship, however, is not simple and suitable approximations must be used. Broadhurst used frequencies up to 4.2 GHz ($\lambda = 7.1cm$) and samples of thicknesses less than .04 cm. l_1 was found experimentally to be about .3 cm. Hence the maximum values of the above arguments can be shown to be less than .26. Using equation (3.16) and the approximation $tanh(u) \approx u$, leads to

$$Y_L \approx Y_0 \frac{\gamma_0(l_1 - l_s) + \epsilon\gamma_0 l_s}{1 + \gamma_0^2(l_1 - l_s)l_s} \tag{3.17}$$

The resulting error is about 7 percent or less. Using the above argument, we can also neglect the second term in the denominator, leading to

$$Y_L \approx Y_0[\gamma_0(l_1 - l_s) + \epsilon\gamma_0 l_s] \tag{3.18}$$

Using equation 3.18, ϵ can be calculated from the measured value of Y_L,

$$\epsilon = \frac{1}{\gamma_0 l_s}[\frac{Y_L}{Y_0} - \gamma_0(l_1 - l_s] \tag{3.19}$$

It should be noted here that equation (3.19) is only valid under the following assumptions:

(i) Pure TEM propagation mode.

(ii) $\frac{2\pi}{\lambda} l_s \leq .25.$

(iii) $\frac{2\pi}{\lambda}(l_1 - l_s) \leq .25.$

Condition (ii) limits the maximum measureable sample thickness to .3 cm at 4 GHz. Broadhurst reported f_c, the upper limit of frequencies that can be used before higher order modes start to propagate, as

$$f_c = 9.5/\sqrt{|\epsilon|} \tag{3.20}$$

This limit depends on the coaxial line dimensions as well as ϵ (as will be shown in Chapter 4).

3.2.2 Probe System

Open-ended coaxial lines can be used successfully in measuring the permittivity of unknown materials (Burdette et al, 1980; Athey et al, 1982; Stuchly et al, 1982). A complete description and analysis of this system will be delayed until the next chapter. However, a brief discussion of the theory of operation is given here for the sake of completeness. Figure 3.4 shows a block diagram of the measurement system. It is basically a standard reflection coefficient measurement system with the probe tip acting as the termination load (either immersed or in contact with the sample). The input reflection coefficient at the probe tip, ρ, is given by

$$\rho = \frac{Z_L - Z_0}{Z_L + Z_0}, \tag{3.21}$$

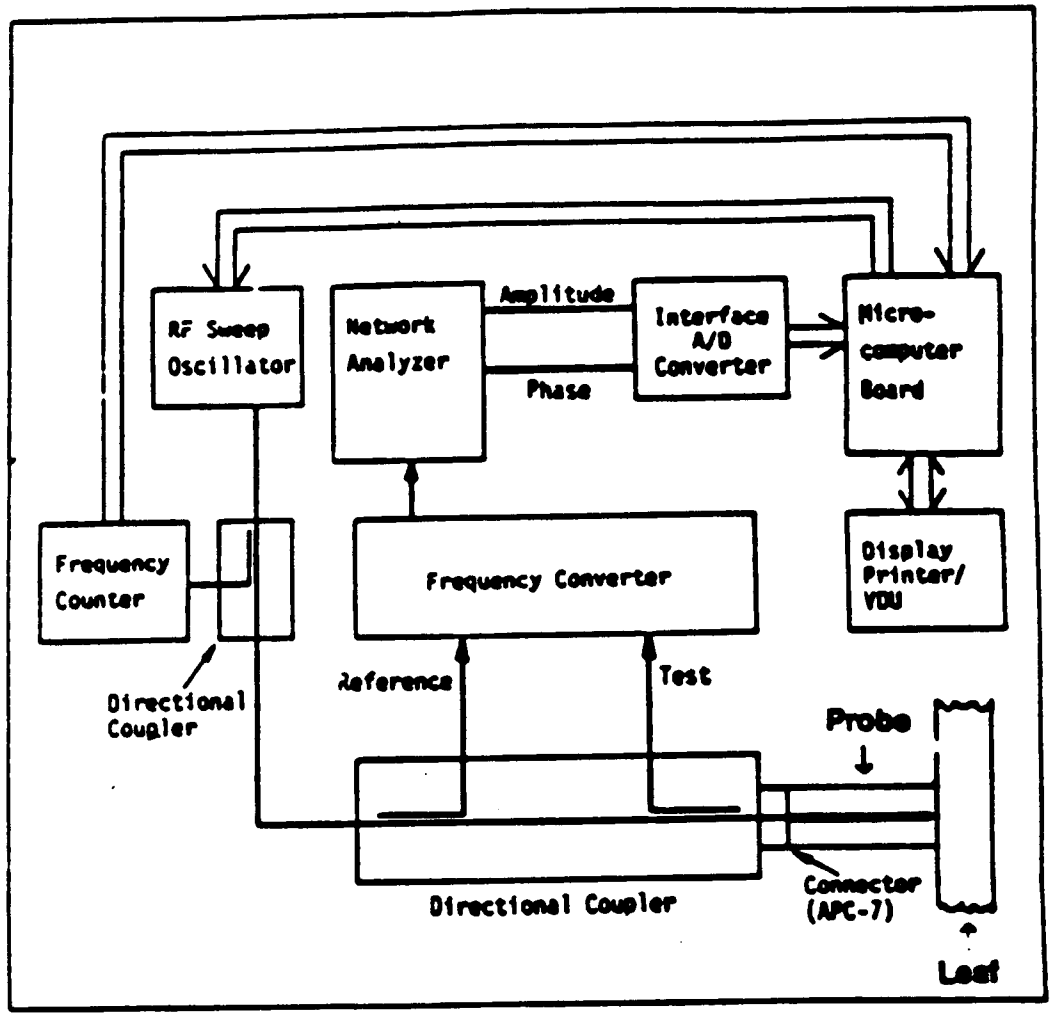

Figure 3.4. Block diagram of the probe dielectric system. Frequency coverage is 0.1-20 GHz.

where Z_0 is the line impedance (50 Ω usually) and Z_L is the load impedance given by (Deschamps, 1962; Burdette et al, 1980)

$$\frac{Z_L(w,\epsilon)}{\eta} = \frac{Z_L(\sqrt{\epsilon}w,\epsilon_0)}{\eta_0}, \tag{3.22}$$

where η_0 and η are the intrinsic impedances of free space and the measured dielectric medium respectively, ϵ_0 and ϵ are the complex dielectric constant of free space and the medium under test respectively, and w is the angular frequency. For a non-magnetic medium where $\mu = \mu_0, Z_L$ simplifies to

$$Z_L(w,\epsilon) = \frac{1}{\sqrt{\epsilon}} Z_L(\sqrt{\epsilon}w,\epsilon_0). \tag{3.23}$$

If the probe equivalent circuit can be modelled analytically, the medium dielectric constant can be retrieved from the measured reflection coefficient; sometimes an iterative solution is required depending upon the complexity of the form of Z_L.

It is possible, albeit difficult, to relate the measured reflection coefficient directly (e.g., the Method of Moments, MOM)to the unknown ϵ (Gajda and Stuchly, 1983). The analysis, e.g. MOM, and processing time would be enormous using this approach. On the other hand, if we choose the frequency range and the line dimensions such that the field distribution around the probe-tip is dominantly capacitive we could develop a lumped-element equivalent circuit which would facilitate the analysis and data precessing.

The equivalent circuit elements could be chosen on the basis of the line dimensions and the operating frequency. In this section only the low frequency

equivalent circuit will be analyzed and the complete one will be discussed in the following chapter.

The input impedance for the low frequency equivalent circuit is given by

$Z_L = 1/j\omega(C_f + C_0)$ in free space,

and $Z_L = 1/j\omega(C_f + \epsilon C_0)$ in the medium. where, C_f is the fringing field inside the teflon, and C_0 is the fringing field outside the teflon and inside the medium. The reflection coefficient can then be expressed as

$$\rho = \frac{1 - jwZ_0(C_f + \epsilon C_0)}{1 + jwZ_0(C_f + \epsilon C_0)}, \tag{3.24}$$

and, solving for ϵ we get

$$\epsilon = \frac{1 - \rho}{jwZ_0C_0(1 + \rho)} - \frac{C_f}{C_0}. \tag{3.25}$$

This equivalent circuit is only valid at frequencies where the line dimensions are small compared to λ; i.e., only the reactive field exists with no radiation. C_f and C_0 are not known and should be estimated using calibration against a standard material such as distilled water. This technique is quite attractive because ϵ can be computed from ρ in a straightforward manner.

3.3 Resonance Technique

In the following two sections a brief description will be given of the use of resonant cavities in the measurement of the microwave dielectric properties of matter.

3.3.1 The Filled-Cavity Approach

A block diagram of a typical cavity measurement system is shown in Fig. 3.5 . A complete theoretical analysis of this problem was given by Harrington (Harrington, 1961). The basic idea is that the dielectric constant of a material filling a cavity is determined by the shift in the resonant frequency f_0 and the change in the quality factor Q (Russ, 1983). An air-filled cavity is assumed to be the reference with f_0 and Q_0; while the dielectric-filled cavity has f_s and Q_s. The dielectric constant can then be calculated from

$$\epsilon_r' = (f_0/f_s)^2, \tag{3.26}$$

and,

$$\epsilon_r'' = \epsilon_r'[\frac{1}{Q_s} - \frac{1}{Q_0}\sqrt{\frac{f_0}{f_s}}]. \tag{3.27}$$

The quality factor Q_i is in general given by

$$Q_i = f_i/\Delta f_i \tag{3.28}$$

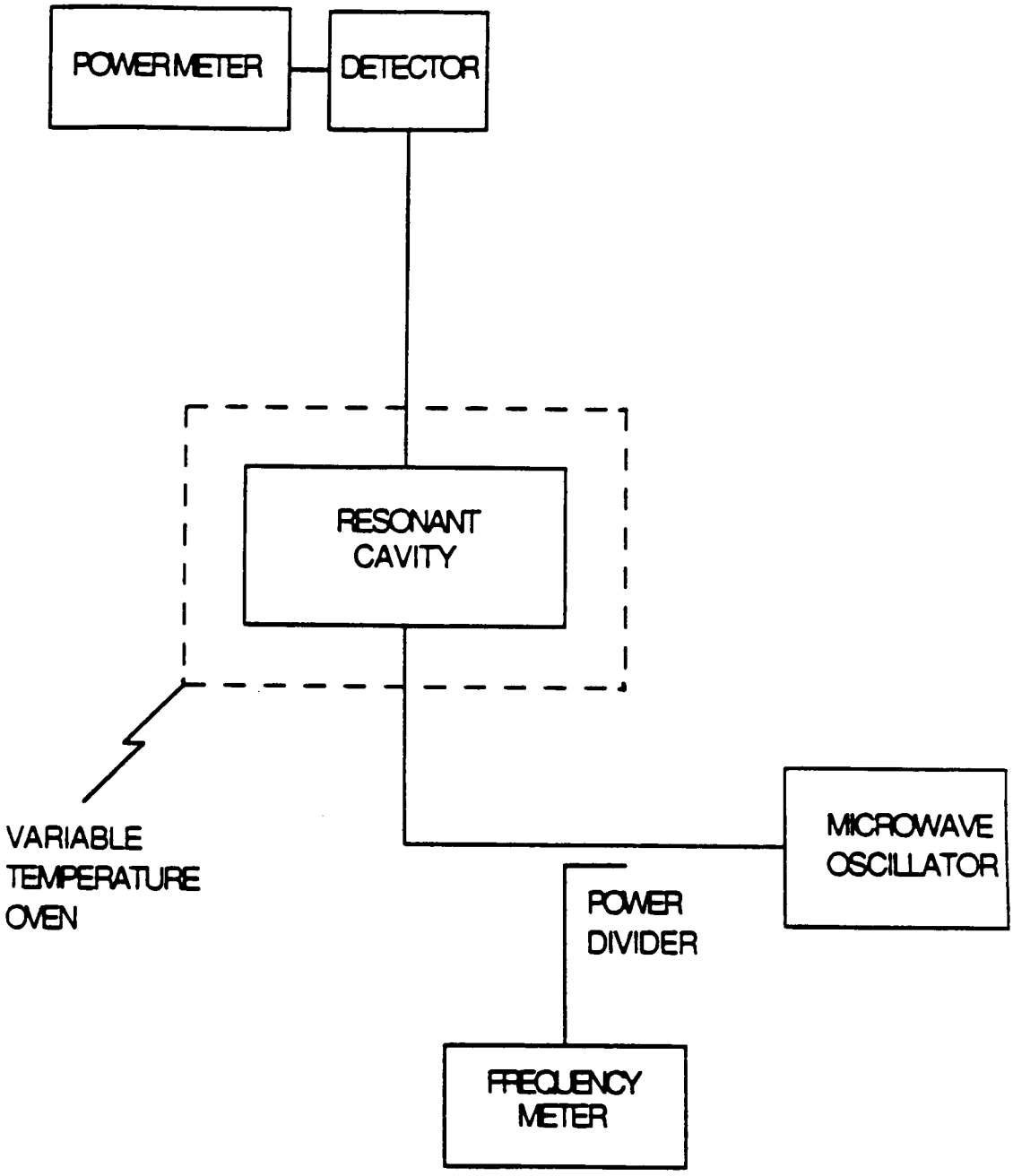

Figure 3.5. Schematic diagram of the measurement set-up for microwave cavity measurements.

where f_i is the resonant frequency and Δf_i is the 3-db bandwidth. Equations (3.26- 3.28) are evidently very simple and easy to use, yet there are two problems encountered:

1. If ϵ_r is too high, an undesirable large frequency shifts and/or reduction in the value of Q would preclude an accurate measurement of f_s and Q_s.

2. For some materials, such as vegetation, it is very difficult to fill the cavity with solid material without some air pockets remaining. This complicates the inference of the dielectric constant of the material.

3.3.2 The Partially-filled Cavity Approach

This technique is also called the perturbation technique. Small resonant frequency shifts are attainable by the proper selection of the sample size. The perturbation analysis is given in details in (Harrington, 1961; Russ, 1983). These derivations were based on the assumption that either the sample volume or its dielectric constant are small enough so that the field structure in the cavity is not substantially changed by the insertion of the sample. The shape of the sample is an important factor in determining the appropriate approximate formula to be used. Spheres, discs, and needles are the most commonly used shapes, and among these the needles are the most popular. Let us take, as an example, a TM_{010} cylindrical cavity with

$$d < 2a \tag{3.29}$$

where, d is the cavity length and a is the cavity radius.

For a cylindrical sample of radius c and length d, (Russ, 1983) shows the derivations leading to

$$\frac{w_s - w_0}{w_0} = -1.855(\epsilon_r - 1)(\frac{c}{a})^2, \tag{3.30}$$

$$w_s' = w_s + j\frac{w_s}{2Q}, \tag{3.31}$$

$$\epsilon_r' = \frac{w_0 - w_s}{1.855 w_s V_v} + 1, \tag{3.32}$$

and

$$\epsilon'' = \frac{w_0}{3.71 w_s v_r}(\frac{1}{Q_s} - \frac{1}{Q_0}), \tag{3.33}$$

where equations 3.32 and 3.33 were derived using equations 3.30, which is only applicable for a needle-shaped sample, and 3.31, which represents the resonant frequency for a lossy circuit. Data processing in this case is very straightforward. However, special care should be taken in the following cases: (i) If the sample length is not equal to the cavity length, a different set of equations is valid (Parkash et al, 1979). (ii) If the sample volume is very small, the changes it produces may not be detectable, and if the sample volume is very large, it could modify the fields, thereby destroying the validity of the perturbation equations.

3.4 Comparison

Table 3.1 provides a summary of the pertinent features of the various microwave dielectric measurement techniques. An analysis of these features will be given next.

3.4.1 Usable Frequency Band

(i) The Waveguide Transmission System

L, S, C, and X band systems are possible frequency bands for the measurements, yet for each band a separate waveguide system is needed. This fact makes measurements across a wide band, e.g. 1-12 GHz, discontinuous due to calibration problems. Also, packing an X-band waveguide is very difficult and it is hard to achieve a homogeneous sample. One of the major limitations of the waveguide system is the possible propagation of higher-order modes in the guide, especially in the upper end of the range. Above X-band, the waveguide size becomes impractically small to use.

(ii) Free-Space System

The free-space system was used successfully in measuring dielectric properties of wet soils and snow samples over the 3-18 GHz (Hallikainen and Ulaby, 1983). The lower frequency limit was imposed by the required sample size and the upper limit by the cut-off frequency of the antennas. A similar system at 37 GHz was also constructed and calibrated. The only high frequency limit seems to be the required smoothness of the sample surface (surface rms roughness should be less

than $\lambda/10$).

(iii) Slotted Line System

Since this system utilizes a TEM cell in a coaxial line, it has a much larger bandwidth compared to a waveguide system (Broadhurst, 1970). Broadhurst reported a slotted line system that operated from 100 kHz to 4.2 GHz but he also concluded that excessive scatter in the data above 1 GHz was due to high-order mode propagation. For the coaxial line used in his experiment the cutoff frequency of these modes is given by

$$f_c = 9.5/\sqrt{|\epsilon|},$$

which means that a moist leaf can be measured up to 1 or 2 GHz without the occurence of moding problems.

(iv) Probe System

Since the probe system is basically an open-ended coaxial line, the usable bandwidth is expected to be as high as that of the slotted line system. In the course of this study, however, it was only attempted to operate the system from 100 MHz to 20 GHz. Reduction in the system sensitivity was observed in the low frequency range and an increase of higher-order mode propagation in the high end. A statisfactory compromise can be achieved by using larger probes at low frequencies and smaller probes at high frequencies as will be discussed in the next chapter.

(v) Resonant Cavity Systems

The frequency of operation is limited to only one single frequency for each cavity.

3.4.2 Measurement Accuracy and Precision

(i) Waveguide System

The relative measurement errors $\Delta\epsilon'/\epsilon'$ and $\Delta\epsilon''/\epsilon''$ were estimated on the basis of the precision specifications of the network analyzer /phase gain indicater. They were compared to those observed during the course of measurement and found to be in complete agreement. The results may be summarized as follows:

(a) $\Delta\epsilon' \leq .15$ and $\Delta\epsilon'' \leq .17$ for all samples tested.

(b) $(\Delta\epsilon'/\epsilon') \leq .9\%$ at 1.4 GHz and $< .7\%$ at 5 GHz for all samples tested.

(c) $\Delta\epsilon''/\epsilon''$ decreases from 37% at low values of ϵ'' to 6% for high values of ϵ''.

The 37% relative precision was observed for $\epsilon'' = .06$ and the standard deviation was $\Delta\epsilon'' = .022$. So, even though the relative precision is large, the absolute precision is small.

(ii) Free-Space System

The total calculated worst case error bounds were plotted against frequency for different sample lengths and for various dielectric constant magnitudes for both ϵ' and ϵ'' and were found to be around 10% (except for very low loss materials where the error can be as high as 60 %). The error bounds include uncertainties in both the equipment and in sample preparation. The system was calibrated for absolute accuracy using polymethyl methacrylate (a low-loss material) and water (a high-loss material) and the errors were within the worst case bounds.

It was found that the system accuracy improves with increasing frequency, magnitude of ϵ, and sample thickness.

(iii) Slotted Line System

The accuracy of measuring the real part was within 10%, while for the imaginary part sizeable errors were reported (Broadhurst, 1970). It was found generally that the accuracy improves at low frequencies. A check of the precision of leaf measurements was conducted by packing the sample, measuring it, unpacking it, then packing it and measuring it again. The previously mentioned procedure was repeated several times for different samples and at different frequencies and an analysis of variance was conducted to separate the instrumental errors from those due to sample variations. The uncertainties in the leaf- thickness measurements amounts to $5 - 10\%$. In general, the total uncertainties in the measurement system was much better than 20%.

(iv) Probe system

Athey et al (part 1, 1982) grouped the errors in their measurement system into two types: (1) Systematic errors and (2) nonsystematic errors. The systematic errors, which are due to the network analyzer system, were assumed to be $\Delta|\rho| = .003$ and $\Delta\phi = .3^0$. The estimated uncertainties around 1 GHz were found to be within 2% for ϵ' and 8% for ϵ''. The nonsystematic errors, on the other hand, were attributed to repeatability of connections, temperature drift, noise, nonperfect probe connector, dirt, imperfect contact with the sample, and inhomogeneities in the substance under test. The system overall accuracy depends on how far the

probe capacitance is from the optimum capacitance value (a discussion of this condition will be given in the next chapter).

The nonsystematic errors can be avoided if proper care is exercised during the measurements and by repeating suspicious data sets. According to Athey (1982), the overall system accuracy and precision were within the limits estimated on the basis of the systematic errors alone.

(v) The Cavity Systems

The precision of the filled cavity measurement system is almost perfect especially if care is taken in replacing the cover and tightening the bolts using a torque wrench. The measurement error for Q_L for a partially filled cavity is $\pm 1.25\%$ (for $Q_L \geq 500$) and $\pm 7\%$ for($Q_L = 200$) (Chao, 1985), which means that the measurement error is negligible for ϵ' and less than $\pm 2\%$ for ϵ'' (compared to 37% in the waveguide system).

However, the smaller the sample volume the larger are the errors associated with ϵ' and ϵ'' due to dimensions measurement errors. These errors can be as large as 10%.

3.4.3 Dielectric Values Limit

It is probably a general rule that the higher the magnitude of ϵ is, the better becomes the accuracy and precision of the measurements, as long as the values of ϵ do not allow higher-order modes to propagate.

3.4.4 Practical Aspects

(1) Sample Size and Preparation

From a vegetation dielectric-measurement-system point of view, the waveguide, the free-space, and the cavity techniques are not suitable because it is impossible to achieve a unity filling factor (because of unavoidable air voids inside the measured sample). Also it is impossible to achieve the smooth surface required for free-space system samples. Slotted line and cavity perturbation measurements on a vegetation sample will always suffer from inaccuracies in thickness measurements.

The probe system on the other hand, requires a relatively thin sample (at most a few leaves-thick). However, special care has to be taken to insure that the pressure applied by the probe against the sample is high enough to ensure good contact, but not too high to cause squeezing of fluid out of the vegetation tissue or changing the vegetation bulk density (as will be discussed in the next Chapter).

(2) Temperature Measurements

The best system for the purpose of making dielectric measurements as a function of temperature is probably the free-space system because there are no metal parts in contact with the sample. The waveguide is probably the hardest because large pieces of metal would need to be insulated. The probe system (as will be shown in the next chapter) operates satisfactorily with regard to temperature measurements.

(3) Field Measurement

The probe system, no doubt, is superior to any other system for field operation because it is the only nondestructive tool capable of measuring samples without destroying them.

Technique Feature	Waveguide System	Free-Space System	Slotted-Line	Probe System	Filled-Cavity	Partially-filled
Usable Band (GHz)	1-2,2-4, 4-8,8-12 4 systems	3-18 1 system	100 KHz-4.2 GHz 2 systems	.05-20.4 1 system, 2 probes	single frequency per cavity	single frequency per cavity
Accuracy Low loss	reasonable	reasonable	bad	bad	the best	very good
Accuracy high loss	very good	good	good	good	Does not work	good
Sample Size	small at HF large at LF	large at HF	reasonable	small	small at HF large at LF	small
Sample Preparation	Easy but lengthy	hard and tedious	easy	easy	hard/ impossible	hard/ impossible
temperature	hard	perfect	hard	easy	perfect	perfect
Field Measurements	hard	hard	hard	easy	hard	hard

Table 3.1 Comparison between different microwave dielectric measurement techniques.

Chapter 4

Open-Ended Coaxial Probe System

4.1 System Description

As previously discussed in section 3.2.2, an open-ended coaxial line and a short monopole probe are found to be viable sensors for dielectric constant measurements at microwave frequencies. We shall restrict the discussion here to only open-ended coaxial line probes. As shown in Fig. 3.4, the main part of the system is the microcomputer-controlled network analyzer (HP 8410C) which is employed to measure the input impedance at the probe tip. The probe translates changes in the permittivity of a test sample into changes in the input reflection coefficient of the probe. The automation of the reflectometry system made data acquisition, correction, and processing a straight forward task in addition to the achieved speed of operation. Indeed, the development of such a system would have been impossible only 15 years ago, since the concept of automated network analyzer measurements was introduced recently.

The open-ended coaxial line probe system operates over a very wide frequency band. The .141" probe model, for example, covers the range extending from .5 GHz to 20 GHz. The overall error bounds for both ϵ' and ϵ'' were found to be within 10 % of the measured values. The 10% figure is very conservative and in some cases it is even better than 1%. Also, since the rounding error in ϵ' and ϵ'' is $\pm.1$, at low dielectric values the relative errors can be too large. The lower frequency limit is set by the degraded sensitivity while the upper limit is determined by the cut-off frequency of the next propagating high-order mode as will be discussed later is section 4.3.2 and 4.3.3. Besides the wide frequency band of operation, the probe has the capability of measuring the dielectric constant of test materials nondestructively and rapidly.

4.2 Analysis

The analysis of the probe system can be divided into the following steps: error correction, equivalent circuit modeling, and calibration and the inverse problem.

4.2.1 Error Correction

There are certain inherent measurement errors when the network analyzer system is used for microwave measurements. These errors can be separated into two categories: (a) instrument errors and (b) test set/connection errors (HP application Note and Burdette, 1980). Instrument errors are those related to random variations due to noise, imperfect conversions in such equipment as the frequency converter, crosstalk, inaccurate logarithmic conversion, nonlinearity

in displays, and overall drift of the system. Test set/connection errors are due to the directional couplers in the reflectometer, imperfect cables, and the use of connector adaptors. Among these two error sources, the latter is the major source of error at UHF and microwave frequencies. These uncertainties are quantified as directivity, source match, and frequency tracking errors. The analytical model used for correcting test set/connection errors is based on the model used by Hewlett-Packard for correcting reflectivity measurements (HP Application note). This model accounts for the three types of systematic errors. Each of them is shown schematically in Fig. (4.1). The measured reflection coefficient can be derived as

$$\rho_{11m} = S_{11} + \frac{S_{12}S_{21}\rho_{11a}}{1 - S_{22}\rho_{11a}} \tag{4.1}$$

S_{11} is the directivity term and is due to (a) direct leakage of the incident signal into the test channel via the reflectometer directional couplers and (b) to further degradation by connectors and adaptors. S_{22} is the source match term and is caused by multiple reflections into the unknown load. The product $(S_{21}S_{12})$ is the frequency tracking term and is due to small variations in gain and phase flatness between the test and reference channels as a function of frequency. The reflection coefficients ρ_{11m} and ρ_{11a} are the measured and actual reflection coefficients, respectively. These three error factors can be determined and calibrated out using three known standard loads with known ρ_{11a} across the required frequency band. Hence, ρ_{11a} can then be determined from

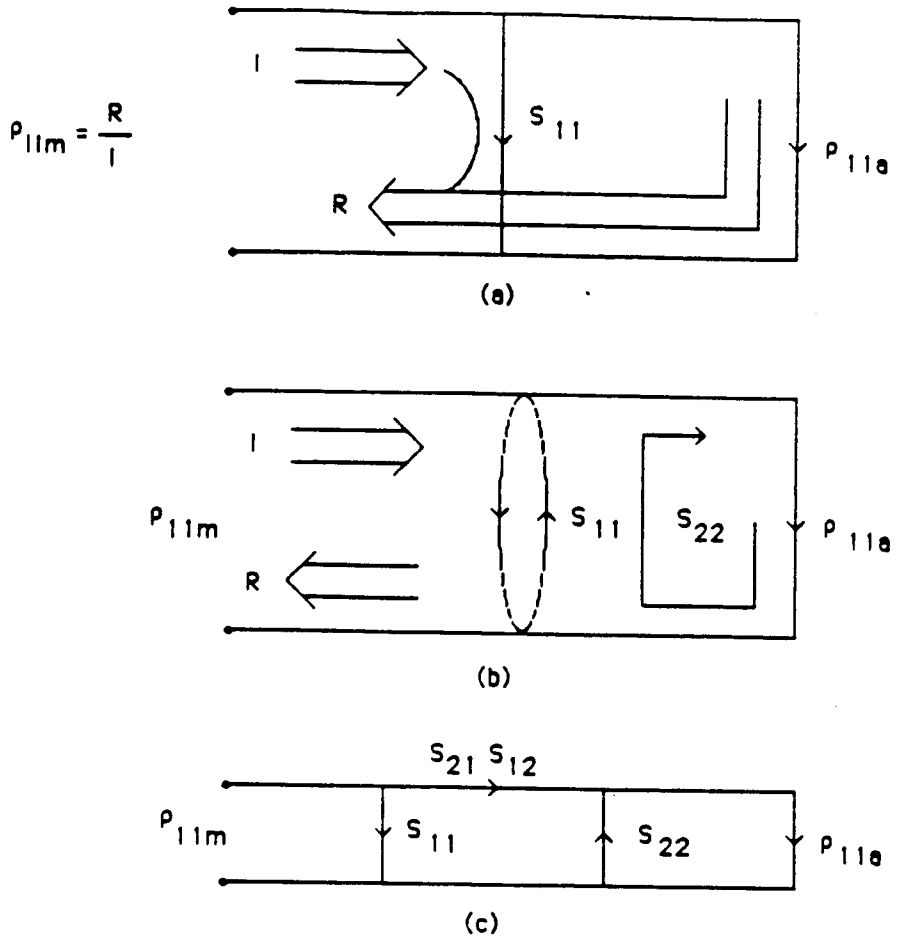

$$\rho_{11m} = \frac{\rho_{11a}(S_{21}S_{12})}{1 - S_{22}\rho_{11a}} + S_{11}$$

$$\rho_{11a} = \frac{\rho_{11m} - S_{11}}{S_{22}(\rho_{11m} - S_{11}) + S_{21}S_{12}}$$

Figure 4.1. Error models used for test set connection errors.

$$\rho_{11a} = \frac{(\rho_{11m} - S_{11})}{S_{22}(\rho_{11m} - S_{11}) + S_{12}S_{21}} \tag{4.2}$$

S_{11} can be determined separately using a sliding matched load termination. The reflection coefficient of the load can be eliminated by multiple load measurements at different path lengths. The loci of these points form a circle whose center is the true directivity error vector. Using short-circuit and open-circuit loads, S_{22} and $S_{12}S_{21}$ can be determined (S_{12} and S_{21} were lumped together because they always appear as a product). Since the open-circuit condition is hypothetical, because of radiation and fringing fields, a correction to $(\rho_{11a})_{O.C.}$ is always made. Also, since the calibration should be done with the probe tip as the reference plane, and since there is no standard short circuit for that situation, liquid mercury has been used as the short circuit termination. This approach proved successfull as long as care is taken to ensure an approximate phase shift of 180^0 from the open-circuit reading. A final remark that should be made here about S_{11} is that its determination is made at the APC-7 connector reference plane and it is used at the probe tip reference plane. This approach neglects the reflections due to the APC-7 connector and any other reflections along the probe especially due to the bent, along the probe line, and any inhomogeneity in the teflon. This approximation is justified by assuming that the APC-7 connector and the probe line are free of defects. This approximation is probably accountable for most of the system errors (accuracy), while instrumental errors can be greatly reduced by data averaging.

4.2.2 Equivalent Circuit Modeling

In general, there are two approaches to handling the probe analysis: an exact electromagnetic treatment or an approximate modeling approach. The exact electromagnetic treatment uses either the variational or the moment methods. These approches are exact, but they have a few problems:

1. Computer- time consuming,

2. The exact inverse problem is impossible, and

3. The loss of accuracy due to the approximate inverse problem is high.

On the other hand, the approximate modeling treameant is less accurate and more efficient in terms of computer time. The model used to describe the probe behavior has, as shown in Fig.(4.2), the following equivalent circuit parameters (Marcuvitz, 1951l; Tai, 1961; Kraszewski and Stuchly, 1983; Gajda and Stuchly, 1983):

1. C_0, the fringing field capacitance,

2. C_f, the fringing field (inside the teflon) capacitance,

3. $B\omega^2$, the increase in the fringing field capacitance with frequency because of the evanescent TM modes excited at the junction discontinuity, and

4. A, the factor representing the radiative discontinuity field.

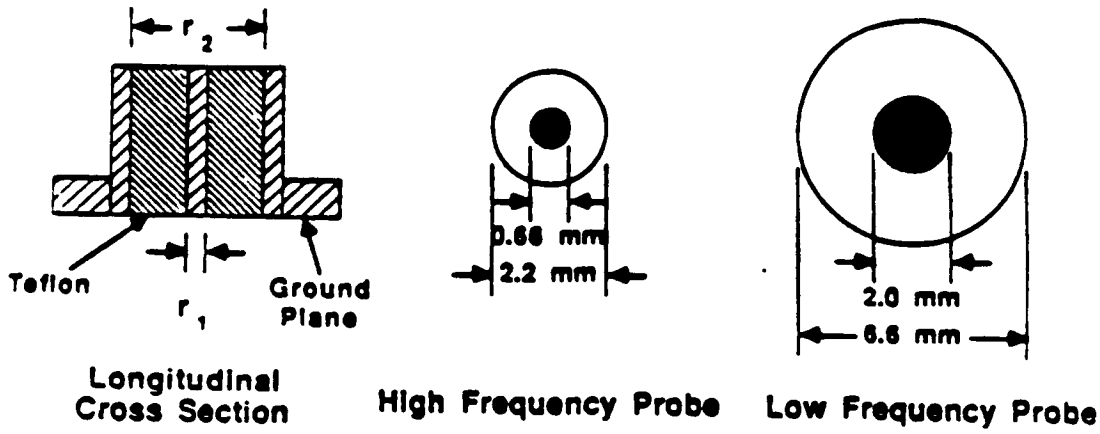

(a) Dielectric Probes

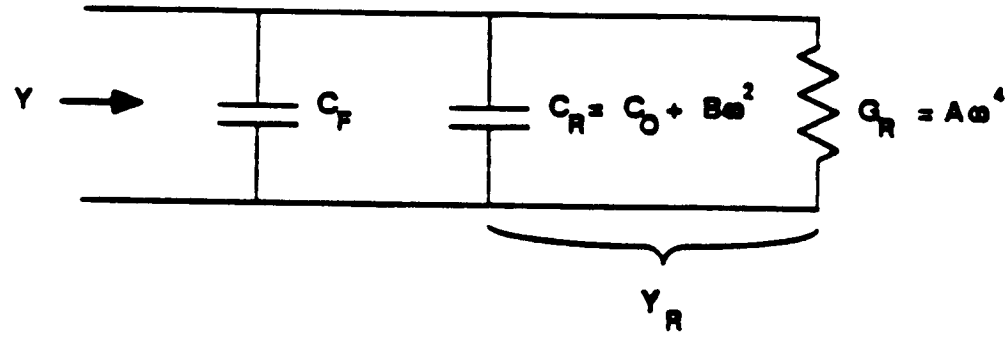

(b) Probe Equivalent Circuit

Figure 4.2. Coaxial probe (a), and its equivalent circuit (b).

C-2

These four parameters are a function of the transmission line dimensions. The admittance in free space is given by

$$Y(\epsilon = 1) = j\omega(C_f + C_0 + B\omega^2) + A\omega^4 \tag{4.3}$$

when the load is a lossy dielectric medium with complex dielectric constant ϵ, $Y(\epsilon)$ is given by:

$$Y(\epsilon) = j\omega(C_f + C_0\epsilon + B\omega^2\epsilon^2) + A\omega^4\epsilon^{2.5} \tag{4.4}$$

This is a linear equation with four unknowns C_f, C_0, B, and A. In order to determine the equivalent circuit unknowns, two standard materials need to be measured to provide two complex equations or four real ones. Usually distilled water and methanol were used for calibration in this work. Equation (4.4) can be solved for the unknown equivalent circuit parameters by solving the matrix equation(4×4).

It is possible to solve this equation for $C_f, C_0, B, and\ A$ using standard matrix techniques (e.g. diagnonal method). After calculating the equivalent circuit paramaters, the system will be ready to process the reflection coefficient data for the unknown materials.

4.2.3 Calibration and the Inverse problem

In calibration we need to solve a (4 x 4) matrix for the equivalent circuit parameters, but in calculating the unknown ϵ of the material under test Equation

(4.4) should be solved for ϵ. This equation is a complex equation of the fifth order. It was found that an easy method for solving it is through an iterative routine. The algorithm used for correction, calibration, and data processing is given in Fig.(4.3).

4.3 Probe Selection

The overall accuracy and precision of any probe system depends on the frequency range of operation, the accuracy of the dielectric constant of the calibration materials, the value of the unknown dielectric, and the nature of the sample under test.

4.3.1 Optimum Capacitance

It has been shown (Stuchly et al, 1974) that for a given accuracy of the reflection coefficient measurement, the accuracy in determining the permittivity ϵ is greatest when

$$C_0 = \frac{1}{wZ_0\sqrt{\epsilon'^2 + \epsilon''^2}} \tag{4.5}$$

where Z_0 is the characteristic impedance of the line. The expression strictly holds only when the uncertainties in the magnetude and phase of the reflection coefficient are approximately the same, i.e., $\Delta\varphi \simeq \frac{\Delta\rho}{\rho}$. For other cases the optimum value of C_0 is different for ϵ' and ϵ''; nontheless, in general the value given by (4.5) is a good compromise. Figures 4.4(a) to (d) show the calculated optimum capacitance for a variety of materials plotted against frequency. Since the

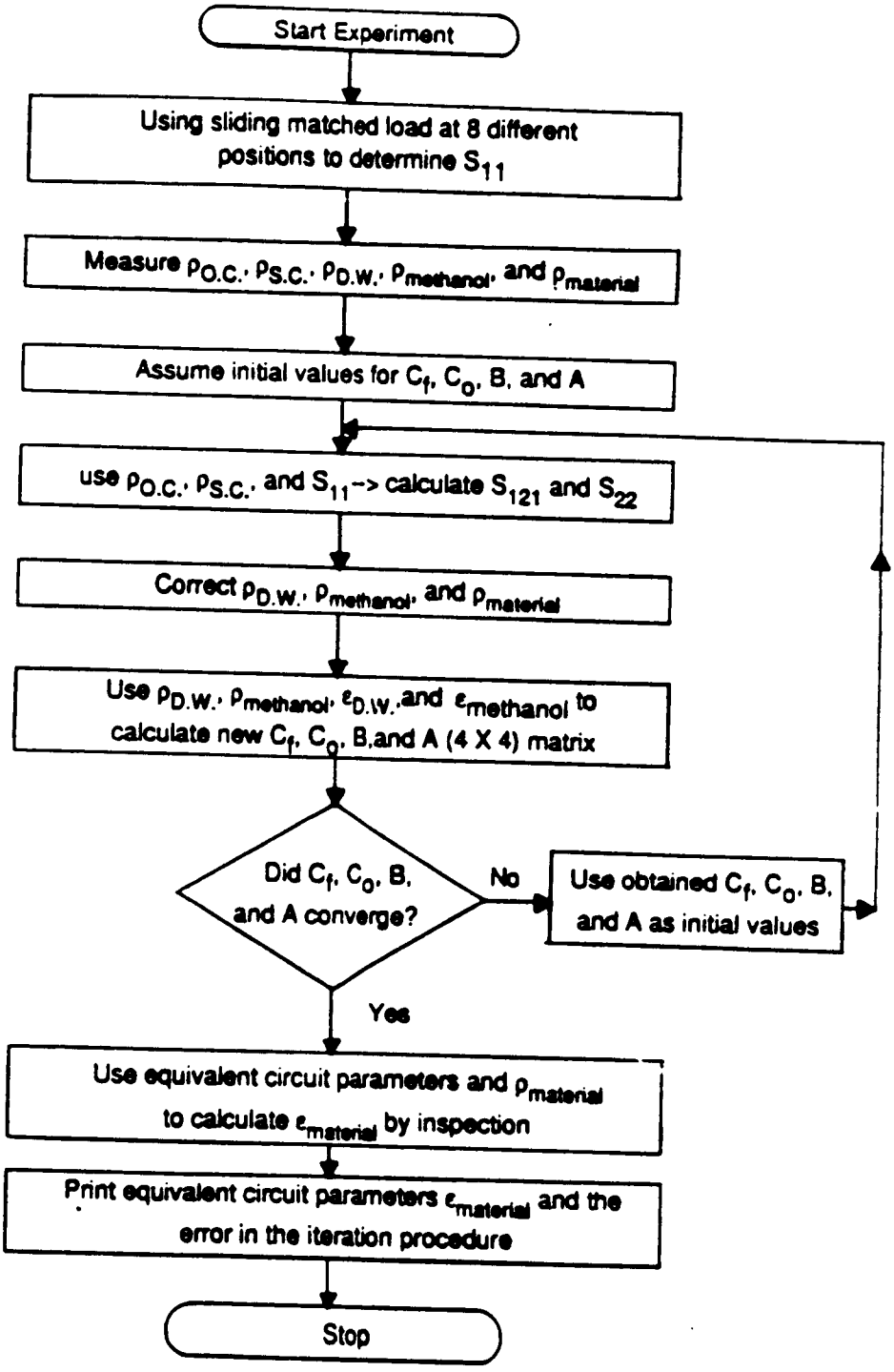

Figure 4.3. Calibration algorithm for the full equivalent circuit parameters, $C_f, C_0, B, and A$.

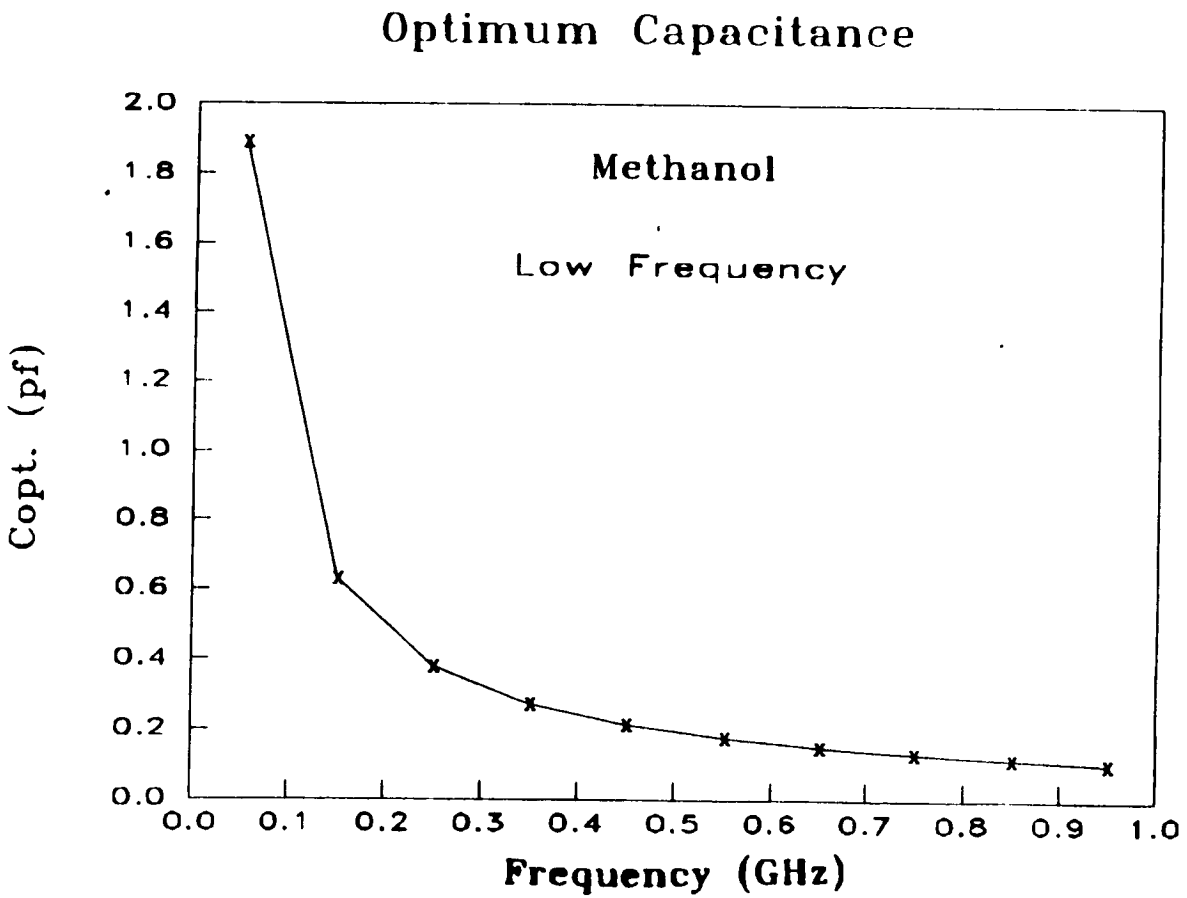

Figure 4.4(a). Calculated optimum capacitance for methanol(0.1-1 GHz).

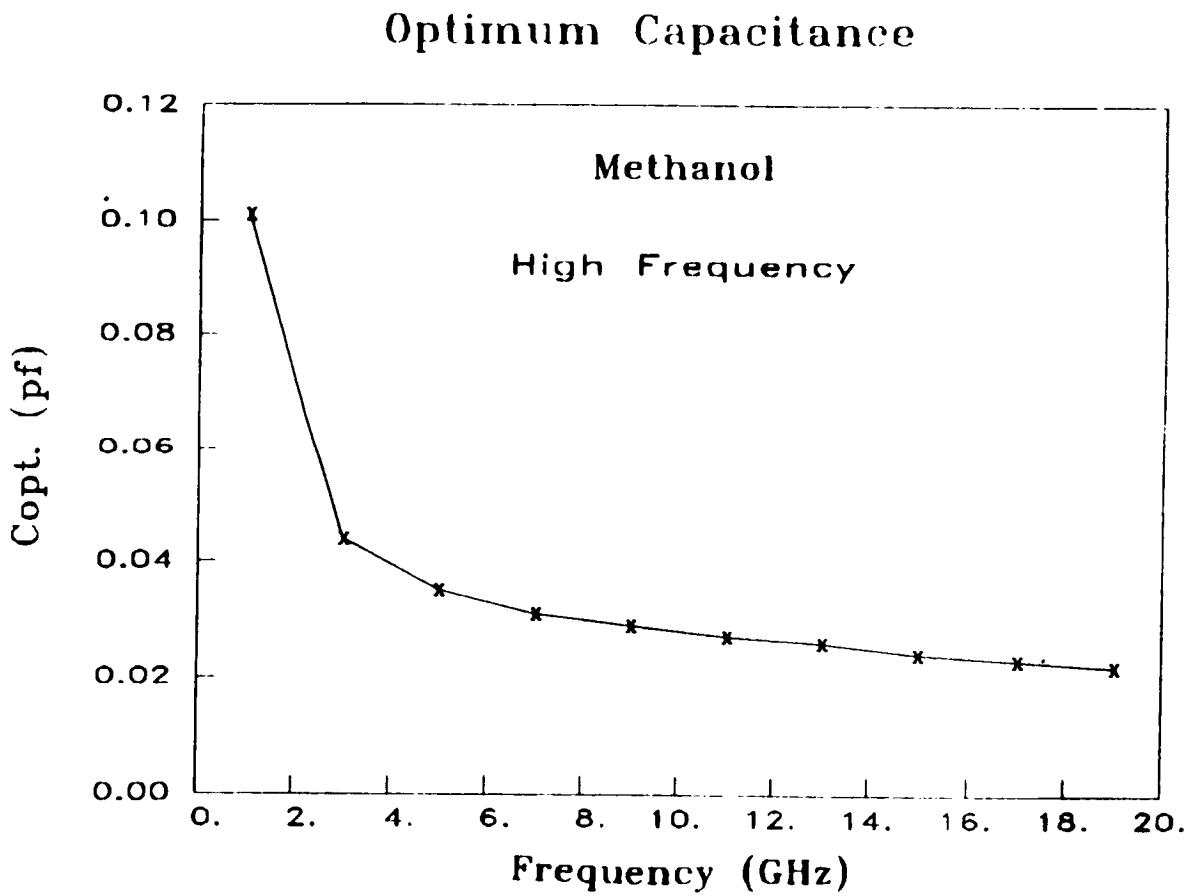

Figure 4.4(b). Calculated optimum capacitance for methanol(1-20 GHz).

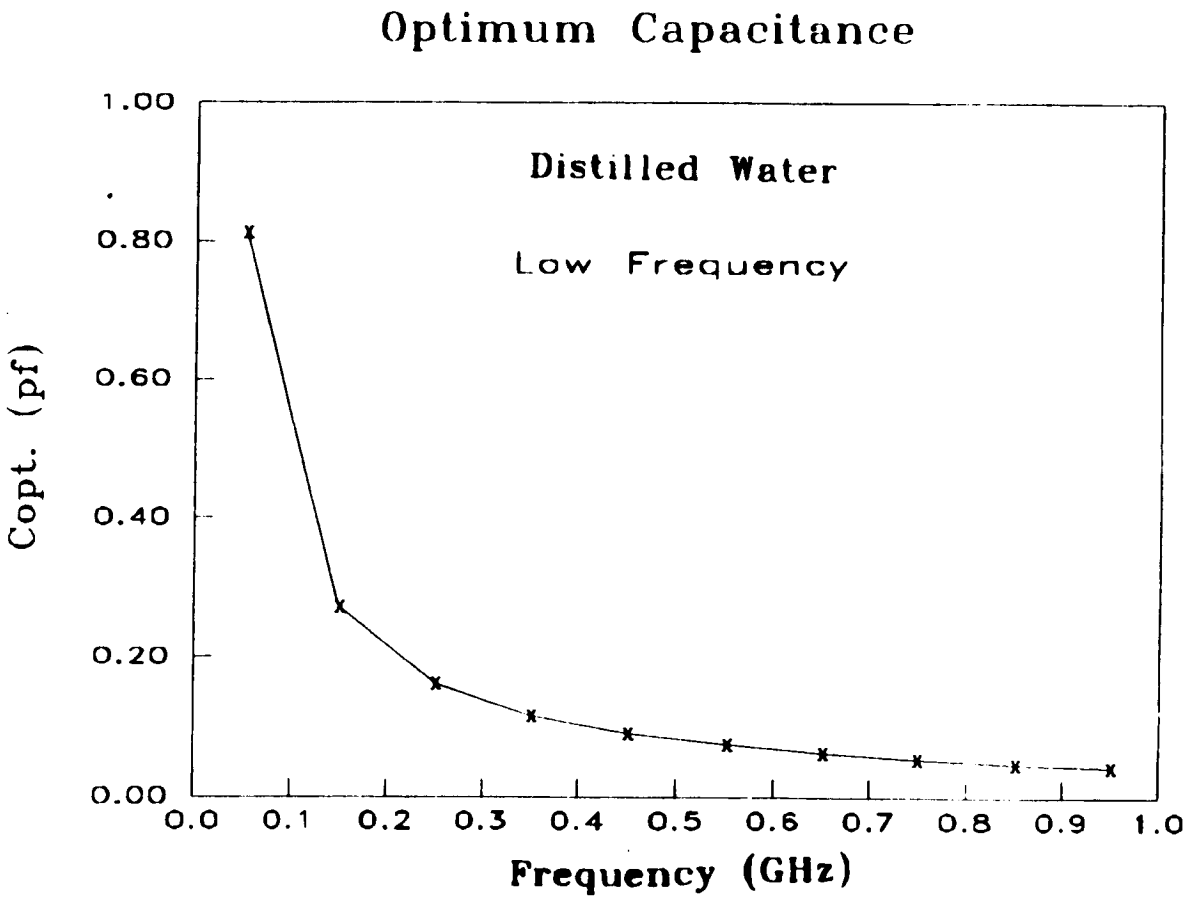

Figure 4.4(c). Calculated optimum capacitance for distilled water(0.1-1 GHz).

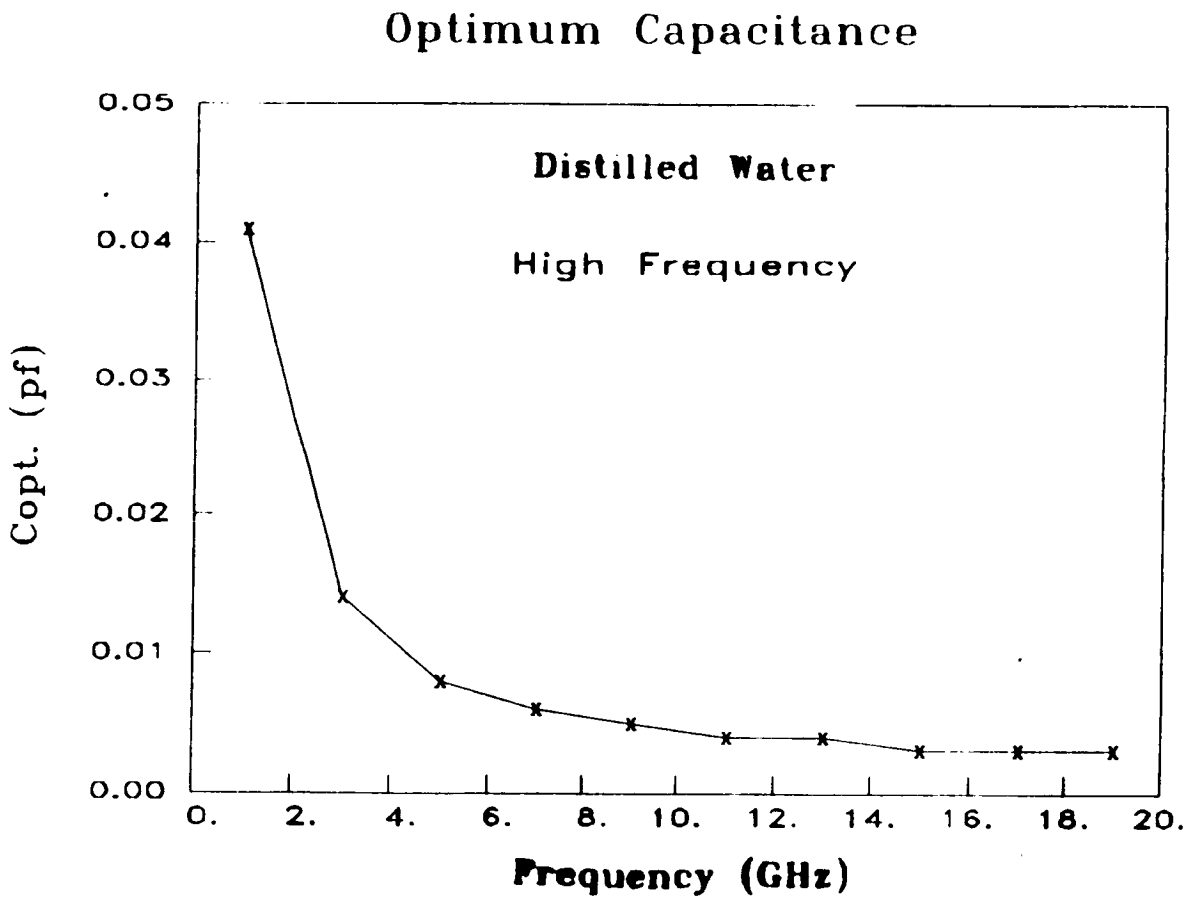

Figure 4.4(d). Calculated optimum capacitance for distilled water(1-20 GHz).

capacitance of an open-ended coaxial line is typically between .02 and .04 pf, the optimum capacitance condition is satisfied for only some materials over a limited frequency range (e.g., distilled water above 2 GHz). The practical situation is not really that stringent and a typical probe can operate satisfactorily over quite a wide band of frequency and range of dielectrics as will be discussed in the next section. The optimum capacitance condition is only useful as a design guideline because the probe would still function satisfactorily in completely different situations, albeit with some degradation in performance.

4.3.2 Sensitivity

The probe translates variations in the permittivity of the test material into variations in the measured amplitude and phase of the reflection coefficient. The variation in the measured phase depends on ϵ'' as well as ϵ'. However, the effect of ϵ'' on $\Delta\varphi$ is of less importance compared to the effect of ϵ' specially at low frequencies. Thus,

$$\Delta\varphi = f(\epsilon', \epsilon'') \approx f(\epsilon').$$

A similar argument for ΔA can lead us to

$$\Delta A = f(\epsilon', \epsilon'') \approx f(\epsilon'')$$

We can define $S^{\varphi}_{\epsilon'}$, the probe phase-sensitivity to ϵ', as

$$S^{\varphi}_{\epsilon'} = limit_{\Delta\epsilon' \longrightarrow 0}[\frac{\Delta\varphi/\varphi}{\Delta\epsilon'/\epsilon'}] \tag{4.6}$$

$$= (\frac{\epsilon'}{\varphi})\frac{\partial\varphi}{\partial\epsilon'} \tag{4.7}$$

We can interpret the sensitivity $S_{\epsilon'}^{\varphi}$ as the ratio of the fractional change in the function φ to the fractional change in the parameter ϵ', provided that the changes are sufficiently small (approaching zero). Similarly, $S_{tan\delta}^{\varphi}$ can be defined as

$$S_{tan\delta}^{\varphi} = (\frac{tan\delta}{\varphi})\frac{\partial\varphi}{\partial tan\delta} \tag{4.8}$$

A third sensitivity term

$$S_{\epsilon''}^{\varphi} = (\frac{\epsilon''}{\varphi})\frac{\partial\varphi}{\partial\epsilon''} \tag{4.9}$$

may also be defined for ϵ''. The corresponding relations for A, where A is the magnitude of the reflection coefficient, can be defined as follows:

$$S_{\epsilon'}^{A} = (\frac{\epsilon'}{A})\frac{\partial A}{\partial\epsilon'}, \tag{4.10}$$

$$S_{tan\delta}^{A} = (\frac{tan\delta}{A})\frac{\partial A}{\partial tan\delta}, \tag{4.11}$$

and

$$S_{\epsilon''}^{A} = (\frac{\epsilon''}{A})\frac{\partial A}{\partial\epsilon''}. \tag{4.12}$$

Figures (4.5)-(4.12) show plots of $S_{\epsilon'}^{\varphi}, S_{\epsilon'}^{A}, S_{\epsilon''}^{\varphi}$, and $S_{\epsilon''}^{A}$, versus frequency for 4 different materials: distilled water, methanol, 1-butanol, and 1-octanol. The following conclusions can be drawn:

1. $S_{\epsilon''}^{A}$ has the highest value especially at low frequencies (Fig.4.6). This shows that ϵ'' has a large sensitivity to the amplitude measurements, and shows how critical the amplitude is in this type of measurements.

2. $S_{\epsilon'}^{\varphi}$ is larger than $S_{\epsilon'}^{A}$ at low frequencies and for high loss materials (Fig.4.8). As the frequency increases, $S_{\epsilon'}^{\varphi}$ decreases while $S_{\epsilon'}^{A}$ increases and they become equal around 5 GHz (for distilled water). This trend continues as

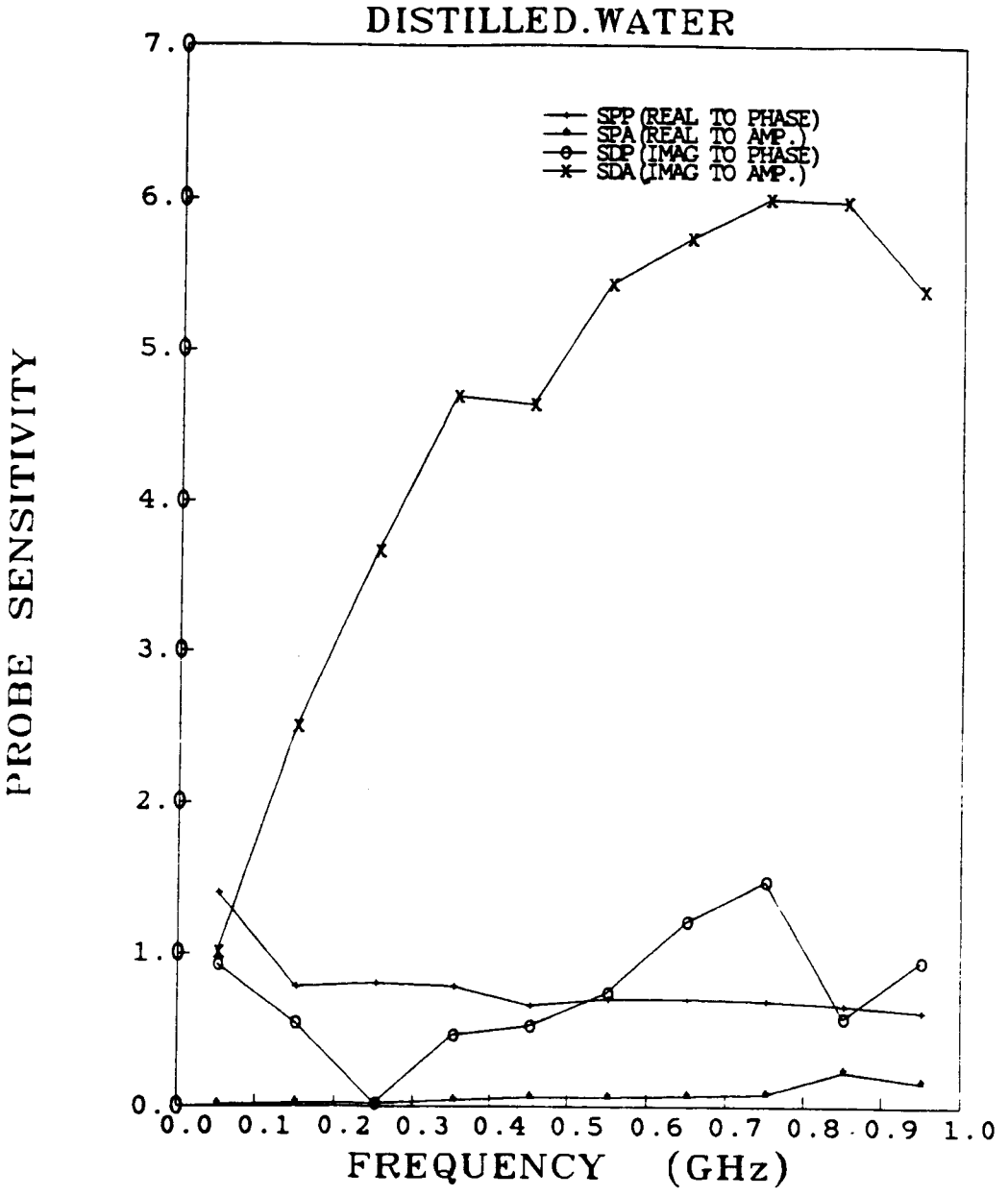

Figure 4.5. Calculated probe sensitivity for distilled water (0.1-1 GHz).

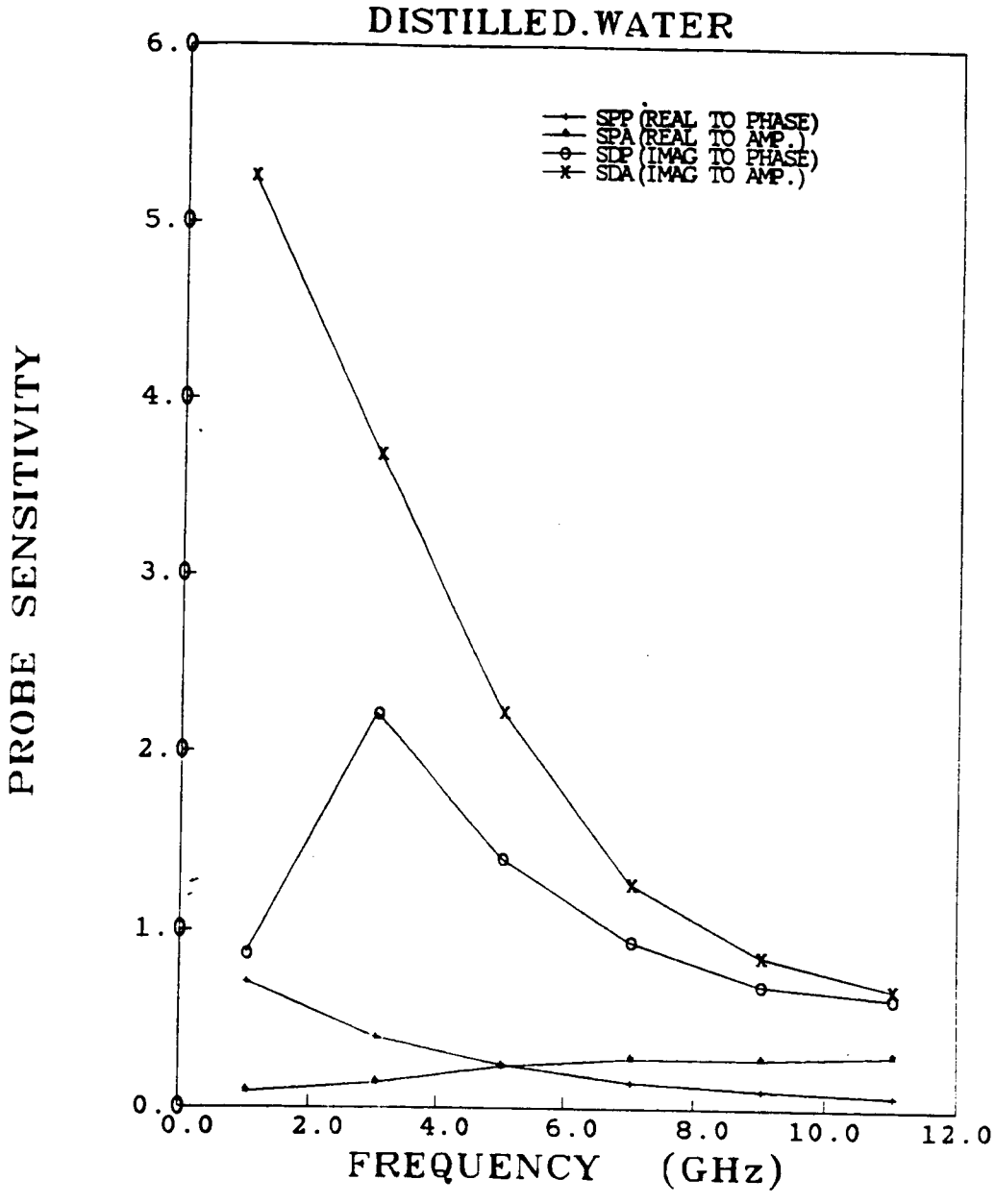

Figure 4.6. Calculated probe sensitivity for distilled water (1-20 GHz).

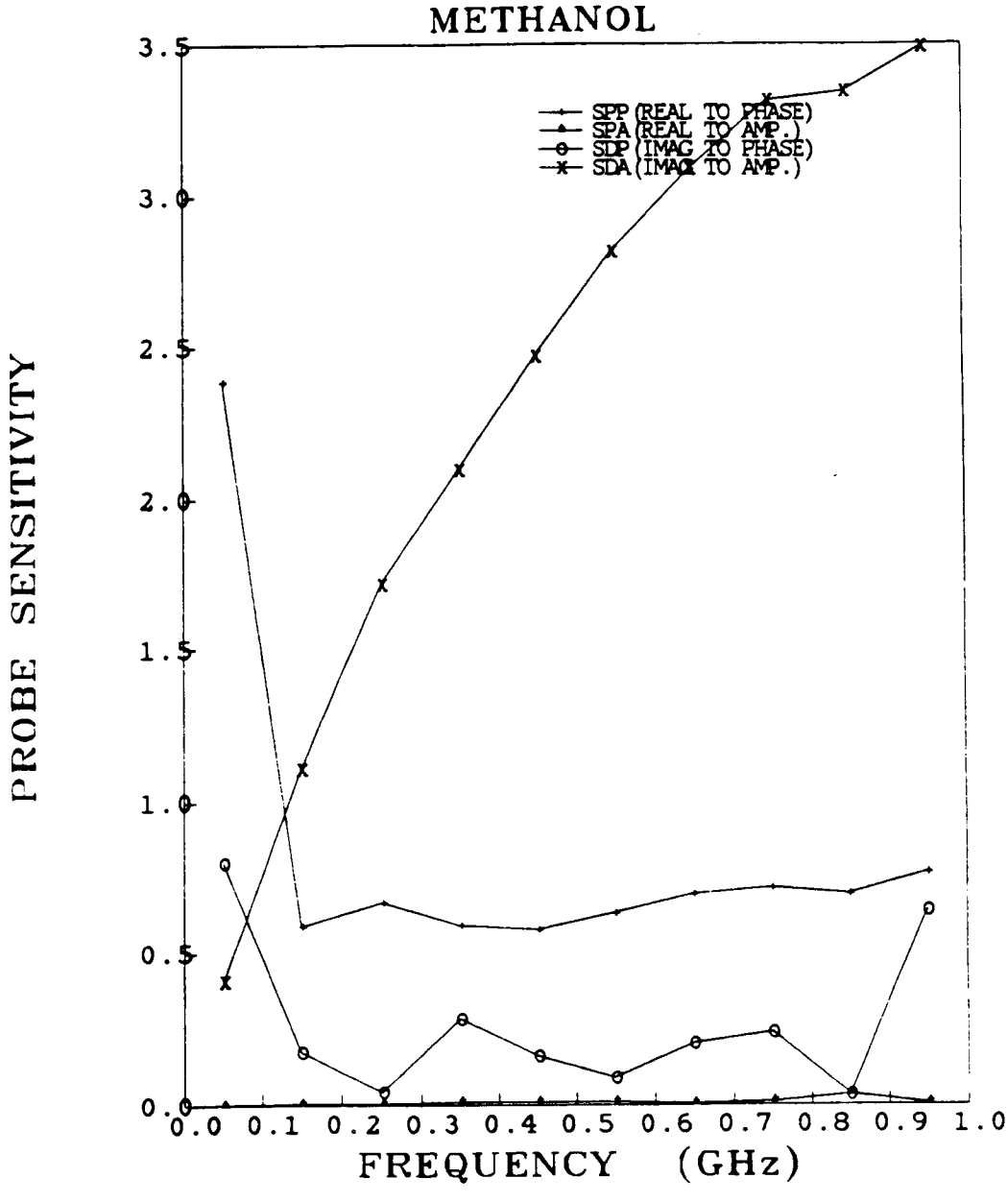

Figure 4.7. Calculated probe sensitivity for methanol (0.1-1 GHz).

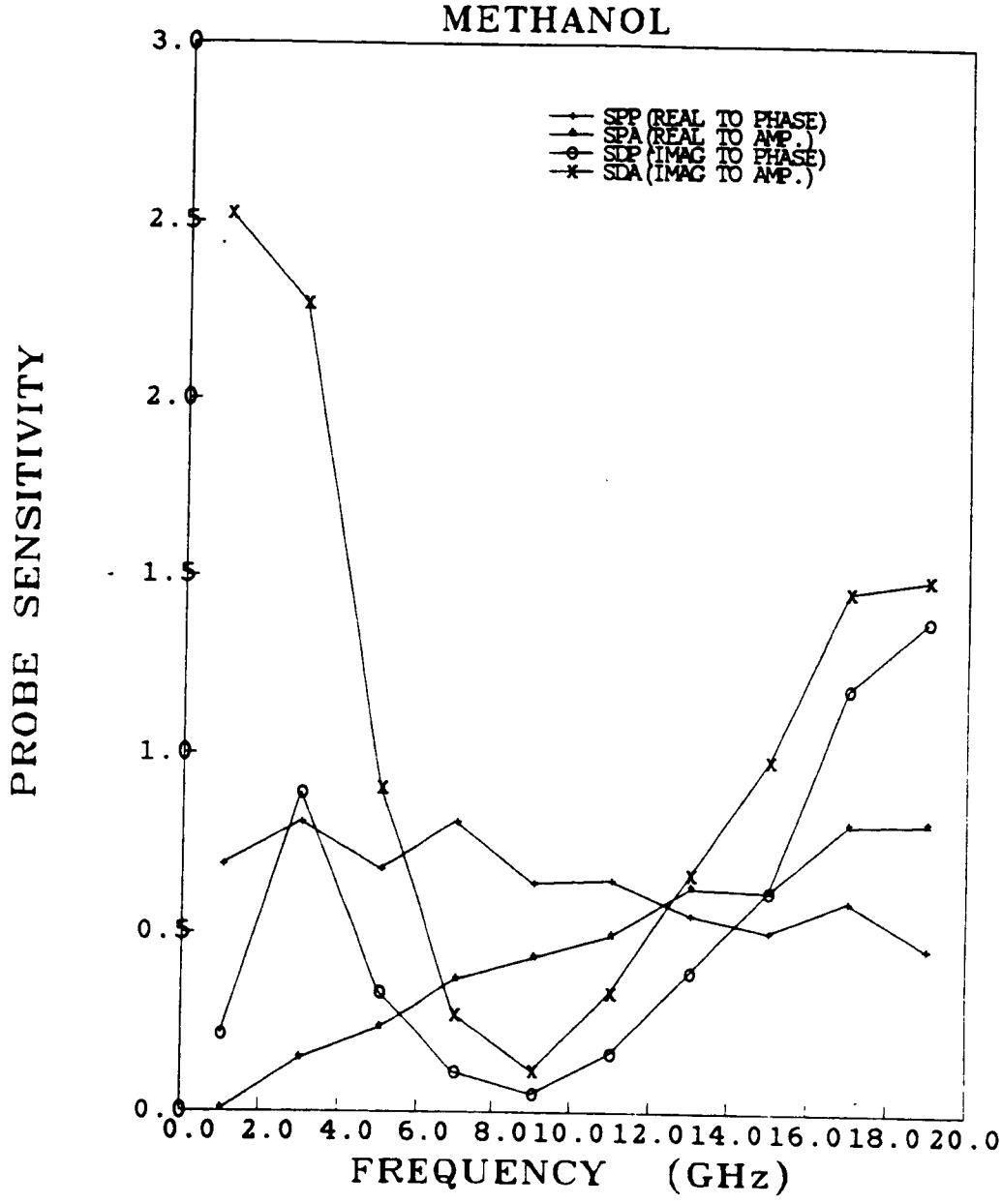

Figure 4.8. Calculated probe sensitivity for methanol (1-20 GHz).

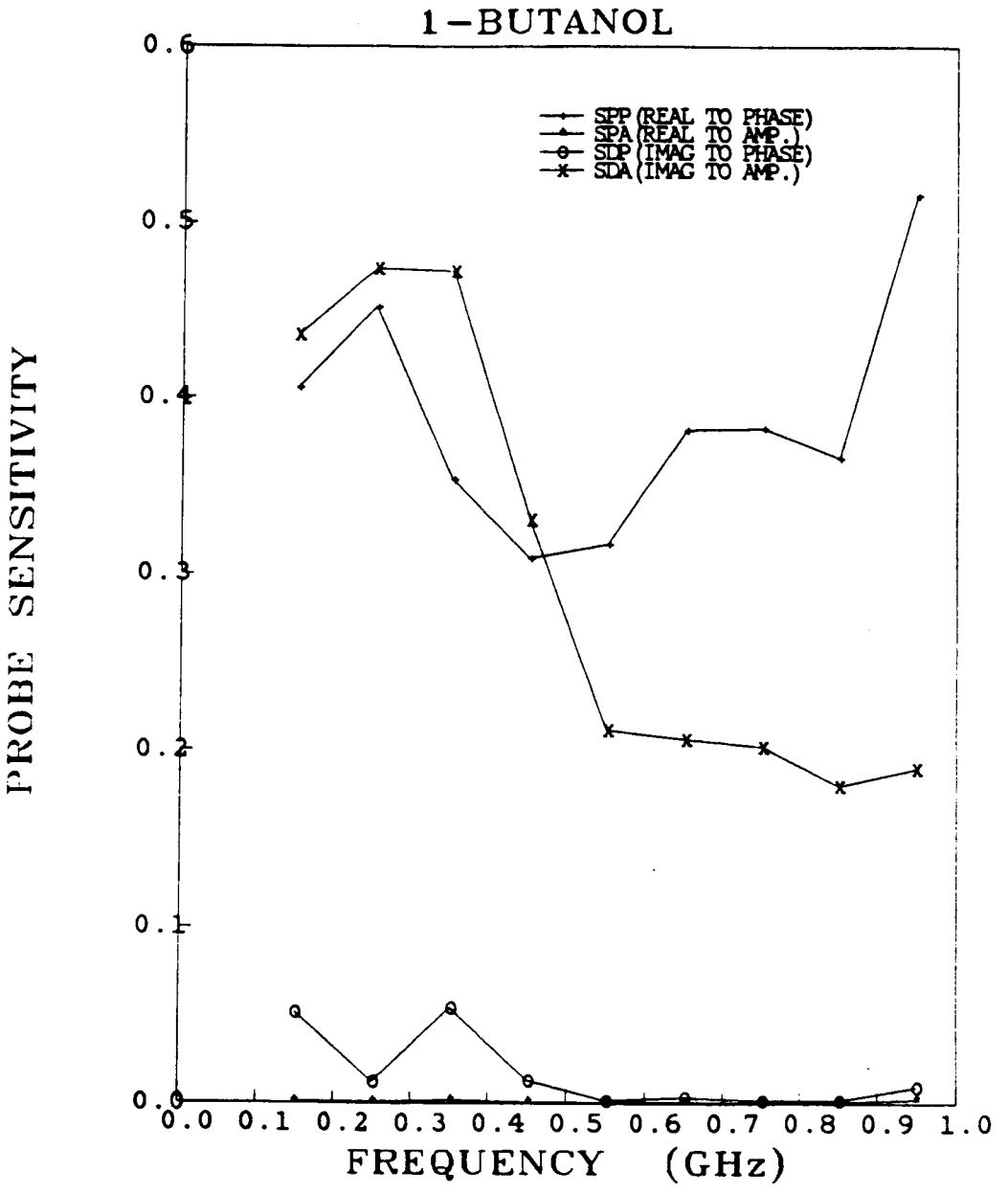

Figure 4.9. Calculated probe sensitivity for 1-butanol (0.1-1 GHz).

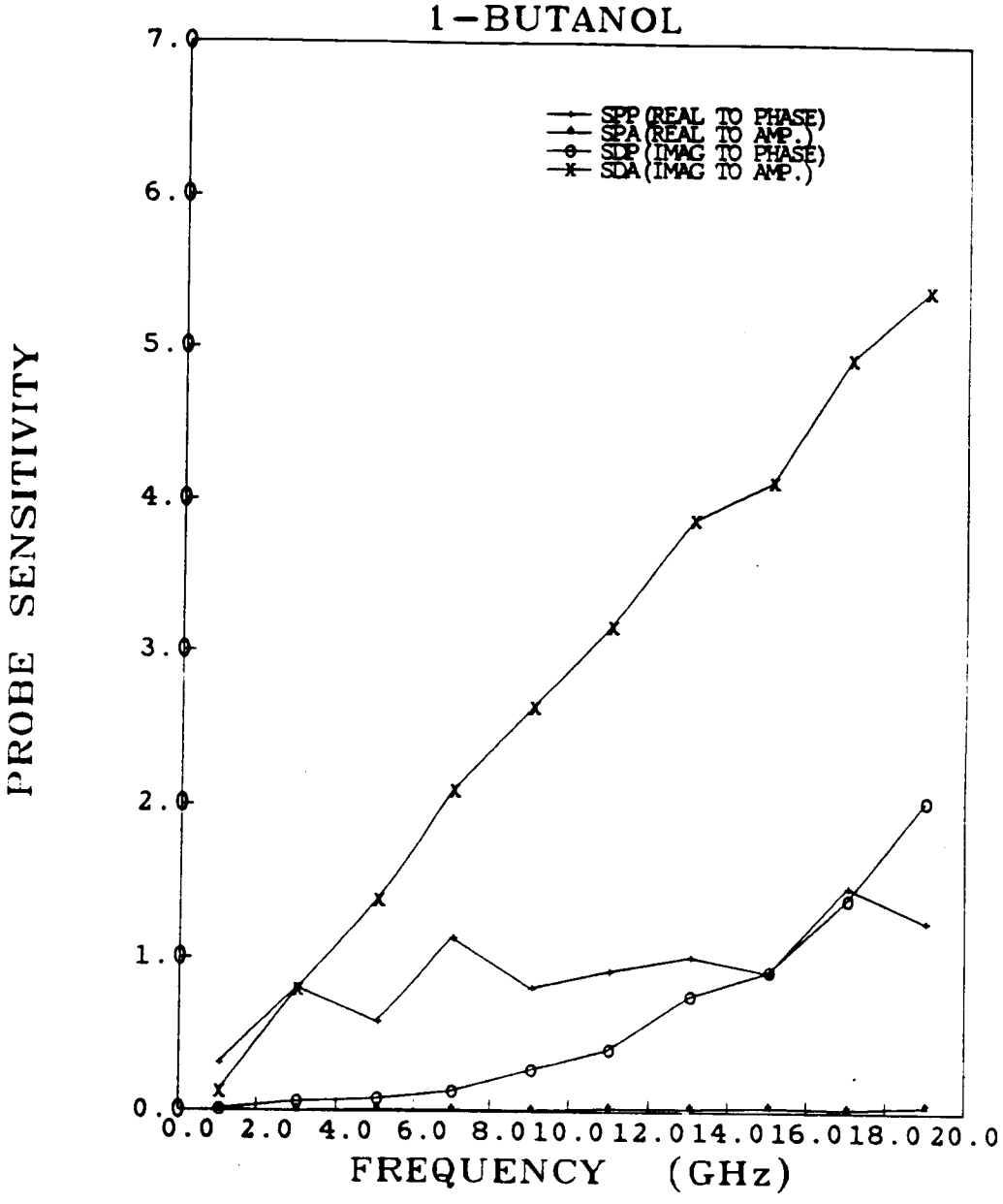

Figure 4.10. Calculated probe sensitivity for 1-butanol (1-20 GHz).

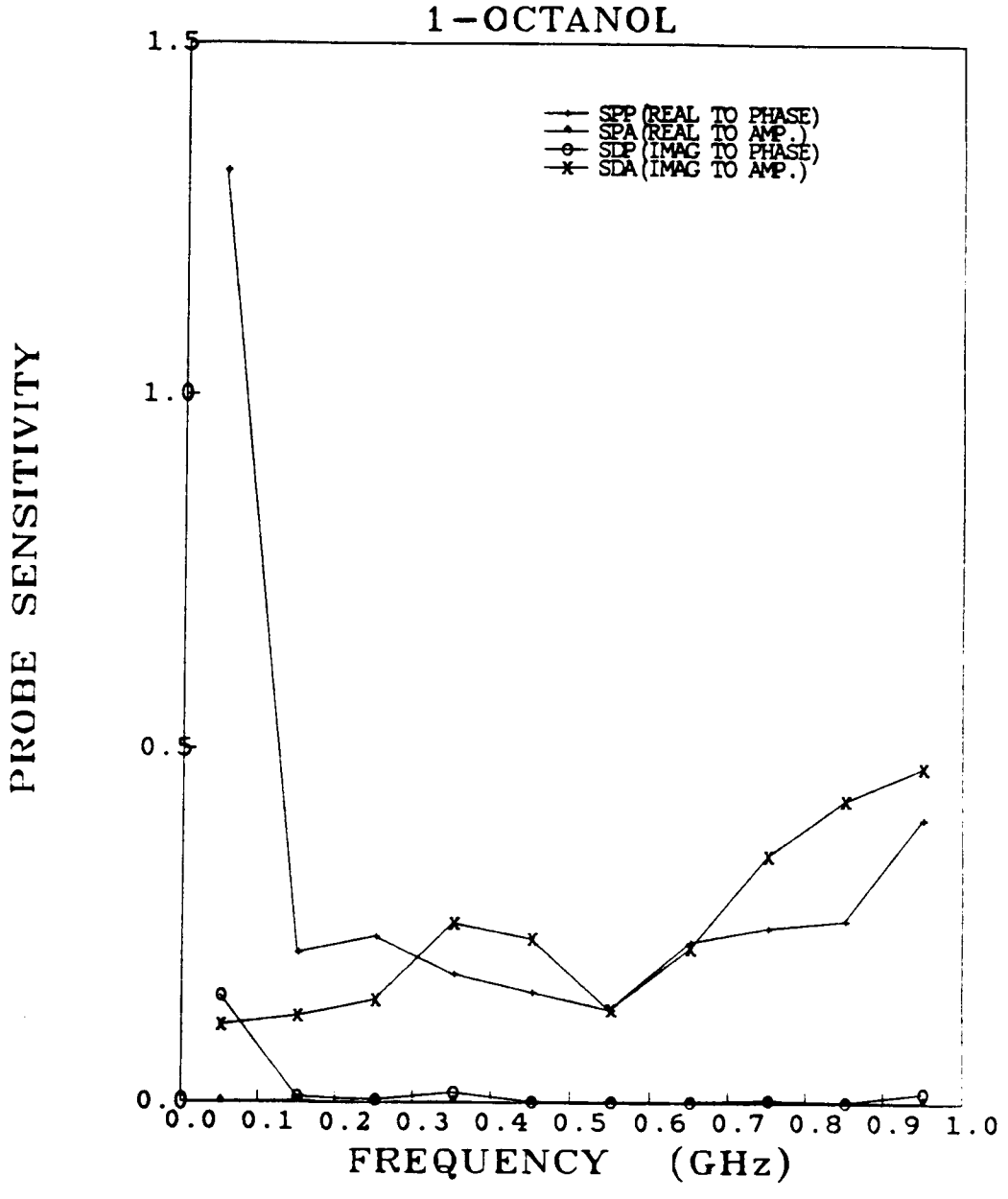

Figure 4.11. Calculated probe sensitivity for 1-octanol (0.1-1 GHz).

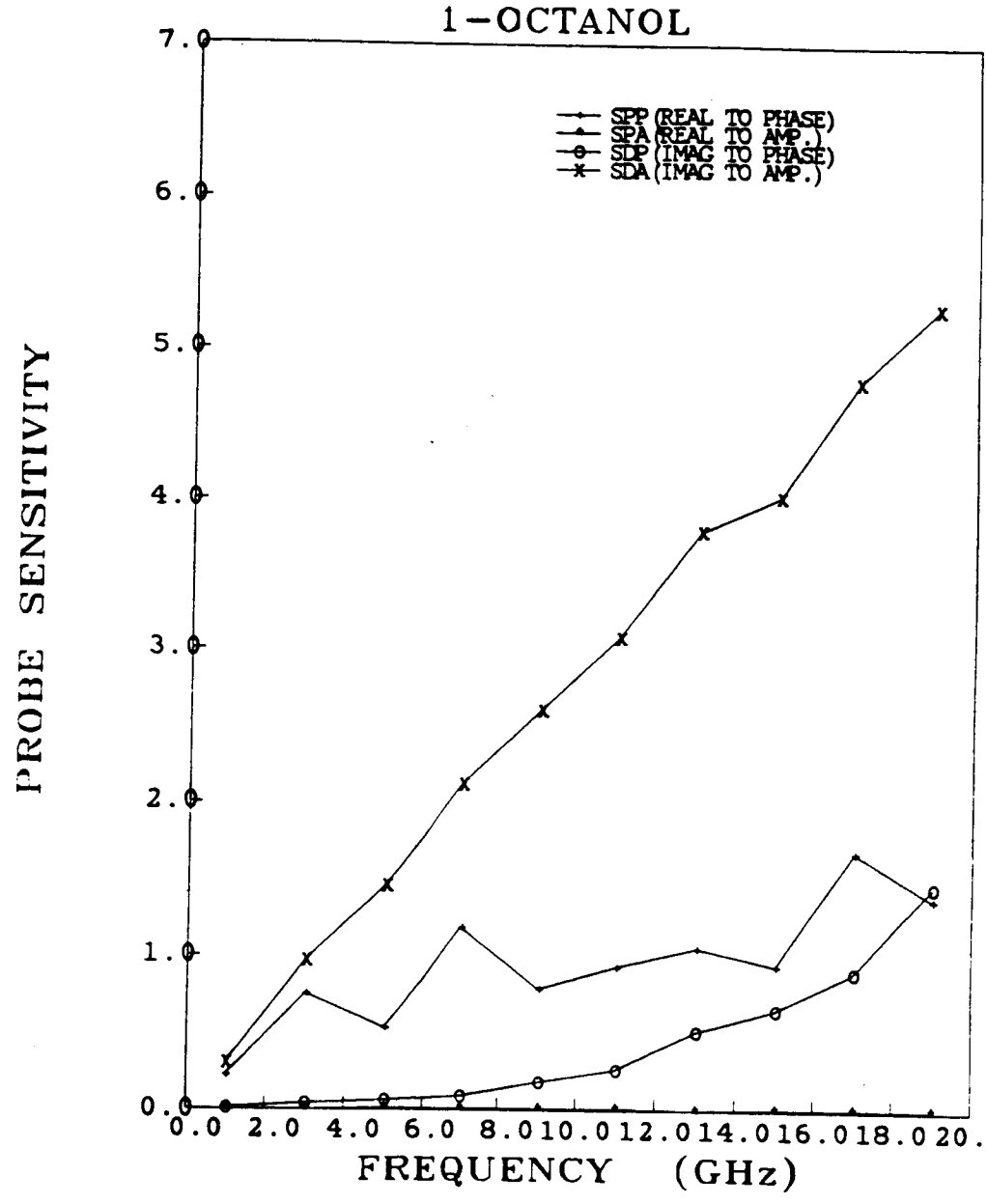

Figure 4.12. Calculated probe sensitivity for 1-octanol (1-20 GHz).

the frequency increases, and $S_{\epsilon'}^{A}$ becomes larger than $S_{\epsilon'}^{\varphi}$. This observation shows the increased importance of the amplitude measurement at high frequencies. In other words, ϵ' at low frequencies depends mainly on φ, while at high frequency it is more sensitive to A. This is due to the increased role of the radiation term $A\omega^4$ in Eq. (4.4) with increasing frequency.

3. $S_{\epsilon''}^{\varphi}$ is generally higher than $S_{\epsilon'}^{A}$ (e.g., Fig.4.7), which shows that ϵ'' is more sensitive to φ than ϵ' is sensitive to A.

4. For 1-Butanol and 1-Octanol (Fig.4.10 to 4.13), $S_{\epsilon''}^{A}$ and $S_{\epsilon''}^{\varphi}$ increase with frequency, $S_{\epsilon'}^{\varphi}$ is roughly constant with frequency, and $S_{\epsilon'}^{A}$ is almost zero.

5. The sensitivity of the probe generally increases with an increase in its diameter (and hence its lumped capacitance and radiation resistance).

4.3.3 Higher Order Modes

Open-ended coaxial lines can be modeled as a simple capacitance, C_0, especially at low frequencies (where the free space wavelength is much larger than the line cross-sectional dimensions). When the frequency of operation increases, the line starts to radiate and the energy is not concentrated in the reactive fringing field any longer. In this situation C_0 increases with frequency due to the increase in the evanescent TM modes being excited at the junction discontinuity. An expression of the form $C_0 + B\omega^2$, where B is a constant dependent on the line dimensions, should be used in place of the constant value C_0. Futhermore, when the medium has a high dielectric constant, these modes may become propagating

modes. The first of these modes is the TM_{01} mode which can propagate when $\lambda_\epsilon \leq 2.03(a-b)$, where λ_ϵ is the wavelengh in the medium, and a and b are the outer and inner line radii. Table (4.1) shows the cut-off wavelengh for the probe types used in this study along with their line dimensions (Athey, 1982):

Cable	type	a(mm)	b(mm)	a/b	λ_c (mm)
.085"	Teflon	.838	.255	3.282	1.177
.141"	Teflon	1.499	.455	3.295	2.129
.250"	Teflon	2.655	.824	3.222	3.764
.350"	Teflon	3.620	1.124	3.221	5.067

Table (4.1): Dimensions and cut-off wavelengths for the TM_{01} mode for the probes used in this study.

If the frequency is high enough such that the wavelength in the medium is shorter than λ_c, moding will occur. To calculate the wavelength in the medium, the following equation can be used (Ulaby et al, 1982):

$$\lambda_\epsilon = \frac{\lambda_0}{\sqrt{\epsilon'}\sqrt{\frac{sec\delta+1}{2}}}$$

where $\lambda_\epsilon, \lambda_0, \epsilon'$ and δ are as defined earlier. In order to avoid the moding problem, care must be taken when materials with high dielectric constants are measured. Usually this probem is encountered in two situations:

1. distilled water and saline solutions at high frequency, and

2. thin samples placed against metal background.

Table (4.2) shows the calculated wavelength in the medium λ_ϵ as a function of frequency for distilled water:

f(GHz)	1	2	4	6	9	10	20	30	40
$(\lambda_\epsilon)_c(mm)$	33.7	16.9	11.7	5.825	4.05	3.70	2.21	1.75	1.49

Table (4.2): $(\lambda_\epsilon)_c$ for distilled water.

From this table we can conclude the following:

1. The .085" probe may be operated at frequencies higher than 40 GHz,

2. The .141" probe may be operated at $f \leq 21$ GHz,

3. The .250" probe may be operated at $f \leq 9$ GHz, and

4. The .350" probe may be operated at $f \leq 6$ GHz.

It was found experimentally, however, that this theoretical limit does not strictly apply. The practical cut-off frequencies are slightly lower than the calculated values. It should be noted that whereas a smaller probe can operate over a wider frequency range, its sensitivities are smaller in magnitude than those of larger probes.

4.3.4 Contact and Pressure Probem

The calibration procedure involves measuring two standard liquids (usually distilled water and methanol). The open-ended coaxial line (with or without a ground plane) is suitable for measuring liquids as long as care is excercised to avoid air bubbles at the probe tip. Also, the fact that the calibration was carried out using liquids made the probe more suitable and more accurate for measuring liquid and semi-liquid materials. Semi-solid materials can also be measured accurately since the surface can deform to comply with the probe tip and achieve a good contact (an example of semi-solid materials is cheese). On the other hand, solid materials are very hard to measure using ordinary probes. When measuring the dielectric constant of a solid material, it is crucial to achieve a perfect contact with the mterial under test particularly in the immediate vicinity of the probe tip. As will be discussed later in this chapter, some new probe designs with very smooth surfaces and ground planes were built, tested

and found suitable to measure solid materials. Measuring vegetation materials, particularly leaves, is usually a problem since any deformation of the plant part would cause an immediate cellular rupture and possible flow of the included liquids, in addition to the change in density with increasing pressure. It was found that for each vegetation material and plant part there is an optimum pressure above which the part will be crushed and below which the contact will not be perfect. This optimum pressure is found experimentally for each part and should be maintained constant during the experiment (a digital scale was used to check pressure). Usually a pressure of few hundred grams applied on the .141" probe tip ($\sim .1cm^2$) is sufficient.

4.4 Probe Calibration

4.4.1 Choice of Calibration Materials

The overall performance of the system depends on the choice of calibration materials as well as the accuracy with which we know their dielectric properties. This section gives few guidelines regarding the selecting of proper materials for a particular application. During the course of this work only distilled water and methanol were used for calibration. The dielectric constant of water is the highest known in the microwave band and that of methanol is approximately one half of it. For wet vegetation materials, it is a good idea to use water as a calibration material. On the other hand, for dry vegetation materials, a different combination may be better. Butanol, e.g., can be used in place of water since its

dielectric constant is about half that of methanol. The calibration liquids should have, in general, the following features:

1. their dielectric properties should be known fairly accurately as a function of frequency and temperature.

2. both must have a reasonably large imaginary part (any lossless material is not suitable for calibration).

3. the dielectric properties of the two materials should be significantly different (e.g., it is not recommended using two saline solutions with different salinities).

4. the two materials should have dielectric values that cover the expected range of the material under test.

4.4.2 Error Analysis

A measurement system usually suffers from three major sources of error, namely the systematic, the random, and the illegitimate errors. The errors in the probe measurement technique can be summed up as follows:

1. Systematic Errors

   (a) System S parameters (S11, S12, S21, and S22),

   (b) Probe model accuracy,

   (c) Experimental conditions and standards, and

(d) Conditions of the sample under test.

2. Random Errors

   (a) Network analyzer precision,

   (b) Harmonic skip problem,

   (c) Noise, and

   (d) Sample conditions.

3. Illegitimate errors

   (a) Blunders, and

   (b) Chaotic.

Before proceeding into quantitative estimation of errors, the following assumptions will be made:

1. The error correction procedure is perfect (for the system S parameters).

2. The sample conditions problem does not exist for liquids (since they are homogeneous and since care was taken to avoid air bubbles at the probe tip).

3. The harmonic skip problem is cured through averaging (of 4 sweeps and 4 independent measurements).

4. Since each time the computer reads the A/D board it actually reads it 30 times, the noise is eliminated.

5. Illegitimate errors can be detected and eliminated by inspection.

Comparing this list to the errors' list, the remaining errors are:

1. Model accuracy, experimental conditions, and standards.

2. Network analyzer precision.

In this analysis, it was assumed that

1. $\Delta\epsilon = \pm 2.\%$,

2. $\Delta A = \pm .05dB$,

3. $\Delta\phi = \pm .3^0$, and

4. Since the number of independent samples is 4, then $\Delta\epsilon$ (4 independent measurements) = $\Delta\epsilon$ (1 measurement)/2. The estimated precision and accuracy of the probe system were evaluated and plotted as shown in Figs. 4.13-4.18 for yellow cheese (.141"), white cheese (.141"), 1-octanol (.250"), 1-octanol (.141"), 1-butanol (.250"), and 1-butanol (.141"), respectively. In order to evaluate the probe performance; several standard materials were measured and plotted along with the calculated values. An example is shown in Figs. 4.19 and 4.20 for 1-butanol.

From this error analysis, it was found that the overall system accuracy and precision are within 10.% (including system and sample errors). The estimated precision and accuracy of the probe system were evaluated and plotted as shown in Fig.(4.19)-(4.20) for 1-Butanol.

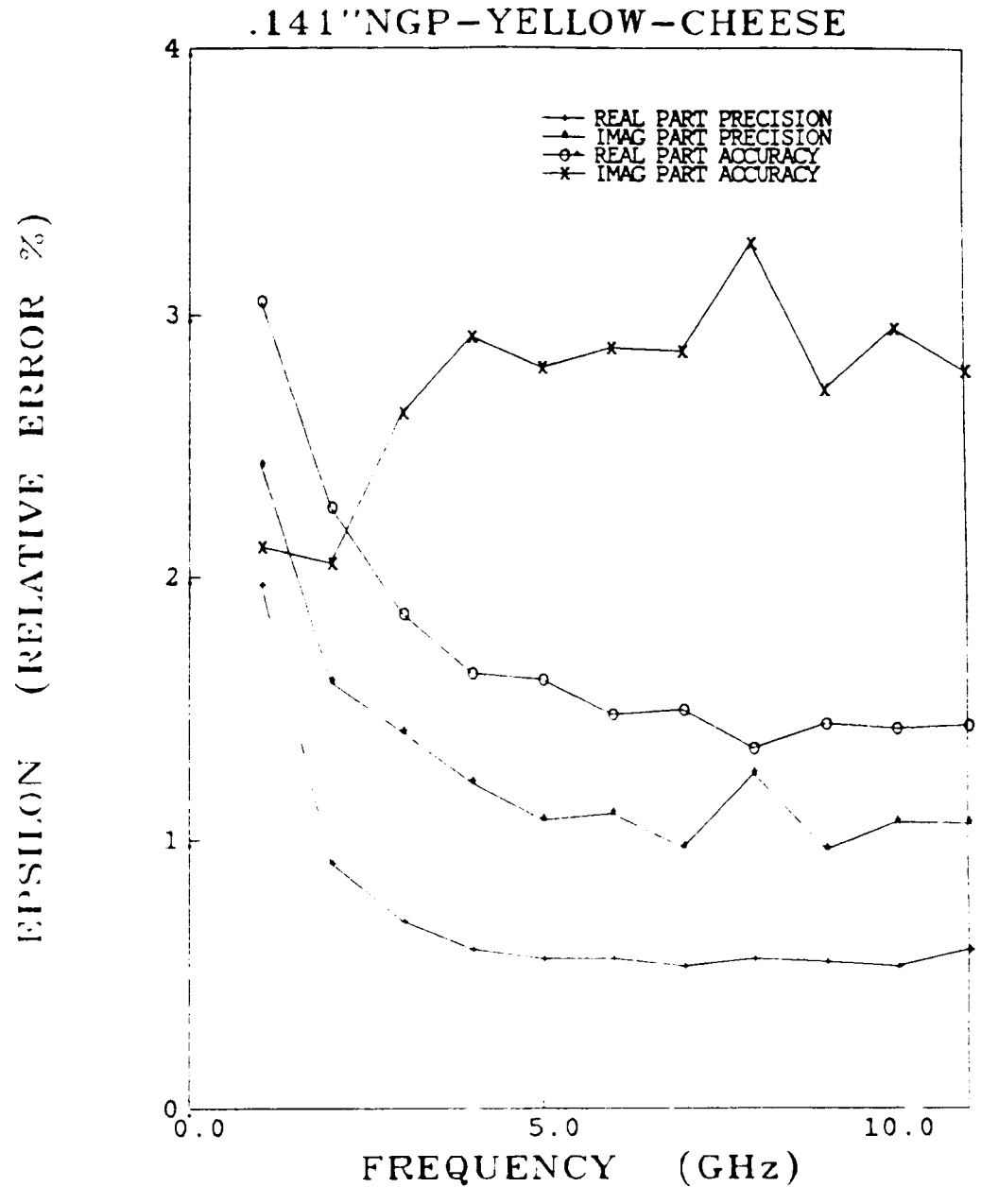

Figure 4.13. Estimated relative errors % for measurements on yellow cheese both accuracy and precision.

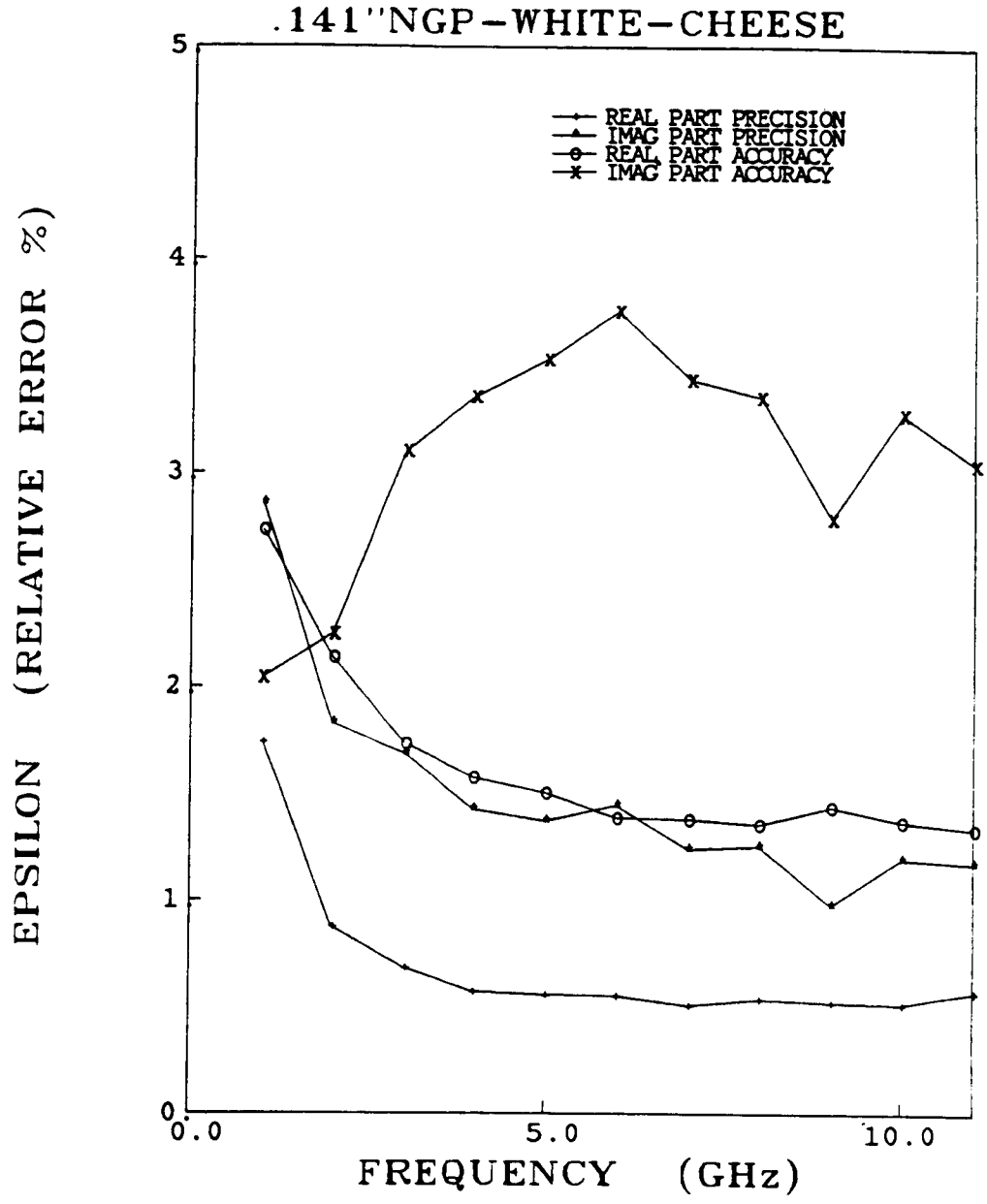

Figure 4.14. Estimated relative errors % for measurements on white cheese both accuracy and precision.

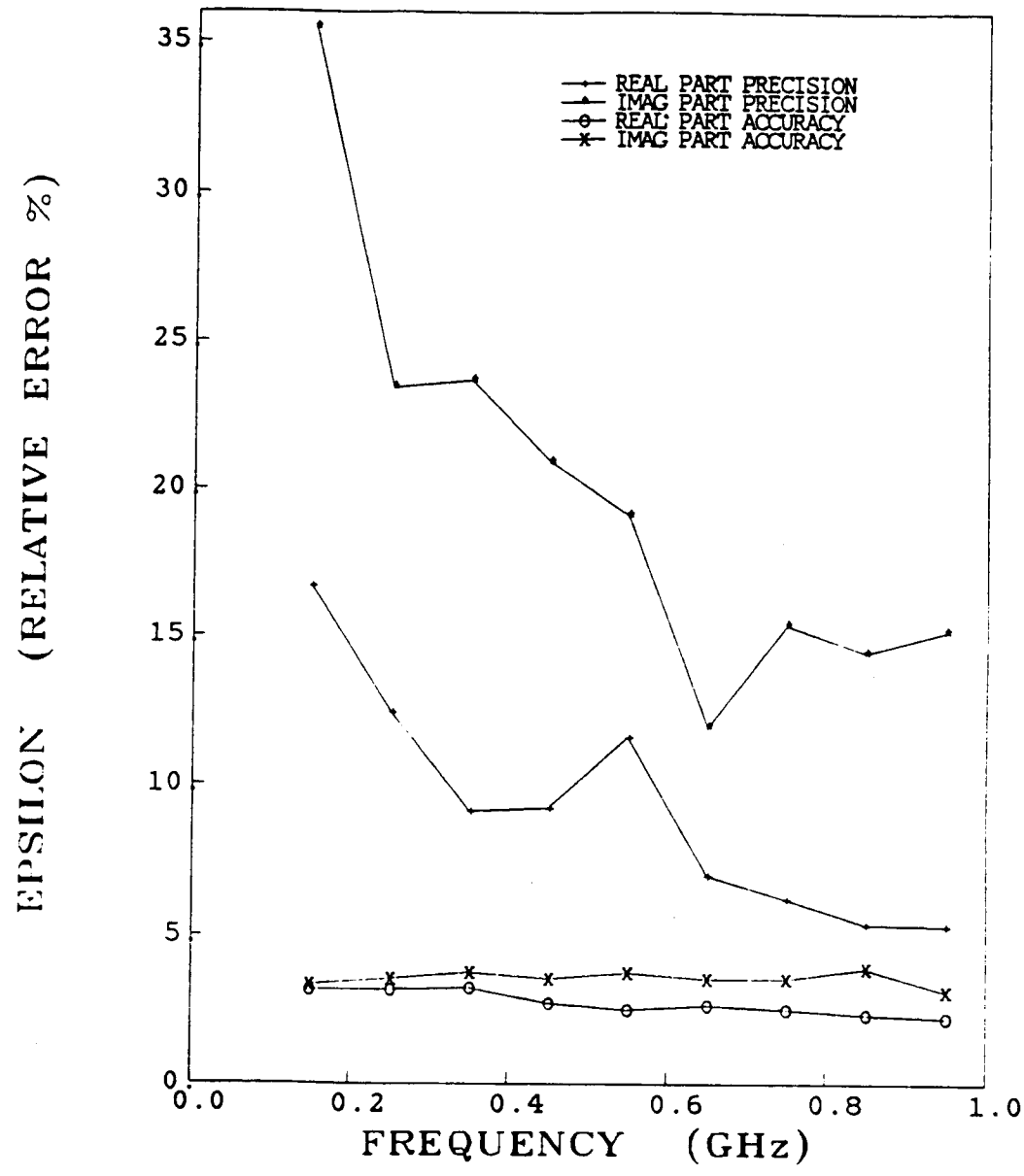

Figure 4.15. Estimated relative errors % for measurements on 1-octanol both accuracy and precision using the 0.250" probe.

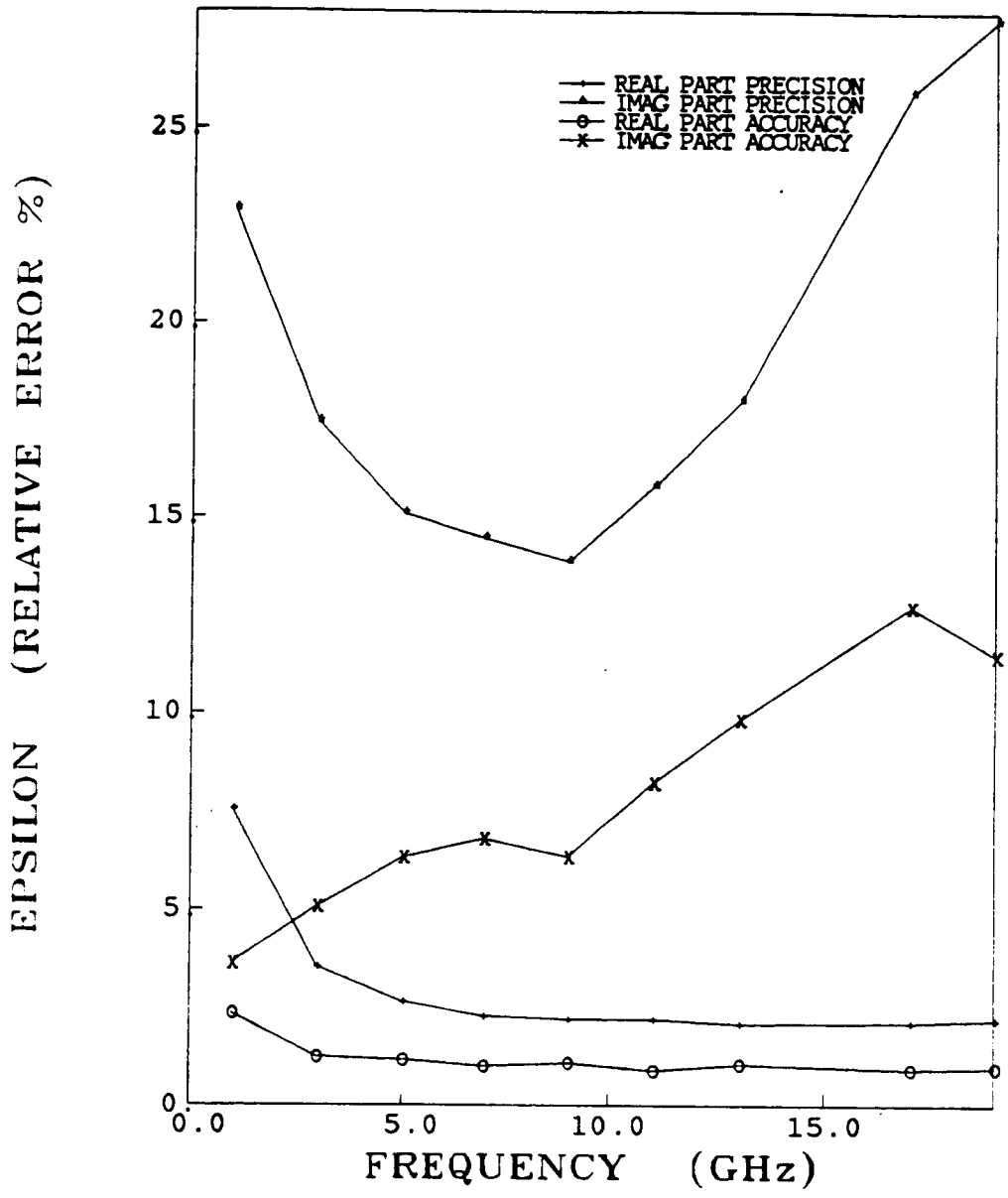

Figure 4.16. Estimated relative errors % for measurements on 1-octanol both accuracy and precision using the 0.141" probe.

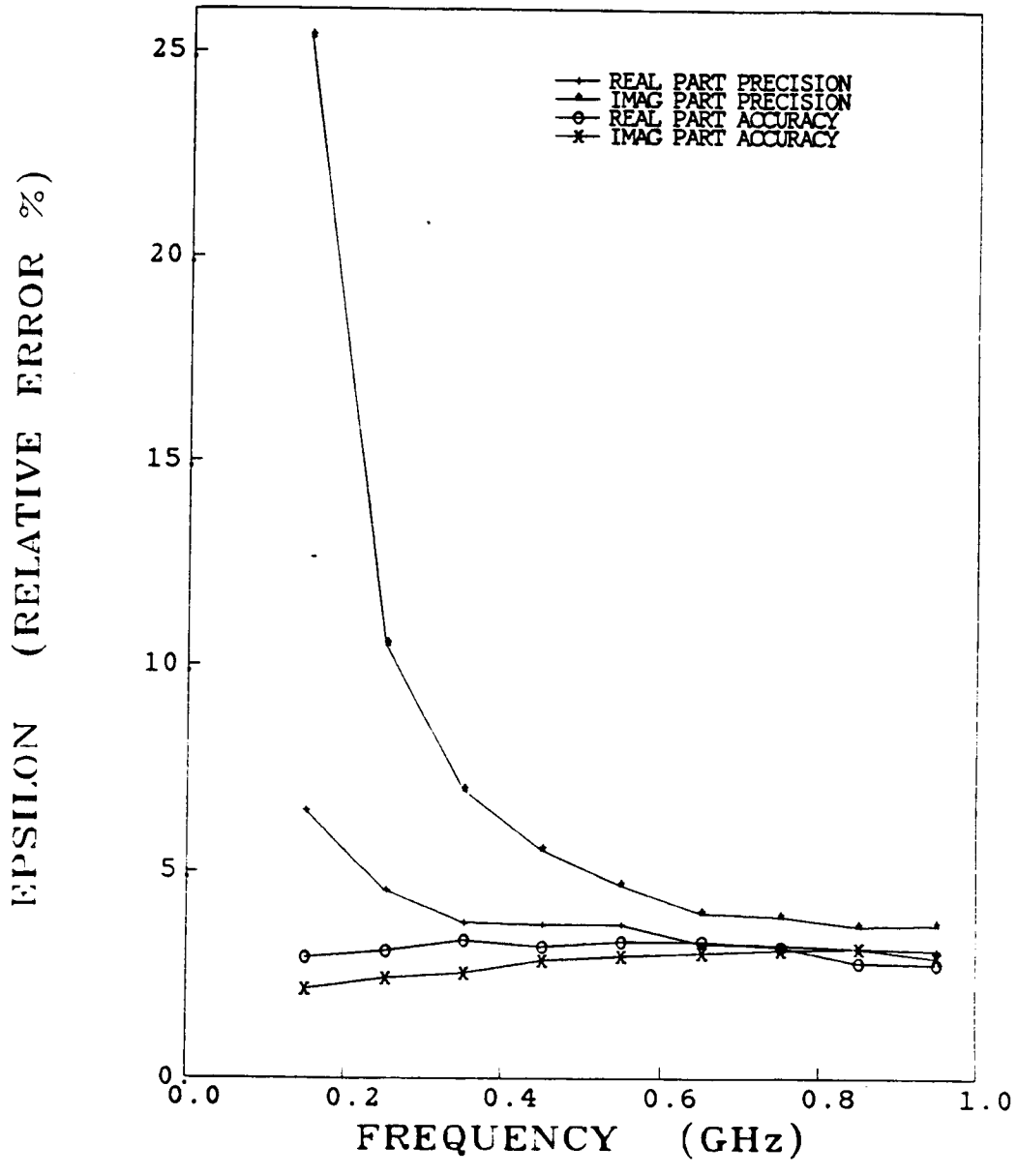

Figure 4.17. Estimated relative errors % for measurements on 1-butanol both accuracy and precision using the 0.250" probe.

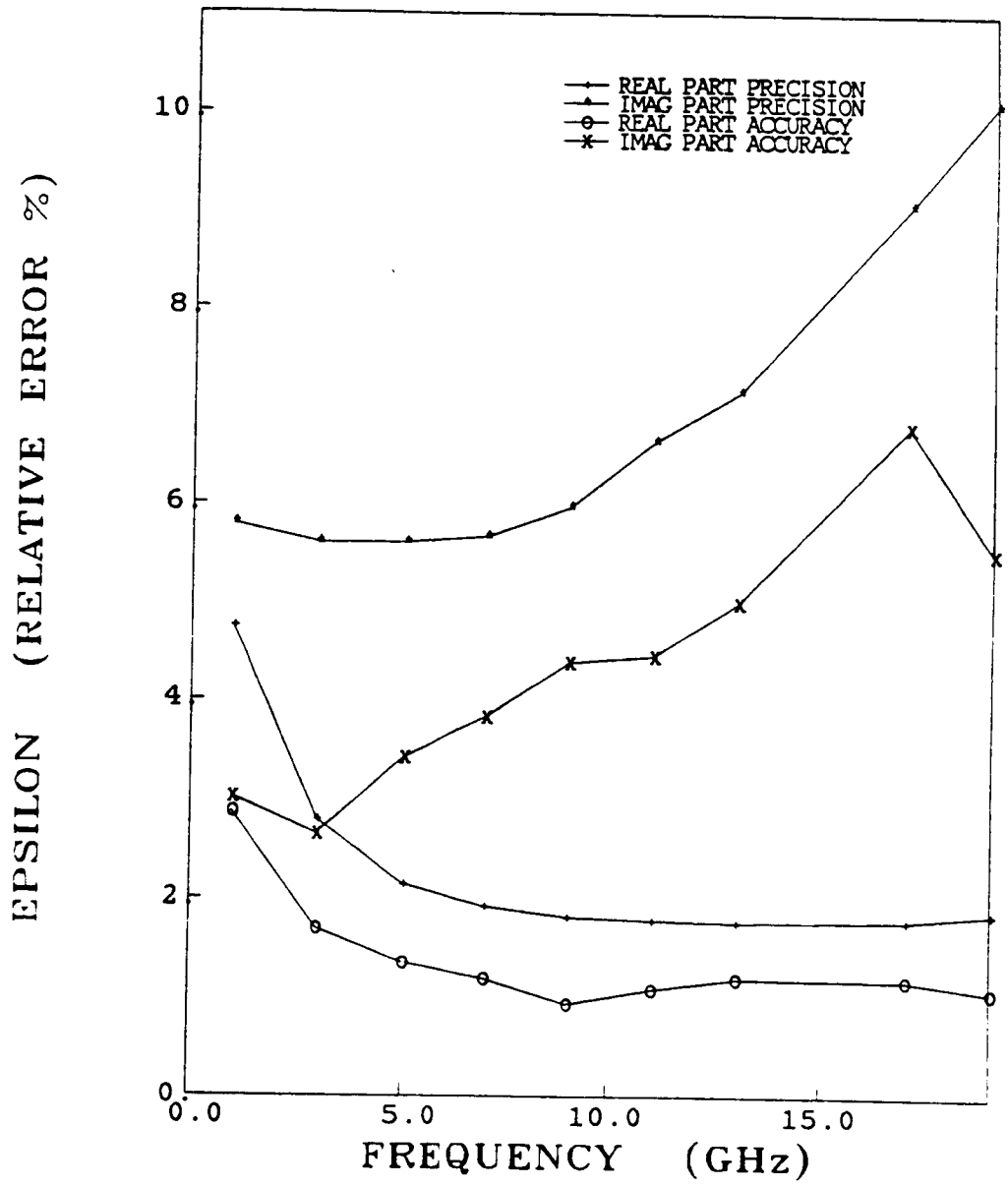

Figure 4.18. Estimated relative errors % for measurements on 1-butanol both accuracy and precision using the 0.141" probe.

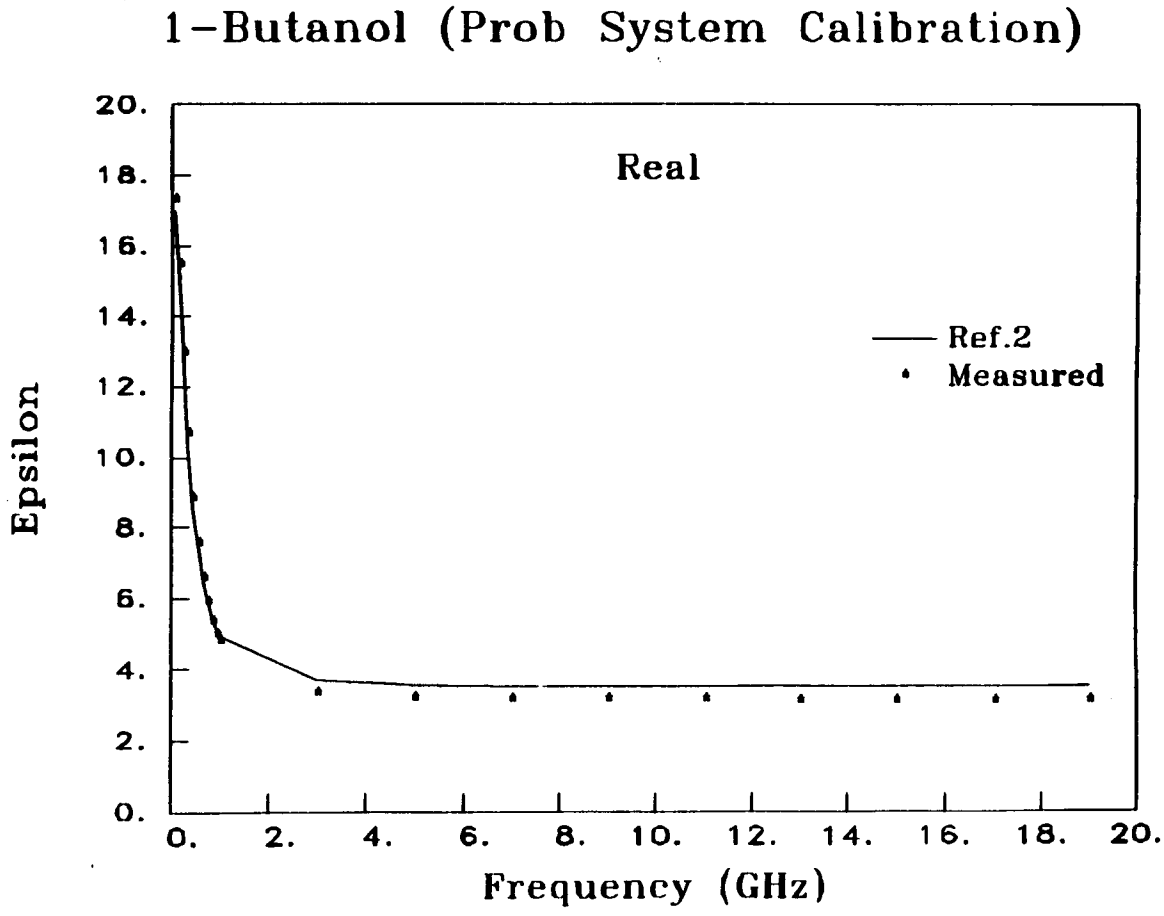

Figure 4.19. Comparison of calculated [ref. 2 is Bottreau et al, 1977] and measured data using the 0.141" probe for 1-butanol (real part).

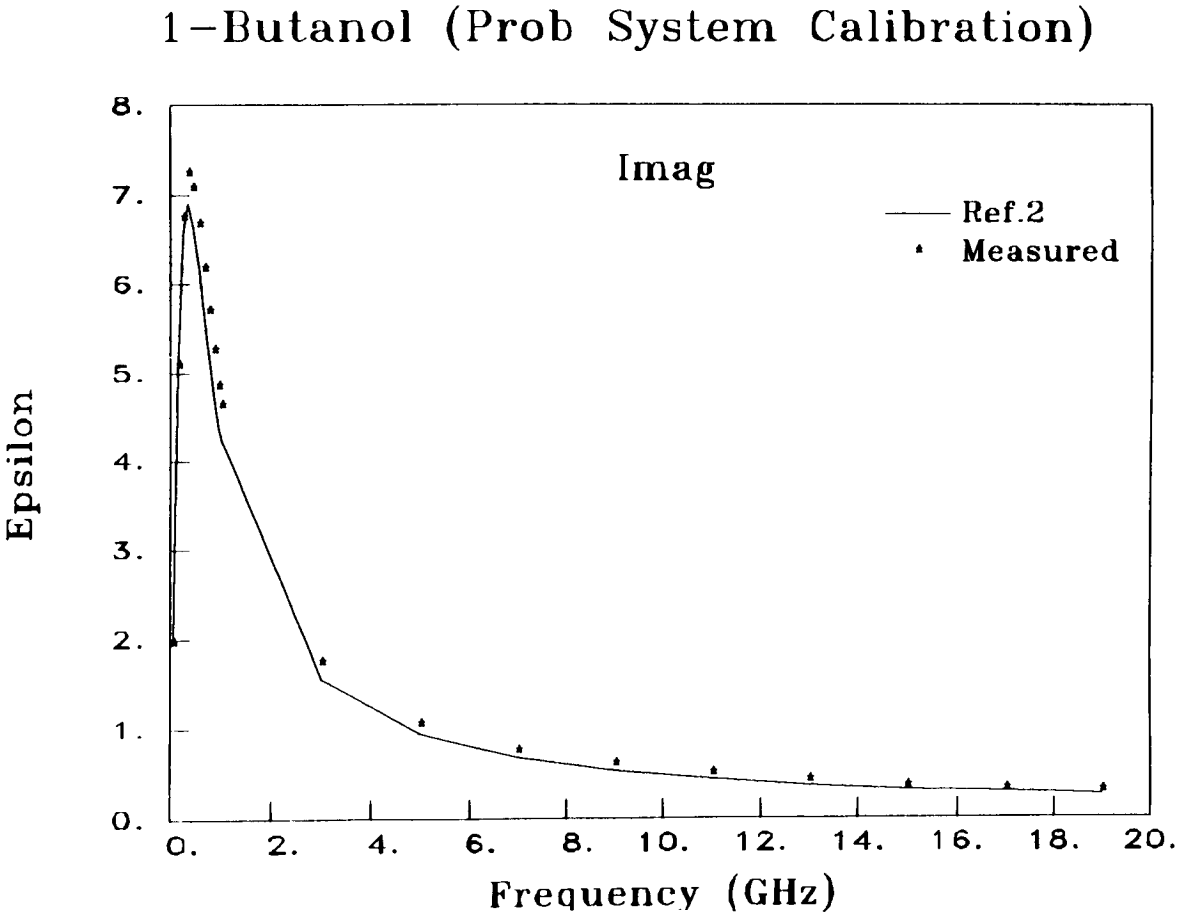

Figure 4.20. Comparison of calculated [ref. 2 is Bottreau et al, 1977] and measured data using the 0.141" probe for 1-butanol (imaginary part).

4.4.3 Thin Sample Measurements

The sample under test was assumed to be a semi-infinite medium. This assumption is impossible to achieve practically; however, it was found that the fringing and radiating fields decay rapidly with distance away from the probe tip. A simple experiment was designed to show the validity of the semi-infinite assumption. A stack of paper sheets, with variable thickness (1 up to 30 sheets), was measured against two different backgrounds. The background materials were selected to be plexiglass and metal in order to provide a large contrast (refer to Fig. 4.21). The results of this measurement are shown in Fig. 4.22(a) to (c). The following observations can be made regarding these figures:

1. One sheet ($\sim$ .1 mm)is too thin and does not satisfy the semi-infinite medium condition.

2. At 1 GHz, at least 30 sheets are required to satisfy the thick sample condition (3 mm).

3. The higher the frequency, the less stringent this condition becomes (at 8 GHz it is about 2 mm).

4. Since paper sheets are practically lossless, this condition is even easier to satisfy for lossy materials.

5. By intuition, we can state that the larger the probe diameter is, the thicker the required sample gets.

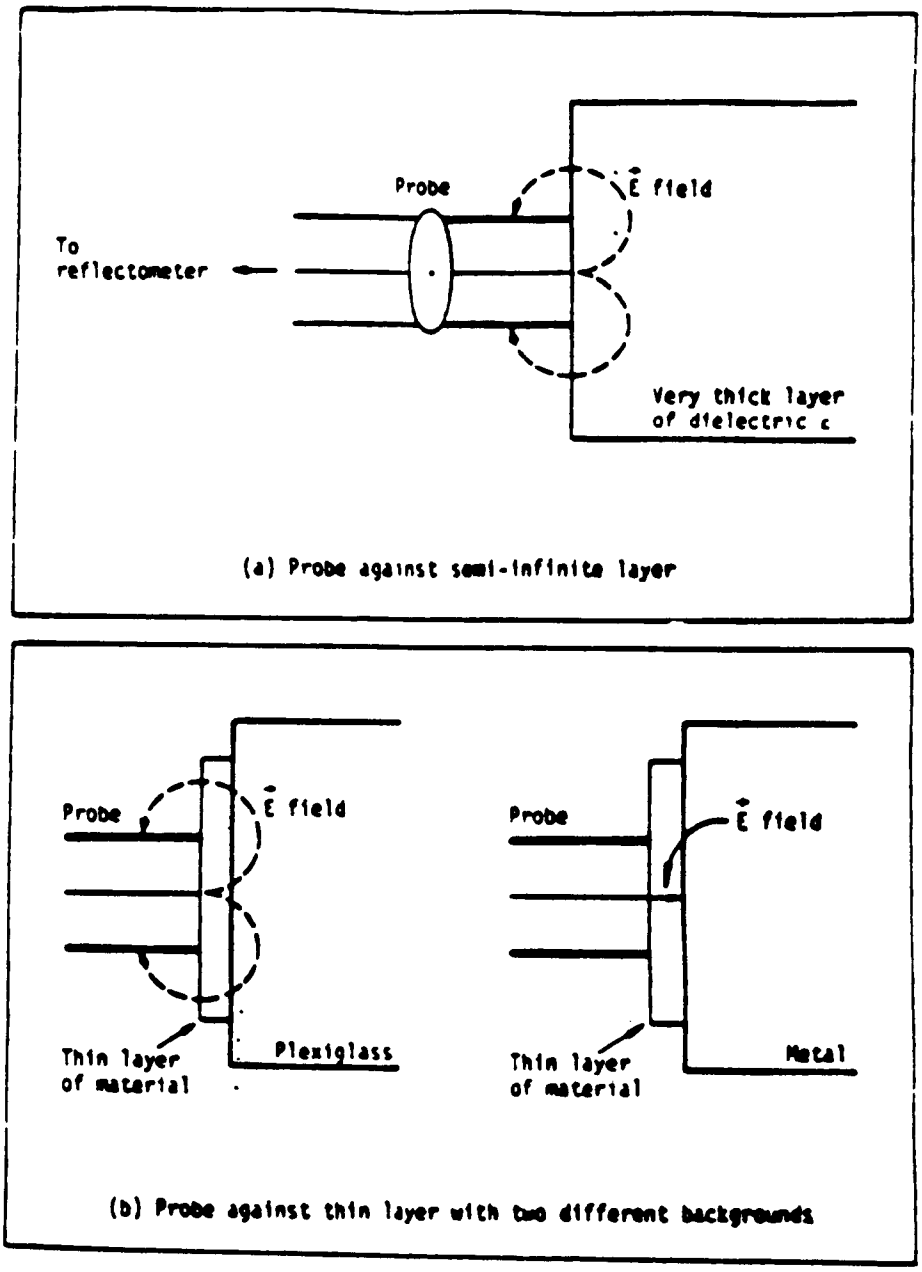

Figure 4.21. Probe technique for measuring dielectric of (a) thick layers and (b) thin layers.

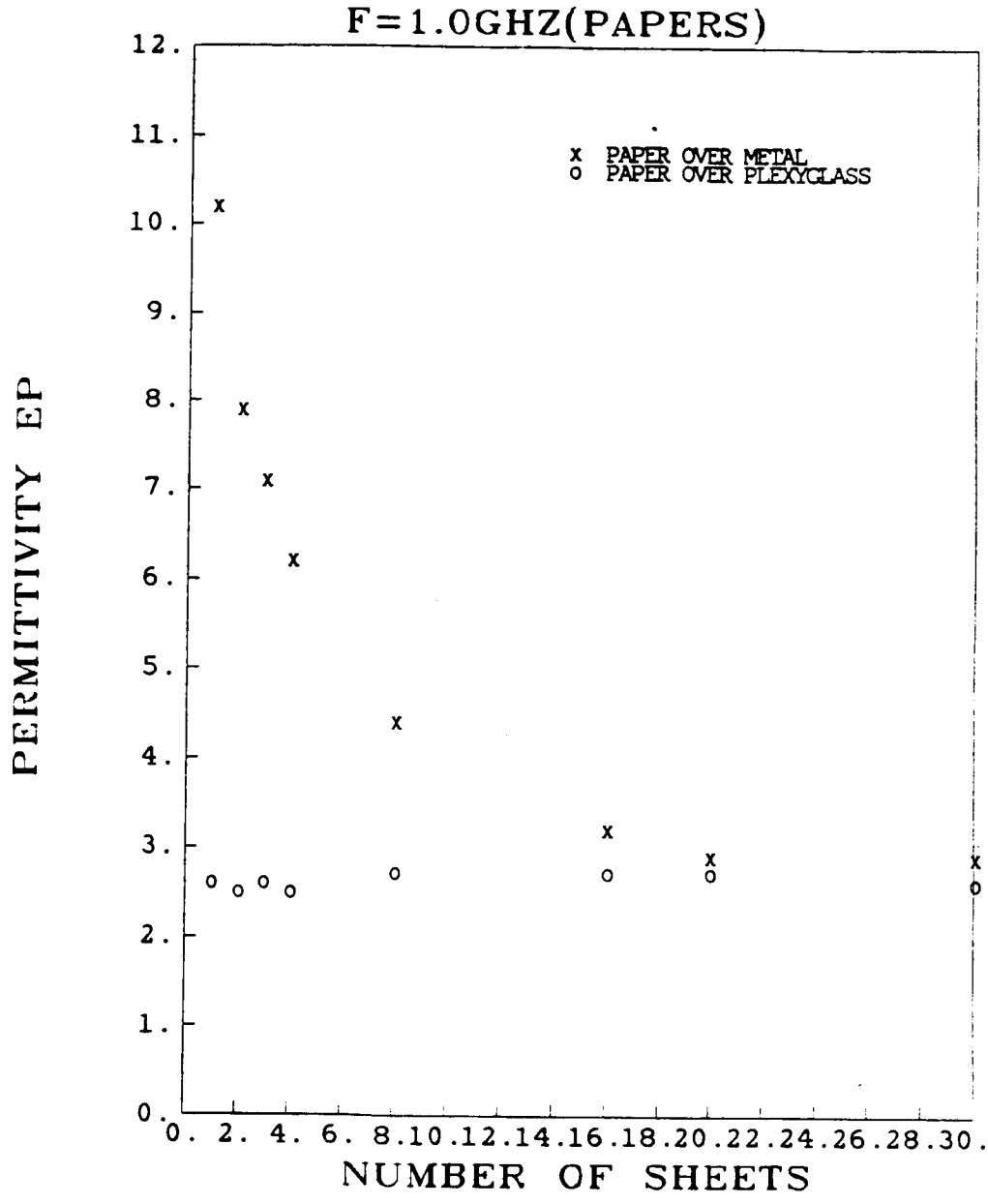

Figure 4.22(a). Comparison of a measured stack of sheets against a metal background and against a plexiglass background versus the stack's thickness at f=1 GHz.

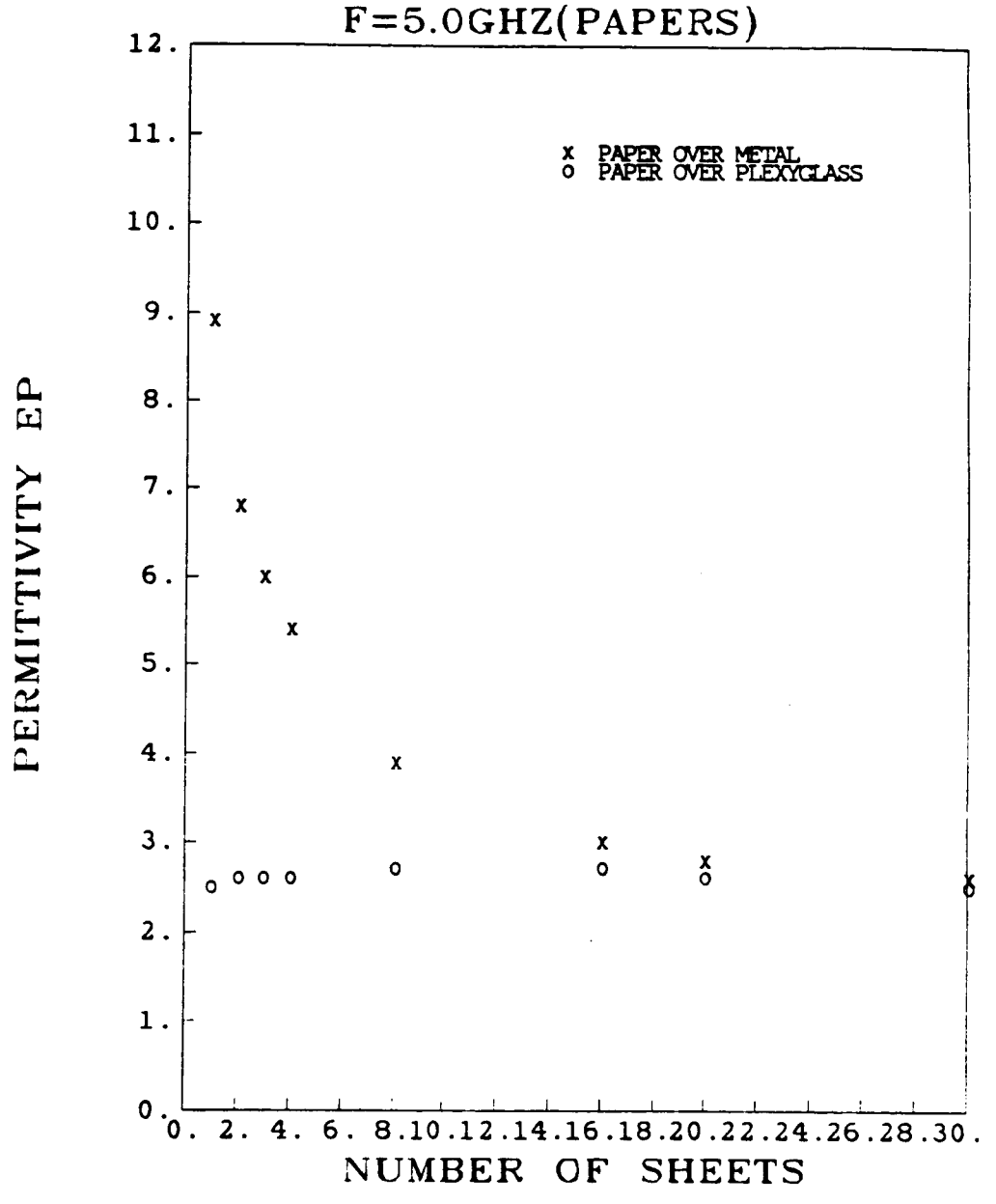

Figure 4.22(b). Comparison of a measured stack of sheets against a metal background and against a plexiglass background versus the stack's thickness at f=5 GHz.

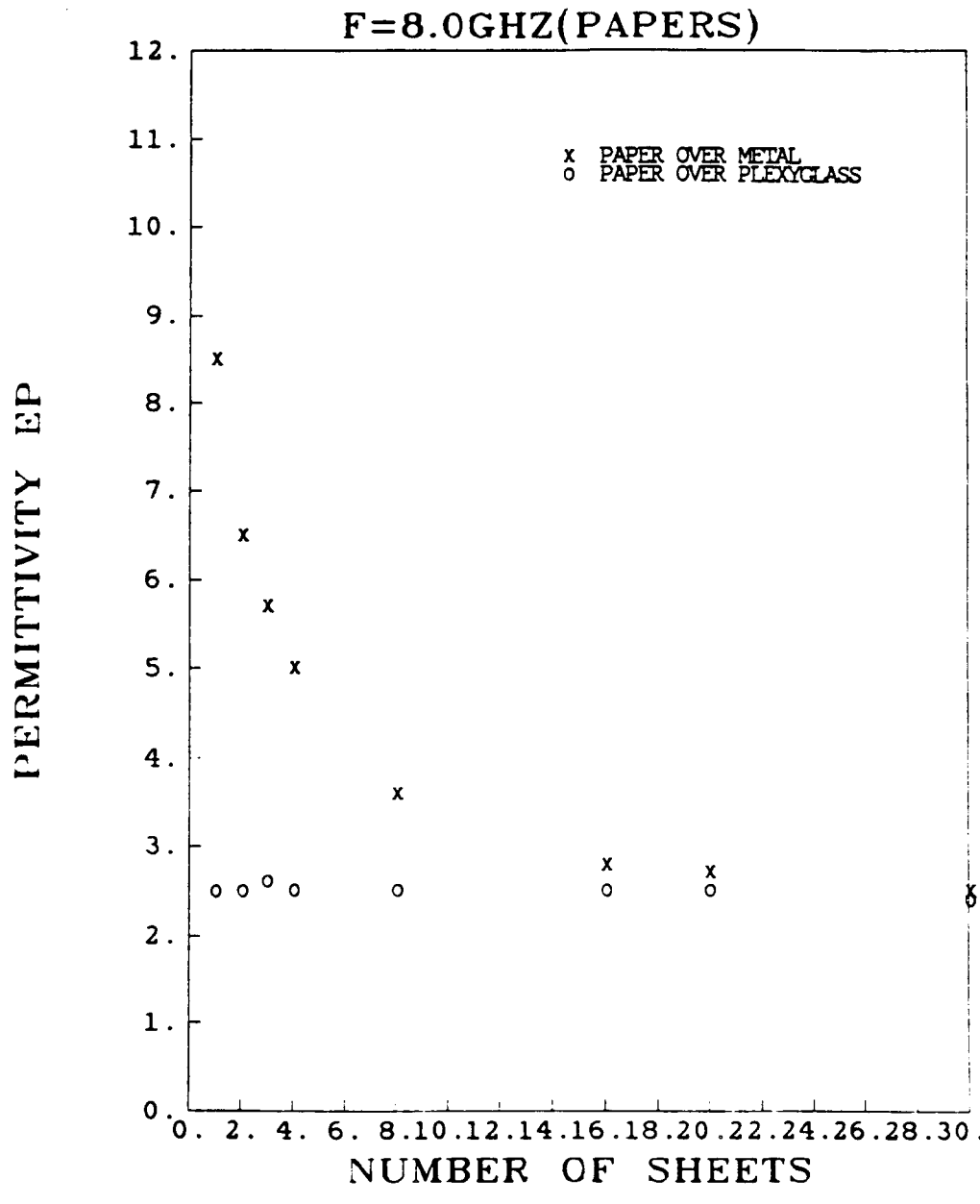

Figure 4.22(c). Comparison of a measured stack of sheets against a metal background and against a plexiglass background versus the stack's thickness at f=8 GHz.

As a rule of thumb, the sample thickness should be approximately equal to the probe radius.

The previous discussion has shown that a sample 3 mm in thickness is suffcient (using the .25" probe) to satisfy the semi-infinite condition for any material and across the entire frequency band of interest (.1-20 GHz). For dielectric measurements of vegetation leaves, however, a single leaf does not have sufficient thickness to satisfy the above conditions. So, a stack of leaves, usually 8 or more, is used and 2 measurements are taken against plexyglass (or teflon) as background and another 2 measurements are taken with a metal background. It is advisable to check that these 4 measurements are consistent and that the variations, if any, can be attributed to sample conditions (and not to sample thickness). In order for the probe to be useful for measuring live or intact plants, it should be able to measure samples that are thinner than the minimum thickness required (3 mm). A semi-empirical formula was developed, tested, and has proved to work satisfactorily over the frequency band of interest. The exact mathematical analysis was fairly complex and hence we took a semi-empirical approach.

Assume that a TEM signal is propagating in medium 1 and impinging on a dielectric slab of known thickness d and known permittivity ϵ_2. The slab is terminated in a semi-infinite medium of dielectric constant ϵ_3 (as shown in Fig. 4.23). If all multiple reflections are considered, we end up with the following general equation for the input impedance at the interface between media 1 and 2 (Ulaby et al, 1982):

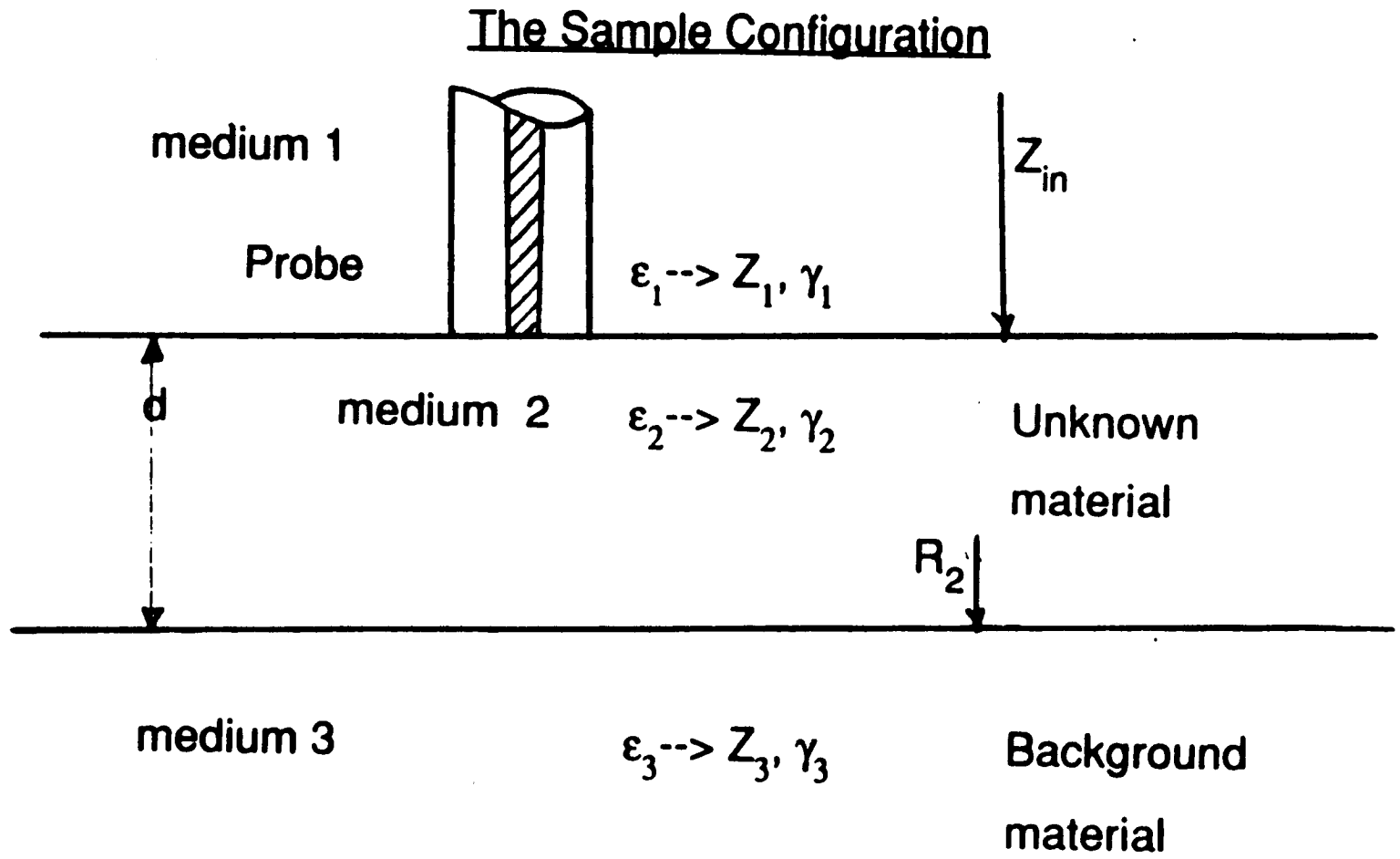

Figure 4.23. Thin sample configuration against a background material (known).

$$Z_{in} = Z_2(\frac{1 + R_2 e^{-j\gamma_2 d}}{1 - R_2 e^{-j\gamma_2 d}}) \tag{4.13}$$

where,

$$R_2 = \frac{Z_3 - Z_2}{Z_3 + Z_2}, \tag{4.14}$$

$$\gamma_2 = \frac{2\pi}{\lambda_0}\sqrt{\epsilon_2}, \tag{4.15}$$

and Z_1, Z_2, and Z_3 are the effective impedances of media 1, 2, and 3, respectively. Equation (4.13) can be rewritten as:

$$e^{-j\gamma_2 d} = (\frac{Y_2 + Y_3}{Y_2 - Y_3})(\frac{Y_2 - Y_{in}}{Y_2 + Y_{in}}), \tag{4.16}$$

where Y_2, Y_3, and Y_{in} are the admittances for media 2, 3, and the input admittance respectively. This equation can be solved for Y_2 by iteration if we know the thickness d, Y_3 of a known background, and the measured Y_{in}. The material under test is generally very thin (e.g., a vegetation leaf), so the error in measuring d can be large, in addition to the fact that the solution is oscillatory and a very strong function of thickness. It was suggested to use two different background materials to eliminate the errors associated with the thickness measurement. We will denote the two different backgrounds by the superscripts 1 and 2; hence,

$$e^{-j\gamma_2 d} = \frac{(Y_2 + Y_3^{(1)})(Y_2 - Y_{in}^{(1)})}{(Y_2 - Y_3^{(1)})(Y_2 + Y_{in}^{(1)})}, \tag{4.17}$$

also,

$$e^{-j\gamma_2 d} = \frac{(Y_2 + Y_3^{(2)})(Y_2 - Y_{in}^{(2)})}{(Y_2 - Y_3^{(1)})(Y_2 + Y_{in}^{(1)})} \tag{4.18}$$

After straightforward manipulation we obtain the general equation:

$$Y_2^2 = \sqrt{\frac{Y_{in}^{(1)}Y_{in}^{(2)}(Y_3^{(1)} - Y_3^{(2)}) + Y_3^{(1)}Y_3^{(2)}(Y_{in}^{(2)} - Y_{in}^{(1)})}{(Y_{in}^{(2)} - Y_{in}^{(1)}) - (Y_3^{(2)} - Y_3^{(1)})}} \tag{4.19}$$

This equation is valid for any 2 media with known $Y_3^{(1)}$ and $Y_3^{(2)}$ and 2 known measured input admittances $Y_{in}^{(1)}$ and $Y_{in}^{(2)}$. A special and useful case can, however, be deduced by putting $Y_3^{(1)} = \infty$ (i.e., medium 1 is metal). Y_2, in this case, will be given by

$$Y_2 = \sqrt{Y_{in}^{(1)}Y_{in}^{(2)} + Y_3^{(2)}(Y_{in}^{(2)} - Y_{in}^{(1)})} \tag{4.20}$$

The admittances of the media are those seen by the probe; hence, they depend on the probe equivalent circuit. A special case can simplify the last expression by assuming the simplest equivalent circuit, which is a capacitor. ϵ_2, in this case, is given by

$$\epsilon_2 = \sqrt{\epsilon_{in}^{(1)}\epsilon_{in}^{(2)} + \epsilon_3^{(2)}(\epsilon_{in}^{(2)} - \epsilon_{in}^{(1)})} \tag{4.21}$$

where ϵ_2, $\epsilon_3^{(2)}$, $\epsilon_{in}^{(1)}$, and $\epsilon_{in}^{(2)}$ are the relative dielectric constants for the sample under test, the second background medium (the first is metal), the measured input ϵ for background material 1 and material 2, respectively. It was found experimentally that Equation (4.21) is valid only at low frequencies, while Equation (4.20) is valid across the entire frequency range of interest (except when the frequency is high enough to cause moding). The validity of this semi-empirical approach

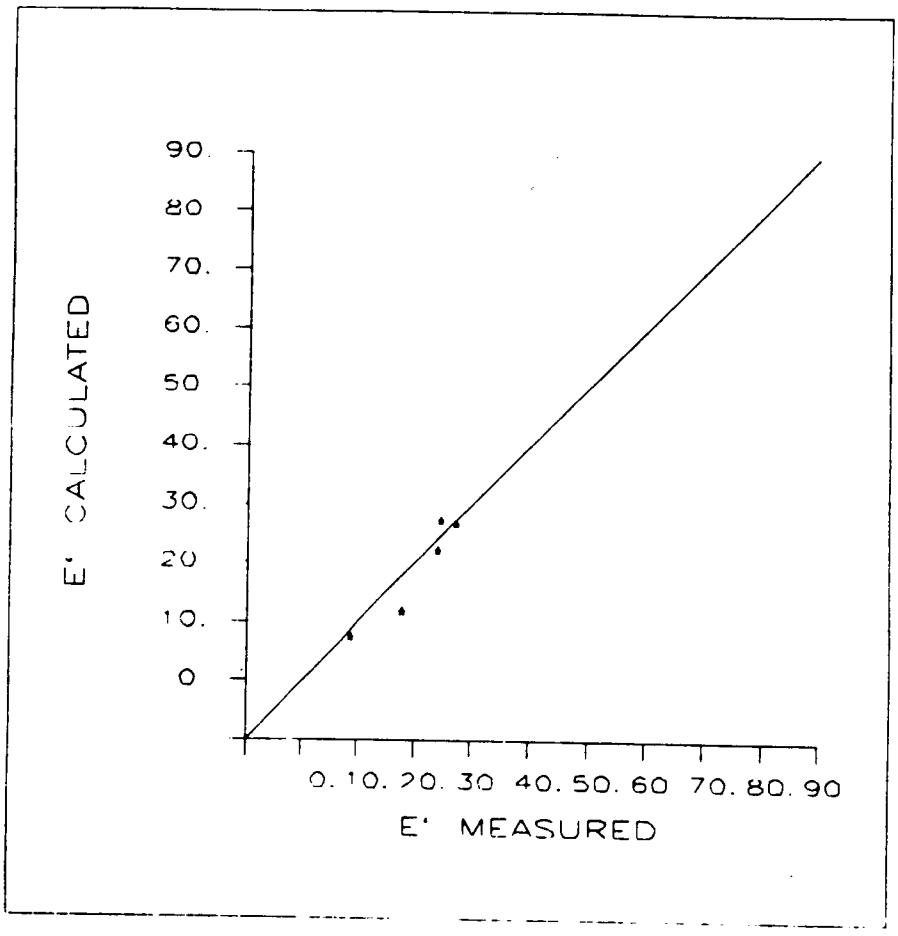

Figure 4.24(a). Evaluation of the thin-thick sample formula (refer to text) for the 0.250" probe at 1 GHz(real part).

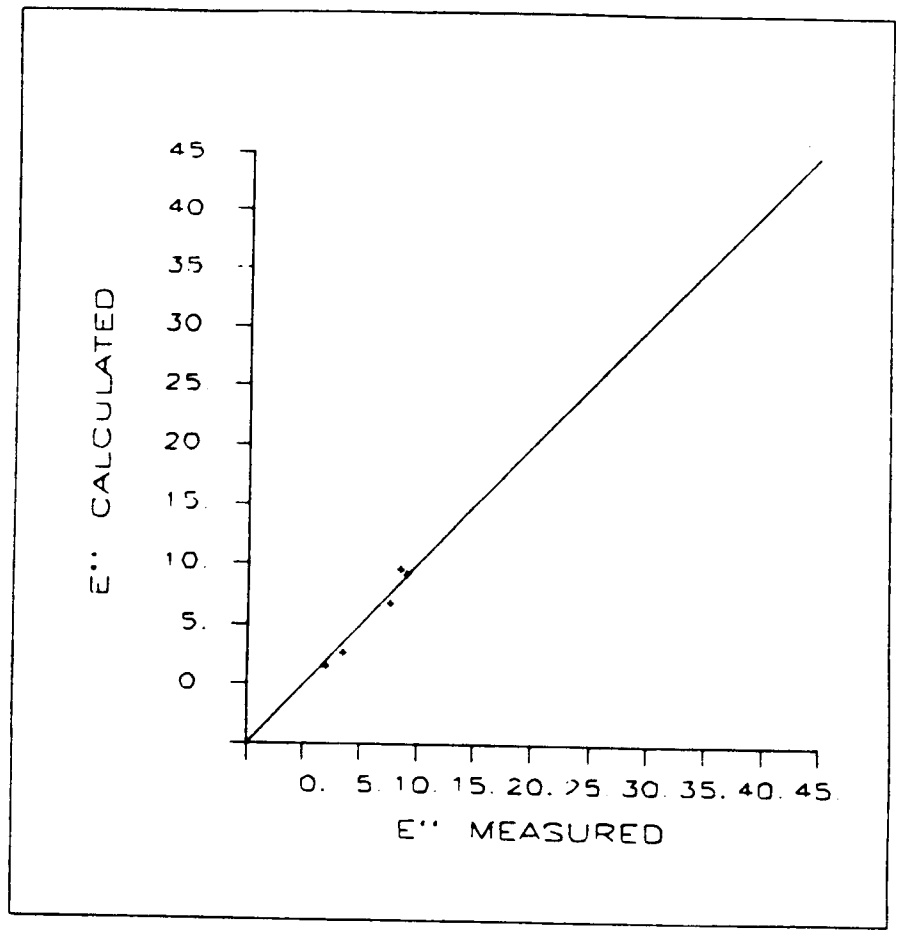

Figure 4.24(b). Evaluation of the thin-thick sample formula (refer to text) for the 0.250" probe at 1 GHz(imaginary part).

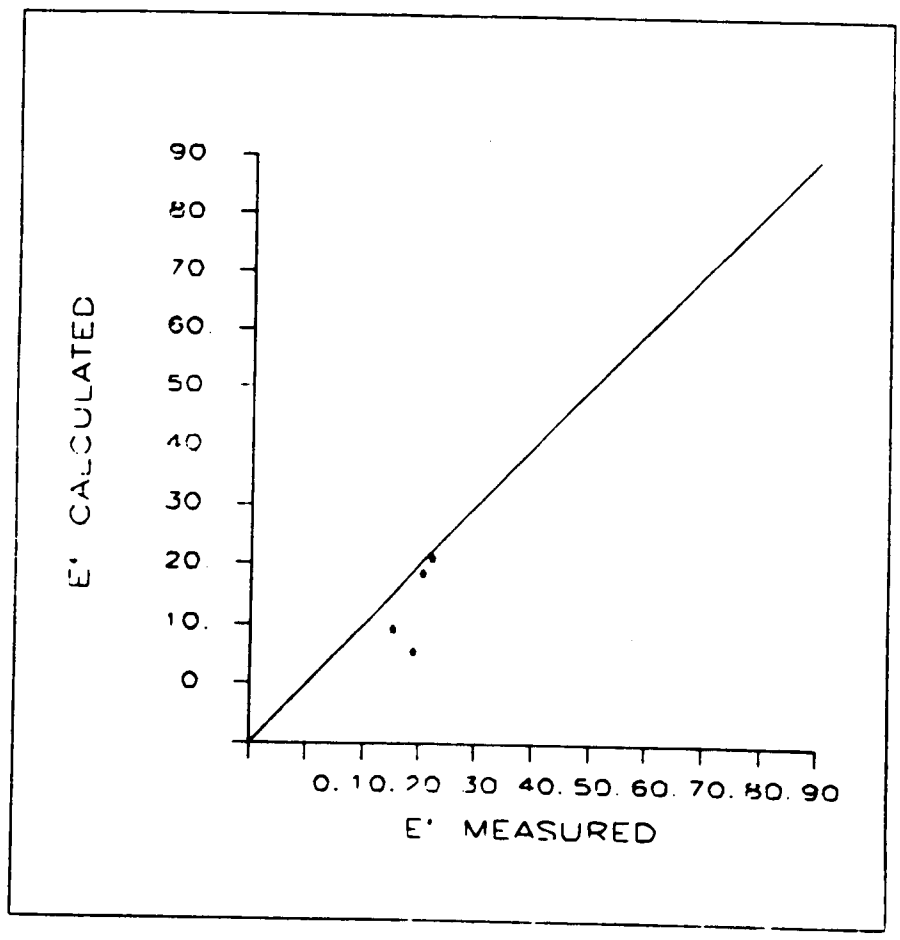

Figure 4.25(a). Evaluation of the thin-thick sample formula (refer to text) for the 0.250" probe at 8 GHz(real part).

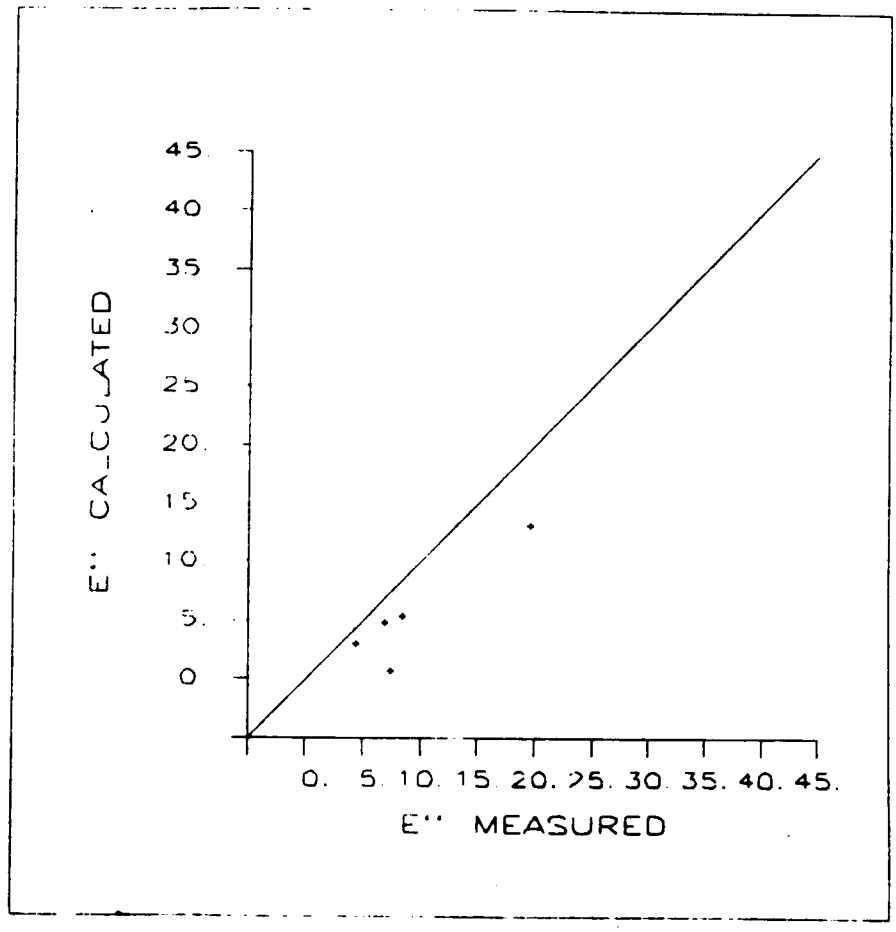

Figure 4.25(b). Evaluation of the thin-thick sample formula (refer to text) for the 0.250" probe at 8 GHz(imaginary part).

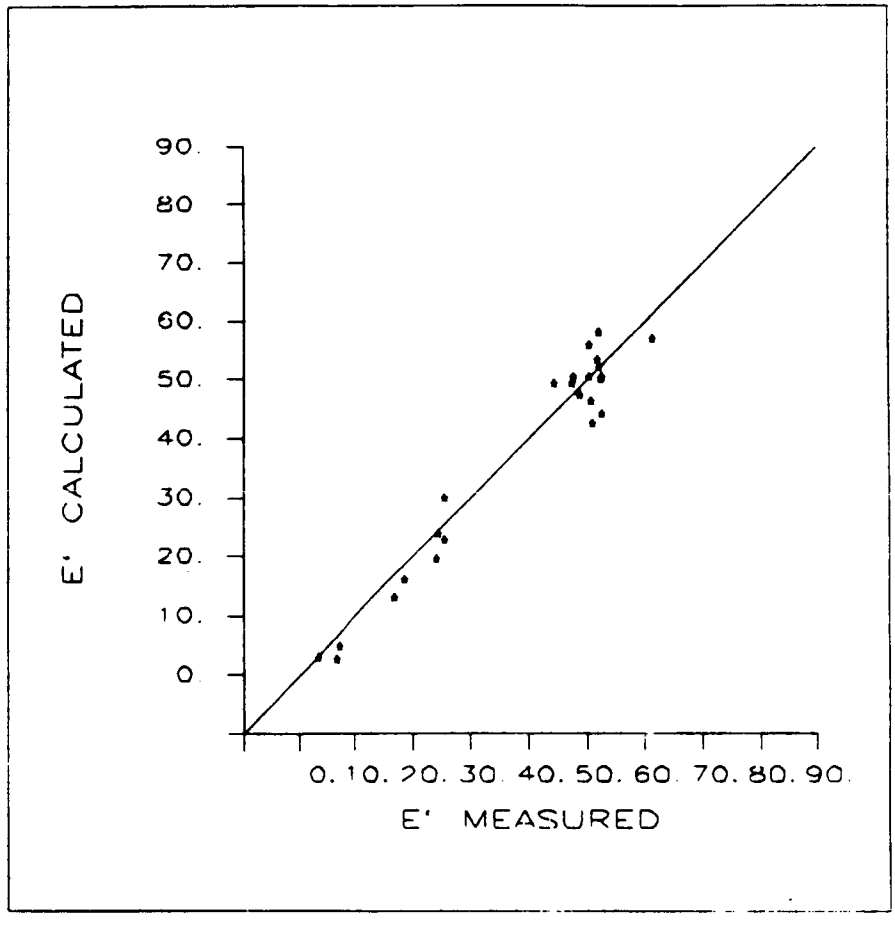

Figure 4.26(a). Evaluation of the thin-thick sample formula (refer to text) for the 0.141" probe at 1 GHz(real part).

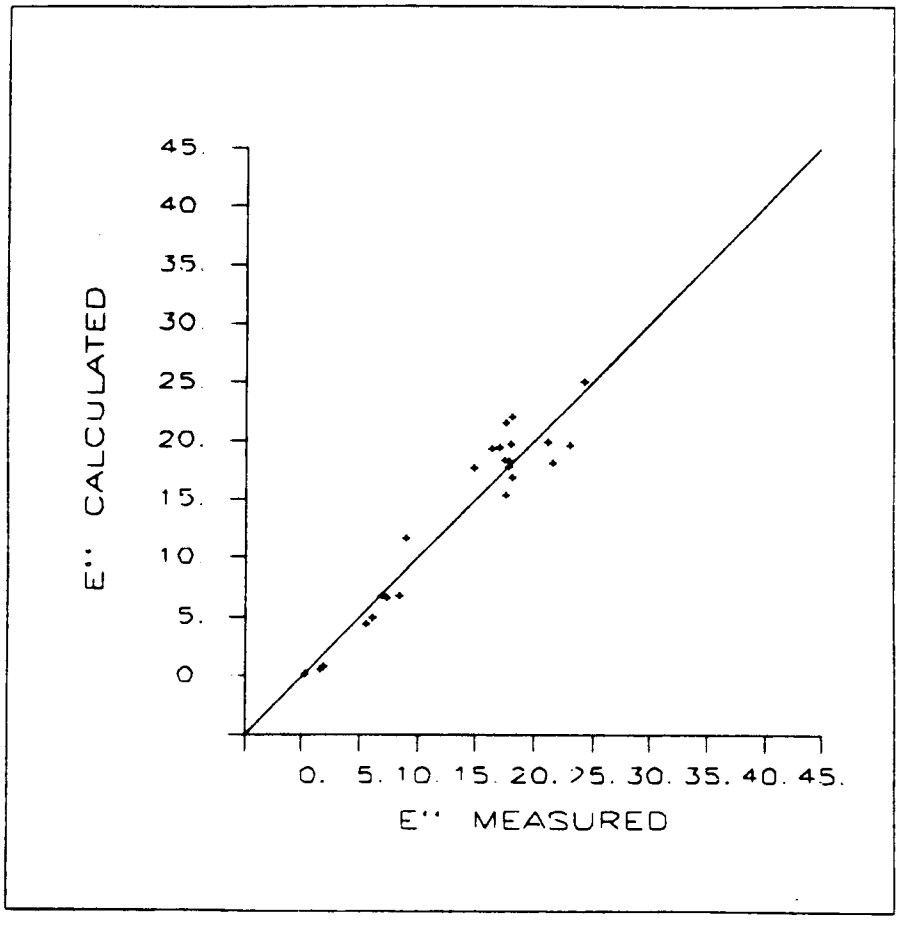

Figure 4.26(b). Evaluation of the thin-thick sample formula (refer to text) for the 0.141" probe at 1 GHz(imaginary part).

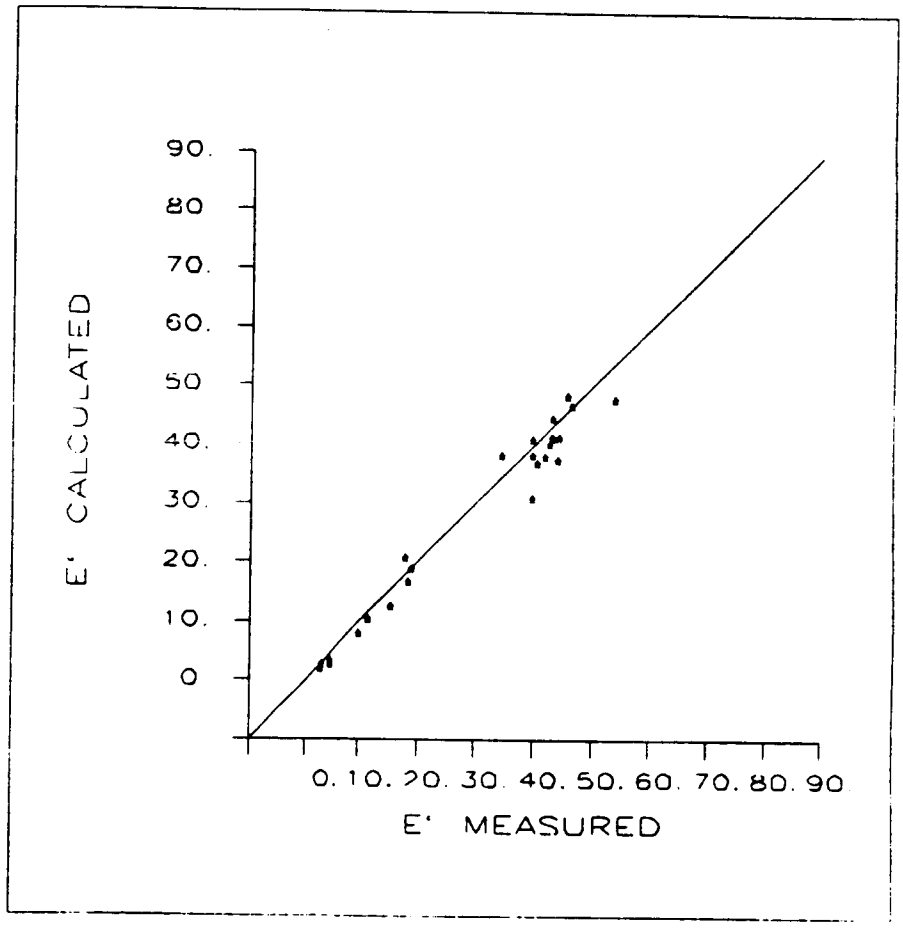

Figure 4.27(a). Evaluation of the thin-thick sample formula (refer to text) for the 0.141" probe at 8 GHz(real part).

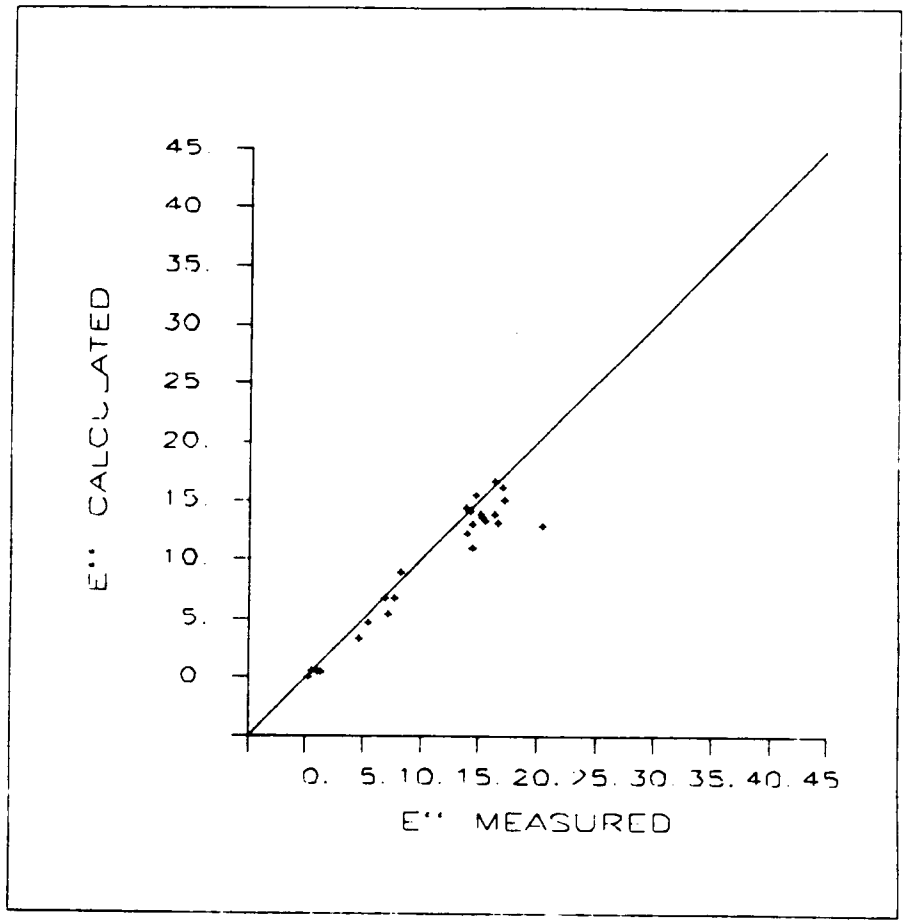

Figure 4.27(b). Evaluation of the thin-thick sample formula (refer to text) for the 0.141" probe at 8 GHz(imaginary part).

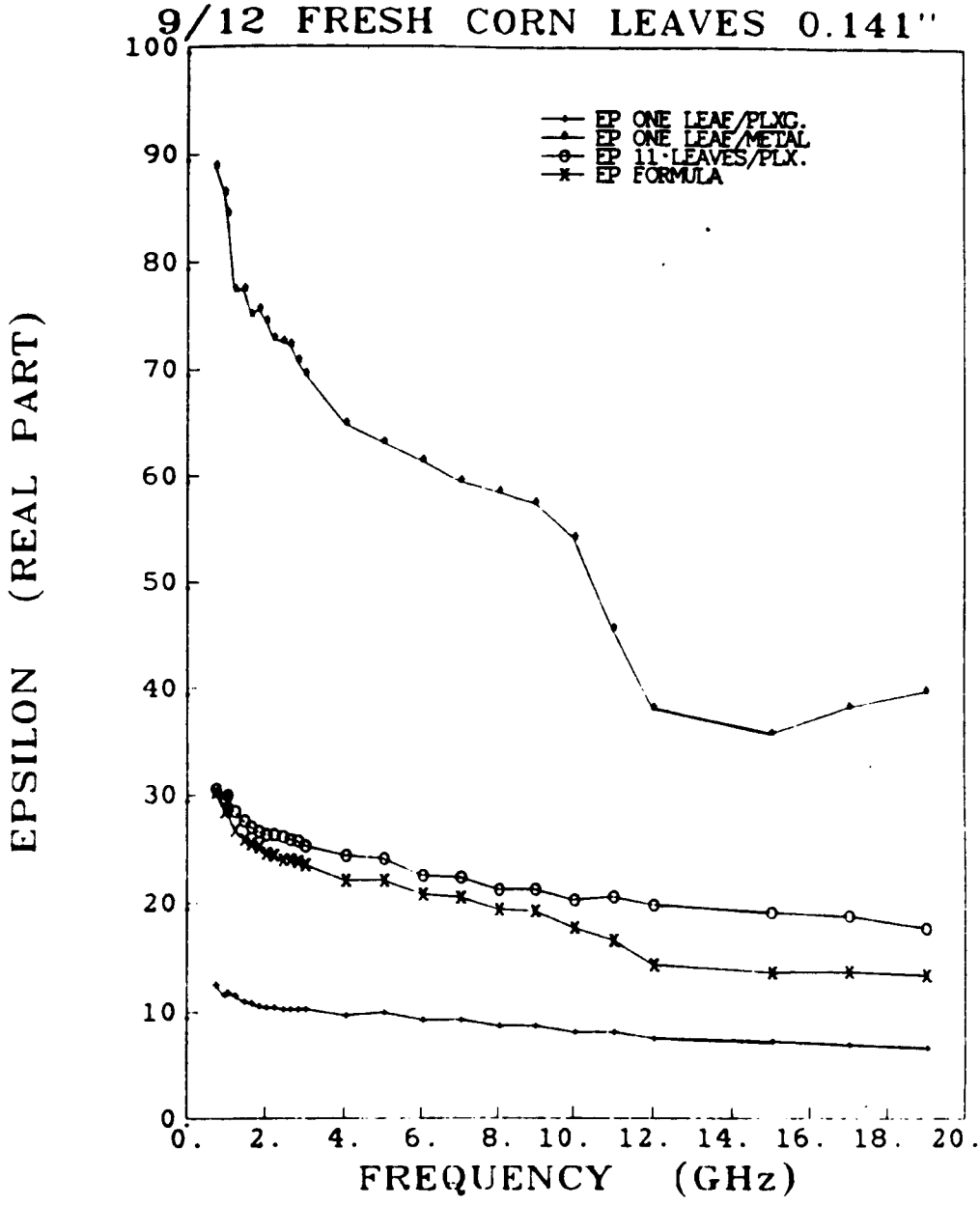

Figure 4.28(a). Spectra of measured one leaf/metal, one leaf/plexiglass, and thick stack/plexiglass along with the calculated values from the thin-thick formula (real parts). Above 11 GHz high-order modes propagation (upper curve) causes large errors.

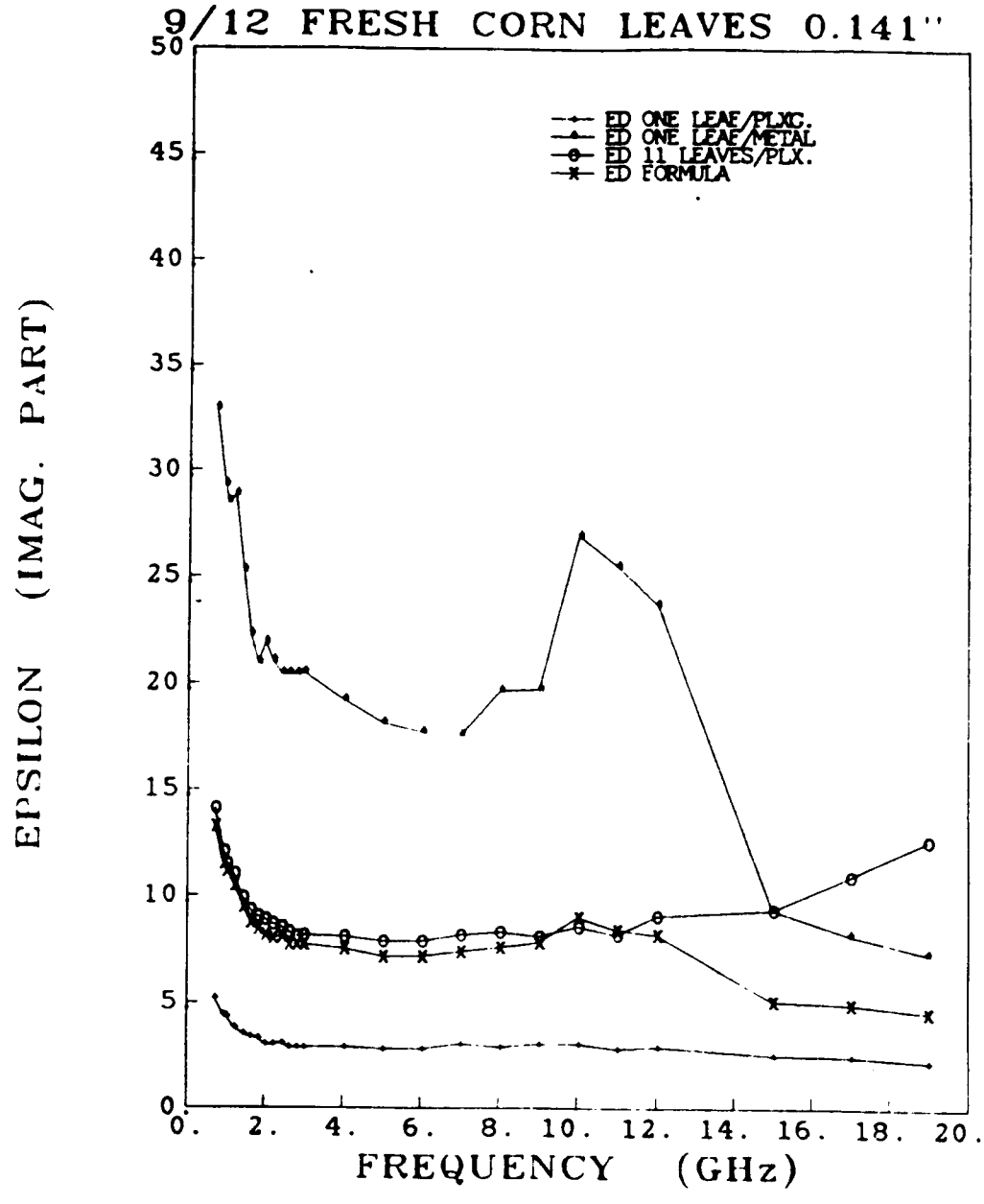

Figure 4.28(b). Spectra of measured one leaf/metal, one leaf/plexiglass, and thick stack/plexiglass along with the calculated values from the thin-thick formula (imaginary parts). Above 11 GHz high-order modes propagation (upper curve) causes large errors.

was tested for a wide frequency range, wide range of dielectric values, and for the .141" probe (Table 4.3). The results were found to be very satisfactory as shown in Table (4.3). Figures (4.24) to (4.27) show how well this approximate model works. Figures 4.28(a) and (b) show spectra of an example of these measurements for thin and thick samples against various backgrounds. The data above 11 GHz was plotted to show how high-order modes can propagate when we use a metal background and a very thin sample. To avoid this problem, however, we can use either a thicker sample or a background material other than metal.

f(GHz)	1	2	4	8
# points	24	25	25	25
ϵ' slope	1.0265	1.0078	1.0026	.9594
ϵ' intercept	-2.03	-1.2728	-1.0795	-.5036
ϵ' variance	15.03	11.51	8.90	7.81
ϵ' ρ	.9776	.9829	.9858	.9849
ϵ'' slope	1.0306	1.0351	.9834	.8726
ϵ'' intercept	-.0707	-.3509	-.2225	.2683
ϵ'' variance	4.38	1.70	1.43	2.34
ϵ' ρ	.9610	.9684	.9660	.9601

Table (4.3): Evaluation of the thin-thick formula for the .141" probe.

4.4.4 Comparison to the Waveguide Transmission System

As was discussed earlier in Chapter 3, the transmission technique is, in general more accurate than the reflection technique. A comparison between both systems provides a useful confirmation of the validity of the probe-system accuracy. The choice of material was a problem since the sample requirements are different for the two techniques. Yellow cheese was finally selected because it is suitable for both systems. As shown in Fig. (4.29) the agreement is very good and the error is within the expected $\pm 5\%$ bounds. This evaluation test gave us confidence in our measurement techniques to go ahead and start measurements on vegetation samples.

4.5 Probe Usage and Limitations-Other Probe Configurations

The standard probes were found to have the following features and limitations:

1. Wide frequency band (.5 - 20 GHz for the .141" and .05 - 9 GHz for the .250").

2. Accurate to within $\pm 5\%$ for all values of ϵ' and to within $\pm 10\%$ for all values of ϵ'' except for low loss materials (because rounding error is ± 0.1).

3. The system is very suitable for temperature measurements.

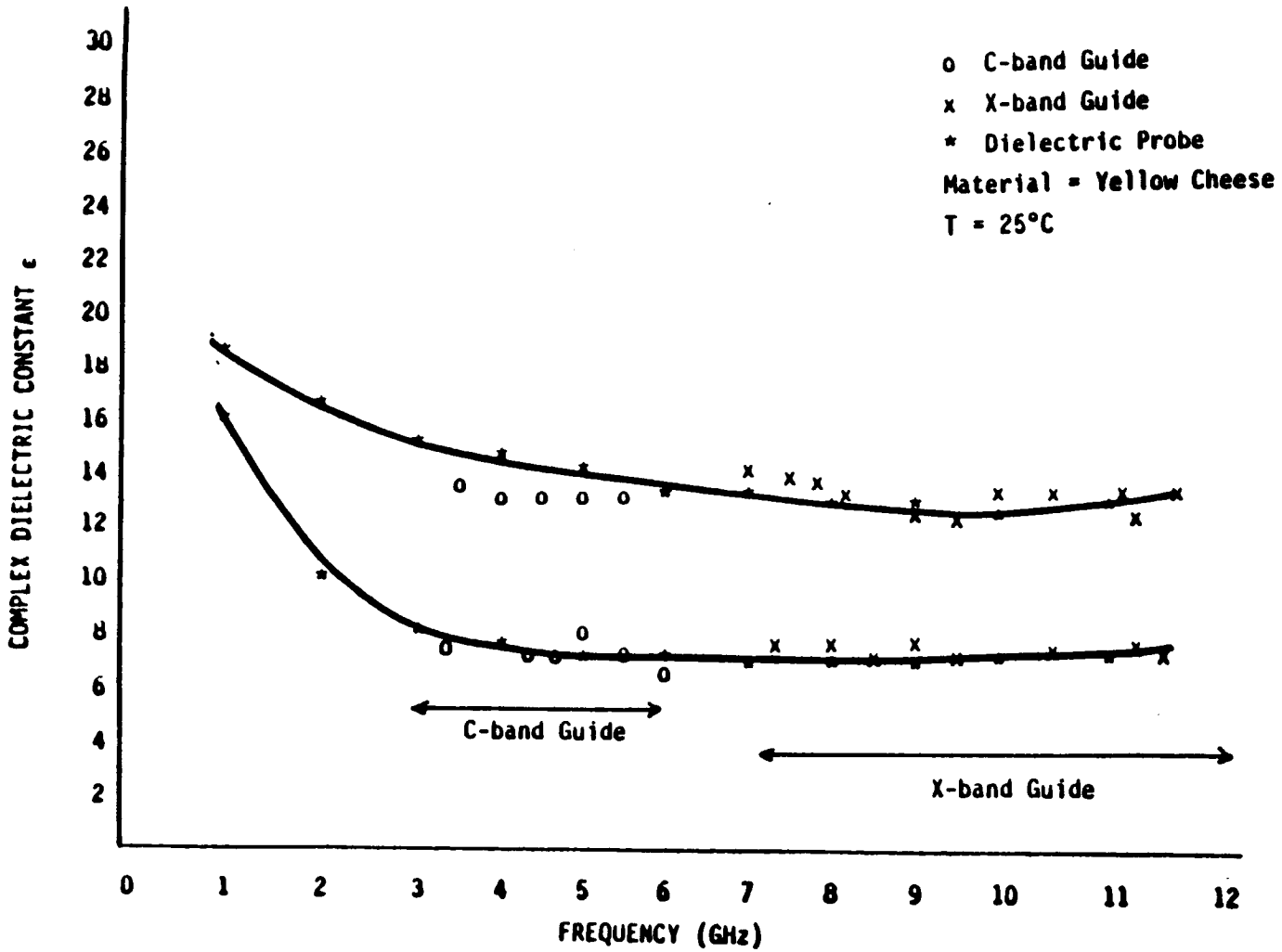

Figure 4.29. Comparison between the probe and the waveguide systems.

4. The system is very suitable for measuring liquid or semi-liquid materials but is difficult to use with solid materials.

5. The probe is suitable for non-destructive and *in-vivo* measurements.

Other Probe Configurations

For standard cables, the ratio $\frac{r_1}{r_2} \approx .3$ and is kept constant in order to maintain Z_0 constant (refer to Fig. 4.2). In order to build an "optimum" probe, it may be necessary to change this ratio to increase the probe sensitivity over a particular frequency band and a given range of ϵ. The cut-off frequency of the first higher-order mode is proportional to $(r_2 - r_1)$ while the sensitivity is proportional to the probe tip area, i.e. to $\pi(r_1^2 - r_2^2)$. Thus we have two major objectives with opposing requirements:

1. To avoid moding $(r_2 - r_1)$ should be small.

2. To increase the sensitivity, $\pi(r_2^2 - r_1^2)$ should be large which means $(r_2 - r_1)$ should be large too.

Preferrably, the ratio $(\frac{r_1}{r_2})$ should be kept constant in order to keep the cable characteristic impedance matched to the probe tip.

Chapter 5

Measurement Results

This chapter presents the experimental results obtained using the open-ended coaxial probe system. Gravimetric moisture content M_g was used in this chapter, instead of the volumetric moisture content M_v, because it is a directly measureable quantity, while M_v is dependent on vegetation density. Vegetation density is very hard to measure, especially for leaves, and the density data measured in this study represents an approximate estimate at best. For the most part, the dielectric data presented in this report will be the actual measurements derived from the probe measurements. In some cases, however, the measured variation of ϵ as a function of moisture will be presented in the form of plots based on regression equations generated using actual data. This is done for the purpose of making presentations clearer in cases where multiple plots are included in a given figure. It should be noted that these regressions provide excellent fits to the data and probably describe the moisture dependence of ϵ better than the actual data. The data presented in this chapter is a subset of that presented in Appendix A. The primary purpose of this chapter is to acquaint the reader with

the observed dielectric behavior. Interpretation and modeling of the data are the subjects of Chapter 6.

5.1 Plant Type, Part, and Location

1. *Plant type*

   Plant types (species) vary depending on the following parameters: (a) density, (b) salinity, (c) bound water content, and (d) how the vegetation material shrinks when it dries out. Salinity and bound water effects are more dominant at low frequency, while density effects are more obvious at low moisture levels. Figure 5.1 shows a comparison between corn (*Zea Mays*) leaves and soybean leaves at 1 GHz. Corn leaves have, in general, higher values of ϵ' and ϵ'' than soybean leaves. The difference can be attributed either to measurement errors in the dielectric constant and moisture content or to physical and physiological differeces. Figure 5.2 shows another comparison between corn stalks and black spruce tree trunk to test the effects of plant type on high density plant parts. The tree samples were measured at moistures less than 40% (graviometric). Corn stalks have a lower ϵ for dry samples, which can be attributed to density effects.

2. *Plant part*

   In order to illustrate the differences between plant parts, we will test two different parts from the same species. Corn leaves and corn stalks are compared at 1 GHz in Fig. 5.3. These two plant parts show comparable

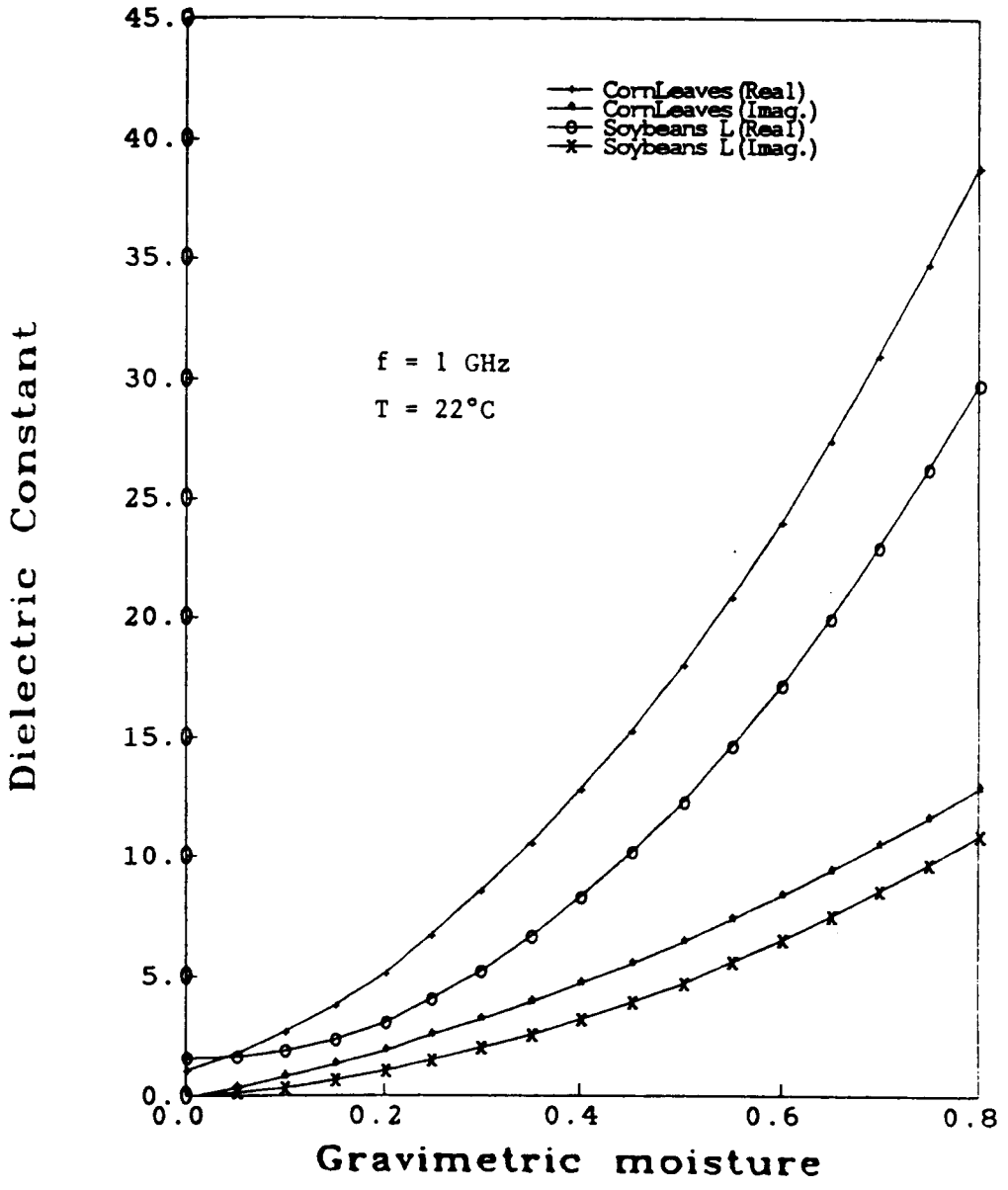

Figure 5.1. Comparison between corn leaves and soybeans leaves. Curves were fitted to measured data using a second order polynomial fit.

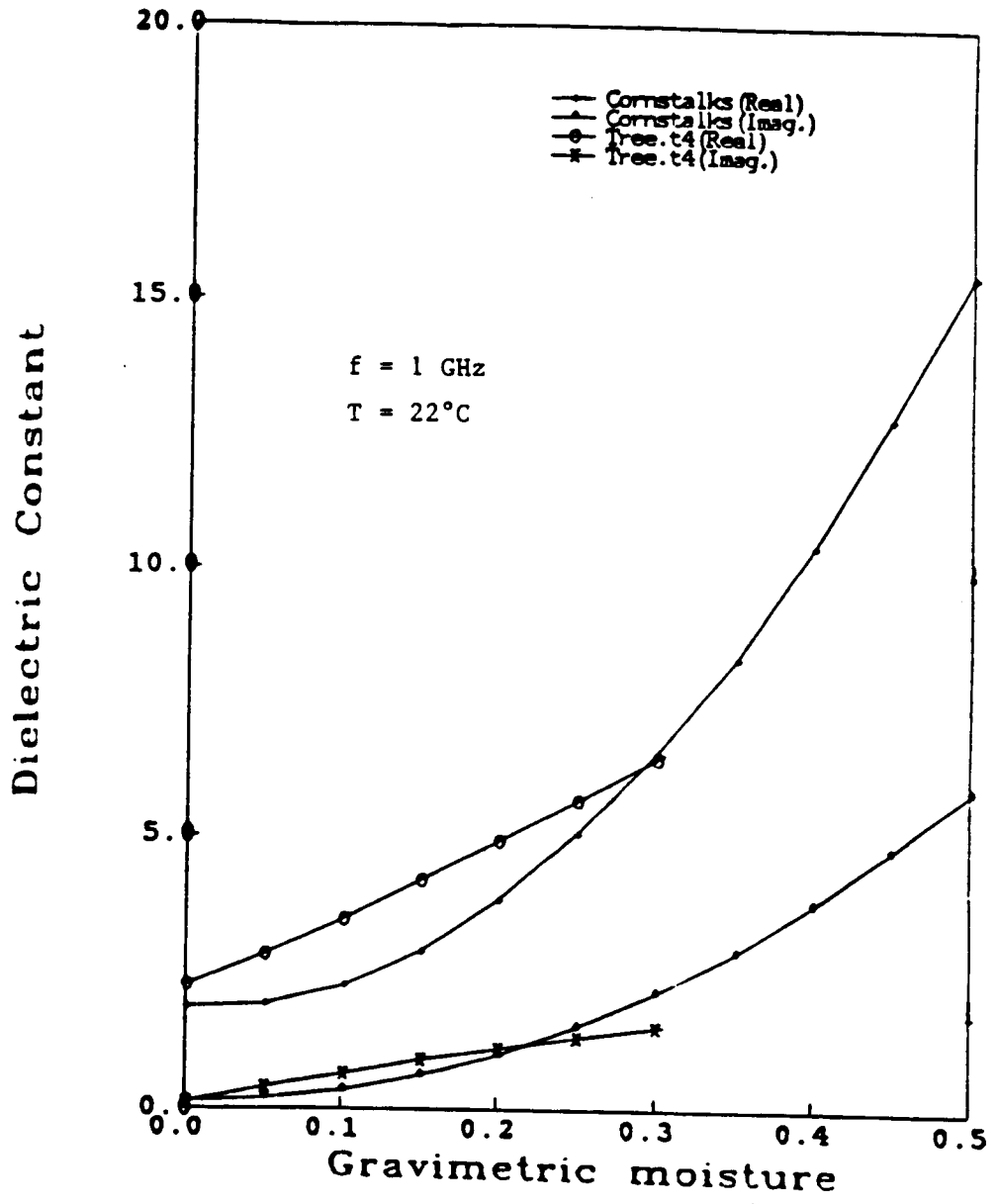

Figure 5.2. Comparison between corn stalks(measured on the inside part) and tree trunk (Black-Spruce). Curves were fitted to measured data using a second order polynomial fit.

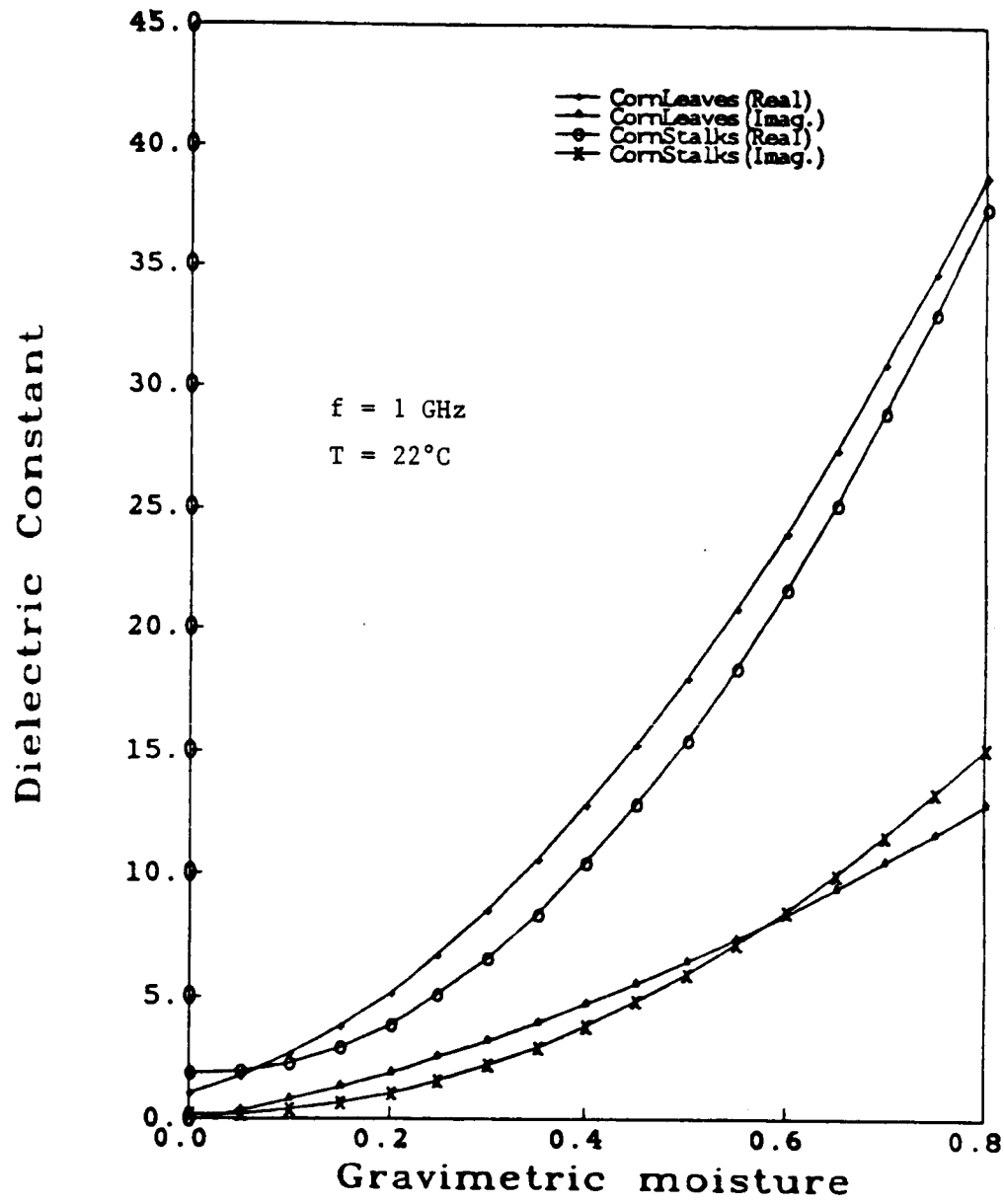

Figure 5.3. Comparison between corn leaves and corn stalks. Curves were fitted to measured data using a second order polynomial fit.

trends and magnitudes for both ϵ' and ϵ'' in spite of the fact that their densities are different.

3. *Part location*

   It was observed that plants have a moisture distribution profile, especially tall plants like corn. Figure 5.4 shows the dependence of ϵ', ϵ'', and M_v on height (above the ground) for a corn stalk of a fresh plant. The measured dielectric constant varies quite significantly as a function of height while the measured volumetric moisture exhibits a weaker dependence. This behavior may be explained by the fact that when the probe is used to measure the dielectric of a corn stalk from the outside sheath, it actually measures ϵ of the sheath (leaf) material surrounding the stalk, and not the stalk itself (because the fringing field of the probe has an effective penetration depth of only few millimeters). The moisture determination, however, is performed for the stalk including the sheath and the inside. Hence, Fig. 5.4 should not be considered quantitatively and the general trend only matters here.

5.2 Frequency Dependence

Figures 5.5 and 5.6 show the frequency behavior of the dielectric constant of corn leaves at different volumetric moisture levels. The trends in these two figures can be compared to those of saline liquid water (refer to Fig. 2.1) and to those of bound water (refer to Fig. 5.18). The low frequency behavior of ϵ'' is similar to those exhibited by both saline and bound water. At high

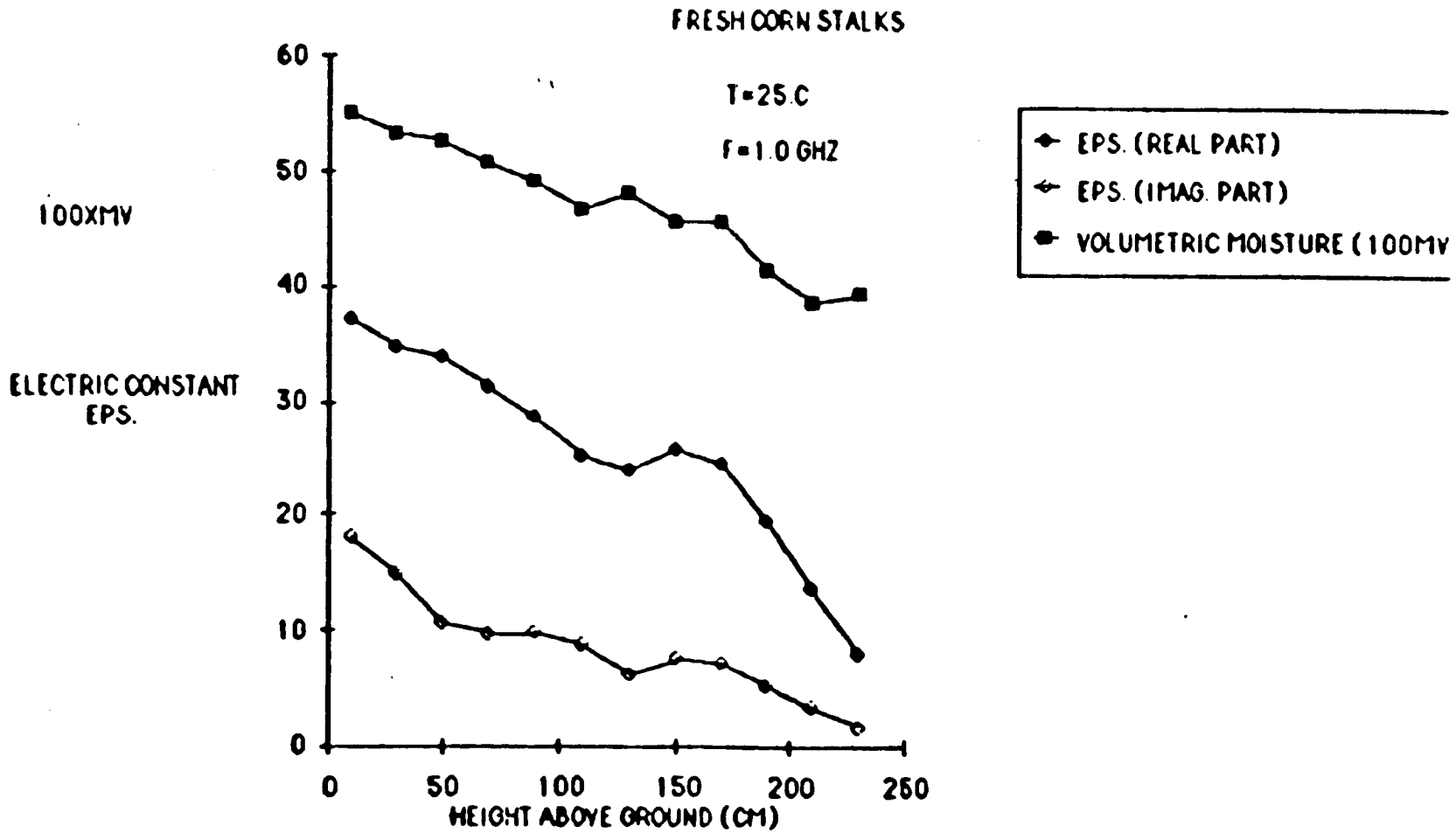

Figure 5.4. Measured dielectric constant and calculated volumetric moisture for fresh corn stalks as a function of height above the ground (cm).

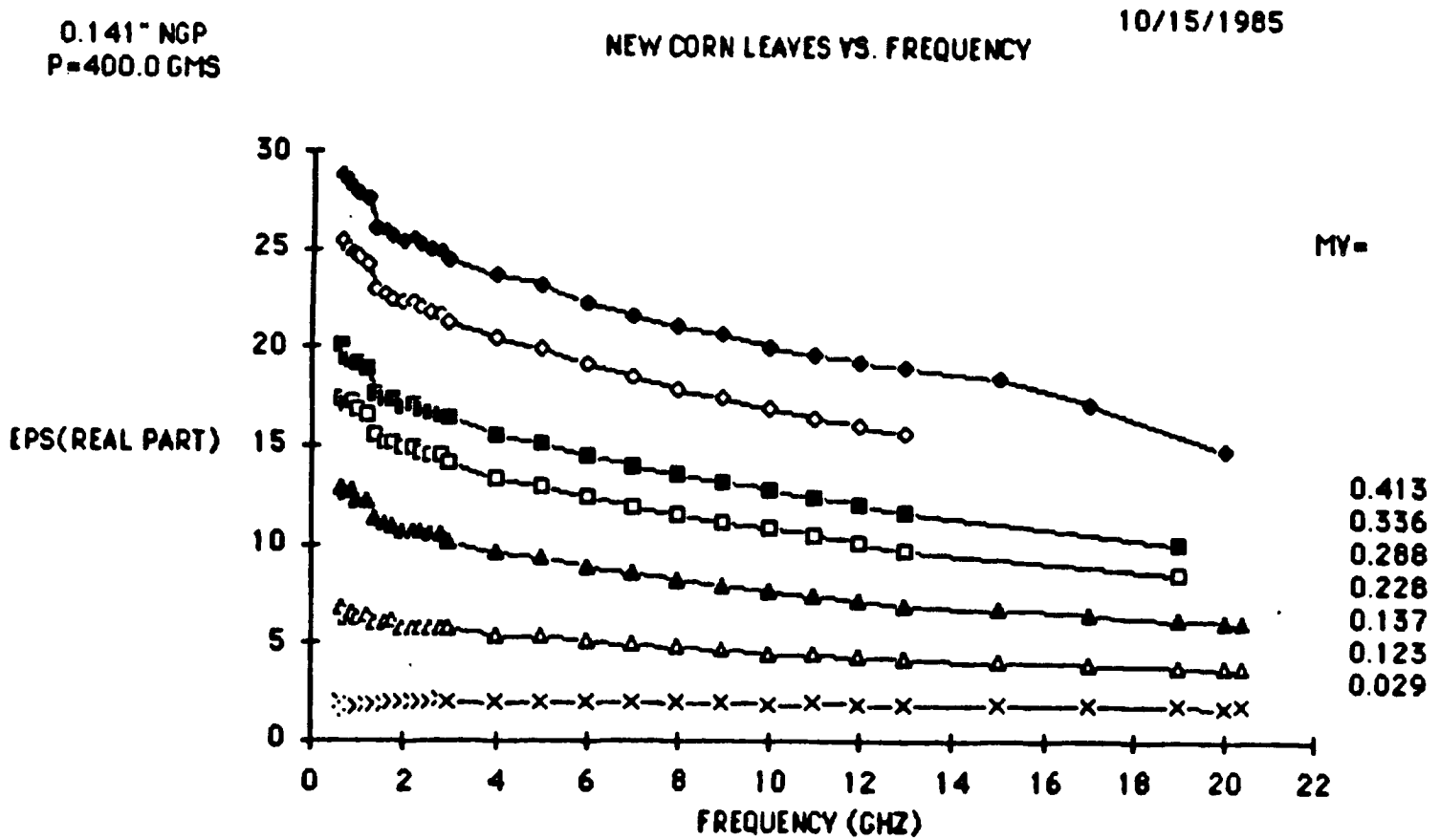

Figure 5.5. Measured spectra of the dielectric constant of corn leaves with volumetric moisture M_v as parameter (real parts).

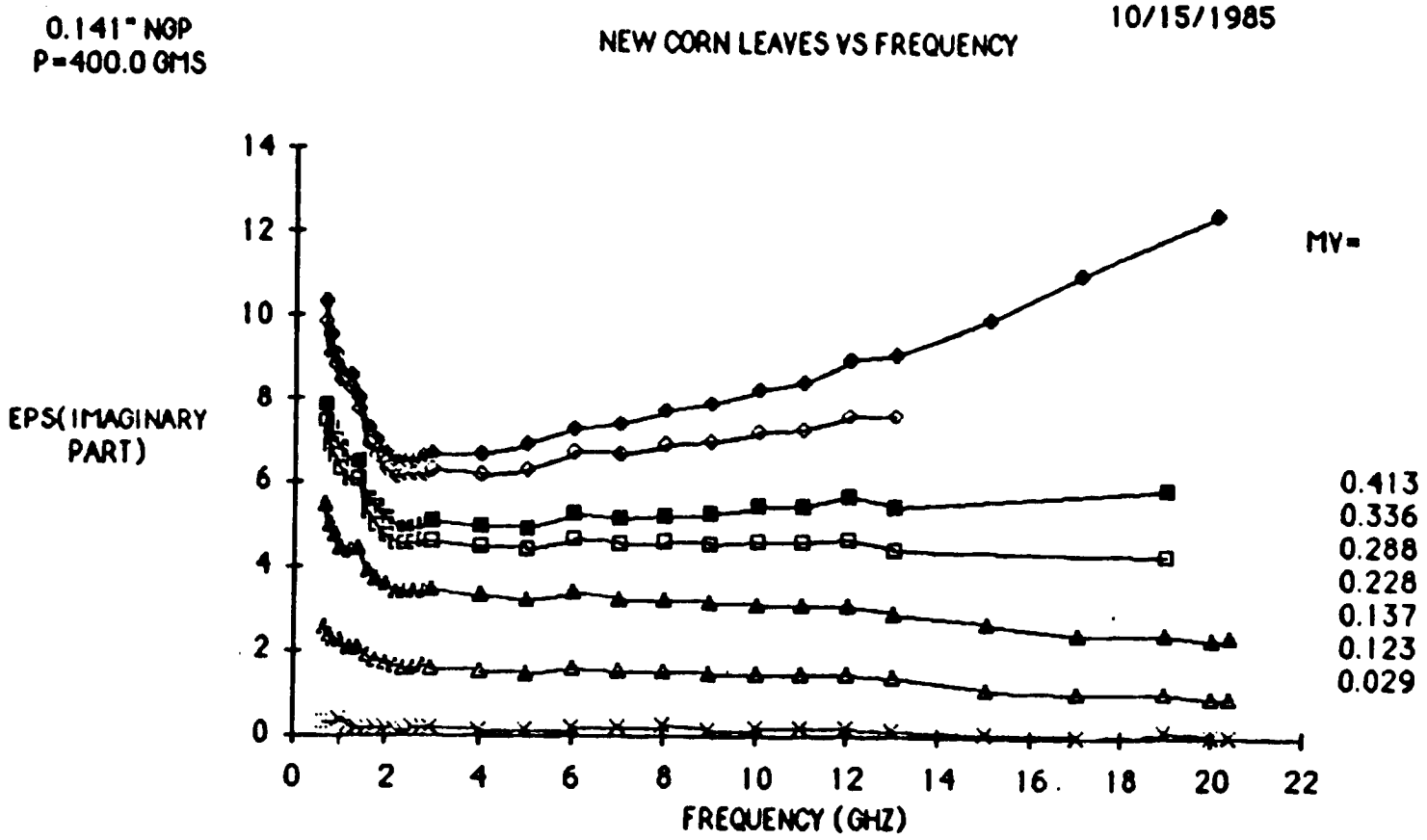

Figure 5.6. Measured spectra of the dielectric constant of corn leaves with volumetric moisture M_v as parameter (imaginary parts).

frequencies , however, ϵ'' increases with f because of the free water component. For the medium to low moisture samples ($M_v \leq .2$), ϵ'' does not increase with increasing f, but stays rather constant or decreases slowly with f. This behavior is attributed to bound-water domination at low moisture levels (because the bound relaxation frequency is below .2 GHz and its Cole-Cole shape factor is .5, ϵ'' exhibits a very slowly varying dependence on f for $f > 2$ GHz, as illustrated in Fig. 5.18). The dielectric loss factor ϵ'' has a minimum around 2 GHz and this minimum becomes less sharp with decreasing moisture content. This minimum separates the low frequency region (where losses are dominated by conductivity and bound water) from the high frequency region (where losses are dominated by free water relaxation with $f_0 = 18$ GHz at room temperature). At $f \leq 3$ GHz, the permittivity ϵ' decreases with increasing frequency at a rate comparable to that observed for bound water. This is discerned from a comparison of Fig. 5.5 with Fig. 5.18. Similar frequency behavior were observed for other vegetation types and parts (refer to Appendix A). Figure 5.7 shows plots for Crassulaceae Echeveria (which has succulent leaves) on an expanded scale covering the .2-2 GHz range. This material has a relatively low salinity (the measured salinity of the extracted liquid was 4 parts per thousands). The real part is almost constant indicating that there is no relaxation process in this frequency range, which means that the bound water content is neglegible and the dielectric loss is dominated by ionic conductivity.

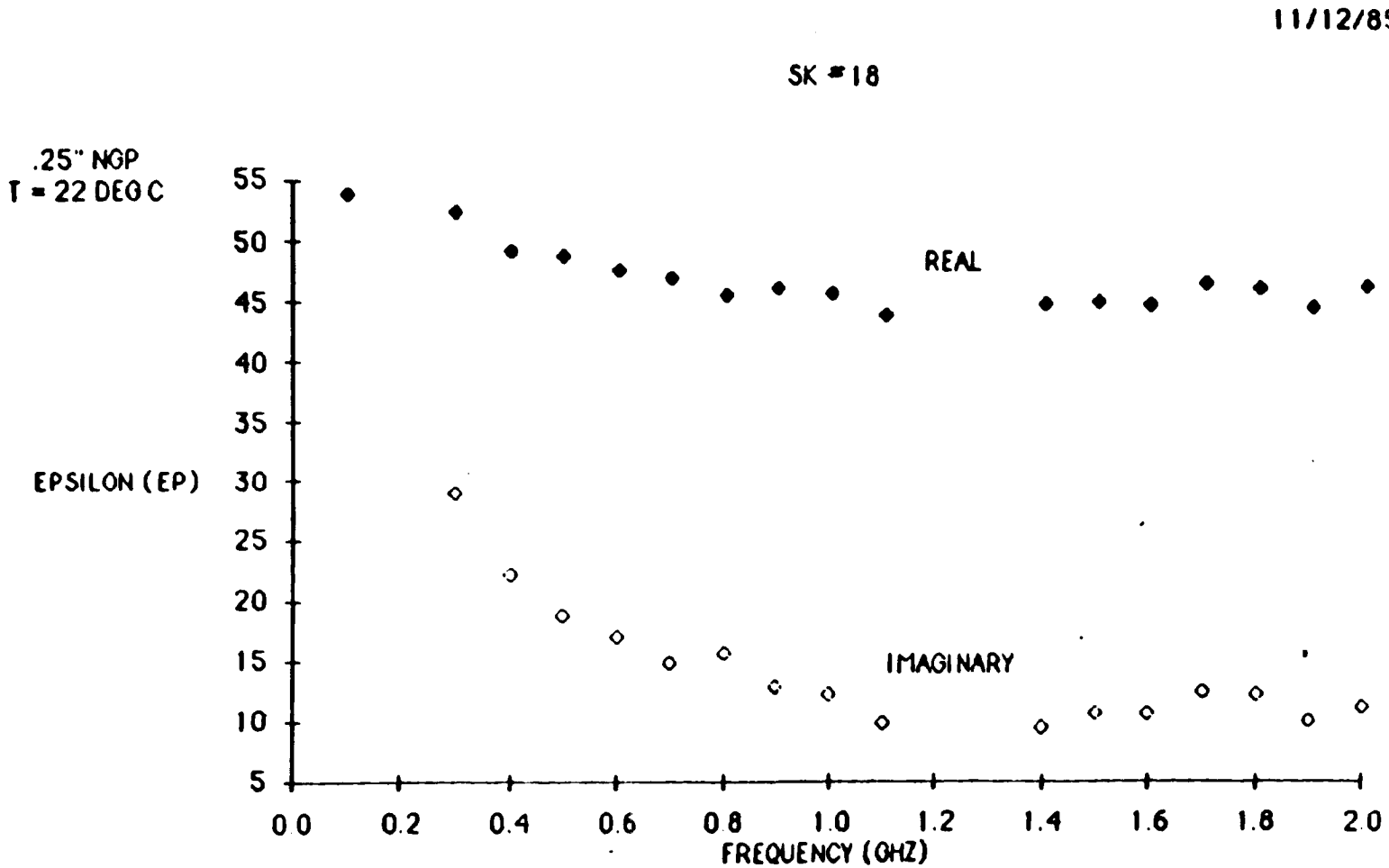

Figure 5.7. Measured spectra of the dielectric constant (real and imaginary parts) at the low frequency band (.1-2 GHz) for Crassulaceae Echeveria leaves.

5.3 Water Content Dependence

Since the main constituent of a plant is liquid water, its dielectric properties are driven by the dielectric properties of liquid water. Liquid water exists in plant tissues in two forms: free and bound. In addition, the free water component usually has a certain amount of dissolved salts, which leads to an ionic conductivity term. It was generally found that ϵ' and ϵ'' are both monotonically increasing functions of water content. Figure 5.8(a) shows the dielectric constant for corn leaves versus M_g at 1, 4, and 17 GHz. As expected, ϵ' increases steadily with increasing M_g and decreases steadily with increasing f. On the other hand, ϵ'' increases steadily with M_g and has a peculiar frequency response: at low moisture levels, $\epsilon''(1\text{ GHz}) \geq \epsilon''(4\text{ GHz}) \geq \epsilon''(17\text{ GHz})$, while at high moisture levels, $\epsilon''(17\text{ GHz}) \geq \epsilon''(1\text{ GHz}) \geq \epsilon''(4\text{ GHz})$. The reason we choose to report dielectric data as a function of gravimetric moisture rather than volumetric moisture is, as discussed earlier, because M_v is not a measureable quantity and it depends on the assumption we make about the dry vegetation density and the manner by which plants lose water (i.e., whether or not they shrink). In some cases, ϵ' was observed to decrease with increasing moisture content at very high moisture contents. An example of this behavior is shown in Fig. 5.8(b). No explanation is available at present for this unexpected behavior.

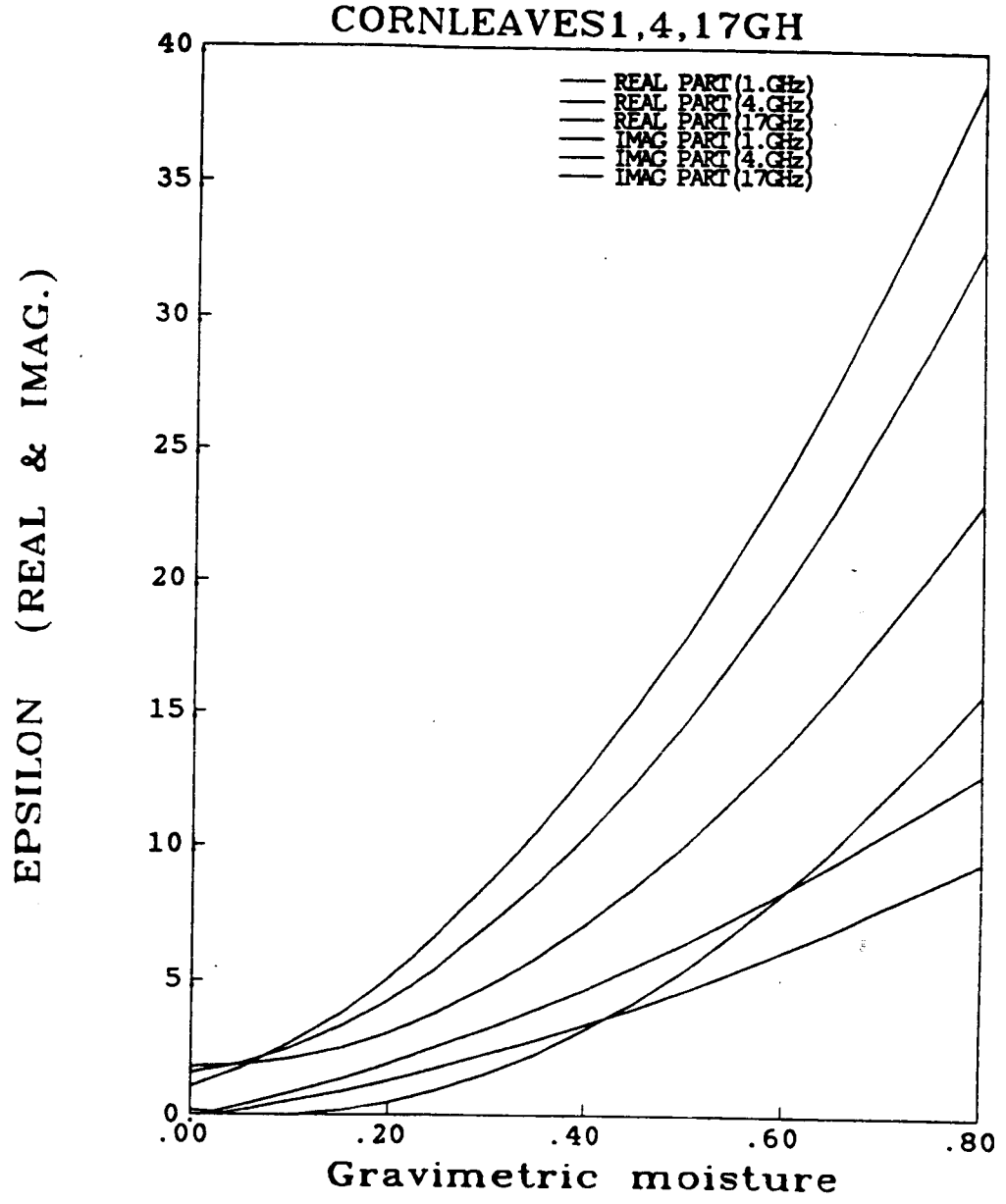

Figure 5.8(a). Measured dielectric constant of corn leaves at 1, 4, and 17 GHz, respectively, with frequency as parameter.

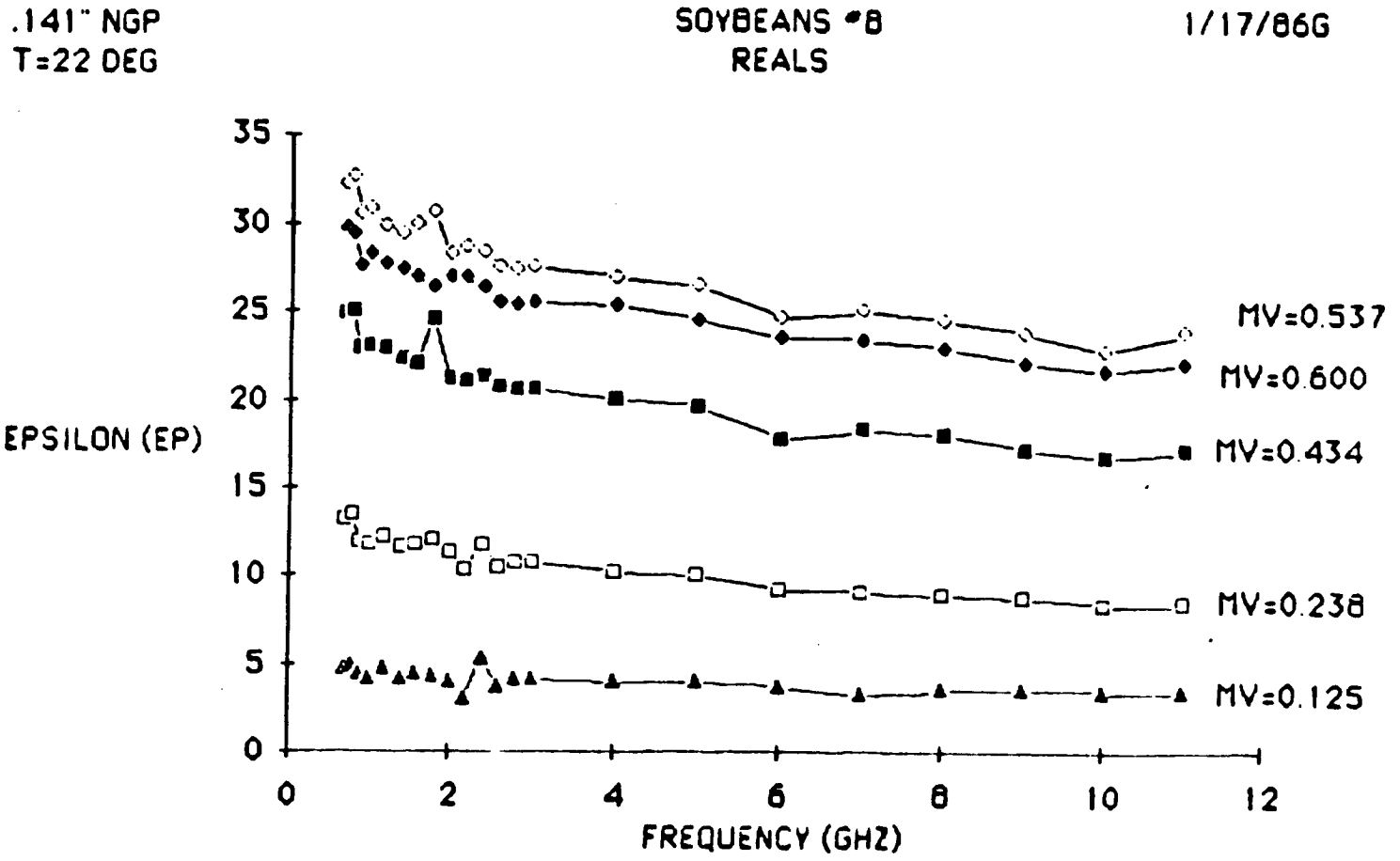

Figure 5.8(b). Measured spectra of the dielectric constant of soybeans leaves with volumetric moisture M_v as parameter (real parts).

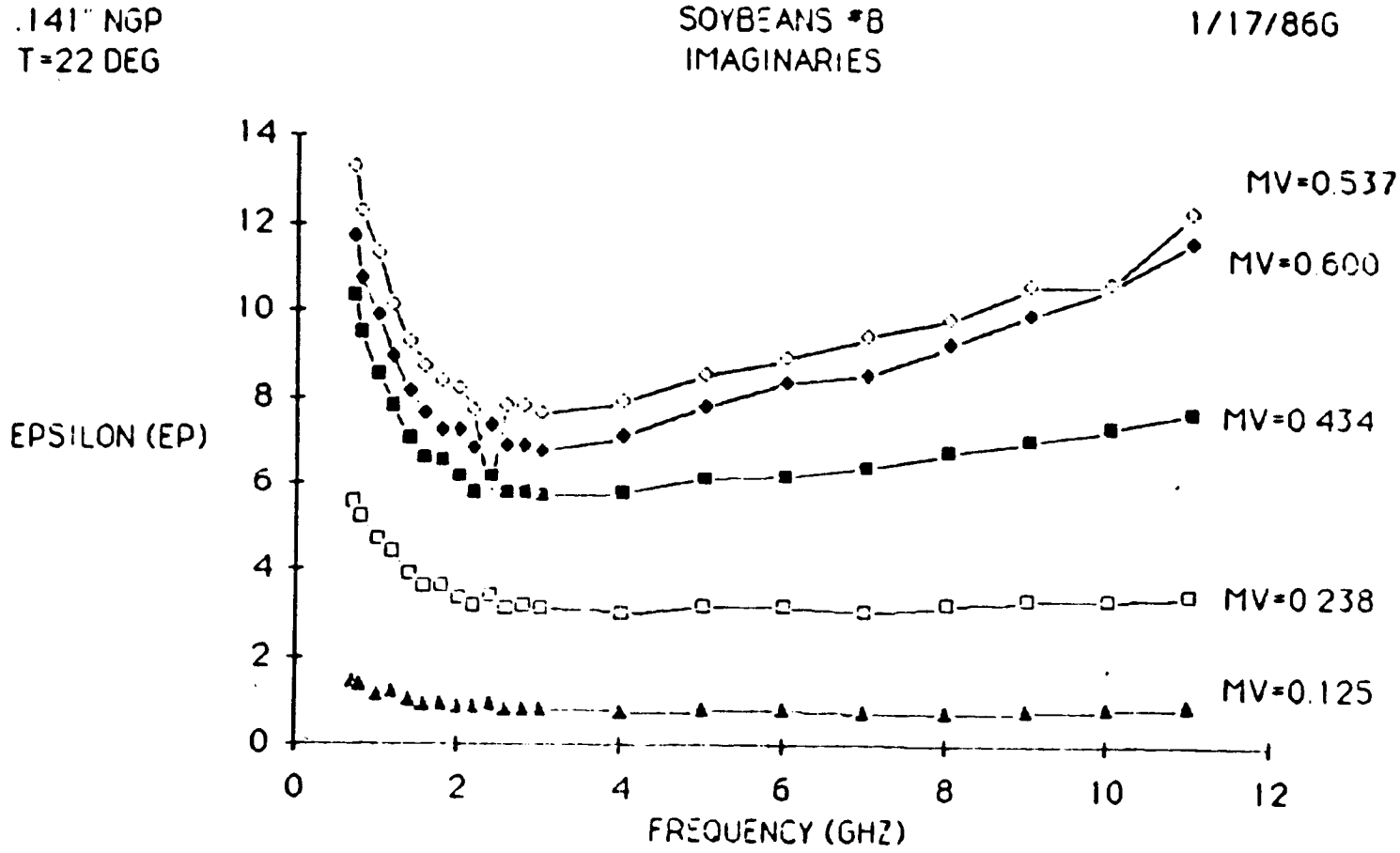

Figure 5.8(c). Measured spectra of the dielectric constant of soybeans leaves with volumetric moisture M_v as parameter (imaginary parts).

5.4 Salinity Effects

The equivalent $NaCl$ salinity, in parts per thousand, is defined as the number of grams of $NaCl$ dissolved in one kilogram of distilled water. The imaginary part of the dielectric constant, ϵ'', can be expressed as:

$$\epsilon'' = \epsilon''_c + \epsilon''_b + \epsilon''_f \tag{5.1}$$

where the subscripts c, b, and f denote the conductivity, bound, and free water terms, respectively. Below 1 GHz , ϵ''_c and ϵ''_b are, in general, much larger than ϵ''_f, while above 4 GHz , ϵ''_f is the dominant factor. We can summarize the loss mechanisms as follows:

1. *conductivity term*

$$\epsilon''_c = \frac{\sigma_{eff}}{\omega\epsilon_0} = \frac{\sigma_e}{f} \tag{5.2}$$

where σ_{eff} is the effective conductivity in $Siemens/m$ and σ_e ($\sigma_e = \sigma_{eff}/2\pi\epsilon_0$) is in sec^{-1}.

2. *bound water term* (refer to Sec. 5.5)

$$\epsilon''_b = \frac{(\epsilon_{sb} - \epsilon_{\infty b})\sqrt{\frac{f}{2f_{0b}}}}{(1 + \sqrt{\frac{f}{2f_{0b}}})^2 + (\frac{f}{2f_{0b}})} \tag{5.3}$$

where ϵ_{sb} and $\epsilon_{\infty b}$ are the static and optical limits for the bound water dielectric constant and f_{0b} is the resonance frequency (the spread relaxation parameter α was assumed to be .5).

3. *free water term*

$$\epsilon''_f = \frac{(\epsilon_{sf} - \epsilon_{\infty f})(\frac{f}{f_{0f}})}{1 + (\frac{f}{f_{0f}})^2} \tag{5.4}$$

where ϵ_{sf}, $\epsilon_{\infty f}$, and f_{0f} are, as defined earlier, the relaxation parameters for free water.

At frequencies in the 1 GHz range, these terms can be approximated as:

1. $\epsilon''_c \simeq \frac{C}{f}$,
2. $\epsilon''_b \simeq \frac{B}{\sqrt{f}}$ $(f \gg f_{0b})$, and
3. $\epsilon''_f \simeq F\sqrt{f}$ $(f \ll f_{0f})$,

where C, B, and F are constants. This approximate approach helps in studying and understanding the low frequency behavior of ϵ'' qualitatively. Unfortunately, both ϵ''_c and ϵ''_b terms decrease steadily with increasing frequency, although ϵ''_b decreases more slowly than does ϵ''_c, which makes it difficult to separate the contribution of these two terms. In order to resolve this problem, we extracted fluids from different plant parts at different moistures and measured their dielectric constant. Table 5.1 shows the measured salinity of included liquids for corn leaves and stalks that had been growing at different heights locations on the corn plant.

moisture	fresh plant			one day		two days	
location	part	$P(tons)$	$S(ppt)$	$P(tons)$	$S(ppt)$	$P(tons)$	$S(ppt)$
upper	leaves	20	6	20	11	25	20
upper	stalks	10	4	20	8	12	6
middle	leaves	15	6	20	14	25	29
middle	stalks	5	5.5	7	7	5	7
		10	5	17	7.5	12	8
lower	leaves	10	6	20	23	25	29
lower	stalks	3	5.5	5	7	5	6
		6	5.5	10	7	10	6
		8	6.5				

Table 5.1: Measured salinity of liquids extracted from corn plants at different pressures (in tons per unit area) and at different plant heights.

The data in Table 5.1 was obtained for three different corn plants from the same canopy. The first was measured while still fresh, the second and the third were measured one and two days later, respectively. Each plant was divided into three parts: upper, middle, and lower sections. Then, liquids from leaves and stalks, in each section, were extracted and measured separately and the

extraction pressure was recorded in tons per unit area. A modified hydraulic press was used to squeeze the juices out of the plant parts. The gravimetric moisture of different sections were measured and the estimated averages of $S(ppt)$ and M_g are given in Table 5.2:

leaves		stalks	
M_g	$S(ppt)$ by measuring ϵ	M_g	$S(ppt)$ by measuring ϵ
.351	29	.669	6
.396	29	.674	4
.521	23	.691	8
.525	20	.733	5
.605	11	.739	7.5
.624	14	.742	7
.646	6	.757	6
.657	6	.779	6
.675	6	.789	7

Table 5.2 Salinity and gravimetric moisture for corn leaves and stalks.

The following observations are offered:

1. It is very difficult to extract liquids from relatively dry leaves ($M_g \leq .3$).

2. Salinity increases with decreasing moisture content, which indicates an increase in concentration of ions with moisture loss.

3. The smallest reported M_g was .35 for corn leaves, while that for corn stalks was .67.

Figure 5.9 shows the measured salinity (in parts per thousands) of corn leaves as a function of volumetric moisture (assuming ρ_{DV}=.33); the maximum measured salinity is around 30 ppt, while the lowest is about 5 ppt. A best fit line for this set of data is shown also; a linear equation relating S to M_g is given by:

$$S = 37 - 46M_g \text{.....(ppt)}, \tag{5.5}$$

or,

$$\sigma_{eff} = 57 - 71M_g \text{.....(m Siemens/cm)}, \tag{5.6}$$

or

$$\sigma_e = 103 - 130\ M_g \text{.....}(as\ defined\ in\ Eq.(5.2)) \tag{5.7}$$

Because of the limited range of M_g for stalks, it was not possible to adequately relate S to M_g for stalks.

The previous three equations should be taken only as approximate estimates of S, σ_{eff},and σ_e because the variability among different species is quite large. Furthermore, large differences in salinity were observed among samples of the same species depending on the stage of growth and geographic location. As

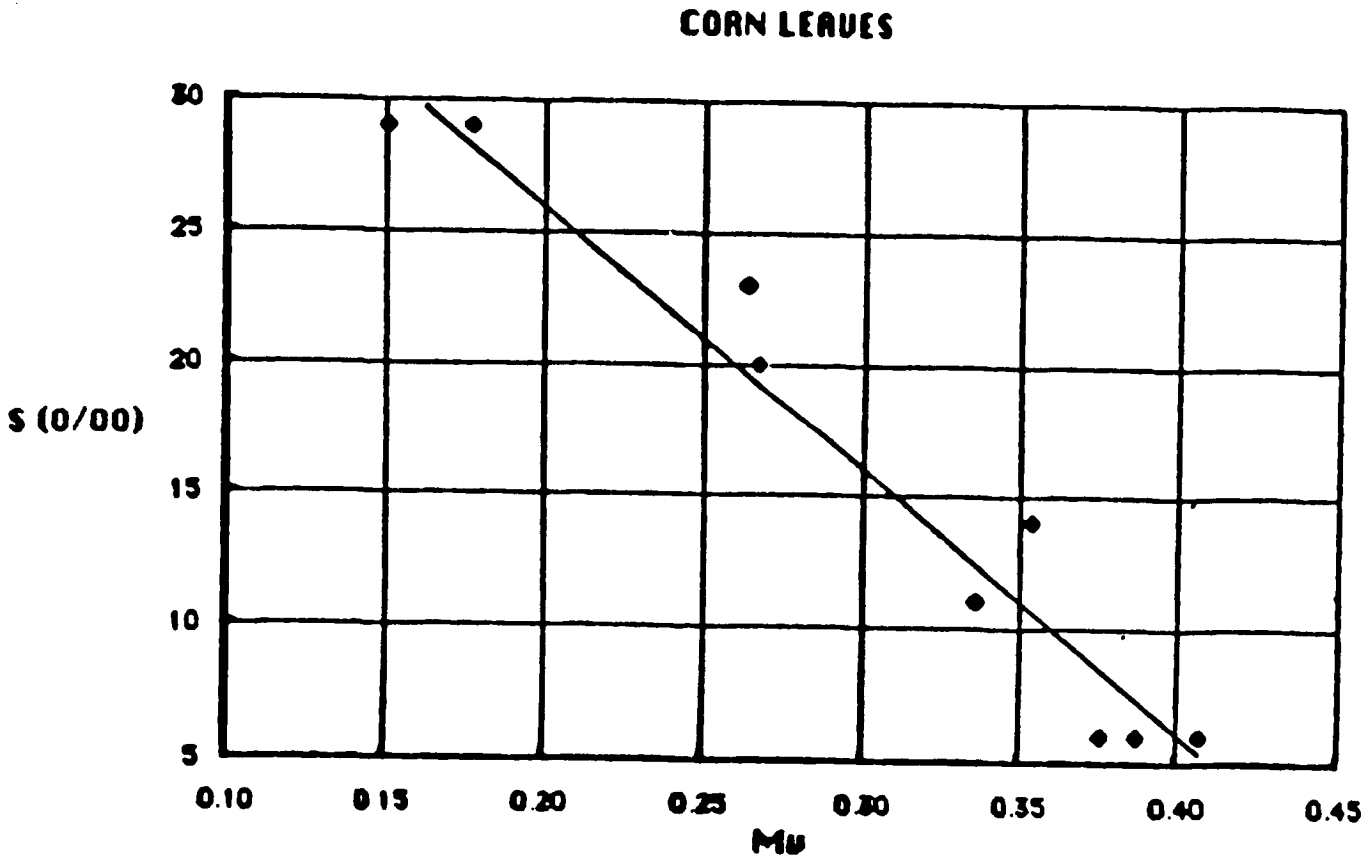

Figure 5.9. Measured salinity in (ppt) for extracted fluids from corn leaves at different volumetric moisture levels, plants were excised and naturally dried.

an example of this variability, the measured salinities of extracted liquids from fresh corn leaves (Ulaby and Jedlicka, 1984) grown near Lawrence, Kansas, were measured to be about 12 *ppt*. As shown in Table 5.1, the measured salinities of fresh corn leaves grown near Ann Arbor, Michigan, were measured to be about 6 *ppt*. This large difference can not be attributed to measurement errors or equipment calibration alone. A comparison between different measurements on corn leaves grown in Kansas (1984) and in Michigan (1985) is given in Table 5.3 (both measured using the same technique, the open-ended coaxial line probe system).

where	when	M_g	f(GHz)	ϵ'	ϵ''	tan(δ)
Kansas	1984	.736	1	33.8	17	.50
		.653	1	30	15	.50
Michigan	1985	.835	1	46	18.5	.4
		.645	1	27	9	.33

Table 5.3: Comparison between measured corn leaves grown in Kansas and Michigan.

Another experiment was conducted in Michigan (December, 1985) on corn leaves and stalks (grown at the University of Michigan Botanical Gardens). The dielectric constant of corn leaves and corn stalks was measured as a function of

frequency for freshly cut plants. Simultaneously, extracted liquids from the same plants were measured in two different ways: (i) Conductivity (mSiemens/cm), using a conductivity meter and (ii) ϵ, using the open-ended coaxial probe, and then by comparing this data to that calculated for saline solutions, an estimate of the effective NaCl salinity can be made. Table 5.4 shows a comparison between these two different approaches:

plant part	P(tons)	S(ppt) ϵ	S(ppt)conductivity meter
leaves	12	8	6.5
stalks	3	8	6.63
stalks	10	7	6.63

Table 5.4: Comparison between salinity measurements using conductivity meter and using dielectric measurement.

Figures 5.10 to 5.12 show spectra of the dielectric constant of extracted liquids along with that for saline solutions with $S = 7$ and 8 *ppt*. The effective salinity inferred from the measured dielectric constant of the liquid is about 20% higher than that measured by the conductivity meter. The latter represents the actual density of free ions present in the solution, whereas the former represents an effective value based on the observed loss factor. The difference may be at-

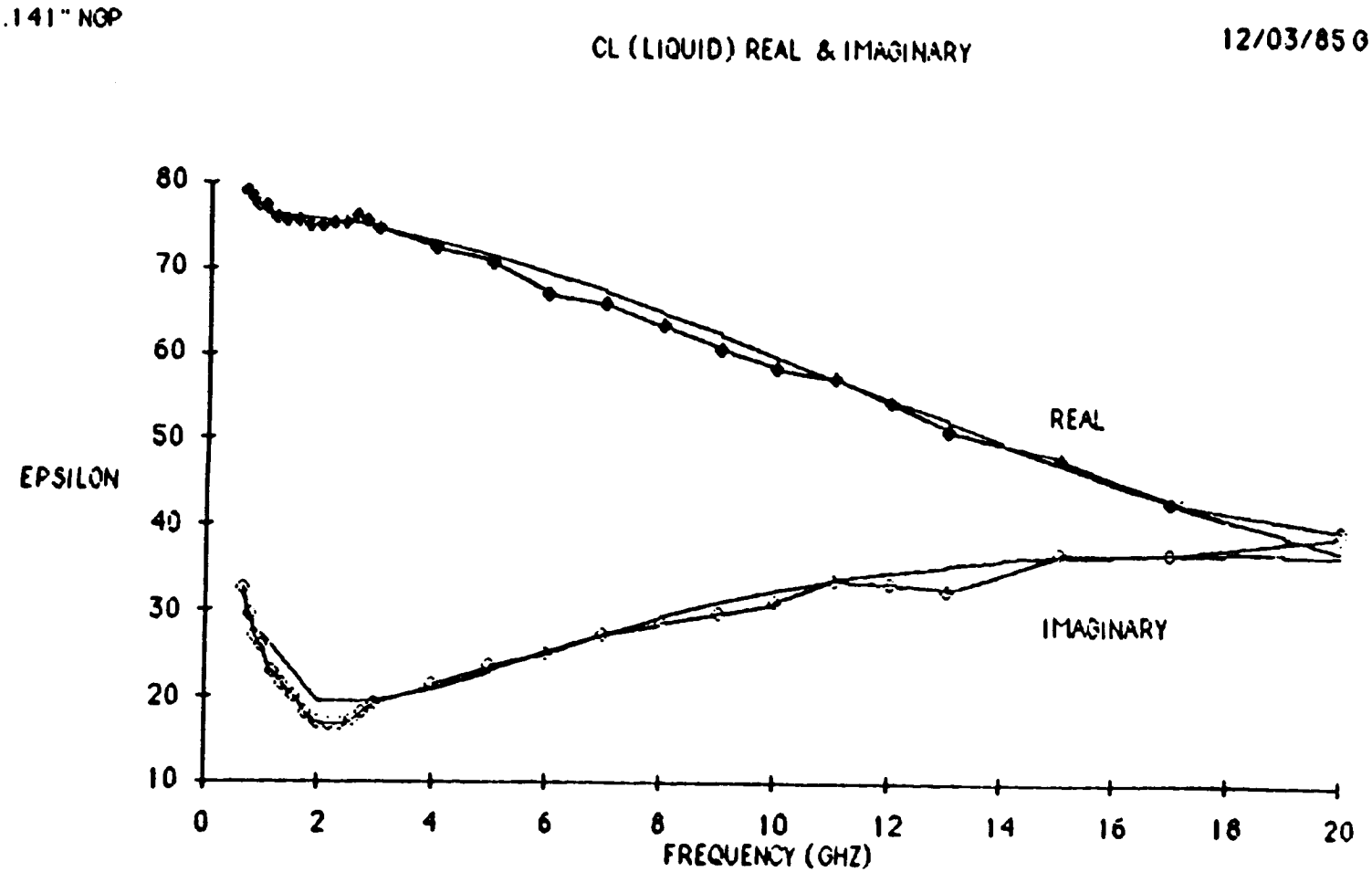

Figure 5.10 Spectra of the extracted fluids from corn leaves. The data points are measured and the solid lines are calculated from [Stogryn, 1971] for saline water solution with 8 ppt salinity.

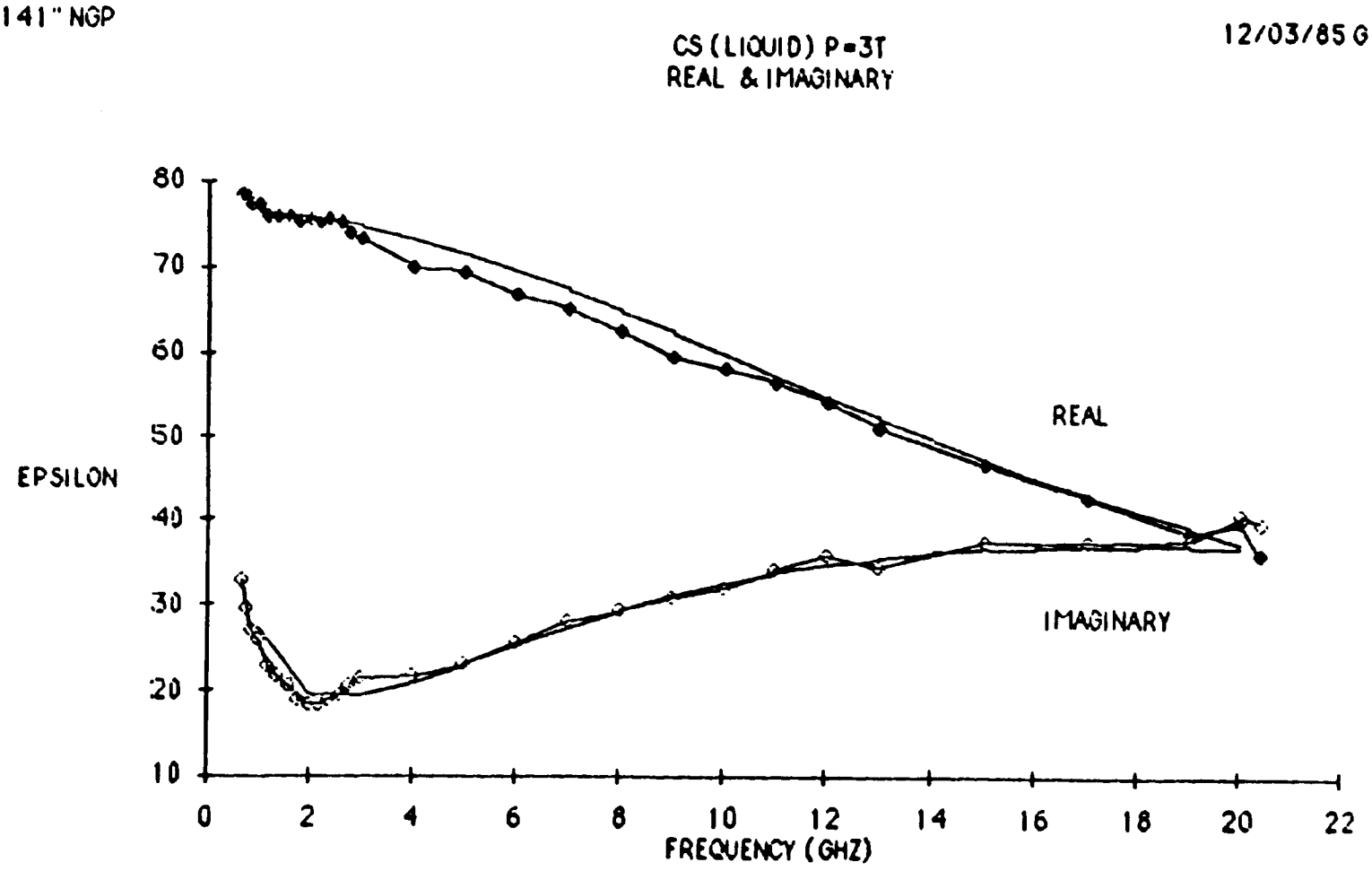

Figure 5.11 Spectra of the extracted fluids from corn stalks. The data points are measured and the solid lines are calculated from [Stogryn, 1971] for saline water solution with 8 ppt salinity.

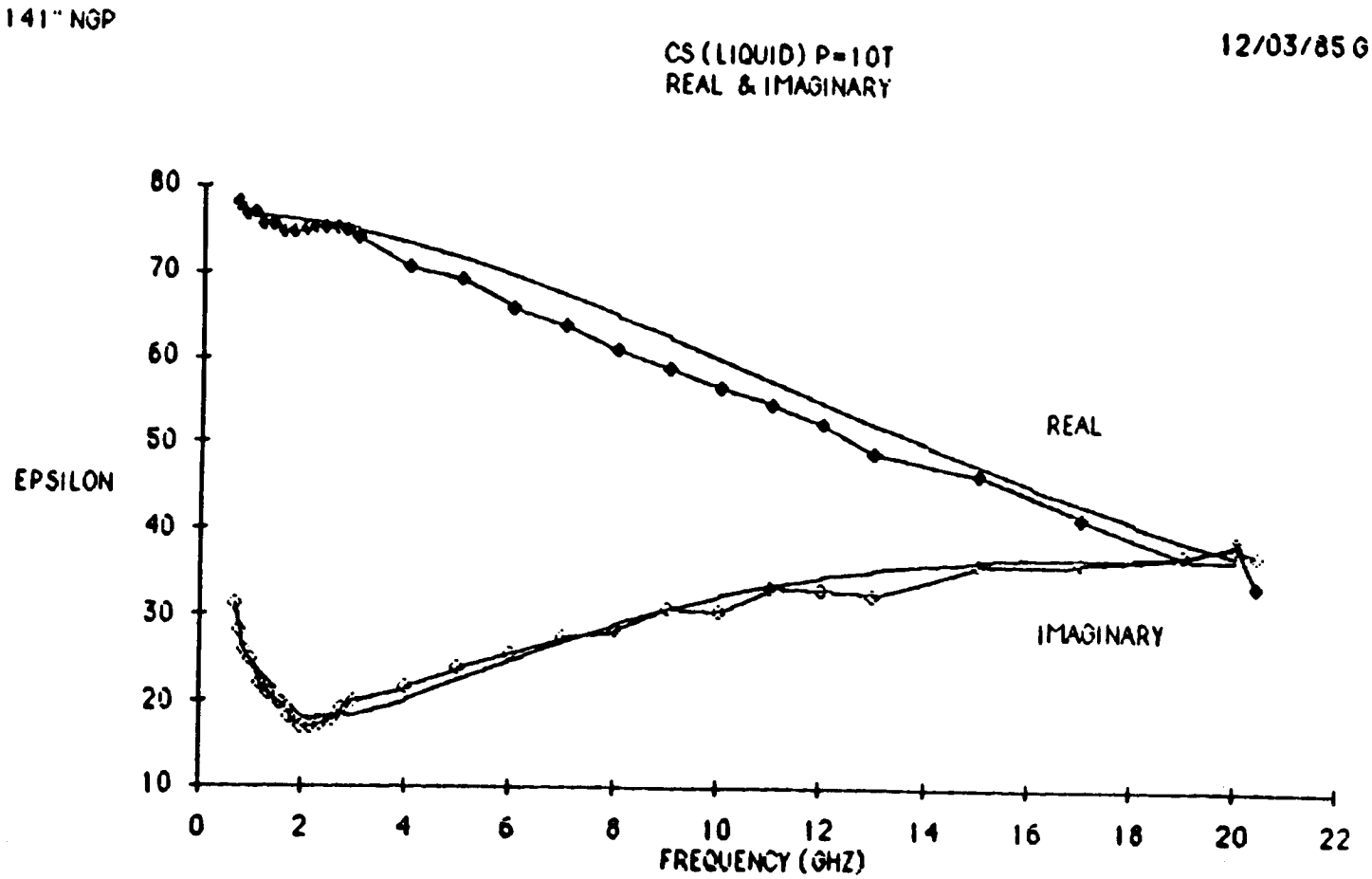

Figure 5.12 Spectra of the extracted fluids from corn stalks. The data points are measured and the solid lines are calculated from [Stogryn, 1971] for saline water solution with 8 ppt salinity (the pressure guage showed 10 tons during the extraction, 3 tons for Figure 5.11).

tributed to the bound-water contribution. Bound water effects do not show as conductivity losses, but rather as dielectric losses. Table 5.5 shows a summary of this experiment at 1 GHz.

part		M_g	$M_v(\rho_{dv} = .33)$	ϵ'	ϵ''	$tan(\delta)$
upper	leaves	.771	.526	34.6	13.3	.383
	stalks(in)	.840	.732	48.8	43.1	.268
	stalks(out)	.781	.650	29.2	8.3	.284
middle	leaves	.813	.589	42.9	15.3	.357
	stalks(in)	.823	.707	48.5	16.7	.344
	stalks(out)	.833	.722	37	13	.351
lower	leaves	.857	.664	44.8	15.8	.353
	stalks(in)	.858	.759	50	15.3	.306
	stalks(out)	.872	.780	45.2	16.9	.374

Table 5.5: Fresh corn leaves and stalks at 1 GHz (Michigan, Dec. 1985, samples grown in Botanical Gardens)

Comparing Tables 5.3 and 5.5 shows a difference between corn leaves measured in the summer of 1985 and those in December, 1985. The dielectric data suggests that the corn plants grown in the Botanical Gardens have more dissolved salts than those grown in the field. The reason for these variations was

not sought in this work: it was our objective, rather, to test plants with different ionic contents and to try to relate their measured salinities to their overall dielectric behavior.

An attempt was made during the course of this study to test plants with exceptionally high ionic contents. We were advised to try desert plants because they are known to have high ionic concentrations (probably to maintain a high osmotic potential). Four plants were selected for this purpose:

1. *Mesembrianthemum Crystallinum* (code: MC)
2. *Cakile Maritima* (code: CM)
3. *Lampranthus Haworthii* (code: LH)
4. *Crassulaceae Echeveria* (code: SK)

Desert plants were very hard to dry out without loss of turgidity. Hence only measurements made on the fresh plants are considered reliable. A summary of these measurements is given in Table 5.6.

part	liquids from leaves				leaves		
plant	s(ppt)	ϵ'	ϵ''	$tan(\delta)$	ϵ'	ϵ''	$tan(\delta)$
MC	5	72.1	18.4	.255	53.7	12.5	.233
CM	10	73.1	33	.451	36.6	20.2	.552
LH					52.6	24.5	.466
SK	4	73.6	15.8	.215	22.6	7.2	.319

Table 5.6. Freshly cut desert plants (at 1 GHz).

Table 5.7 presents the results of a test made to compare ϵ for potatoes, apples, and tomatoes and to relate the measured ϵ to the salinity of the extracted liquids.

part	solid			liquids			
material	ϵ'	ϵ''	$tan(\delta)$	ϵ'	ϵ''	s(ppt)	$tan(\delta)$
potatoes	64.1	24.7	.385	71.3	24.1	7	.338
tomatoes	73.5	16.3	.222	74.5	16	4	.215
apples	63.5	8.7	.137	72.2	6.4	.8	.089

Table 5.7: Dielectric of potatoes, tomatoes, and apples ($M_g \geq .8$ and $f = 1$ GHz).

It is observed that $tan(\delta)$ of the solid plant material is generally higher than that for the extracted liquids, which may be due to the added losses contributed by bound water. Figure 5.13 illustrates the effects of salinity by comparing the dielectric constants of potatoes and apples as a function of frequency.

5.5 Bound Water Effects

As discussed in the previous section, the effects of bound water and salinity are similar and they tend to mask each other, especially in the 1-5 GHz frequency range. Therefore, two steps were taken to remedy this problem:

1. The measurement frequency range was extended down to .1 GHz, and
2. Special circumstances were sought that would allow the study of bound-water effects in isolation of salinity effects.

To achieve the first step, the dielectric system was modified and the probe section was calibrated so that it could operate at as low a frequency as 50 MHz, as discussed in Chapter 4. In order to study the bound water without the "shadow" of the ionic conductivity, it is necessary to use a material with known bound water concentration. Sucrose (table sugar) is such a material (Sayre, 1932). It was reported that each molecule of sucrose can bind to six molecules of water. Since the molecular weights of water and sucrose are known to be 18.01534 and 342.30 respectively, we can write,

$$X_b = 6(\frac{18.01534}{342.30})X = (\frac{6}{19})X \tag{5.8}$$

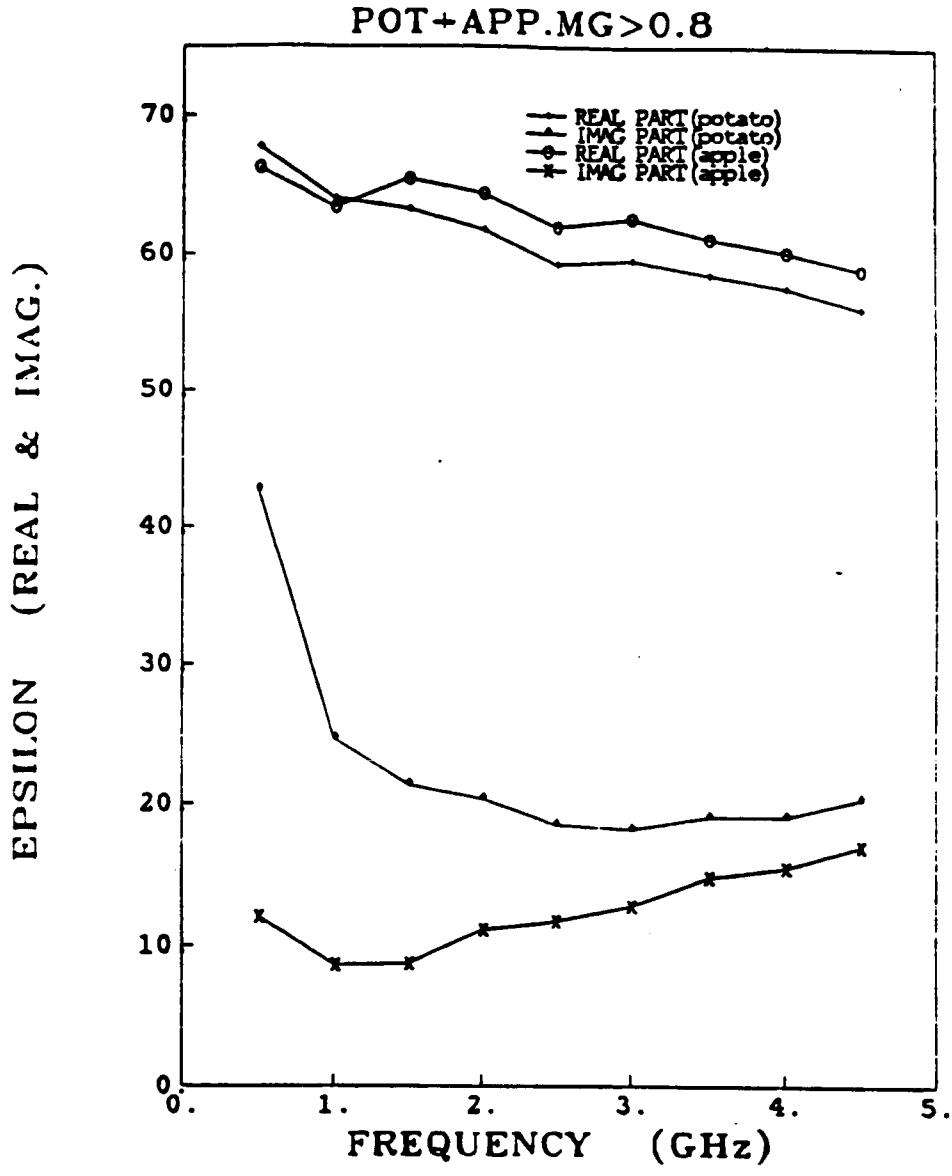

Figure 5.13. Measured spectra of the dielectric properties of potatoes and apples. The measured salinity of the extracted fluids were 7 and 0.8 ppt, respectively.

where X_b is the mass ratio of bound water to total water and $X = \frac{S}{W}$ is the ratio of sucrose weight to water weight. So, given X, we can calculate X_b and X_f, the mass ratio of free water to total water, as:

$$X_f = 1 - (\frac{6}{19})X. \tag{5.9}$$

Volume-Fraction Calculations

1. Dissolve $S(gm)$ of sucrose into $W(gm)$ of distilled water. Hence,

$$X = \frac{S}{W}. \tag{5.10}$$

2. A, the concentration (per cent), is given by:

$$A = \frac{100S}{S+W}, \%. \tag{5.11}$$

3. Use a Chemistry Handbook to read ρ(the density in g/cm^3) corresponding to A.

4. The total volume of solid sucrose is:

$$V_s = [\frac{S - W(\rho - 1)}{\rho}], cm^3 \tag{5.12}$$

5. The total volume of water is:

$$V_w = W, cm^3 \tag{5.13}$$

6. The volume fraction of solid sucrose is:

$$v_s = \frac{V_s}{V_s + V_w} \tag{5.14}$$

7. The volume fraction of water is:

$$v_w = \frac{V_w}{V_s + V_w} \tag{5.15}$$

8. The volume fraction of bound water is:

$$v_b = V_w(\frac{6}{19}X) \tag{5.16}$$

9. The volume fraction of free water is:

$$v_f = v_w(1 - \frac{6}{19}X). \tag{5.17}$$

Table 5.8 gives the volume fractions of some of the sucrose solutions measured in the course of this work.

sucrose#	X	v_s	v_b	v_f	ϵ'	ϵ''	$tan(\delta)$	f_0(GHz)
water	0	0	0	1	79.1	4.1	.052	18
A	.5	.239	.120	.641	65	10	.154	8.4
B	1	.385	.194	.421	51.9	14	.270	3.9
C	1.5	.485	.244	.271	40.2	15.4	.383	2.2
D	2	.559	.279	.162	31.1	14.4	.463	1.1
E	2.5	.613	.306	.081	23.4	12.1	.517	.44
F	3	.655	.327	.018	18.5	9.9	.535	.21
G	3.17	.667	.333	0	17.4	9.3	.534	.178

Table 5.8: Volume fractions and dielectric constants of sucrose solutions at 1 GHz.

Samples A though G were prepared such that they cover a wide range of the bound-water volume fractions that may exist in a plant material. A peculiar, yet useful, observation is that the ratio v_s/v_b is always equal to 2. In Chapter six, this feature will be used to calculate the volume fractions for vegetation samples. The dielectric properties of these samples were measured as a function of frequency at two different frequency bands:

1. *Low band* .2-2 GHz using the .25" probe, and

2. *High band* .5-20.4 GHz using the .141" probe.

A sample of the results is shown in Figs. 5.14 to 5.17 for sucrose solutions A, D and G. The dielectric loss factor ϵ'' is relatively small for distilled water at .2 GHz, but it increases rapidly as v_b is increased. Conductivity measurements were carried out on these samples to test their ionic contents and the results showed no dissolved ionic concentrations. It is clear that these high losses are caused by a dipolar relaxation mechanism and not by conductivity effects. Table 5.8 shows the measured ϵ' and ϵ'' at 1 GHz for different sucrose concentrations. Also given is the relaxation frequency f_0 corresponding to each concentration, calculated using an optimization program (BMDP) that fits the spectral data to a Cole-Cole equation of the form:

$$\epsilon = \epsilon_\infty + \frac{\epsilon_s - \epsilon\infty}{1 + (jf/f_0)^{1-\alpha}} \tag{5.18}$$

For sucrose solution $\#G$, which contains no free water,

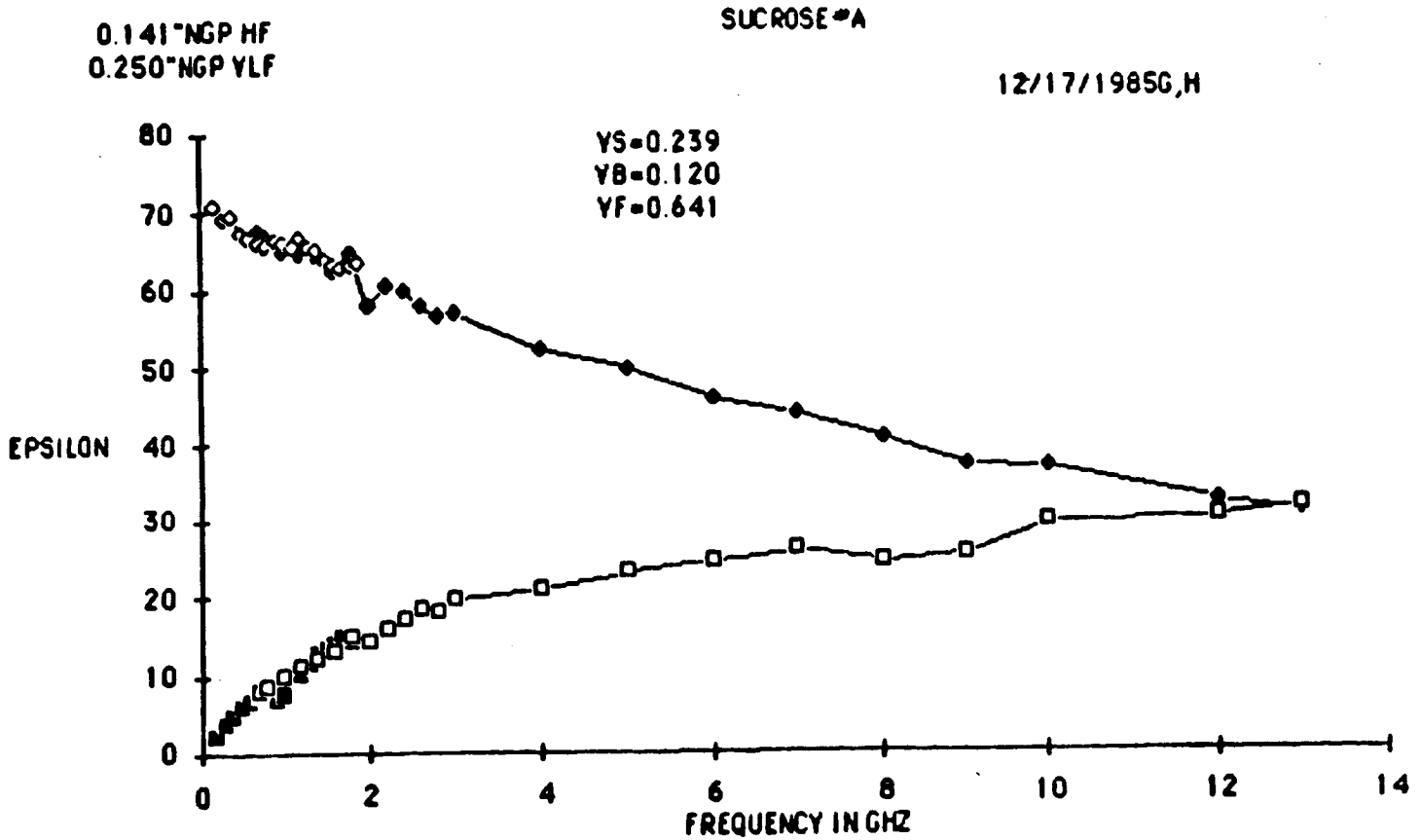

Figure 5.14. Measured spectra of the sucrose solution (A) with x=0.5. Two probes were used to measure the lower (.25") and upper (.141") bands. $V_s, V_b, and V_f$ are sucrose, bound, and free water volume fractions, respectively.

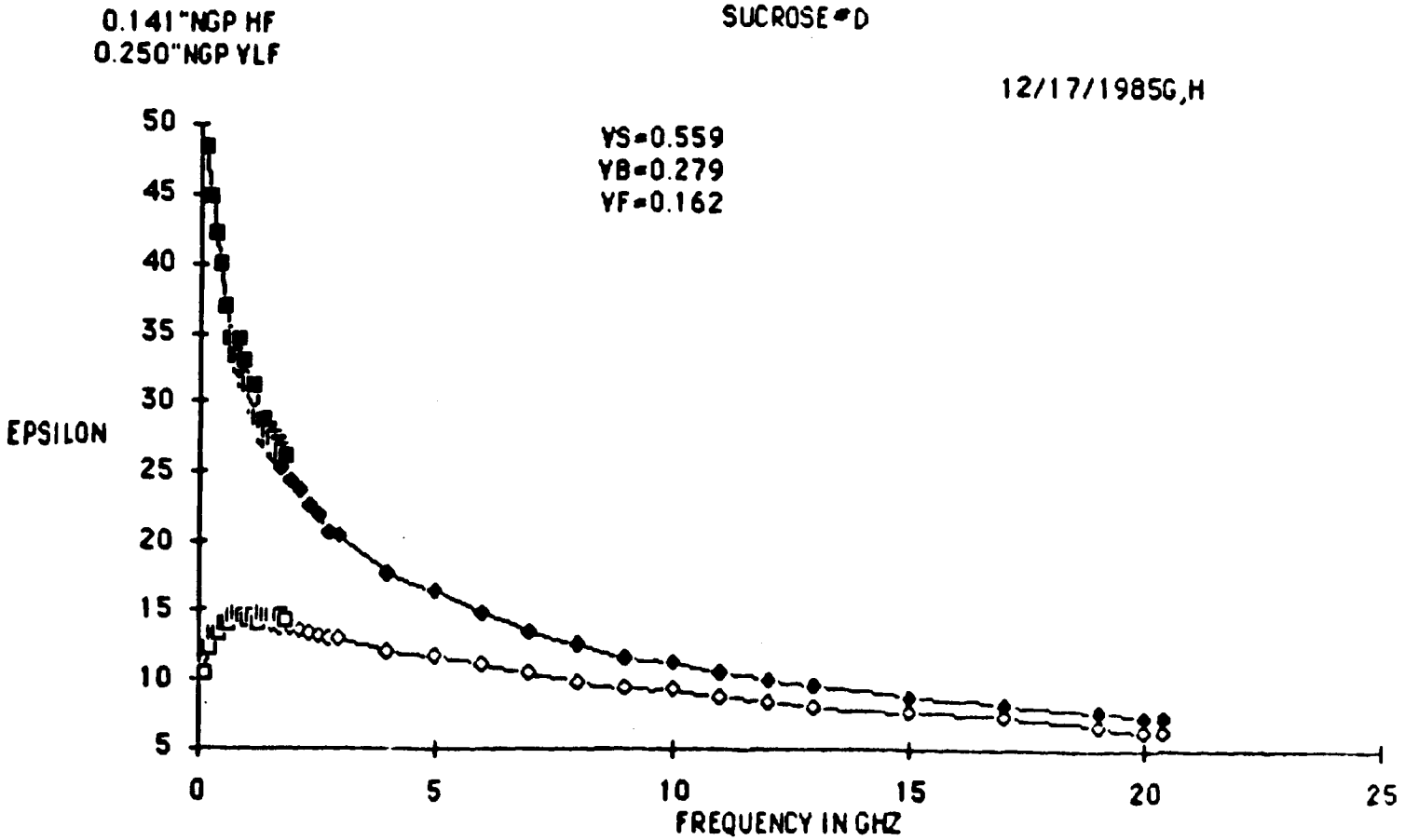

Figure 5.15. Measured spectra of the sucrose solution (D) with x=2. Two probes were used to measure the lower (.25") and upper (.141") bands. $V_s, V_b, and V_f$ are sucrose, bound, and free water volume fractions, respectively.

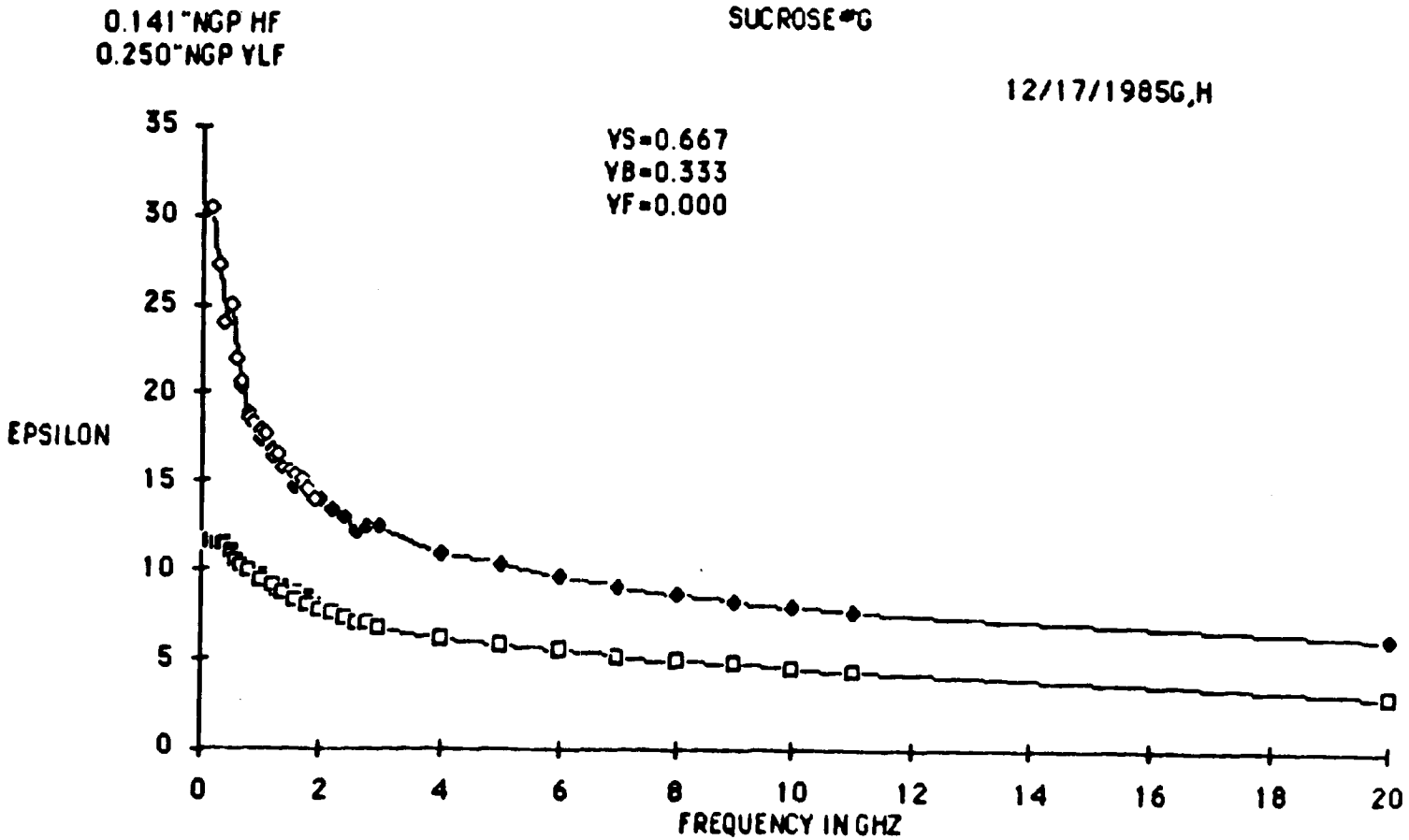

Figure 5.16. Measured spectra of the sucrose solution (G) with x=3.17. Two probes were used to measure the lower (.25") and upper (.141") bands. $V_s, V_b, and V_f$ are sucrose, bound, and free water volume fractions, respectively.

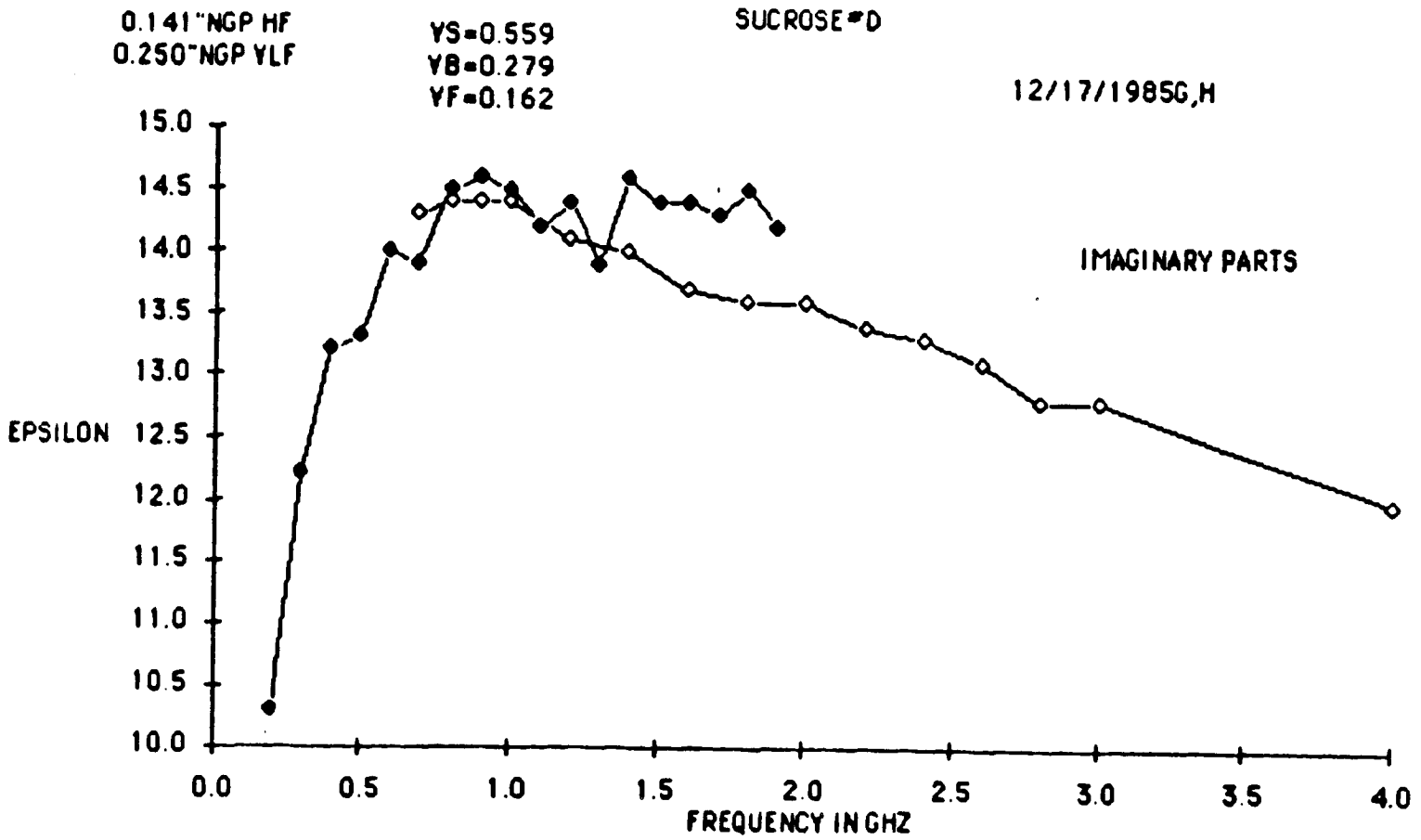

Figure 5.17. Measured spectrum of the imaginary part for sucrose solution (D) with x=2. The peak is at around 1 GHz. The agreement between the two sets of data produced by two different probes is fairly good.

$$\epsilon = 2.9 + \frac{56}{1 + (jf/.178)^{.5}} \tag{5.19}$$

where f is in GHz and the relaxation parameters α is .5. Figure 5.18 shows Eq. (5.19) plotted with the measured data points. This type of frequency response is rarely observed in plants because salinity effects are present also, and what we observe is the result of the combined spectra of both, especially in frequency range below 5 GHz.

The observed spectrum of sucrose solutions is not really unique; a similar type of behavior was observed for the following materials:

1. *Dextrose* Fig.5.19 shows the spectrum of a dextrose solution of concentration $X = 2$. This curve, when compared to sucrose solution D (Fig. 5.15), is found to bear strong resemblence in shape, although the two are slightly different in magnitude.

2. *Silica gel,* Fig. 5.20 shows the spectrum for silica gel of concentration $X = .5$. This curve is to be compared to that of sucrose A. Again they are similar but vary slightly in level and in the frequency at which ϵ' and ϵ'' intersect (silica gel at 20 GHz and sucrose A at 13 GHz).

3. *Gelatin,* Fig. 5.21 shows the spectrum for gelatin at a concentration of $X = 1$. Comparing this figure to that for sucrose B shows large differences indicating that sucrose and gelatin have different binding properties.

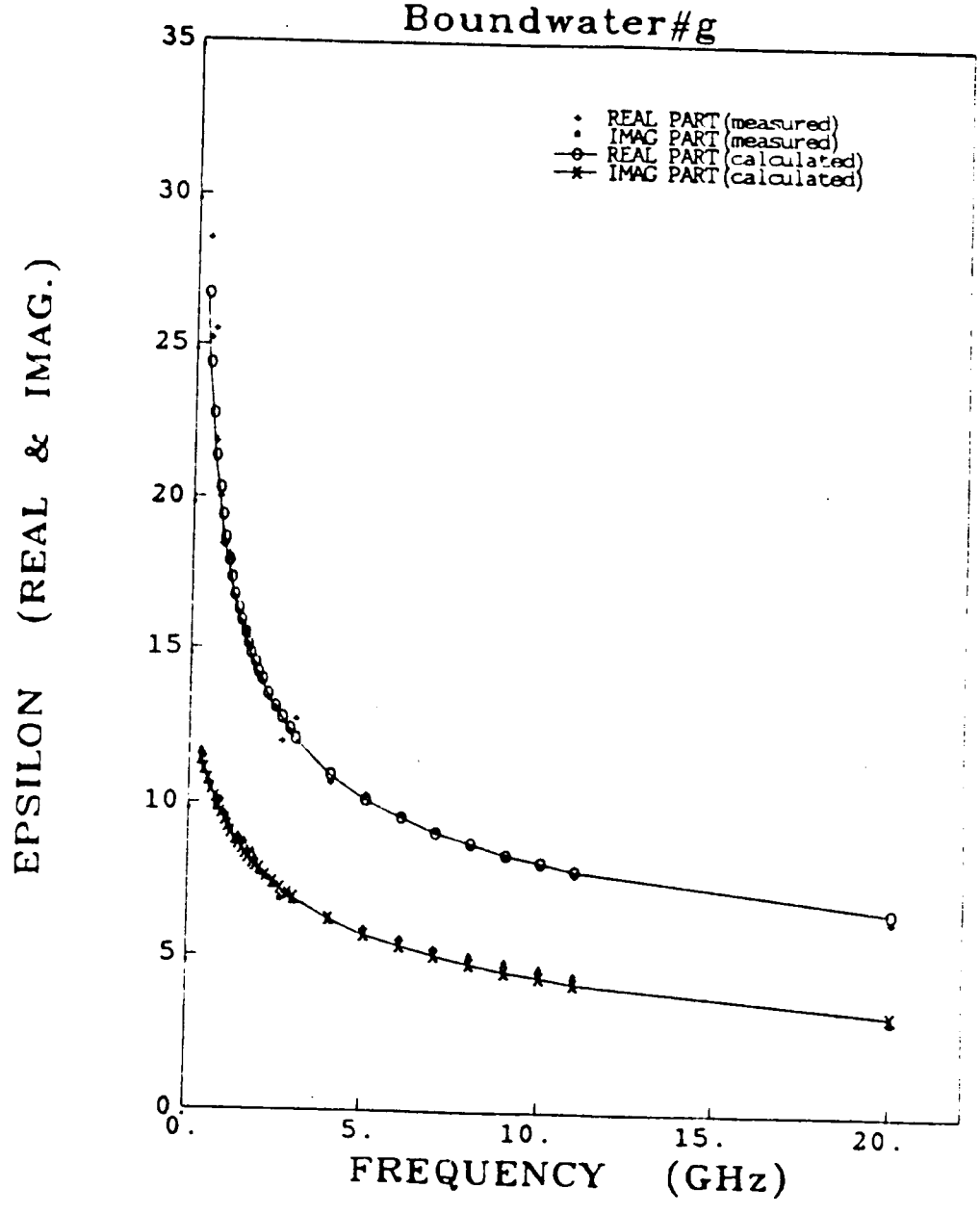

Figure 5.18. Spectra for the sucrose solution (G) with x=3.17. The data points are measured and the solid lines are calculated using Equation 2.18 in the text.

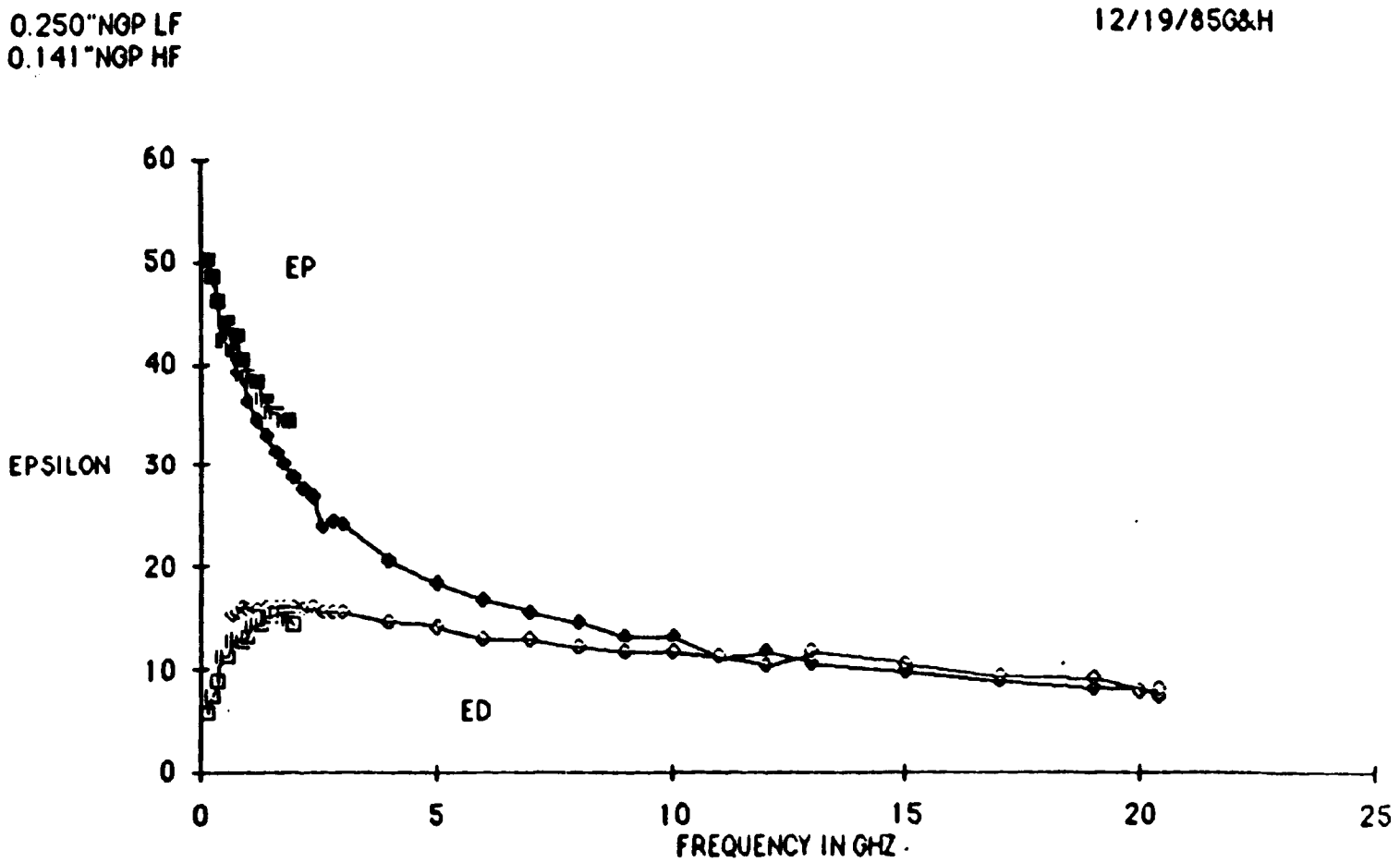

Figure 5.19. Measured spectra for dextrose solution with x=2. Two probes were used to measure the lower(.25") and upper(.141") bands.

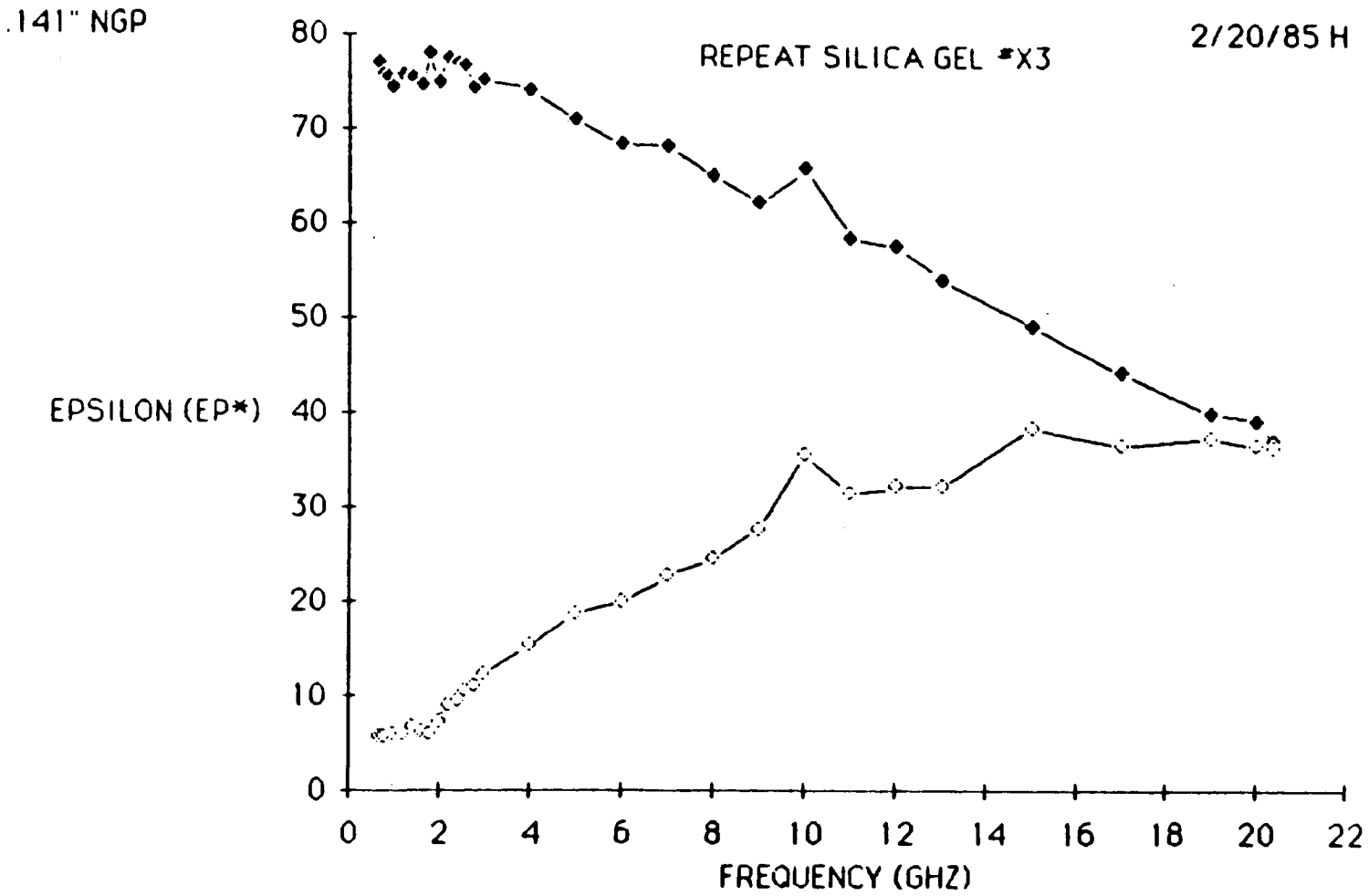

Figure 5.20. Measured spectra for Silica gel (X3) with x=0.5.

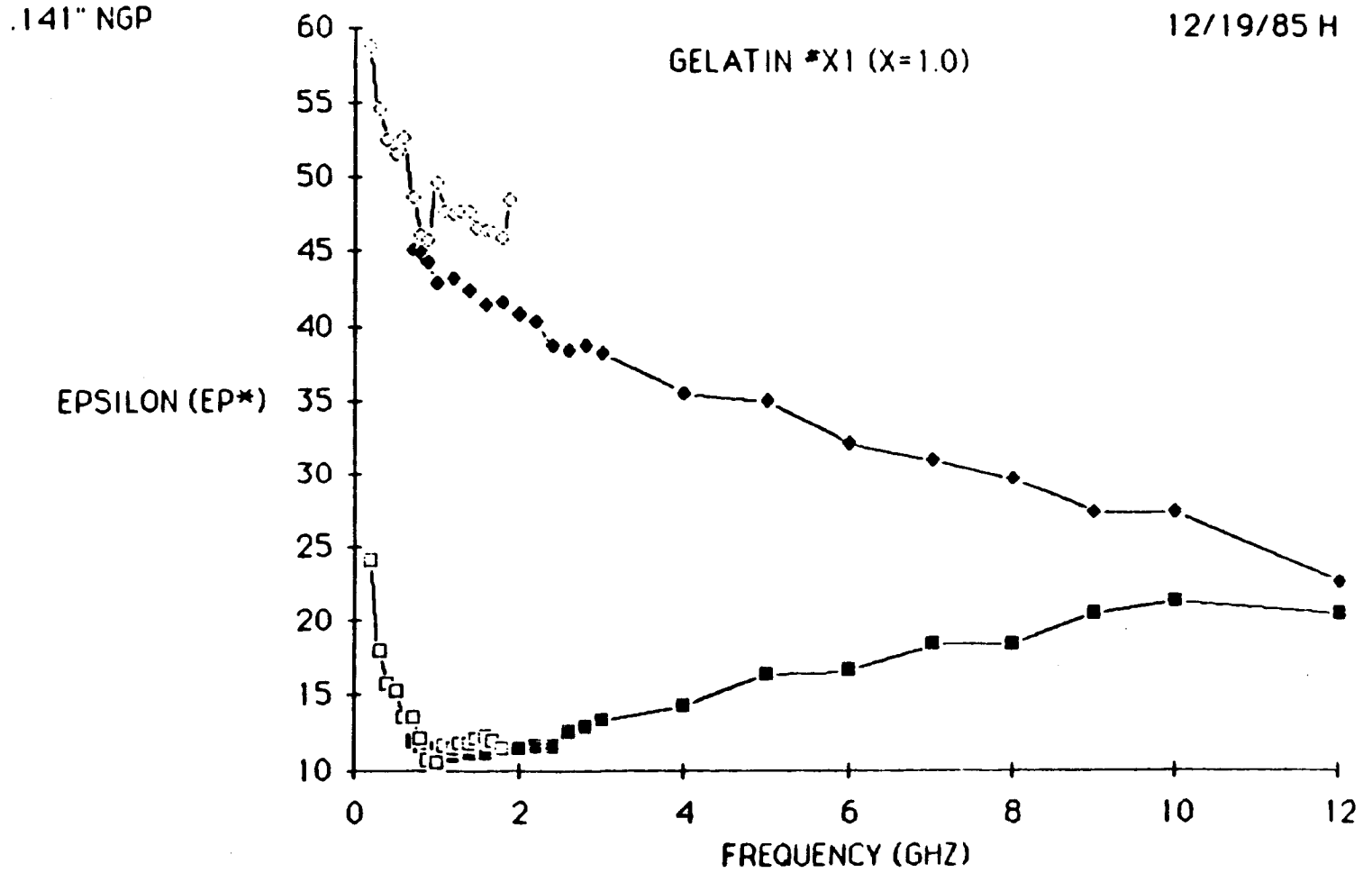

Figure 5.21. Measured spectra for Gelatin (X1) with x=1. Two probes were used to measure the lower(.25") and upper(.141") bands.

4. *Starch,* Fig. 5.22 shows the spectrum of a starch mixture at $X = 1$. This figure is to be compared to sucrose B. It can be observed that starch can bind more water than sucrose can (for the same concentration).

5. *Accacia,* Fig. 5.23 shows the behavior of accacia (arabic gum) mixture with water at $X = .8$. Similar to starch, accacia shows a larger binding capacity compared to sucrose solutions.

6. *Natural honey,* Fig. 5.24 shows the spectrum of natural honey. If we compare this spectrum to sucrose G, we note that ϵ, at e.g. $f = .5$ GHz, drops from about (26-j11) for sucrose G to about (14 - j7) for honey. This behavior is governed by the molecular arrangement by which water binds itself to the host molecule.

7. *Miscellaneous* materials including egg white, egg yolk, and human skin (finger tips) as shown in Figs. 5.25 to 5.27, respectively. Table 5.12 summarizes these measurements at $f = 1$ GHz.

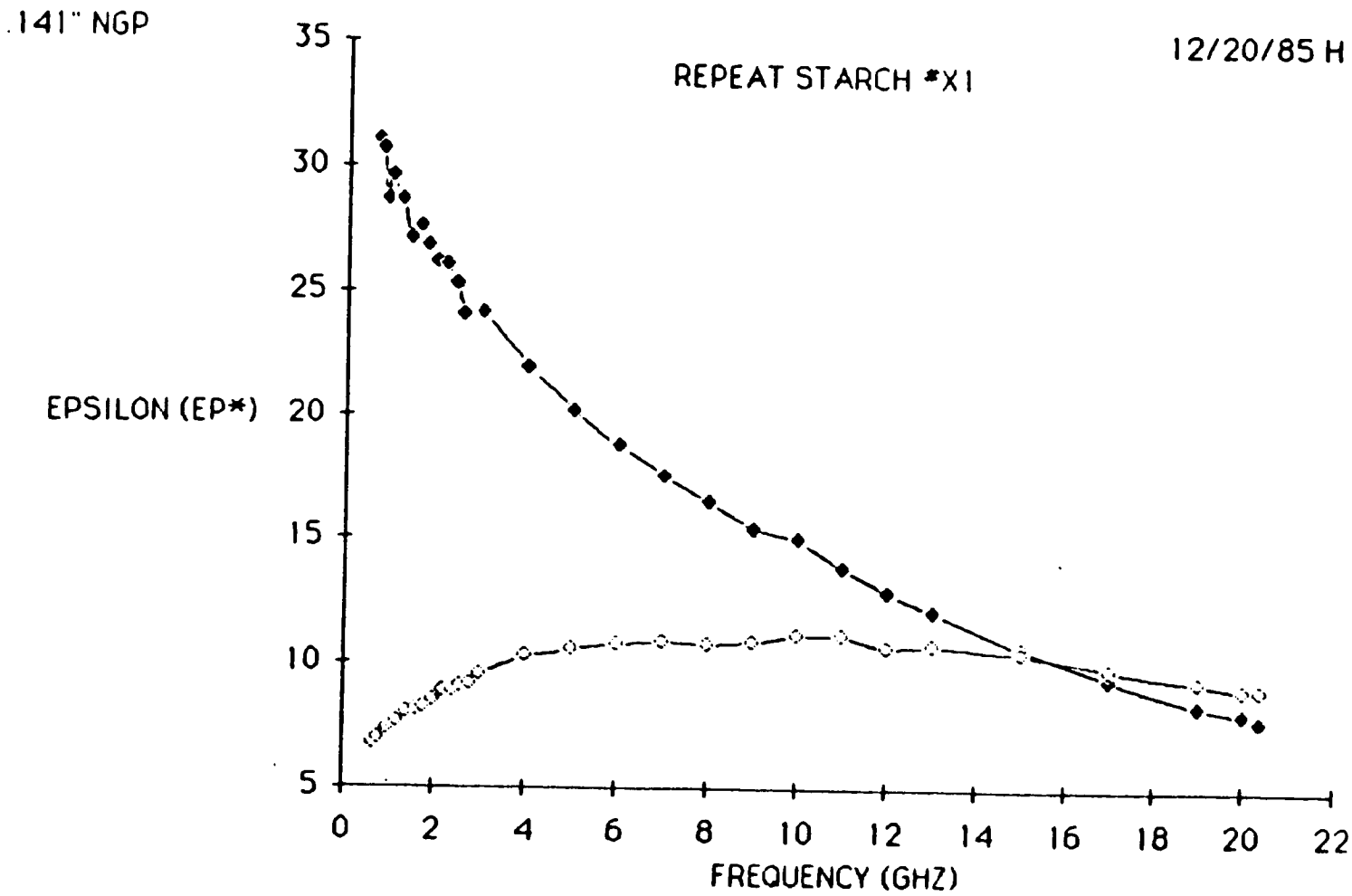

Figure 5.22. Measured spectra for starch solution with x=1.

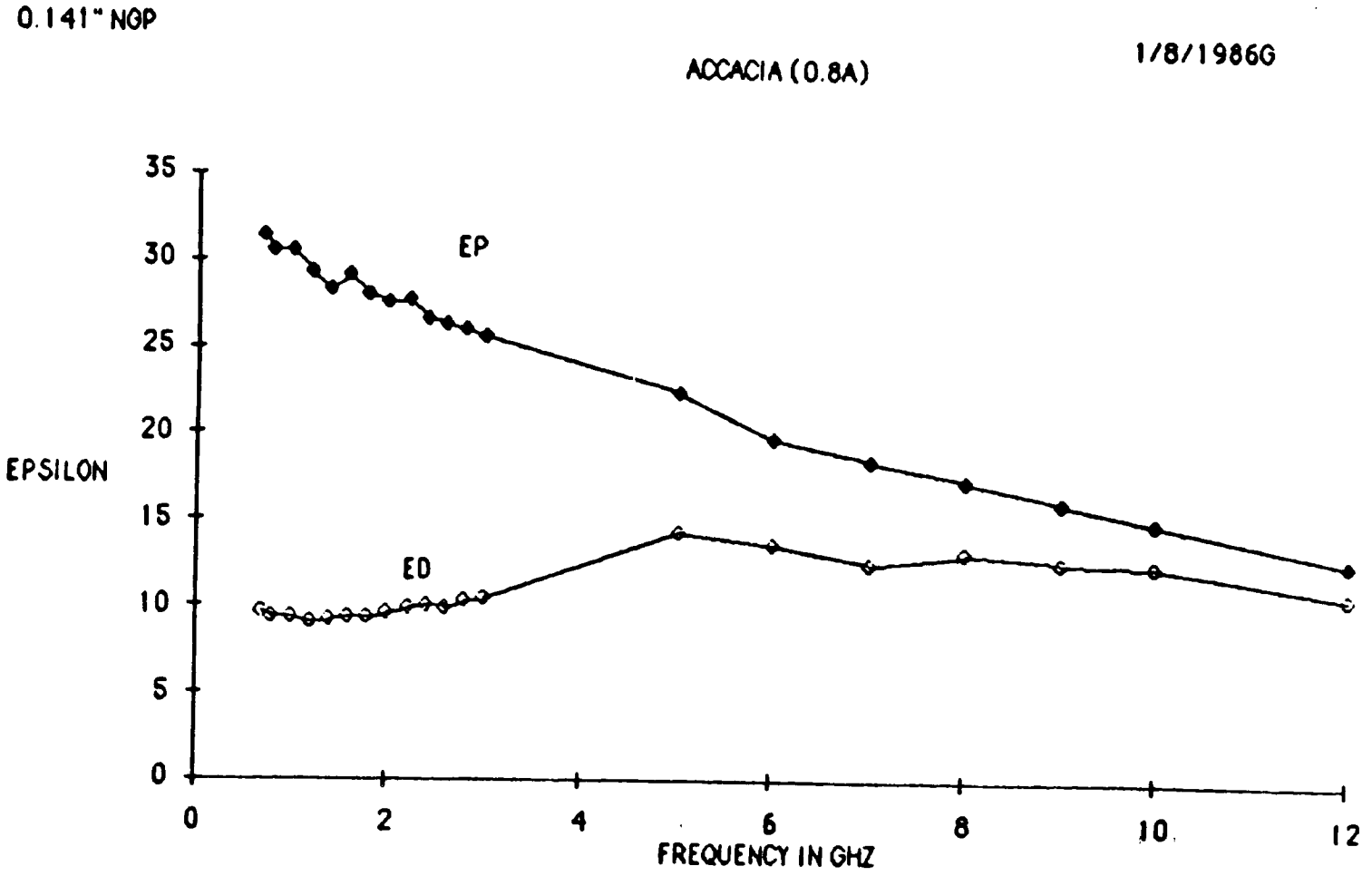

Figure 5.23. Measured spectra for Accacia (Arabic Gum) solution with x=0.8.

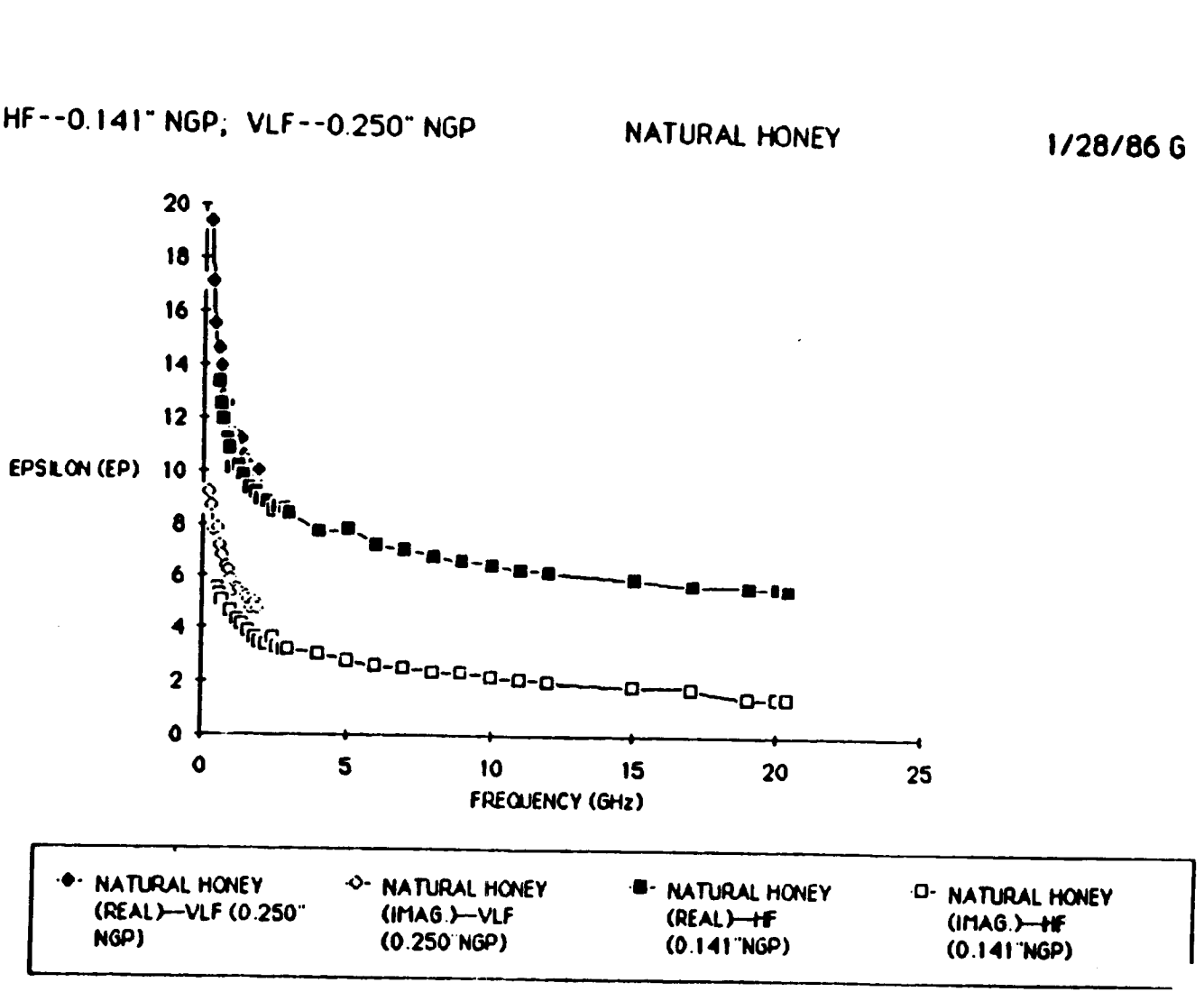

Figure 5.24. Measured spectra for natural honey. Two probes were used to measure the lower(.25") and upper(.141") bands.

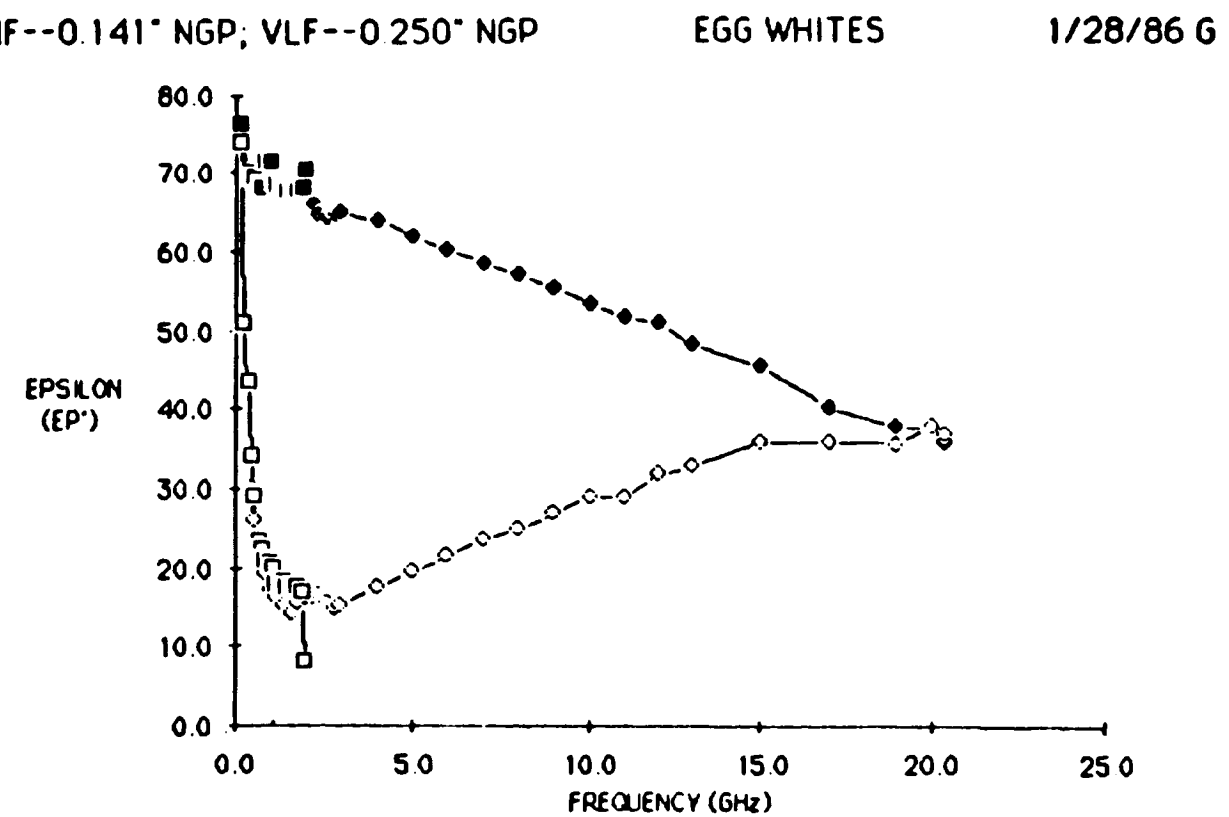

Figure 5.25. Measured spectra for egg white. Two probes were used to measure the lower(.25") and upper(.141") bands.

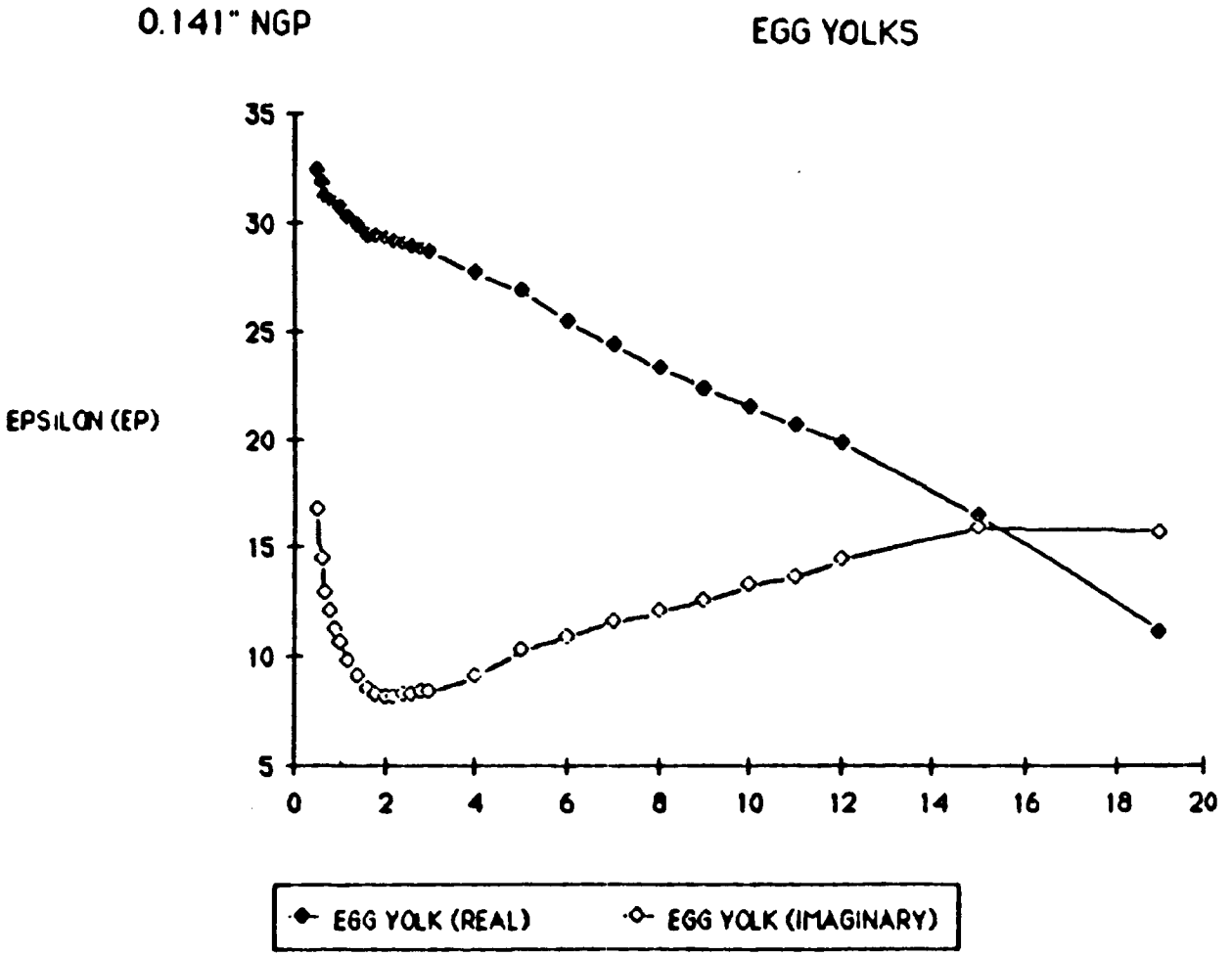

Figure 5.26. Measured spectra for egg yolks.

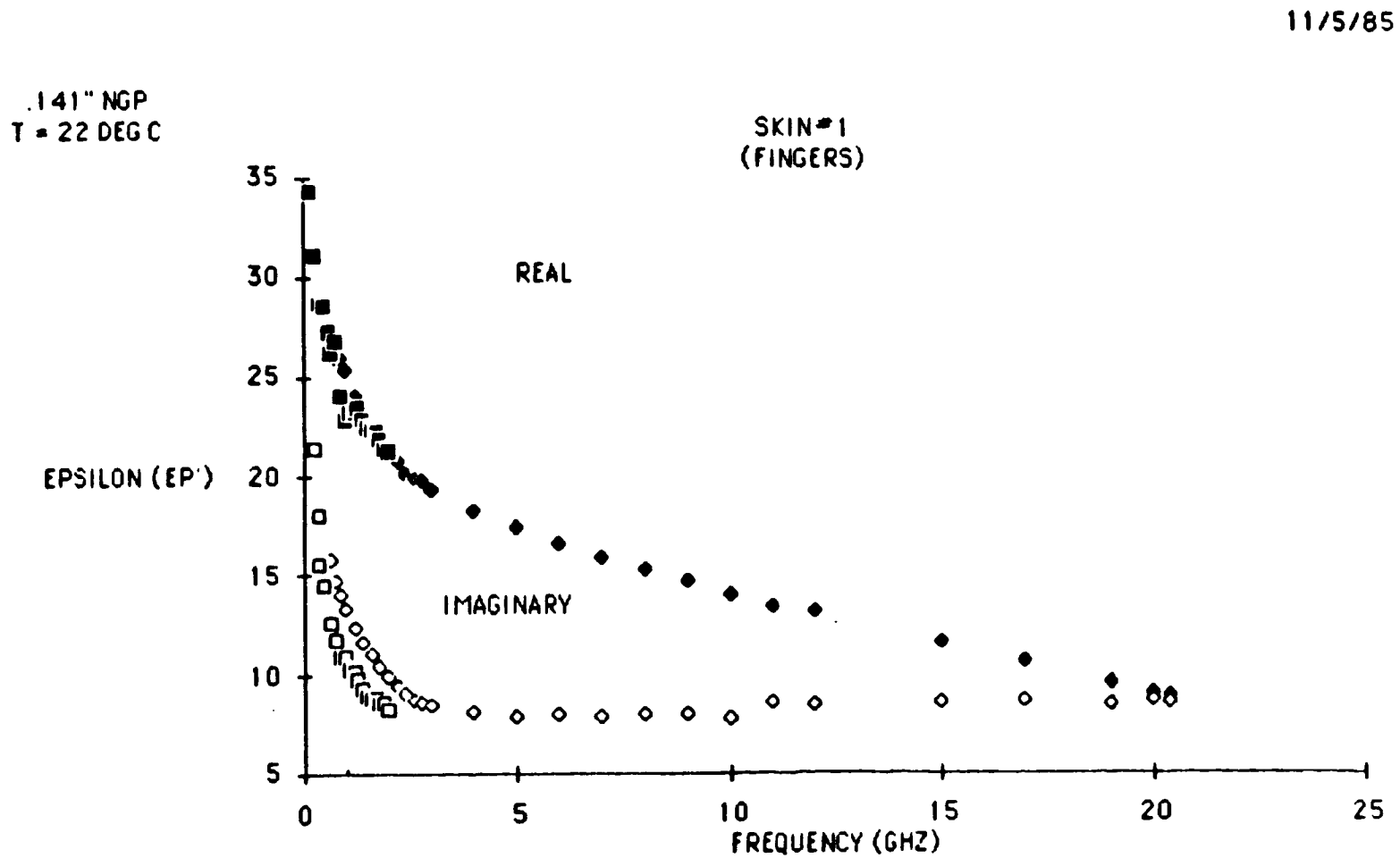

Figure 5.27. Measured spectra for human skin (finger tips). Two probes were used to measure the lower(.25") and upper(.141") bands.

material	X	ϵ'	ϵ''	$tan(\delta)$
distilled water	0	79.1	4.1	.052
sucrose#A	.5	65	10	.154
sucrose#B	1	51.9	14	.270
dextrose#$X3$	.5	67	7.5	.112
dextrose#$X1$	1	62	12.5	.093
gelatin#$X3$	.5	55	12	.218
gelatin#$X1$	1	44	12	.273
starch#$X3$	.5	57	9	.158
starch#$X1$	1	28	7.5	.268
accacia	.8	31	9	.290
natural honey		11	5	.455
egg white		70	20	.286
egg yalk		31	10	.323
skin		23	12.5	.543

Table 5.9: Measured ϵ' and ϵ'' of various materials (some with known water-binding capacity, X=solid weight/water weight)at 1 GHz.

5.6 Temperature Effects

A temperature experiment was devised and conducted to study:

1. the dielectric properties of plants at temperatures above, below, and at the freezing-point discontinuity, and

2. the properties of bound water as a function of temperature.

A.Free Water

Before we start discussing the data measured for plants, it is useful to first review the dielectric properties of liquid water because the latter govern the behavior of the former. Figures 5.28 to 5.30 show the dielectric properties of liquid water as a function of temperature (above freezing) for different frequencies (1, 4, 8 and 20 GHz) and salinities (0, 4 and 8 ppt). The following observations may be made:

1. $\frac{\partial \epsilon'}{\partial T}$ (at 1 and 4 GHz) is, in general, small in magnitude and negative in sign.

2. $\frac{\partial \epsilon'}{\partial T}$ (at 8 and 20 GHz) is large and positive in sign.

3. $\frac{\partial \epsilon'}{\partial S}$ is small and negative (S is salinity in ppt).

4. The relaxation frequency, f_0, decreases with T.

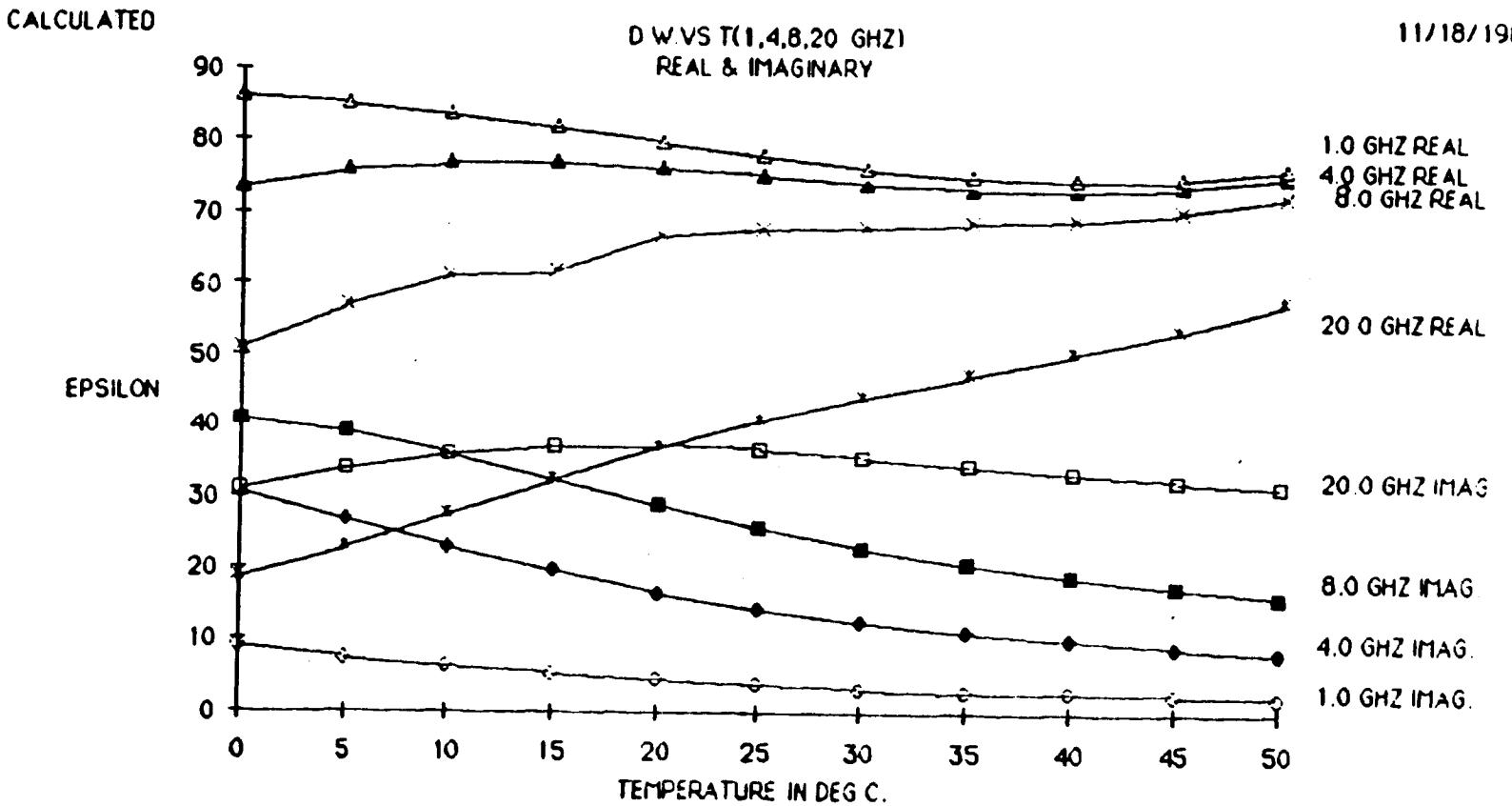

Figure 5.28. Dielectric constant behavior versus temperature with frequency as parameter for distilled water (s=0 ppt). Calculated from [Stogryn, 1971].

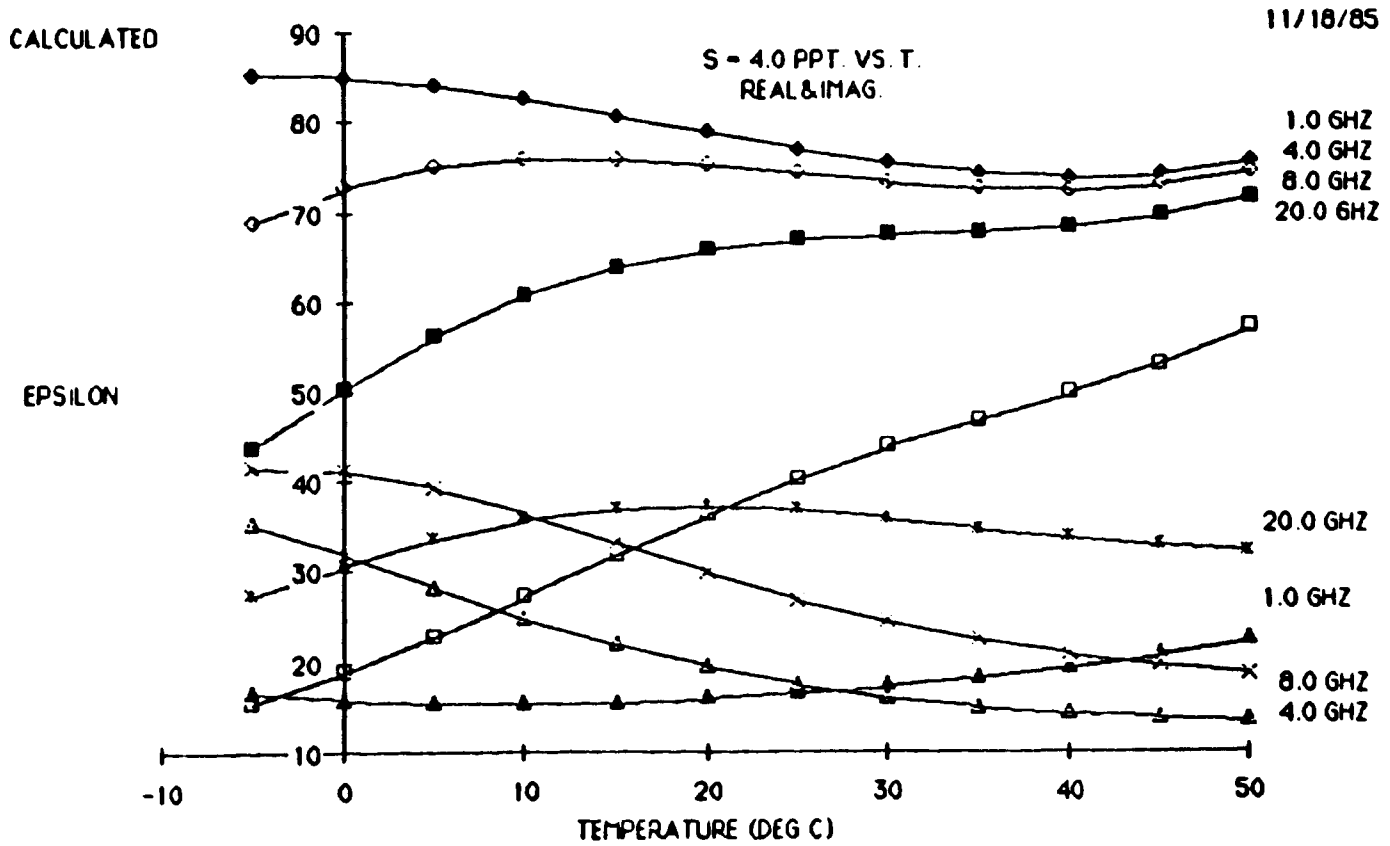

Figure 5.29. Dielectric constant behavior versus temperature with frequency as parameter for saline water solution (s=4 ppt). Calculated from [Stogryn, 1971].

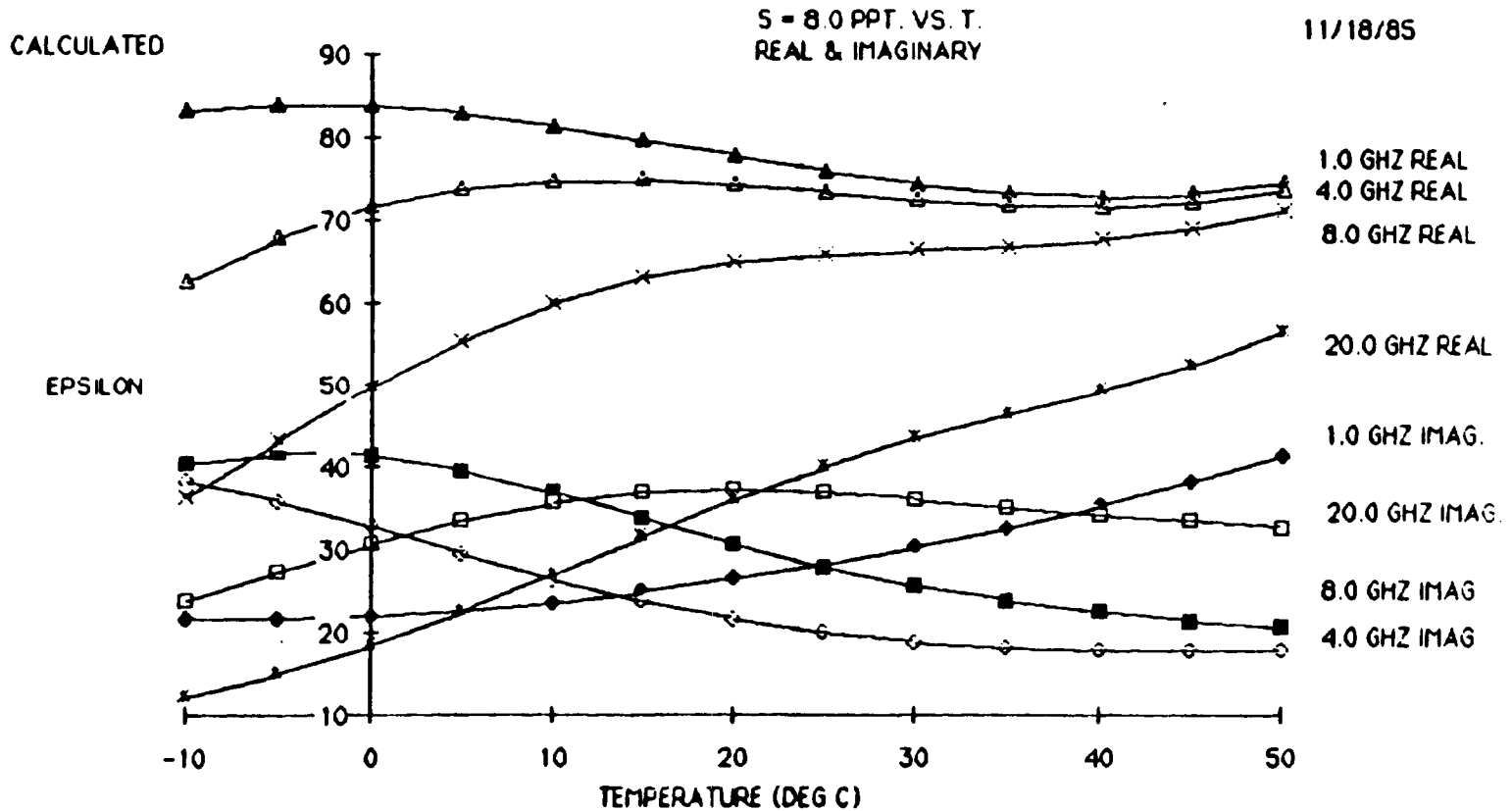

Figure 5.30. Dielectric constant behavior versus temperature with frequency as parameter for saline water solution (s=8 ppt). Calculated from [Stogryn, 1971].

5. ϵ''(at 4, 8, and 20 GHz) is driven mainly by the free-water relaxation process; it has a negative temperature-coefficient, $\frac{\partial \epsilon''}{\partial T}$, below resonance and a positive one above resonance.

6. ϵ'' is very sensitive to conductivity at 1 GHz, $\frac{\partial \epsilon''}{\partial T}$ (at f=1 GHz and S=0) is negative because $f \leq f_0$, while $\frac{\partial \epsilon''}{\partial T}$ (at f=1 GHz and S=4 and 8 ppt) is positive due to conductivity effects.

Table 5.10 summarizes the temperature properties of water in its different forms:

	free-water relaxation			conductivity	bound-water relaxation		
$\frac{\partial \epsilon''}{\partial T}$	$f \leq f_0$	$f = f_0$	$f \geq f_0$	$f \leq$ 4GHz	$f \leq f_0$	$f = f_0$	$f \geq f_0$
	($f_0 \simeq$ 18 GHz)				($f_0 \simeq$ .178GHz)		
f in GHz	-ve	zero	+ve	+ve	-ve	zero	+ve
1 GHz	small -ve			large +ve	large +ve		
4 GHz	medium -ve			medium +ve	medium +ve		
10 GHz	large -ve			neglegible	small +ve		
20 GHz	small +ve			neglegible	small +ve		

Table 5.10: Liquid water temperature coefficients.

B.Bound Water

As shown in Table 5.10, the dielectric properties of free-water and bound-water as a function of temperature are similar, except in that the relaxation frequency is a 100 times smaller and the spectrum is more flat for bound water($\alpha = .5$). The dielectric behavior of bound water is studied through the study of concentrated sucrose solutions. Figures 5.49 to 5.51 show the measured dielectric properties of a concentrated sucrose solution as a function of temperature. The general behavior of bound water agrees with that expected in Table 5.10.

C.Vegetation Material

experiment # 1

Fatshedera leaves were used for the first temperature experiment. The temperature inside the environmental chamber was measured accurately but the stability of the temperature sensing circuit is only $\pm.5^0C$. The temperature sensing devices, i.e. the thermistor and the thermocouple, were placed as close as possible to the sample under test, and sufficient time was allowed so that the chamber may reach equilibrium before ϵ is measured. The steady state condition is hard to identify, since there is no way by which we can check the temperature difference between the sample and the surrounding air. An air blower was used for this purpose, but blowing air, especially hot air, increases evaporation from the sample. The longer we wait, to attain steady-state conditions, the larger is the moisture loss from the sample and of course the more tedious the experiment becomes. It was found that waiting for 30 minutes, after resetting the temperature,

before taking the dielectric measurement is an acceptable compromise.

Figures 5.31 to 5.34 show plots of ϵ versus T at 1, 4, 8, and 20 GHz. The gravimetric moisture of the sample was .745 before the experiment started and .711 after the measurements were completed. The sample lost 5% of its original M_g during the experiment. The following observations may be made:

1. The freezing-point discontinuity takes place at well below 0^0C. Freezing actually happens at around -7^0C, which is attributed to a *super-cooling* (or *under-cooling*) effect (Levitt, 1956). Figure 5.35 shows reported data on corn plants with and without *Pseudomonas Syringae* (Bacteria that act like ice nuclei between -2 and -5^0C). The untreated plants were able to withstand temperatures as low as -8^0C before significant damage was observed.

2. $\frac{\partial \epsilon'}{\partial T}$(1 GHz) is small and negative,

3. $\frac{\partial \epsilon'}{\partial T}$(4 GHz) is small and positive,

4. $\frac{\partial \epsilon'}{\partial T}$(8 and 20 GHz) is large and positive,

5. $\frac{\partial \epsilon''}{\partial T}$(1 GHz) is large and positive,

6. $\frac{\partial \epsilon''}{\partial T}$(4 and 8 GHz) is small and negative, and

7. ϵ''(20 GHz) has a minimum around 20^0C.

Comparing these properties to liquid water shows great similarity, except for the imaginary part at 20 GHz. The imaginary part ϵ'' at 20 GHz is not similar to

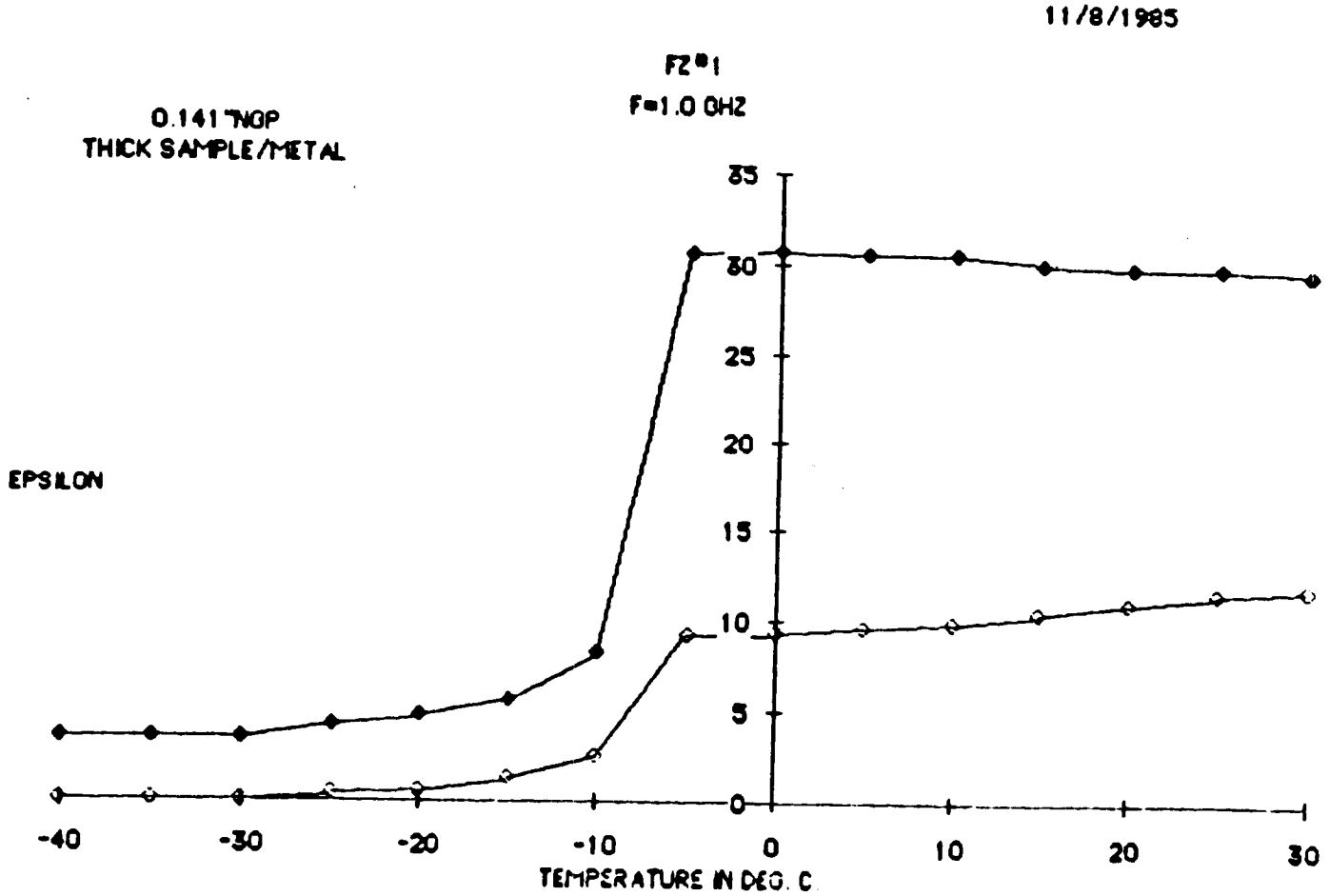

Figure 5.31. Measured dielectric constant versus temperature from -40^0C to $+30^0C$ at 1 GHz for Fatshedera leaves. M_g(before) = 0.745 and M_g(after) = 0.711.

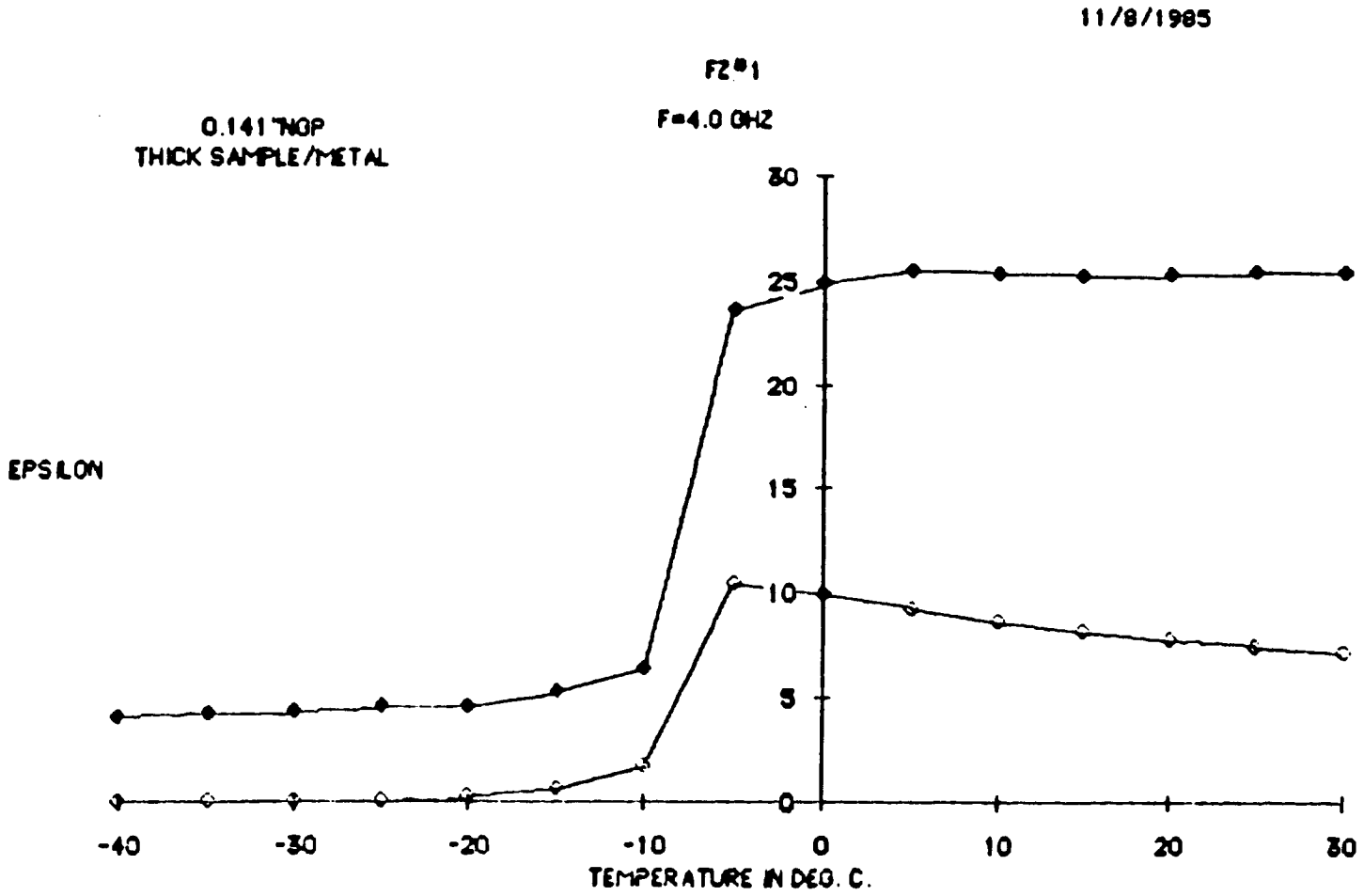

Figure 5.32. Measured dielectric constant versus temperature from -40^0C to $+30^0C$ at 4 GHz for Fatshedera leaves. M_g(before) = 0.745 and M_g(after) = 0.711.

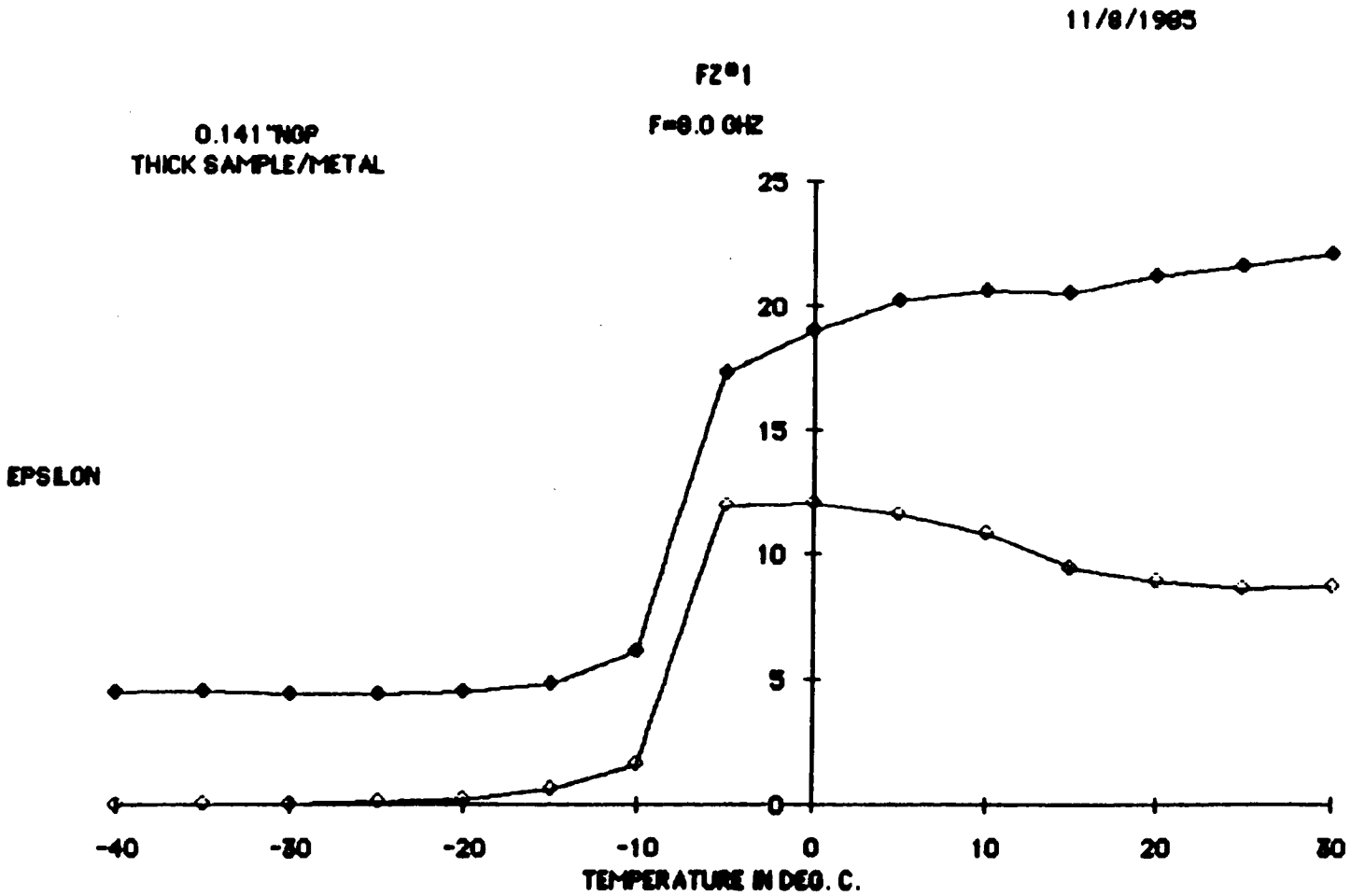

Figure 5.33. Measured dielectric constant versus temperature from -40^0C to $+30^0C$ at 8 GHz for Fatshedera leaves. M_g(before) = 0.745 and M_g(after) = 0.711.

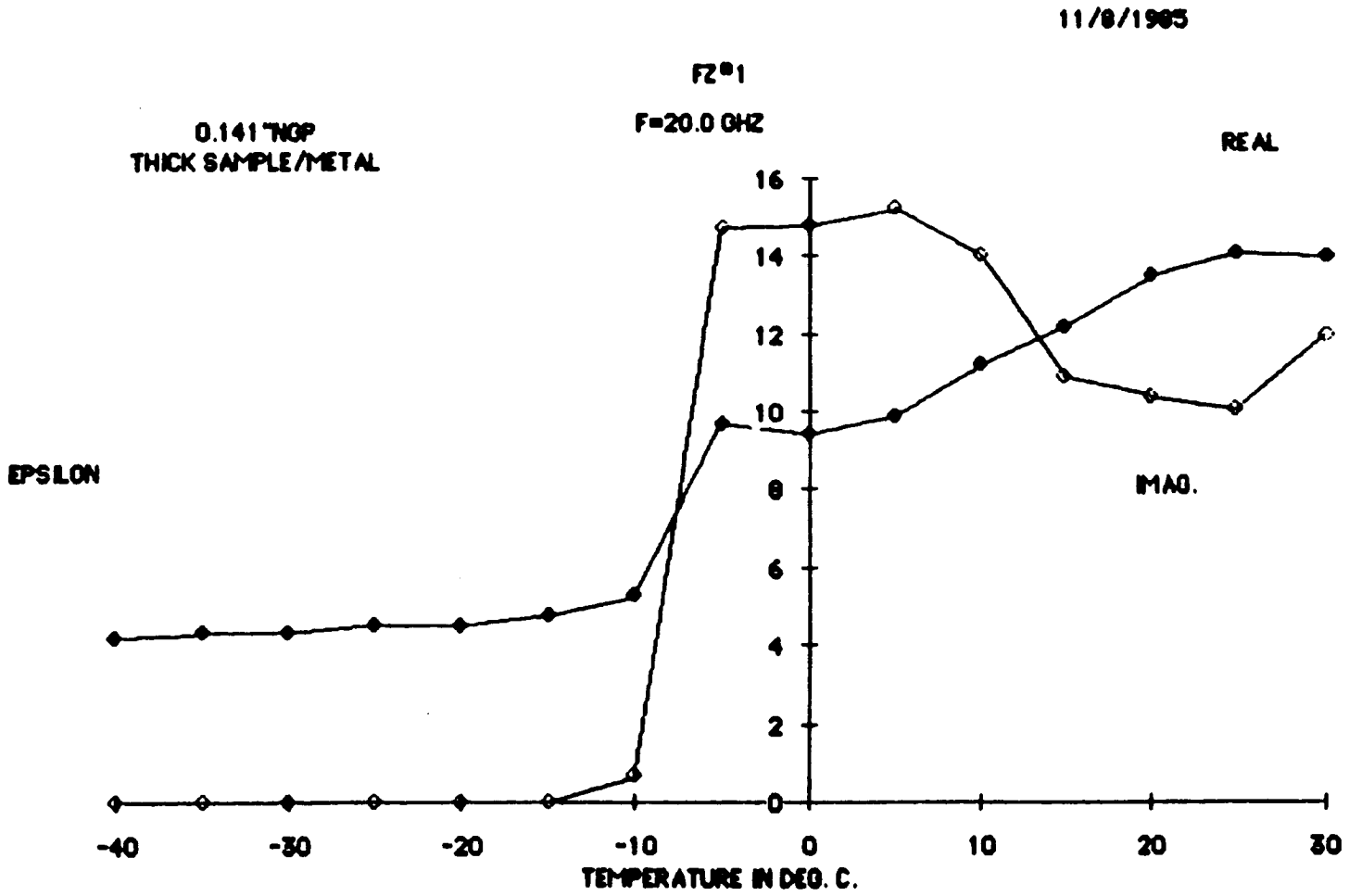

Figure 5.34. Measured dielectric constant versus temperature from -40^0C to $+30^0C$ at 20 GHz for Fatshedera leaves. M_g(before) = 0.745 and M_g(after)

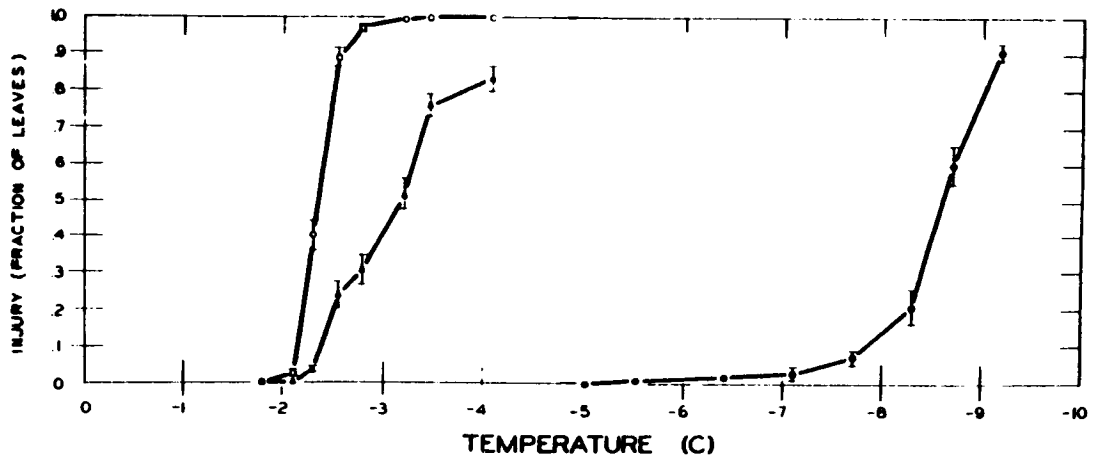

Frost damage as a function of temperature to corn seedlings with and without leaf populations of Pseudomonas syringae. Plants were sprayed with P. syringae suspensions (≈ 0.5 ml/plant) of 3 x 10^8 cells/ml (○) or 3 x 10^5 cells/ml (△) and incubated in a mist chamber for 24 hours. Other plants remained untreated (●). Then the plants were placed in a growth chamber at 0° C and cooled at 0.05° C/minute. Groups of plants were removed from the chamber at the temperatures shown on the abscissa. Data are represented as means ± standard error (vertical bars).

Figure 5.35. [Levitt, 1956].

that of liquid water. Figures 5.36 to 5.38 show the frequency response of ϵ, both real and imaginary, at different temperatures ($-40^0C \leq T \leq +30^0C$). Note the sudden change in level between the spectra measured at $T \geq -5^0C$ and those measured at $T \leq -10^0C$.

Experiment # 2

The fact that the Fatshedera leaves freeze at around -10^0C poses a question: Do other plants have similar freezing behavior?. To answer this question, a leaf sample from the plant (a tropical banana-like plant) with M_g=.839 was tested. This time, care was excercised to allow more time for the chamber to reach steady state and, also, ϵ was sampled more frequently at temperatures around freezing (25 times). Figure 5.39 shows ϵ versus T ($-45^0C \leq T \leq 50^0C$) at 10 GHz. Since, for this experiment, we really do not care about the frequency response, only the 1 GHz data is shown. The rest of the data is given in Appendix B. Figure 5.39 shows the usual above-freezing behavior of ϵ at low frequencies; $\frac{\partial \epsilon'}{\partial T}$ is small and negative and $\frac{\partial \epsilon''}{\partial T}$ is large and positive. The freezing temperature is below -8^0C and the change in level, as shown in Fig. 5.39, is very steep. Below freezing, however, ϵ'' continues to have a non-zero value down to -25^0C. Below -30^0C, ϵ'' is almost zero (indeed we should always bear in mind that the data processing procedure has a $\pm.1$ accuracy due to rounding error alone). But, in spite of the poor overall system accuracy at low ϵ values, conclusive evidence shows the existence of unfrozen water in plants below the freezing temperature of free water. Figure 5.40 shows an example of ϵ versus f at $T = -15^0C$, it is clear

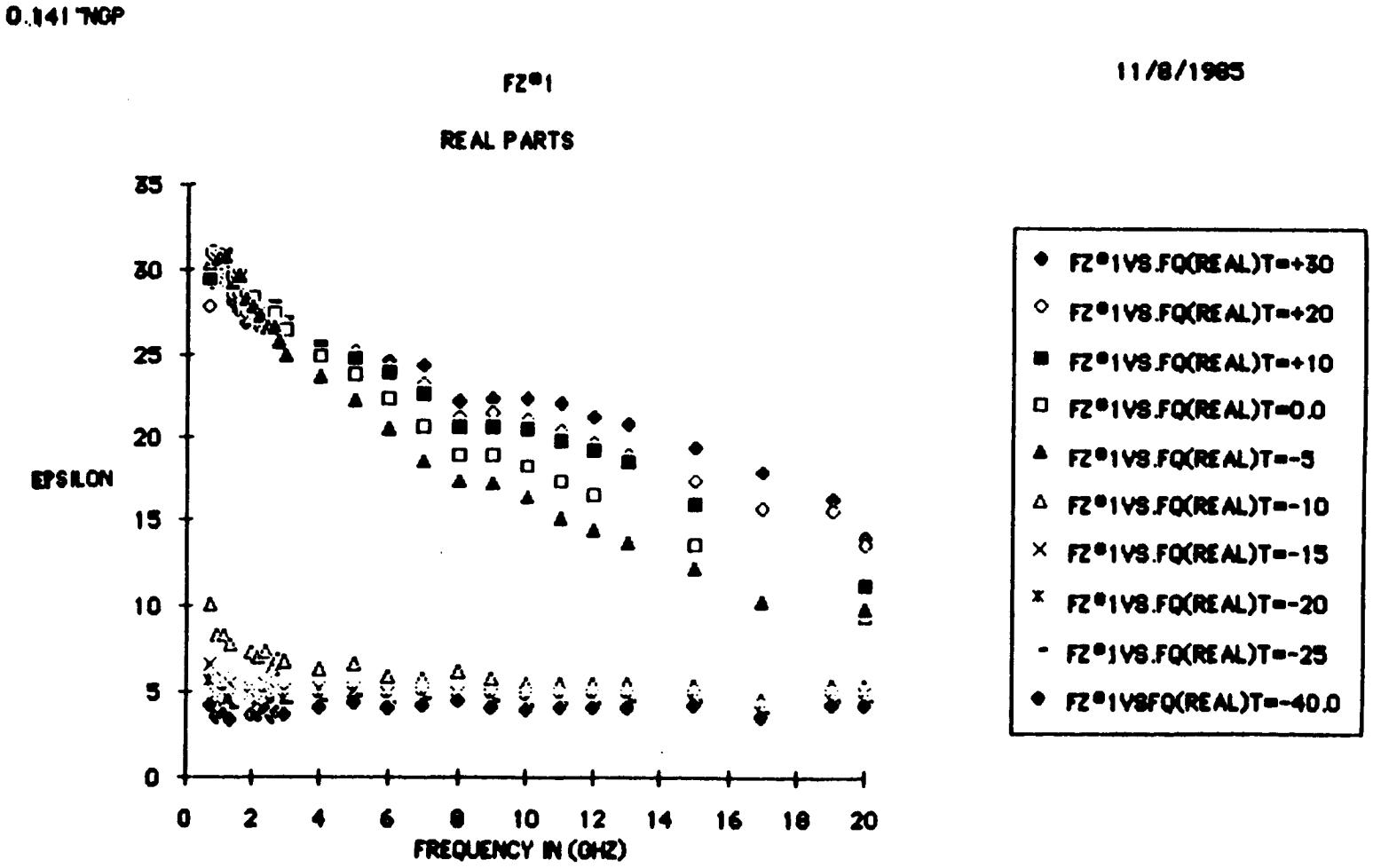

Figure 5.36. Measured spectra for Fatshedera leaves with temperature as parameter (real parts) M_g(before) = 0.745 and M_g(after) = 0.711.
= 0.711.

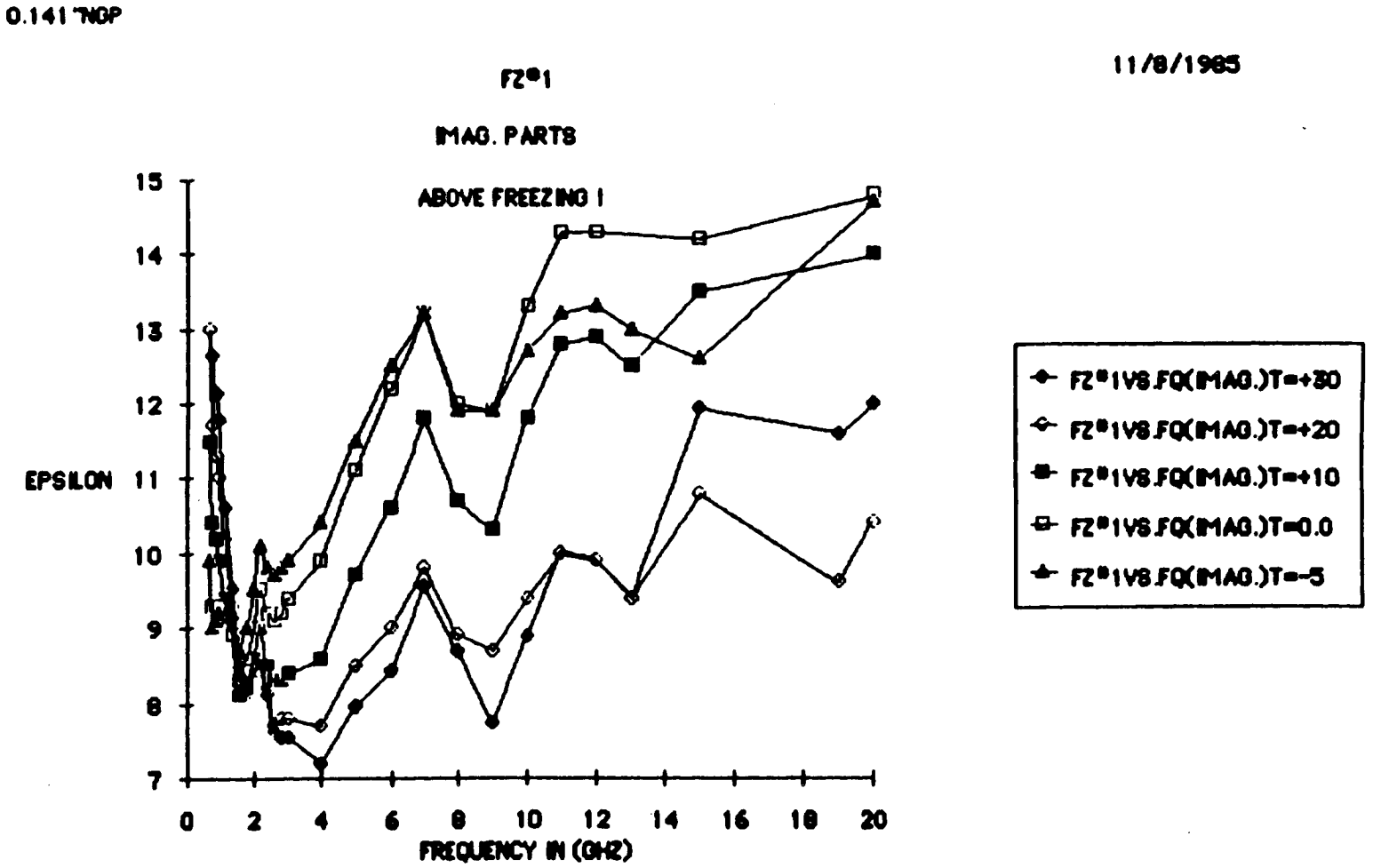

Figure 5.37. Measured spectra for Fatshedera leaves with temperature above freezing as parameter (imaginary parts) M_g(before) = 0.745 and M_g(after) = 0.711.

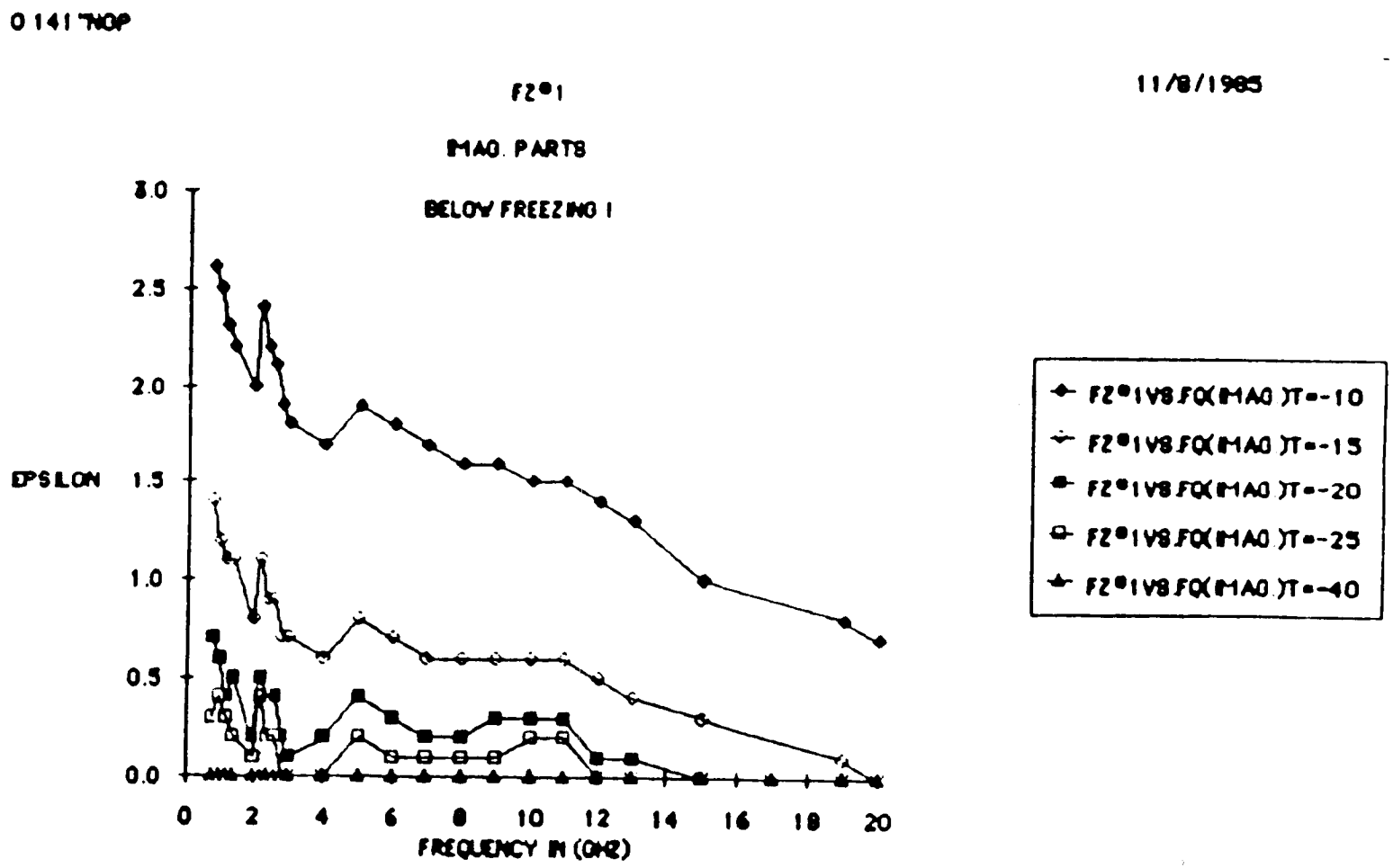

Figure 5.38. Measured spectra for Fatshedera leaves with temperature below freezing as parameter (imaginary parts) M_g(before) = 0.745 and M_g(after) = 0.711.

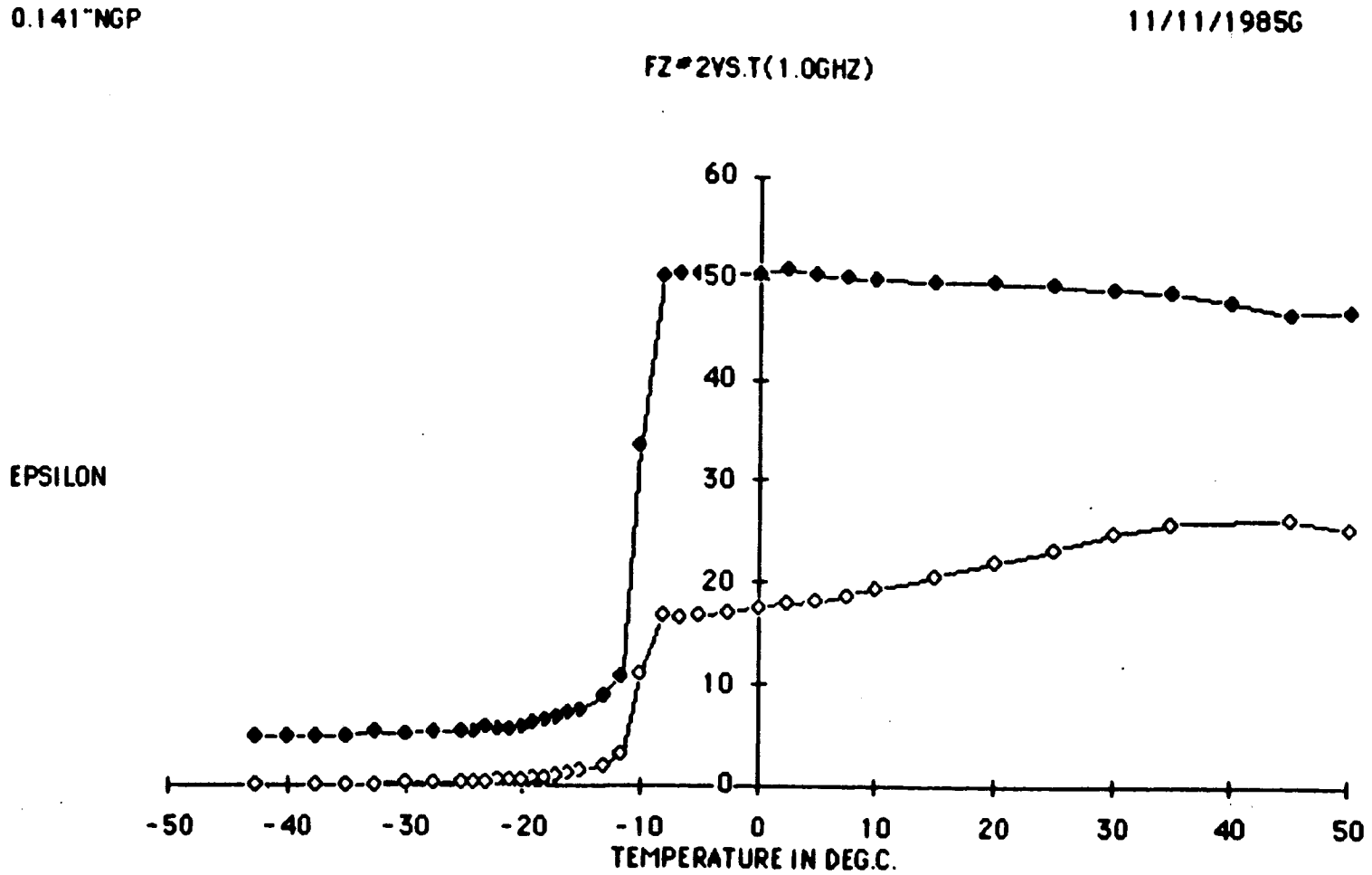

Figure 5.39. Measured dielectric constant versus temperature from -45^0C to $+50^0C$ at 1 GHz for a tropical tree leaves. M_g(before) = 0.839 and M_g(after) = 0.818.

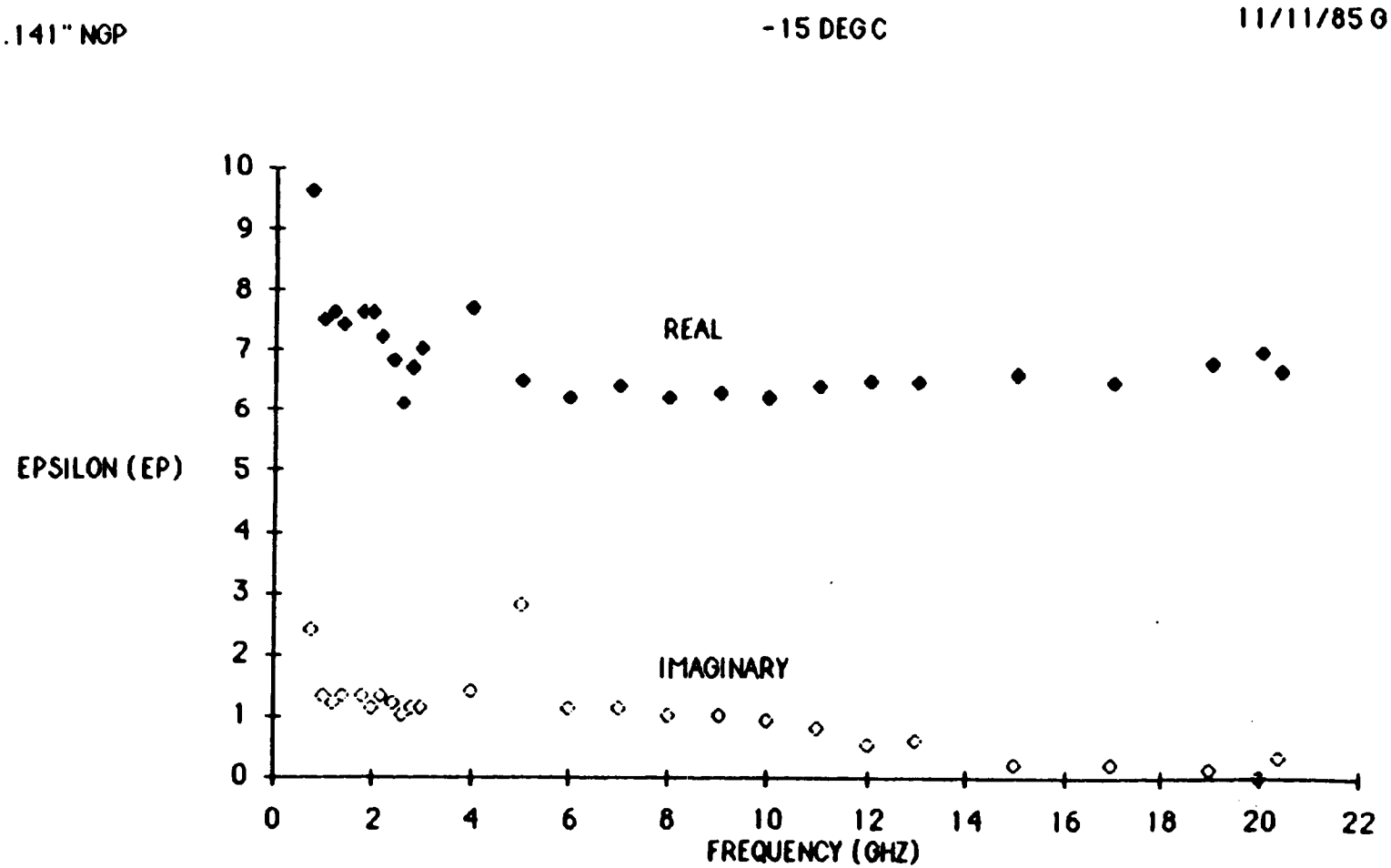

Figure 5.40. Measured spectra for a tropical tree leaves at -15^0C.

that ϵ'' has a much larger value than that of ice. Figure 5.39 also shows that the terminal value of ϵ below -40^0C is about (5-j0). Since ϵ of dry vegetation (bulk vegetation + air) is $\simeq 1.7 - j0$, and ϵ of ice is $\simeq 3.15 - j0$, ϵ of the mixture can not be larger than that of ice unless liquid water is present. The observed value of $\epsilon' \simeq 5$ is attributed to ϵ' of *bound-water ice*. It has, probably, a value much higher than that of free-water ice ($\simeq$ 10 !).

Experiment # 3

In the previous two experiments we have shown the similarity between the dielectric spectra of liquid water and plant materials. Also, the low freezing temperature of plant samples, the super-cooling effects, was briefly discussed. The third experiment was designed to test a plant sample undergoing two cycles of freezing and thawing. Again, we chose Fatshedera leaves with high moisture content (M_g=.736 before and =.718 after the experiment). Figures 5.41 and 5.42 show the general behavior of ϵ versus T at 1, 4, and 8 GHz. Above freezing, the temperature dependence of ϵ'' is consistent with that of free water. Below freezing, ϵ''(1 GHz)$\geq$ ϵ''(8 GHz)$\geq$ ϵ''(4 GHz), but the levels are too close to the lower limit of the system's measurement capability to make quantitative comparisons.

Figures 5.43 and 5.44 show a freezing cycle side by side with a thawing cycle. The hystresis behavior was completely unexpected because it implies a different freezing temperature for water in the two directions. Hence, another experiment

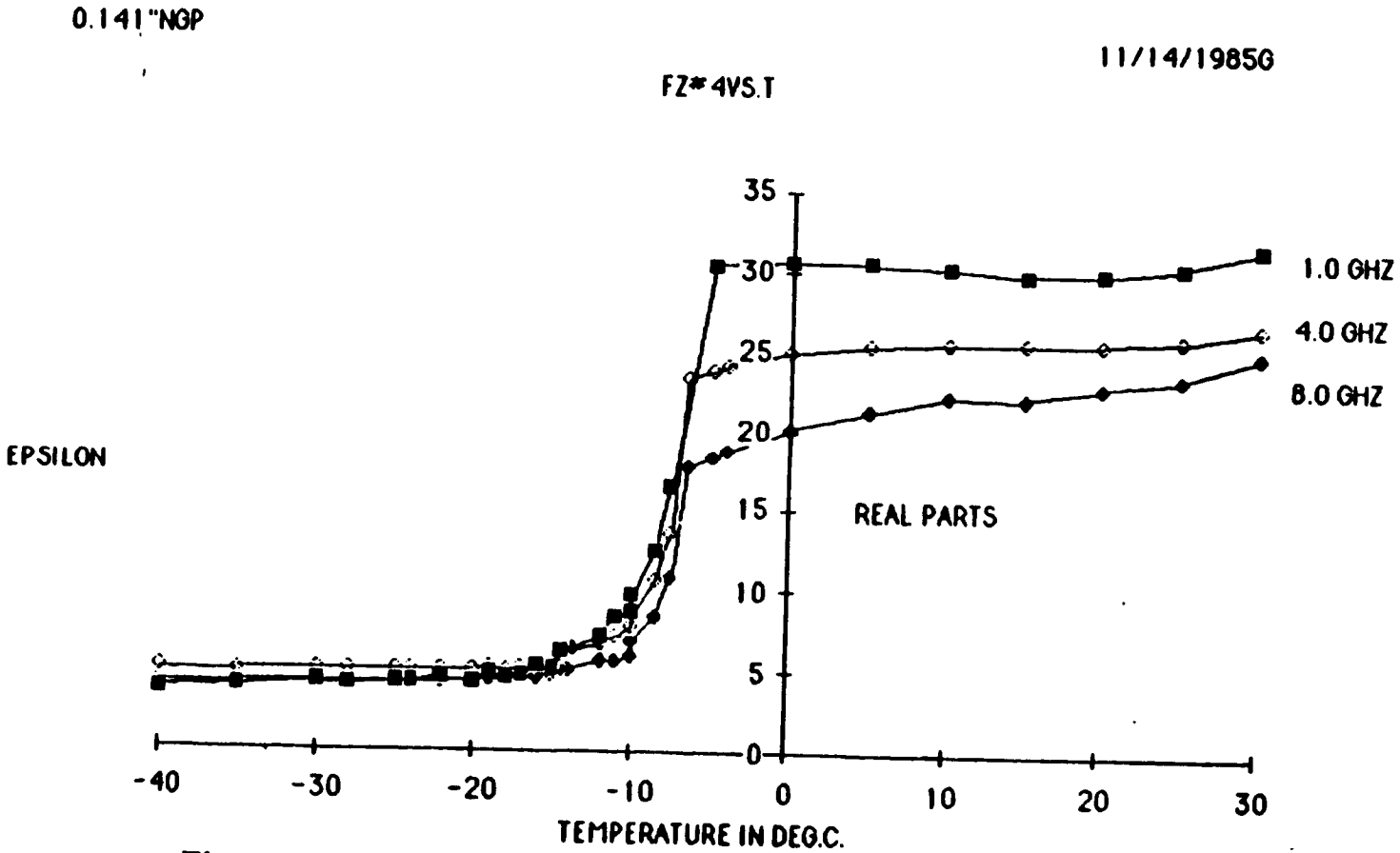

Figure 5.41. Measured dielectric constant versus temperature from -40^0C to $+30^0C$ with frequency as parameter for Fatshedera leaves (real parts). M_g(before) = 0.736 and M_g(after) = 0.718.

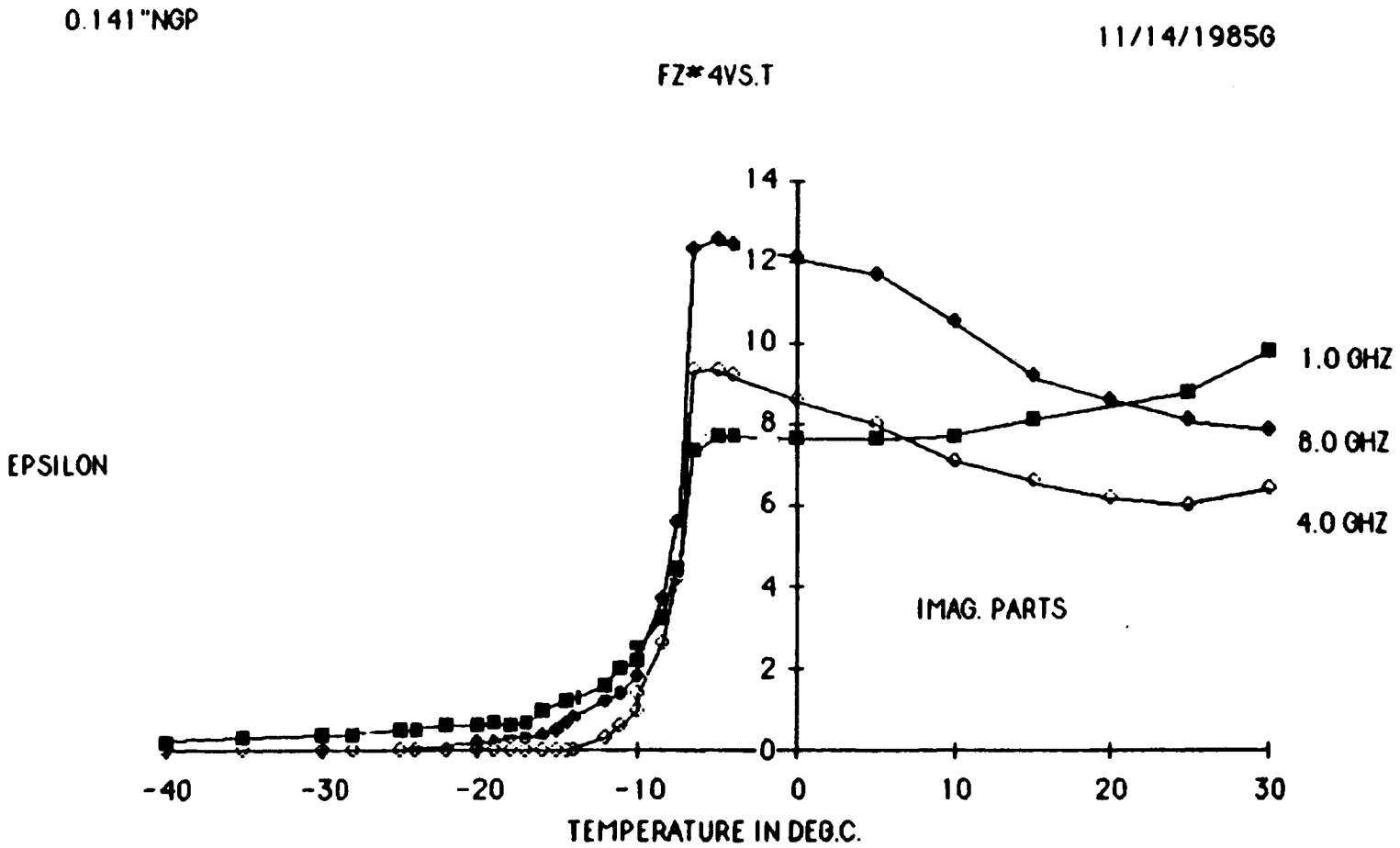

Figure 5.42. Measured dielectric constant versus temperature from -40^0C to $+30^0C$ with frequency as parameter for Fatshedera leaves (imaginary parts). M_g(before) = 0.736 and M_g(after) = 0.718.

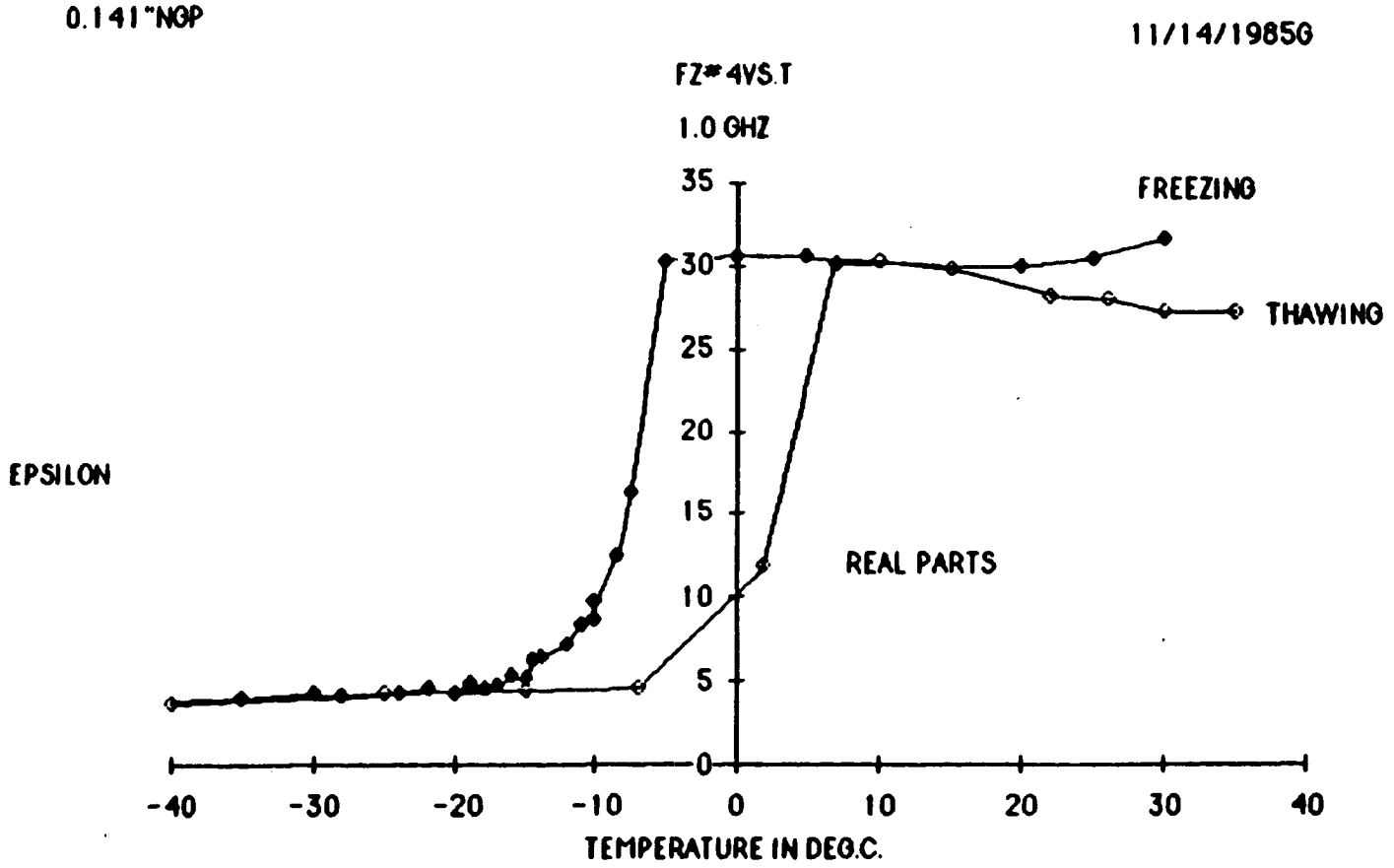

Figure 5.43. Measured dielectric constant versus temperature from -40^0C to $+30^0C$ at 1 GHz for Fatshedera leaves. A freezing-thawing cycle is shown for the real part.

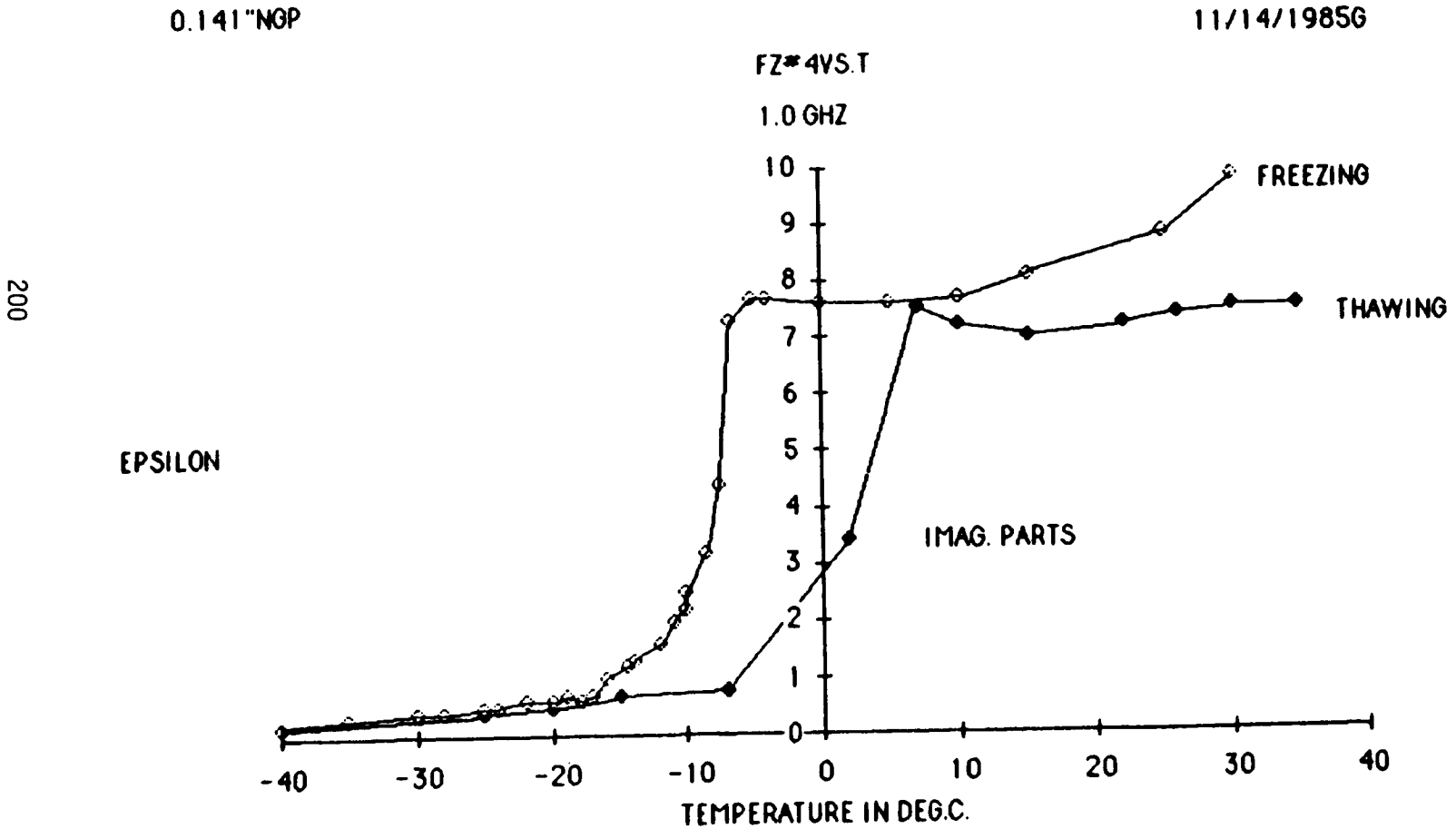

Figure 5.44. Measured dielectric constant versus temperature from -40^0C to $+30^0C$ at 1 GHz for Fatshedera leaves. A freezing-thawing cycle is shown for the imaginary part.

was conducted with particular concentration on the freezing region.

Experiment # 4

During this experiment, freezing, thawing, and refreezing cycles were conducted very slowly on corn leaves with high moisture, M_g(before)=.835 and M_g(after)=.781. The dielectric constant behavior versus temperature for f=1, 4, and 8 GHz is plotted in Figs. 5.45 and 5.46. The following observations may be made:

1. Above and below freezing, the behavior is close to that observed for Fatshedera.

2. The freezing point discontinuity occurs between $(-5.3^0 C and -7.7^0 C)$, similar to Fatshedera leaves.

Figures 5.47 and 5.48 show the freezing, thawing, and refreezing cycles at 1 GHz. The hystresis pattern observed earlier in Figs. 5.43 and 5.44 were apparently real but exagerated. The difference in level is, probably, due to loss of moisture during the experiment.

Experiment # 5

As mentioned earlier, the behavior of bound water in biological tissues is not well understood. This shortcoming is attributed, at least in part, to the following reasons:

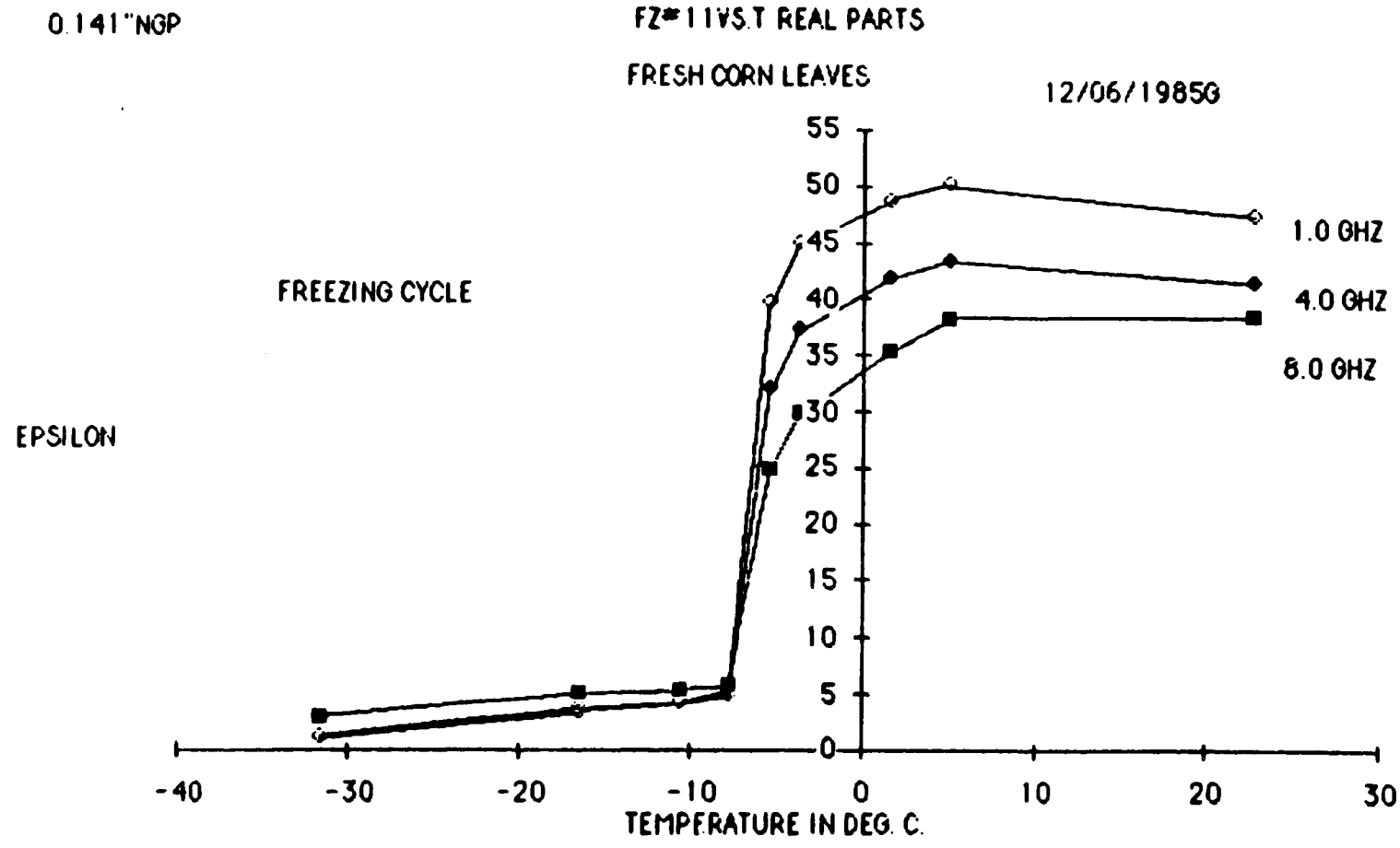

Figure 5.45. Measured dielectric constant versus temperature from -35^0C to $+30^0C$ with frequency as parameter for corn leaves (real parts). M_g(before) = 0.835 and M_g(after) = 0.781.

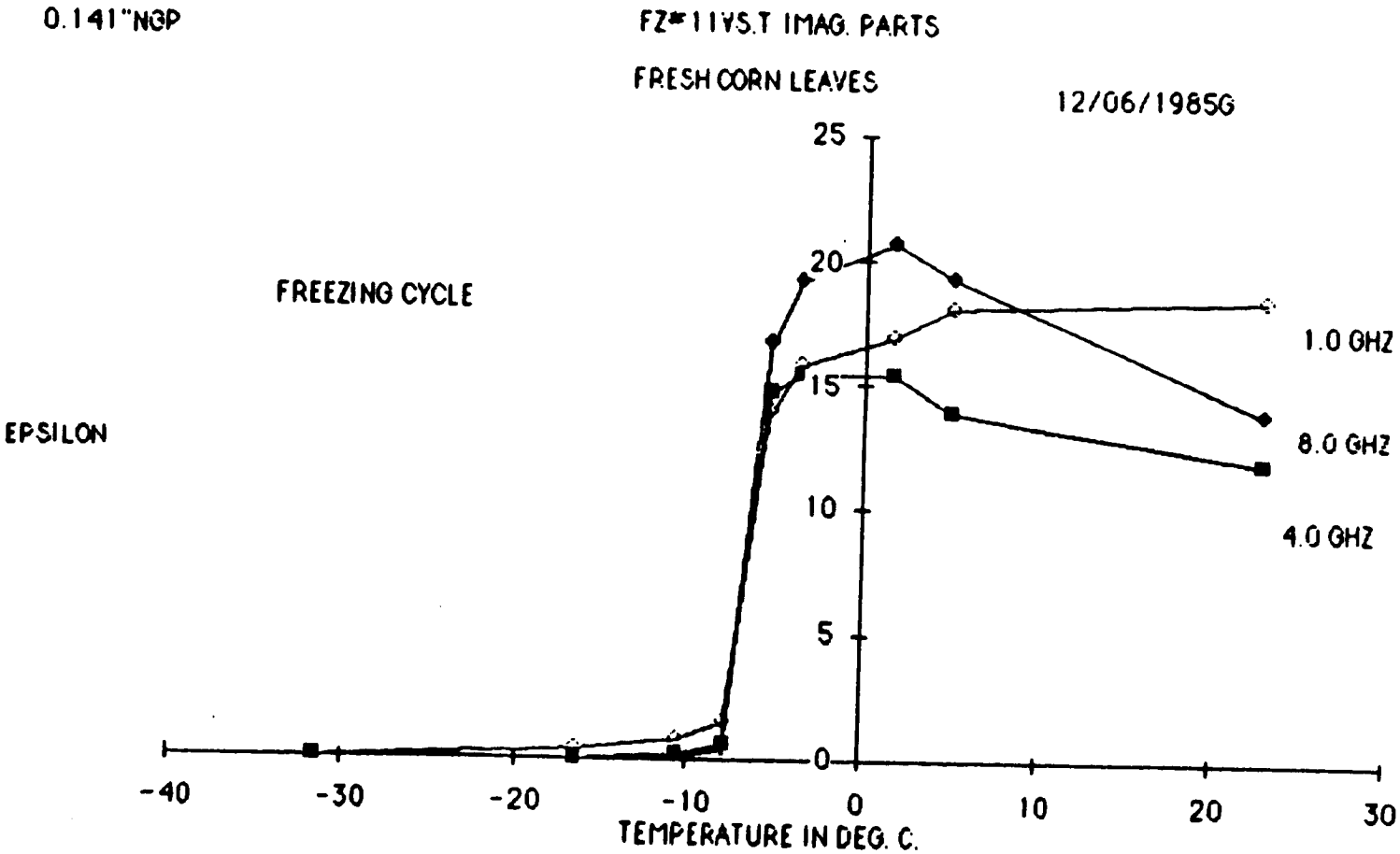

Figure 5.46. Measured dielectric constant versus temperature from -35^0C to $+30^0C$ with frequency as parameter for corn leaves (imaginary parts). M_g(before) = 0.835 and M_g(after) = 0.781.

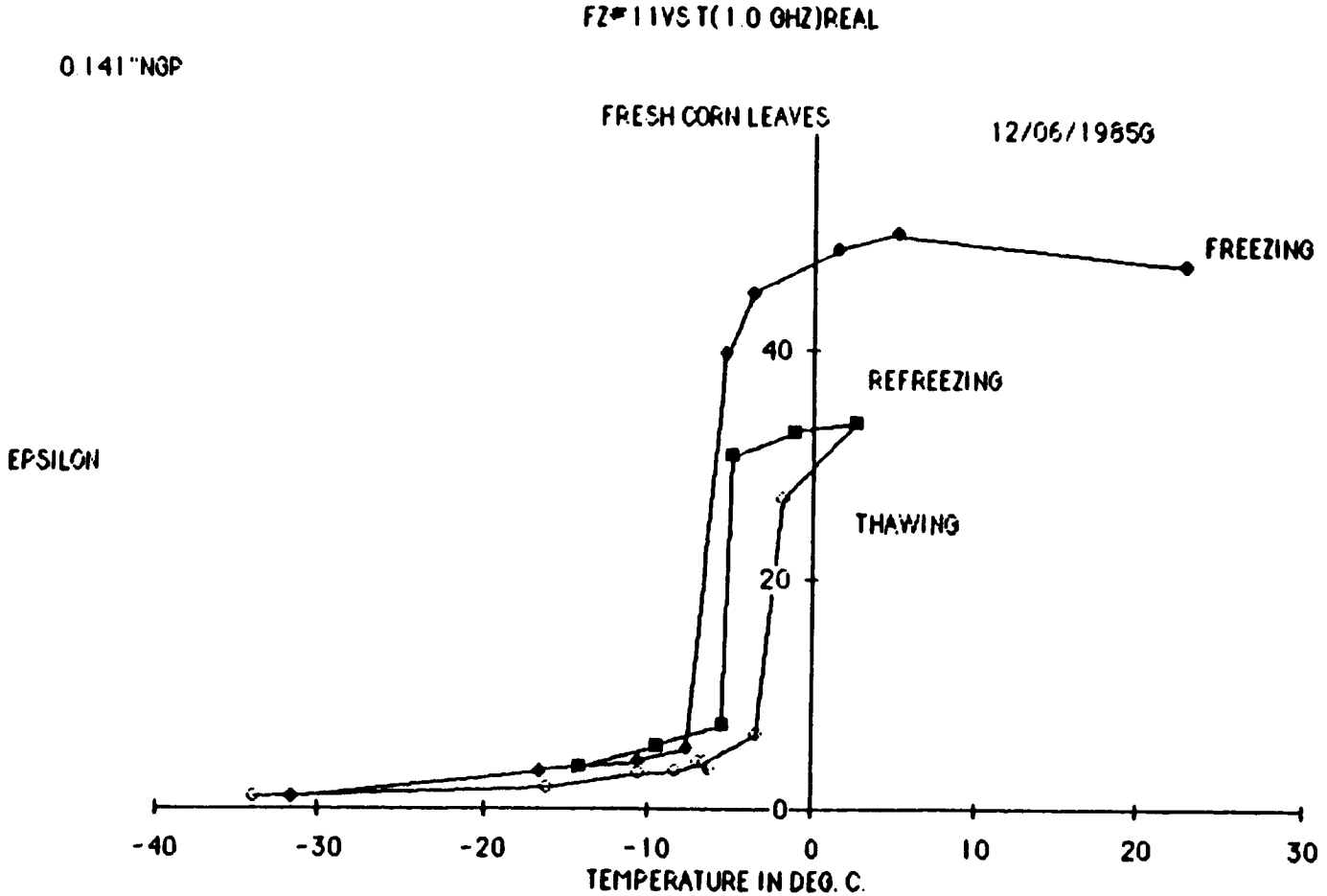

Figure 5.47. Measured dielectric constant versus temperature from -35^0C to $+30^0C$ at 1 GHz for corn leaves. A freezing-thawing-freezing cycle is shown for the real part.

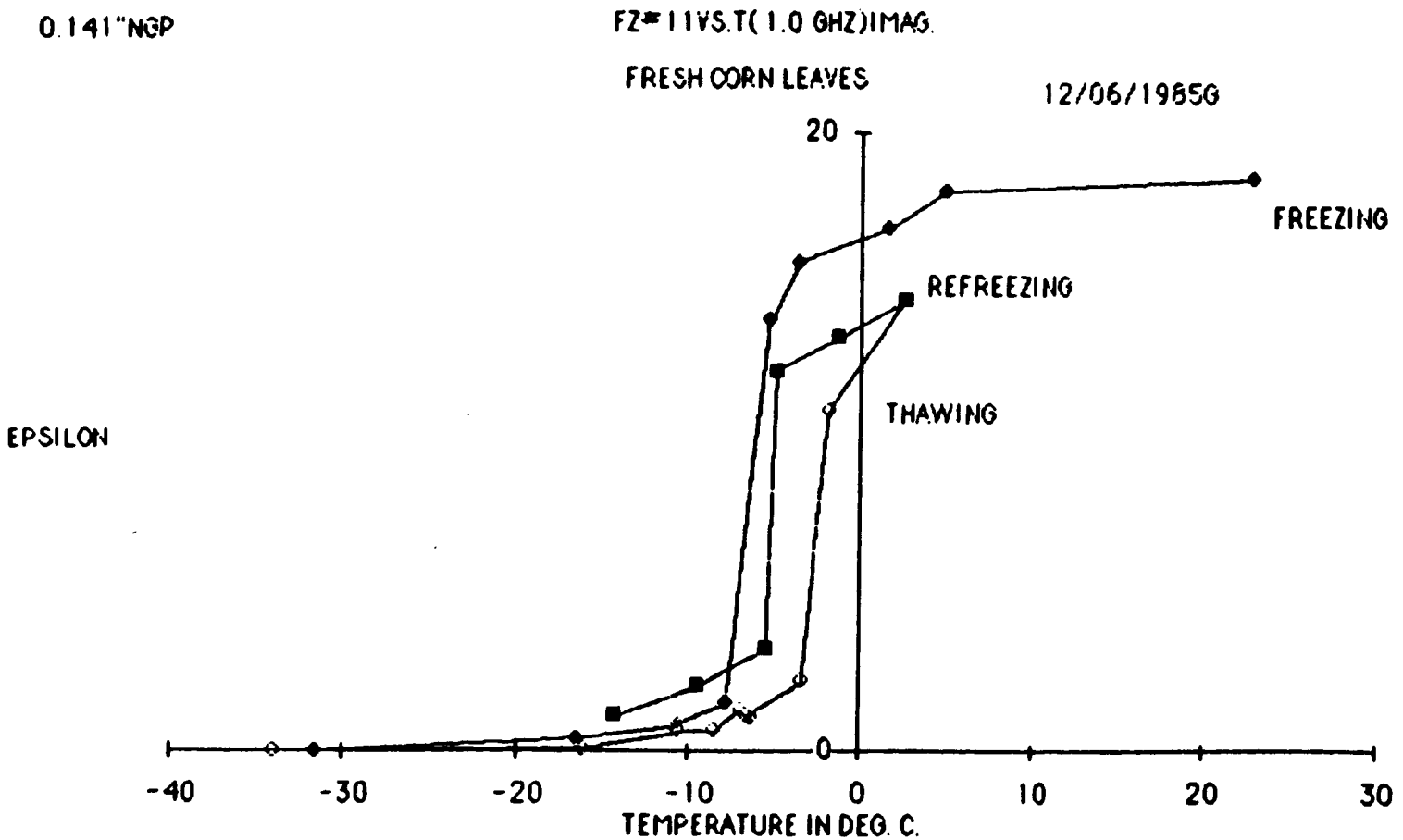

Figure 5.48. Measured dielectric constant versus temperature from -35^0C to $+30^0C$ at 1 GHz for corn leaves. A freezing-thawing-freezing cycle is shown for the imaginary part.

1. It is impossible to isolate or obtain pure bound water (otherwise it would not be bound), so we usually measure the combined properties of bound water, the binding surface material (e.g. sucrose), and other materials (e.g. free water) at the same time.

2. We do not know for sure whether bound water has unique properties, irrespect of the binding material, or not. So, measured properties for one material may not be generalized to others. For example, compare the spectrum of sucrose solution $\#B$ to that of starch sloution $\#X1$ (Table 5.9).

3. Bound water relaxation takes place at frequencies well below 1 GHz. Unfortunately, in this band losses due to ionic conductivity are very large, which makes it difficult to separate the two processes.

Our approach, as will become evident in Chapter 6, is to study the dielectric properties of bound water in sucrose solutions and assume that these properties represent bound water in plant materials. In order to study the temperature behavior of sucrose solutions, a concentrated solution was prepared (with v_F=0, v_B=.33, and v_S=.67) and it will be referred to as sucrose #9 (it is similar to sucrose $\#G$ that was reported in previous sections). Figures 5.49 and 5.50 show the temperature behavior of sucrose #9 as a function of T ($-15^0C \leq T \leq 55^0C$) for f= .2, .6, 1, and 1.9 GHz. The reason bound water was measured at these low frequencies is to be able to study its relaxation properties. Figure 5.49 shows that the real part has a monotonic increase with T. On the other hand, Fig. 5.50

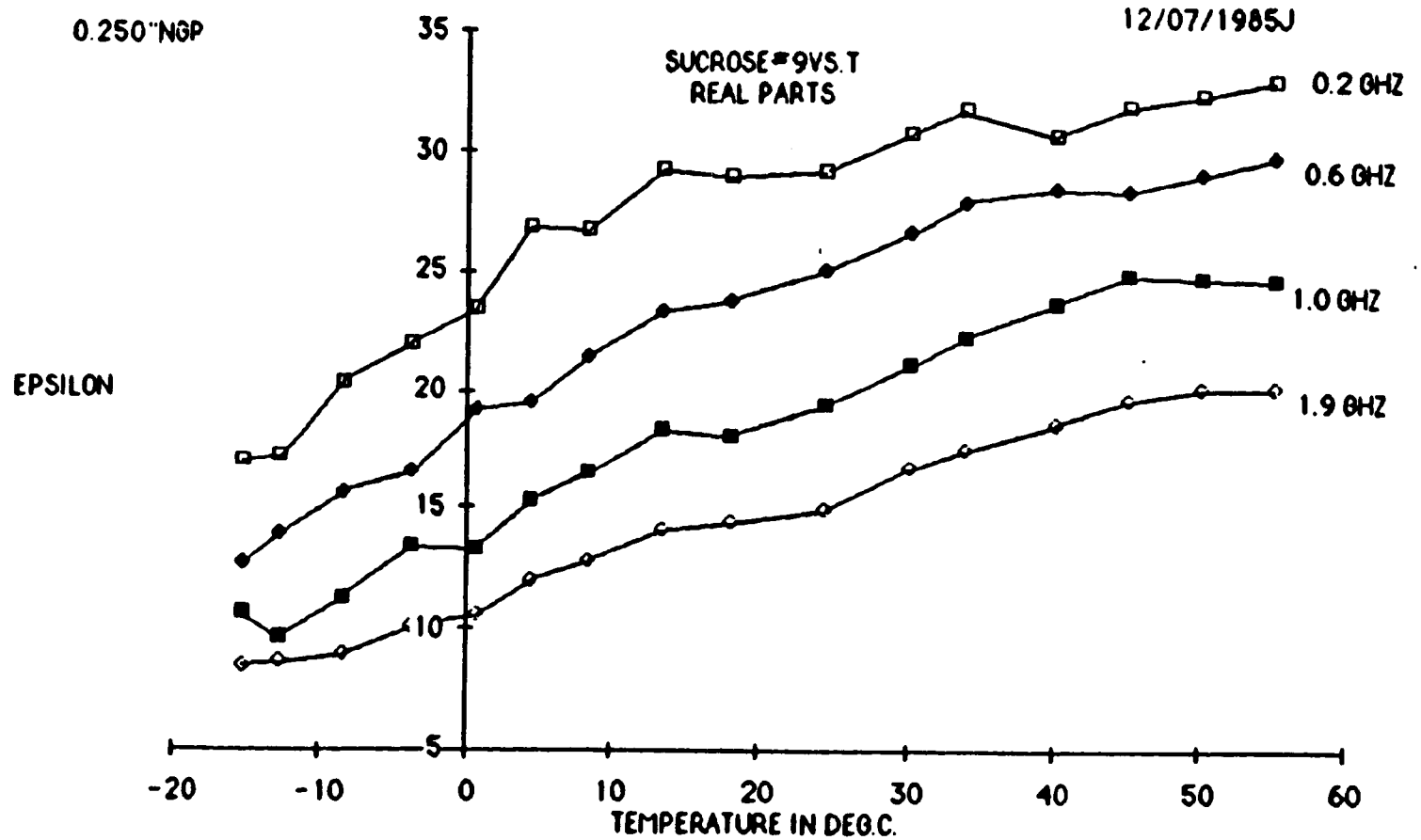

Figure 5.49. Measured dielectric constant versus temperature from -20^0C to $+50^0C$ with frequency as parameter for sucrose solution (#9 or G) for the real partrs.

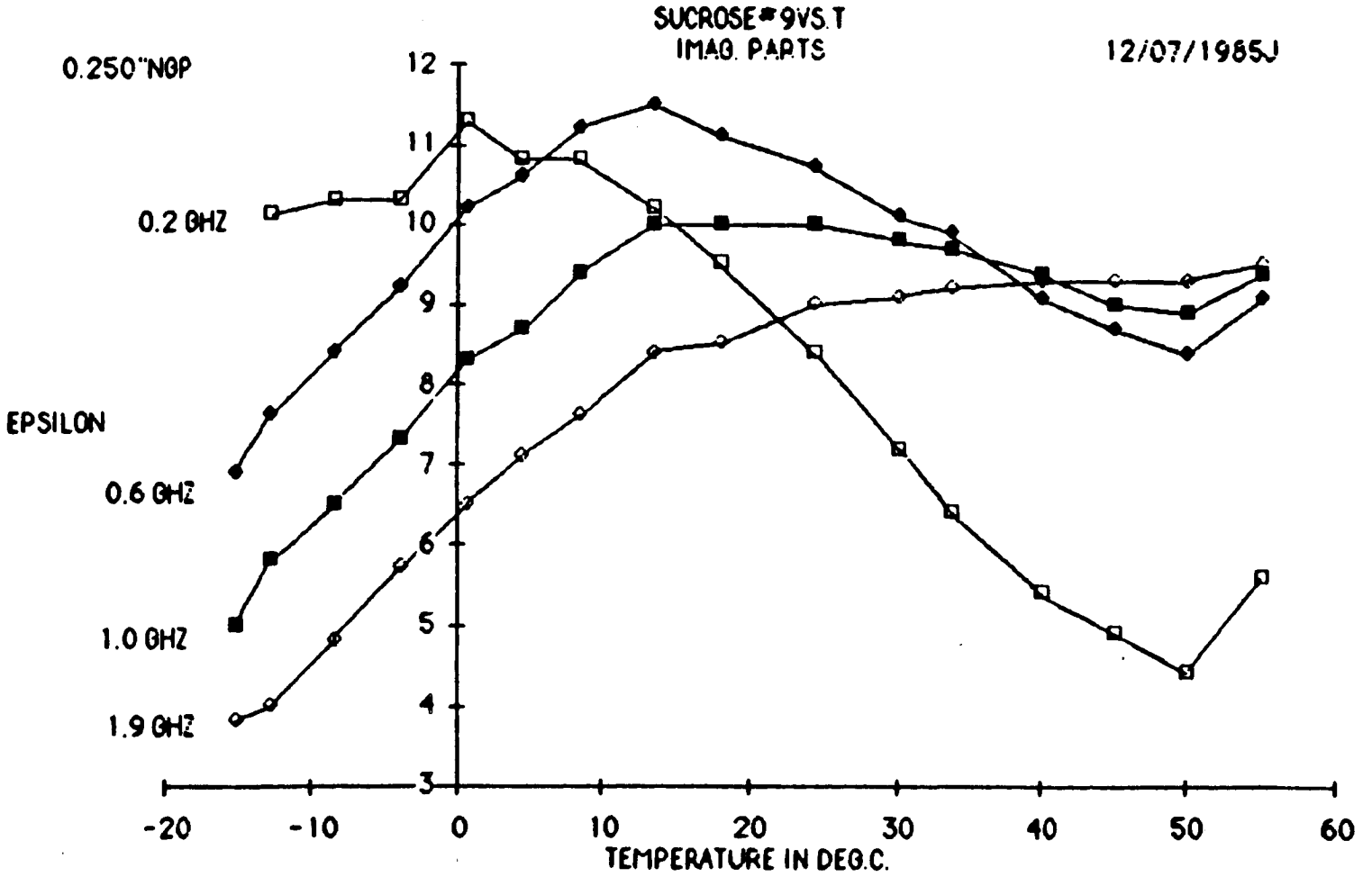

Figure 5.50. Measured dielectric constant versus temperature from -20^0C to $+50^0C$ with frequency as parameter for sucrose solution (#9 or G) for the imaginary partrs.

shows that the imaginary part has a peak at a frequency-dependent temperature, e.g. ϵ''(.2 GHz) peaks at 0^0C, ϵ''(.6 GHz) peaks at $+15^0C$, ϵ''(1 GHz) peaks at $+25^0C$, and ϵ''(1.9 GHz) peaks at $+55^0C$. In order to study the effects of deep freezing on sucrose solutions, another experiment was performed on sucrose #9 over the range $-80^0C \leq T \leq +30^0C$, and the results are shown in Fig. 5.51. It is interesting to note that there is no sharp freezing point discontinuity and that $\epsilon(T = -80^0C) = 6 - j0$.

5.7 Density Effects

A quantitative definition of density will be given in Chapter 6, and for the time being, the term density will be used in the qualitative sense. In order to compare the effects of density variations, we will need to compare either different parts of the same species (e.g. corn leaves and corn stalks) or the same parts from different species (e.g. corn stalks and Black Spruce tree wood). Comparison between corn leaves and corn stalks, at 1 GHz, is shown in Fig. 5.3. These two parts have similar dielectric properties except, perhaps, at the dry end. When M_g=0, corn stalks have a higher dielectric constant than corn leaves. Comparison between the dielectric constants of corn stalks and the trunk of a Black Spruce tree at 2 GHz are shown in Fig. 5.53. There are obvious differences in the general trend, but again ϵ' at M_g=0 is larger for the tree sample, which has a higher density. The density effects are not well understood because it is very hard to measure the density, especially that of a leaf, accurately.

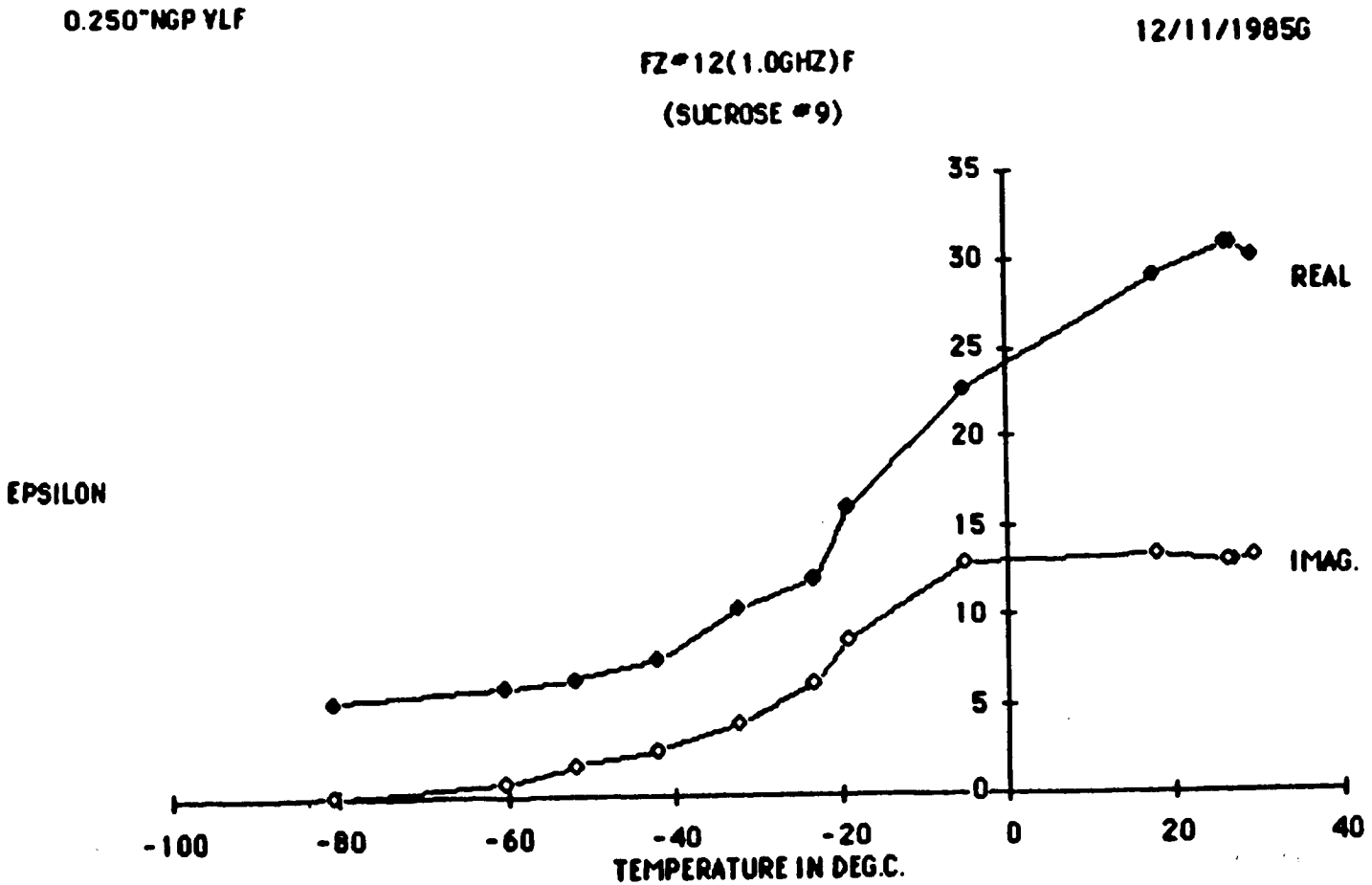

Figure 5.51. Measured dielectric constant versus temperature from -80^0C to $+30^0C$ at 1 GHz for sucrose solution (#9 or G). The measured solution in this case is not exactly (#9 or G) because of solid sucrose precipitation at low temperatures.

Measurements conducted on a poplar tree trunk showed large variations between measured ϵ at various parts on the trunk cross section. It was observed that ϵ increases inwardly while the moisture content (M_g) was found to be constant. The only explanation of this phenomena is density variations of wood from one ring to the other, increasing in density inwardly. Table 5.11 shows a summary of the results at 1 and 5 GHz, respectively.

f(GHz)	location	ϵ'	ϵ''	tan(δ)	M_g
1	bark(side)	7.5	1.3	.173	.48
1	bark(section)	17.73	5.07	.286	.48
1	first ring	23.17	4.7	.203	.49
1	second ring	21.95	6.01	.274	.50
1	central ring	32.8	8.3	.253	.50
1	average	20.63	5.08	.246	.49
5	bark(side)	7.1	1.5	.211	.48
5	bark(section)	14.4	5.5	.382	.48
5	first ring	20.3	6.9	.340	.49
5	second ring	19	6.7	.353	.50
5	central ring	29.2	10	.343	.50
5	average	18	6.1	.339	.49

Table (5.11): Measured data for Poplar tree trunk at 1 and 5 GHz.

Chapter 6

Modeling Efforts

In order to model the dielectric properties of vegetation parts, e.g. leaves, we must first examine: (i) the dielectric properties of the vegetation constituents, (ii) their volume fractions, and (iii) the proper mixing formula by which the information from (i) and (ii) may be combined to calculate the dielectric of the mixture ϵ. These pieces of information will be discussed separately in Sections 6.1 to 6.3.

Section 6.3 contains the results of different physical, semi-empirical, and empirical models. Also, the use of statistical regression to model the dielectric behavior of vegetation independent of plant type or part is considered. No attempt will be made to model the temperature dependence of the dielectric constant of vegetation; such a development would require further work, both experimentally and analytically.

6.1 Liquid Water Dielectric Properties

6.1.1 Distilled Water

For pure water, it is assumed that the ionic conductivity is zero which means that there are no free ions to contribute to the total loss (especially at low frequencies). The frequency dependence is given by the Debye equations (2.13)-(2.15):

$$\epsilon_w^* = \epsilon_{w\infty} + \frac{\epsilon_{ws} - \epsilon_{w\infty}}{1 + j\omega\tau} \tag{6.1}$$

where ϵ_{ws} and $\epsilon_{w\infty}$ are the static and optical limit of the dielectric constant of liquid water, respectively, and τ is the relaxation time constant.

The importance of liquid water at microwave frequencies stems from the fact that its relaxation frequency ($f_w = 1/2\pi\tau$) lies in the microwave band. For example,

$$f_w(0^0C) \simeq 9\text{GHz} \tag{6.2}$$

and

$$f_w(20^0C) \simeq 17\text{GHz} \tag{6.3}$$

6.1.2 Saline Water

A saline solution is defined as a solution that contains free ions, whether or not these ions are organic in nature. The salinity, S, of a solution is defined as the total mass of dissolved solid salts in grams in one kilogram of solution. An equivalent Debye-like equation could be used to represent saline solutions in the

following modified form

$$\epsilon'_{sw} = \epsilon_{sw\infty} + \frac{\epsilon_{sws} - \epsilon_{sw\infty}}{1 + (\frac{f}{f_{sw0}})^2} \tag{6.4}$$

and

$$\epsilon''_{sw} = \frac{(\epsilon_{sws} - \epsilon_{sw\infty})(\frac{f}{f_{sw}})}{1 + (\frac{f}{f_{sw}})^2} + \frac{\sigma_i}{2\pi\epsilon_0 f} \tag{6.5}$$

where the subscript sw refers to saline water, σ_i is the ionic conductivity in $Siemens/m$, and ϵ_0 is the free space dielectric constant ($\epsilon_0 = 8.854 \times 10^{-12} f/m$).

6.1.3 Temperature Effects

For any relaxation process, temperature affects $\epsilon_s, \epsilon_\infty, and\ f_0$. However, the change in ϵ_∞ is negligible, that in ϵ_s is small, and that in f_0 is of major importance. Referring to Sec. 2.1.1, we can write Eq. (2.18) to (2.20) as

$$\tau = A \exp(\frac{\Delta H}{RT}) \tag{6.6}$$

$$\frac{\partial(\ln \tau)}{\partial(\frac{1}{T})} = \frac{\Delta H}{R} \tag{6.7}$$

$$\tau = \frac{h}{KT} \exp(\frac{-\Delta S}{R}) \exp(\frac{\Delta H}{RT}) \tag{6.8}$$

where the notation used here is the same as elsewhere in this text. Referring to (Ulaby et al, 1986), we can write the equations for liquid water as a function of temperature (^0C) and salinity (ppt) as:

$$\epsilon_\infty = 4.9 (\simeq independent\ of\ temperature\ and\ salinity), \tag{6.9}$$

$$2\pi\tau_w(T) = 1.1109 \times 10^{-10} - 3.824 \times 10^{-12}T + 6.938 \times 10^{-14}T^2 - 5.096 \times 10^{-16}T^3, \tag{6.10}$$

$$\epsilon_{w0}(T) = 88.045 - 0.4147T + 6.295 \times 10^{-4}T^2 + 1.075 \times 10^{-5}T^3, \tag{6.11}$$

$$\epsilon_{sw0}(T, S_{sw}) = \epsilon_{sw0}(T, 0)a(T, S_{sw}), \tag{6.12}$$

$$\epsilon_{sw0}(T, 0) = 87.134 - 1.949 \times 10^{-1}T - 1.276 \times 10^{-2}T^2 + 2.491 \times 10^{-4}T^3, \tag{6.13}$$

$$a(T, S_{sw}) = 1.0 + 1.613 \times 10^{-5}TS_{sw} - 3.656 \times 10^{-3}S_{sw} + 3.210 \times 10^{-5}S_{sw}^2 - 4.232 \times 10^{-7}S_{sw}^3, \tag{6.14}$$

$$\tau_{sw}(T, S_{sw}) = \tau_{sw}(T, 0)b(T, S_{sw}), \tag{6.15}$$

$$b(T, S_{sw}) = 1.0 + 2.282 \times 10^{-5}TS_{sw} - 7.638 \times 10^{-4}S_{sw} - 7.760 \times 10^{-6}S_{sw}^2 + 1.105 \times 10^{-8}S_{sw}^3, \tag{6.16}$$

$$\sigma_i(T, S_{sw}) = \sigma_i(25, S_{sw}) \exp -\phi, \tag{6.17}$$

$$\sigma_i(25, S_{sw}) = S_{sw}[0.18252 - 1.4619 \times 10^{-3} S_{sw} + 2.093 \times 10^{-5} S_{sw}^2 - 1.282 \times 10^{-7} S_{sw}^3], \tag{6.18}$$

$$\Delta = 25 \; - \; T, \tag{6.19}$$

and

$$\phi = \Delta[2.033 \times 10^{-2} + 1.266 \times 10^{-4}\Delta + 2.464 \times 10^{-6}\Delta^2$$

$$- S_{sw}(1.849 \times 10^{-5} - 2.551 \times 10^{-7}\Delta + 2.551 \times 10^{-8}\Delta^2)]. \tag{6.20}$$

6.1.4 Bound Water

According to the results presented in Chapter 5, the Cole-Cole equation provides a reasonable fit to the dielectric data measured for sucrose. The Cole-Cole equation is given by

$$\epsilon_b = \epsilon_{\infty b} + \frac{\epsilon_{sb} - \epsilon_{\infty b}}{1 + (jf/f_{0b})^{(1-\alpha_b)}} \tag{6.21}$$

where α_b is a Cole-Cole relaxation parameter. For the volume fractions v_b =.33, v_f =0, and v_s =.67, the relaxation parameter was found to be α_b =.5, f_{0b} =.178, $\epsilon_{\infty b}$ =2.9, and ϵ_{sb} =59, in which case (6.21) may be rewritten in the following form:

$$\epsilon_b' = \epsilon_{\infty b} + \frac{(\epsilon_{sb} - \epsilon_{\infty b})(1 + \sqrt{\frac{f}{2f_{0b}}})}{1 + 2\sqrt{\frac{f}{2f_{0b}}} + 2(\frac{f}{2f_{0b}})} \tag{6.22}$$

$$\epsilon_b'' = \frac{(\epsilon_{sb} - \epsilon_{\infty b})\sqrt{\frac{f}{2f_{0b}}}}{1 + 2\sqrt{\frac{f}{2f_{0b}}} + 2(\frac{f}{2f_{0b}})}. \tag{6.23}$$

The assumption made in this chapter is that the dielectric properties of the sucrose solutions may be generalized to other materials, e.g., other carbohydrates and starches. As discussed earlier in Chapter 5, this assumption is not always valid, but in the absence of detailed information about the dielectric properties of all of the major organic and inorganic constituents of vegetation material, the assumption shall be considered adequate for the time being.

6.1.5 Temperature Effects (Bound Water)

The temperature measurements conducted for sucrose solutions were discussed in Sec. 5.6 (experiment#5) and the results were shown in Fig. (5.49) to (5.50) . This data will now be used to model the temperature-dependence of the parameters in the Cole-Cole equation. From $f_{0b} = 1/2\pi\tau$ and Eq.(6.8),

$$\tau = \frac{h}{KT} \exp(\frac{-\Delta S}{R}) \exp(\frac{\Delta H}{RT}), \tag{6.24}$$

we can write

$$f_{0b} = A_f T \exp \frac{-B_f}{T}, \tag{6.25}$$

where $A_f = \frac{K}{h} \exp \frac{\Delta s}{R}$, $B_f = (\frac{\Delta H}{R})$, and T is in K.

A linear model was assumed for ϵ_s, ϵ_∞, and α_b as follows:

$$\epsilon_s = A_s + B_s T, \tag{6.26}$$

$$\epsilon_\infty = A_\infty + B_\infty T, \tag{6.27}$$

and

$$\alpha_b = A_\alpha + B_\alpha T. \tag{6.28}$$

Using regression techniques (BMDP software library), the constants were estimated and the model can be represented by:

$$\epsilon_b(f,T) = \epsilon_{\infty b}(T) + \frac{\epsilon_{sb}(T) - \epsilon_{\infty b}(T)}{1 + [jf/f_{0b}(T)]^{1-\alpha_b(T)}}, \tag{6.29}$$

$$\epsilon_{sb}(T) = 35.461 + 0.262T(^0C), \tag{6.30}$$

$$\epsilon_{\infty b}(T) = 6.457 - 0.146T(^0C), \tag{6.31}$$

$$\alpha_b(T) = 0.207 + 0.007T(^0C), and \tag{6.32}$$

$$f_{0b}(T) = 1.296T(K) \exp \frac{-1882.238}{T(K)}. \tag{6.33}$$

An evaluation of the overall accuracy of this model was performed and the results are given in Table 6.1.

The quantities in the table are:

$RSS \equiv$ *Residual sum of squares*,

$EMSE \equiv$ *Estimated Mean Square Error*,

$N \equiv$ *number of data points*,

$\rho \equiv$ *correlation coefficient*,

$b \equiv$ *intercept(scatter plot)*,

$a \equiv$ *slope(scatter plot)*,

where, for a given variable X, a and b have the following meaning:

$$X(predicted) = aX(observed) + b. \tag{6.34}$$

For sucrose solution #9, the frequency range was .2GHz< f < 2GHz, the temperature range was $-6^0C < T < 30^0C$, and the volume fractions were: $v_s = .67$, $v_b = .33$, and $v_f = 0$.

	RSS	$EMSE$	N	ρ	b	a
ϵ'	340.1	1.447	237	.984	-.090	1.005
ϵ''	114	.494	237	.932	.688	.904

Table (6.1) Statistics associated with the regression fits given by (6.30) to (6.33).

The strategy used in this optimization procedure, similar to that used elsewhere in this chapter, was to rely on the fact that the model is more sensitive to ϵ'' than it is to ϵ'. Six parameters were optimized using the ϵ'' data; they are $A_f, B_f, A_s, B_s, A_\alpha, and\ B_\alpha$. Then, A_∞ and B_∞ were optimized using the ϵ' data and the other six parameter values already determined. The relaxation parameters calculated from the equations given in this section at room temperature should match those for sucrose#9. The fact that they do not quite match may be due to a slight change in the sucrose solution concentration.

The overall fit is reasonably adequate for our purposes but a more elaborate model may be needed for future work.

6.2 Volume Fraction Calculations

6.2.1 Assumptions and Definitions

The density measurement of plant materials is, in general, tedious and inaccurate. Furthermore, the density of the bulk vegetation material with no air present is not known. So, certain assumptions have to be made in order to model the vegetation medium. The most important assumption is the one related to the question of whether or not vegetation material shrinks in volume when it loses water. For a material like a corn leaf, the assumption is made that the volume occupied by the bulk vegetation and by air is independent of the moisture content of the leaf, and that when a leaf loses moisture, its volume shrinks by the volume of the lost water.

Some of the terms used in this chapter need to be defined, although some of them were used in earlier chapters with or without proper definition.

The gravimetric moisture (wet basis) M_g may be determined from knowledge of the wet weight of the plant sample W_v and its dry weight W_d,

$$M_g = \frac{(W_v - W_d)}{W_v}. \tag{6.35}$$

The vegetation density (wet basis) ρ_v can be determined by measuring the weight W_v and the volume V_v of the vegetation sample, $\rho_v = W_v/V_v$. The volume may be determined using a displacement technique in which the leaf is inserted in an oil bath and the increase in volume is measured (McKinley, 1983).

The volumetric moisture (wet basis) M_v is given by

$$M_v = M_g \rho_v. \tag{6.36}$$

The dry vegetation density ρ_{DV} is the density of the dry material and is usually less than 1 g/cm^3.

The bulk vegetation density ρ_{BV} is the bulk density of the vegetation material without air.

In the next section, we shall derive expressions for the various volume fractions used in the dielectric models in Sections 6.3. These and related quantities are defined as follows:

$\eta \equiv \frac{\rho_{DV}}{\rho_{BV}}$,

$v_v(Max) \equiv$ volume fraction of solid vegetation,

$v_b(Max) \equiv$ maximum volume fraction that bound water can occupy,

$v_v \equiv$ volume fraction of solid vegetation that actually binds some water,

$v_{vr} \equiv$ volume fraction of solid vegetation that does not bind any water $0 \leq v_v \leq v_v(Max)$,

$v_b \equiv$ volume fraction of bound water,

$v_f \equiv$ volume fraction of free water,

$v_a \equiv$ volume fraction of air, and

$v_{vb} \equiv$ volume fraction of the total vegetation-bound water mixture$(= v_b + v_v)$.

6.2.2 Volume Fractions For a Sample That Shrinks

Volumetric moisture can be derived for a vegetation sample with known M_g and ρ_{DV} as follows:

$$M_g = \frac{water\ weight}{total\ weight} = \frac{water\ weight}{water\ weight + dry\ vegetation\ weight} \tag{6.37}$$

Since the density of water is $1g/cm^3$,

$$M_g = \frac{water\ volume}{water\ volume + \rho_{DV}(total\ volume - water\ volume)} \tag{6.38}$$

or,

$$M_g = \frac{M_v}{M_v + \rho_{DV}(1 - M_v)}, \tag{6.39}$$

from which we can obtain:

$$M_v = \frac{M_g}{M_g + \frac{1-M_g}{\rho_{DV}}} \tag{6.40}$$

This expression was used throughout this text to calculate M_v. The other relevant expressions are:

$v_v(Max) = \eta(1. - M_v)$,

$v_b(Max) = \frac{v_v(Max)}{x}$, where $x = 2$ for sucrose solutions and may vary for different materials(see Sec. 6.2.4); this formulation implies that water exists only as bound water for gravimetric moisture equal to or less than .2 and that bound water can not exceed this value,

$v_b = v_b(Max)$ if $M_v \geq v_b(Max)$,

$v_b = M_v$ if $M_v \leq v_b(Max)$,

$v_f = M_v - v_b$,

$v_v = xv_b$,

$v_{vb} = v_v + v_b$,

$v_a = 1 - v_v(Max) - M_v$, and

$v_{vr} = v_v(Max) - v_v$.

Figures (6.1) to (6.3) were calculated assuming $\rho_{DV} = .33\ g/cm^3$, $\rho_{BV} = 1.60\ g/cm^3$, and $x = 2$. Figure (6.1) shows $v_a, v_f, v_b, and\ v_v$ plotted versus M_g; figure (6.2) shows $M_v, v_f, v_b, and\ v_v$ plotted versus M_g; and Fig. (6.3) shows $M_v, v_v, v_{vr}, and\ v_v(Max)$ plotted versus M_g.

6.2.3 Volume Fractions For a Sample That Does Not Shrink

In this case, when the sample loses water (due to evapotranspiration), an equal volume of air is acquired (may be through the pores). The volume of the sample stays constant throughout the drying process. This situation does not seem realistic, but the shrinking assumption may not be exact either, and the actual case probably lies somewhere between these two limits. Again the volumetric moisture can be derived from M_g and ρ_{DV} as follows:

$$M_g = \frac{water\ weight}{total\ weight} = \frac{water\ weight}{water\ weight + dry\ vegetation\ weight} \tag{6.41}$$

but the weight of dry vegetation is constant (independent of moisture, since the volume fraction of the bulk vegetation, v_v, does not change), and dry vegetation weight $= \rho_{BV} v_v = \rho_{DV}$ hence,

$$M_g = \frac{water\ volume}{water\ volume + \rho_{BV}(bulk\ vegetation\ volume)} \tag{6.42}$$

Again, by dividing by the total volume, we will get

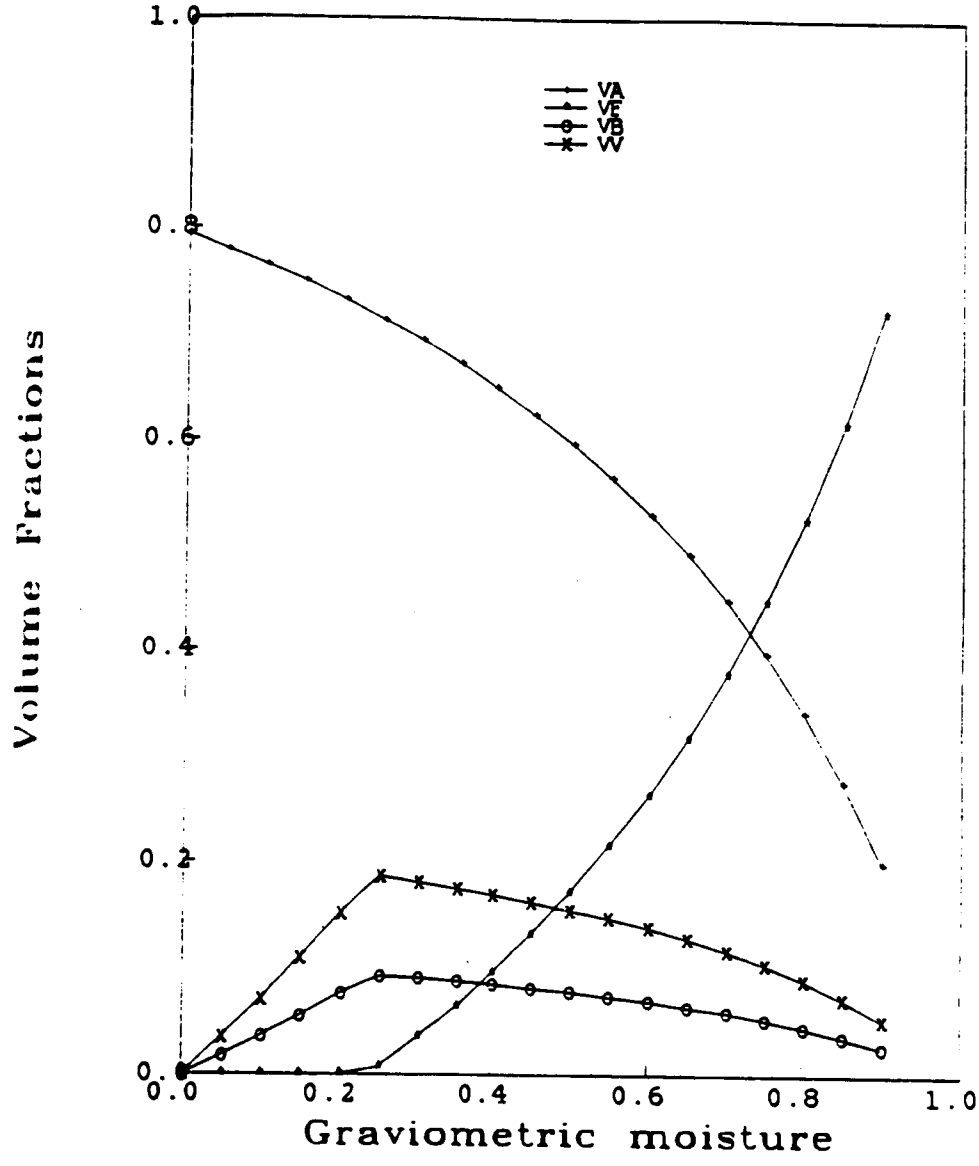

Figure 6.1. Calculated volume fractions for a vegetation sample that shrinks. V_a, V_f, V_b, and V_v are the volume fractions of air, free, bound water, and bulk vegetation material that binds water, respectively.

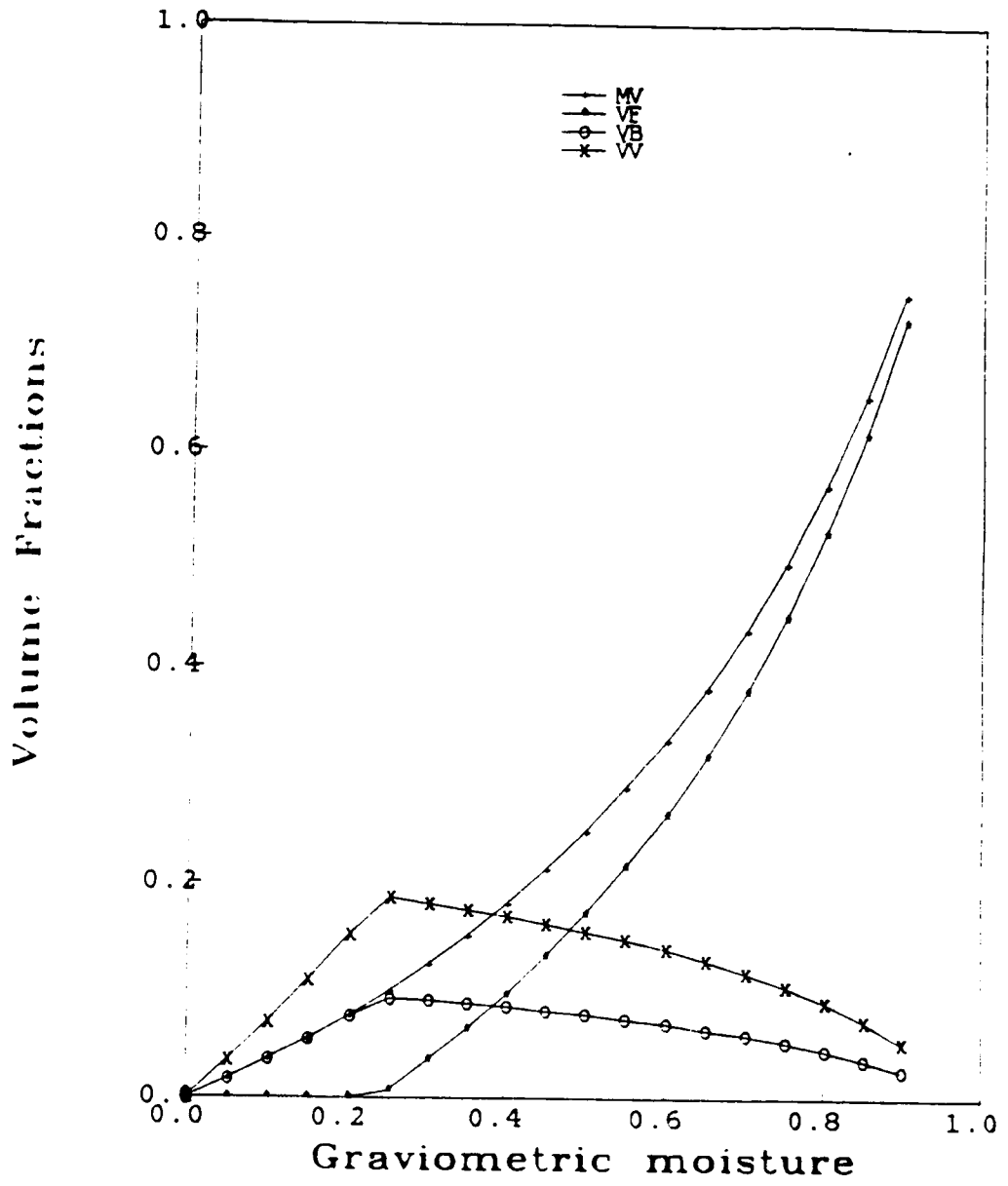

Figure 6.2. Calculated volume fractions for a vegetation sample that shrinks. M_v, V_f, V_b, and V_v are the volume fractions of water, free water, bound water, and bulk vegetation material that binds water, respectively.

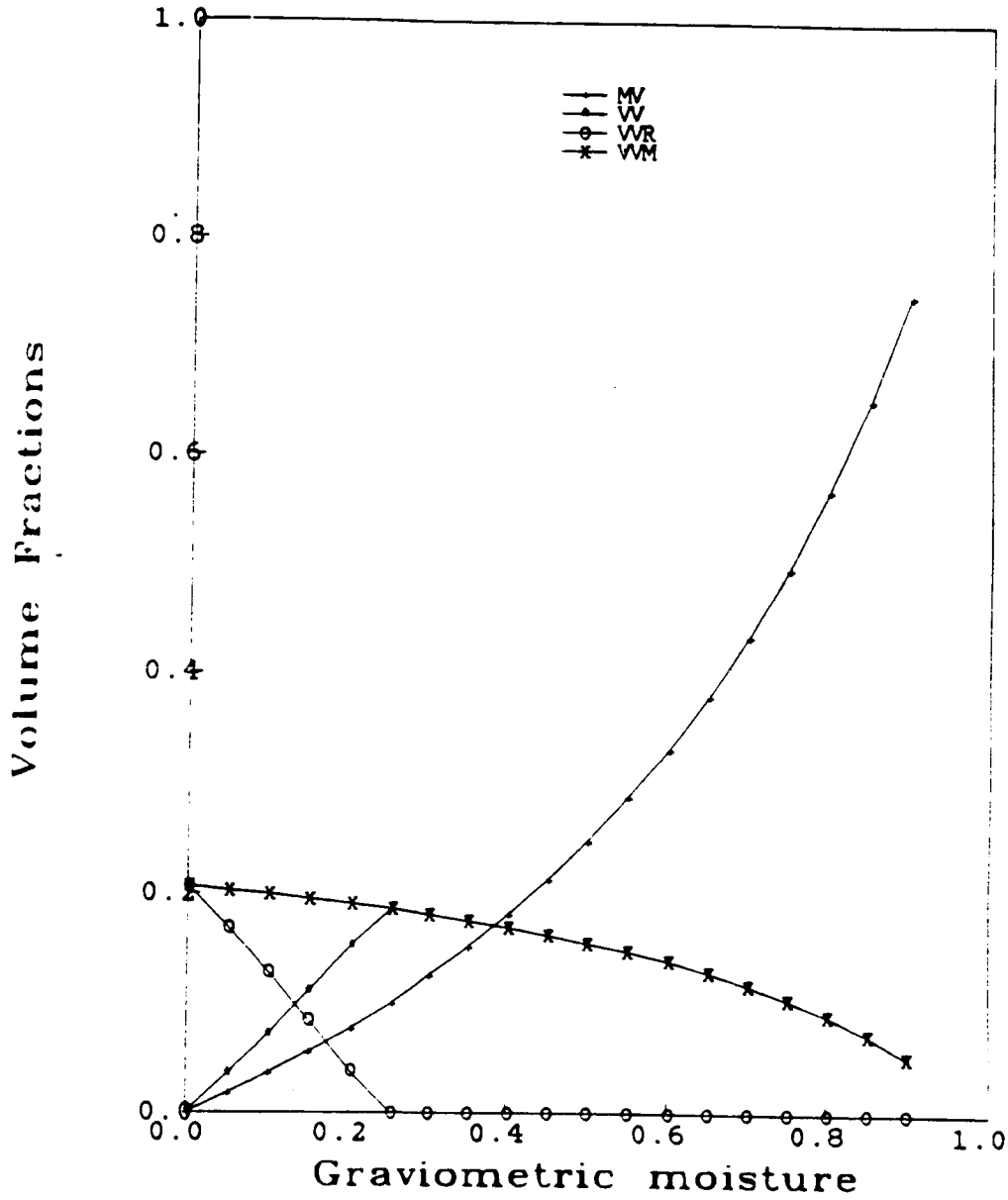

Figure 6.3. Calculated volume fractions for a vegetation sample that shrinks. M_v, V_v, V_{vr}, and V_{vm} are the volume fractions of water, bulk vegetation material that binds water, remaining bulk material that does not bind water, and the total or maximum bulk material, respectively.

$$M_g = \frac{M_v}{M_v + \rho_{DV}}, \tag{6.43}$$

and M_v will be,

$$M_v = \frac{M_g \rho_{DV}}{1 - M_g}. \tag{6.44}$$

The expressions given previously for $v_b(Max)$, v_b, v_f, v_v, v_{vb}, v_a, and v_{vr} remain unchanged; the only changes are:

1. M_g has an upper limit, $M_g(Max) = \frac{1}{1+\rho_{DV}}$, and

2. $v_v(Max) = \eta$.

Figures (6.4) to (6.6) were calculated assuming $\rho_{DV} = .33\ g/cm^3$, $\rho_{BV} = 1.60\ g/cm^3$, and $x = 2$. Figure (6.4) shows $v_a, v_f, v_b, and\ v_v$ plotted versus M_g; figure (6.5) shows $M_v, v_f, v_b, and\ v_v$ plotted versus M_g; and Fig. (6.6) shows $M_v, v_v, v_{vr}, and\ v_v(Max)$ plotted versus M_g.

6.2.4 Volume Fractions For Sucrose solutions

As discussed earlier in Sec. 5.5, the volume fractions for a sucrose solution of $S(g)$ sucrose and $W(g)$ water are given by:

$X = \frac{S}{W}$,

$A\% = \frac{100S}{S+W} = \frac{100X}{X+1}$,

from The Chemistry Handbook (1986), the density $\rho(g/cm^3)$ is tabulated in terms of $A\%$,

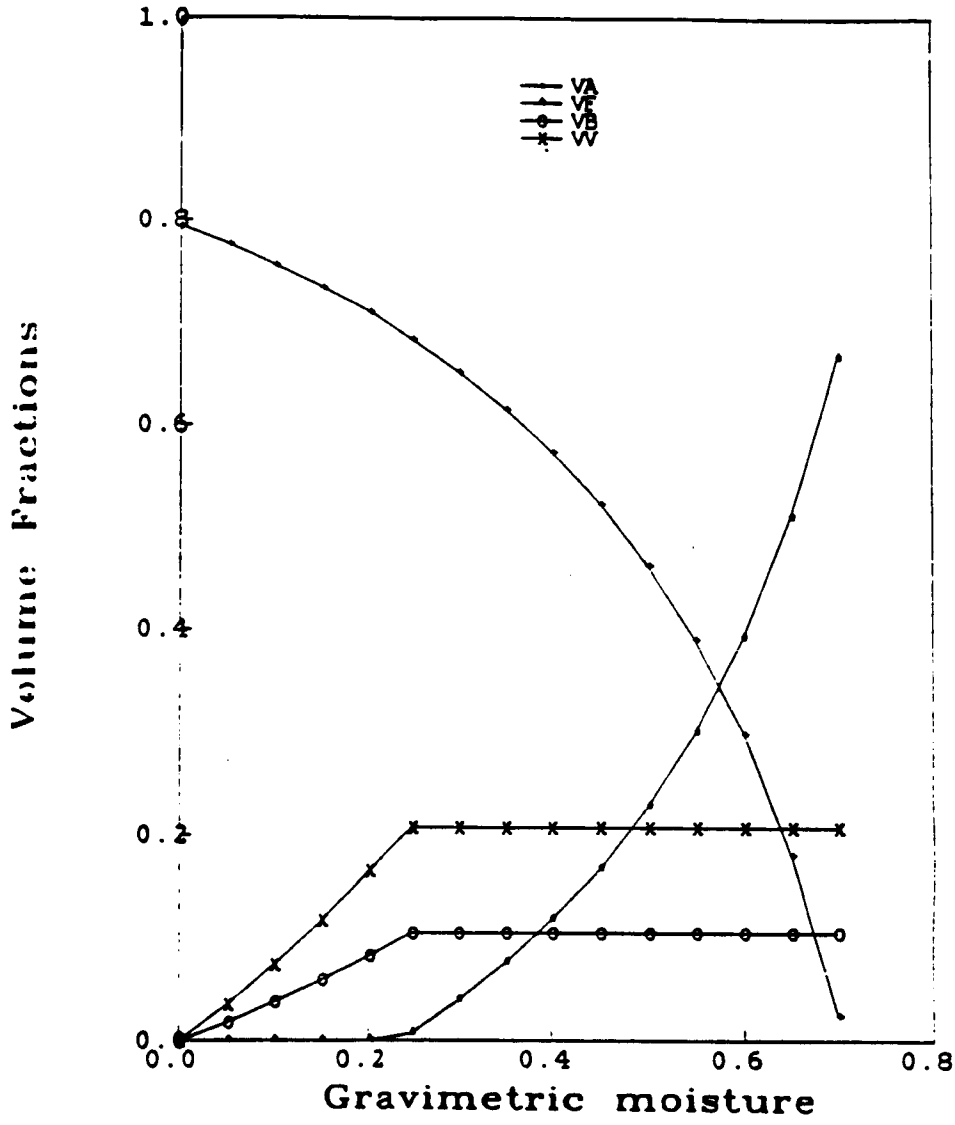

Figure 6.4. Calculated volume fractions for a vegetation sample that does not shrink. V_a, V_f, V_b, and V_v are the volume fractions of air, free, bound water, and bulk vegetation material that binds water, respectively.

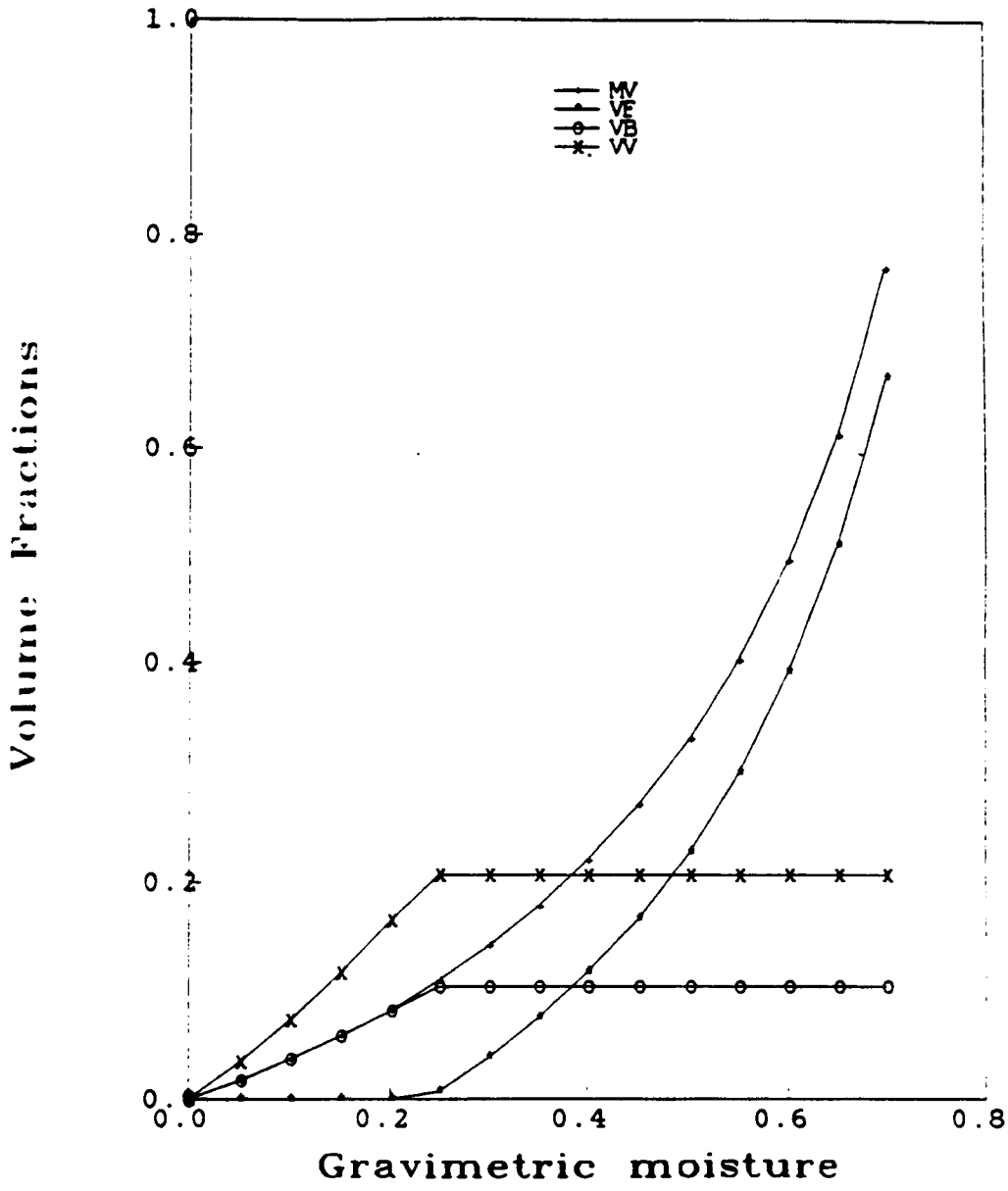

Figure 6.5. Calculated volume fractions for a vegetation sample that does not shrink. M_v, V_f, V_b, and V_v are the volume fractions of water, free water, bound water, and bulk vegetation material that binds water, respectively.

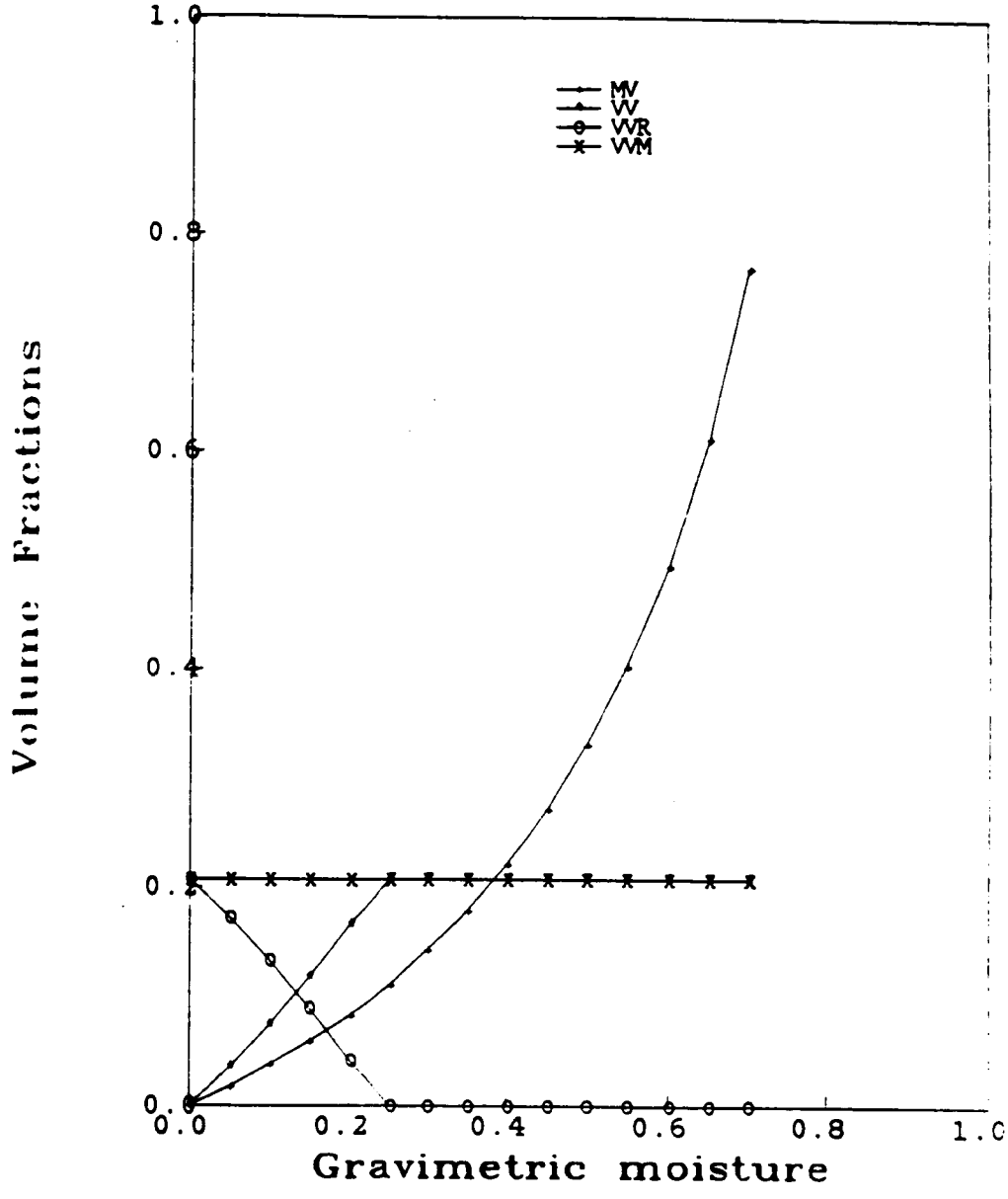

Figure 6.6. Calculated volume fractions for a vegetation sample that does not shrink. M_v, V_v, V_{vr}, and V_{vm} are the volume fractions of water, bulk vegetation material that binds water, remaining bulk material that does not bind water, and the total or maximum bulk material, respectively.

$V_s = \frac{S-W(\rho-1)}{\rho}(cm^3)$,

$V_w = W(cm^3)$,

$v_s = \frac{V_s}{V_s+V_w}$,

$v_w = \frac{V_w}{V_s+V_w}$,

$v_b = v_w(\frac{6}{19})X$, and

$v_f = v_w(1-\frac{6}{19})X$.

Table 5.8 shows these volume fractions for different solution concentrations. We observe that the ratio $\frac{v_s}{v_b}$ is always a constant, approximately equal to 2.

6.3 Models

6.3.1 DeLoor's model, Discs, and $\epsilon^* = \epsilon_m$

As discussed in Sec. 2.2.1, DeLoor's mixing model depends on the following parameters: (1) the depolarization factors, A_i, of the included particles, and (2) ϵ^*, the effective relative dielectric constant near an inclusion-host boundary.

According to Tan (1981), DeLoor's model with parameters $\epsilon^* = \epsilon_h$ and $A_i = (0,0,1)$ provides a good fit when compared with the measured data for grass samples. He treated vegetation as a two component mixture consisting of dry vegetation and free water. Tan's data set, however, was limited to single-frequency measurements made at 9.5 GHz. For this study, we shall assume that vegetation materials consist of four components: (1) air, (2) free water, (3) bound water, and (4) bulk vegetation. Knowing that bound water is held by bulk vegetation materials (e.g. Carbohydrates and Starches) and assuming a constant

ratio between v_v and v_b (e.g. $\frac{v_v}{v_b} = 2$ for sucrose solutions, as shown in Table 5.8), we can reduce the components into three:

1. If $M_v \geq v_b(Max)$, the three volume fractions are: $v_a, v_{vb} = v_v + v_b, and\ v_f$,

2. If $M_v < v_b(Max)$, the three volume fractions are: $v_a, v_{vb} = v_v + v_b, and\ v_{vr}$.

As discussed earlier, $v_{vr} = v_v(Max) - v_v$ while $v_f = 0$.

DeLoor's model for disc-shaped, randomly-oriented, and randomly-distributed inclusions ($A_j = 0, 0, 1$) and $\epsilon^* = \epsilon_m$ was found to fit our measured data better than Deloor's other models. This model is known to give the *upper limit* of ϵ, while sphere-shaped inclusions with $\epsilon^* = \epsilon_h$ gives the *lower limit* (refer to Eq.2.34). The equation describing the upper limit is given by:

$$\epsilon_m = \epsilon_h + \sum_{i=1}^{n} \frac{v_i}{3}(\epsilon_i - \epsilon_h)(2 + \frac{\epsilon^*}{\epsilon_i}) \tag{6.45}$$

or for a three-component mixture:

$$\epsilon = \frac{\epsilon_a + \frac{2}{3}v_{vb}(\epsilon_b - \epsilon_a) + \frac{2}{3}v_f(\epsilon_f - \epsilon_a)}{1 - \frac{1}{3}v_{vb}(1 - \frac{\epsilon_a}{\epsilon_b}) - \frac{1}{3}v_f(1 - \frac{\epsilon_a}{\epsilon_f})} \tag{6.46}$$

for $M_v \geq v_b$(Max).

DeLoor's model is asymmetrical, and the choice of the host material is not completely arbitrary. The host material should be the material with the largest volume fraction among the constituent components. In Eq. (6.46), ϵ_h was put equal to ϵ_a since air has the largest volume fraction. On the other hand, when $M_v < v_b(Max)$ we can use:

$$\epsilon = \frac{\epsilon_a + \frac{2}{3}v_{vb}(\epsilon_b - \epsilon_a) + \frac{2}{3}v_{vr}(\epsilon_v - \epsilon_a)}{1 - \frac{1}{3}v_{vb}(1 - \frac{\epsilon_a}{\epsilon_b}) - \frac{1}{3}v_{vr}(1 - \frac{\epsilon_a}{\epsilon_v})} \tag{6.47}$$

where $\epsilon_a = 1$, $\epsilon_v = 4.1$ (this value was reported for solid sucrose and was assumed for the bulk vegetation material), and the rest of the variables are as defined earlier in this chapter.

A regression analysis on measured data for corn leaves was conducted to optimize the model parameters. These parameters were ρ_{DV}, ρ_{BV}, $x(\equiv \frac{v_x}{v_b})$, S_m (maximum salinity), and S_s (slope of salinity curve, $s = S_m - S_s M_g$).

The optimized values are as follows:

$\rho_{DV} = .322$,

$\rho_{BV} = .978$,

$x \equiv \frac{v_x}{v_b} = 2.398$,

$S_m = 30.307\ ppt$, and

$S_s = 34.417\ ppt$.

ϵ_f and ϵ_b were calculated for each sample given T, f, and s using the equations listed in Sec. 6.1. Table 6.2 shows the model accuracy for the data measured on corn leaves for $M_g \leq .7$, $.7GHz \leq f \leq 20.4$ GHz, and at $T = 22^0C$.

	RSS	$EMSE$	N	ρ	b	a
ϵ'	3883.82	5.745	676	.981	.179	.821
ϵ''	245.1	.365	676	.979	.197	.949

Table 6.2 Model accuracy for corn leaves, DeLoor's model with $A_j = (0, 0, 1)$ and $\epsilon^* = \epsilon_m$ at $T = 22^0C$.

It is obvious from this last table that the model fits ϵ'' much better than it fits ϵ'. Again, it was our strategy to use the model sensitivity to ϵ'' to optimize all the model parameters. The model was then evaluated for ϵ'. Figures (6.7) to (6.9) show frequency spectra of the model compared to the measured data for three different moistures (M_g =.681, .333, and .168).

6.3.2 Debye's model (two relaxation spectra)

Since the dielectric properties of plants are controlled by the dielectric properties of water, in its various forms, and since Debye's equations can adequately model water properties, it was assumed that a Debye-like equation is suitable for modeling the dielectric properties of vegetation.

The proposed model is:

$$\epsilon = \epsilon_\infty + \left(\frac{\epsilon_{sf} - \epsilon_{\infty f}}{1 + j\frac{f}{f_{0f}}} - j\frac{\sigma_{eff}}{\omega\epsilon_0}\right)v_f + \left(\frac{\epsilon_{sb} - \epsilon_{\infty b}}{1 + (j\frac{f}{f_{0b}})^{(1-\alpha_b)}}\right)v_{vb} \qquad (6.48)$$

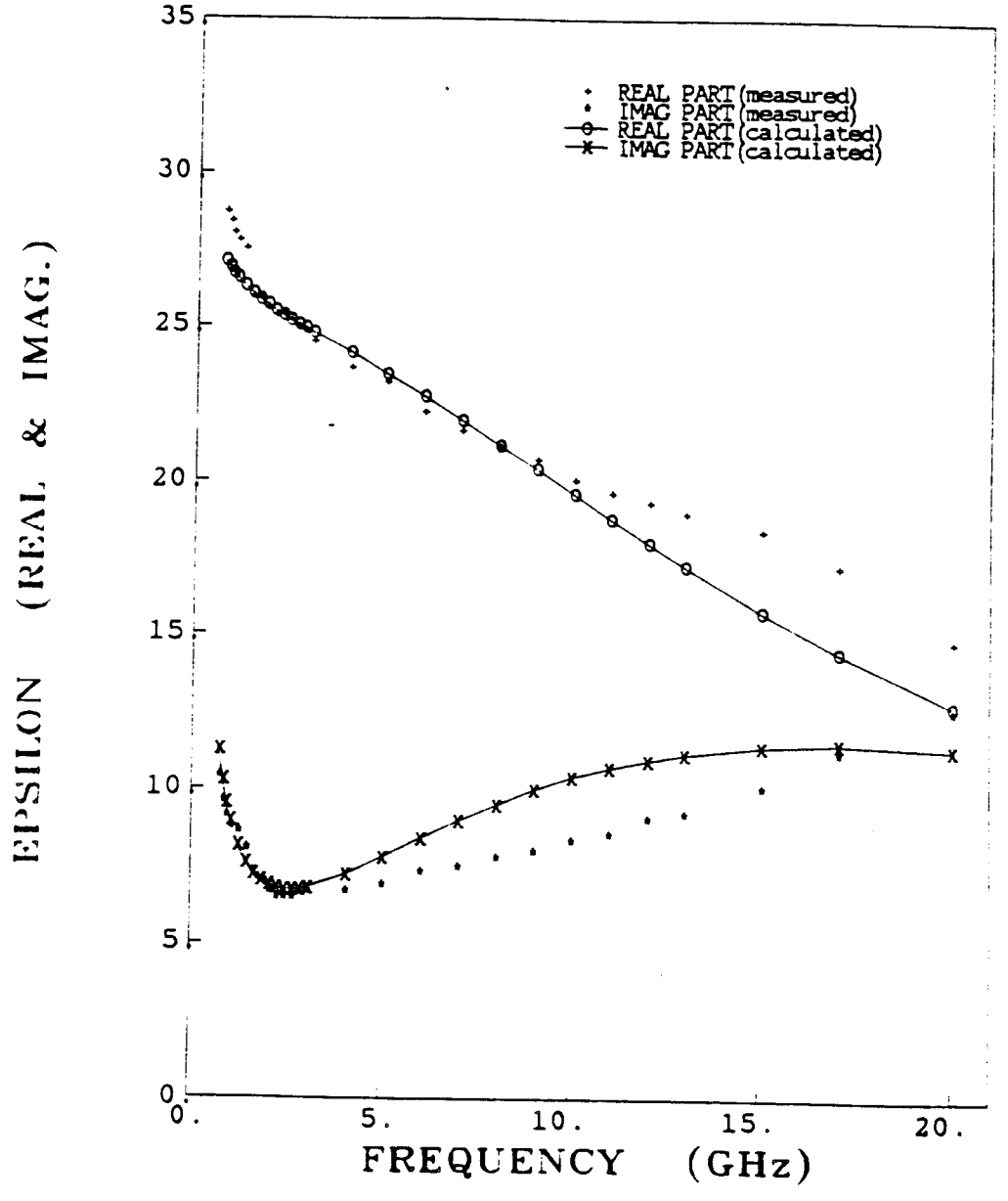

Figure 6.7. Comparison of calculated and measured dielectric spectra for corn leaves using DeLoor's model for randomly oriented and randomly distributed discs at T=22^{0}C for M_g=0.681.

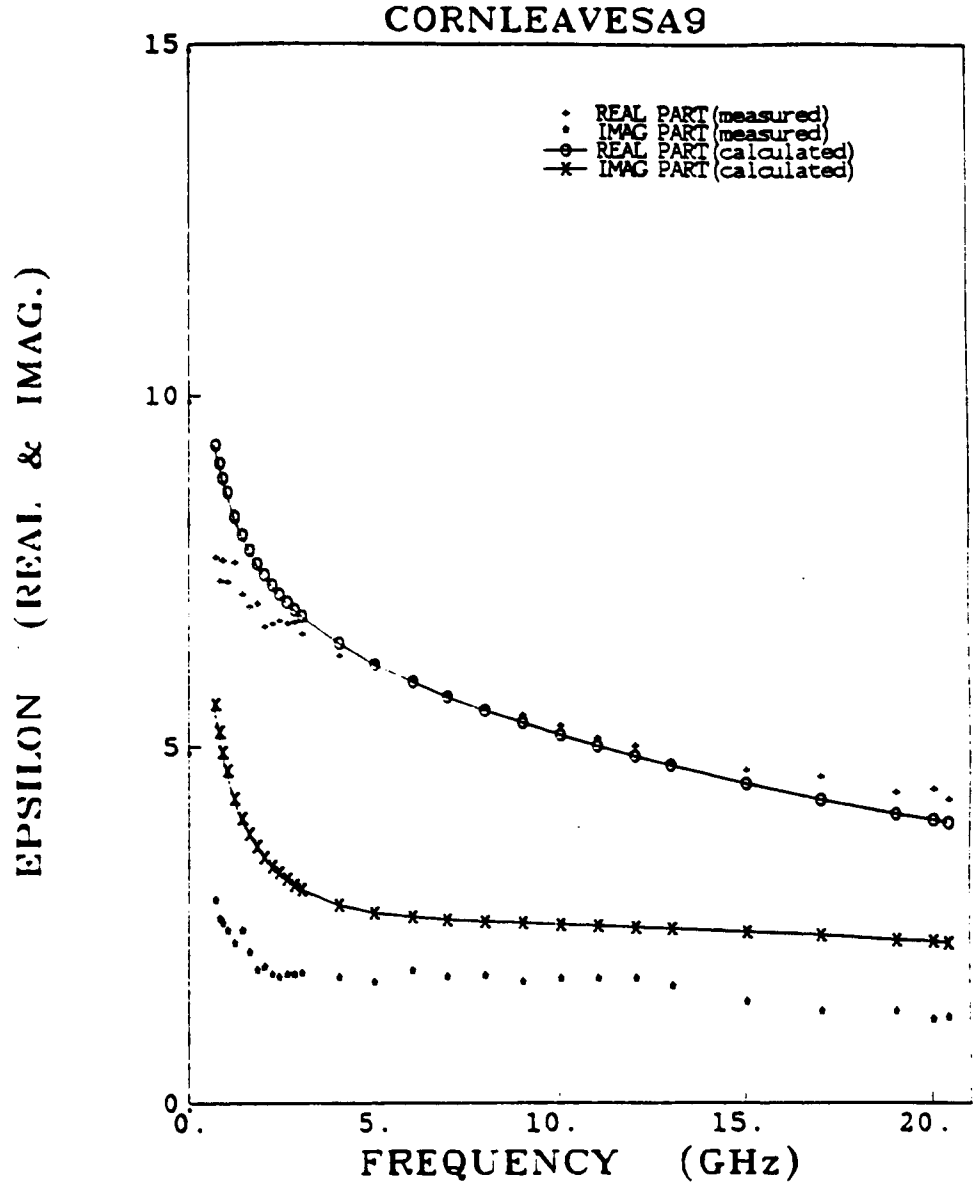

Figure 6.8. Comparison of calculated and measured dielectric spectra for corn leaves using DeLoor's model for randomly oriented and randomly distributed discs at T=22°C for M_g=0.333.

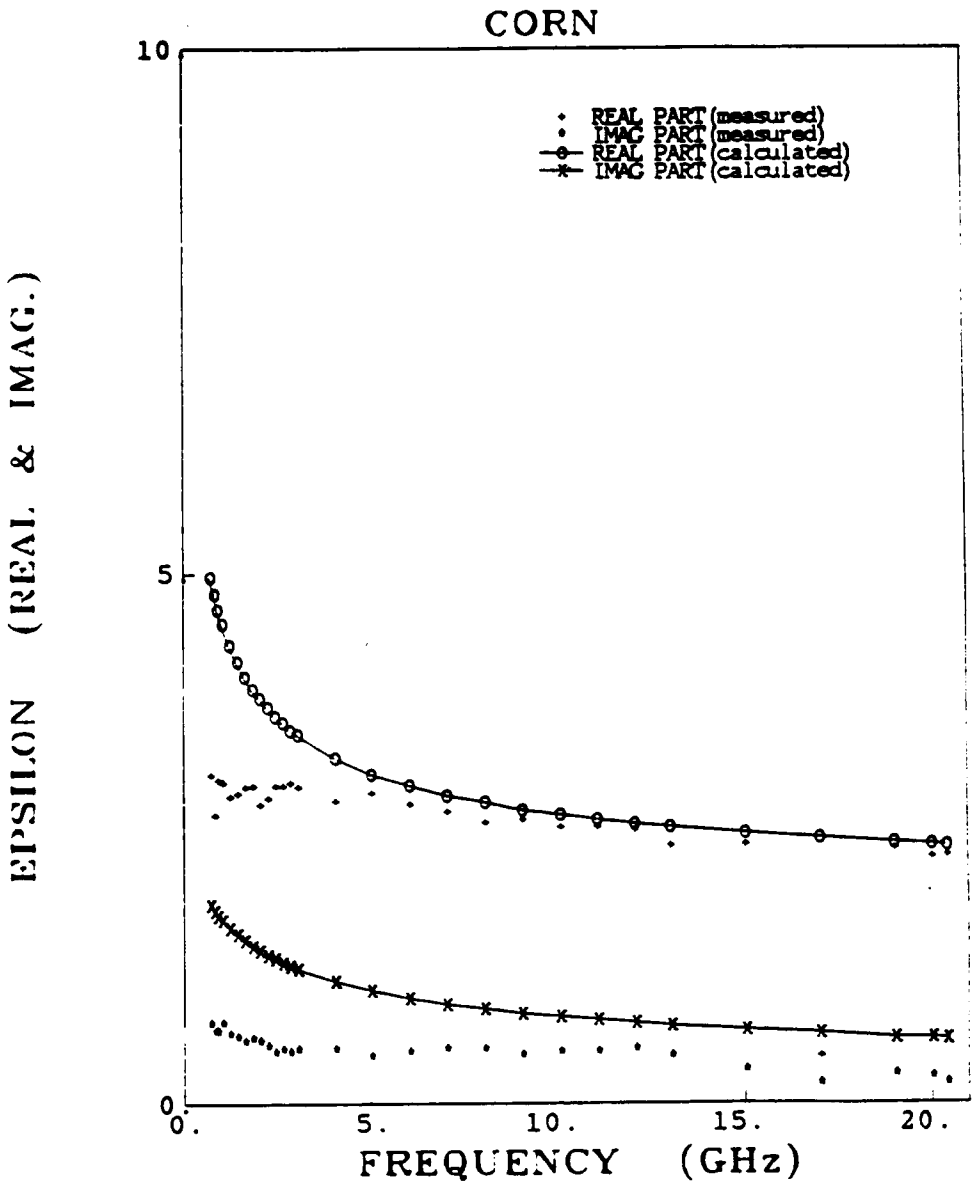

Figure 6.9. Comparison of calculated and measured dielectric spectra for corn leaves using DeLoor's model for randomly oriented and randomly distributed discs at T=22^{0}C for M_g=0.168.

where $\epsilon_\infty = A + BM_v$, ϵ_{sf}, $\epsilon_{\infty f}$, f_{0f}, and σ_{eff} are free water relaxation parameters as defined in Sec.6.1.1, ϵ_{sb}, $\epsilon_{\infty b}$, f_{0b}, and α_b are bound water relaxation parameters as defined in Sec.6.1.4. This model was tested on data taken at room temperature; from Section 6.1.3 and 6.1.4, $(\epsilon_{sf} - \epsilon_{\infty f}) \simeq 75$, $f_{0f} \simeq 18$GHz, $(\epsilon_{sb} - \epsilon_{\infty b}) \simeq 55$, and $f_{0b} \simeq .178$ GHz. The conductivity term $\frac{\sigma_{eff}}{\omega\epsilon_0}$ was written in a slightly modified form, as

$$\epsilon_c'' = \frac{\sigma_e}{f} v_f \tag{6.49}$$

Furthermore, the conductivity term, which is proportional to salinity, can be expressed as:

$$\sigma_e = P - Qv_f \tag{6.50}$$

where P and Q are constants that depend on the plant type (or in general depend on the ionic content of the sample). This conductivity term was found to vary between different species and even for the same species grown in different geographic locations, as discussed earlier in Sec. 5.4. This Debye-like model was found to fit the data very well in terms of magnitudes and trends. The optimized parameters for ϵ'' (i.e., ρ_{DV}, ρ_{BV}, x, P, and Q) were used as constants when optimizing the remaining parameters of ϵ' (A and B). The optimized values are: $\rho_{DV} = .238$, $\rho_{BV} = 1.255$, $x = 2$, $A = 1.861$, $B = 12.913$, $P = 53.506$, $Q = 121.041$, and $\alpha_b = .501$.

Hence, Eq. (6.48) becomes:

$$\epsilon = (1.861+12.913M_v)+(\frac{75.}{1.+j\frac{f}{18.0}}-j\frac{53.506-121.041v_f}{f})v_f+(\frac{55.}{1.+(j\frac{f}{0.178})^{0.499}})v_{vb} \tag{6.51}$$

Table 6.3 shows the model accuracy for the data measured on corn leaves ($M_g \leq .7, .7\text{GHz} \leq f \leq 20.4\text{GHz}$), and at $T = 22^0C$).

	RSS	$EMSE$	N	ρ	b	a
ϵ'	1412.2	1.947	676	.983	.292	.969
ϵ''	254.9	.379	676	.978	.084	.968

Table 6.3 Model accuracy for corn leaves data, Debye-like model at $T = 22^0C$.

Comparing Table 6.3 (Debye's model) to 6.2 (DeLoor's model) shows that Deloor's model provides a slightly better fit for ϵ'', whereas the Debye-like model provides a much better fit for ϵ'. Figures (6.10) to (6.12) show frequency spectra of the measured data and the values calculated according to the Debye-like model. Also, Fig. (6.13) to (6.16) show the dielectric properties of corn leaves (measured and calculated) as a function of M_g for f =1, 4, 12, and 20 GHz. These plots, indicate that the model is in good agreement with the data over the frequency

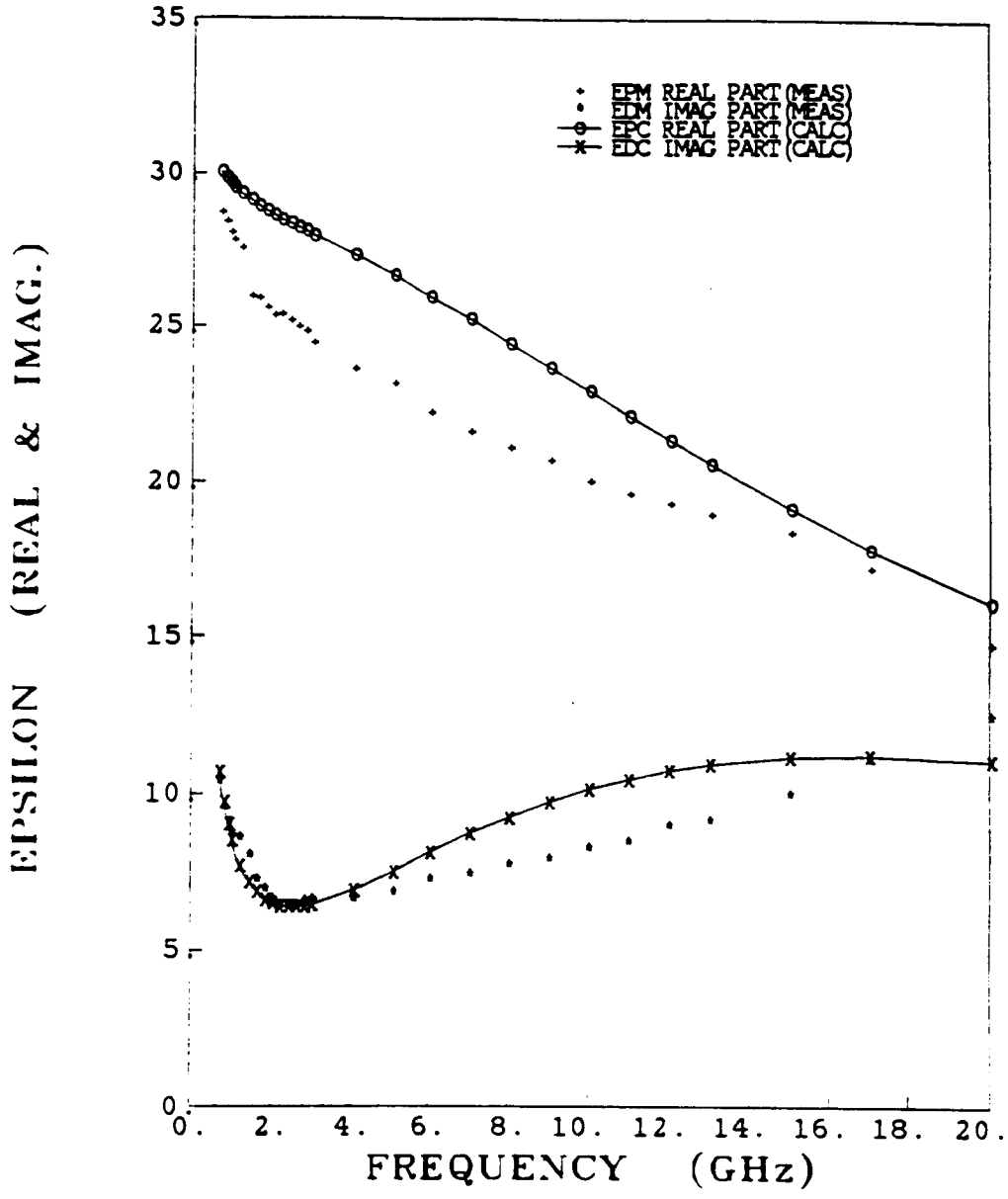

Figure 6.10. Comparison of calculated and measured dielectric spectra for corn leaves using a Debye-like model with two relaxation spectra at T=22^{0}C for M_g=0.681.

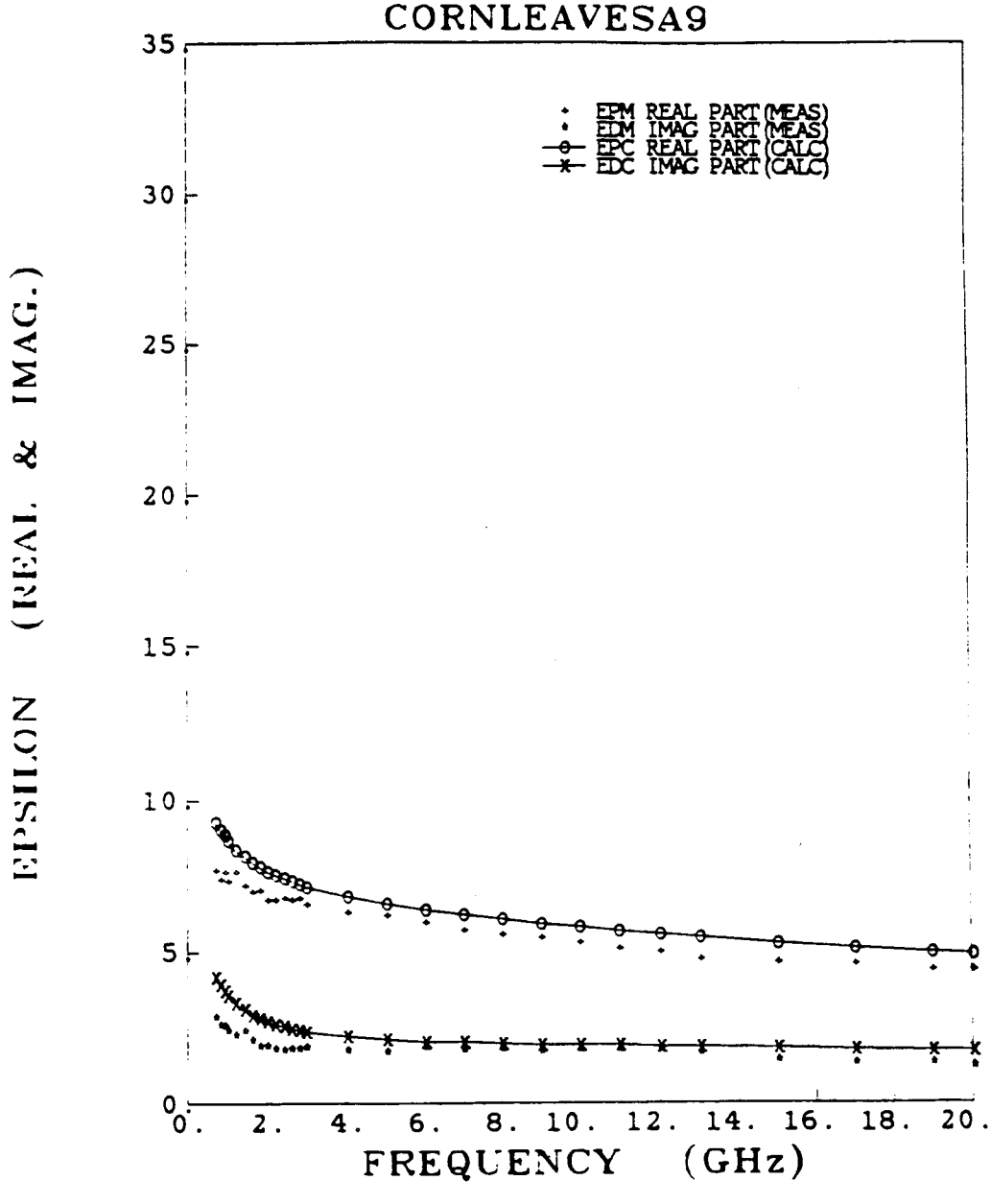

Figure 6.11. Comparison of calculated and measured dielectric spectra for corn leaves using a Debye-like model with two relaxation spectra at T=22^{0}C for M_g=0.333.

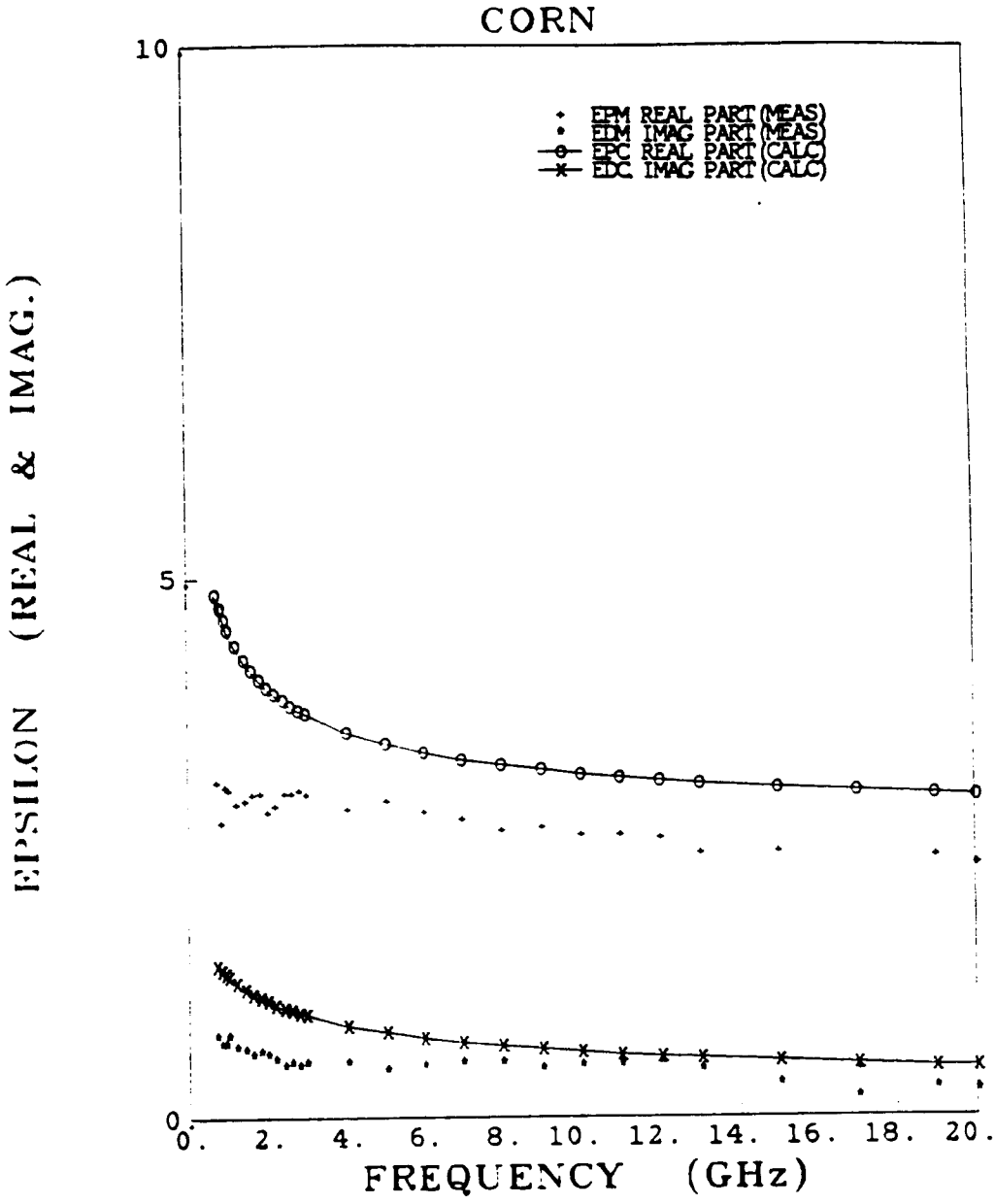

Figure 6.12. Comparison of calculated and measured dielectric spectra for corn leaves using a Debye-like model with two relaxation spectra at T=22^{0}C for M_g=0.168.

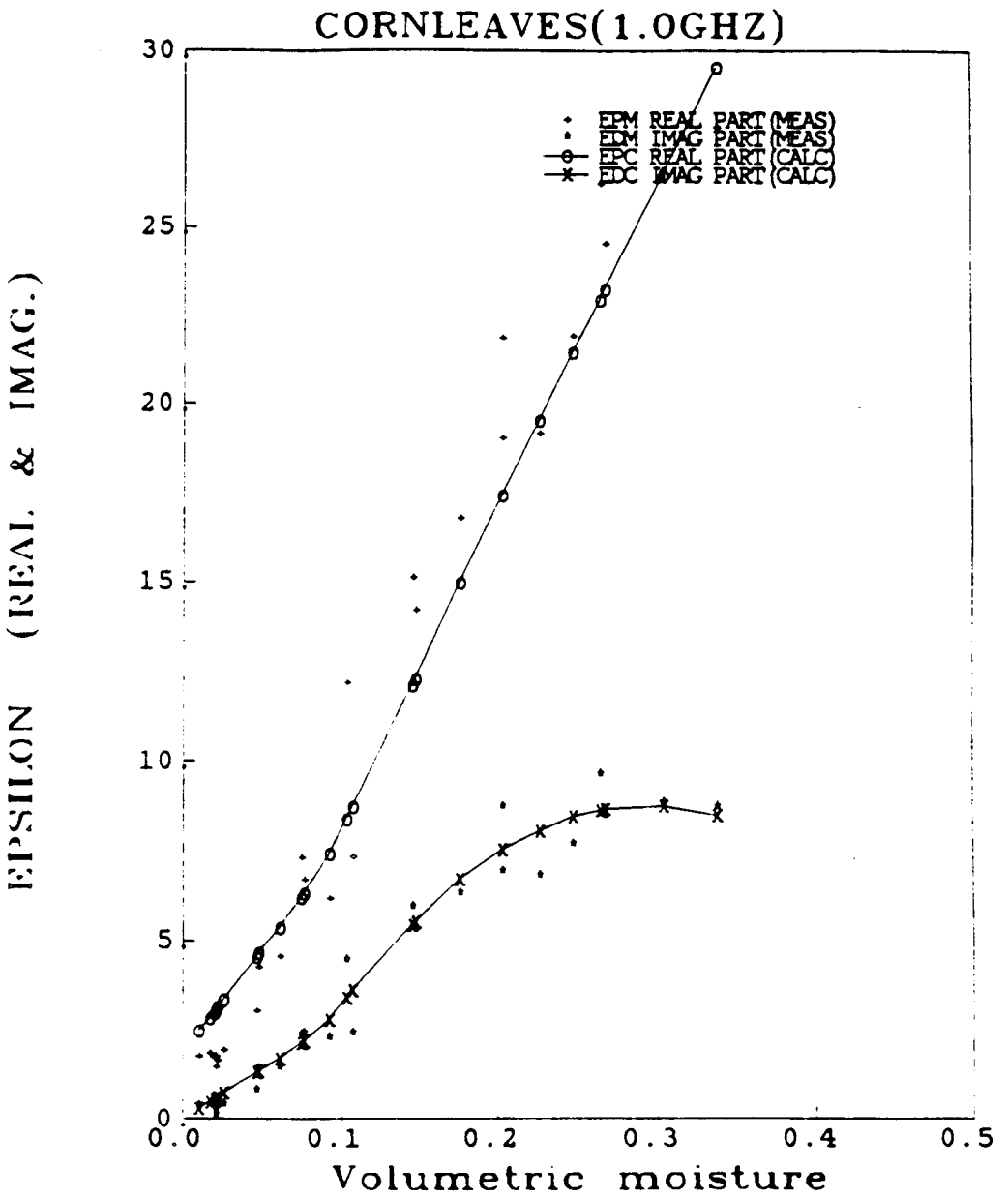

Figure 6.13. Comparison of calculated and measured dielectric constant versus moisture for corn leaves using a Debye-like model with two relaxation spectra (f=1 GHz).

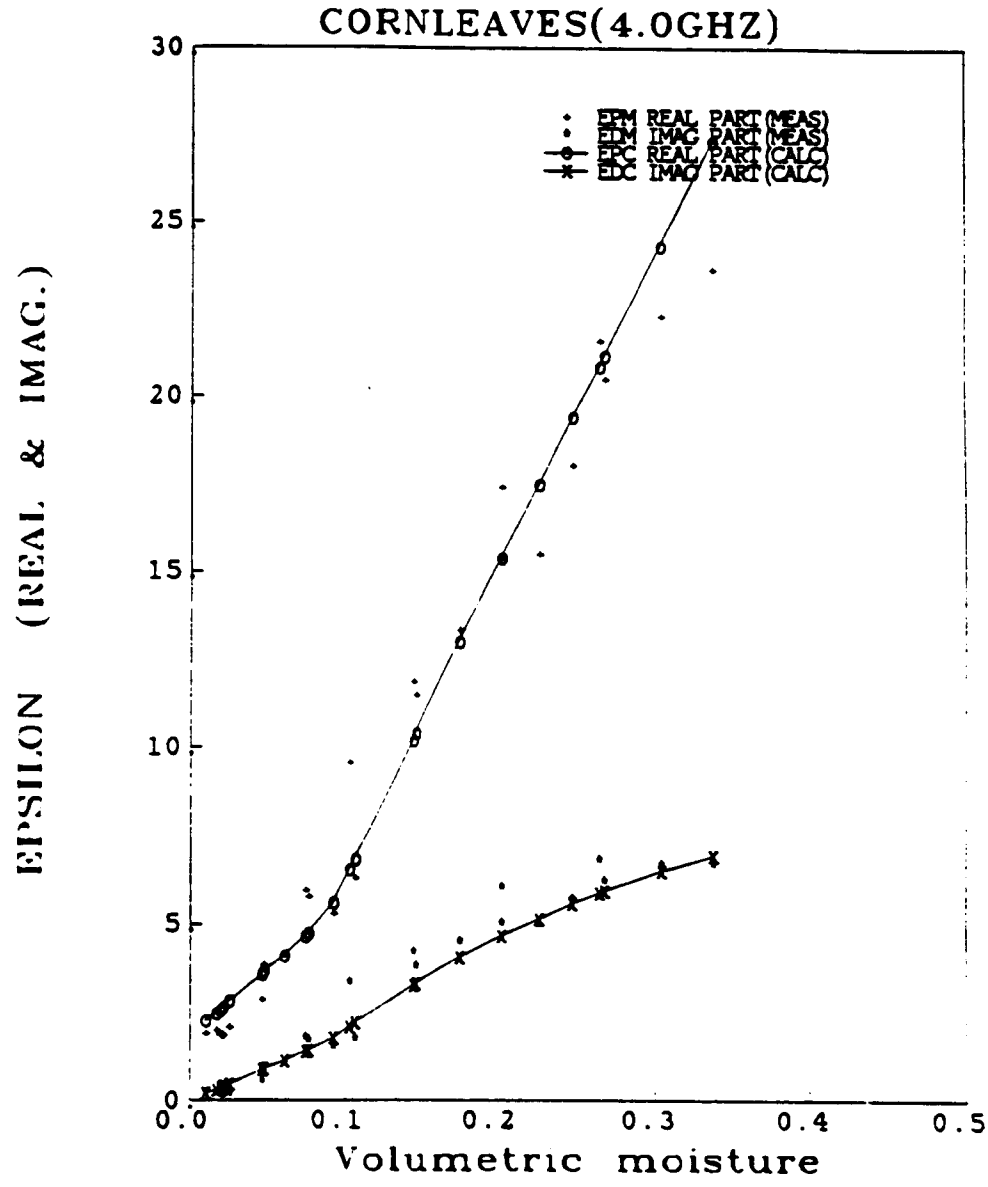

Figure 6.14. Comparison of calculated and measured dielectric constant versus moisture for corn leaves using a Debye-like model with two relaxation spectra (f=4 GHz).

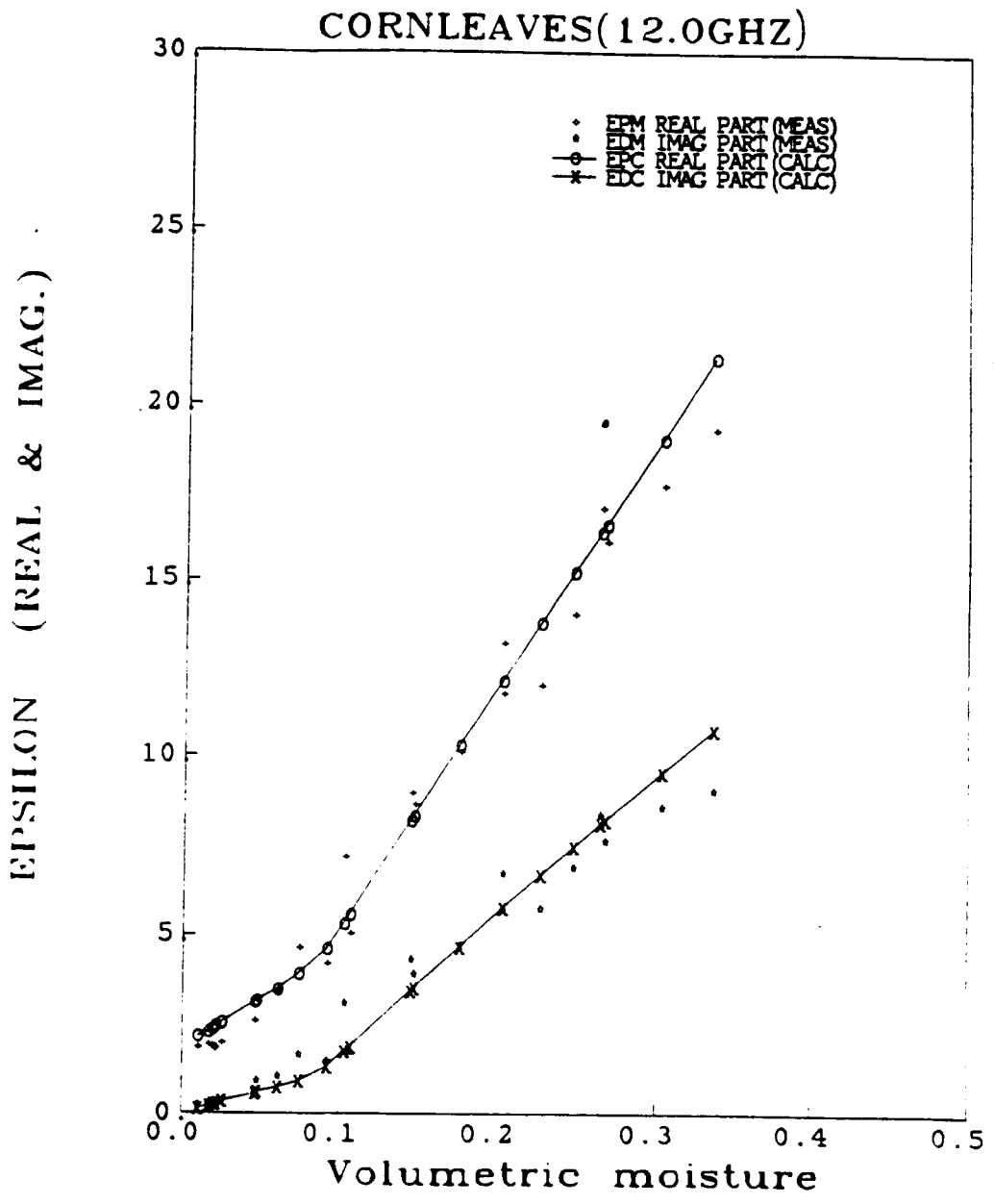

Figure 6.15. Comparison of calculated and measured dielectric constant versus moisture for corn leaves using a Debye-like model with two relaxation spectra (f=12 GHz).

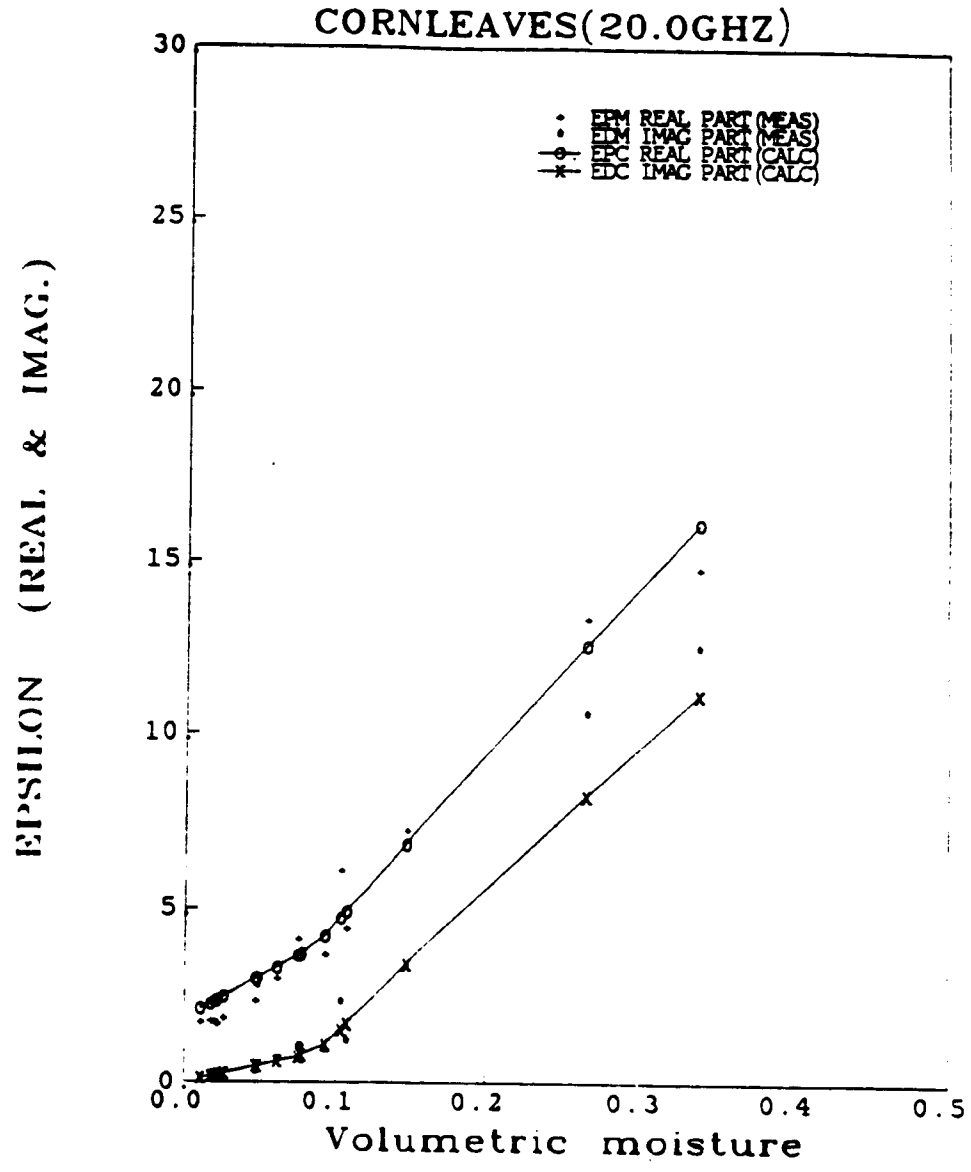

Figure 6.16. Comparison of calculated and measured dielectric constant versus moisture for corn leaves using a Debye-like model with two relaxation spectra (f=20 GHz).

and moisture ranges encountered. Two interesting features about this model are: (1) it is symmetrical and (2) it is linear. The second feature was used to test the effects of each of the water components separately:

$$\epsilon'_t = \epsilon'_f(free\ water) + \epsilon'_b(bound\ water) + \epsilon'_{av}(air + vegetation), and \qquad (6.52)$$

$$\epsilon''_t = \epsilon''_f(free\ water) + \epsilon''_b(bound\ water) + \epsilon''_c(conductivity). \qquad (6.53)$$

These terms were plotted separately and are shown in Fig.(6.17) to (6.22). It is interesting to note the following:

1. At low frequencies (e.g., $f < 5$ GHz), ϵ'_f drops very slowly with increasing frequency while ϵ'_b drops sharply. This feature suggests a visual method to inspect the existence of bound water in biological tissues and to estimate its volume relative to free water (refer, e.g., to Fig. (5.27) for the dielectric spectrum of human skin which shows how abundantly bound water may exist in these tissues).

2. At higher frequencies, however, ϵ'_f drops fast while ϵ'_b stays essentially constant (f >5 GHz).

3. ϵ'_{av} (air+vegetation) is constant as a function of frequency and varies slightly with moisture while ϵ''_{av} is neglegible.

4. ϵ''_c drops drastically with frequency, and its effects are practically neglegible above 5 GHz.

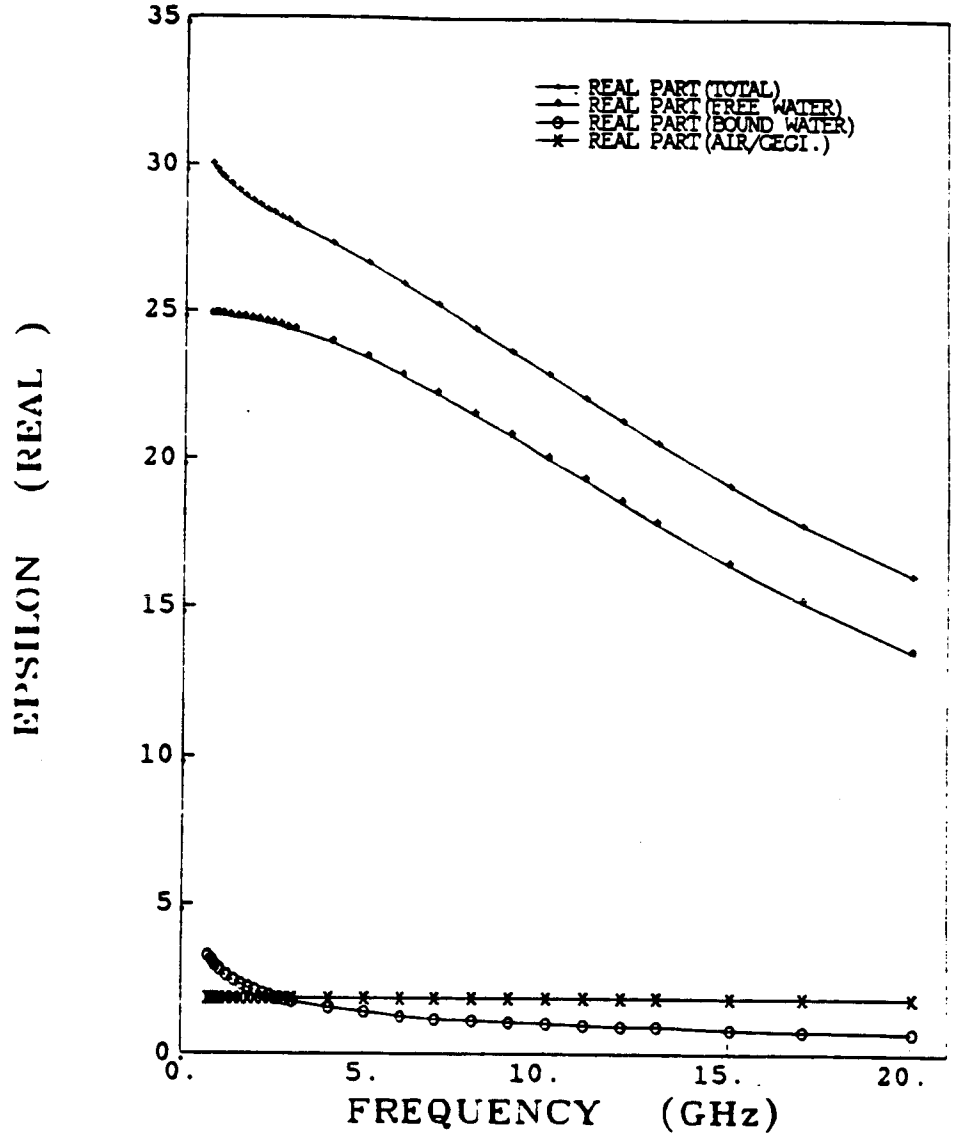

Figure 6.17. Calculated real parts spectra of all components for corn leaves using a Debye-like model with two relaxation spectra. (M_g = 0.681).

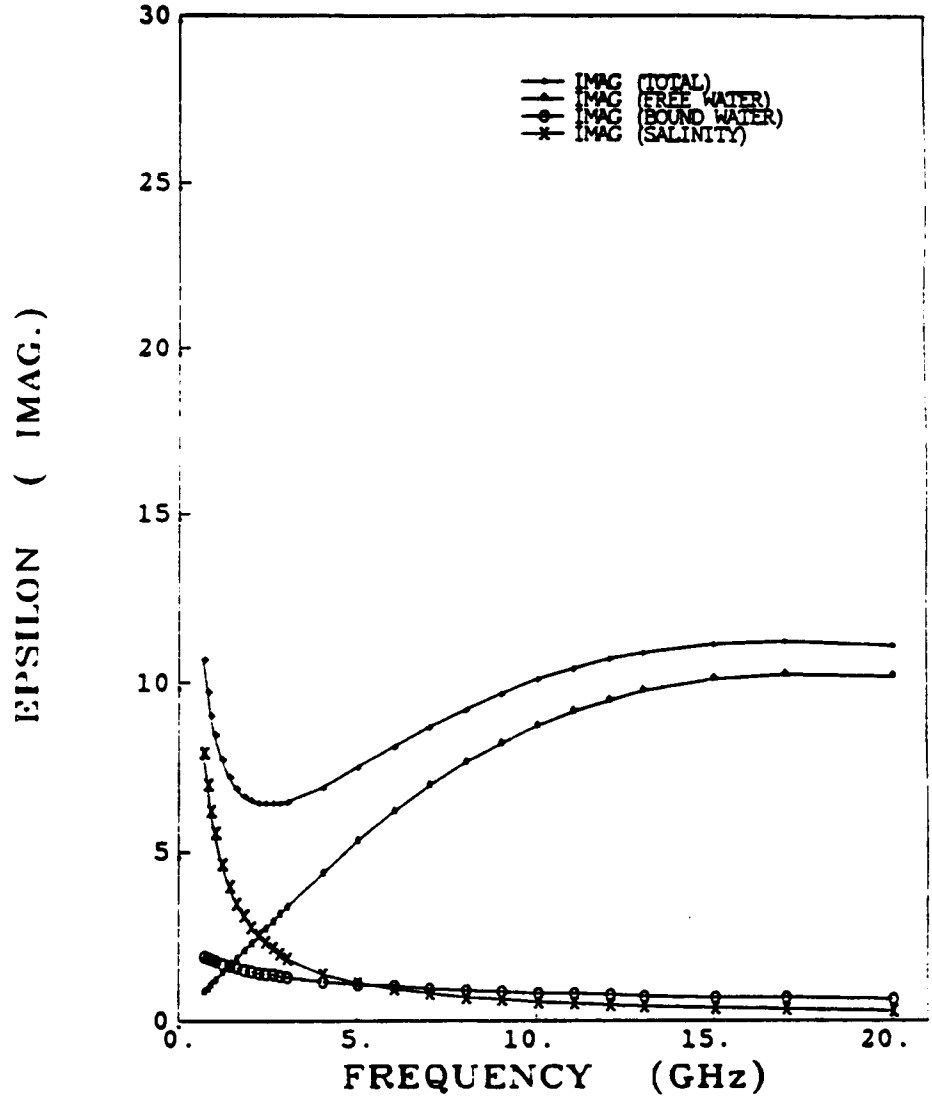

Figure 6.18. Calculated imaginary parts spectra of all components for corn leaves using a Debye-like model with two relaxation spectra. ($M_g = 0.681$)

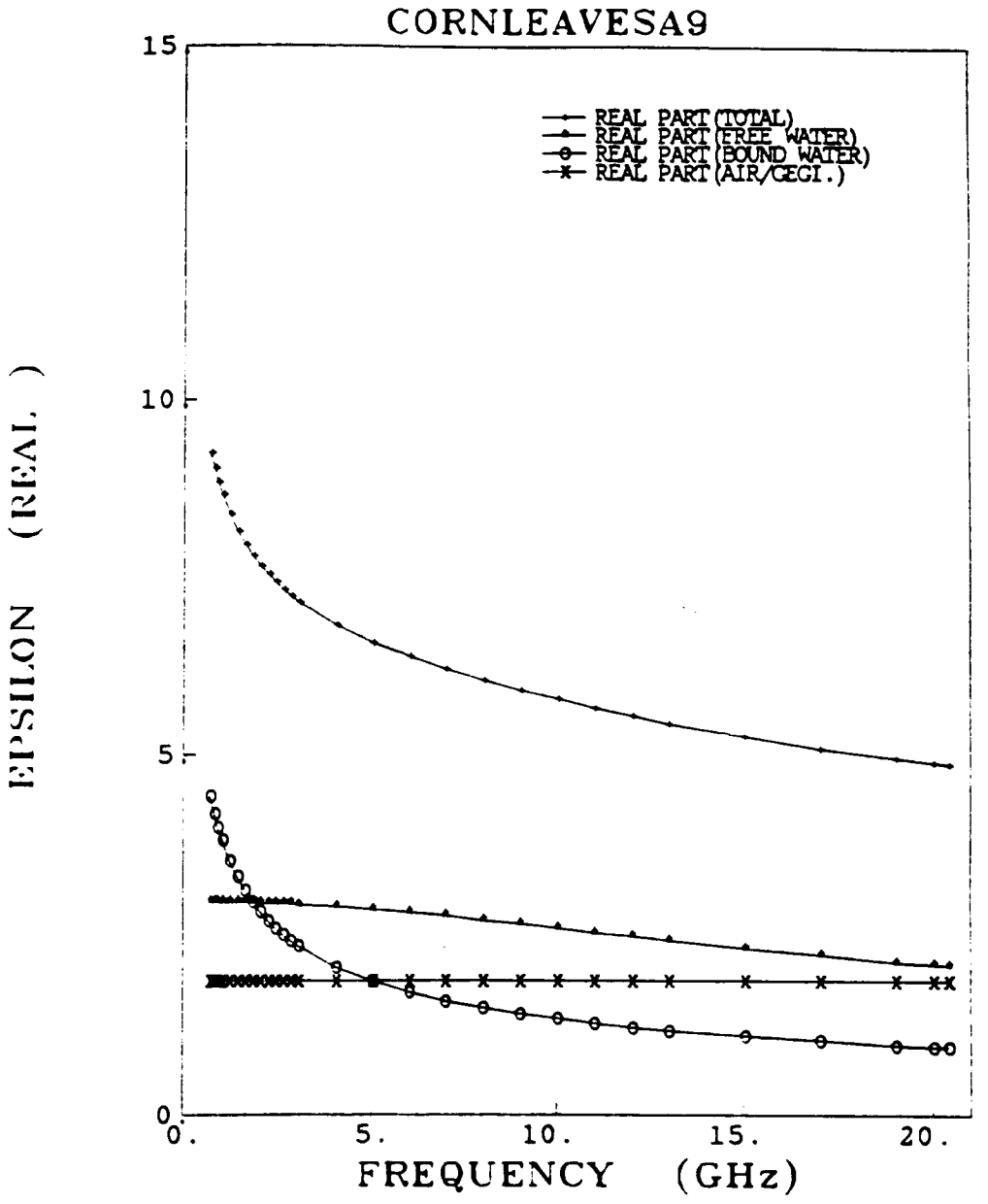

Figure 6.19. Calculated real parts spectra of all components for corn leaves using a Debye-like model with two relaxation spectra. ($M_g = 0.333$).

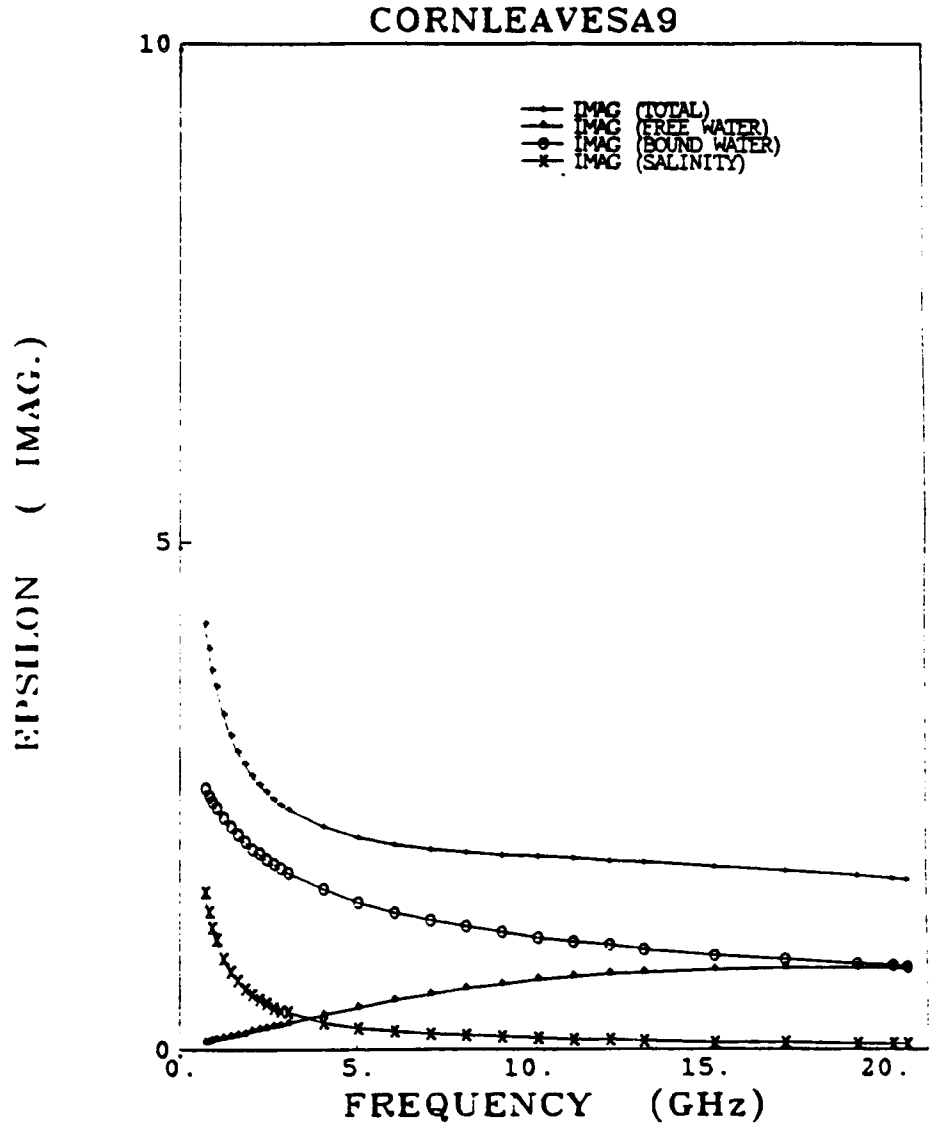

Figure 6.20. Calculated imaginary parts spectra of all components for corn leaves using a Debye-like model with two relaxation spectra. ($M_g = 0.333$)

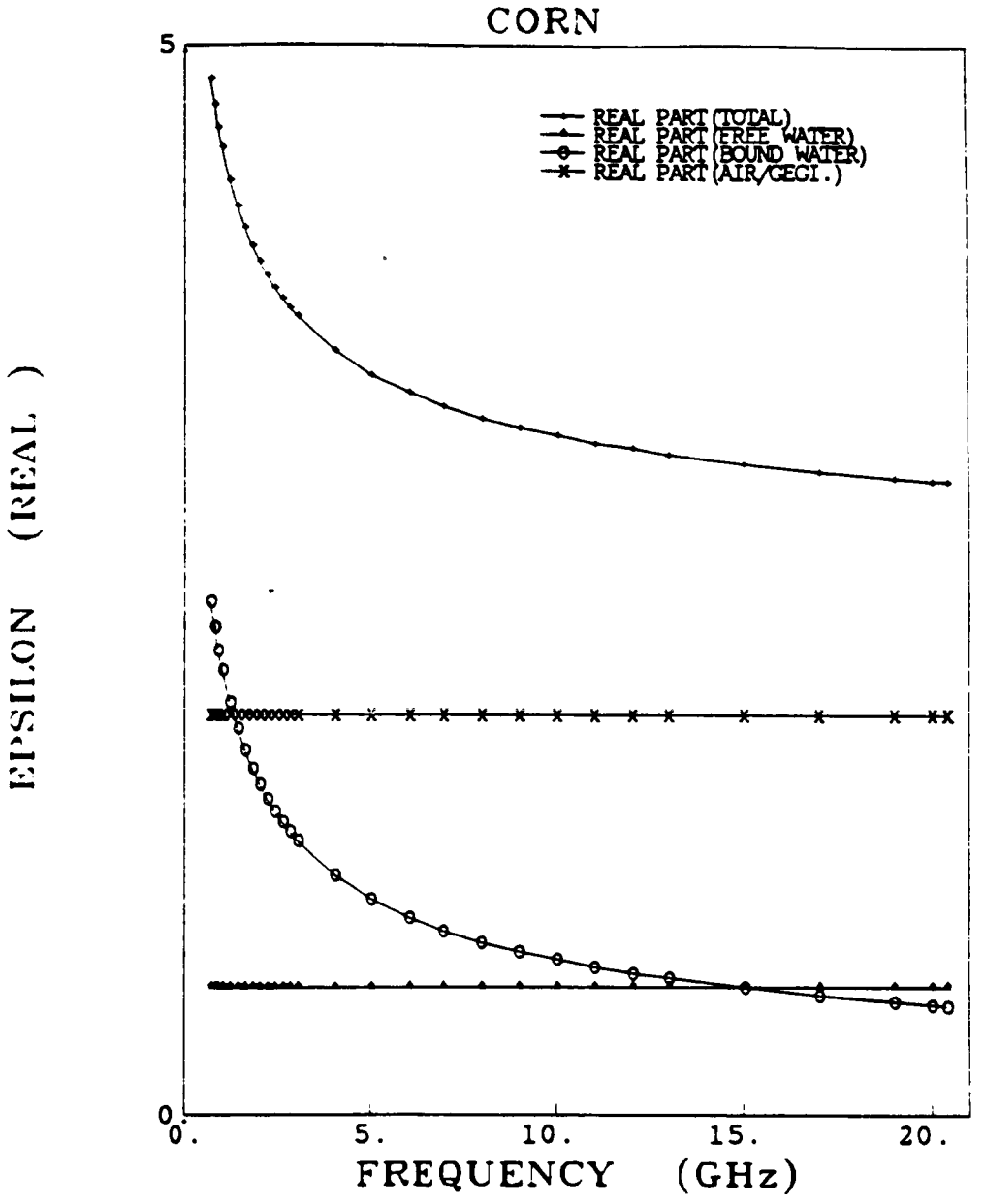

Figure 6.21. Calculated real parts spectra of all components for corn leaves using a Debye-like model with two relaxation spectra. ($M_g = 0.168$).

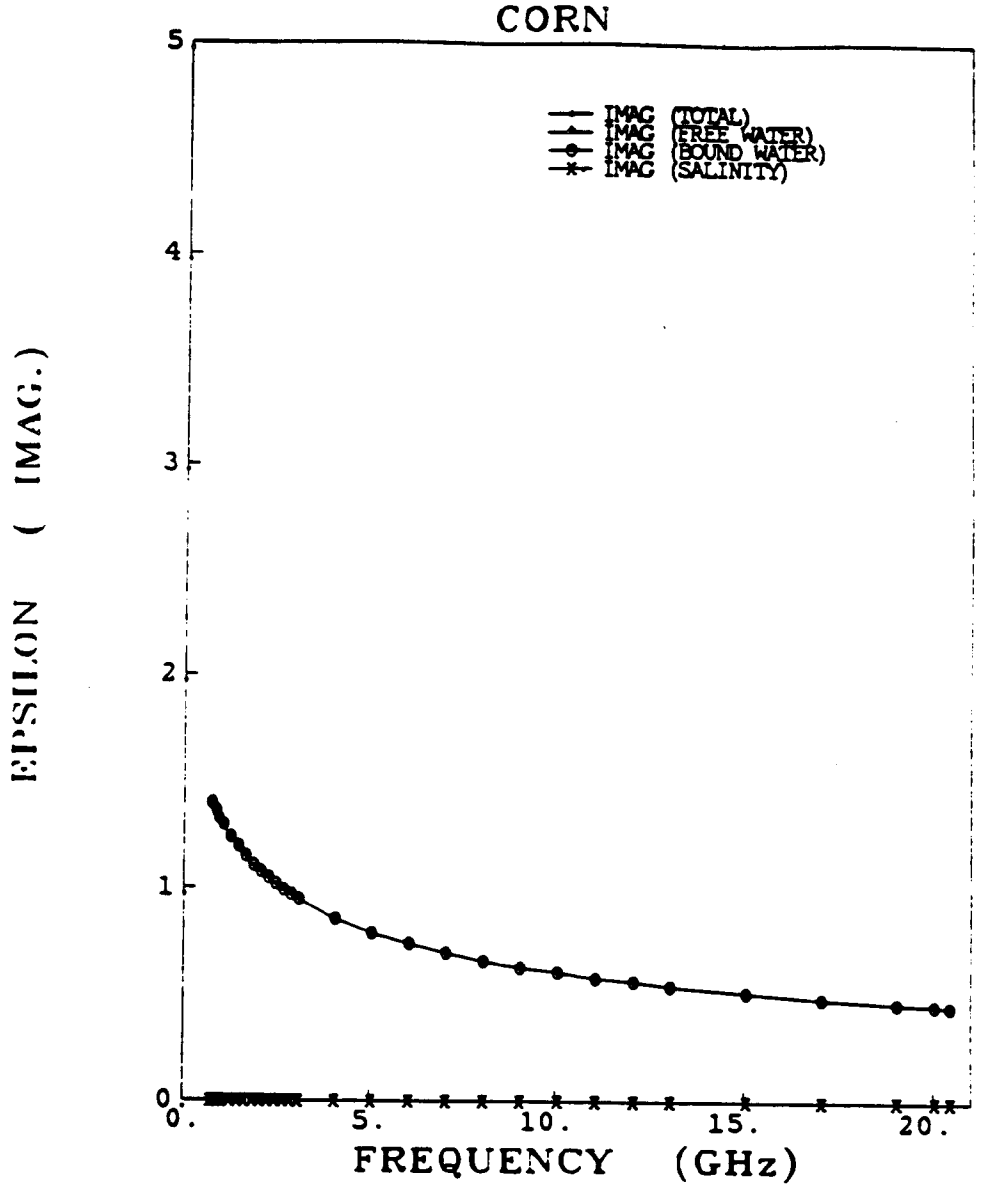

Figure 6.22. Calculated imaginary parts spectra of all components for corn leaves using a Debye-like model with two relaxation spectra. ($M_g = 0.168$)

5. ϵ_f'' increases with frequency and it has a broad peak around 18 GHz.

6. ϵ_b'' decreases with frequency but with a much slower rate than ϵ_c''. Since bound-water relaxation has a relaxation parameter $\alpha_b = .5$, the spectrum of ϵ_b'' is very broad (the half-peak points are separated by about 80 decades!).

7. In general, free water dominates at high moistures, while bound water dominates at low moistures.

6.3.3 Birchak model (Semi-empirical)

The Birchak model is one of the most attractive semi-empirical models because it is simple and symmetrical. It is given as:

$$\epsilon^\alpha = v_a\epsilon_a^\alpha + v_{vr}\epsilon_v^\alpha + v_f\epsilon_f^\alpha + v_{vb}\epsilon_b^\alpha, \tag{6.54}$$

where the variables are as defined earlier, and α is a free parameter. If $\alpha = .5$, it is called the refractive model. Again, we tested this model using the measured dielectric data for corn leaves with the following assumptions: $\rho_{DV} = .33$, $\rho_{BV} = 1.60$, and $x(\equiv \frac{v_v}{v_b}) = 2$. Equation 5.5 was used for salinity, $s = 37 - 46M_g$. The only parameter to be optimized in this case was α and it was found to be .873. For these parameters, Table 6.4 shows the model accuracy when tested against the measured data.

	RSS	$EMSE$	N	ρ	b	a
ϵ'	1772.02	2.621	676	.984	-.182	.935
ϵ''	413	.612	676	.975	.264	1.030

Table 6.4 Model accuracy for corn leaves, Birchak model ($\alpha = .873$) at $T = 22^0C$.

The model accuracy in this case is very good especially if we remember that only one free parameter was used to fit the data. Figures (6.23) to (6.25) show examples of the frequency spectrum of the model compared to the measured data.

6.3.4 Polynomial fit (empirical model)

Polynomial fits are usually very versatile, easy to use, and they can be made to fit almost any set of data (provided that the order of the polynomial is suitable). On the other hand, these models have, in general, no physical significance and they require that many coefficients be estimated. The following polynomial expressions were found to fit the corn leaves data very well:

$$\epsilon' = (.429 + .074f) + (14.620 - .834f)M_g + (39.396 - .616f)M_g^2, \qquad (6.55)$$

and

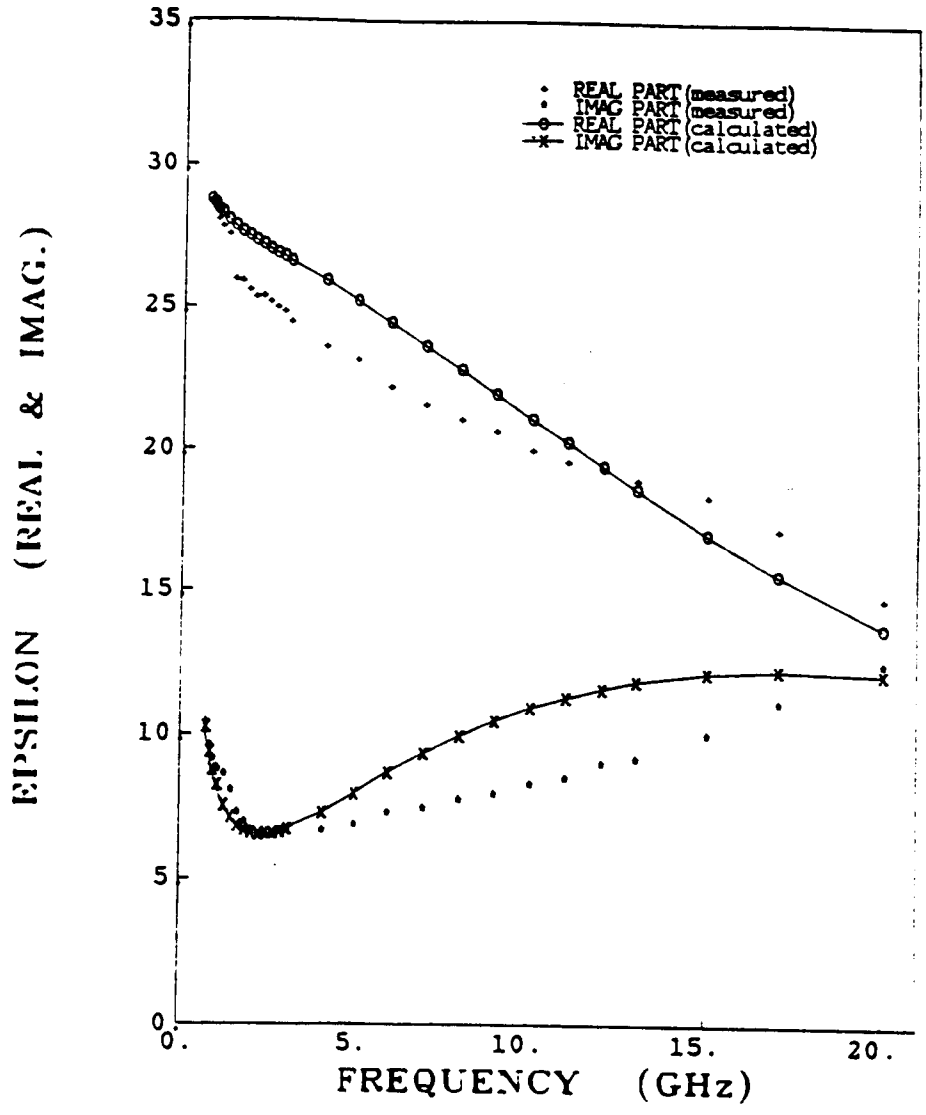

Figure 6.23. Comparison of calculated and measured dielectric spectra for corn leaves using Birchak's model ($M_g = 0.681$).

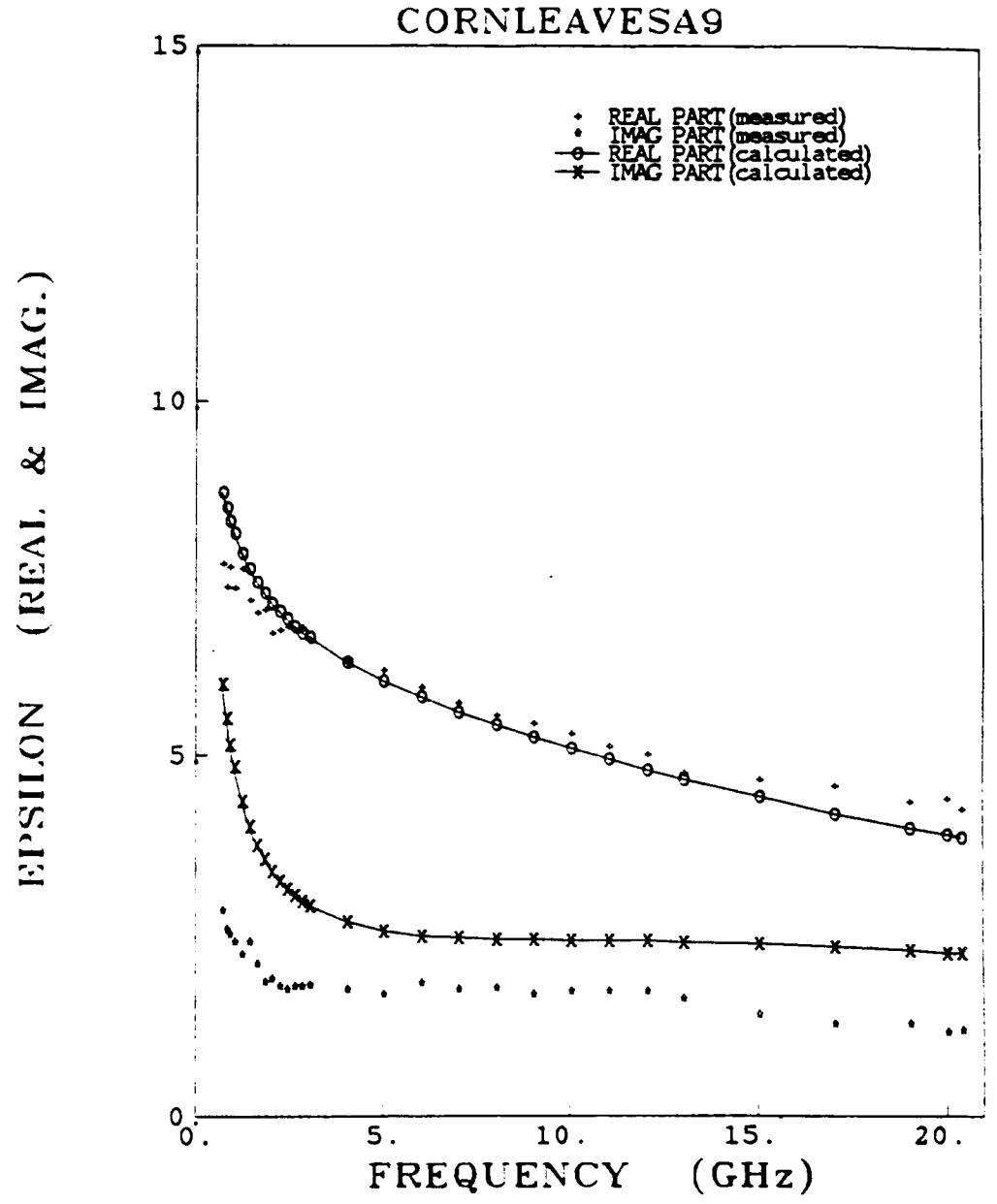

Figure 6.24. Comparison of calculated and measured dielectric spectra for corn leaves using Birchak's model ($M_g = 0.333$).

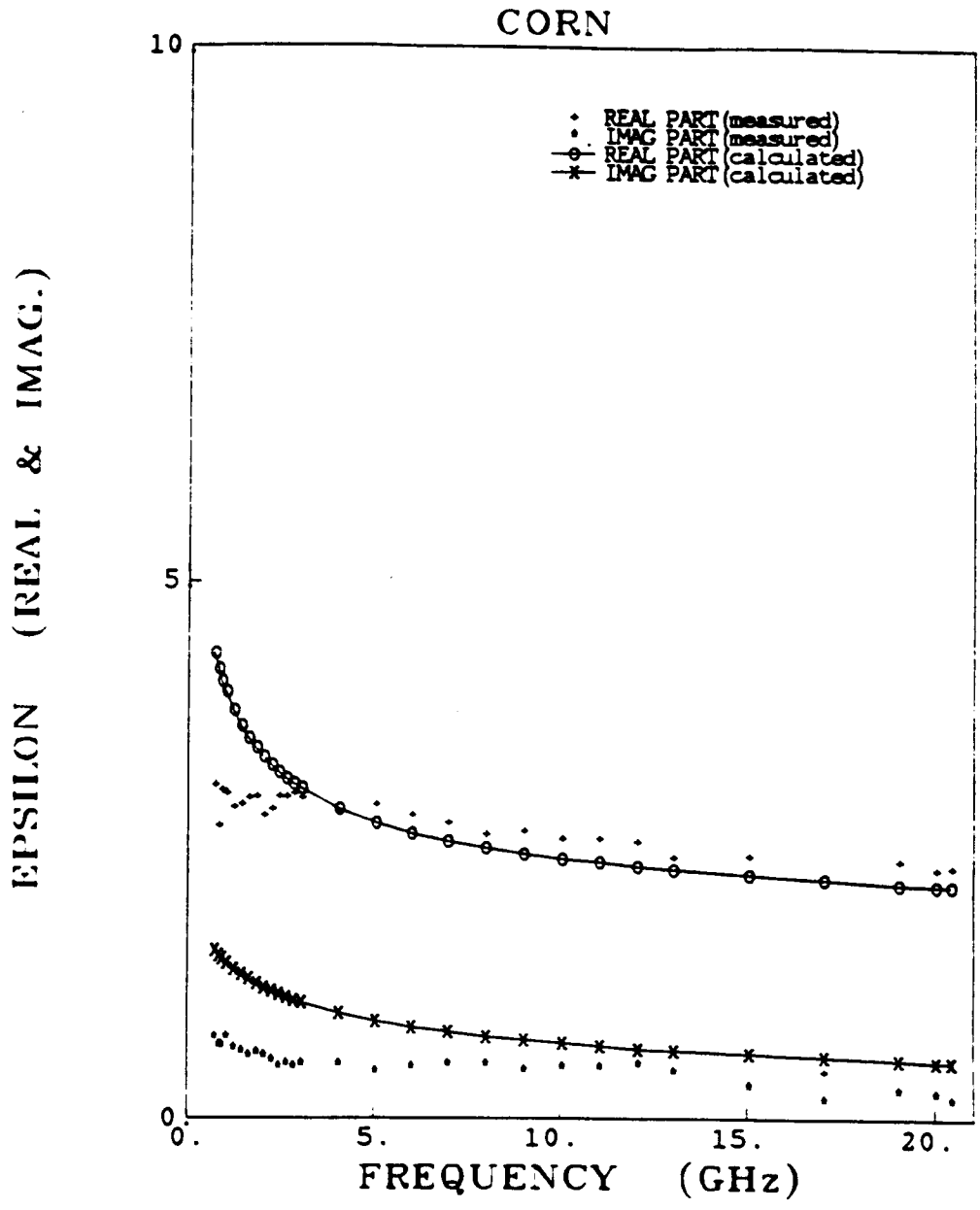

Figure 6.25. Comparison of calculated and measured dielectric spectra for corn leaves using Birchak's model ($M_g = 0.168$).

$$\epsilon'' = (6.590 - \frac{.977}{f} - .559f)M_g + (.463 + \frac{9.368}{f} + 1.617f)M_g^2. \qquad (6.56)$$

The expression for ϵ'' was obtained after several trials to determine which powers of f are the most appropriate. Table 6.5 shows the model accuracy for the polynomial fit.

	RSS	$EMSE$	N	ρ	b	a
ϵ'	885.8	1.322	676	.989	.210	.978
ϵ''	235.4	.351	676	.980	.230	.943

Table 6.5 Model accuracy for corn-leaves data, Polynomial fit at $T = 22^0C$.

It is surprising how well this model fits the measured data, albeit it includes 12 coefficients whose values were selected by regressing the model against the data. Figures (6.26) to (6.28) compare spectra calculated using the polynomial model with the measured data.

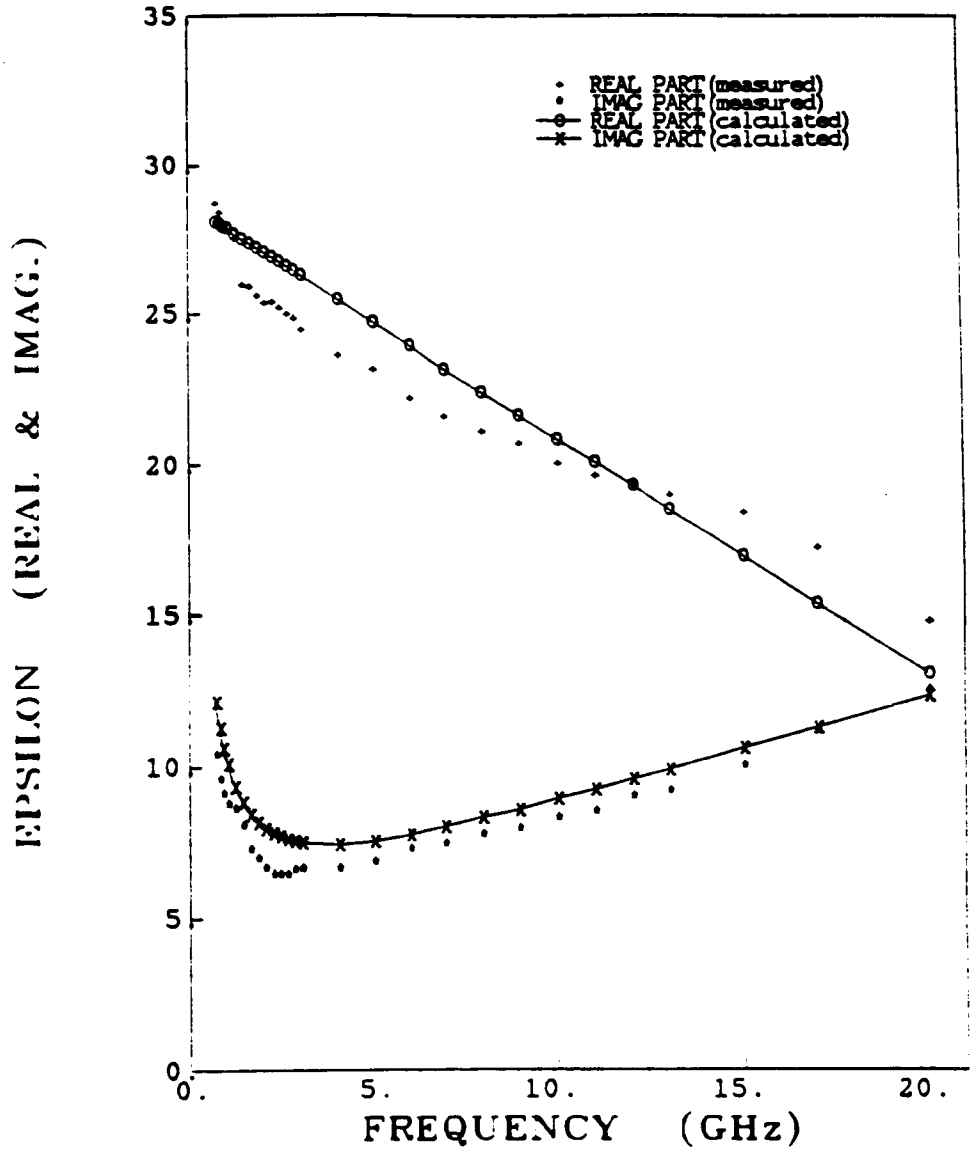

Figure 6.26. Comparison of calculated and measured dielectric spectra for corn leaves using a polynomial fit ($M_g = 0.681$).

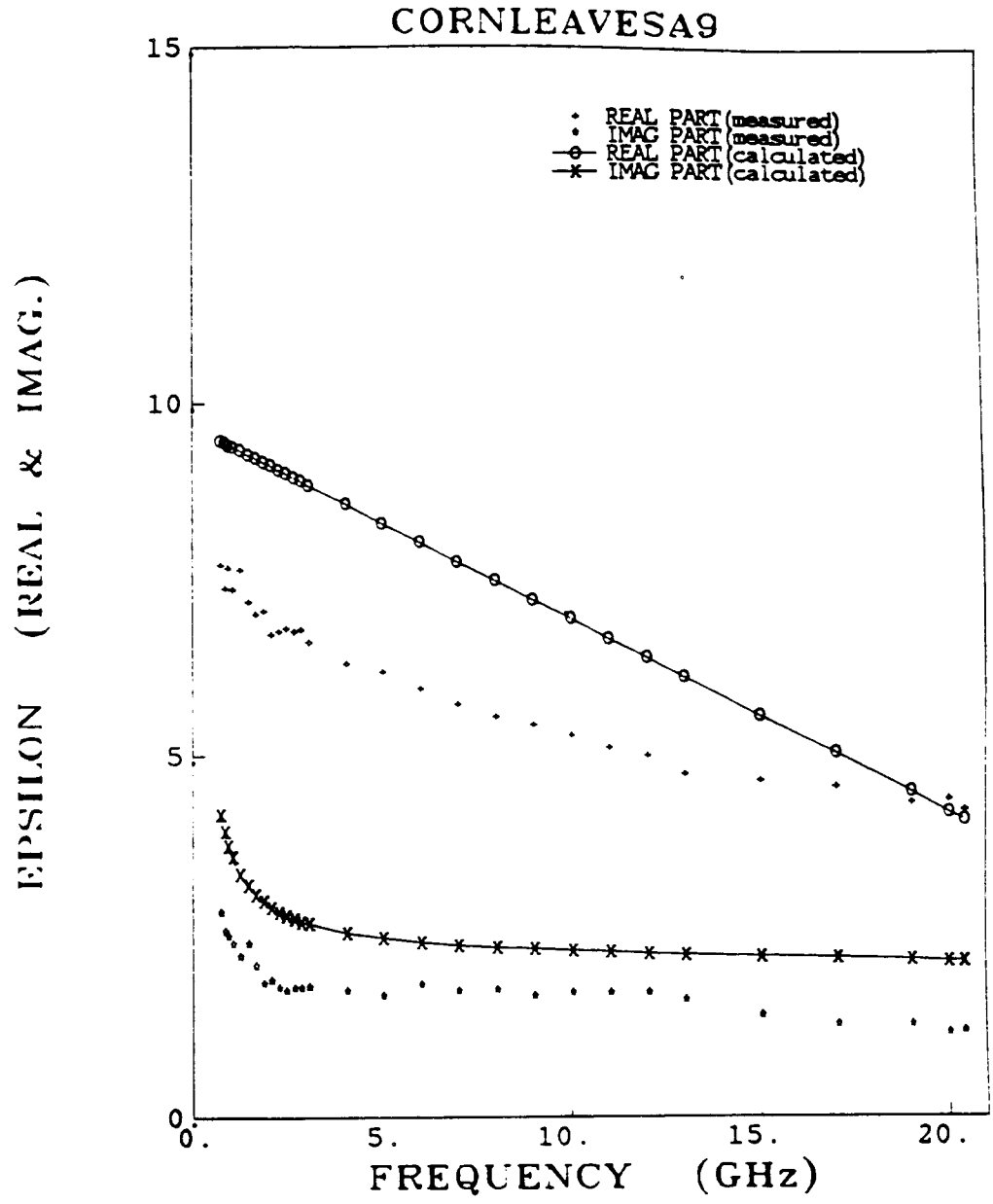

Figure 6.27. Comparison of calculated and measured dielectric spectra for corn leaves using a polynomial fit ($M_g = 0.333$).

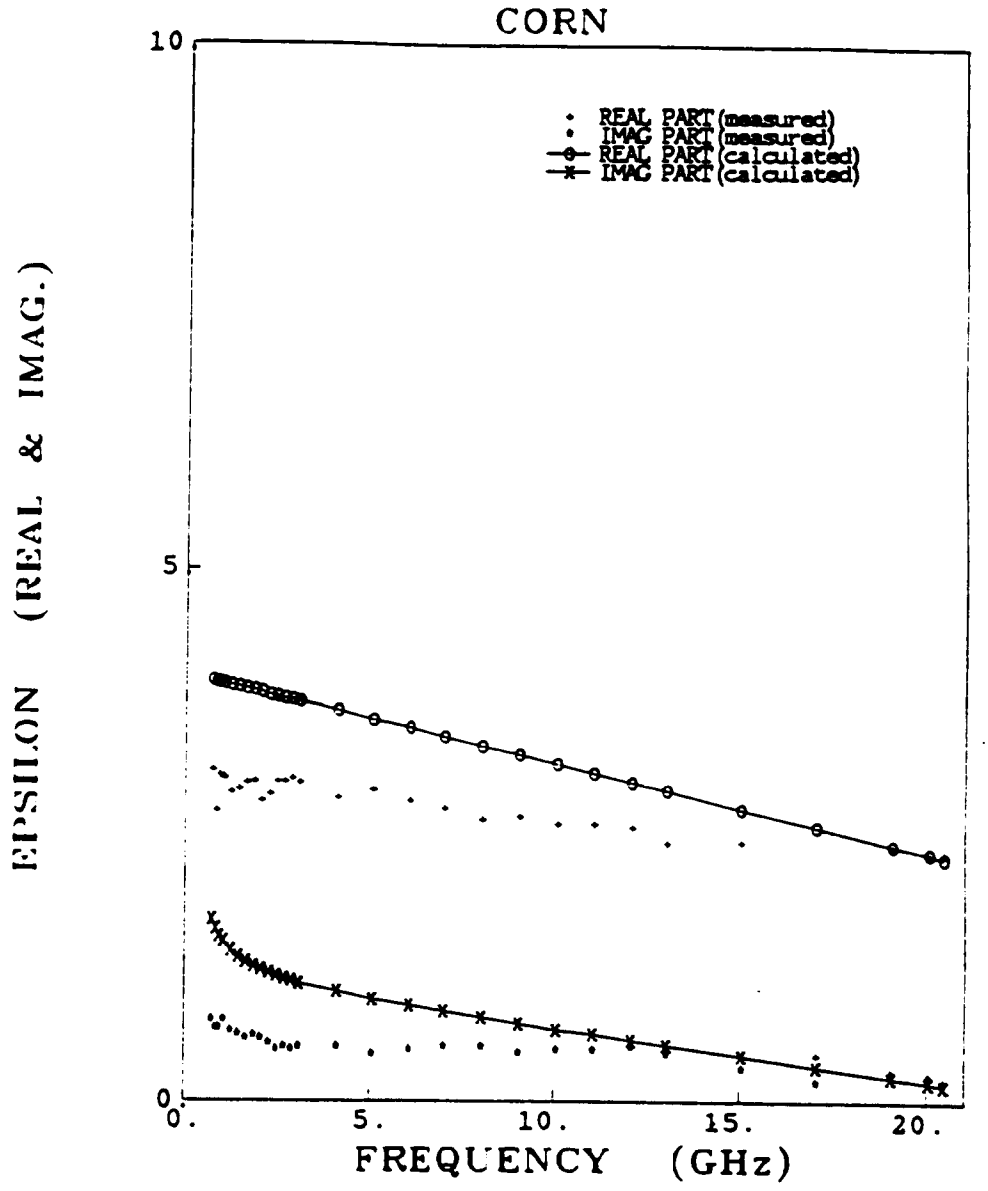

Figure 6.28. Comparison of calculated and measured dielectric spectra for corn leaves using a polynomial fit ($M_g = 0.168$).

6.3.5 Single-Phase Single-Relaxation Spectrum Debye Model

In the previous sections, a vegetation sample was considered as a heterogeneous mixture with four components: (1) vegetation bulk material, (2) air, (3) free water, and (4) bound water. A different approach is adopted in this section which assumes liquid water to have one phase which is neither free nor bound. It is difficult to satisfactorily define what is meant by bound water. It is generally agreed (Sayre, 1932) that bound water is that portion of the total water content that does not show some of the common properties of liquid (bulk) water. Since the binding forces generated by solid materials, like e.g. sucrose, are continuous and decay with increasing distance from the surfaces of their molecules, bound water actauly exists under various conditions of binding forces. The first layer of water, being the closest to the solid molecules and consequently the most tightly held by their surfaces, is considered to represent the "real" bound water. The further apart water molecules are from solid molecules, the weaker the attraction forces become. At a sufficient distance (corresponding to a sparsely concentrated solution), these attraction forces become small enough so as to consider all the water as free.

In this section we will consider the liquid water in a plant tissue as having a uniform single-phase spectrum with effective characteristics that are neither those of free water nor those of bound water. The attraction forces exerted by solid molecules on water molecules, in general, limit the mobility of the free dipoles and their ability of alignment with a time-varying electric field. Consequently,

C-4

the effective resonance frequency of a sucrose solution is less than that of free water. This effect may be treated as if the solution has an effective temperature lower than its physical temperature.

1. *Sucrose Solutions*

Let us choose a parameter that represents the concentration of a solution:

$$y = v_s/M_v \tag{6.57}$$

where v_s is the volume fraction of the solid material (solute) and M_v is that of the solvent. We may assume, arbitrarily, that the effective temperature depression ΔT caused by a concentation y is

$$\Delta T = -A_T y \tag{6.58}$$

where A_T is a constant that depends on the solute type but is independent of concentration. The effective temperature, T_e, of the solution is then defined as

$$T_e = T_p + \Delta T \tag{6.59}$$

where T_p is the physical temperature of the solution. Now, having the effective temperature, we can calculate the resonance frequency $f_{0w}(T_e)$

using the formulation derived by Stogryn (1971) for free water (see Section 6.1.3).

The quantity $\Delta_w(\equiv \epsilon_s - \epsilon_\infty)$ for liquid water is assumed to vary linearly with effective temperature,

$$\Delta_w = A_\Delta - B_\Delta T_e \tag{6.60}$$

where A_Δ and B_Δ are constants and T_e is in Kelvins. The values of A_Δ and B_Δ are derived from Equation 6.12 by considering only terms to first order. Similarly, the Cole-Cole relaxation spread parameter α is assumed to vary with y as:

$$\alpha = A_\alpha(1 - \exp -B_\alpha y) \tag{6.61}$$

where A_α and B_α are constants. The Debye model for a single-phase liquid is given as:

$$\epsilon = \epsilon_v v_s + [\epsilon_{\infty w} + \frac{\Delta_w}{1 + (jf/f_{0w})^{1-\alpha}}]M_v \tag{6.62}$$

Using the data measured for sucrose solutions A through G, regression analysis provided the following results:

$A_T = 67.290$,

$A_\Delta = 195.110$,

$B_\Delta = .371$,

$A_\alpha = .509$,

$B_\alpha = 1.035$,

$\epsilon_v = 2.442$, and $\epsilon_{\infty w} = 1.0$. Table 6.6 lists the statistical measures of the model fit to the data.

	RSS	EMSE	N	ρ	b	a
ϵ'	741.4	2.463	302	.997	-.630	1.027
ϵ''	254.5	.857	302	.980	.454	.962

Table 6.6 Model accuracy of Single-Phase Debye Model as applied to the sucrose solutions data at $T = 22^0C$.

Figures (6.23)-(6.29), which show the measured and calculated data for various sucrose solutions, indicate that the model is in very good agreement with the measured data.

2. *Corn Leaves*

To test the single-relaxation Debye model for vegetation data, we shall use the same parameter y to represent the tissue volume fractions, in exactly the same manner it was used for sucrose solutions. Consequently, we shall use the same expressions obtained from the sucrose-solutions optimization

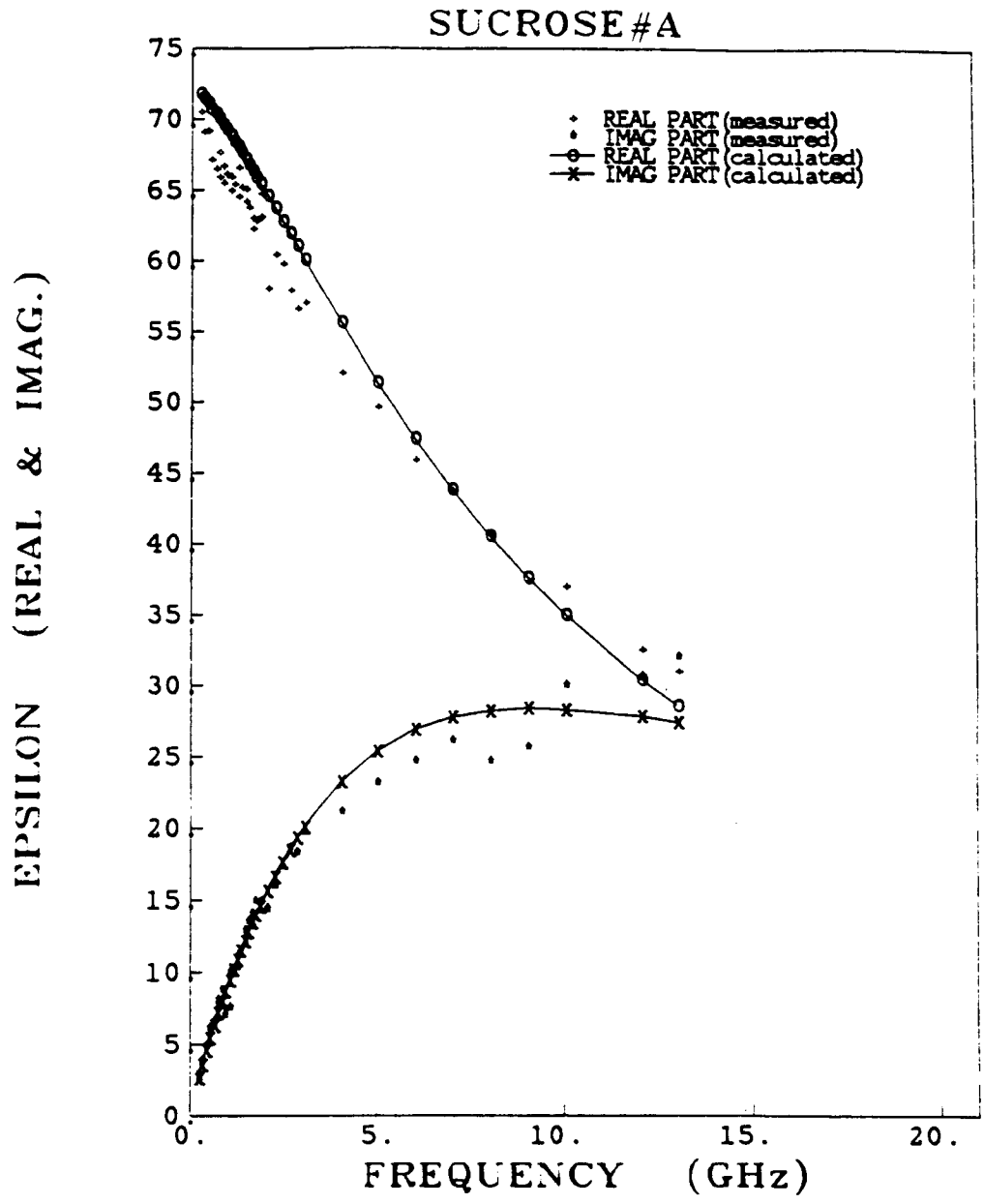

Figure 6.29. Comparison of calculated and measured dielectric spectra for sucrose solution (A) using a Debye-like model with a single variable relaxation spectrum ($V_s = 0.239$ and $M_v = 0.761$).

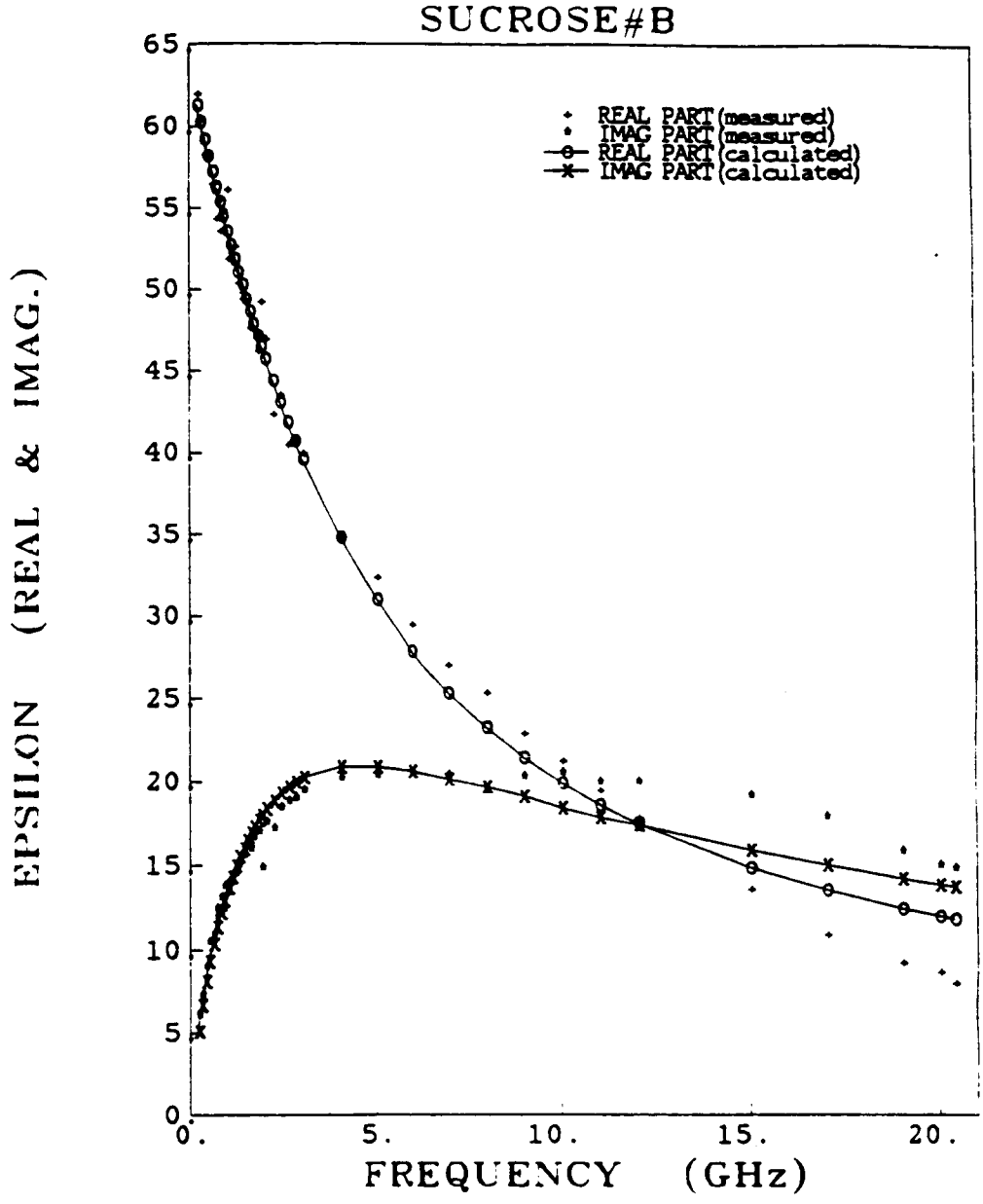

Figure 6.30. Comparison of calculated and measured dielectric spectra for sucrose solution (B) using a Debye-like model with a single variable relaxation spectrum ($V_s = 0.385$ and $M_v = 0.615$).

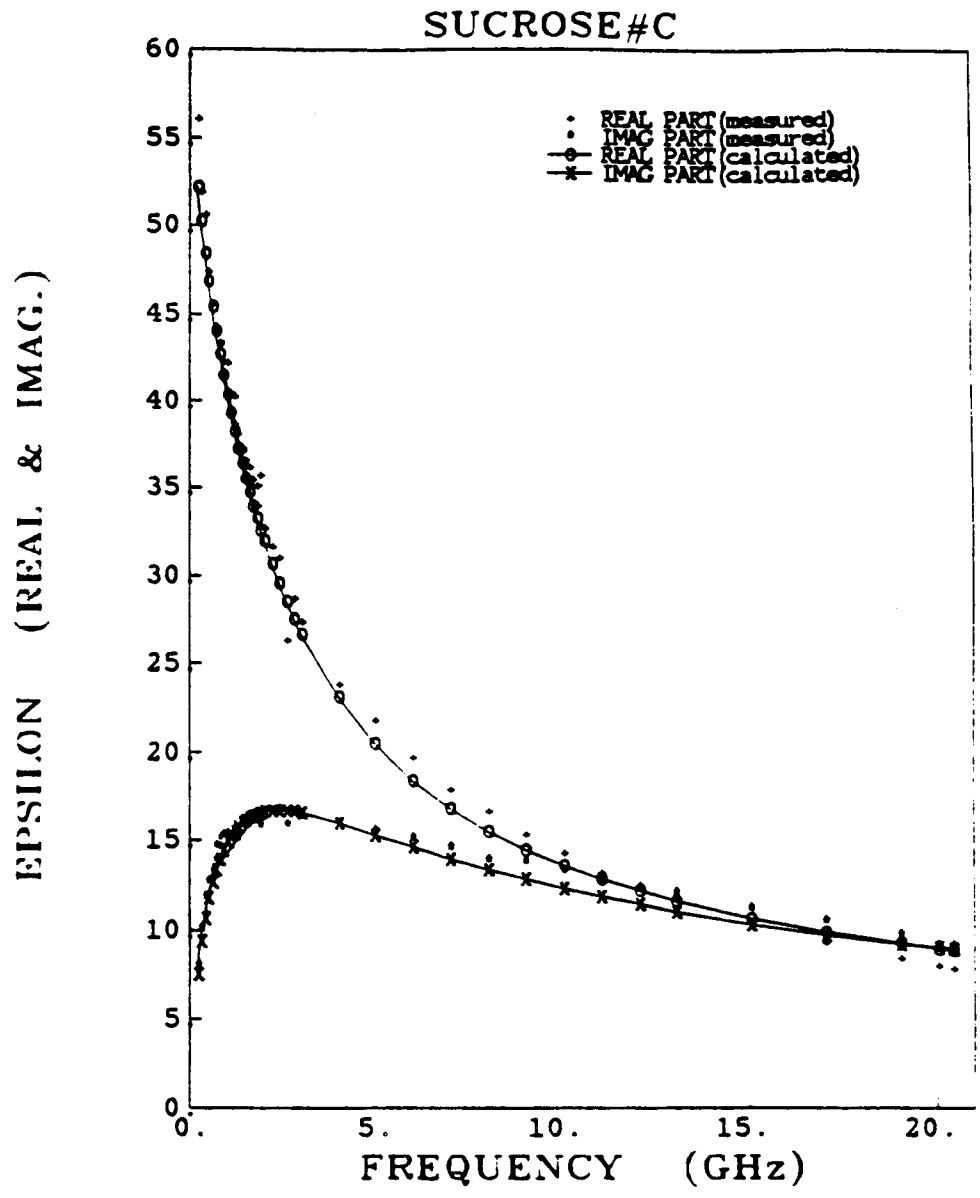

Figure 6.31. Comparison of calculated and measured dielectric spectra for sucrose solution (C) using a Debye-like model with a single variable relaxation spectrum ($V_s = 0.485$ and $M_s = 0.515$).

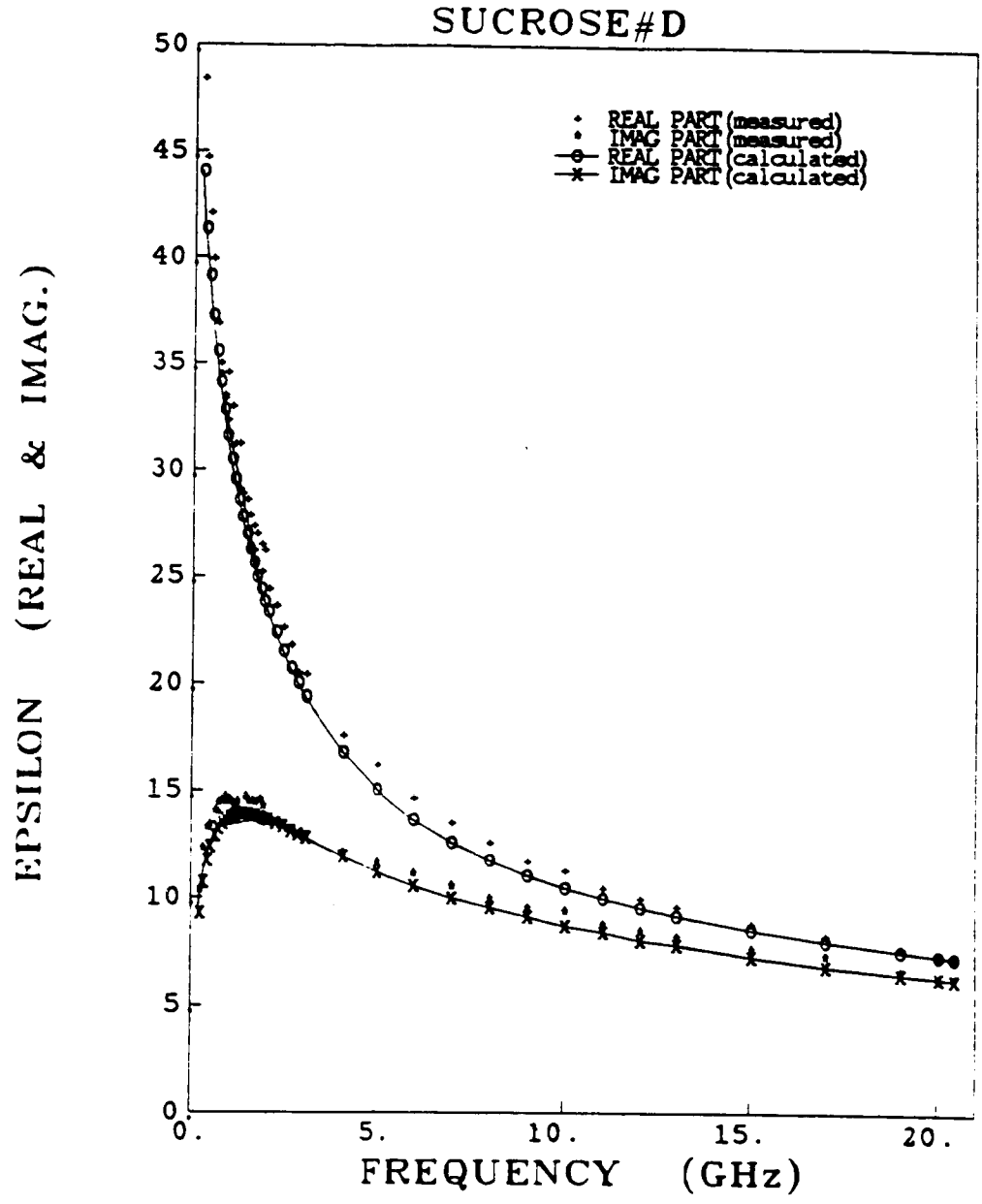

Figure 6.32. Comparison of calculated and measured dielectric spectra for sucrose solution (D) using a Debye-like model with a single variable relaxation spectrum ($V_s = 0.559$ and $M_v = 0.441$).

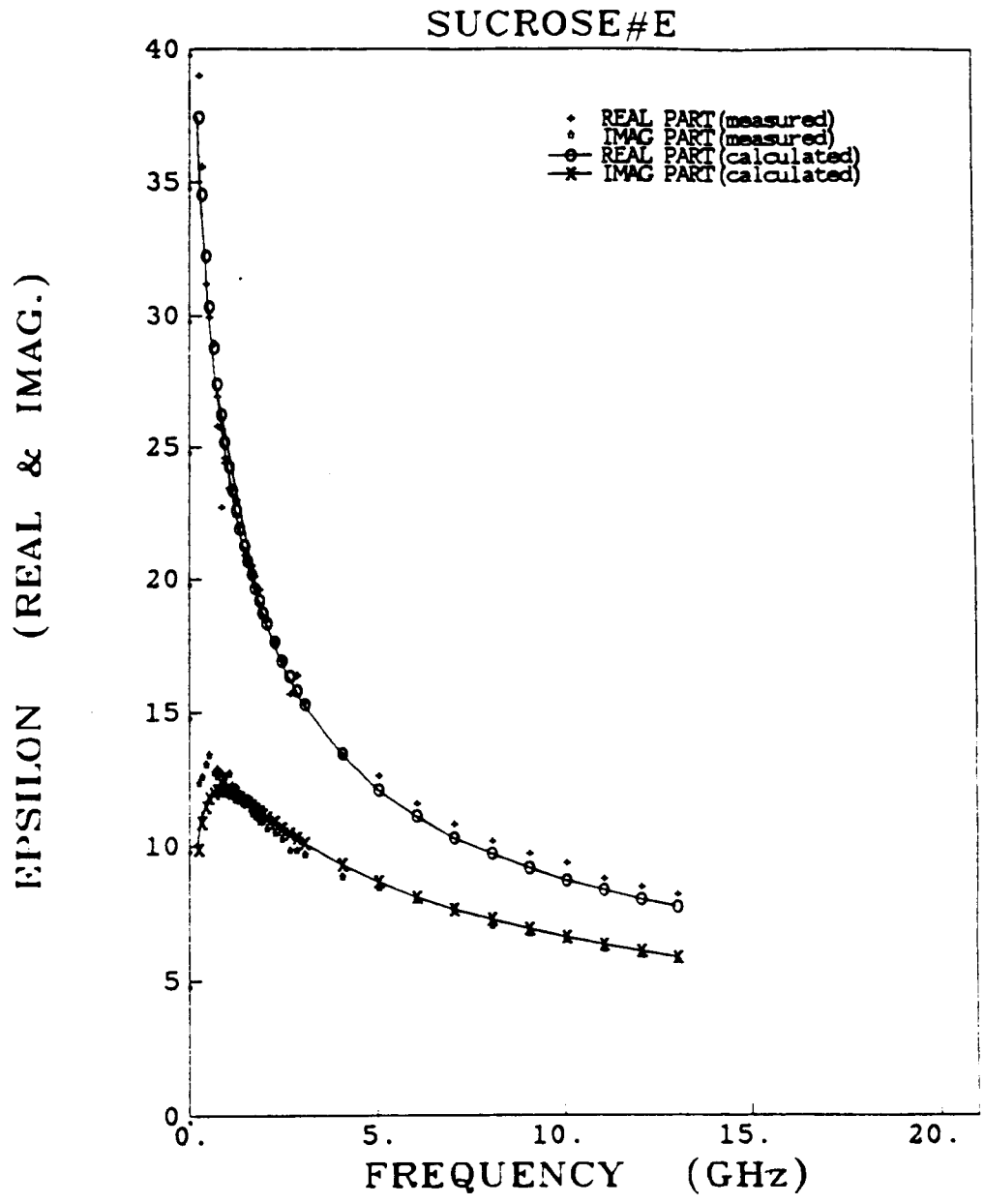

Figure 6.33. Comparison of calculated and measured dielectric spectra for sucrose solution (E) using a Debye-like model with a single variable relaxation spectrum ($V_s = 0.613$ and $M_v = 0.387$).

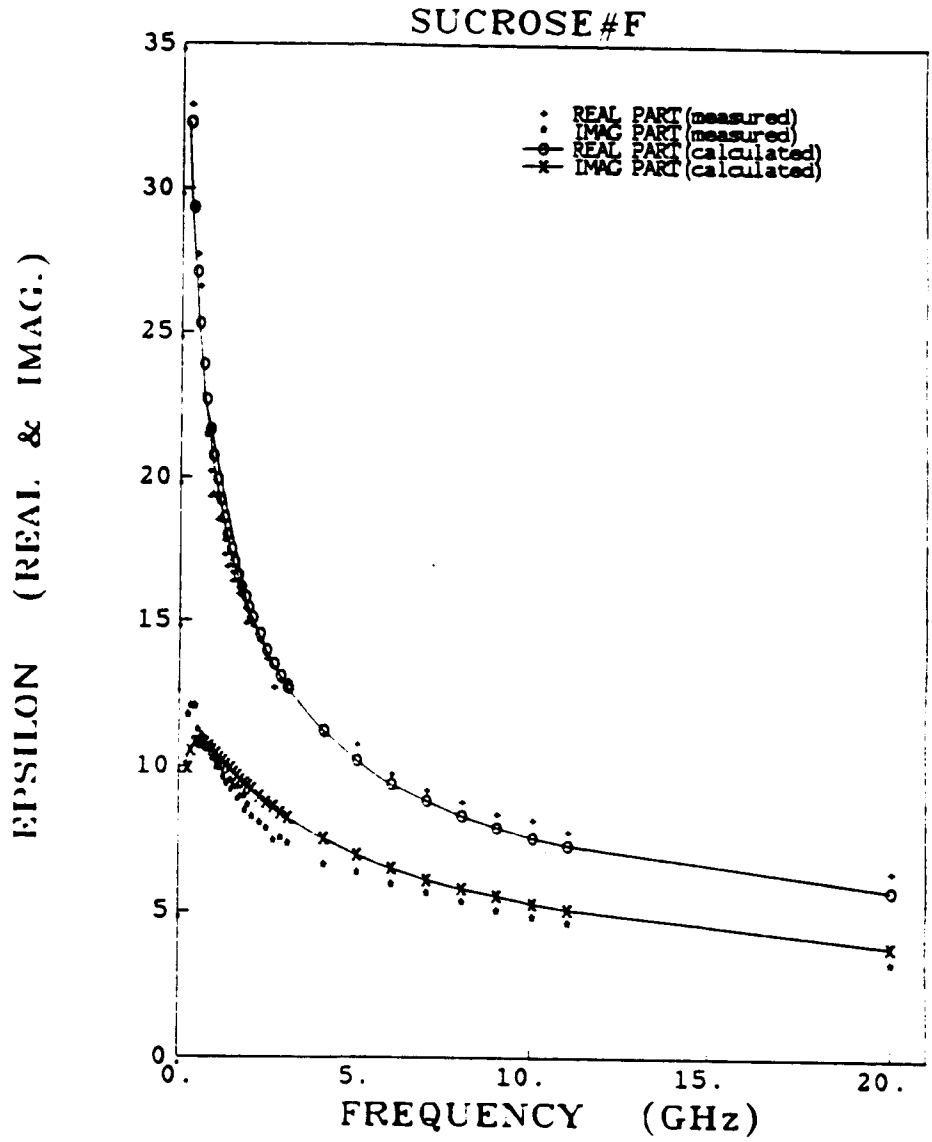

Figure 6.34. Comparison of calculated and measured dielectric spectra for sucrose solution (F) using a Debye-like model with a single variable relaxation spectrum ($V_s = 0.655$ and $M_v = 0.345$).

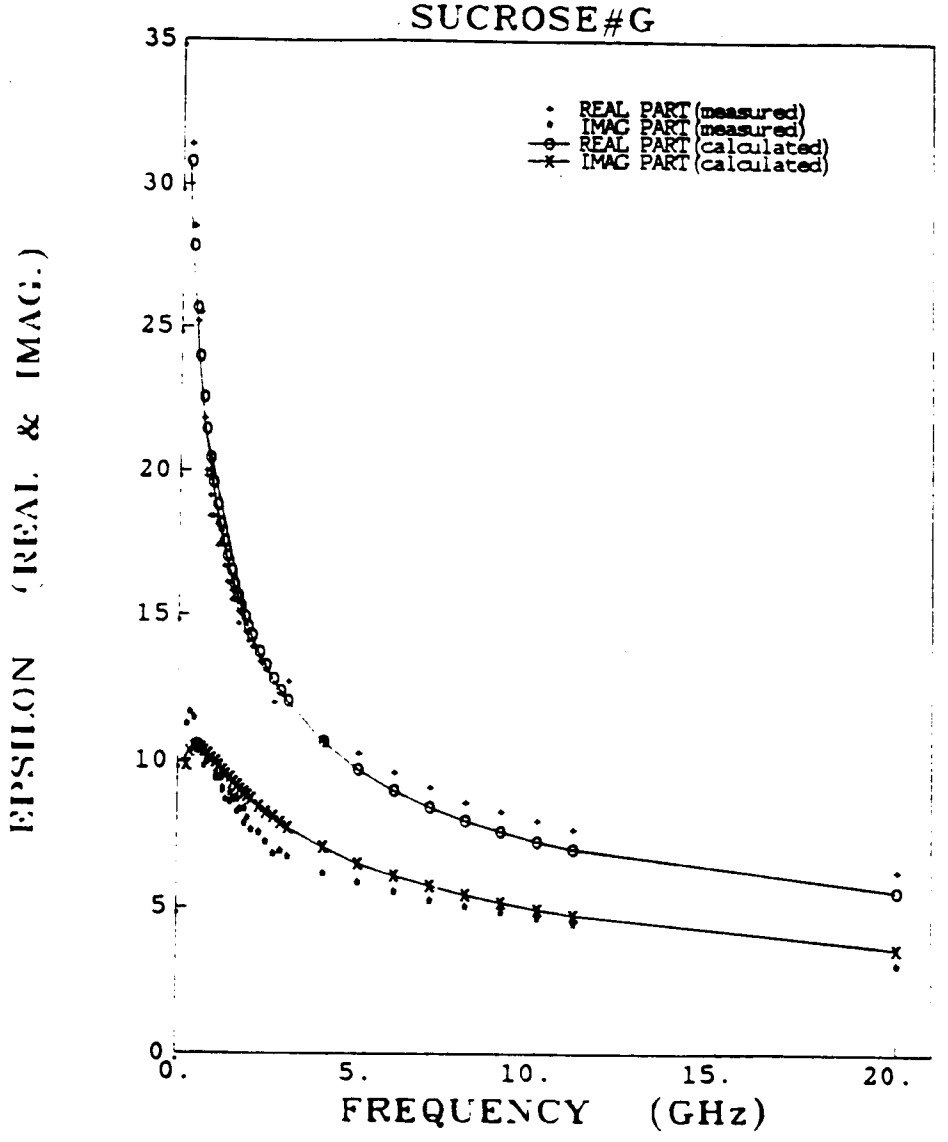

Figure 6.35. Comparison of calculated and measured dielectric spectra for sucrose solution (G) using a Debye-like model with a single variable relaxation spectrum ($V_s = 0.667$ and $M_v = 0.333$).

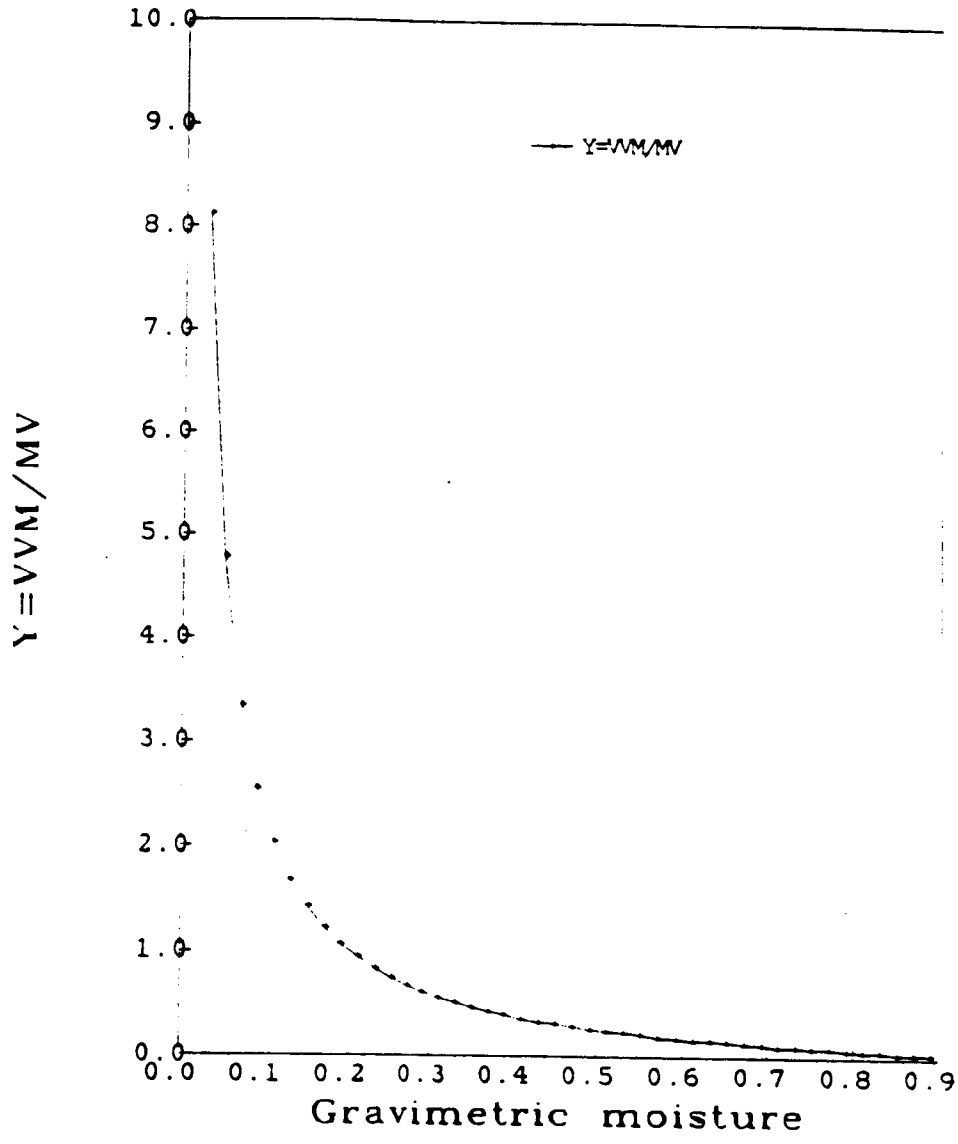

Figure 6.36. For the single phase model, y(V_{vm}/M_v) is plotted against gravimetric moisture M_g.

to model the data for corn leaves. These expressions are:

$$y = v_s/M_v, \tag{6.63}$$

$$\Delta T = -67.290y, \tag{6.64}$$

$$T_e = T_p + \Delta T(\mathrm{K}), \tag{6.65}$$

$f_{0w}(T_e)$ is according to the expressions given in Stogryn (1971),

$$\Delta_w = 195.110 - .371T_e(\mathrm{K}), and \tag{6.66}$$

$$\alpha = .509(1 - \exp -1.035y). \tag{6.67}$$

The Expressions for the volume fractions are:

$$M_v = \frac{M_g}{M_g + \frac{1-M_g}{\rho_{DV}}}, \tag{6.68}$$

and

$$v_s = v_v(Max.) = \eta(1 - M_v). \tag{6.69}$$

In order to calculate v_s and M_v, we have to assume values for ρ_{DV} and ρ_{BV}.

$$\eta = \rho_{DV}/\rho_{BV}. \tag{6.70}$$

The model may be written in the following form:

$$\epsilon = \epsilon_\infty + [\frac{\Delta_w}{1+(jf/f_{0w})^{1-\alpha}} - j\sigma/f]M_v \tag{6.71}$$

where $\epsilon_\infty = A_\infty + B_\infty M_v$ and $\sigma_e = A_\sigma - B_\sigma M_v$. Using corn leaves data and regression analysis (BMDP), the following values were selected for the unknown parameters:

$\rho_{DV} = .154\ g/cm^3$,

$\rho_{BV} = 3.978\ g/cm^3$,

$A_\infty = 1.656$,

$B_\infty = 24.374$,

$A_\sigma = 37.396$, and

$B_\sigma = 18.892$.

Table 6.7 gives the statistical parameters associated with fitting the model to the data.

	RSS	EMSE	N	ρ	b	a
ϵ'	1063.99	1.579	676	.987	.230	.976
ϵ''	390.60	.580	676	.969	.439	.923

Table 6.7 Model accuracy for corn leaves data, Single-Phase Debye Model, $T = 22^0C$.

Figure (6.30) shows a plot of the parameter y as a function of gravimetric moisture, and Fig. (6.31) shows how the resonance frequency varies with gravimetric moisture. When $M_g = 1$ (pure water), $f_0 = 18$ GHz while when $M_g = 0$, $f_0 = 0$. The volume fractions calculated using the optimized values of ρ_{DV} and ρ_{BV} are shown in Fig.(6.32). Figure (6.33)-(6.43) show frequency spectra for corn leave, at selected moisture conditions, plotted against the model. Similarly, Figs. (6.44)-(6.51) show dielectric plots for corn leaves as a function of M_g. The model, in general, fits the measured data very well (at least as good as the two-phase Debye model does).

Tables 6.8 and 6.9 provide comparison of the overall performance of the five models considered in this Chapter.

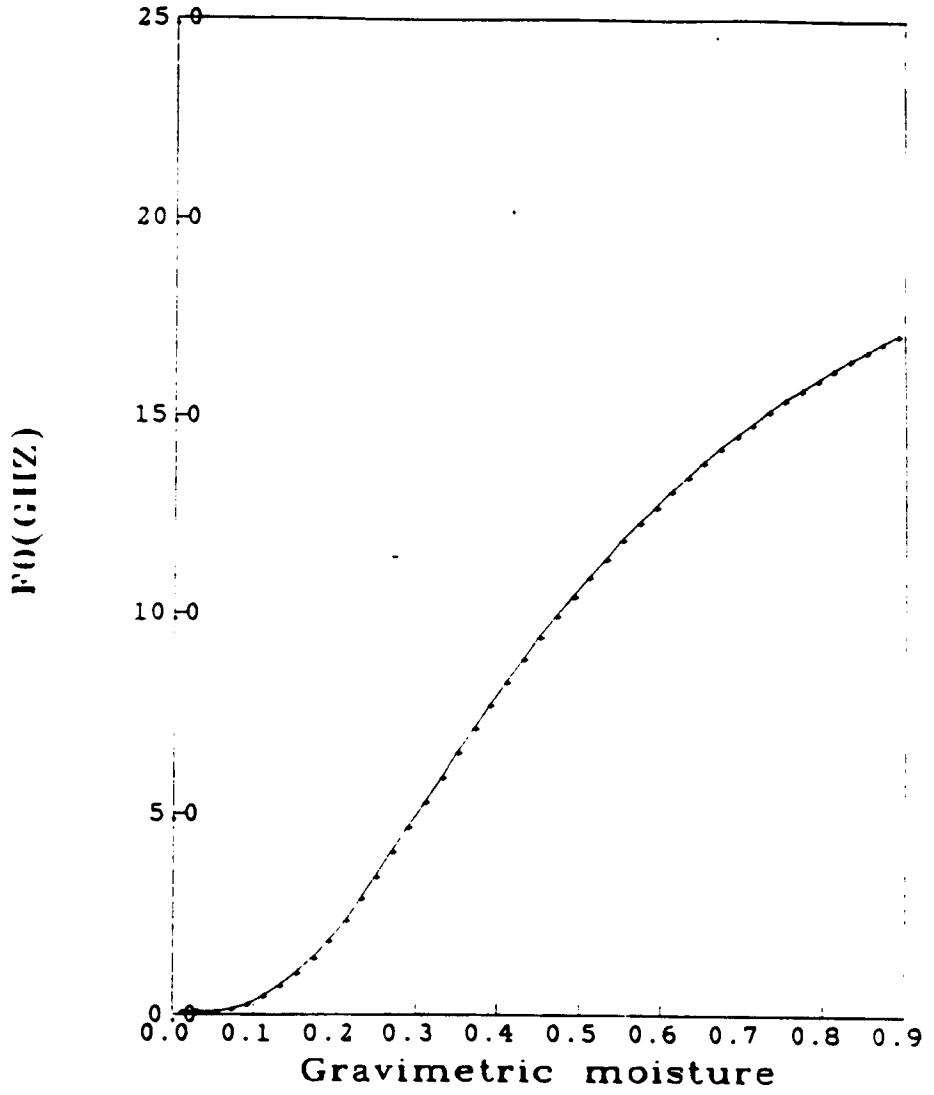

Figure 6.37. The effective resonant frequency f_0(GHz) of the single water phase versus gravimetric moisture M_g.

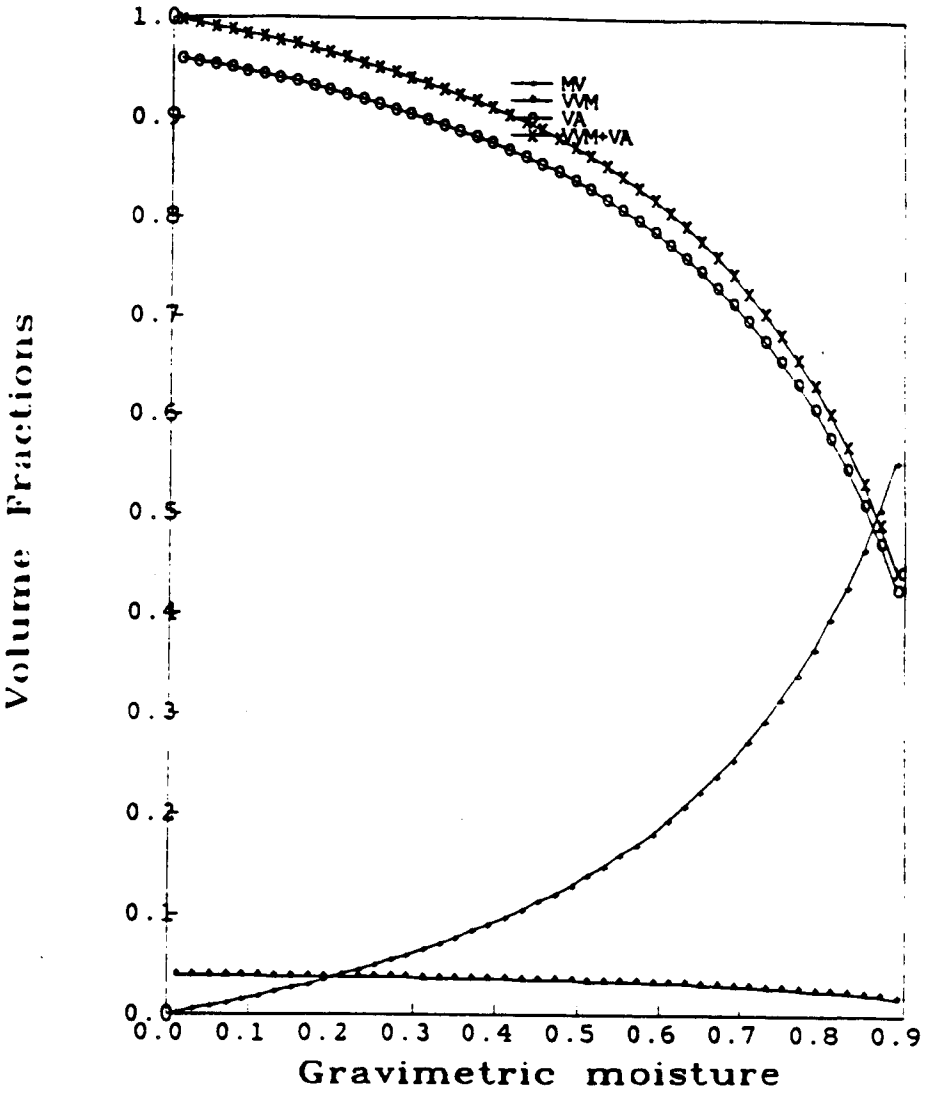

Figure 6.38. Volume fractions of corn leaves as calculated from the single phase model. M_v, V_{vm}, Va, and $V_{vm} + V_a$ are the volume fractions of water, bulk vegetation material, air, and dry vegetation material, respectively.

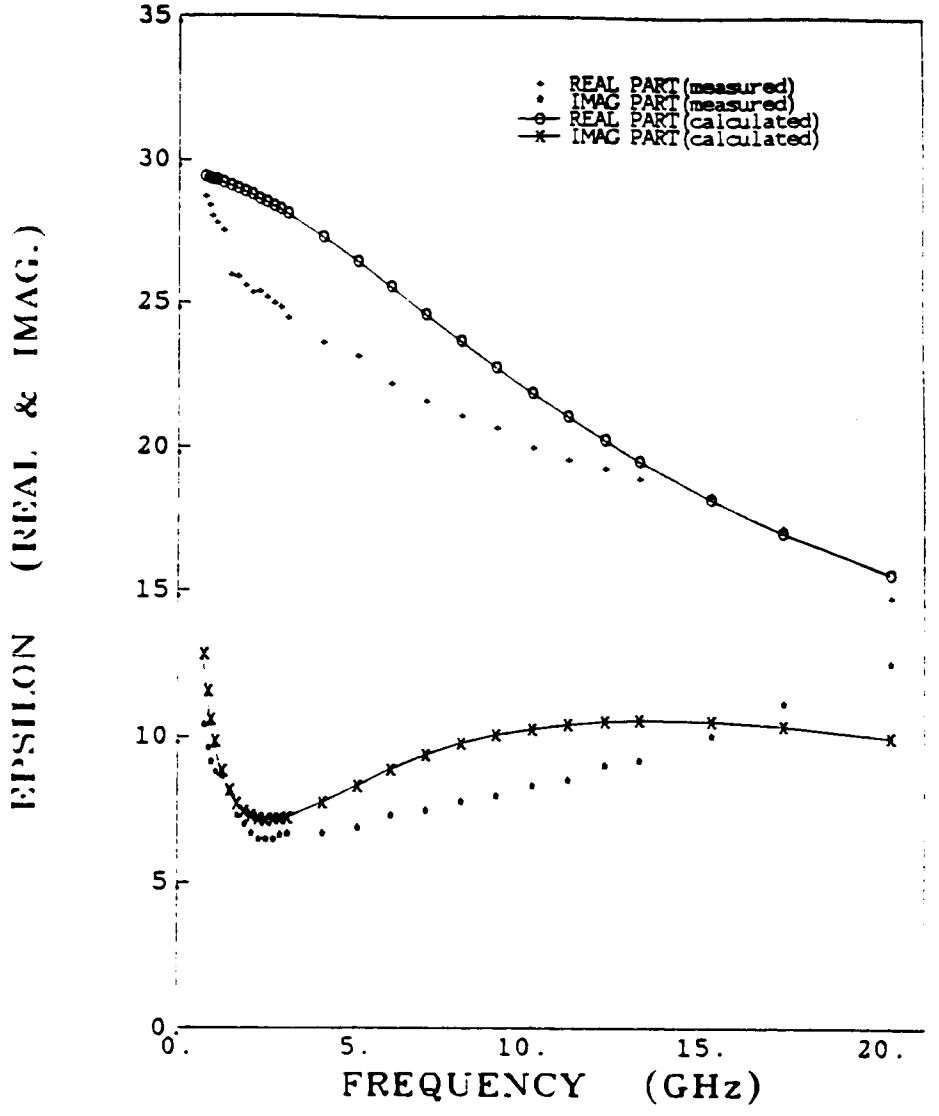

Figure 6.39. Comparison of calculated and measured dielectric spectra for corn leaves using a Debye-like model with a single relaxation spectrum (variable) for $M_g = 0.681$.

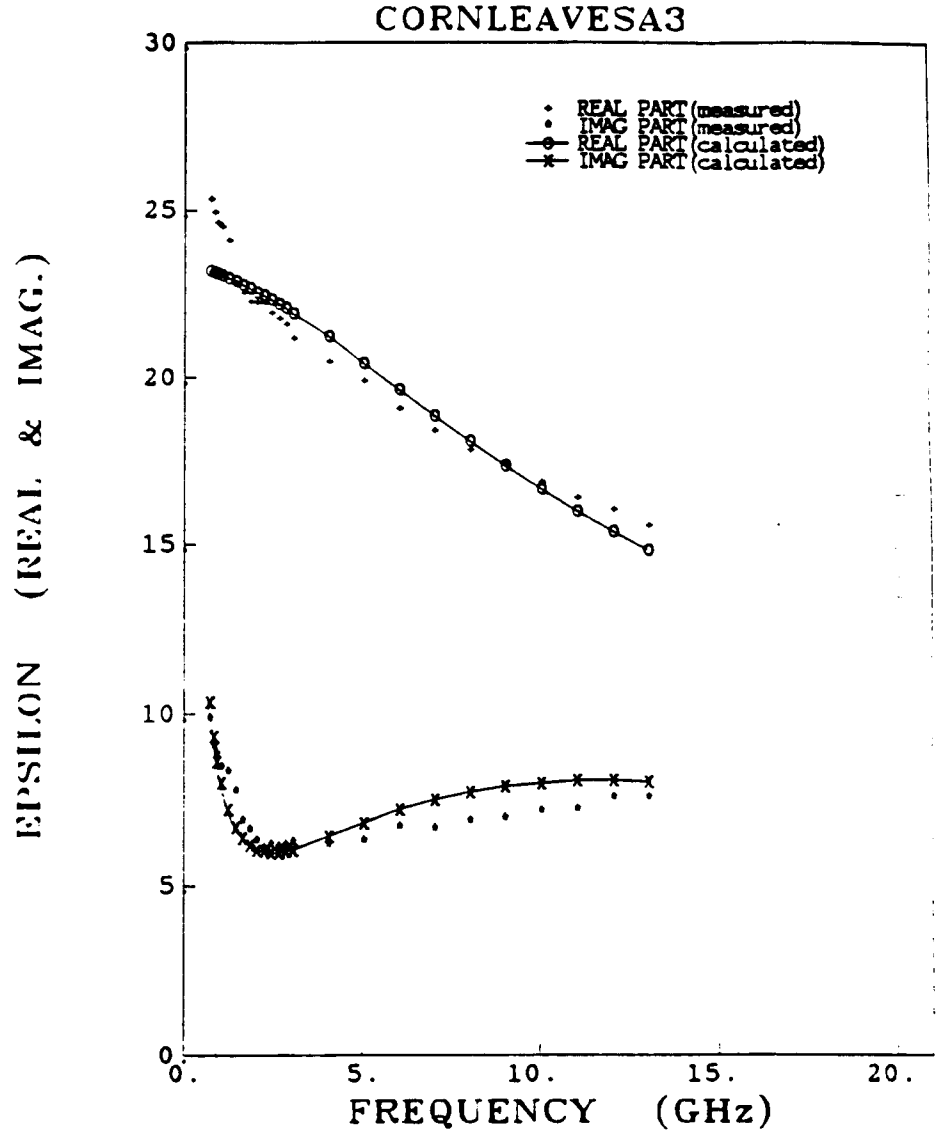

Figure 6.40. Comparison of calculated and measured dielectric spectra for corn leaves using a Debye-like model with a single relaxation spectrum (variable) for $M_g = 0.605$.

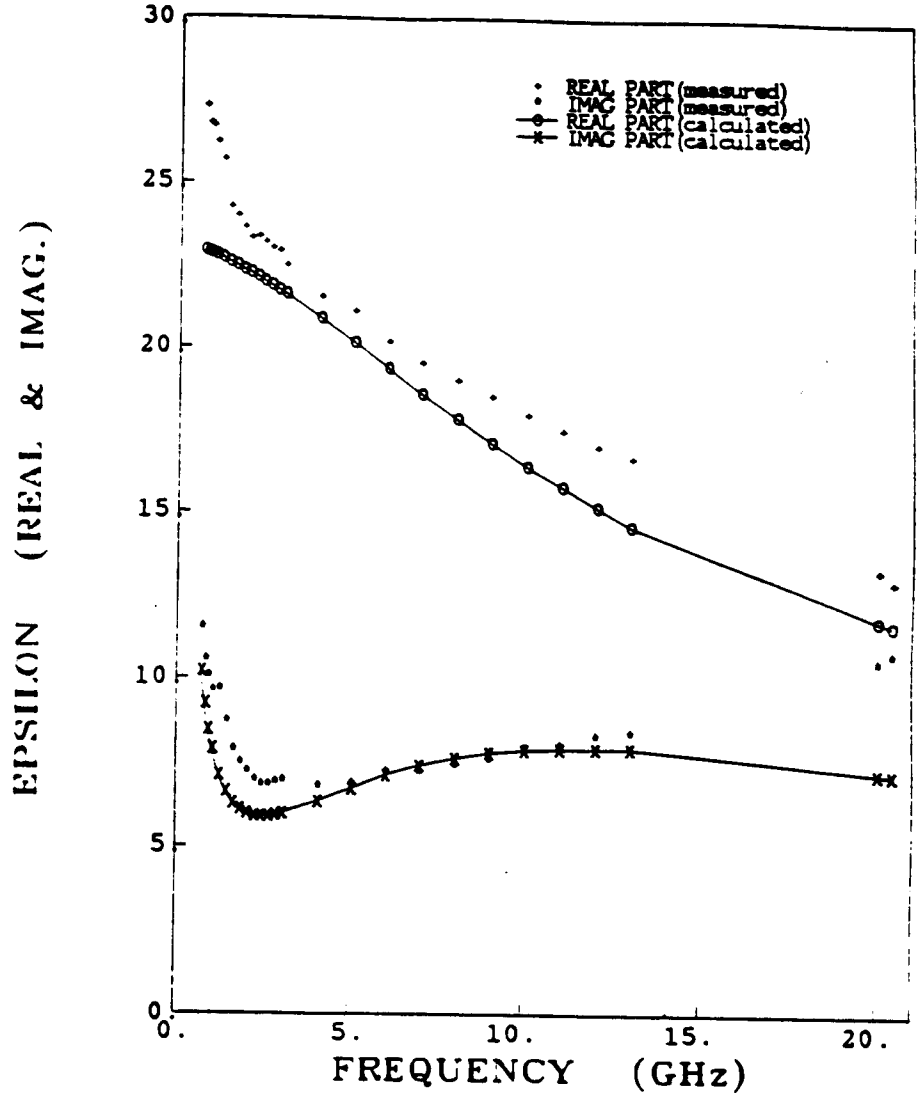

Figure 6.41. Comparison of calculated and measured dielectric spectra for corn leaves using a Debye-like model with a single relaxation spectrum (variable) for $M_g = 0.601$.

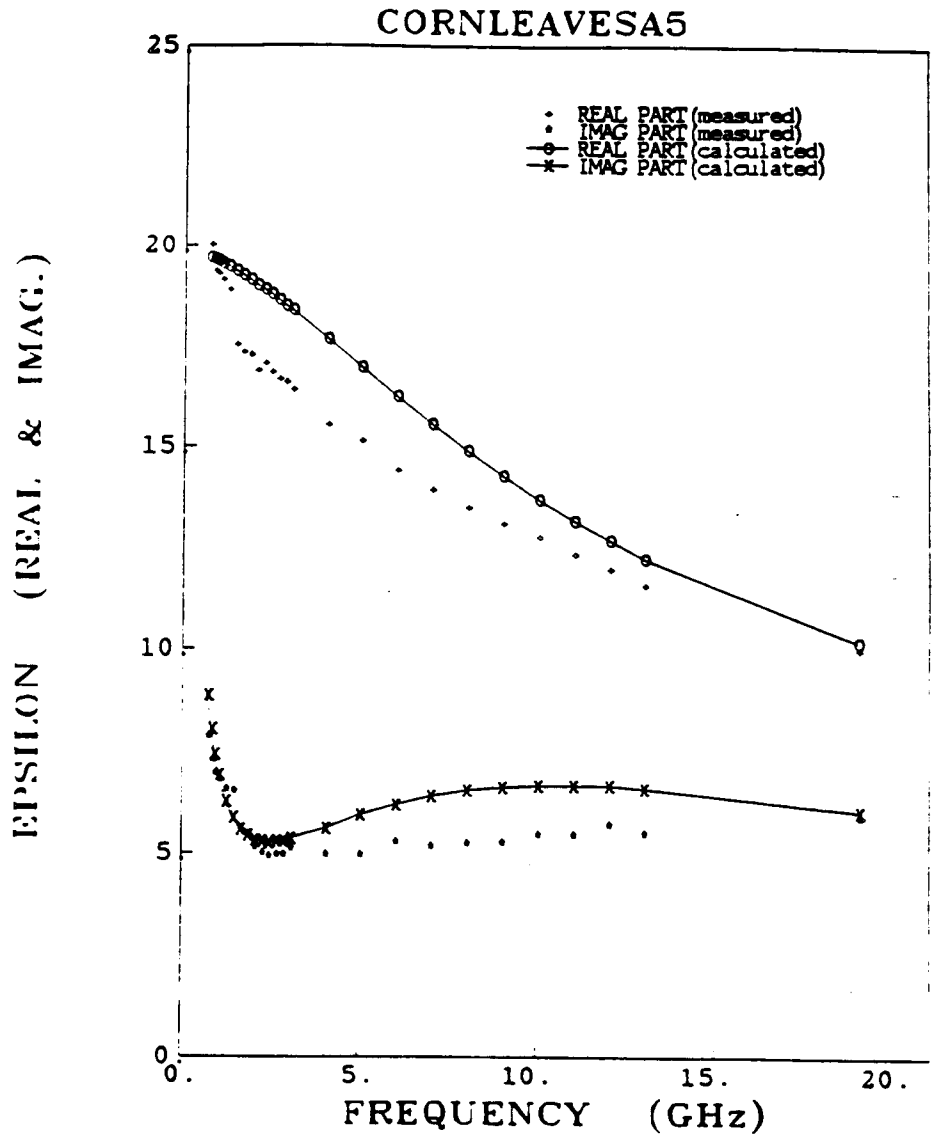

Figure 6.42. Comparison of calculated and measured dielectric spectra for corn leaves using a Debye-like model with a single relaxation spectrum (variable) for $M_g = 0.551$.

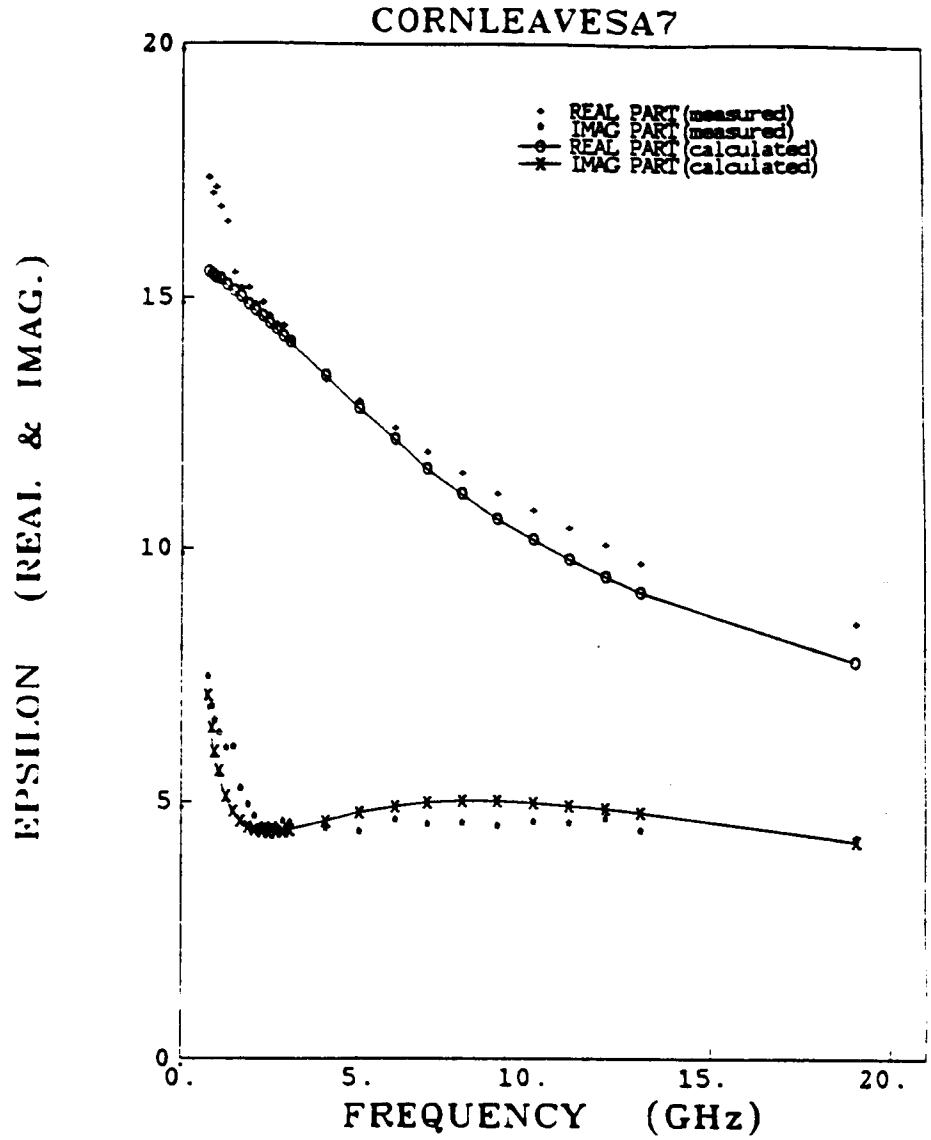

Figure 6.43. Comparison of calculated and measured dielectric spectra for corn leaves using a Debye-like model with a single relaxation spectrum (variable) for $M_g = 0.472$.

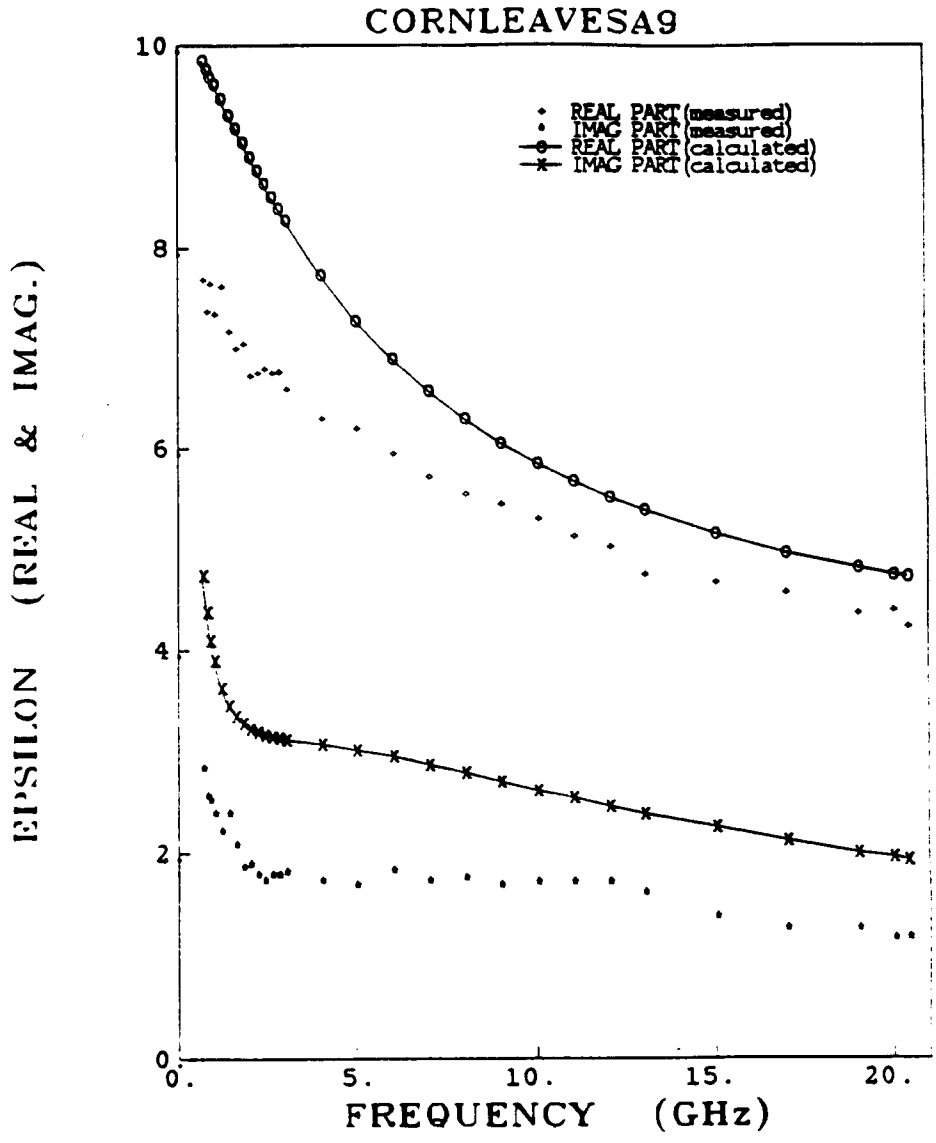

Figure 6.44. Comparison of calculated and measured dielectric spectra for corn leaves using a Debye-like model with a single relaxation spectrum (variable) for $M_g = 0.333$.

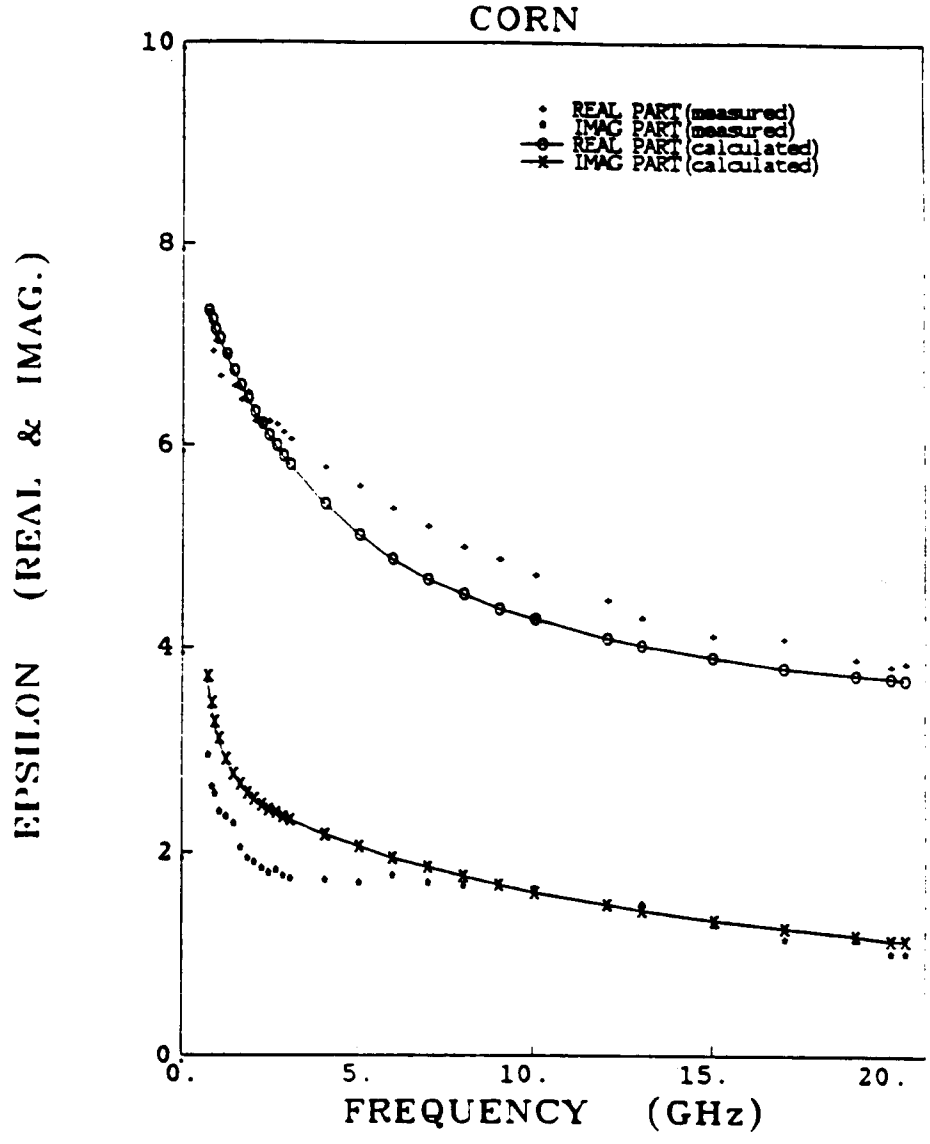

Figure 6.45. Comparison of calculated and measured dielectric spectra for corn leaves using a Debye-like model with a single relaxation spectrum (variable) for $M_g = 0.258$.

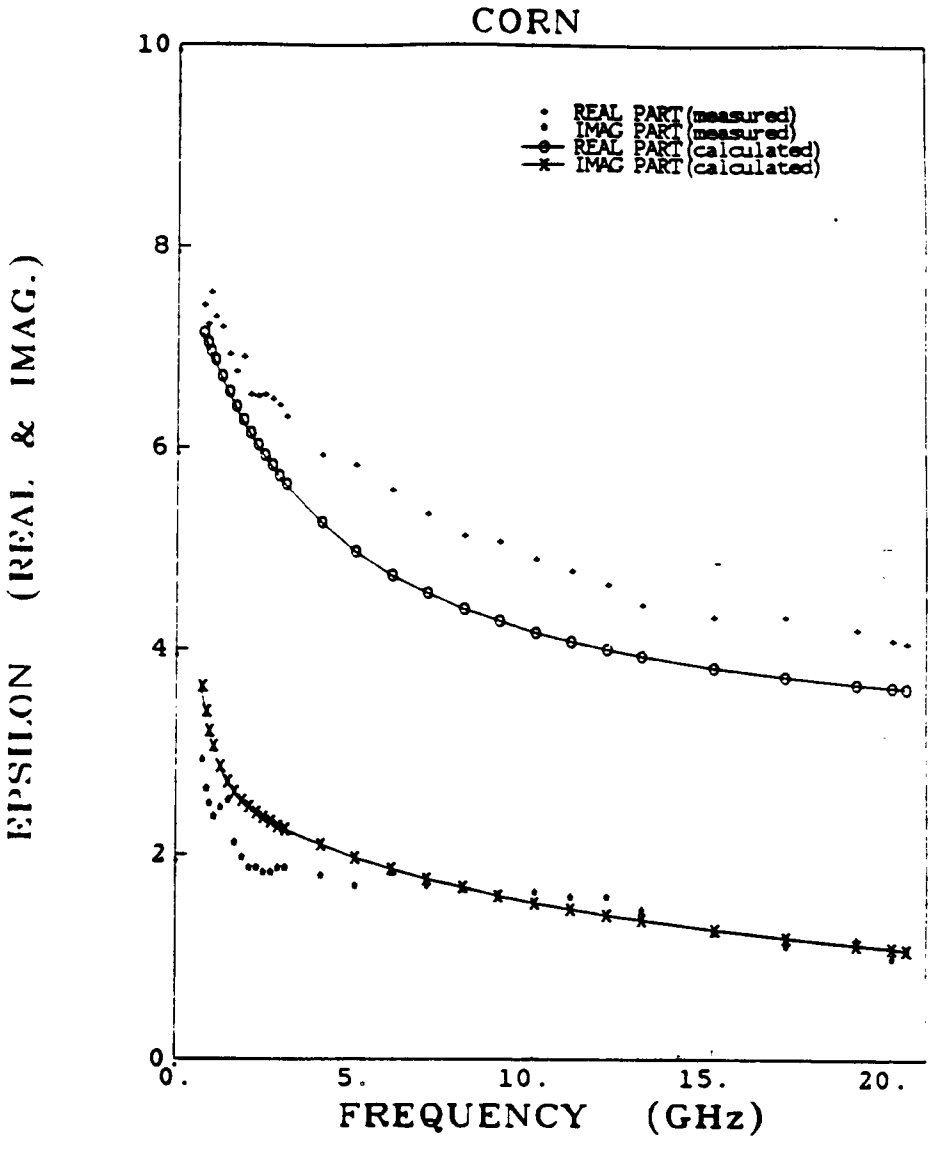

Figure 6.46. Comparison of calculated and measured dielectric spectra for corn leaves using a Debye-like model with a single relaxation spectrum (variable) for $M_g = 0.252$.

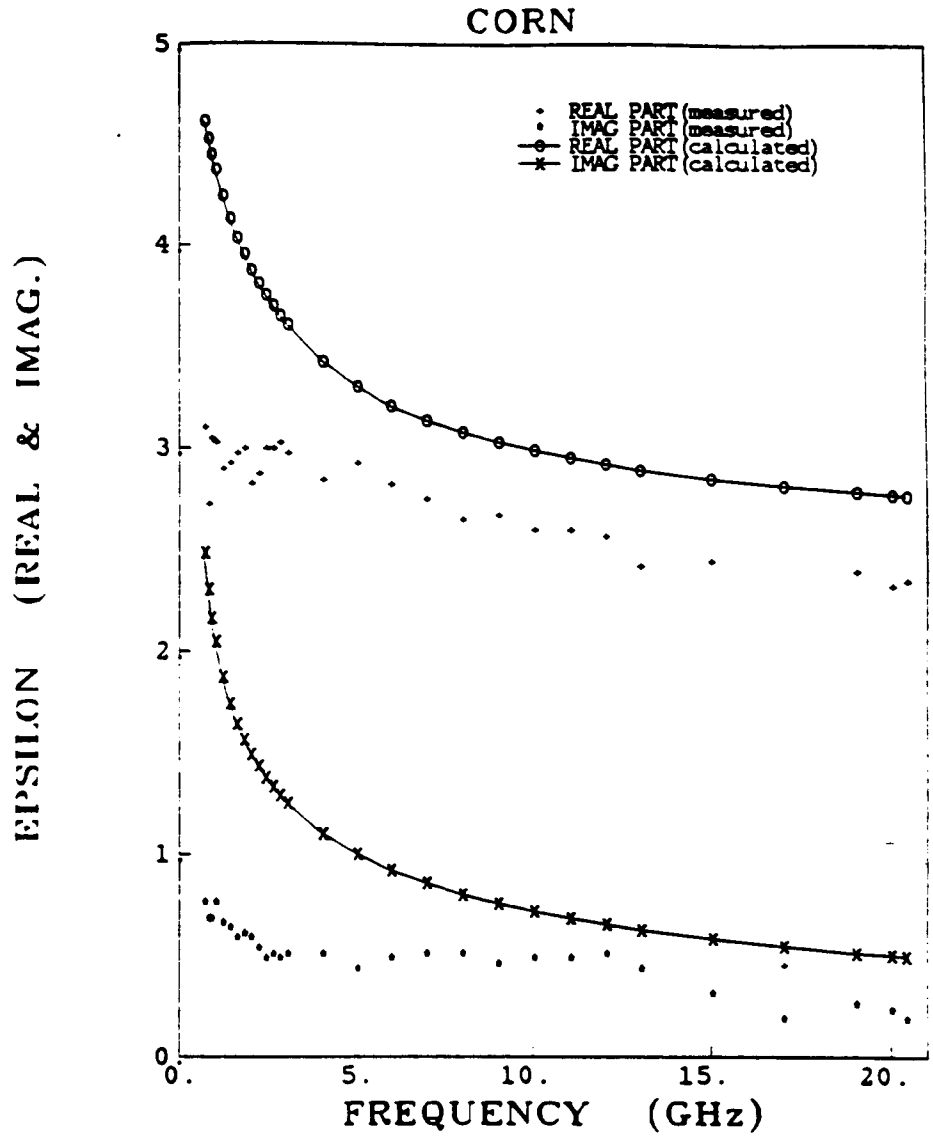

Figure 6.47. Comparison of calculated and measured dielectric spectra for corn leaves using a Debye-like model with a single relaxation spectrum (variable) for $M_g = 0.168$.

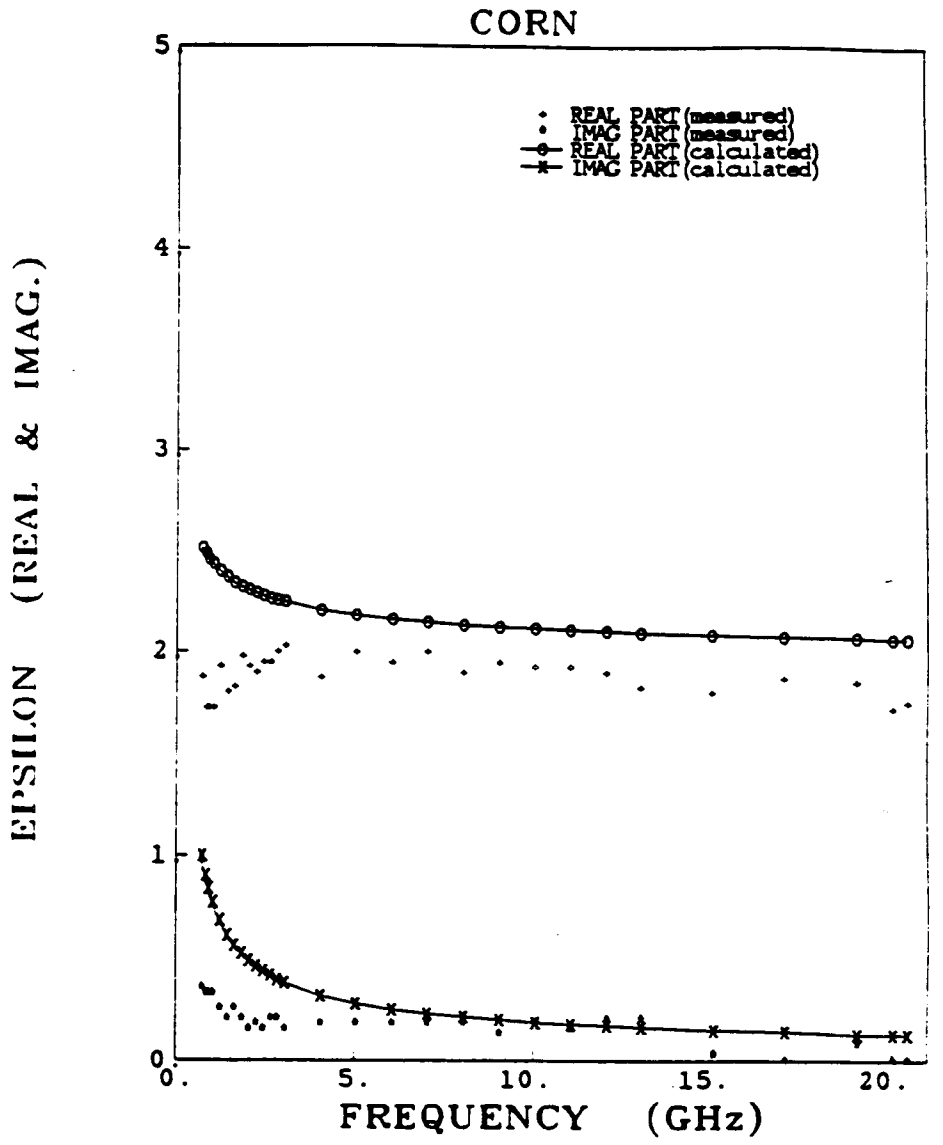

Figure 6.48. Comparison of calculated and measured dielectric spectra for corn leaves using a Debye-like model with a single relaxation spectrum (variable) for $M_g = 0.074$.

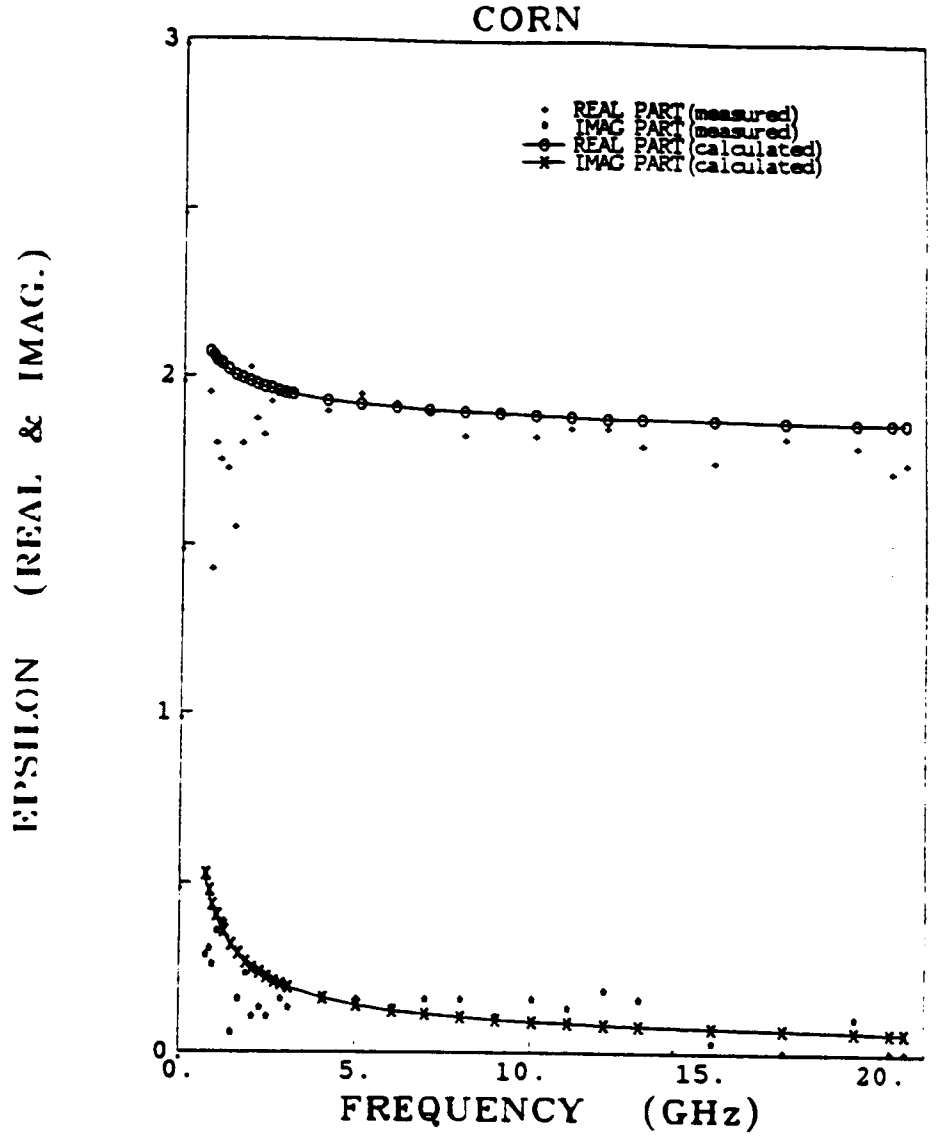

Figure 6.49. Comparison of calculated and measured dielectric spectra for corn leaves using a Debye-like model with a single relaxation spectrum (variable) for $M_g = 0.041$.

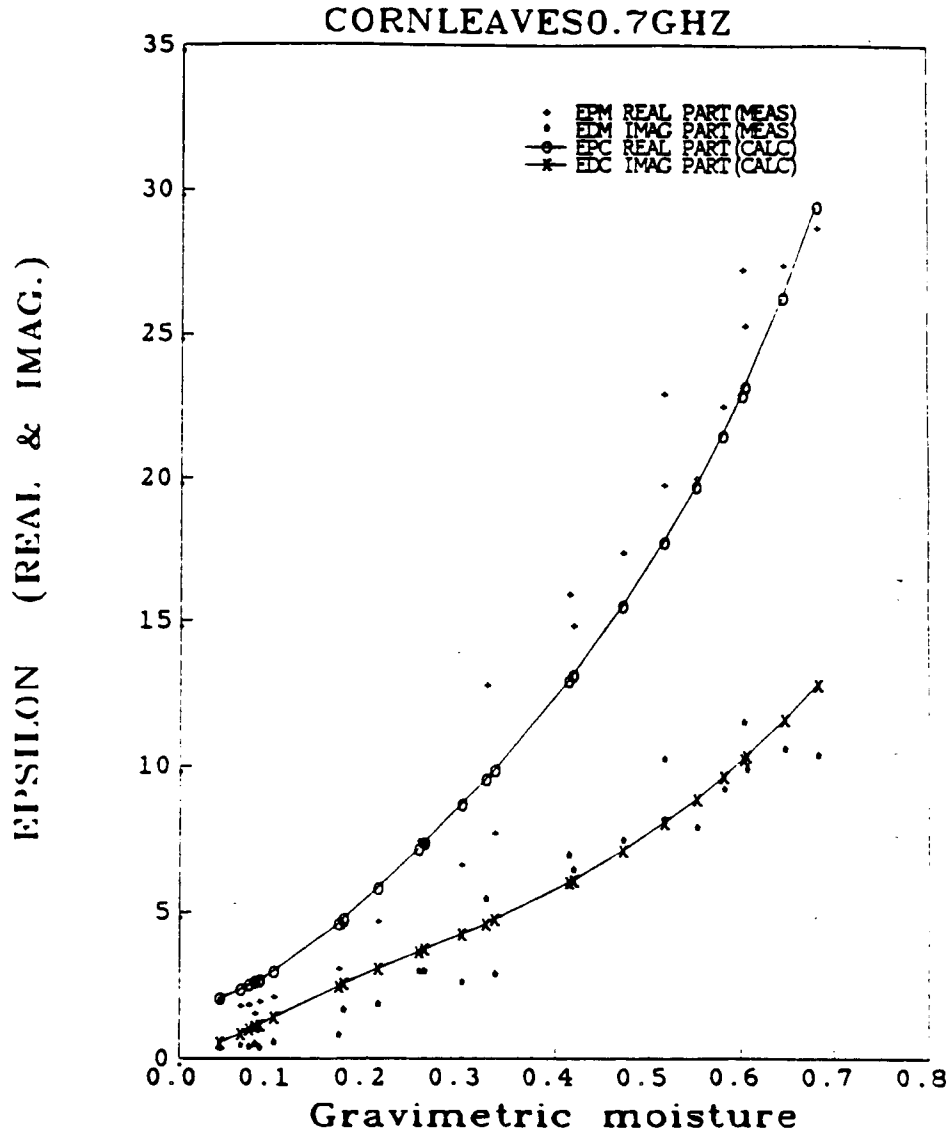

Figure 6.50. Comparison of calculated and measured dielectric constant versus moisture for corn leaves using a Debye-like model with a single variable relaxation spectrum for f = 0.7 GHz.

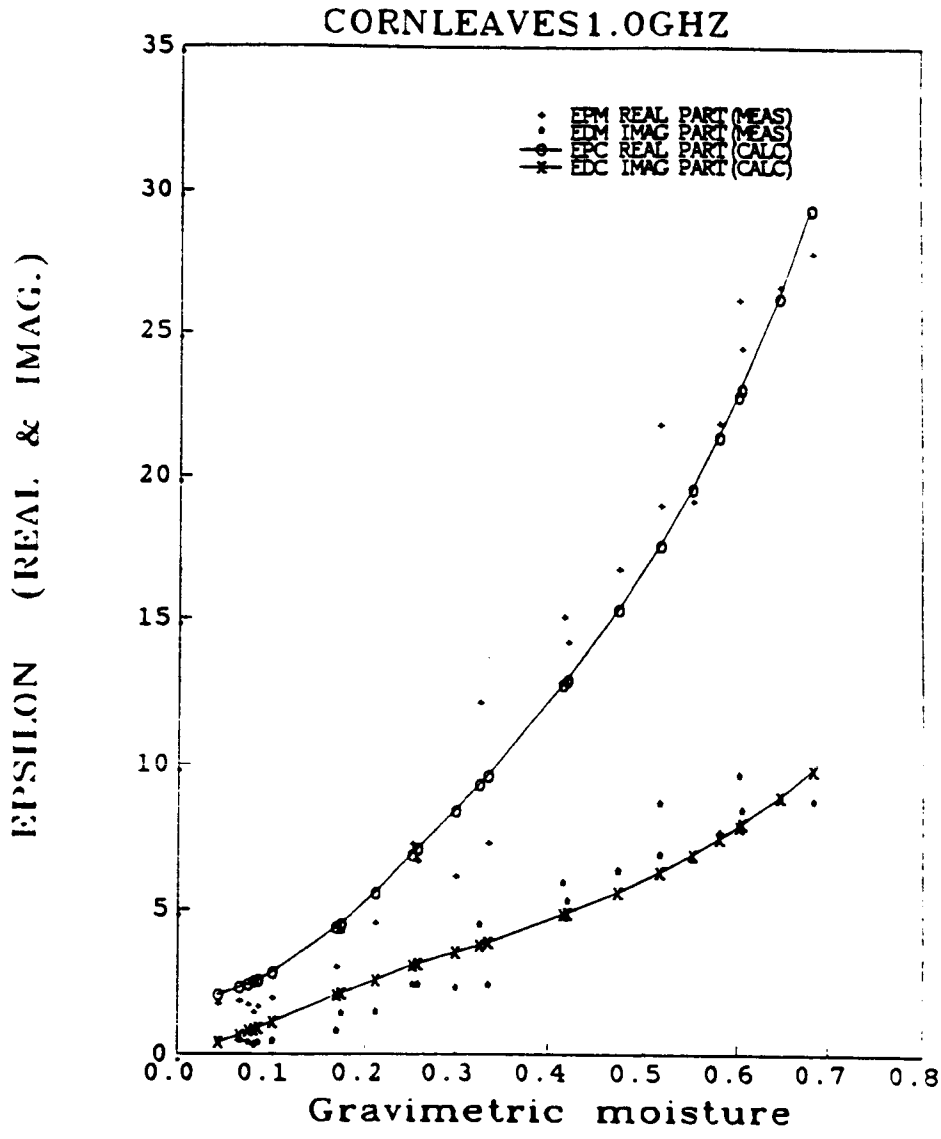

Figure 6.51. Comparison of calculated and measured dielectric constant versus moisture for corn leaves using a Debye-like model with a single variable relaxation spectrum for f = 1 GHz.

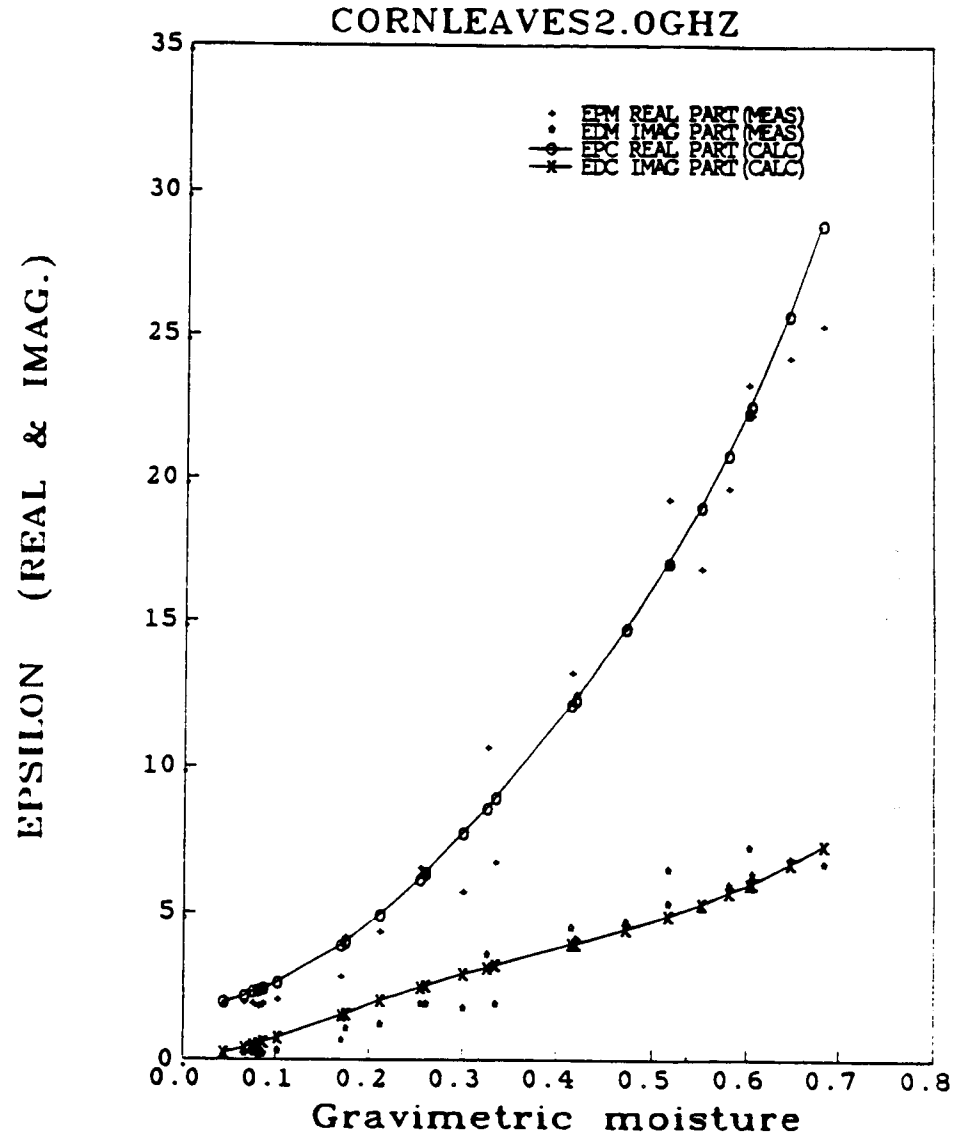

Figure 6.52. Comparison of calculated and measured dielectric constant versus moisture for corn leaves using a Debye-like model with a single variable relaxation spectrum for f = 2 GHz.

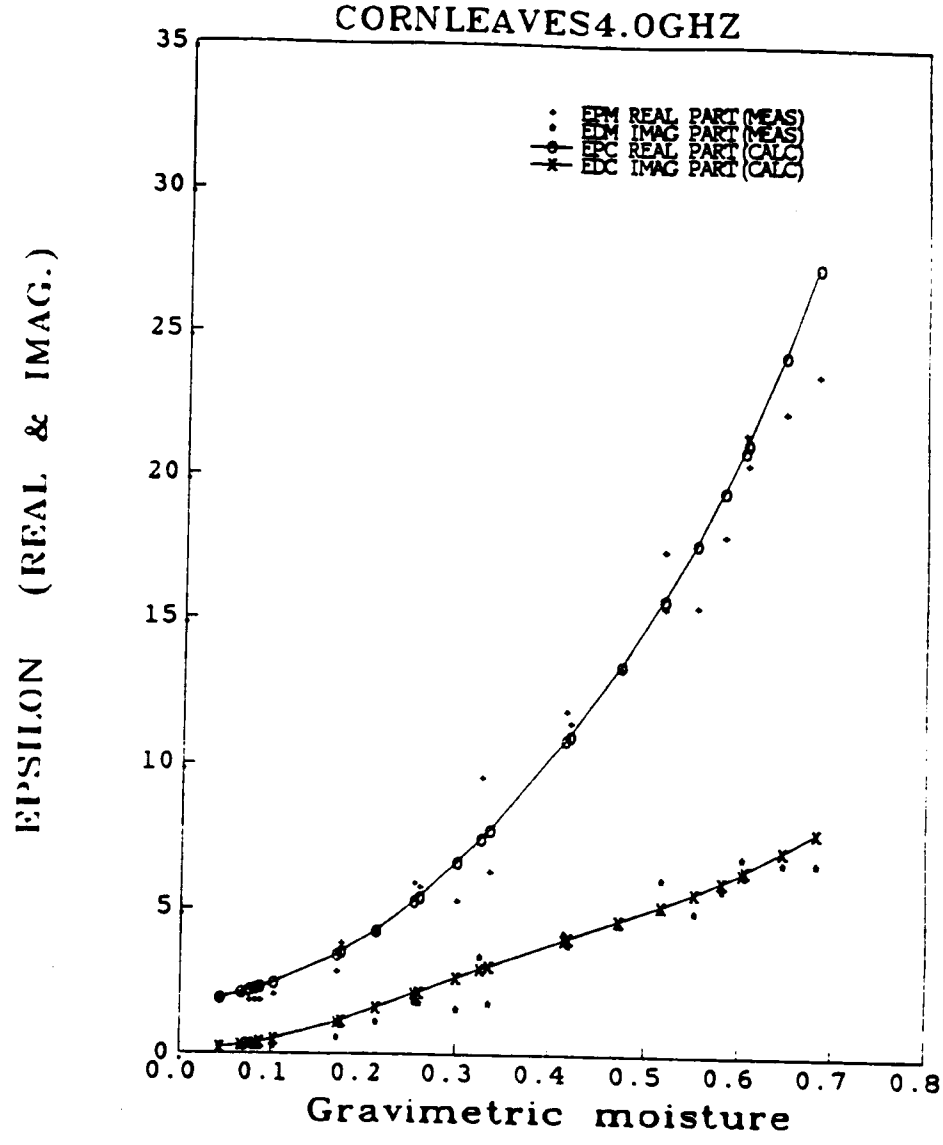

Figure 6.53. Comparison of calculated and measured dielectric constant versus moisture for corn leaves using a Debye-like model with a single variable relaxation spectrum for f = 4 GHz.

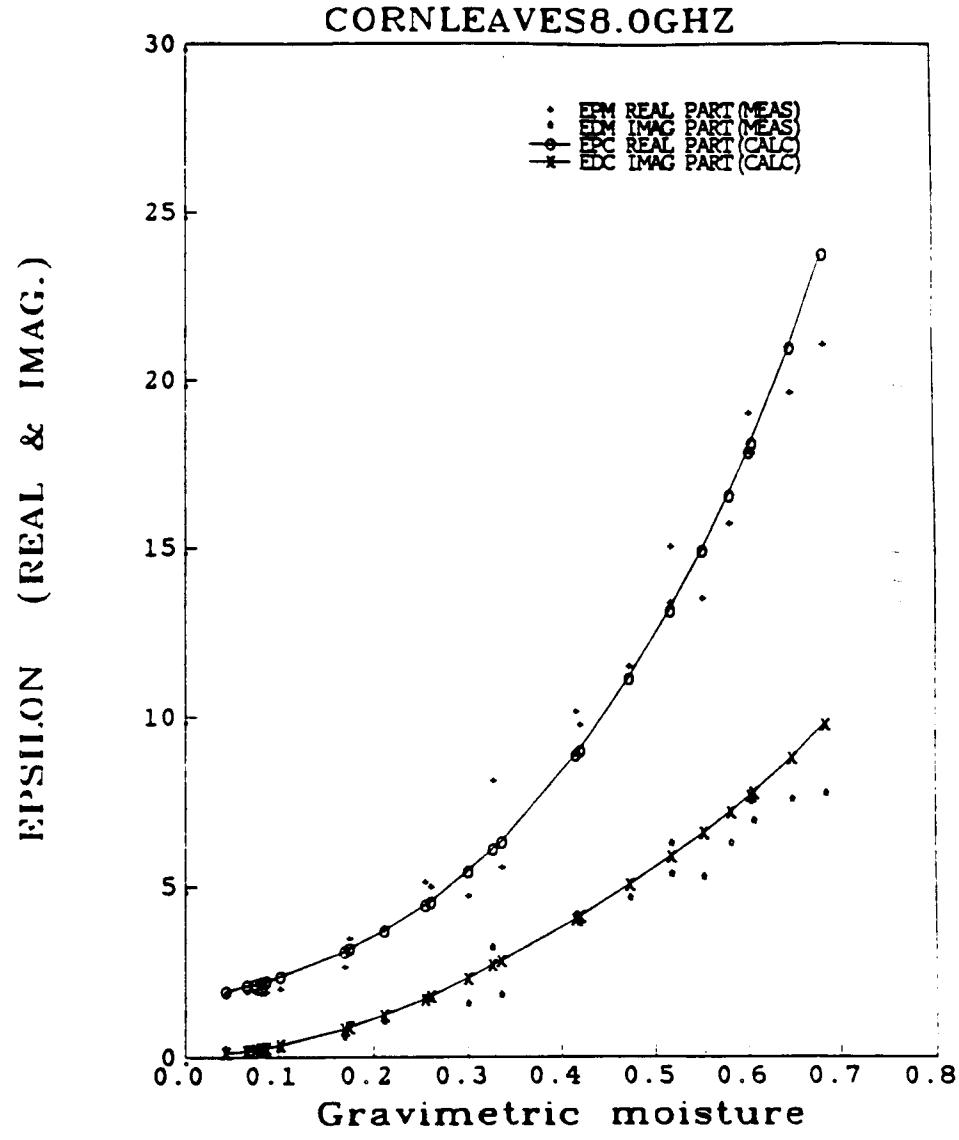

Figure 6.54. Comparison of calculated and measured dielectric constant versus moisture for corn leaves using a Debye-like model with a single variable relaxation spectrum for f = 8 GHz.

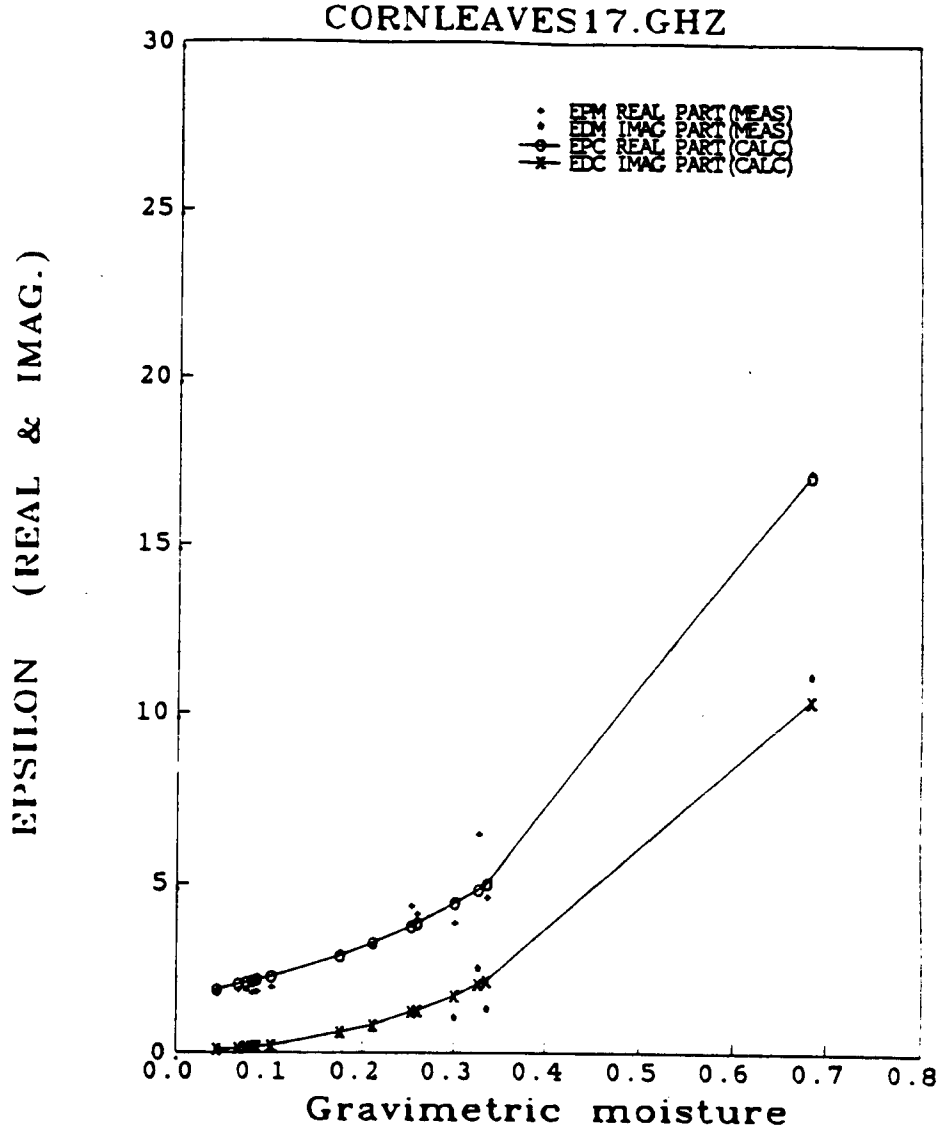

Figure 6.55. Comparison of calculated and measured dielectric constant versus moisture for corn leaves using a Debye-like model with a single variable relaxation spectrum for f = 17 GHz.

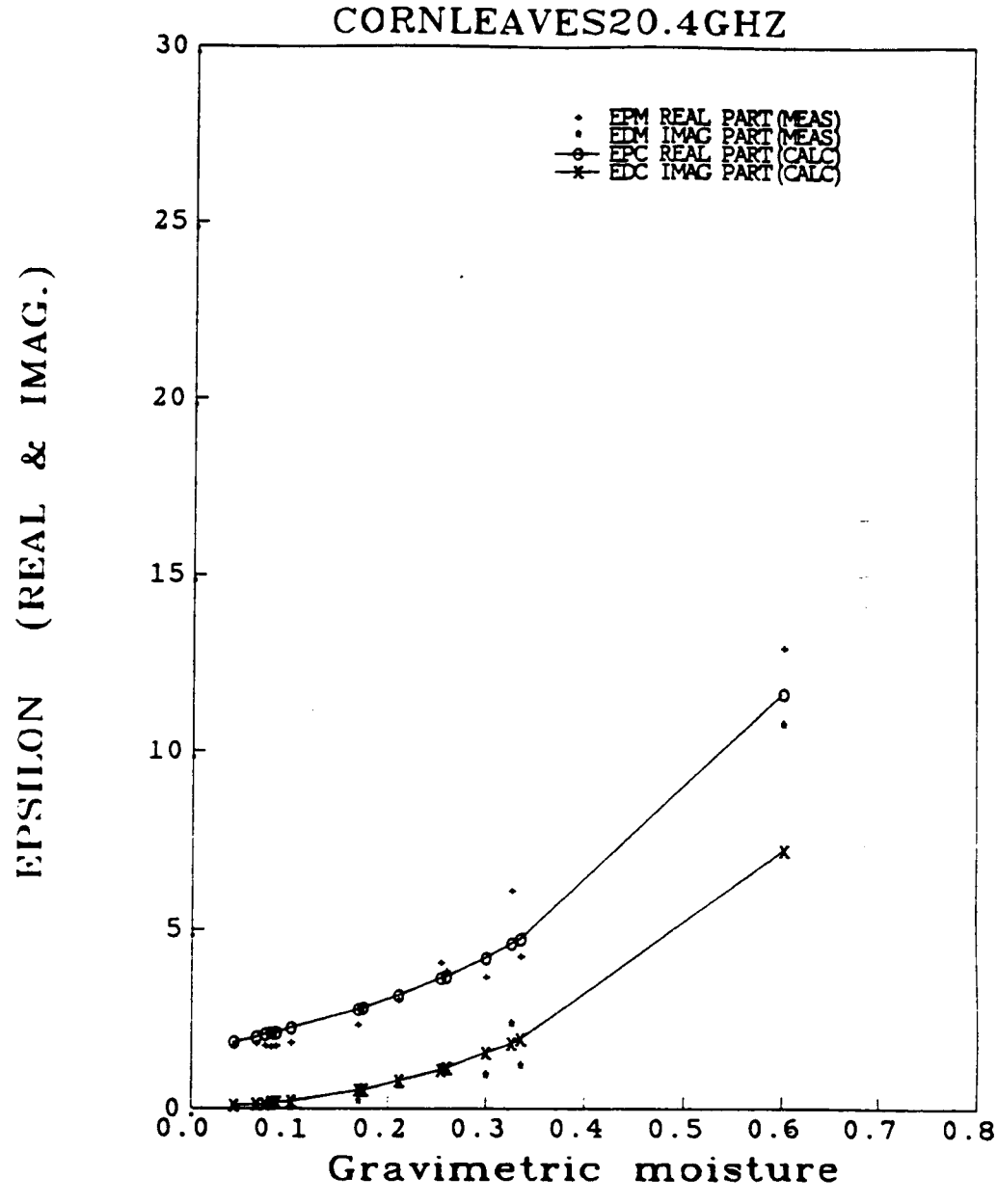

Figure 6.56. Comparison of calculated and measured dielectric constant versus moisture for corn leaves using a Debye-like model with a single variable relaxation spectrum for f = 20.4 GHz.

model	DeLoor's	Debye	Birchak	Polynomial	Debye (Single)
# parameters ϵ'	0	2	0	6	2
RSS	3883.82	1412.2	1772.02	885.8	1063.99
$EMSE$	5.745	1.947	2.621	1.322	1.579
N	676	676	676	676	676
ρ	.981	.983	.984	.989	.987
b	.179	.292	-.182	.210	.230
a	.821	.969	.935	.978	.976

Table 6.8 Comparison between different models for corn leaves data at 22^0C (real parts).

model	DeLoor's	Debye	Birchak	Polynomial	Debye (Single)
# parameters ϵ''	5	5	1	6	4
RSS	245.1	254.9	413	235.4	390.60
$EMSE$	.365	.379	.612	.351	.580
N	676	676	676	676	676
ρ	.979	.978	.975	.980	.969
b	.197	.084	.264	.230	.439
a	.949	.968	1.030	.943	.923

Table 6.9 Comparison between different models for corn leaves data at 22^0C (imaginary parts).

Chapter 7

Conclusions and Recommendations

This chapter provides a summary of the major conclusions reached during the course of this study and proposes recommendations for future work.

7.1 Conclusions

7.1.1 Measurement System

Open-ended coaxial probes were found to be viable sensors for making dielectric constant measurements at microwave frequencies. They have the following features:

1. They can be operated over a wide frequency band (e.g., .05-20.4 GHz for the .141" probe).

2. They are easy to use; no sample preparation, in general, is required.

3. They provide results in near real-time (when used with an automatic network analyzer).

4. Non-destructive measurements of plant parts (or any living tissue) are possible.

5. Temperature measurements are easy.

6. Measurement accuracy is fairly good (5% or better for liquids).

7. The sample thickness need only be comparable to the probe diameter.

8. It is possible to deduce ϵ of a thin sheet of material from two independent measurements made against two known background materials with infinite electrical thicknesses.

9. The probe system is very sensitive to contact and pressure at the probe tip. It is extremely accurate for liquids where contact and pressure are not crucial problems. For semi-solids, like plant parts, it is possible to use a pressure guage to control pressure and use care to insure good contact between the sample and the probe. However, because of errors caused by imperfect contact between the probe tip and the material under test, the variability of the measured ϵ was found to be about 10% ($\sigma/\mu = .10$). By designing the experiment to fit the required precision of the data, a choice of N (number of independent measurements) can be made.

7.1.2 Measurements

1. The measurements covered a variety of plant types; some of them were not reported because of time and space limitations.

2. The overall frequency band of the measurement system was .05 to 20.4 GHz; however, most of the measurements on plant parts were performed from .7 to 20.4 GHz. Higher-order mode propagation determined the upper end of the frequency range while probe sensitivity governed the lower end of the frequency range.

3. Plants were measured at various moisture levels from freshly cut to very dry.

4. Also, the salinity of the fluids extracted from leaves and stalks was measured by a conductivity meter.

5. Temperature measurements were conducted on different plant leaves between -40^0C and $+50^0C$. These samples were found to freeze at temperatures below 0^0C (between -5 and -10^0C) due to supercooling effects. Some of these temperature experiments involved exposing the sample to a freezing-thawing-freezig cycle to investigate a hysteresis-like behavior.

6. In order to study bound water effects in plant materials, a series of dielectric measurements were conducted on sucrose, dextrose, starch, and other plant constituents known to form chemical bonds with water molecules.

Various sucrose solutions of different concentrations were measured as a function of frequency and temperature. The knowledge gained from these measurements confirmed the existence and importance of bound water in living tissues, and the technique made it possible to study this form of water in the absence of the effects of salinity on the dielectric constant of the water-vegetation mixture.

7.1.3 Modeling

The dielectric properties of liquid water in all its forms (free, bound, and saline water) were summarized. The volume fraction models were established for a vegetation sample that shrinks and for one that does not. Both models were tested and we concluded that although the real situation lies between these two extremes, the shrinking model is closer to reality. Given the dielectric constant and the volume fractions of the sample constituents, various mixing models were tested and compared to dielectric data measured for corn leaves at room temperature ($T = 22^0C$). DeLoor's mixing model fits the data when $\epsilon^* = \epsilon_m$ and $(A_j = 0, 0, 1)$ which is the model for randomly-oriented and randomly-distributed disc-shaped inclusions (known as DeLoor's upper limit). Birchak model was tested and found satisfactory. Debye's model was tested (with one and with two relaxation spectra) and found to yield very good results. Also, a polynomial fit was developed for easy calculations. Because our knowledge about the physical properties of plants is still limited, we had to use free parameters in the models. The fewer these free parameters are, the more useful the model becomes.

7.2 Recommendations

7.2.1 Measurement System

1. The use of the HP8510 network analyzer will enhance the system capabilities:

   - Frequency band .01 to 20.4 GHz in one sweep.
   - The time domain feature will help eliminate the reflections from the various discontinuities (e.g., connectors and bends), while allowing the measurement of the reflection from the probe tip (using FFT and a time gate). Consequently, the system will have better overall accuracy.
   - Similarly, measurement precision will improve because of the general built-in high quality features of the HP8510 such as automatic frequency-locking (no harmonic skip problem).
   - Easy to program and fast data acquisition and processing.

2. The calibration algorithm can be modified by replacing the equivalent circuit model with an exact electromagnetic solution (e.g., MOM), which will improve the overall accuracy of the system.

3. The frequency range may be extended beyond 20.4 GHz by using .085" probes with connectors that operate at millimeter wavelengths.

4. New probe tip configurations may be developed to better suit the measurement of solid materials (e.g., rocks).

5. The possibility of using open-ended waveguides to perform dielectric measurements should be explored.

7.2.2 Measurements and modeling

Extensive measurements and modeling efforts need to be performed on plant materials to:

1. Generate a database of plant dielectric properties as a function of:
   - plant type, part, and location,
   - plants with very high moisture contents,
   - plants with low salinity (may be fresh water aquatic plants),
   - plants with very high salinity content,
   - temperature for $-40^0C \leq T \leq +50^0C$ with freezing-thawing-freezing cycles.
2. Develop a complete dielectric model for bound water (one or two relaxation spectra) as a function of concentration, frequency, temperature, and the binding material.
3. Investigate, more thoroughly, the freezing point discontinuity, the under (super) cooled effects, and the hysteresis-like behavior observed in $\epsilon - T$ curves.
4. Further investigate the single-phase model of liquid water (refer to Sec. 6.3.5). This model suggests that liquid water exists in solute and colloidal

solutions as one continuous phase with an effective temperature lower than room temperature by a value that is proportional to the type and concentration of the solid material. The effective temperature calculated for a particular solution has a corresponding ϵ_s and f_0 for the liquid water phase. The model fits the sucrose solutions and the corn leaves data (at least as good as the two-phase model). Another approach to the single-phase model can be suggested as follows: since, according to Debye's relaxation formulation, the ability of the molecular dipole to orient itself with a time-varying electromagnetic field depends on the viscosity of the medium, it is possible to consider that solutions have viscosities that are different from that of free water. Consequently, solutions have dielectric relaxation spectra that are different from that for pure water.

5. Conduct experiments on pressure-volume curves:

   Pressure-volume (P-V) curves can be generated on roots, shoots, or leaves using two methods: (i) samples are dehydrated inside a pressure chamber, and the sap is collected and weighed as the pressure is incrementally increased, or (ii) excised samples are allowed to dry outside the pressure chamber by evapotranspiration, then they are weighed periodically to determine sap loss, and their corresponding balance pressure is determined in a pressure chamber. These two methods were compared in (Ritchie et al, 1984). Such an experiment is important because the extracted sap samples may be used to determine:

(a) the salinity distribution (by measuring ionic content of the extracted fluids using a conductivity meter) as a function of pressure, and

(b) the bound water distribution (by measuring the dielectric constant of the extracted liquids) as a function of pressure.

The two methods described earlier for generating (P-V) curves are tedious, time consuming, and destructive. We can investigate the possibility of using the probe dielectric measurement system to predict the (P-V) curves without actually destroying the sample. The probe system, in this case, can be used as a fast and non-destructive tool to monitor plant physiological parameters such as volume-averaged osmotic potential at full turgor ($\psi\pi_0$) and volume-averaged water potential at zero turgor (ψ_z).

6. Study the dielectric constant profiles in plants as a function of height above the ground surface. Also, more measurements should be conducted to study the azimuthal profiles of the dielectric constant of tree trunks.

7. Study density effects by testing plants with high density (e.g., some tree branches are very dense) and other plants with low density (e.g., Coleus leaves).

8. Develop a general model for the dielectric properties of plant materials that incorporates all their physical parameters. Special attention should be given to the temperature effects in general and to the freezing point discontinuity in particular. Freezing point discontinuity is a transitional

state and the measured data showed a hysteresis behavior that has been attributed to supercooling behavior. Also, the properties of bound water at low temperatures should be considered.

REFERENCES

1. Athey, T. W., M. A. Stuchly, and S. S. Stuchly (1984), "Measurement of Radio Frequency Permittivity of Biological Tissues With an Open-Ended Coaxial Line: Part I," IEEE Transactions On Microwave Theory And Techniques, vol. MTT-30, No. 1, January 1982, pp. 82-86.
2. Birchak, J. R., C. G. Gardner, J. E. Hipp, and J. M. Victor (1974), "High Dielectric Constant Microwave Probes For Sensing Soil Moisture," Proceeding of IEEE, vol. 62, No. 1, January 1974, pp. 93-98.
3. Bose, T. K., A. M. Bottreau, and R. Chahine (1986), "Develpment Of A Dipole Probe For The Study Of Dielectric Properties Of Biological Substances In Radiofrequency And Microwave Region With Time-Domain Reflectometry," IEEE Transactions On Instrumentation And Measurement, Vol. IM-35, No. 1, March 1986.
4. Bottreau, A. M., Y. D. Dutuit, and J. Moreau (1977), "On Multiple Reflection Time Domain Method In Dielectric Spectroscopy: Application To The Study Of Some Normal Primary Alcohols," J. Chem. Phys., Vol. 66, No. 8, 15 April 1977.
5. Broadhurst, M. G. (1970), "Complex Dielectric Constant And Dissipation Factor Of Foliage," NBS Report 9592, October 1970.
6. Burdette, E. C., F. L. Cain, and J. Seals (1980), "In Vivo Probe Measurement Technique For Determining Dielectric Properties At VHF Through Microwave Frequencies," IEEE Transaction On Microwave Theory And Techniques, Vol. MTT-28, No. 4, April 1980, pp. 414-427.
7. Carlson, N. L. (1967), "Dielectric Constant Of Vegetation At 8.5 GHz," TR 1903-5, Electroscience Laboratory, The Ohio State University, Columbus Ohio, 1967.
8. Carver, K. R., C. Elachi, and F. T. Ulaby (1985), "Microwave Remote Sensing from Space," Proceeding of the IEEE, Vol. 73, No. 6, June 1985.
9. Debye, P. (1929), Polar Molecules, Dover, New York.

10. Deschamps, G. A. (1962), " Impedance Of An Antenna In A Conducting Medium," IRE Trans. Antennas Propagat., Sept. 1962, pp. 648-650.

11. DeLoor, G. P. (1956), "Dielectric Properties Of Heterogeneous Mixtures," Thesis, Leiden. Also (1964) Appl. Sci. Res., B11, pp. 310-320.

12. DeLoor, G. P. (1968), "Dielectric Properties Of Heterogeneous Mixtures Containing Water," J.Microwave Power, vol. 3, pp. 67-73.

13. DeLoor, G. P. (1982), "The Dielectric Properties Of Wet Materials," Invited paper presented at the 1982 International Geoscience And Remote Sensing Symposium (IGARSS'1982), June 1-4, 1982.

14. Dobson, M. C. , F. T. Ulaby, M. A. El-Rayes, and M. Hallikainen (1983), "Micrwave Dielectric Behavior Of Wet Soil Part II: Four-Component Dielectric Mixing Model," RSL Technical Report 545-2, University of Kansas Center for Research, Inc., Lawrence, Kansas.

15. Dobson, M. C. , F. T. Ulaby, M. A. El-Rayes, and M. Hallikainen (1985), "Micrwave Dielectric Behavior Of Wet Soil Part II: Four-Component Dielectric Mixing Model," IEEE Trans.Geosci.Rem.Sens., GE-23, January 1985.

16. Dumanskii, A. (1933), "Die Bestimmung Der Menge Des Gebundenen Wassers In Dispersen Systemen," Kolloid-z. 65, 178-184(1933).

17. Gajda, G., and S. S. Stuchly (1983), "Numerical Analysis Of Open-Ended Coaxial Lines," IEEE Trans. Microwave Theory Tech., Vol. MTT-31, pp. 380-384, 1983.

18. Hallikainen, M. T., and F. T. Ulaby (1983), "A Free-Space System For Dielectric Measurements In The 3-18 GHz Frequency Range," University Of Kansas Center For Research, Inc., Lawrence, KS, RSL Tech. Rep. 543-3, 1983.

19. Hallikainen, M. T., F. T. Ulaby, M. C. Dobson, and M. A. El-Rayes (1984), "Dielectric Measurements Of Soils In The 3- To 37-GHz Band Between -50C And 23C," Proceeding of IGARSS'84 Symposium, Strasbourg 27-30 August 1984, pp. 163-168.

20. Hallikainen, M. T., F. T. Ulaby, M. C. Dobson, M. A. El-Rayes, and L. Wu (1985), "Microwave Dielectric Behavior Of Wet Soil-Part I: Empirical Models And Experimental Observations From 1.4 To 18 GHz," IEEE Trans. Geosci.Remote Sensing, Vol. GE-23, No. 1, pp. 25-34, January 1985.

21. Hallikainen, M. T., F. T. Ulaby, M. C. Dobson, and M. A. El-Rayes, May 1986, "Microwave Dielectric Behavior of Wet Soil, Part III: The Effects of Frequency, Soil Texture, and Temperature," Radiation Laboratory Technical Report 022486-1-T, Electrical Engineering and Computer Science Department, The University of Michigan, Ann Arbor, Michigan 48109.

22. Harrington, R. F. (1961), "Time-Harmonic Electromagnetic Fields," McGraw-Hill, New York, 1961.

23. Hasted, J. B. (1973), "Aqueous Dielectrics," Chapman and Hall, London.

24. Hewlett-Packard Application Note 221 (1977), "Semi-automated Measurements Using The 8410 Microwave Network Analyzer and The 9825A Desk-Top Computer," Mar. 1977.

25. Hoekstra, P., and W. T. Doyle (1971), "Dielectric Relaxation Of Surface Adsorbed Water," Journal Of Colloid and Interface Science, Vol. 36, No. 4, Aug. 1971.

26. Jedlicka, R. P. (1983), "Resonant-Cavity Dielectric Measurements Of Vegetation," RSL Tech. Memo 591-1, Remote Sensing Laboratory, University Of Kansas Center For Research, Inc., Lawrence, KS 66045-2969, May 1983.

27. Jordan, B. P., R. J. Sheppard, and S. Szwarnowski (1978), "The Dielectric Properties Of Formamide, Ethanedoil, and Methanol," J. Phys. D: Appl. Phys., Vol. 11, 1978 (Printed In Great Britain).

28. Klien, L. A., and C. T. Swift (1977), "An Improved Model For The Dielectric Constant Of Sea Water At Microwave Frequencies," IEEE Trans. Antennas Propag., AP-25, pp. 104-111.

29. Koets, P. (1931), "Water Adsorption On Silica Gel," Proc. Acad. Sci. Amsterdam 34, 420-426 (1931).

30. Kramer, P. J. (1955), "Bound Water", Encycl. Plant Physiol. 1, pp. 223-242 (1955).

31. Kramer, P. J. (1983), "Water Relations Of Plants," Academic Press, 1983.

32. Kraszewski, A., and S. S. Stuchly (1983), "Capacitance Of Open-Ended Dielectric-Filled Coaxial Lines-Experimental Results," IEEE Transactions On Instrumentation And Measurement, Vol. IM-32, No. 4, December 1983.

33. Kraus, J. D., and K. R. Carver (1973), "Electromagnetics," McGraw-Hill, 1973.

34. Lane, J., and J. Saxton (1952), "Dielectric Dispersion In Pure Polar Liquids At Very High Radio Frequencies, III. The Effect Of Electrolytes In Solution," Proc. Roy. Soc., 214A, pp. 531-545.

35. Levitt, J., and G. W. Scarth (1936), "Frost-Hardening Studies With Living Cells," Canad. J. Res., Sect. C14, pp. 267-305 (1936).

36. Levitt, J. (1956), "The Hardiness Of Plants," Academic Press Inc., Publishers, New York, n.Y., 1956.

37. Levitt, J. (1980), "Response Of Plants To Environmental Stress," 2nd Ed., Vol. 2 Academic Press, New York.

38. Marcuvitz, N. (1965), "Waveguide Handbook," New York, Dover 1965.

39. Marinesco, N. (1931), "Polarisation Dielectrique Et Structure Des Colloides," J. Chim. Physic. 28, 51-91 (1931).

40. McKinley, M. S. (1983), "Vegetation Density Measurements," Remote Sensing Laboratory, RSL Technical Memorandum 591-2, June 1983.

41. Nelson, S. O. (1978), "Electrical Properties Of Grain And Other Food Materials," J. Food Proc. And Preserv., 2, pp. 137-154.

42. Parkash, A., J. K. Valid, and A. Mansingh (1979), "Measurement Of Dielectric Parameters At Microwave Frequencies By Cavity Perturbation Technique," IEEE Trans. Microwave Theory Tech., Vol. MTT-27, pp. 791-795, 1979.

43. Pethig, R. (1979), "Dielectric And Electronic Properties Of Biological Materials," New York: Wiley, 1979.

44. Poulder, D., and J.H. Van Santen (1946), "The Effective Permittivity Of Mixtures Of Solids," Physica, Vol. XII, No. 5, 1946, pp. 257-271.

45. Razani, M. (1982), "Microwave Radiometric Sensitivity To Soil Moisture Under Vegetation Cover," Ph.D. Thesis 1982, The University Of Kansas, ECE Department.

46. Shuh-Han, C. (1985), "Measurements Of Microwave Conductivity And Dielectric Constant By The Cavity Perturbation Method And Their Errors," IEEE Trans. On Microwave Theory And Techniques, Vol. MTT-33, No. 6, June 1985, pp. 519-526.

47. Siminova E. F. (1939), "Change Of Hydrophilic Properties Of Roots And Leaves Of Sugar Beets", Kolloid-z.5, 749-754 (1939).

48. Stogryn, A. (1971), "Equation For Calculating The Dielectric Constant Of Saline Water", IEEE Trans. Microwave Theory And Techniques, MIT-19, pp. 733-736.

49. Stuchly, S. S., M. A. Rzepecka, and M. F. Iskander (1974), "Permittivity Measurements At Microwave Frequencies Using Lumped Elements," IEEE Transaction On Instrumentation And Measurements, Vol. IM-23, No. 1, March 1974.

50. Stuchly, M. A., T. W. Athey, G. M. Samaras, and G. E. Taylor (1982), "Measurement Of Radio Frequency Permittivity Of Biological Tissues With An Open-Ended Coaxial Line: Part II. Experimental Results," IEEE Transaction On Microwave Theory And Techniques, Vol. MTT-30, No. 1, January 1982, pp. 87-92.

51. Tai, C. T. (1961), "Characteristics Of Linear Antenna Elements," in Antenna Engineering Handbook, H. Jasik, ed. New York: McGraw-Hill, 1961, Ch.3, pp. 2.

52. Tan, M. S. (1981), "Microwave Measurements And Modeling Of The Permittivity Of Tropical Vegetation Samples", Applied Physics, Vol.25, pp. 351-355, 1981.

53. Ulaby, F. T., R. K. Moore, and A. K. Fung (1981), "Microwave Remote Sensing," Vol. 1, Reading, MA: Addison-Wesley, 1981.

54. ——(1982), "Microwave Remote Sensing," Vol. 2, Reading, MA: Addison-Wesley, 1982.

55. ——(1986), "Microwave Remote Sensing," Vol. 3, Reading, MA: Addison-Wesley, 1986.

56. Ulaby, F. T. and R. P. Jedlicka (1984), "Microwave Dielectric Properties Of Plant Materials," IEEE Trans. Geosci. Rem. Sens., GE-22, pp. 406-414.

57. Ulaby, F. T., and M. A. El-Rayes (1986), "Microwave Dielectric Spectrum Of Vegetation Material," IEEE Proceedings of IGARSS'86 Symposium, Sept. 8-11, 1986, Zurich, Switzerland.

58. Ulaby, F. T., and M. A. El-Rayes (1986), "Dispersion Spectrum Of The Dielectric Constant Of Vegetation," Proceedings of the International Union of Radio Science, Wave Propagation And Remote Sensing, July 28-August 1, 1986, Hanover, New Hampshire.

59. Von Hippel, A. R. (1954), "Dielectric Materials And Applications," MIT Press, Cambridge, MA..

APPENDIX A

Dielectric Data at Room Temperature

This appendix contains the dielectric data for some vegetation materials at room temperature. The set consists of eight parts:

1. Sucrose solutions (A.1 - A.8)
   Seven sucrose solutions, with different concentrations, are reported. Some of them were already given in Chapters 5 and 6, but the whole set is presented here for the sake of completeness.

2. Comparison between corn leaves and soybean leaves (A.9 - A.13) at 1, 2, 4, 8, and 17 GHz.

3. Comparison between corn leaves and corn stalks (A.14 - A.20)
   The measurements were taken on the inside part of the stalk (not on the sheath) at .7, 1, 2, 4, 8, 17, and 20 GHz.

4. Comparison between the model developed in Sec. 6.3.2 (solid line) with $\rho_{DV} = .52$ and the Measured data for corn stalks at .7, 1, 2, 4, 8, 12, and 20 GHz (A.21 - A.27).

5. Measured dielectric spectra for Aspen leaves with M_g as parameter for M_g = .28, .57, and .86 (A.28 - A.29).

6. Measured dielectric spectra for Black Spruce tree trunk with M_g as parameter for M_g = 0, .136, .257, .38, and .52 (A.30 - A.31).

   Also, for the same samples, measured dielectric data versus M_g for f = 1, 2, 4, and 8 GHz (A.32 - A.35).

7. Measured dielectric spectra for Balsam Fir trees (branches, trunk, and leaves). Since the leaves are needle-like, a single needle was measured against two different backgrounds (teflon and metal). (A.36 - A.45)

8. Comparison of measured dielectric data for corn stalks and corn leaves between those reported in (Ulaby and Jedlicka, 1984) and those reported in this work at different frequencies (A.46 - A.50). Differences are mainly attributed to samples variability.

Appendix A

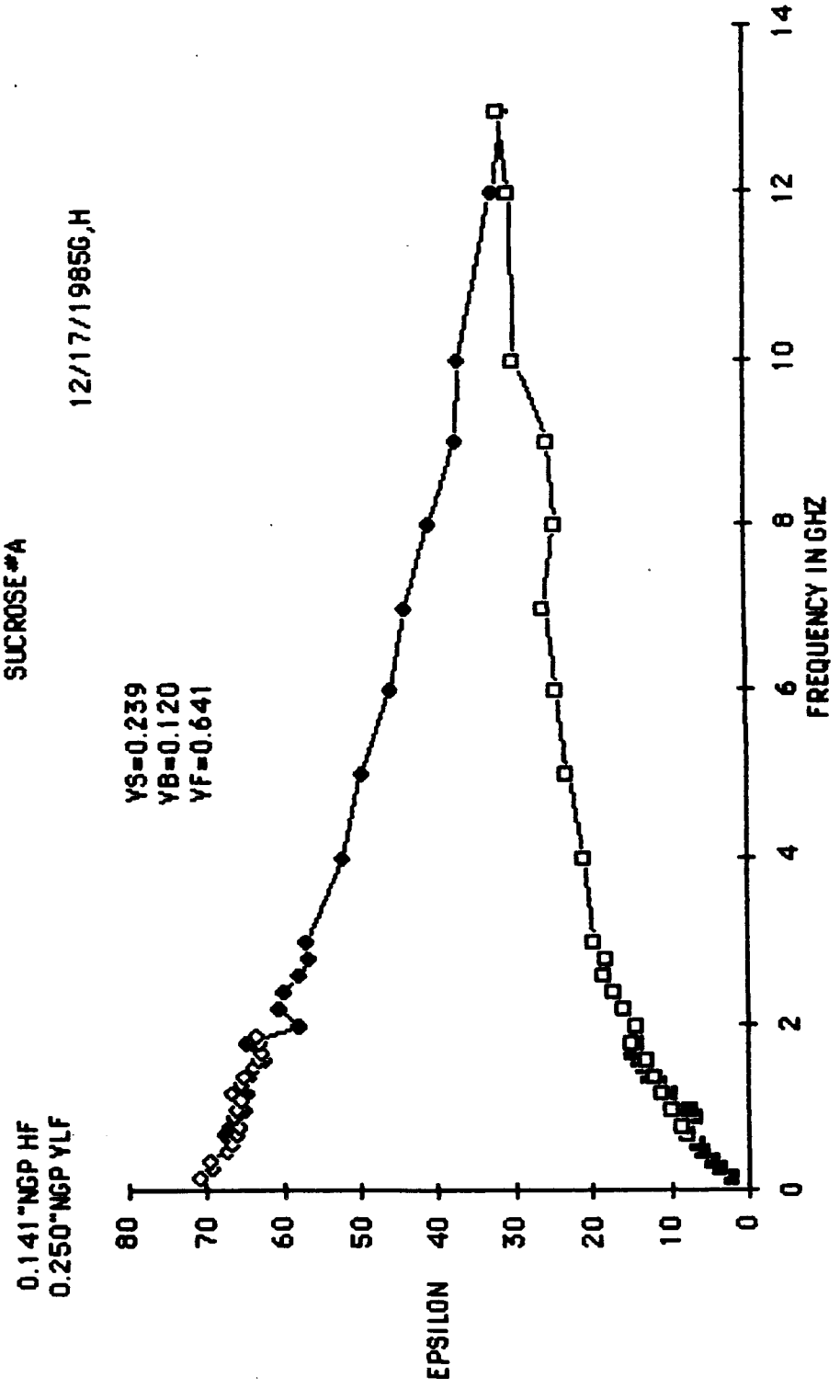

Figure A.1

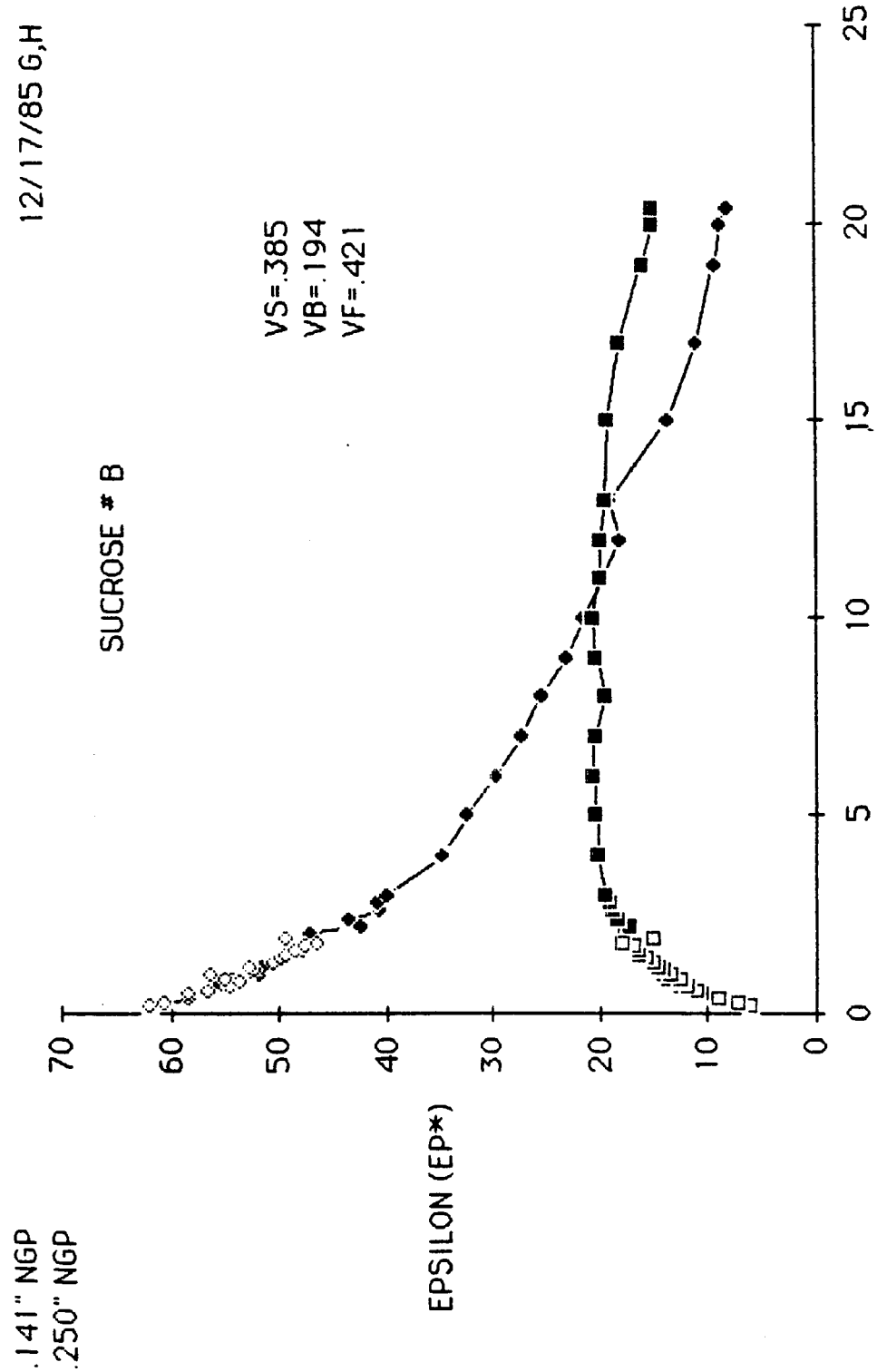
12/17/85 G,H
SUCROSE # B
VS=.385
VB=.194
VF=.421
.141" NGP
.250" NGP
EPSILON (EP*)
FREQUENCY (GHZ)
70
60
50
40
30
20
10
0
0
5
10
15
20
25

Figure A.2

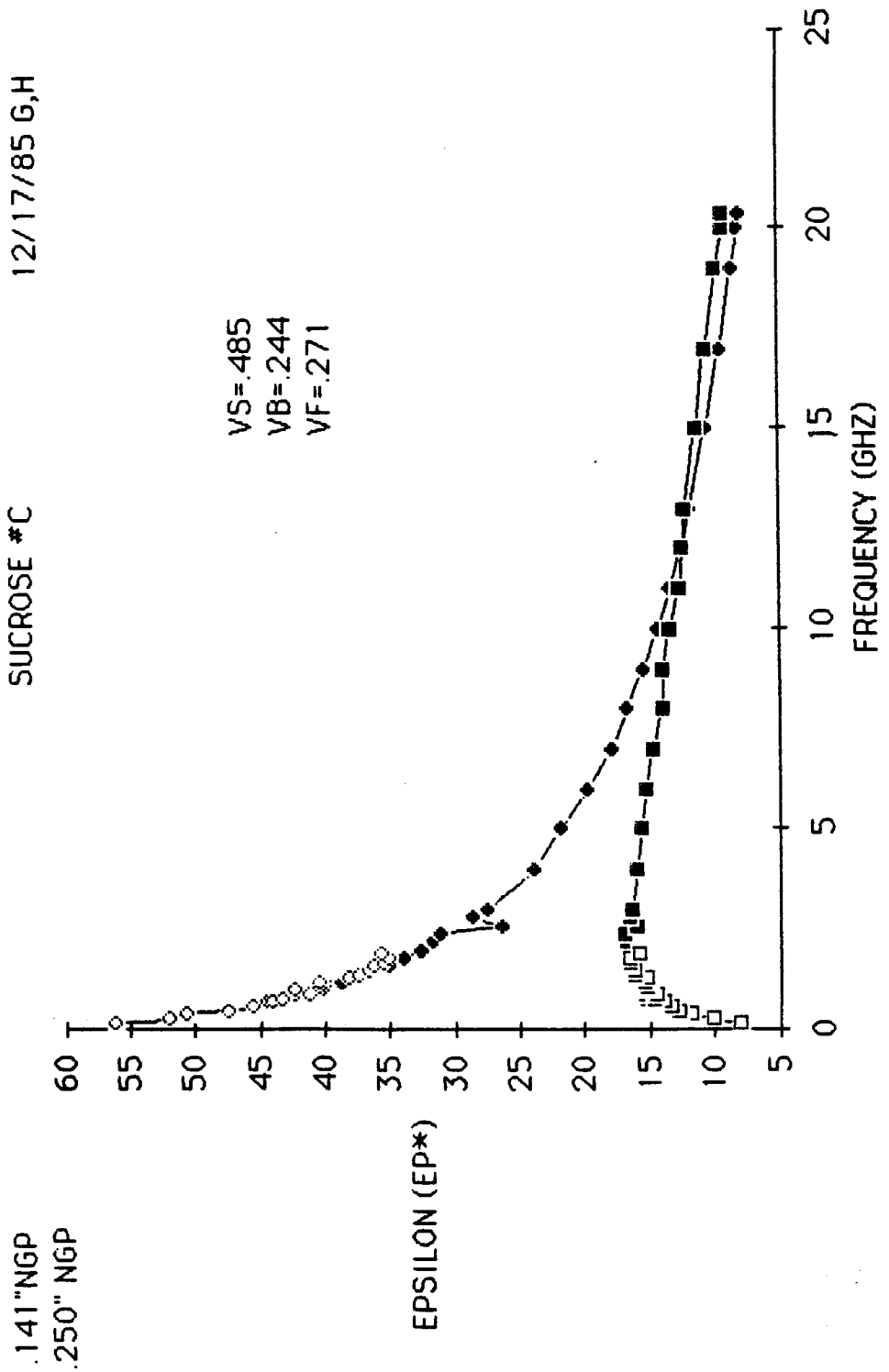
12/17/85 G,H
SUCROSE *C
VS=.485
VB=.244
VF=.271
.141"NGP
.250" NGP
EPSILON (EP*)
FREQUENCY (GHZ)
60
55
50
45
40
35
30
25
20
15
10
5
0
5
10
15
20
25

Figure A.3

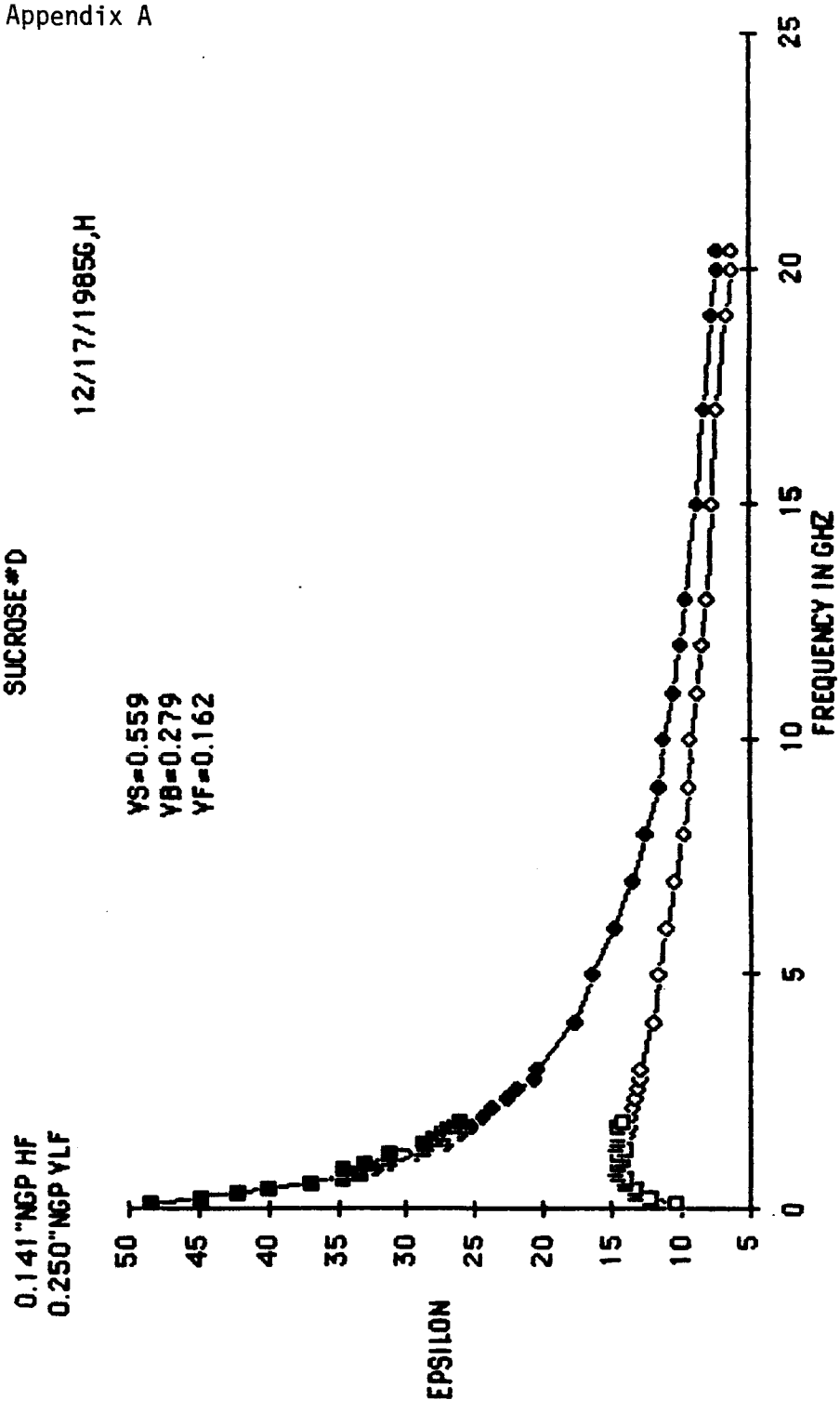
SUCROSE*D
12/17/1985G,H
YS=0.559
YB=0.279
YF=0.162
0.141"NGP HF
0.250"NGP YLF
EPSILON
FREQUENCY IN GHZ
50
45
40
35
30
25
20
15
10
5
0
5
10
15
20
25

Figure A.4

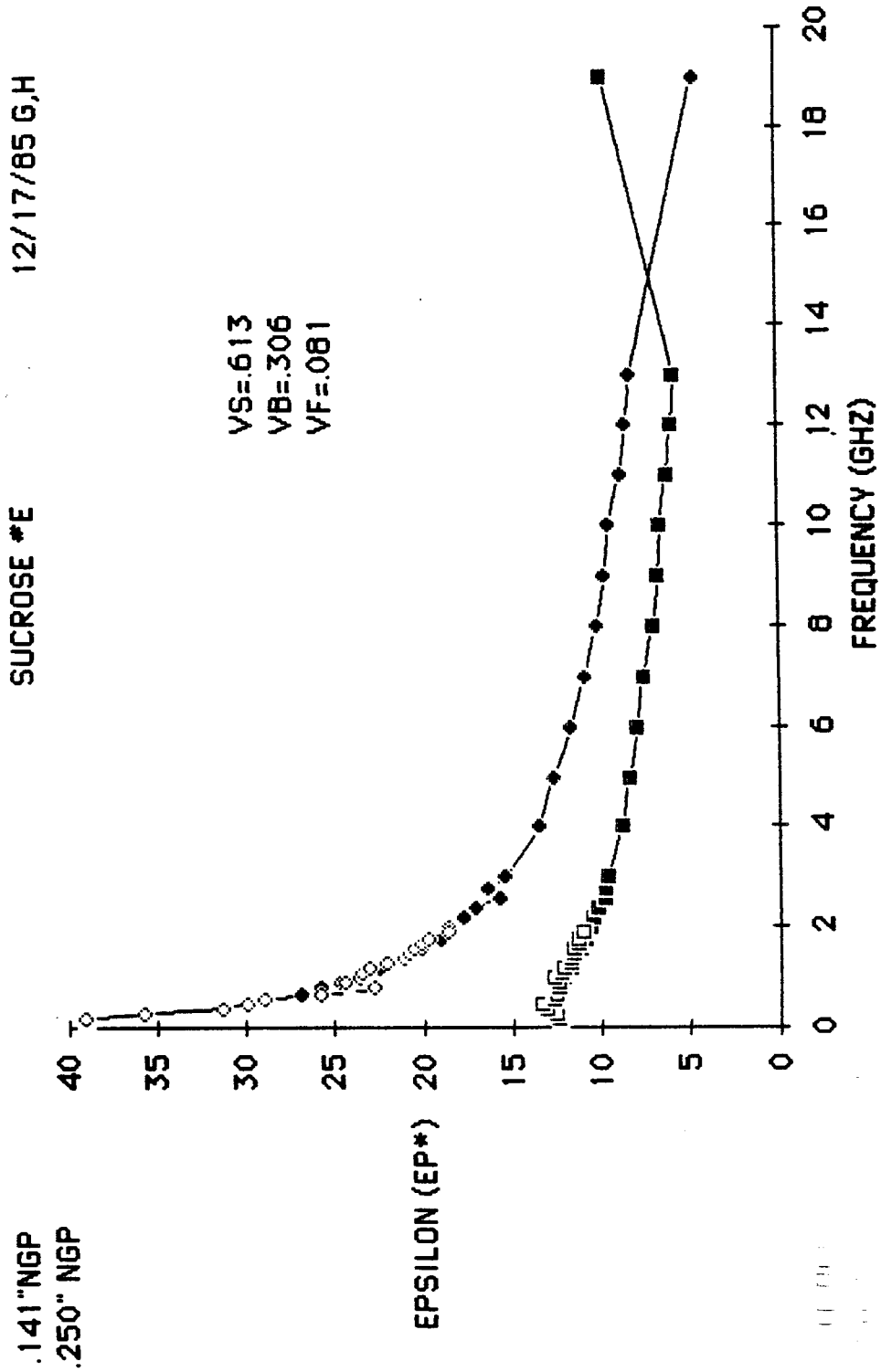
SUCROSE *E
12/17/85 G,H
VS=.613
VB=.306
VF=.081
.141"NGP
.250" NGP
EPSILON (EP*)
FREQUENCY (GHZ)
0
5
10
15
20
25
30
35
40
0
2
4
6
8
10
12
14
16
18
20

Figure A.5

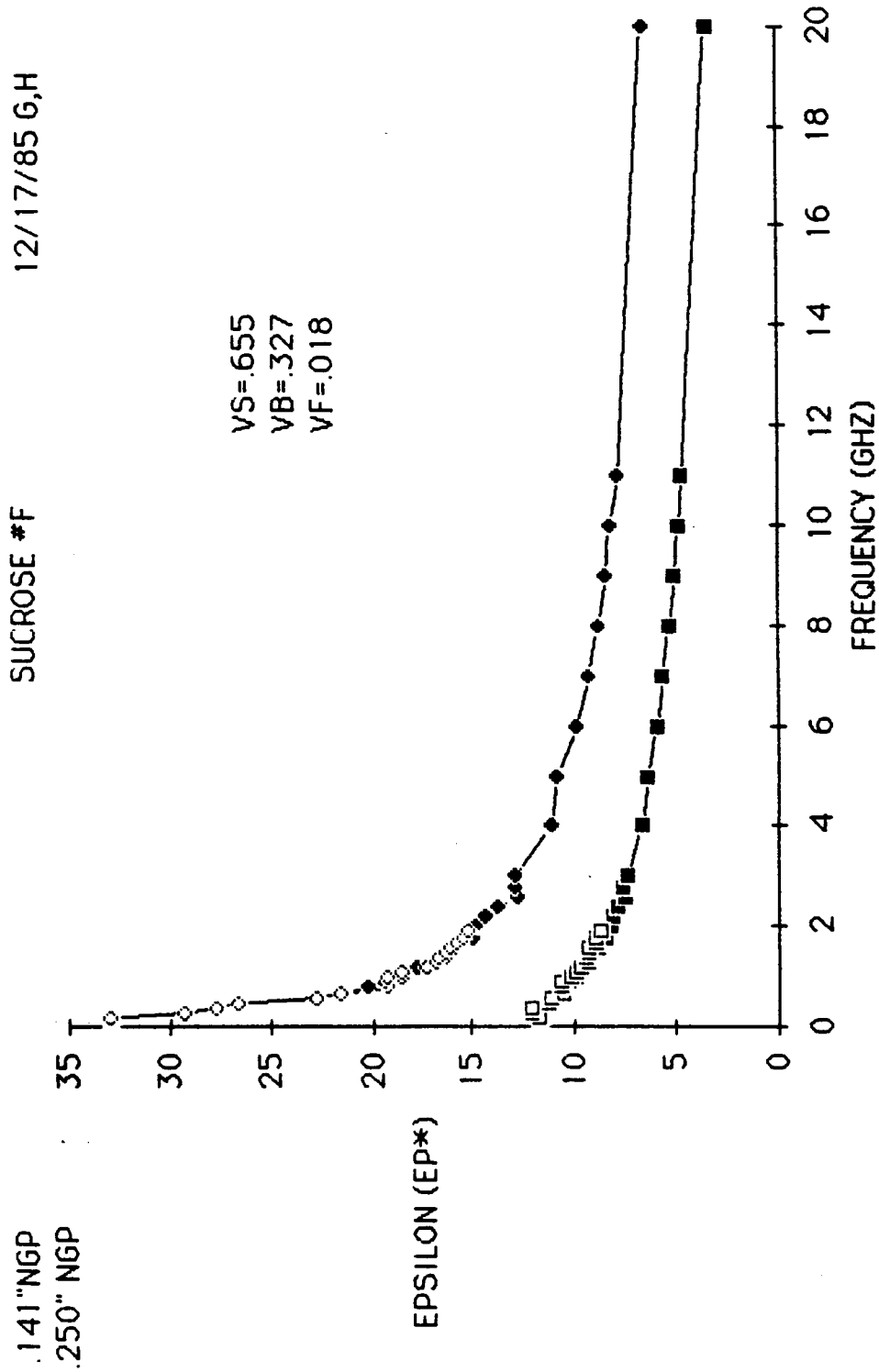
12/17/85 G,H
SUCROSE #F
VS=.655
VB=.327
VF=.018
.141"NGP
.250" NGP
EPSILON (EP*)
FREQUENCY (GHZ)
0
5
10
15
20
25
30
35
0
2
4
6
8
10
12
14
16
18
20

Figure A.6

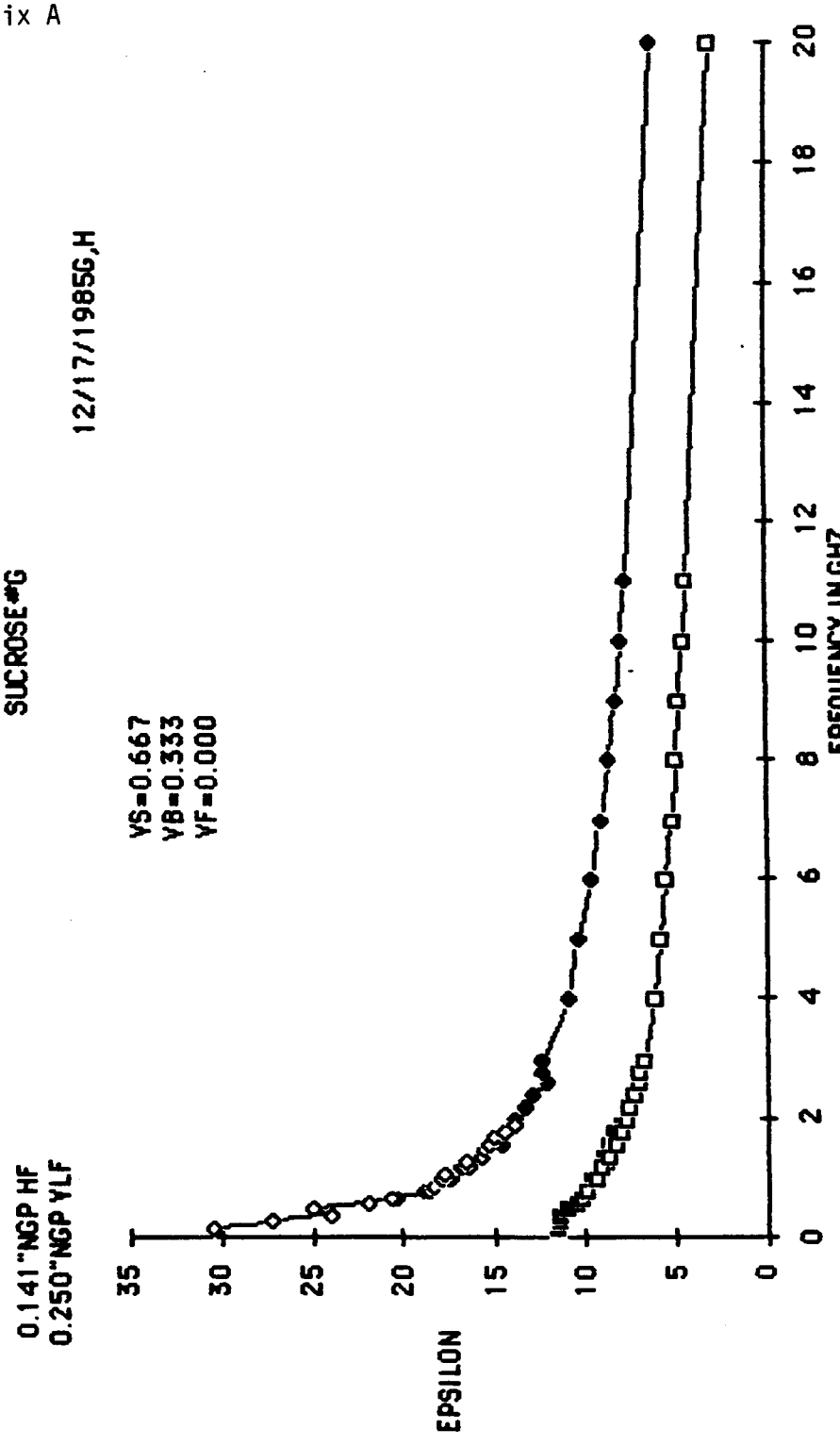
0.141"NGP HF
0.250"NGP YLF
SUCROSE@G
12/17/1985G,H
VS=0.667
VB=0.333
VF=0.000
EPSILON
FREQUENCY IN GHZ
35
30
25
20
15
10
5
0
0
2
4
6
8
10
12
14
16
18
20

Figure A.7

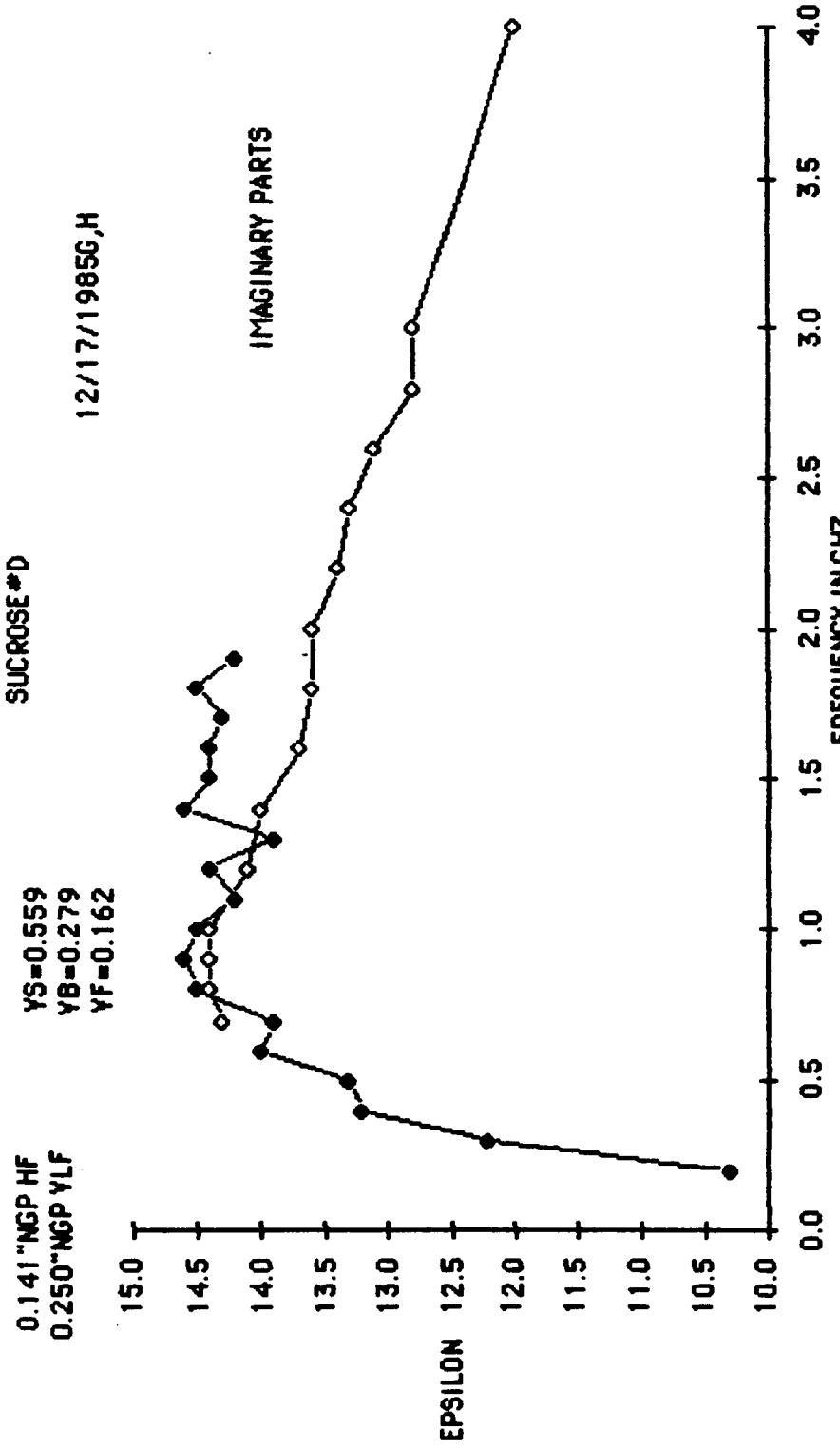
SUCROSE*D
12/17/1985G,H
IMAGINARY PARTS
YS=0.559
YB=0.279
YF=0.162
0.141"NGP HF
0.250"NGP YLF
EPSILON
FREQUENCY IN GHZ
15.0
14.5
14.0
13.5
13.0
12.5
12.0
11.5
11.0
10.5
10.0
0.0
0.5
1.0
1.5
2.0
2.5
3.0
3.5
4.0

Figure A.8

Appendix A

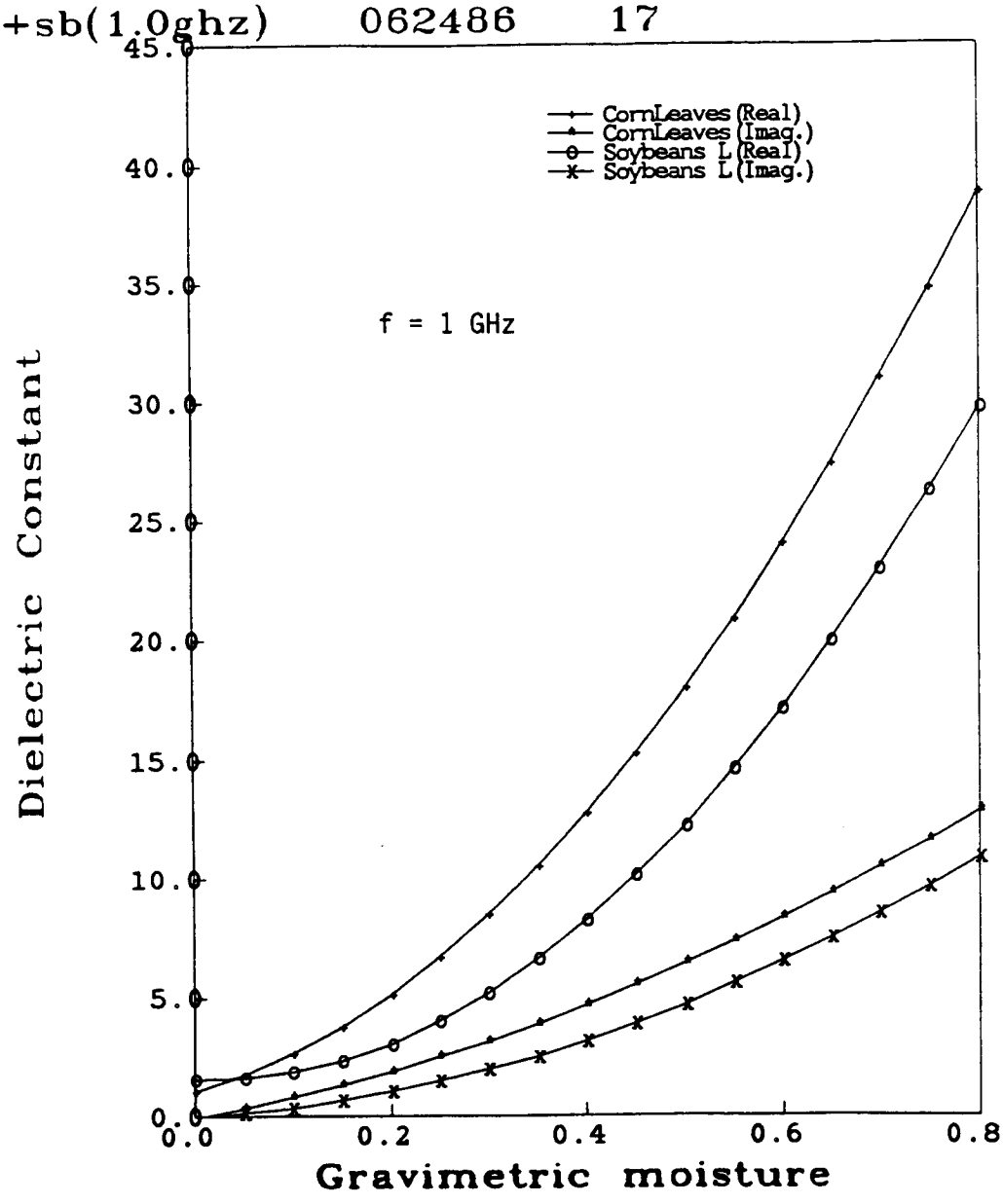

Figure A.9

Appendix A

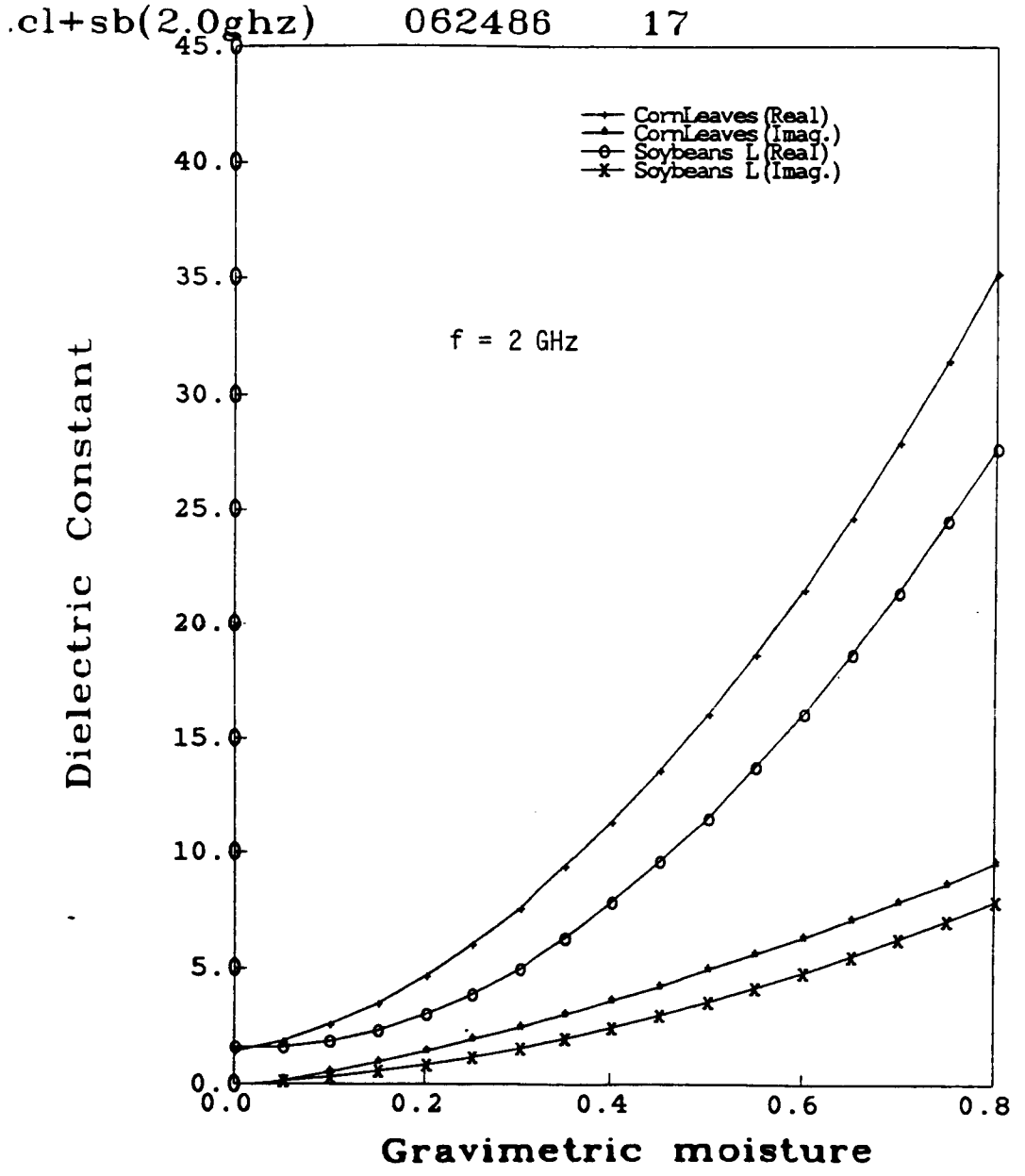

Figure A.10

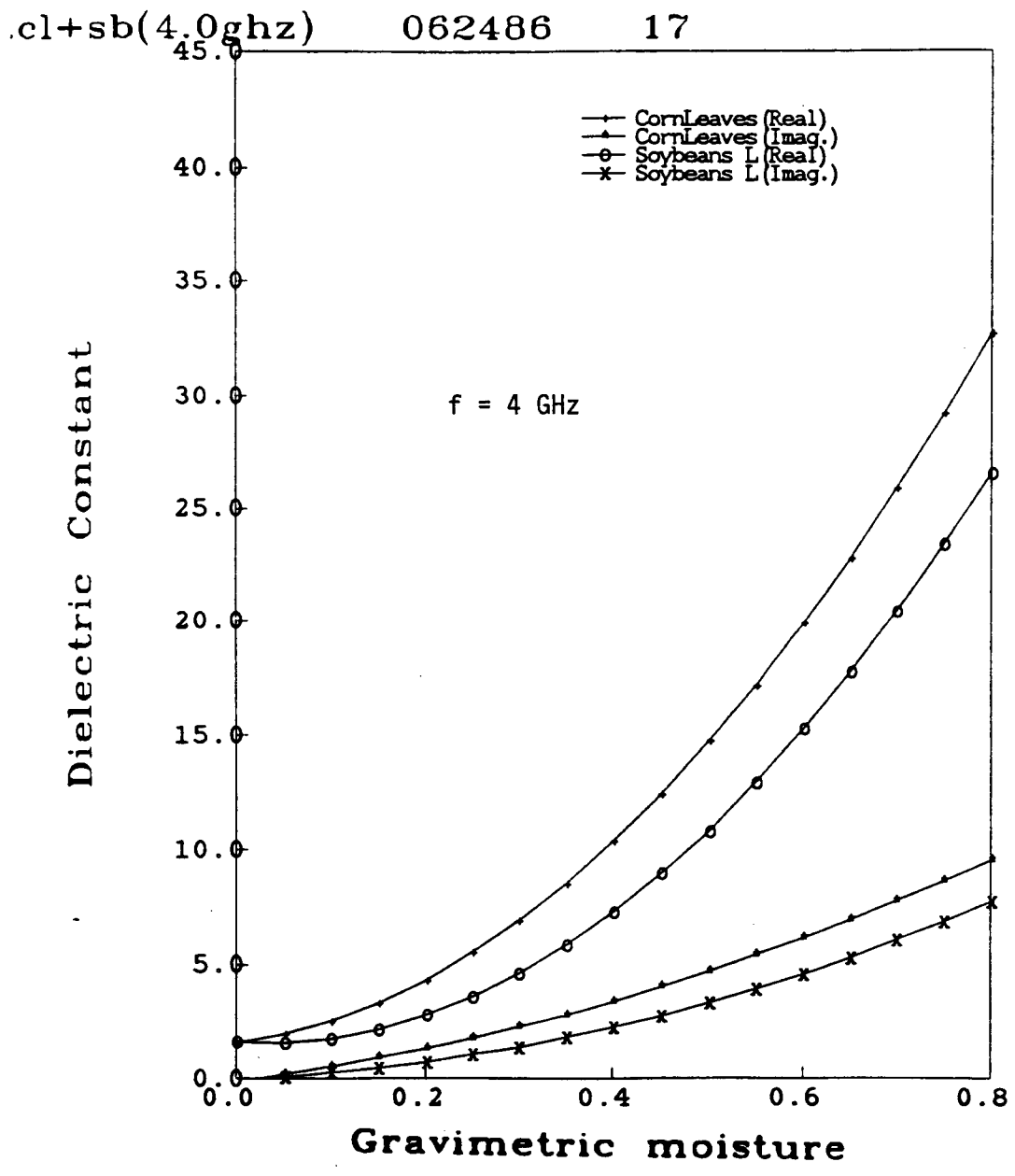
.cl+sb(4.0ghz) 062486 17
CornLeaves(Real)
CornLeaves(Imag.)
Soybeans L(Real)
Soybeans L(Imag.)
f = 4 GHz
Dielectric Constant
Gravimetric moisture
45.0
40.0
35.0
30.0
25.0
20.0
15.0
10.0
5.0
0.0
0.0
0.2
0.4
0.6
0.8

Figure A.11

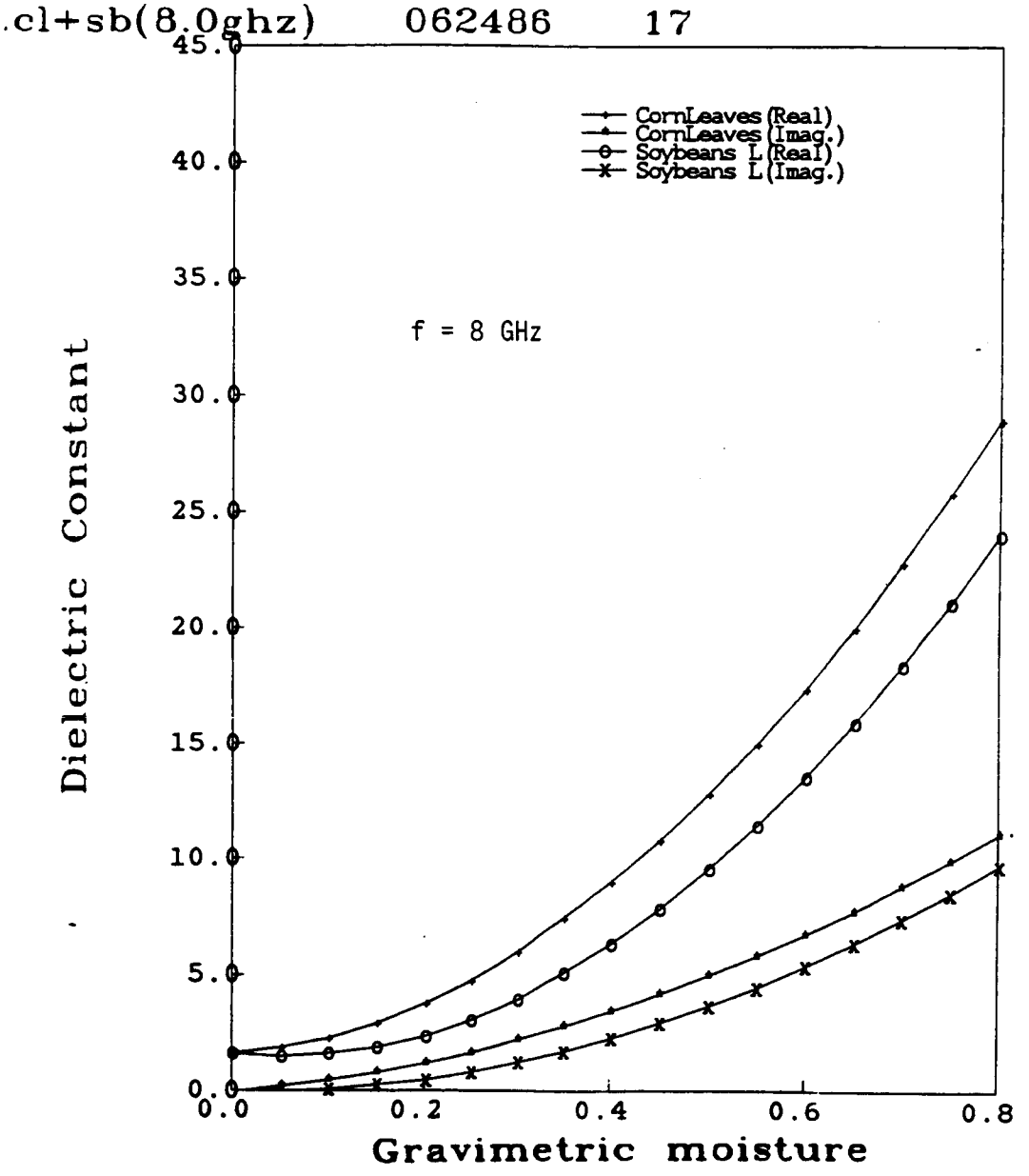
.cl+sb(8.0ghz) 062486 17
CornLeaves (Real)
CornLeaves (Imag.)
Soybeans L (Real)
Soybeans L (Imag.)
f = 8 GHz
Dielectric Constant
45.0
40.0
35.0
30.0
25.0
20.0
15.0
10.0
5.0
0.0
0.0
0.2
0.4
0.6
0.8
Gravimetric moisture

Figure A.12

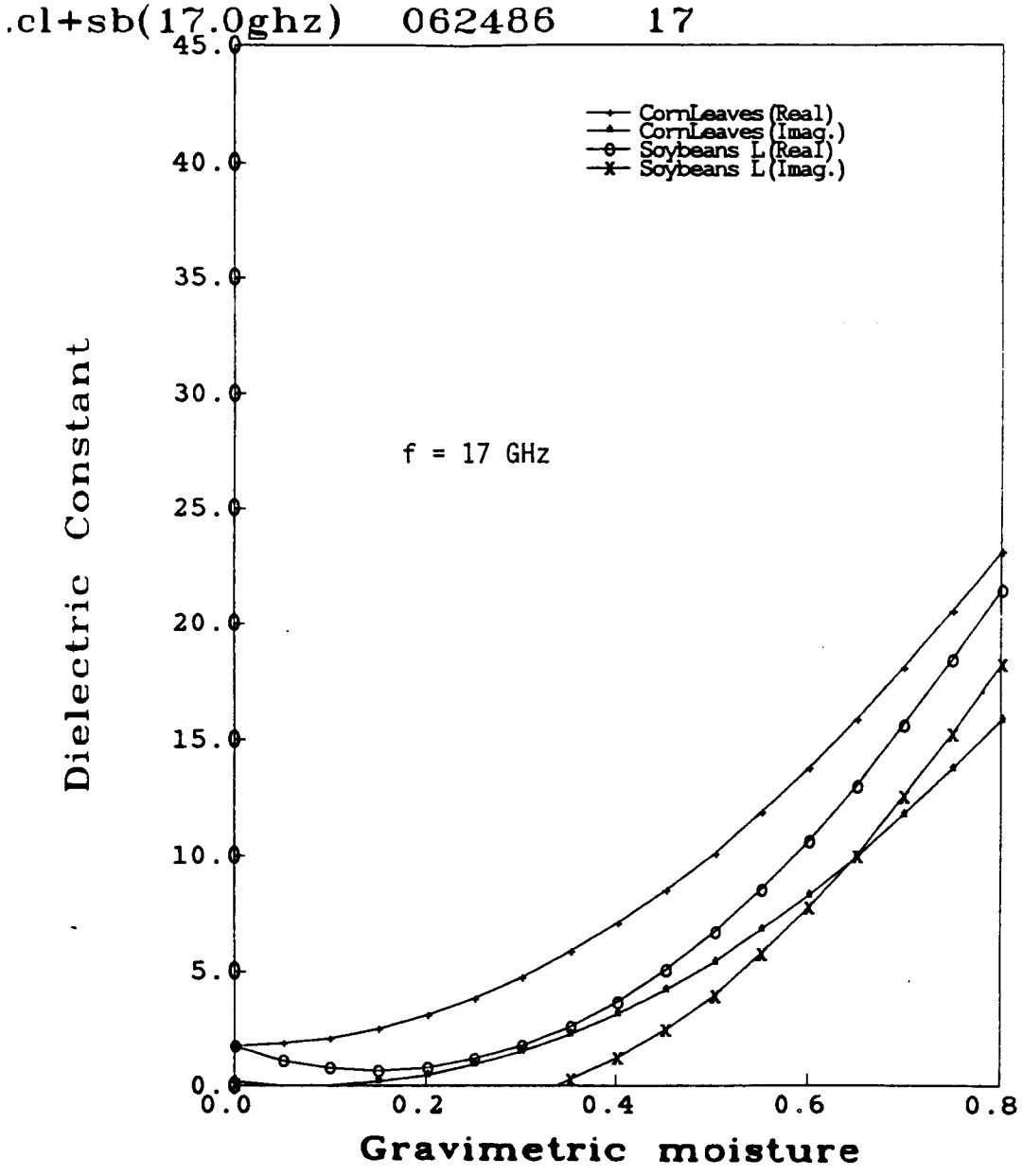
.cl+sb(17.0ghz) 062486 17
CornLeaves (Real)
CornLeaves (Imag.)
Soybeans L (Real)
Soybeans L (Imag.)
f = 17 GHz
Dielectric Constant
Gravimetric moisture
45.0
40.0
35.0
30.0
25.0
20.0
15.0
10.0
5.0
0.
0.0
0.2
0.4
0.6
0.8

Figure A.13

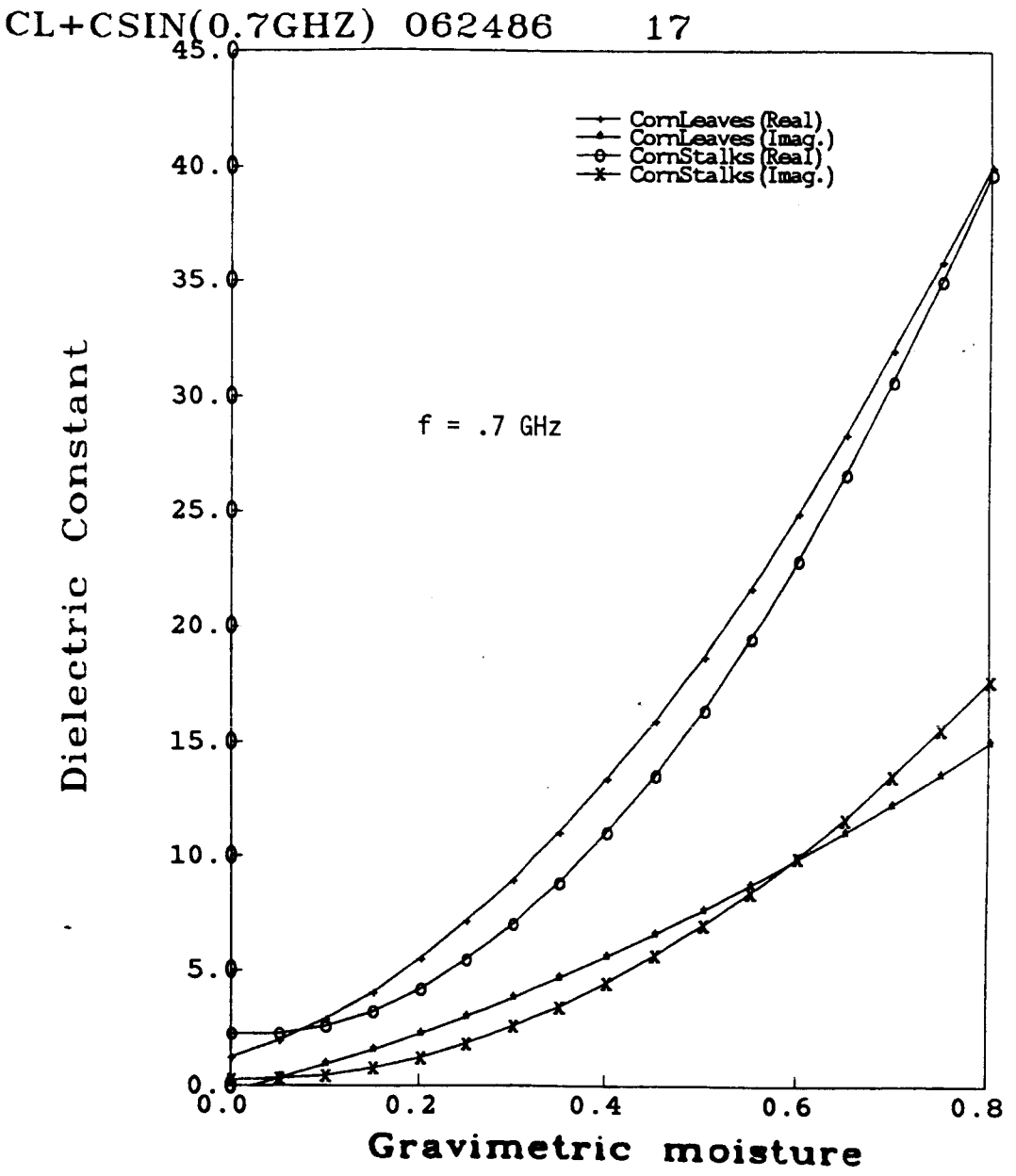
CL+CSIN(0.7GHZ) 062486 17
CornLeaves (Real)
CornLeaves (Imag.)
CornStalks (Real)
CornStalks (Imag.)
f = .7 GHz
Dielectric Constant
Gravimetric moisture
45.0
40.0
35.0
30.0
25.0
20.0
15.0
10.0
5.0
0.
0.0
0.2
0.4
0.6
0.8

Figure A.14

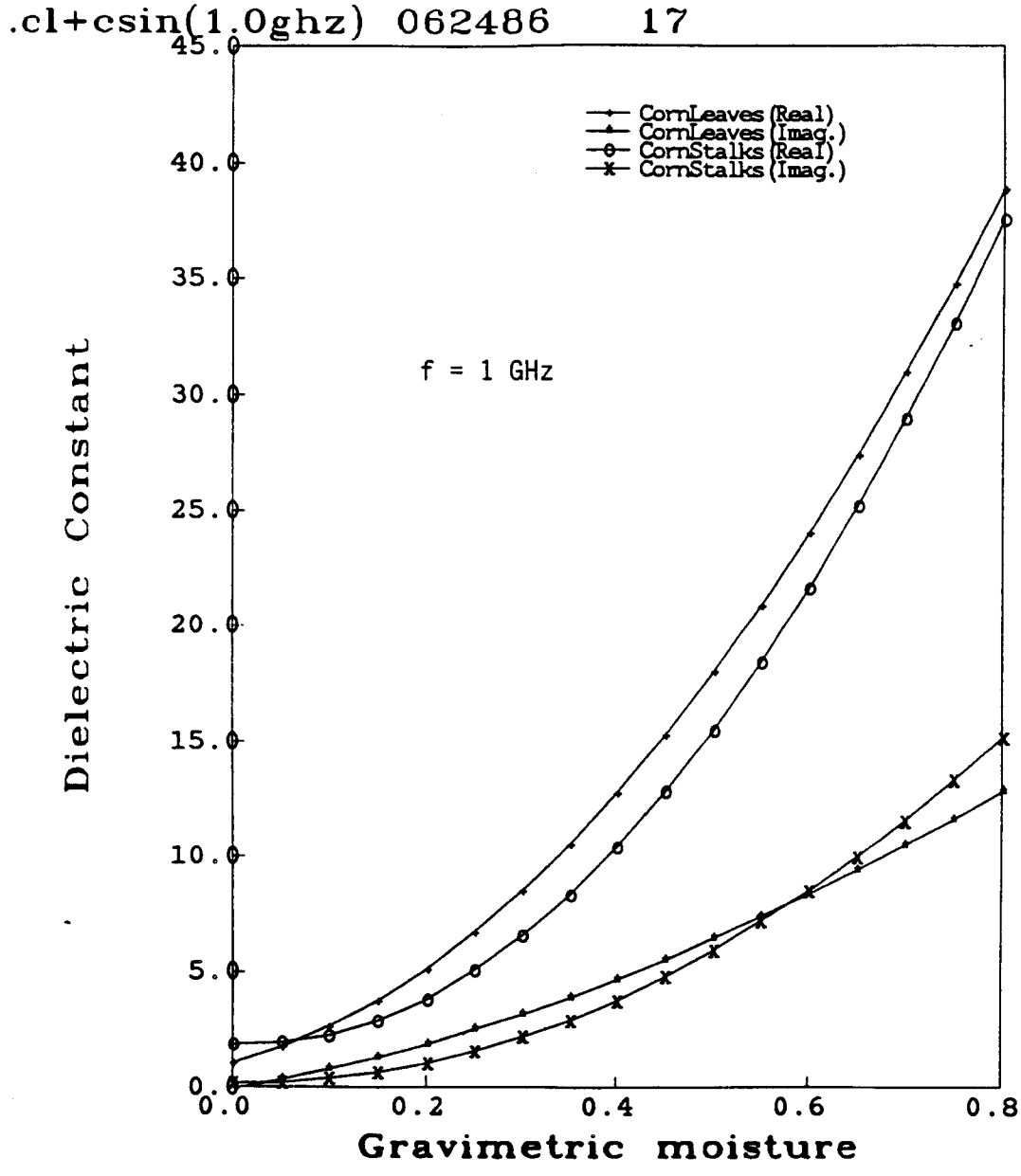
.cl+csin(1.0ghz) 062486 17
CornLeaves(Real)
CornLeaves(Imag.)
CornStalks(Real)
CornStalks(Imag.)
f = 1 GHz
Dielectric Constant
Gravimetric moisture
45.0
40.0
35.0
30.0
25.0
20.0
15.0
10.0
5.0
0.
0.0
0.2
0.4
0.6
0.8

Figure A.15

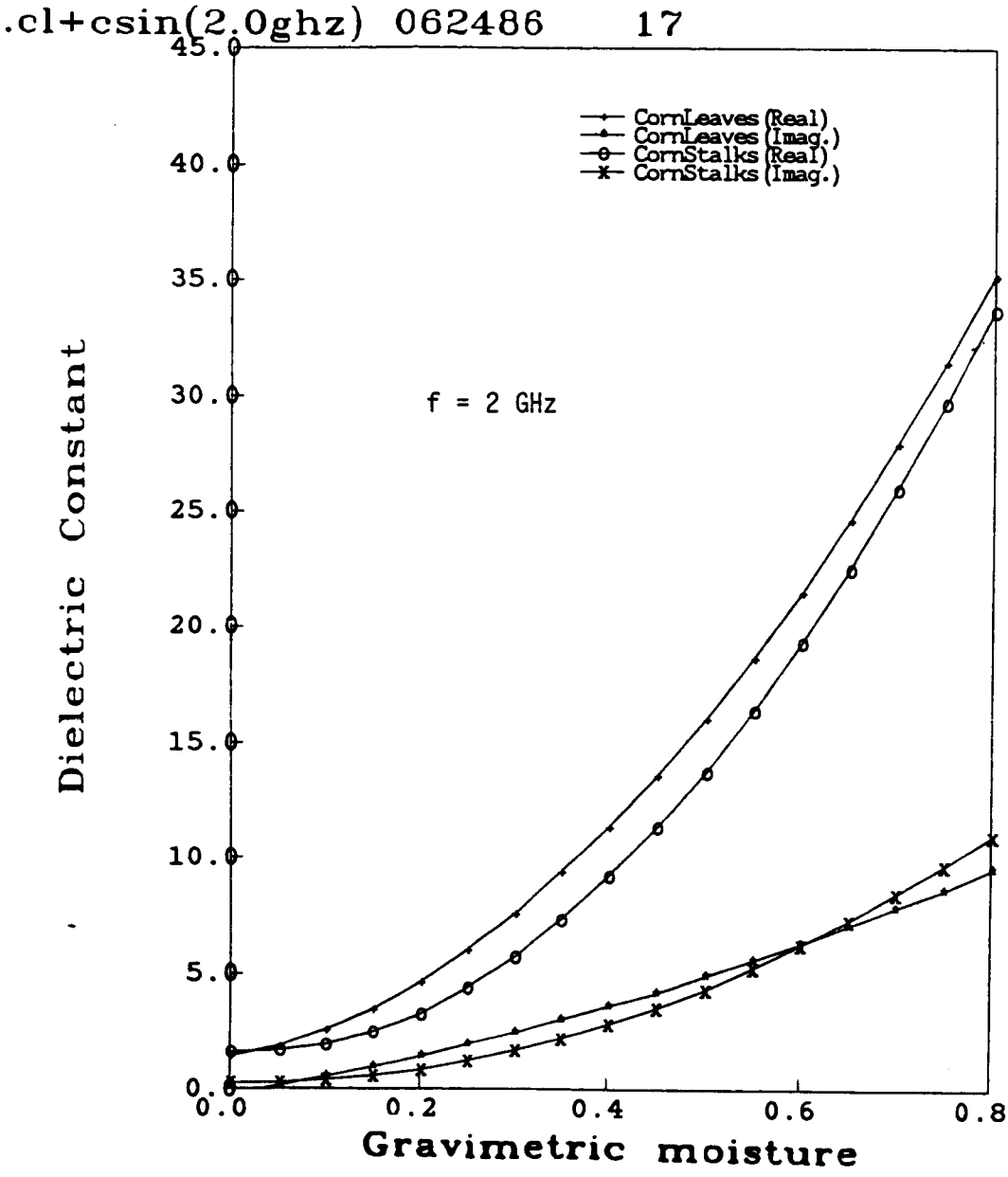
.cl+csin(2.0ghz) 062486 17
CornLeaves (Real)
CornLeaves (Imag.)
CornStalks (Real)
CornStalks (Imag.)
f = 2 GHz
Dielectric Constant
Gravimetric moisture
45.0
40.0
35.0
30.0
25.0
20.0
15.0
10.0
5.0
0.0
0.0
0.2
0.4
0.6
0.8

Figure A.16

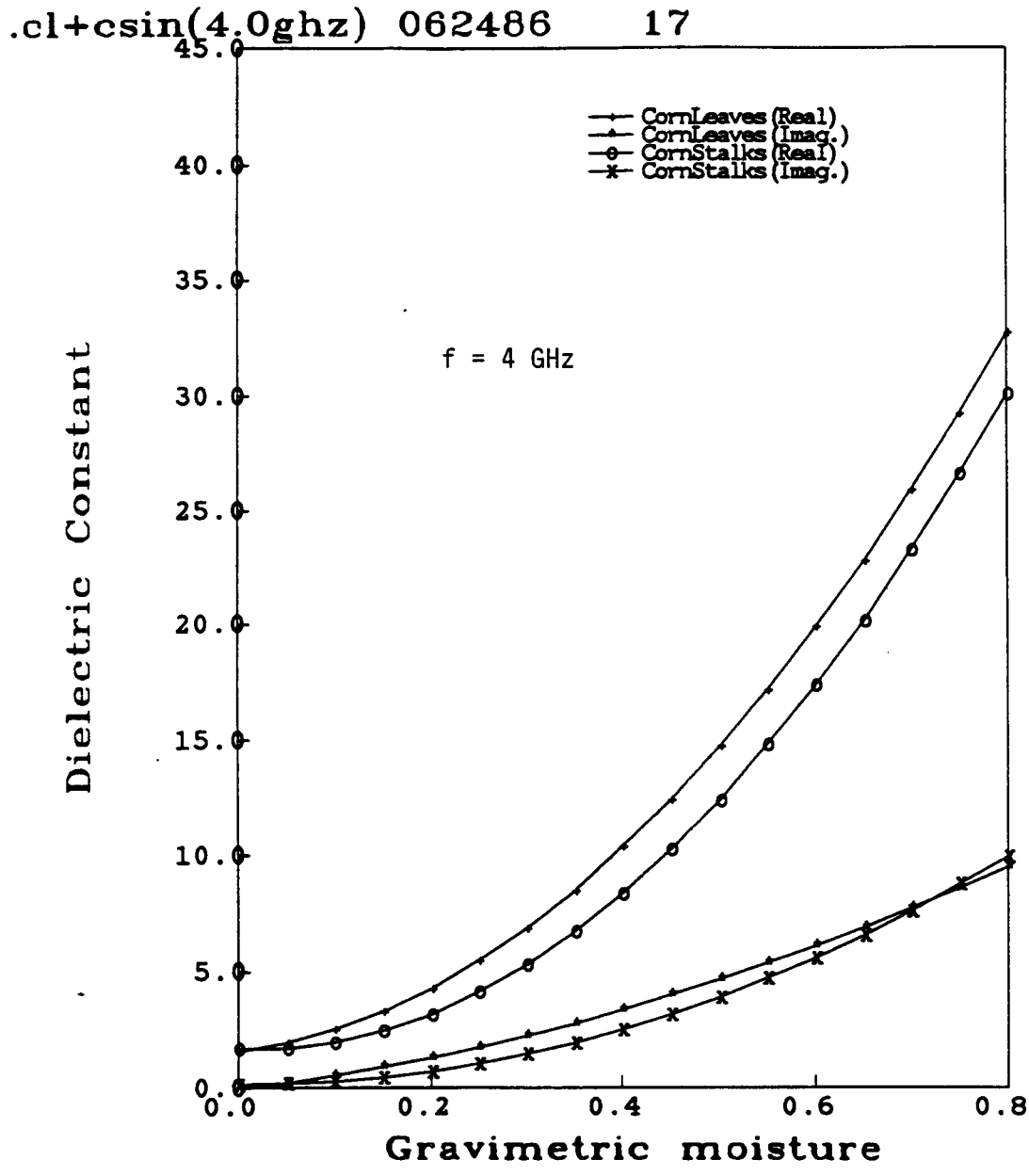
.cl+csin(4.0ghz) 062486 17
CornLeaves(Real)
CornLeaves(Imag.)
CornStalks(Real)
CornStalks(Imag.)
f = 4 GHz
Dielectric Constant
Gravimetric moisture
45.0
40.0
35.0
30.0
25.0
20.0
15.0
10.0
5.0
0.0
0.0
0.2
0.4
0.6
0.8

Figure A.17

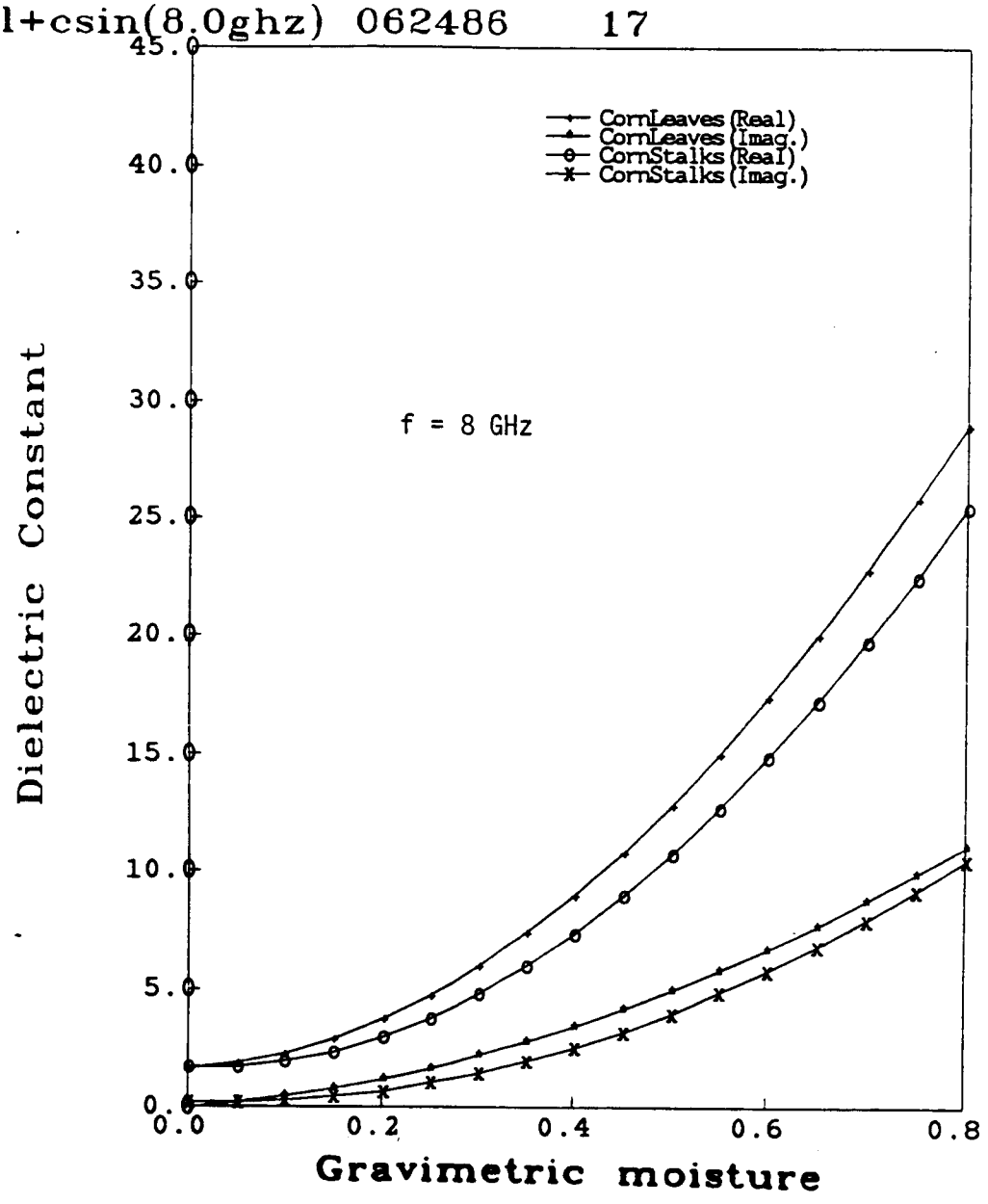
.cl+csin(8.0ghz) 062486 17
CornLeaves (Real)
CornLeaves (Imag.)
CornStalks (Real)
CornStalks (Imag.)
f = 8 GHz
Dielectric Constant
Gravimetric moisture
45.0
40.0
35.0
30.0
25.0
20.0
15.0
10.0
5.0
0.0
0.0
0.2
0.4
0.6
0.8

Figure A.18

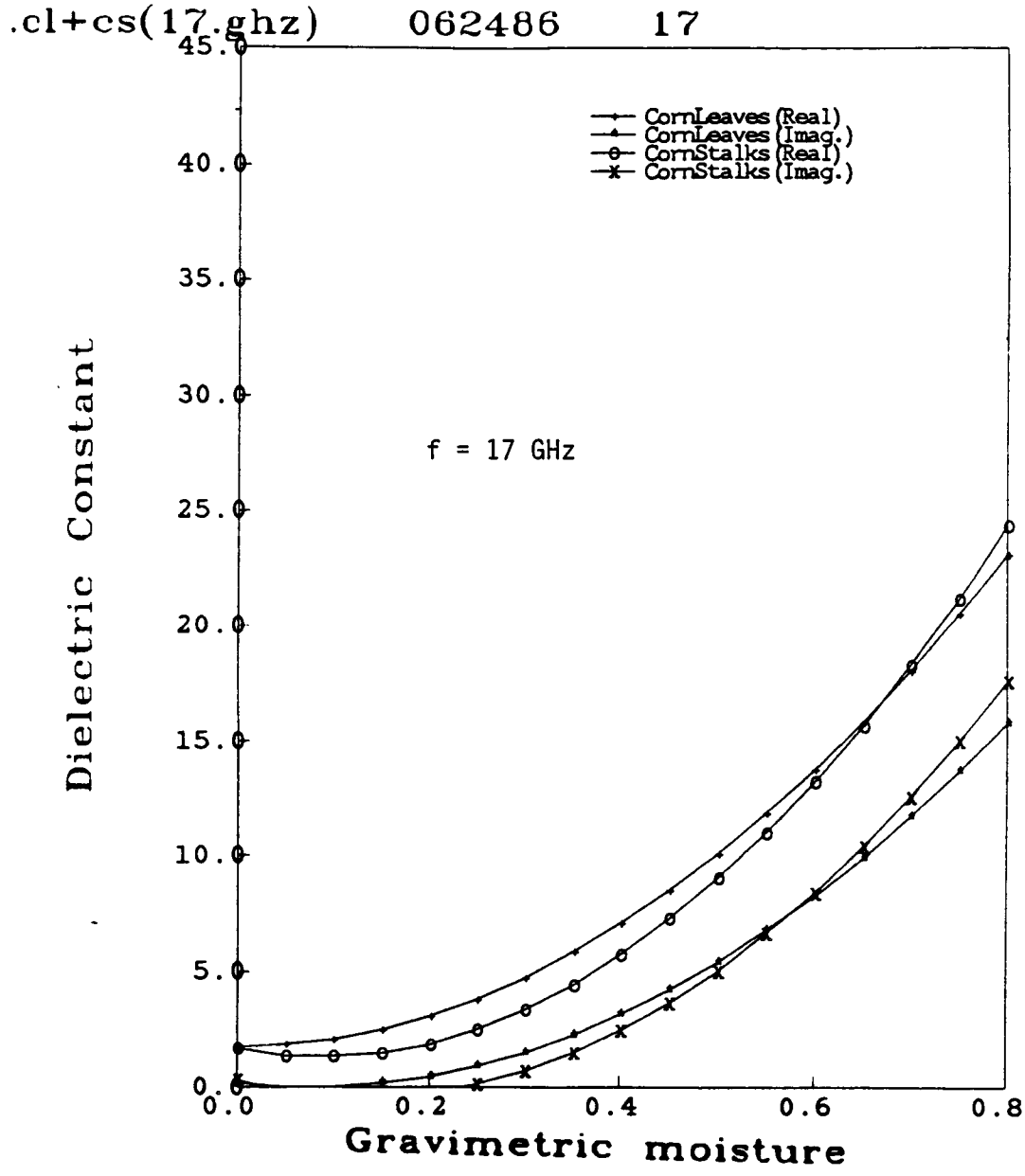
.cl+cs(17.ghz) 062486 17
CornLeaves(Real)
CornLeaves(Imag.)
CornStalks(Real)
CornStalks(Imag.)
f = 17 GHz
Dielectric Constant
Gravimetric moisture
45.0
40.0
35.0
30.0
25.0
20.0
15.0
10.0
5.0
0.0
0.0
0.2
0.4
0.6
0.8

Figure A.19

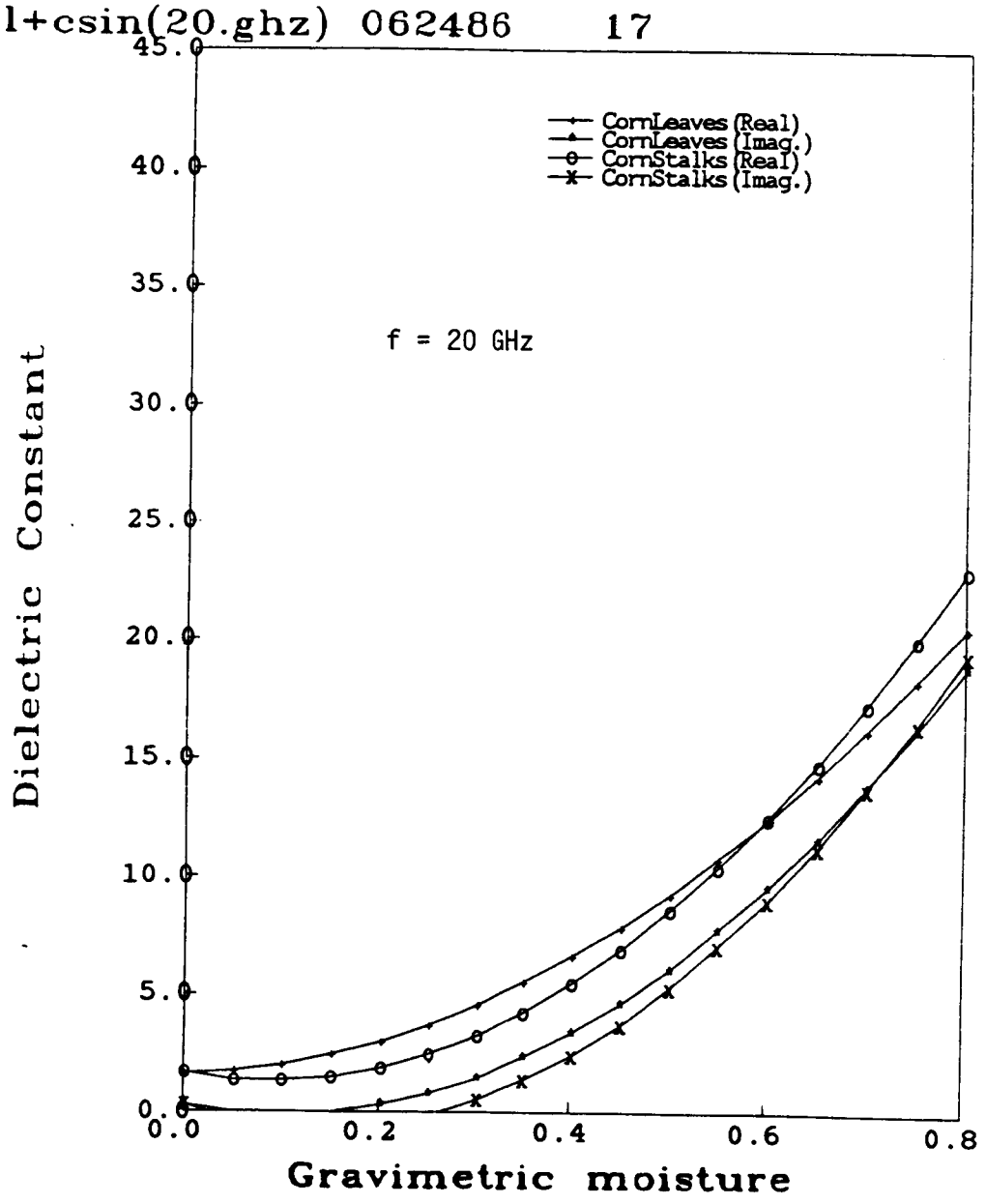
.cl+csin(20.ghz) 062486 17
CornLeaves (Real)
CornLeaves (Imag.)
CornStalks (Real)
CornStalks (Imag.)
f = 20 GHz
Dielectric Constant
Gravimetric moisture
45.0
40.0
35.0
30.0
25.0
20.0
15.0
10.0
5.0
0.0
0.0
0.2
0.4
0.6
0.8

Figure A.20

Appendix A

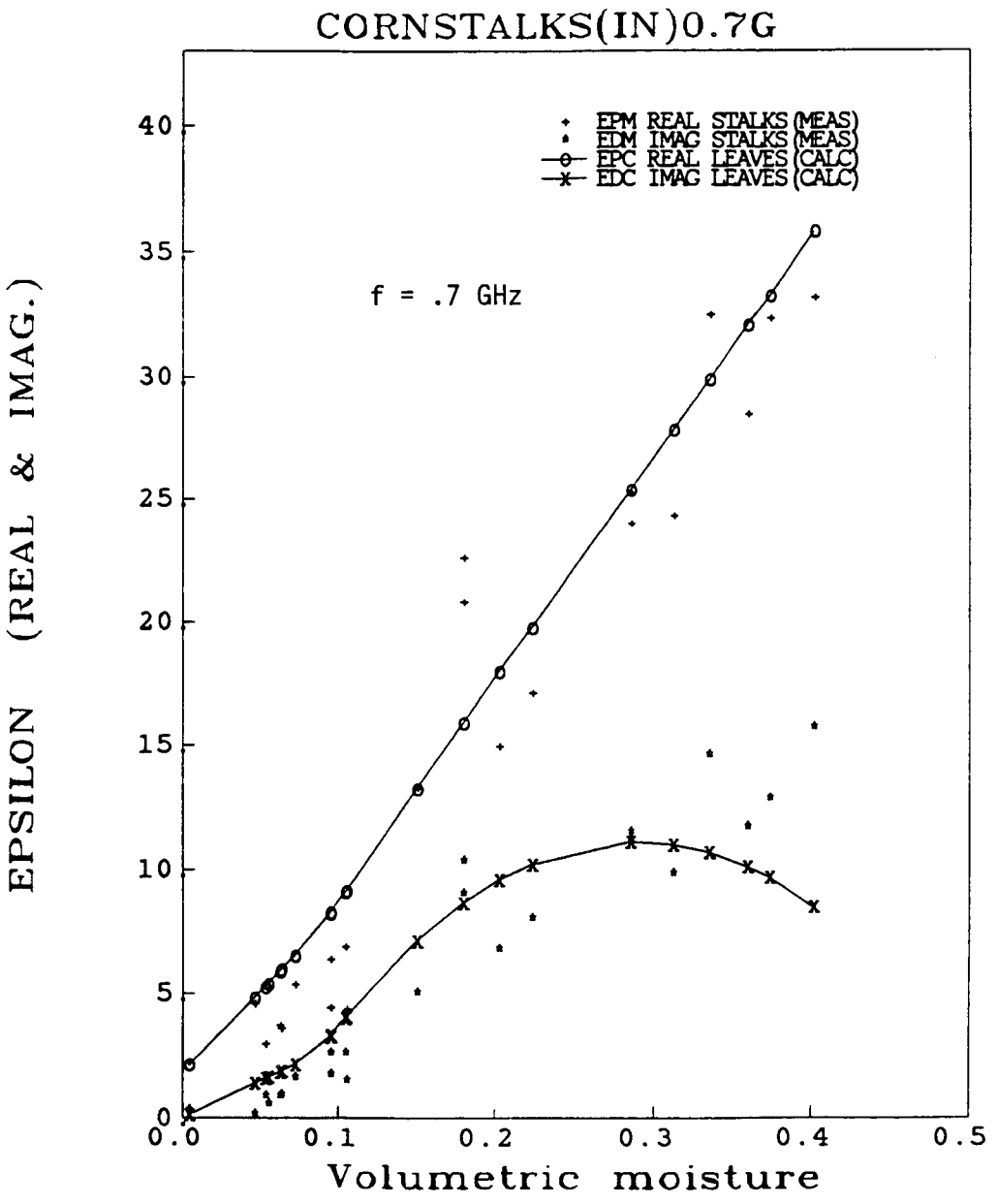

Figure A.21

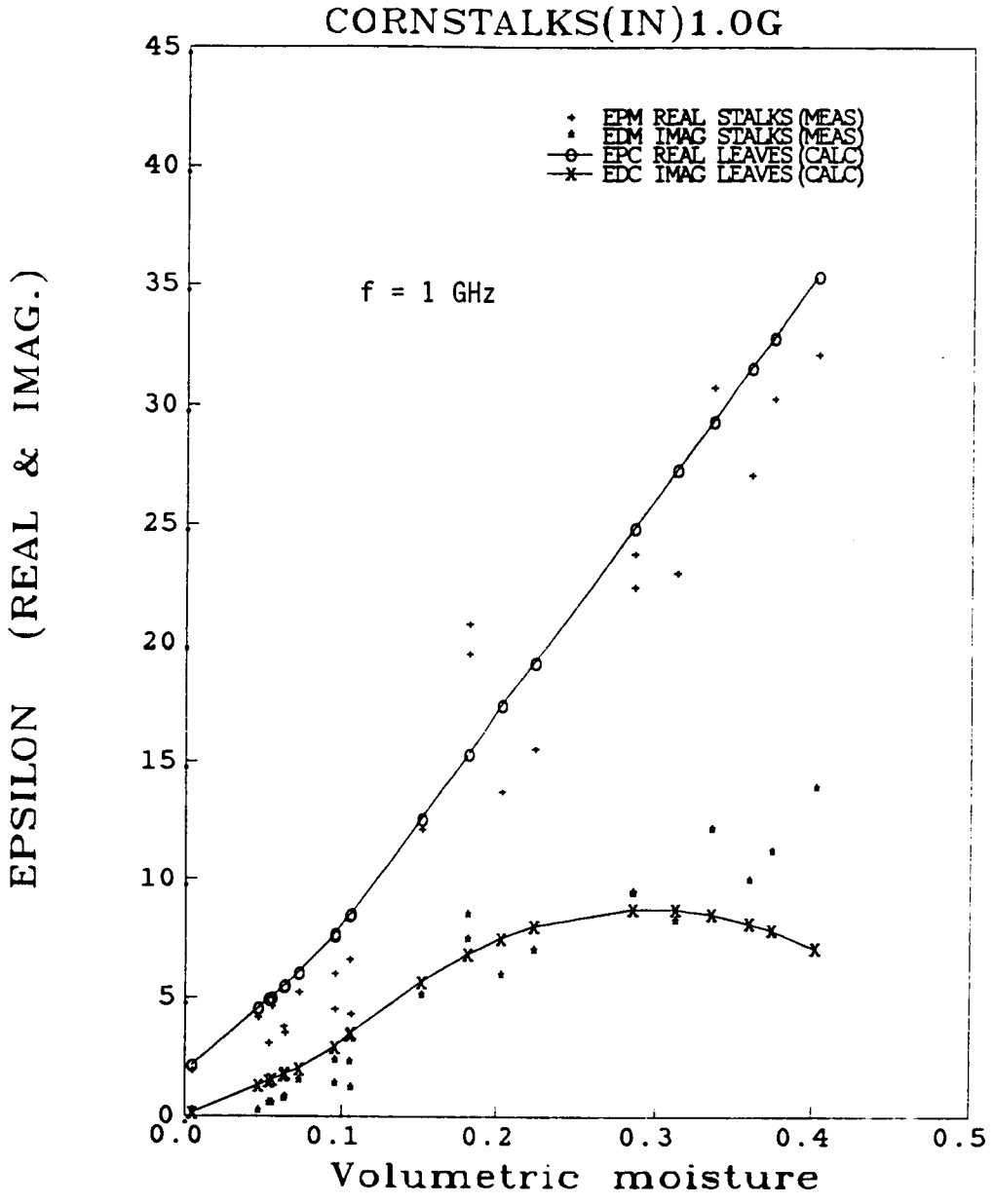
CORNSTALKS(IN)1.0G
EPM REAL STALKS (MEAS)
EDM IMAG STALKS (MEAS)
EPC REAL LEAVES (CALC)
EDC IMAG LEAVES (CALC)
f = 1 GHz
EPSILON (REAL & IMAG.)
Volumetric moisture
0
5
10
15
20
25
30
35
40
45
0.0
0.1
0.2
0.3
0.4
0.5

Figure A.22

Appendix A

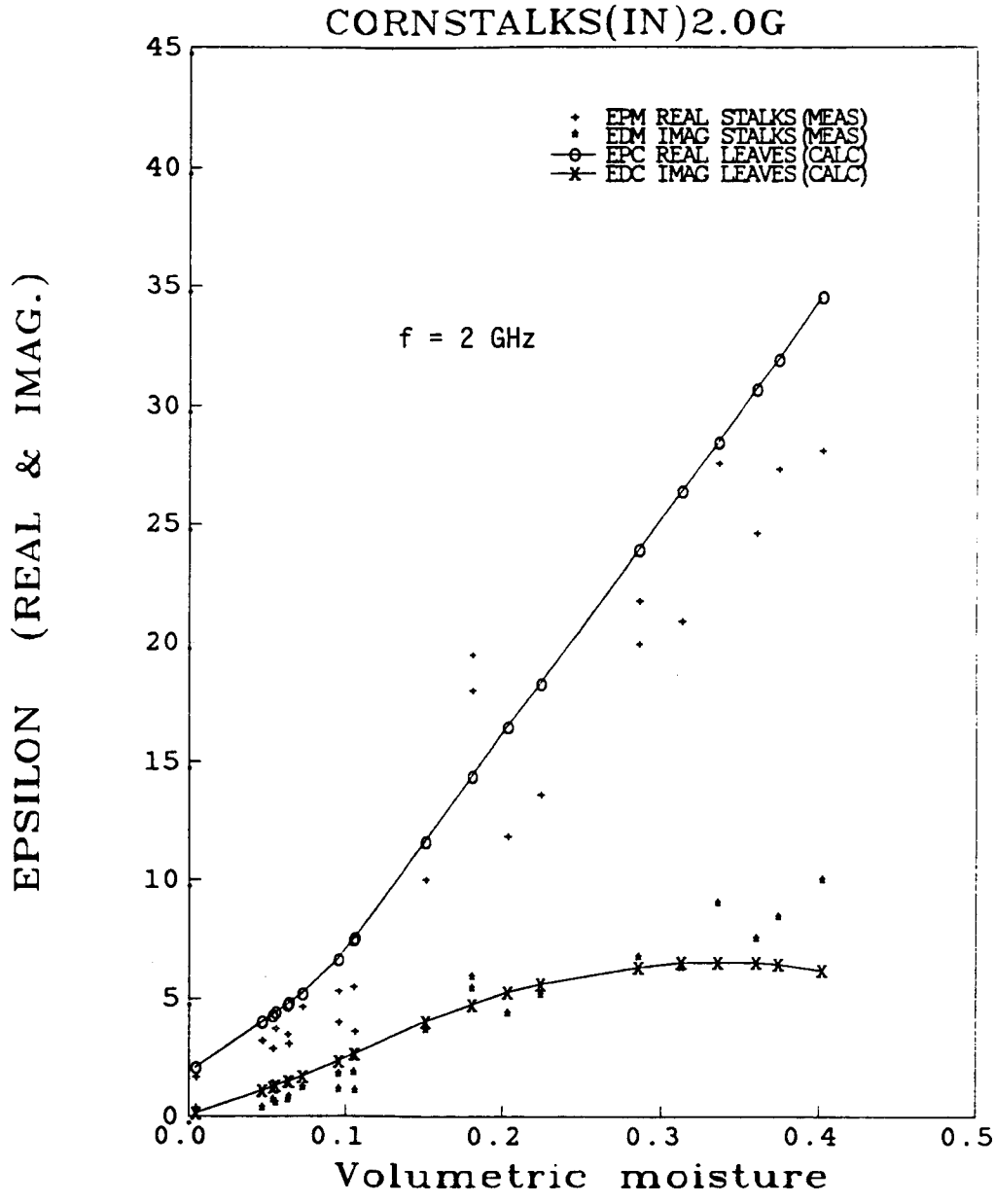

Figure A.23

Appendix A

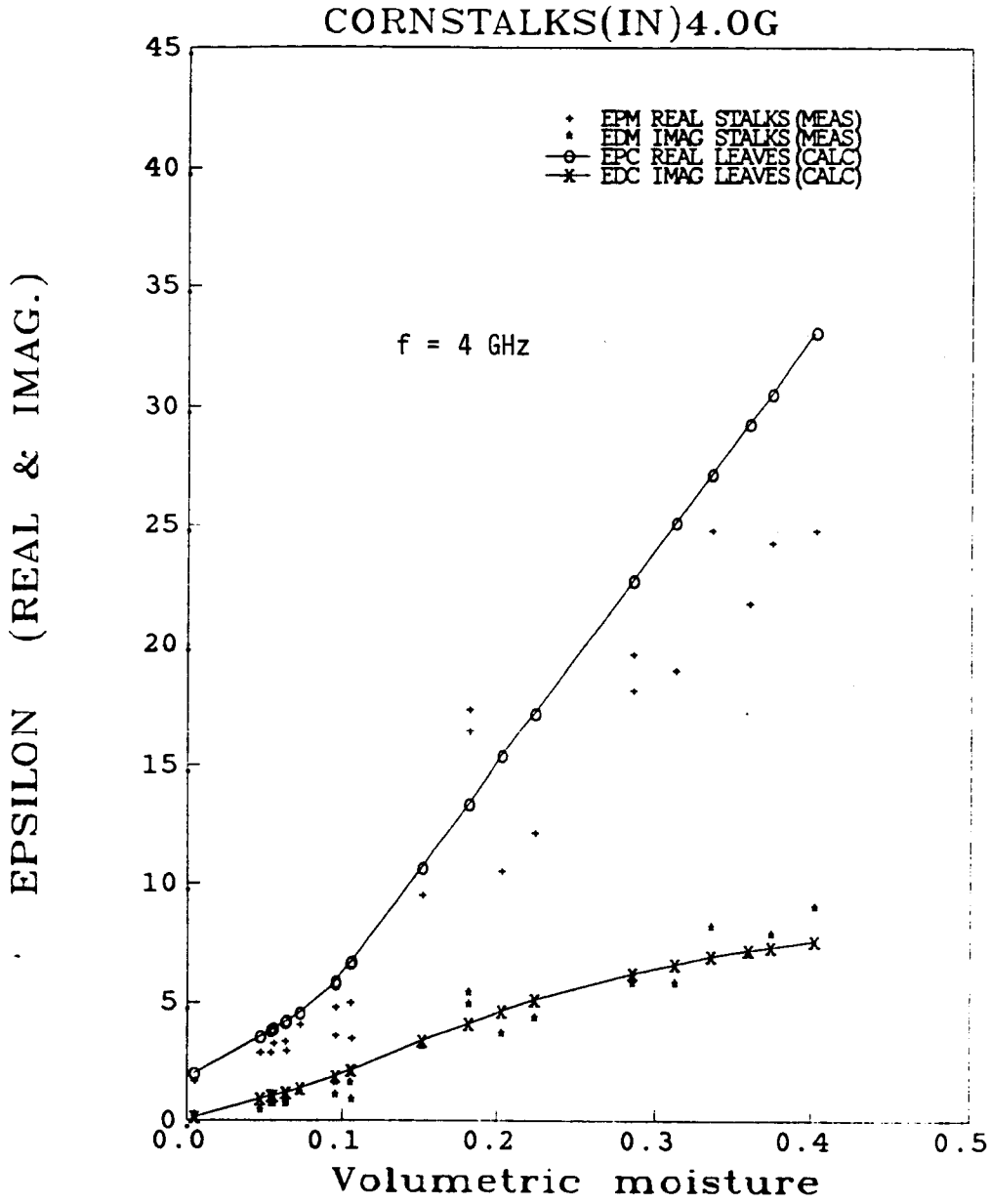

Figure A.24

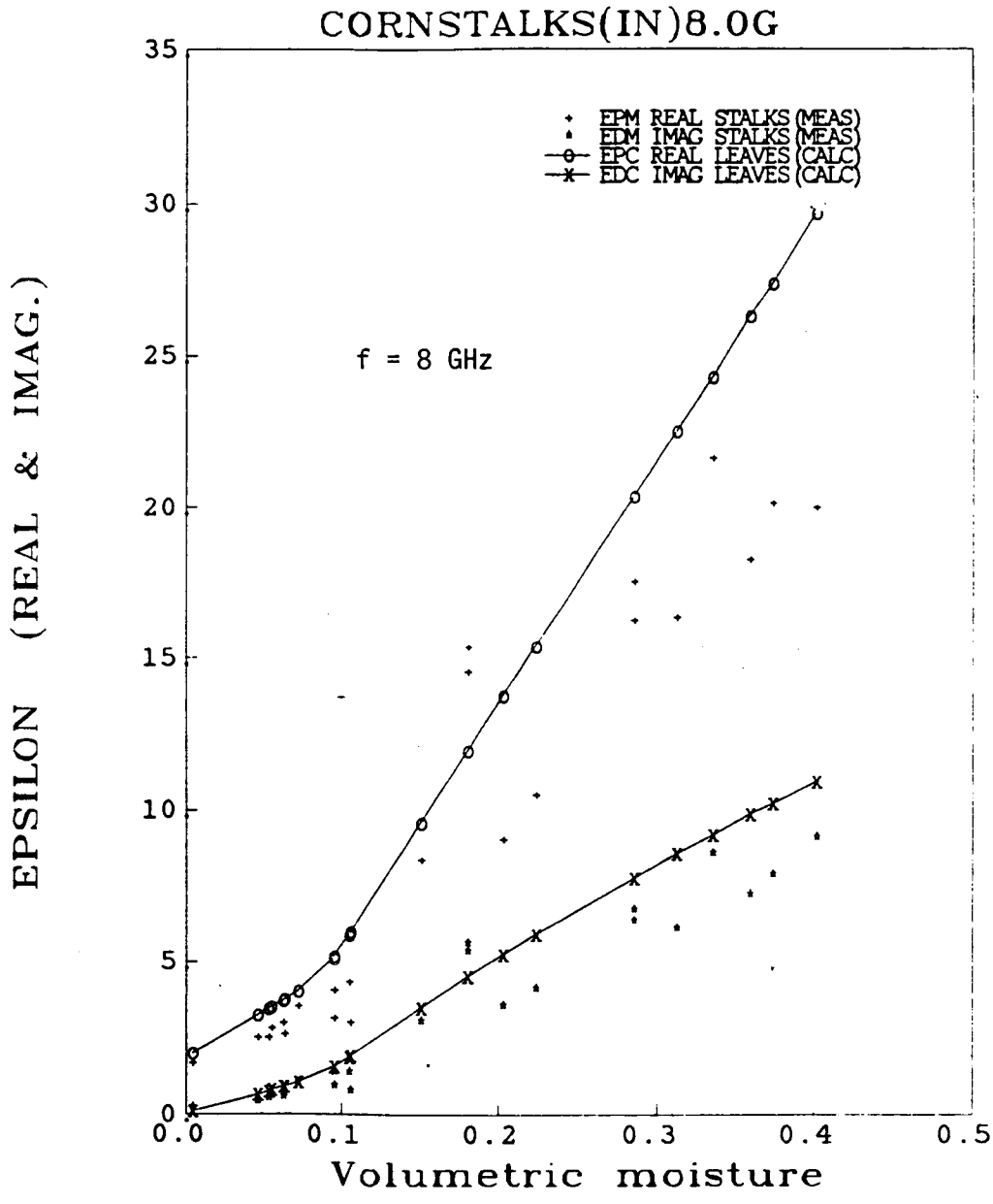
CORNSTALKS(IN)8.0G
EPM REAL STALKS (MEAS)
EDM IMAG STALKS (MEAS)
EPC REAL LEAVES (CALC)
EDC IMAG LEAVES (CALC)
f = 8 GHz
EPSILON (REAL & IMAG.)
Volumetric moisture
0
5
10
15
20
25
30
35
0.0
0.1
0.2
0.3
0.4
0.5

Figure A.25

Appendix A

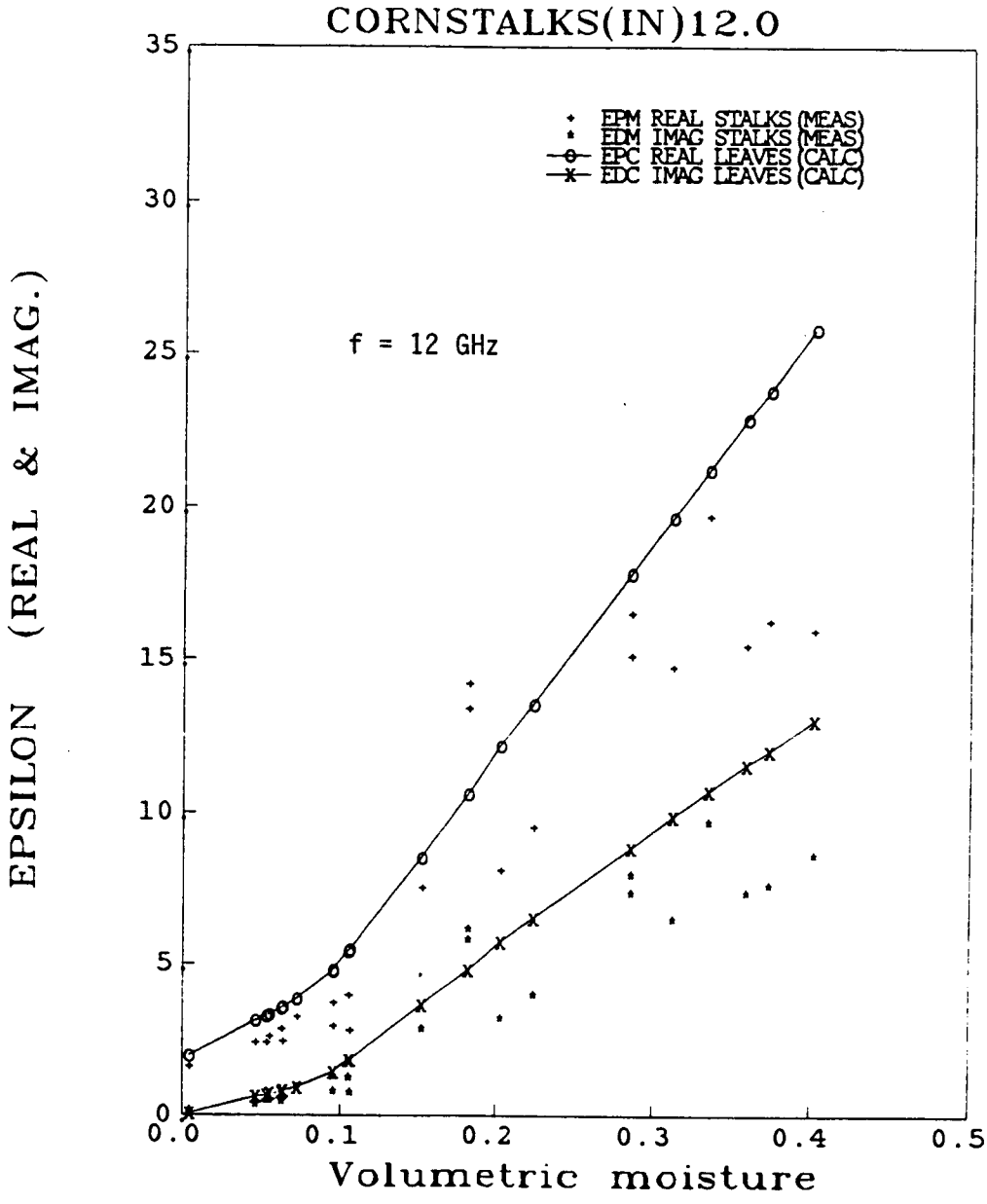

Figure A.26

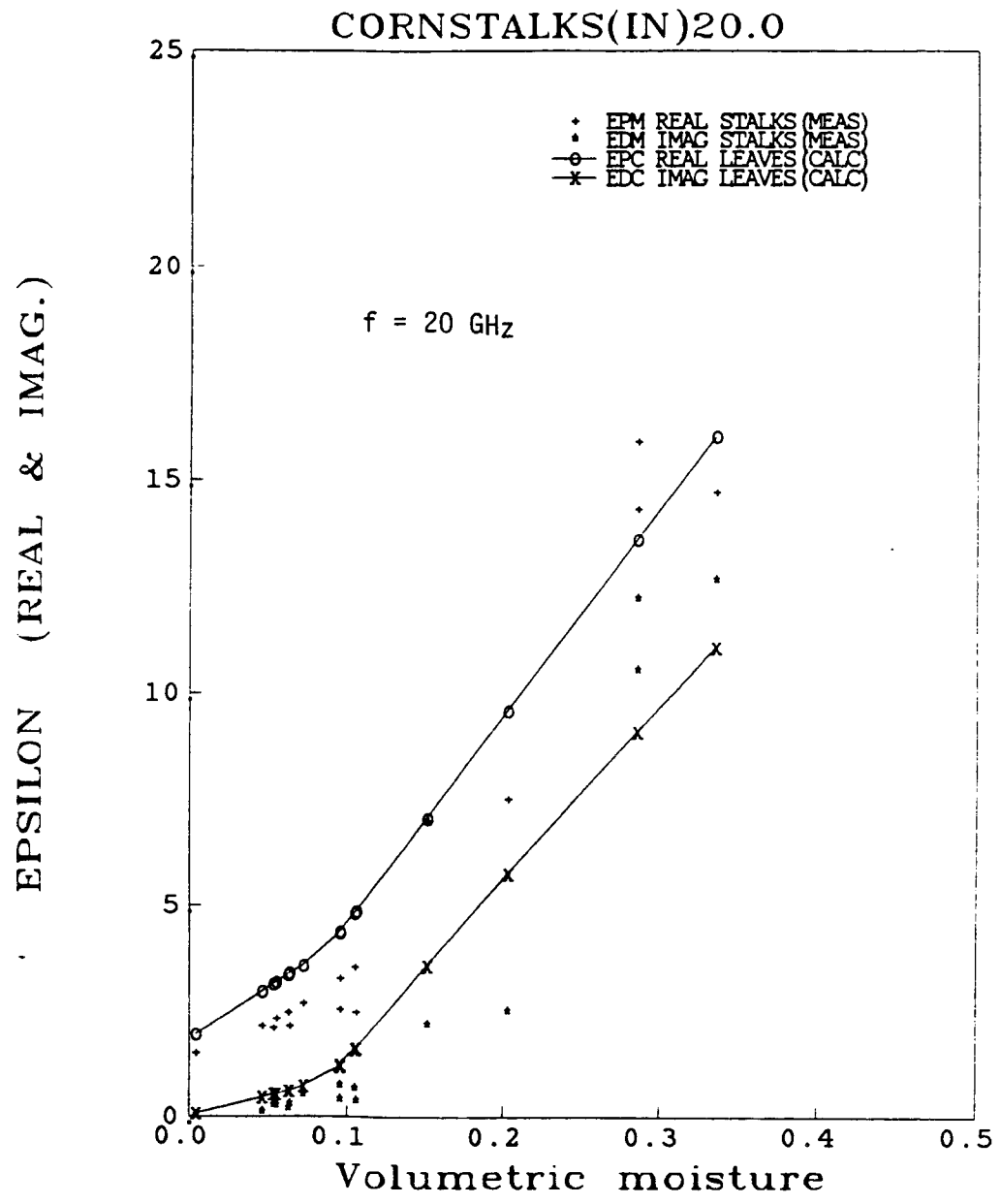
CORNSTALKS(IN)20.0
EPM REAL STALKS (MEAS)
EDM IMAG STALKS (MEAS)
EPC REAL LEAVES (CALC)
EDC IMAG LEAVES (CALC)
f = 20 GHz
EPSILON (REAL & IMAG.)
Volumetric moisture
0
5
10
15
20
25
0.0
0.1
0.2
0.3
0.4
0.5

Figure A.27

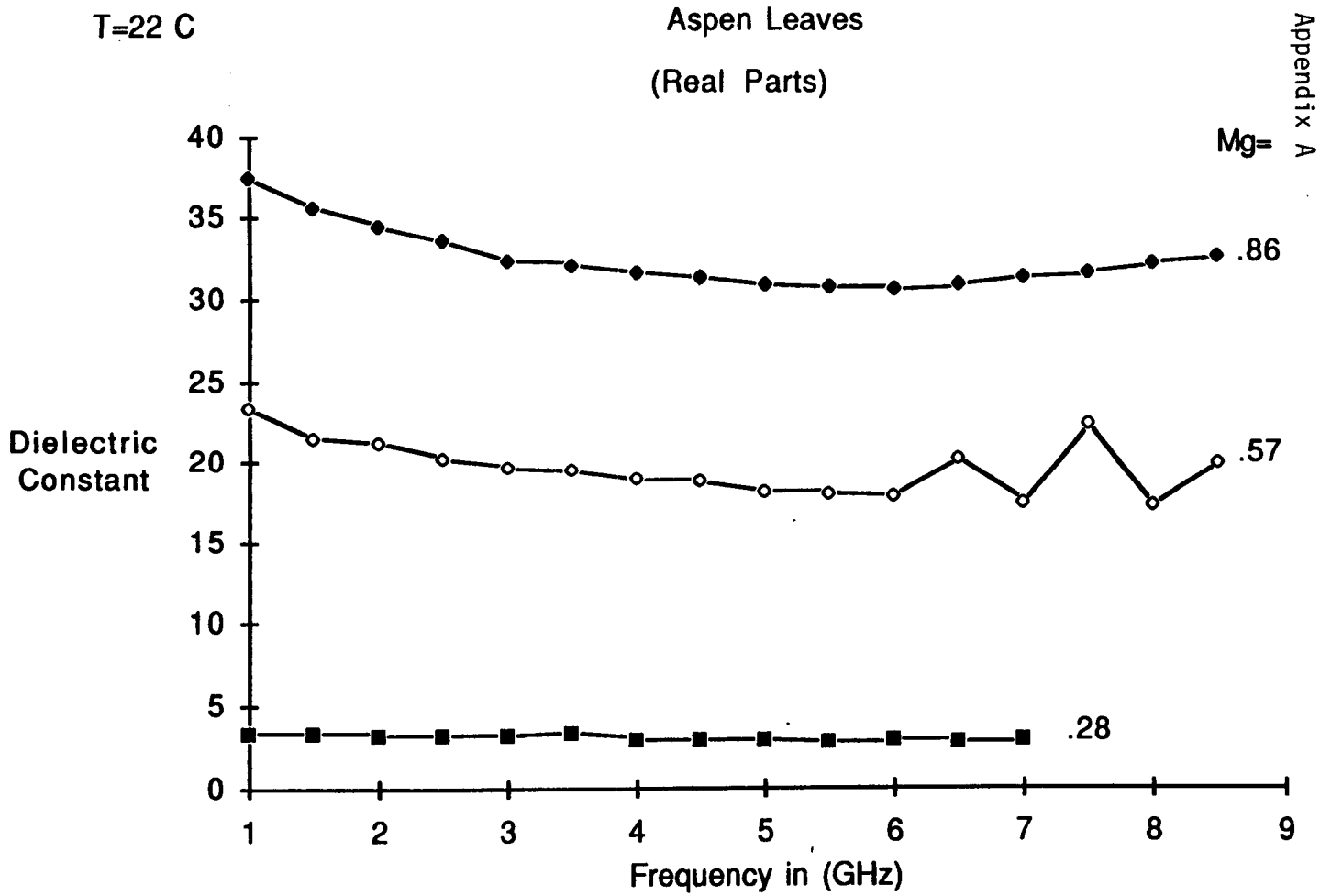
T=22 C
Aspen Leaves
(Real Parts)
Mg=
.86
.57
.28
Dielectric Constant
40
35
30
25
20
15
10
5
0
1
2
3
4
5
6
7
8
9
Frequency in (GHz)

Figure A.28

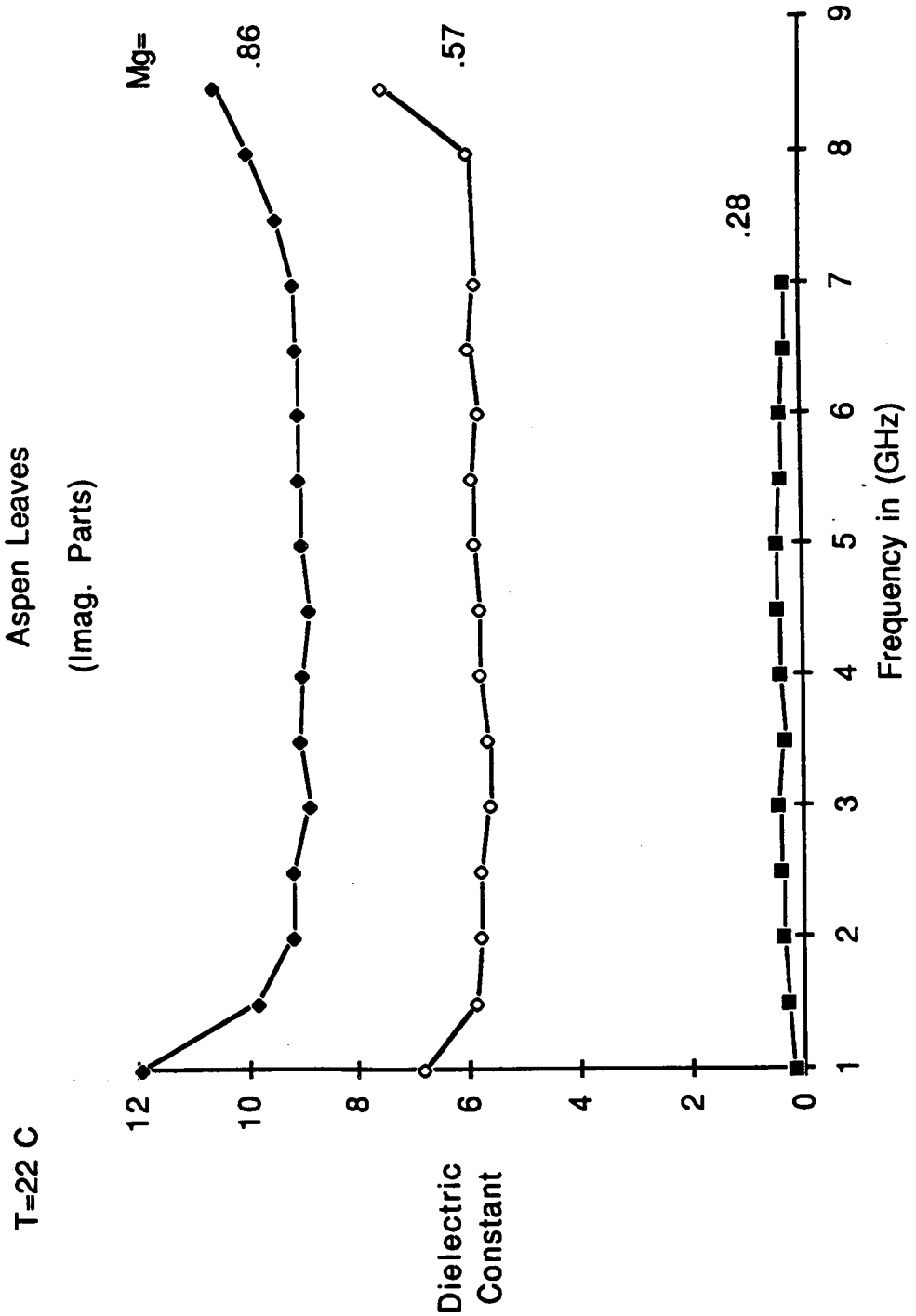
Aspen Leaves
(Imag. Parts)
T=22 C
Mg=
.86
.57
.28
Dielectric Constant
Frequency in (GHz)
12
10
8
6
4
2
0
1
2
3
4
5
6
7
8
9

Figure A.29

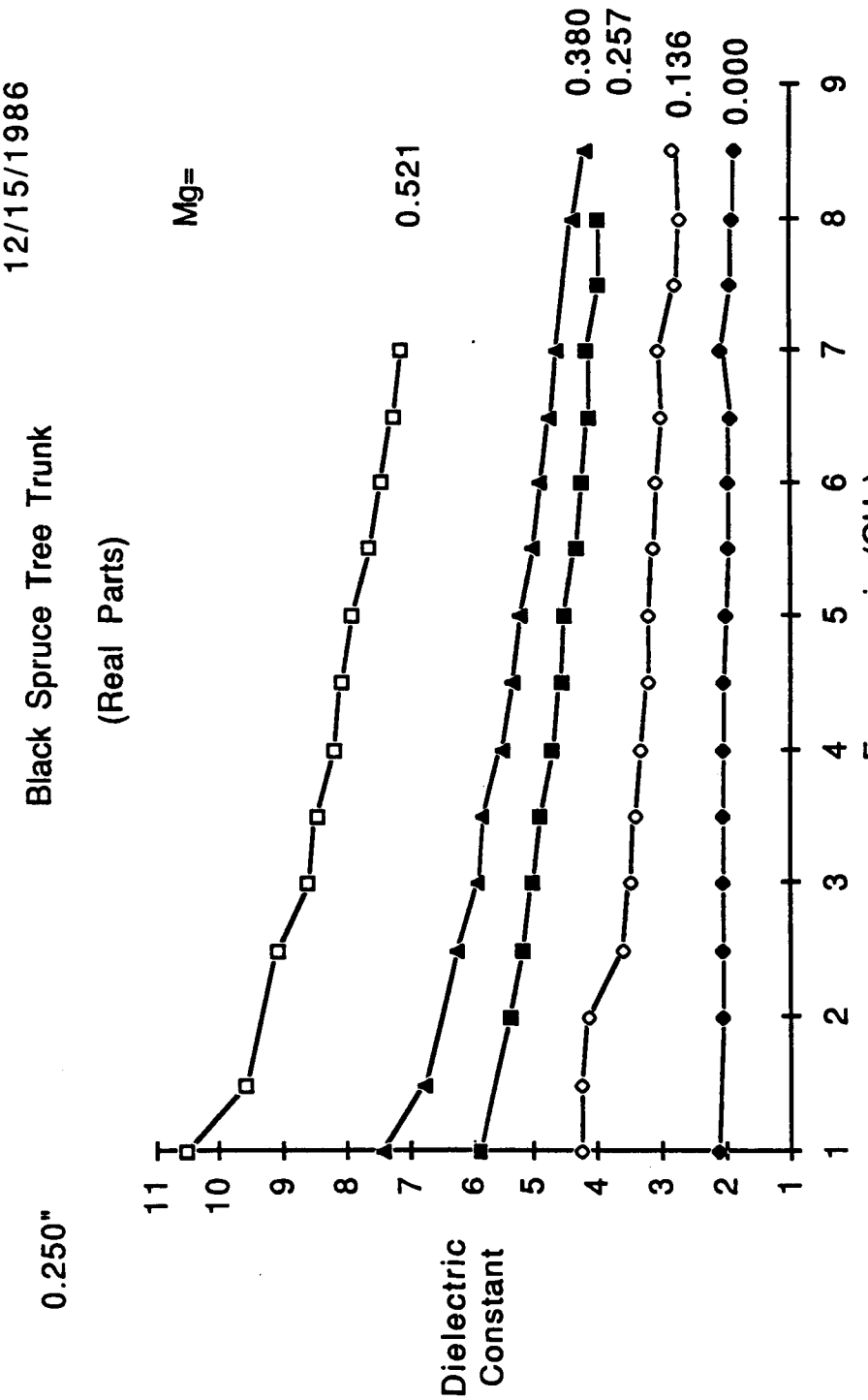
0.250"
Black Spruce Tree Trunk
12/15/1986
(Real Parts)
Mg=
0.521
0.380
0.257
0.136
0.000
Dielectric Constant
Frequency in (GHz)
11
10
9
8
7
6
5
4
3
2
1
1
2
3
4
5
6
7
8
9

Figure A.30

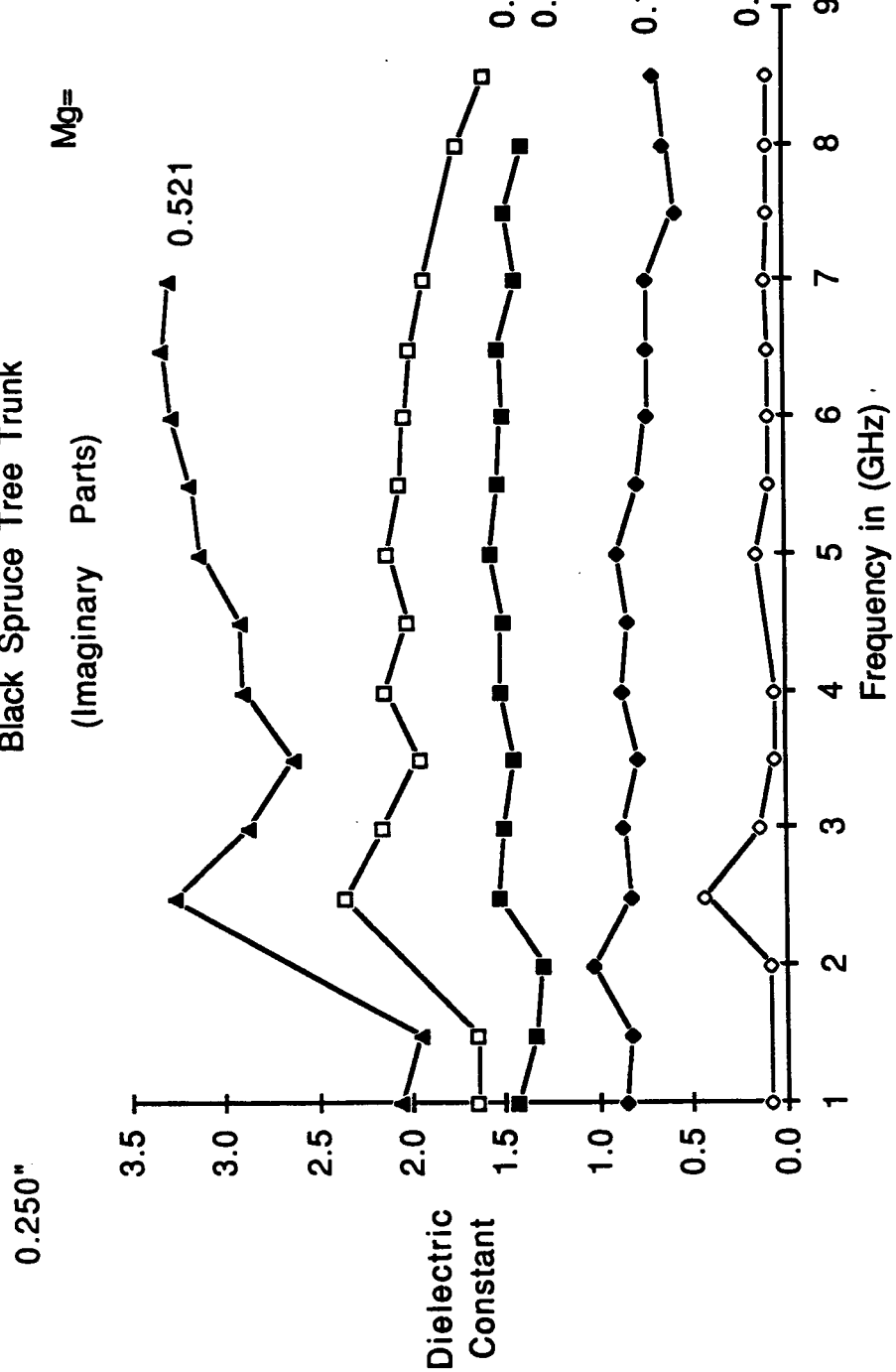
Black Spruce Tree Trunk
12/15/1986
(Imaginary Parts)
Mg=
0.521
0.380
0.257
0.136
0.000
0.250"
Dielectric Constant
Frequency in (GHz)
3.5
3.0
2.5
2.0
1.5
1.0
0.5
0.0
1
2
3
4
5
6
7
8
9

Figure A.31

0.250"

12/15/1986

Black Spruce Tree Trunck
f=1.0 GHz

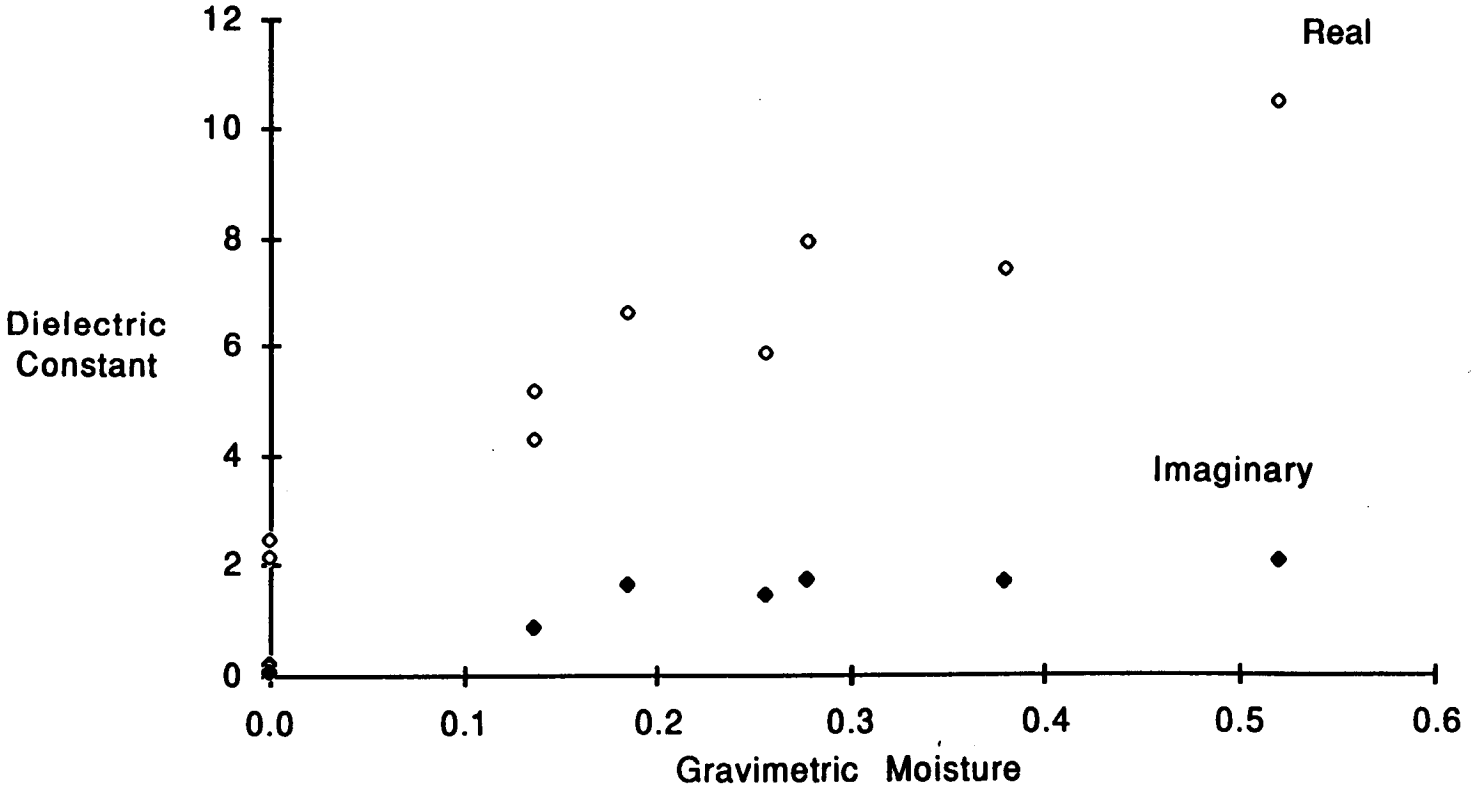

Figure A.32

0.250"

12/15/1986

Black Spruce Tree Trunck
f = 2.0 GHz

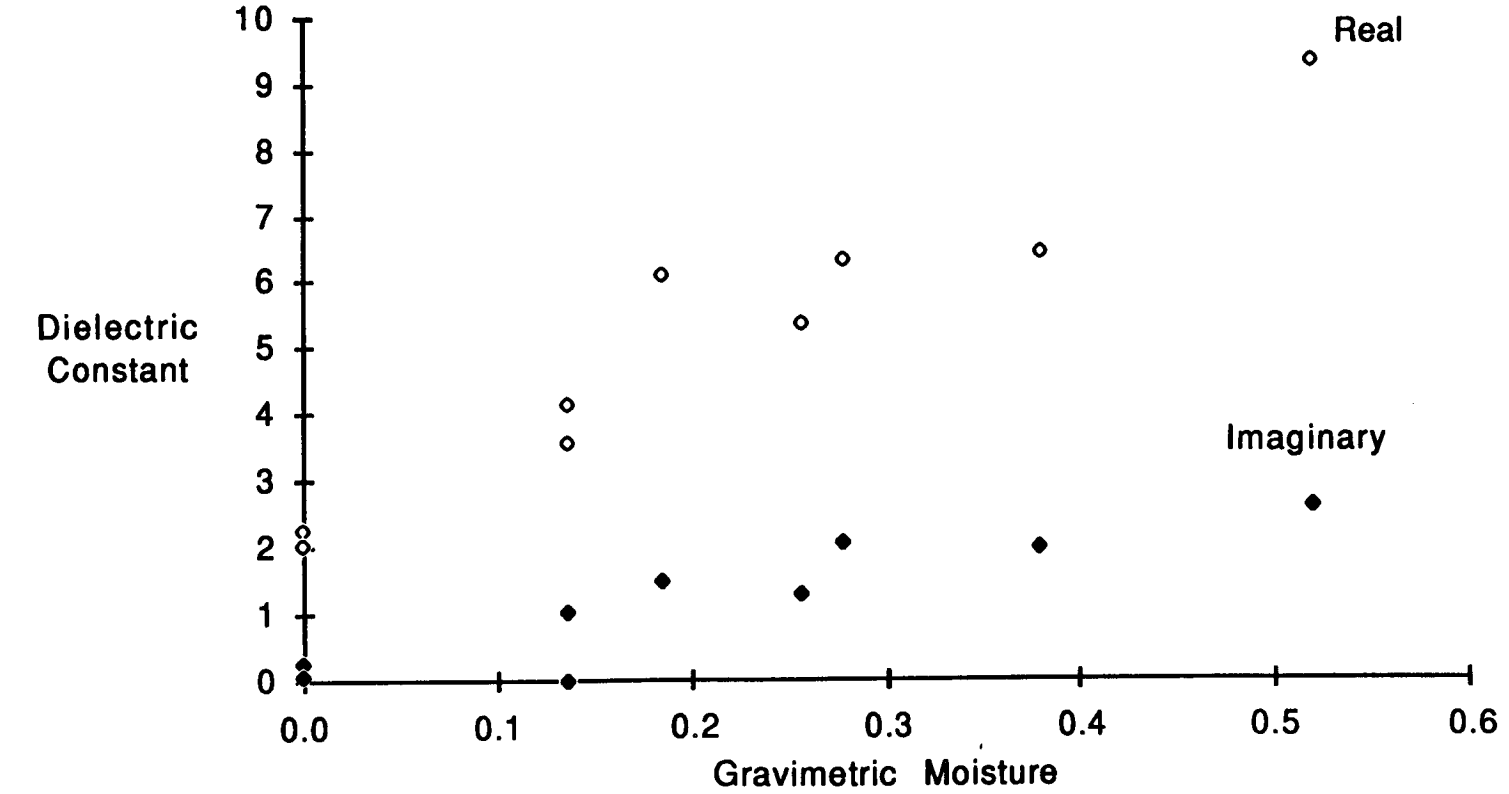

Figure A.33

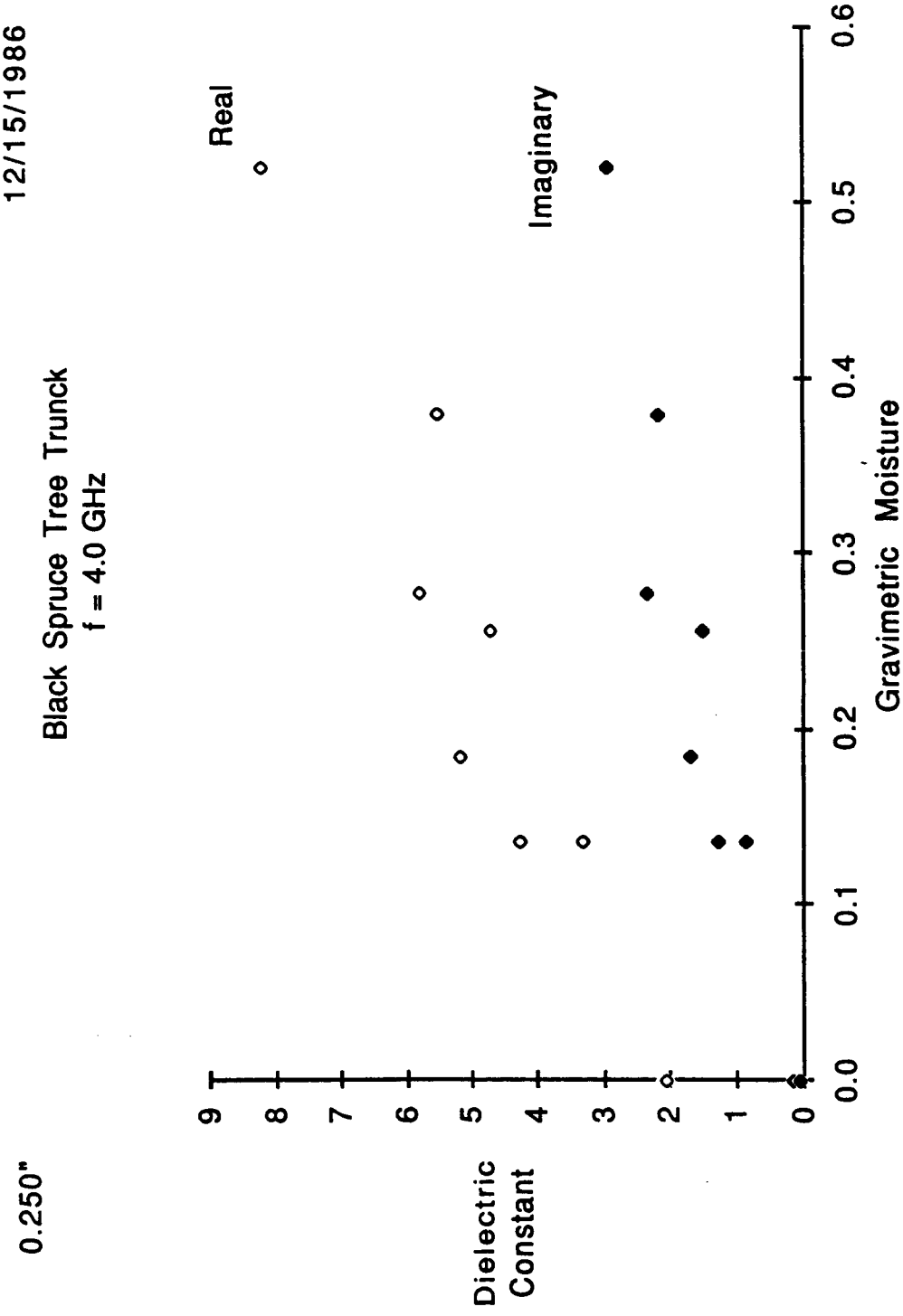
12/15/1986
Black Spruce Tree Trunck
f = 4.0 GHz
0.250"
Real
Imaginary
Dielectric Constant
Gravimetric Moisture
0
1
2
3
4
5
6
7
8
9
0.0
0.1
0.2
0.3
0.4
0.5
0.6

Figure A.34

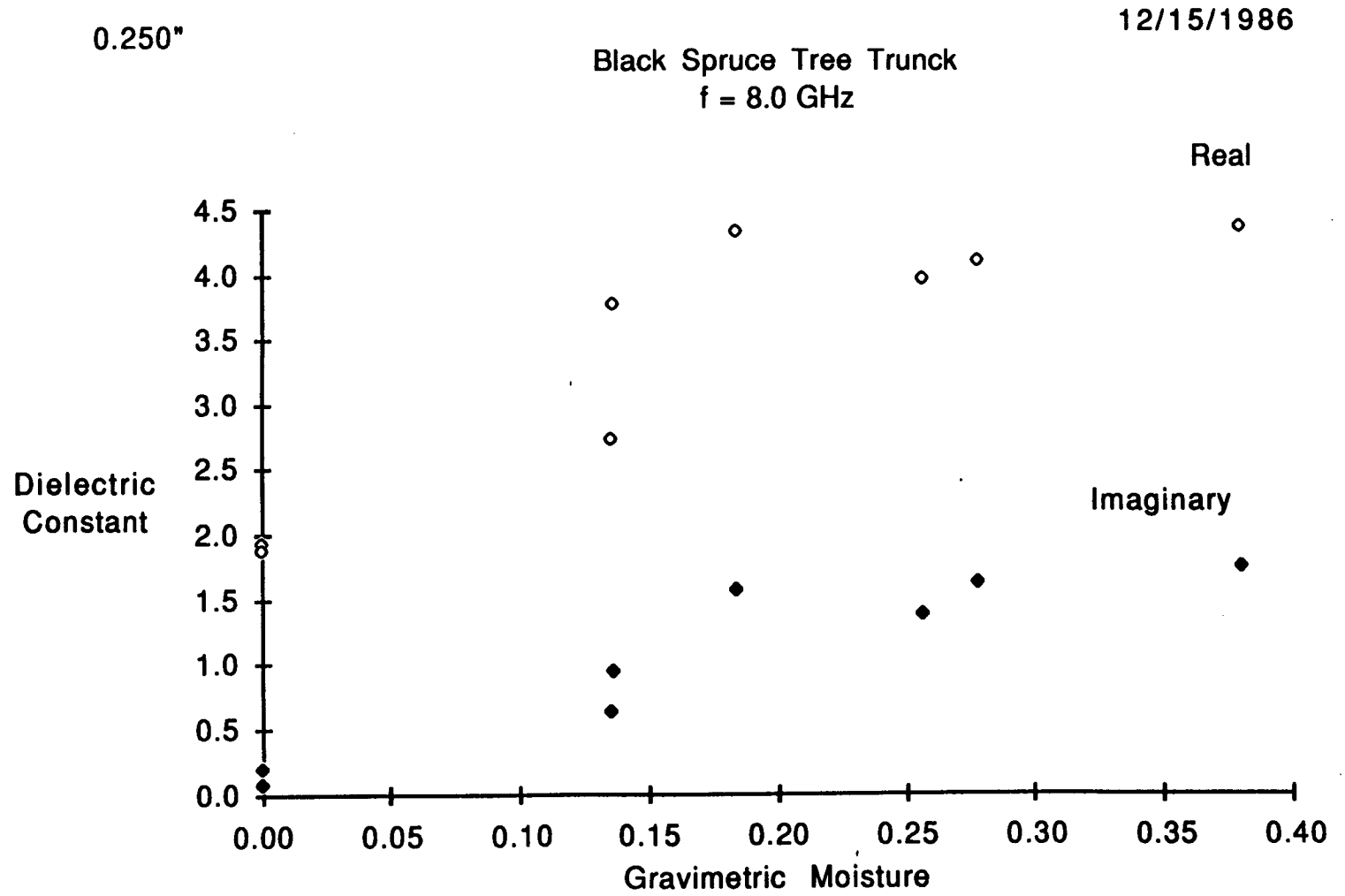
0.250"
12/15/1986
Black Spruce Tree Trunck
f = 8.0 GHz
Real
Imaginary
Dielectric Constant
ε
4.5
4.0
3.5
3.0
2.5
2.0
1.5
1.0
0.5
0.0
0.00
0.05
0.10
0.15
0.20
0.25
0.30
0.35
0.40
Gravimetric Moisture

Figure A.35

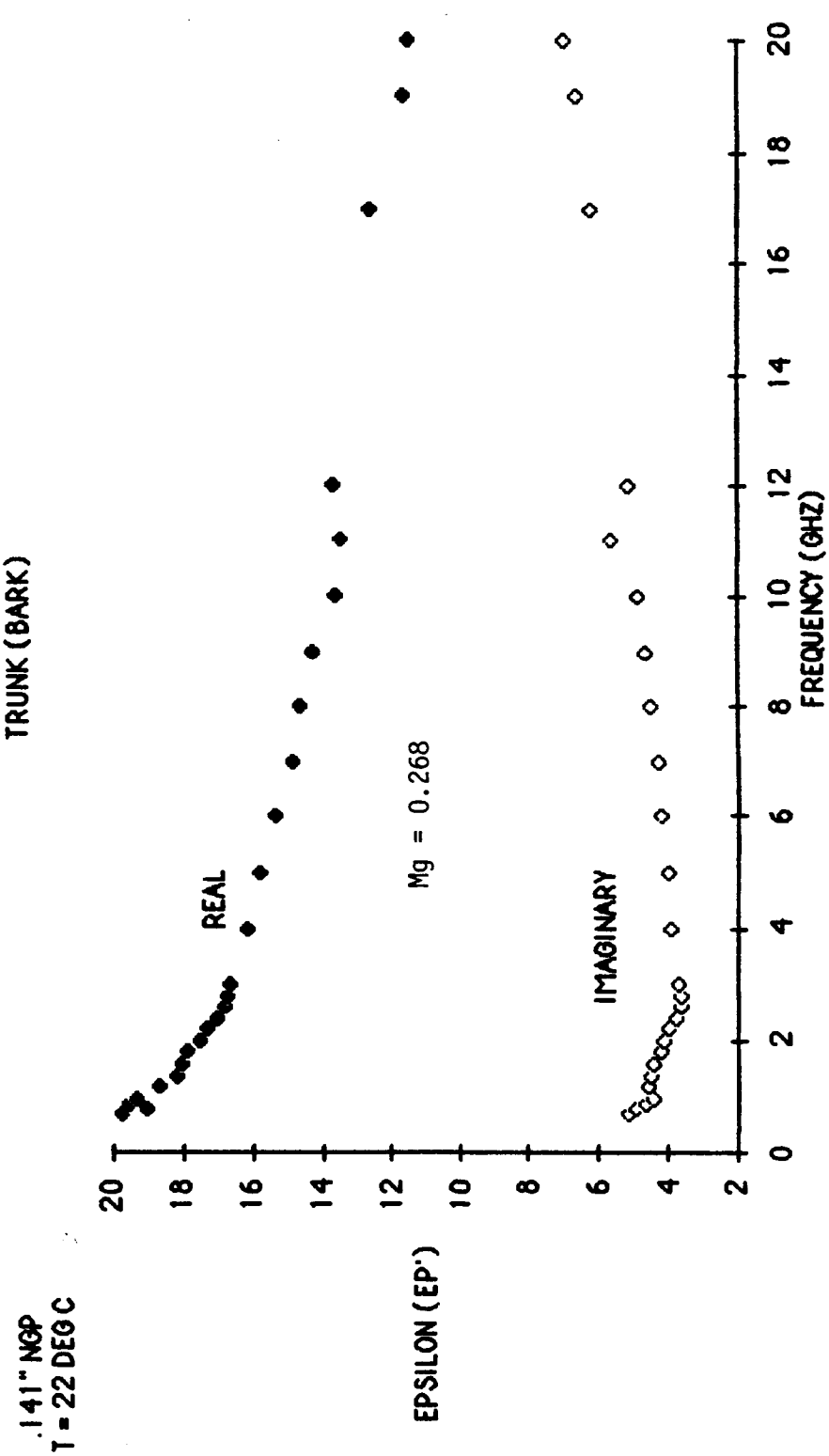
11/5/85
BALSAM FIR
TRUNK (BARK)
.141" NGP
T = 22 DEG C
EPSILON (EP')
REAL
IMAGINARY
Mg = 0.268
FREQUENCY (GHZ)
20
18
16
14
12
10
8
6
4
2
0
2
4
6
8
10
12
14
16
18
20

Figure A.36

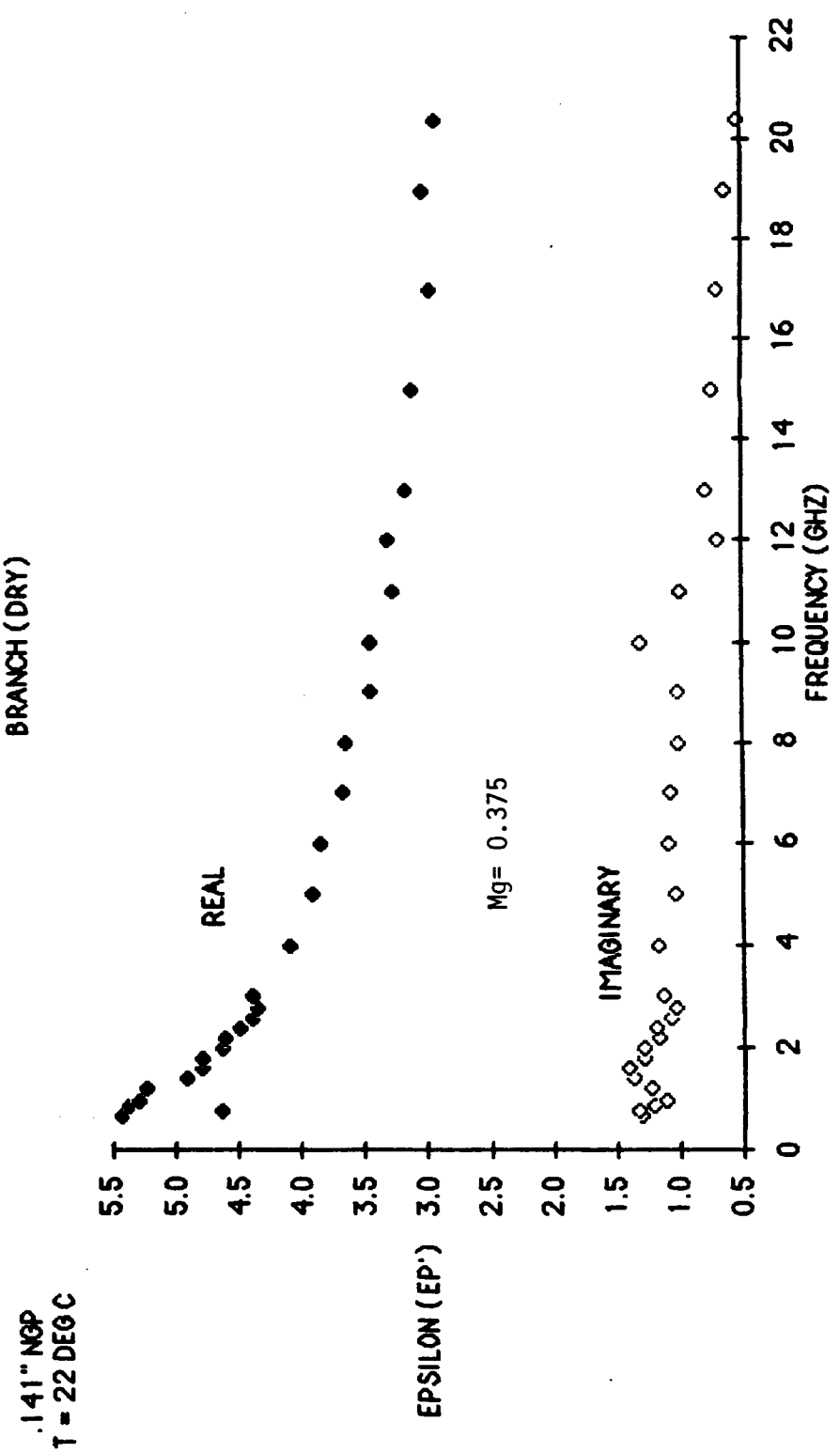
11/5/85
BALSAM FIR
BRANCH (DRY)
.141" NGP
T = 22 DEG C
REAL
IMAGINARY
Mg= 0.375
EPSILON (EP')
FREQUENCY (GHZ)
5.5
5.0
4.5
4.0
3.5
3.0
2.5
2.0
1.5
1.0
0.5
0
2
4
6
8
10
12
14
16
18
20
22

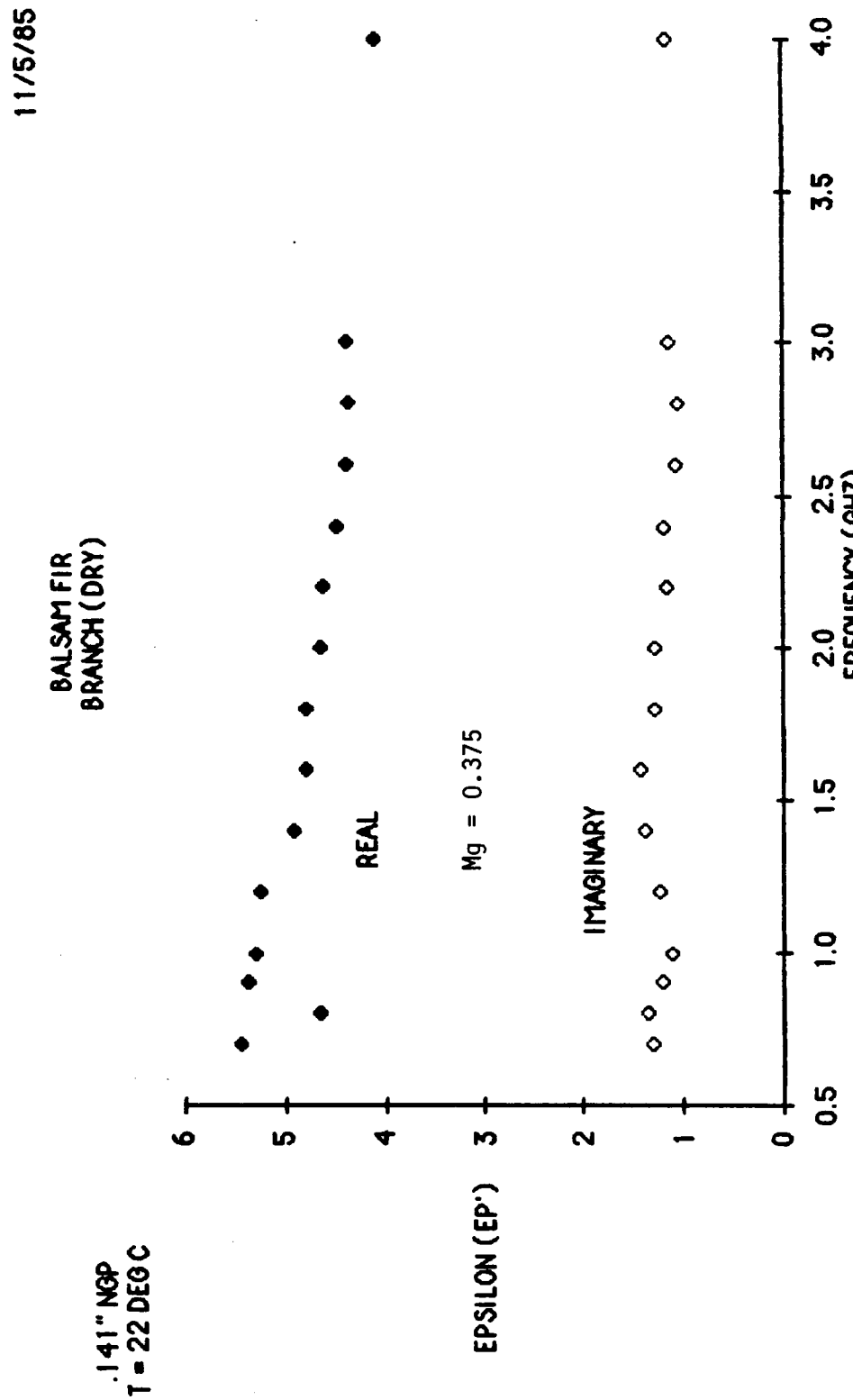
11/5/85
BALSAM FIR
BRANCH (DRY)
.141" NGP
T = 22 DEG C
EPSILON (EP')
REAL
IMAGINARY
Mg = 0.375
FREQUENCY (GHZ)
0
1
2
3
4
5
6
0.5
1.0
1.5
2.0
2.5
3.0
3.5
4.0

Figure A.38

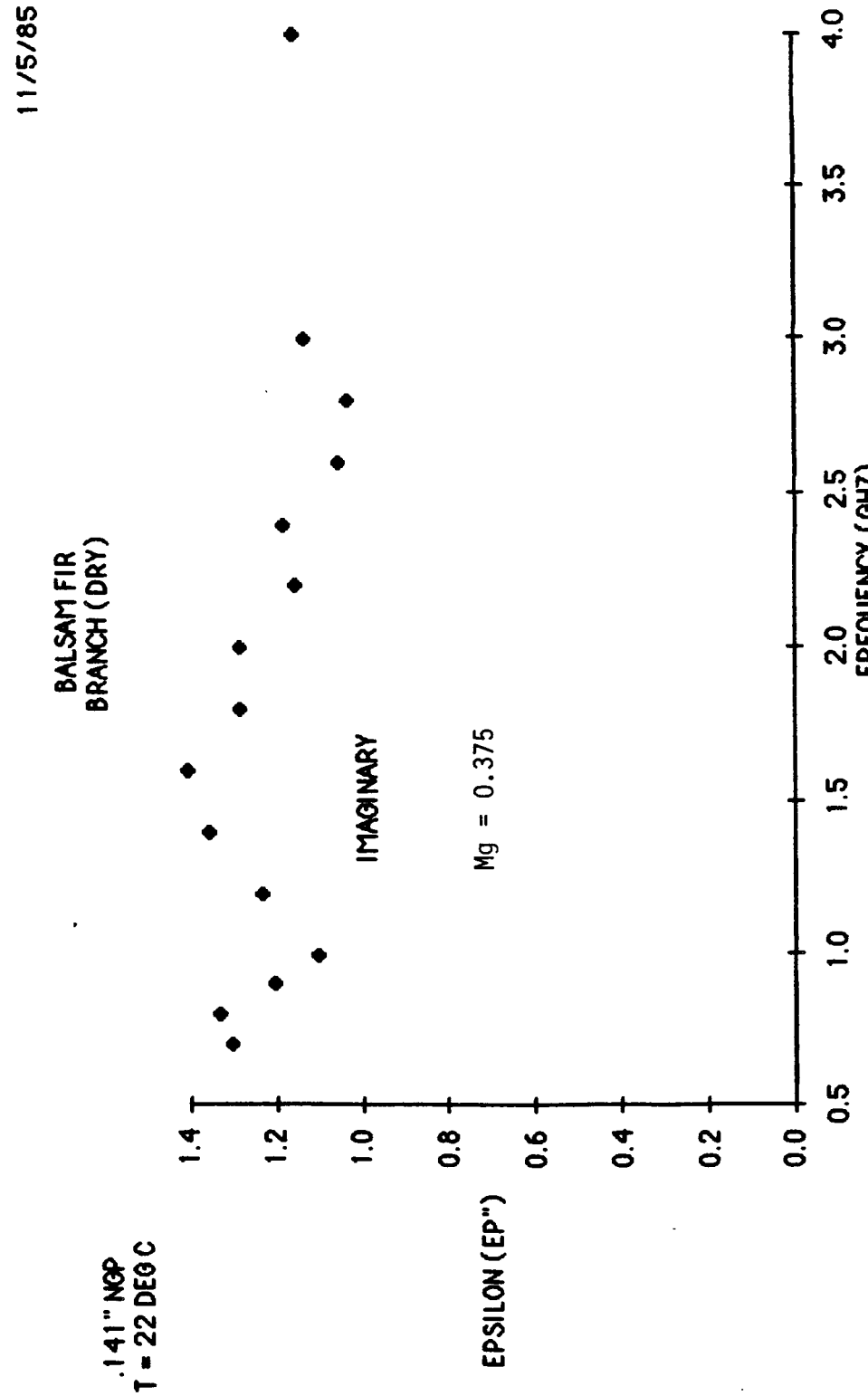
11/5/85
BALSAM FIR
BRANCH (DRY)
IMAGINARY
Mg = 0.375
.141" NGP
T = 22 DEG C
EPSILON (EP")
FREQUENCY (GHZ)
1.4
1.2
1.0
0.8
0.6
0.4
0.2
0.0
0.5
1.0
1.5
2.0
2.5
3.0
3.5
4.0

Figure A.39

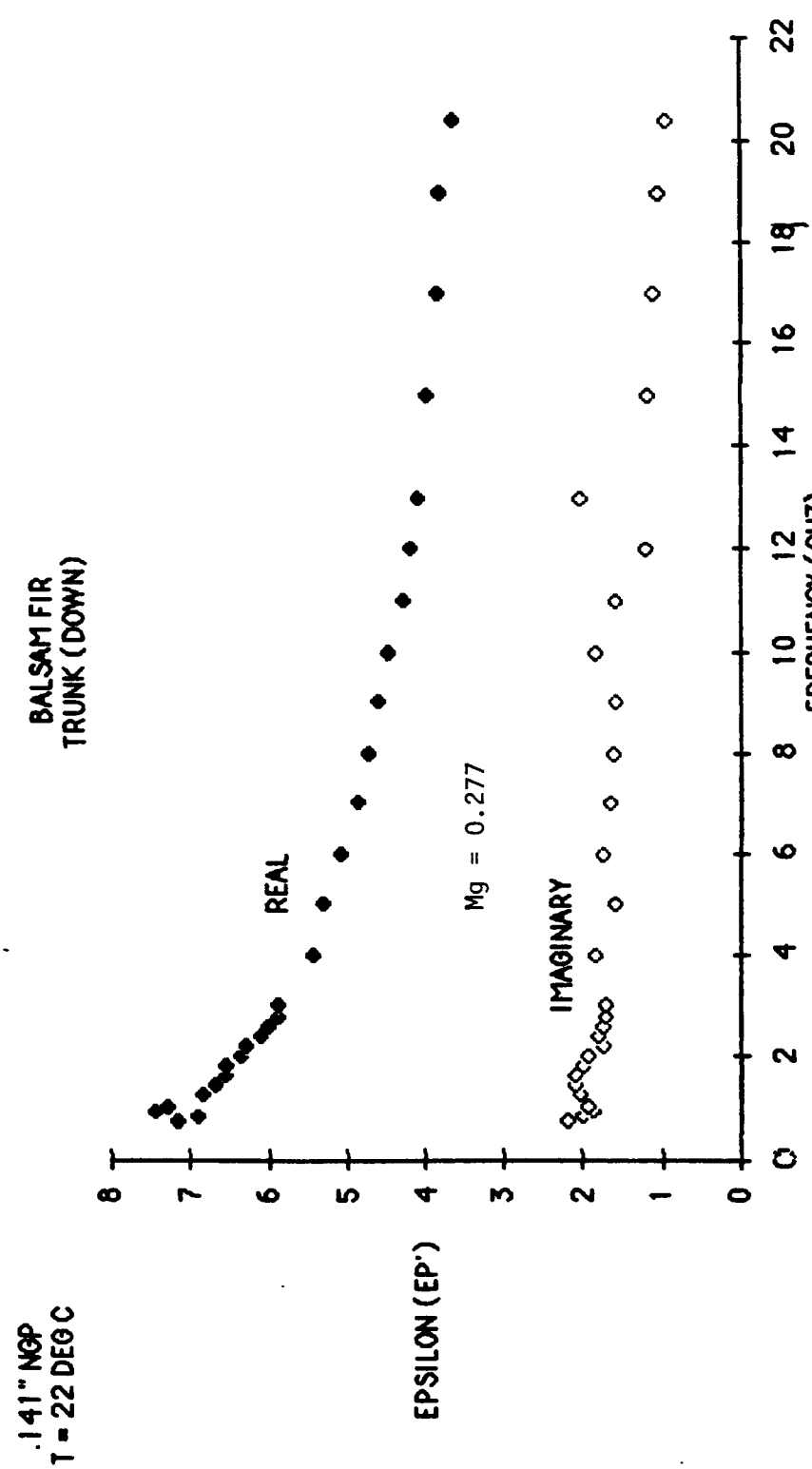
11/5/85
BALSAM FIR
TRUNK (DOWN)
.141" NOP
T = 22 DEG C
REAL
IMAGINARY
Mg = 0.277
EPSILON (EP')
FREQUENCY (GHZ)
0
1
2
3
4
5
6
7
8
0
2
4
6
8
10
12
14
16
18
20
22

Figure A.40

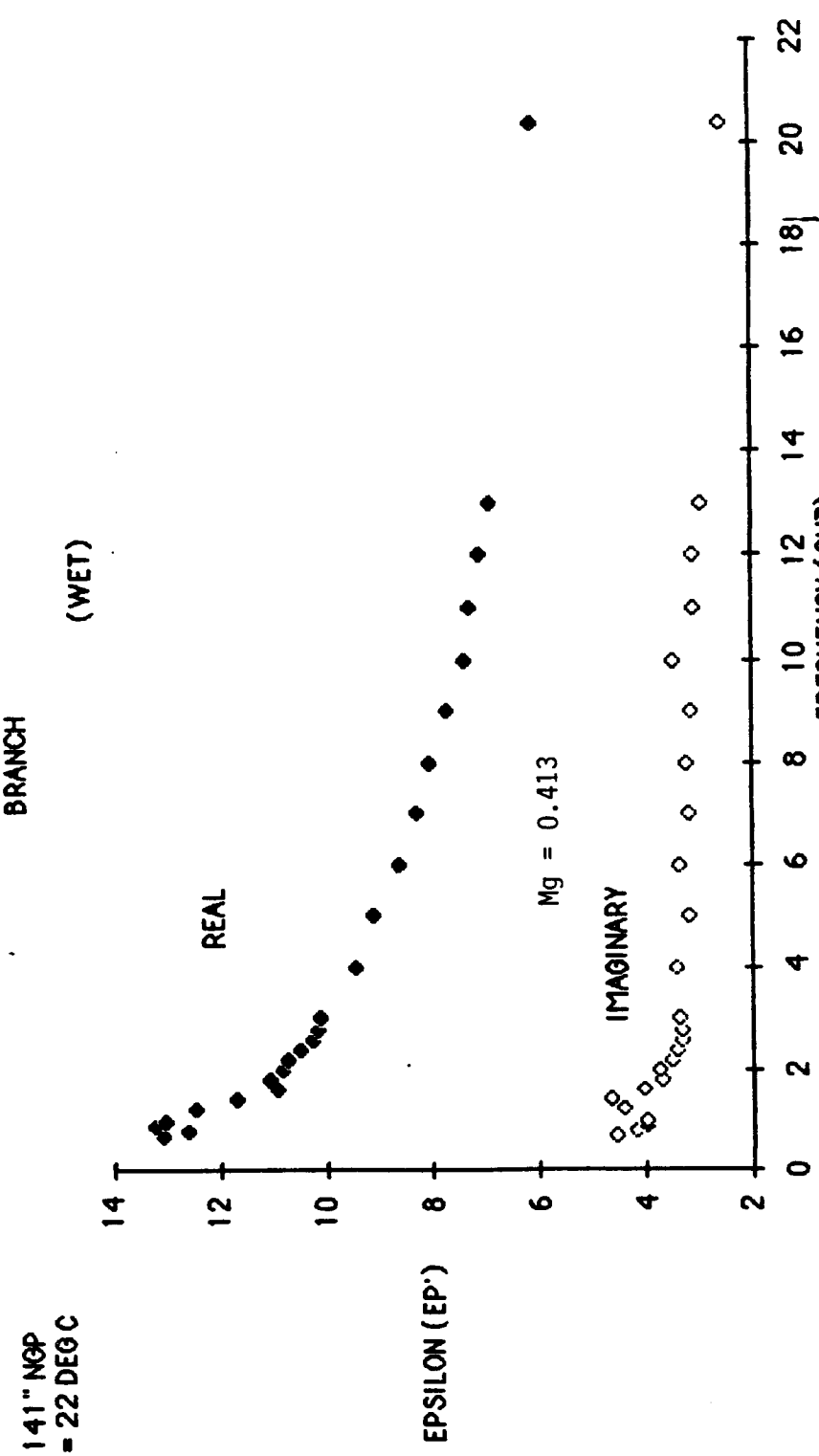
11/5/85
BALSAM FIR
BRANCH
(WET)
.141" NGP
T = 22 DEG C
REAL
IMAGINARY
Mg = 0.413
EPSILON (EP')
FREQUENCY (GHZ)
14
12
10
8
6
4
2
0
2
4
6
8
10
12
14
16
18
20
22

Figure A.41

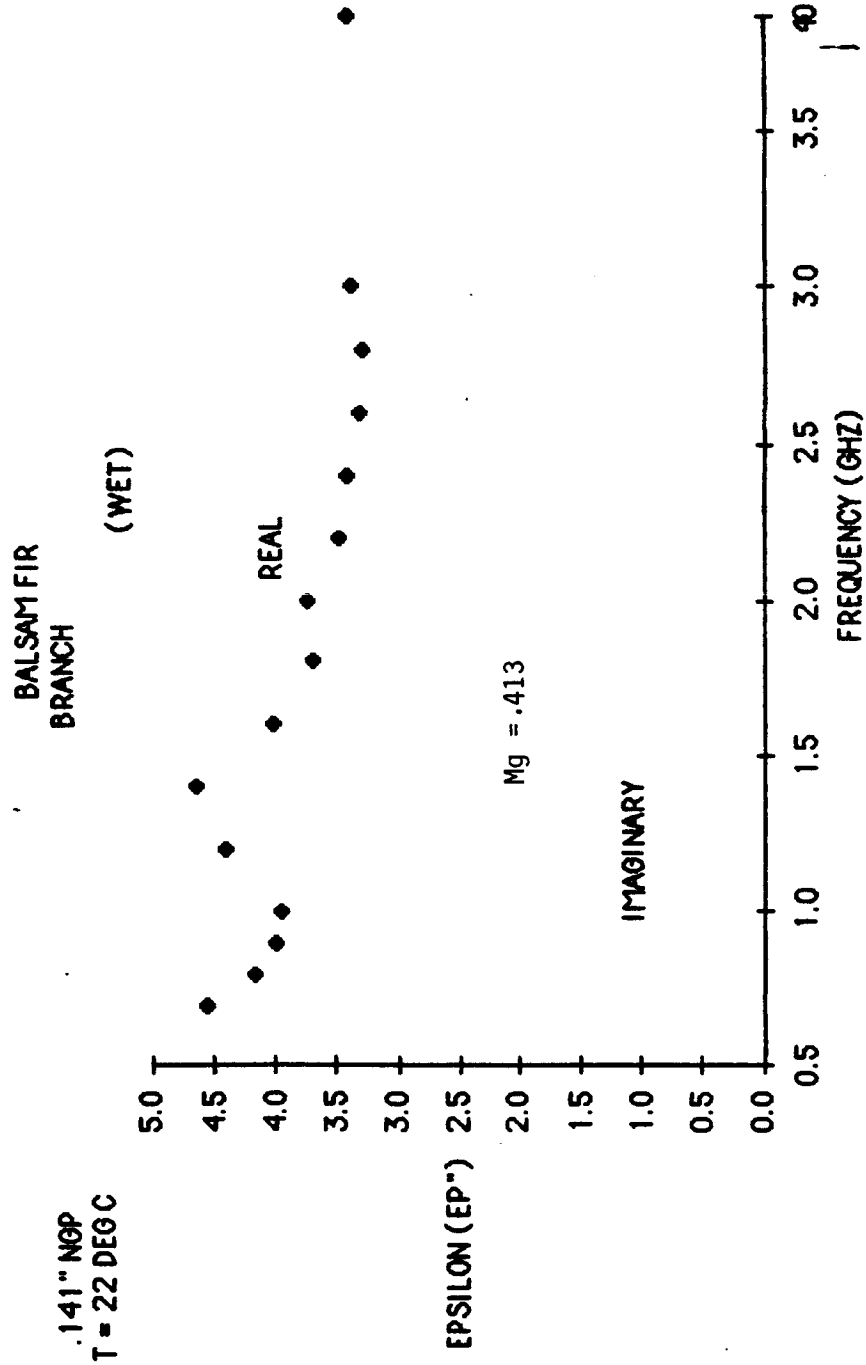
BALSAM FIR
BRANCH
(WET)
REAL
IMAGINARY
Mg = .413
.141" NGP
T = 22 DEG C
EPSILON (EP")
FREQUENCY (GHZ)
5.0
4.5
4.0
3.5
3.0
2.5
2.0
1.5
1.0
0.5
0.0
0.5
1.0
1.5
2.0
2.5
3.0
3.5
4.0

Figure A.42

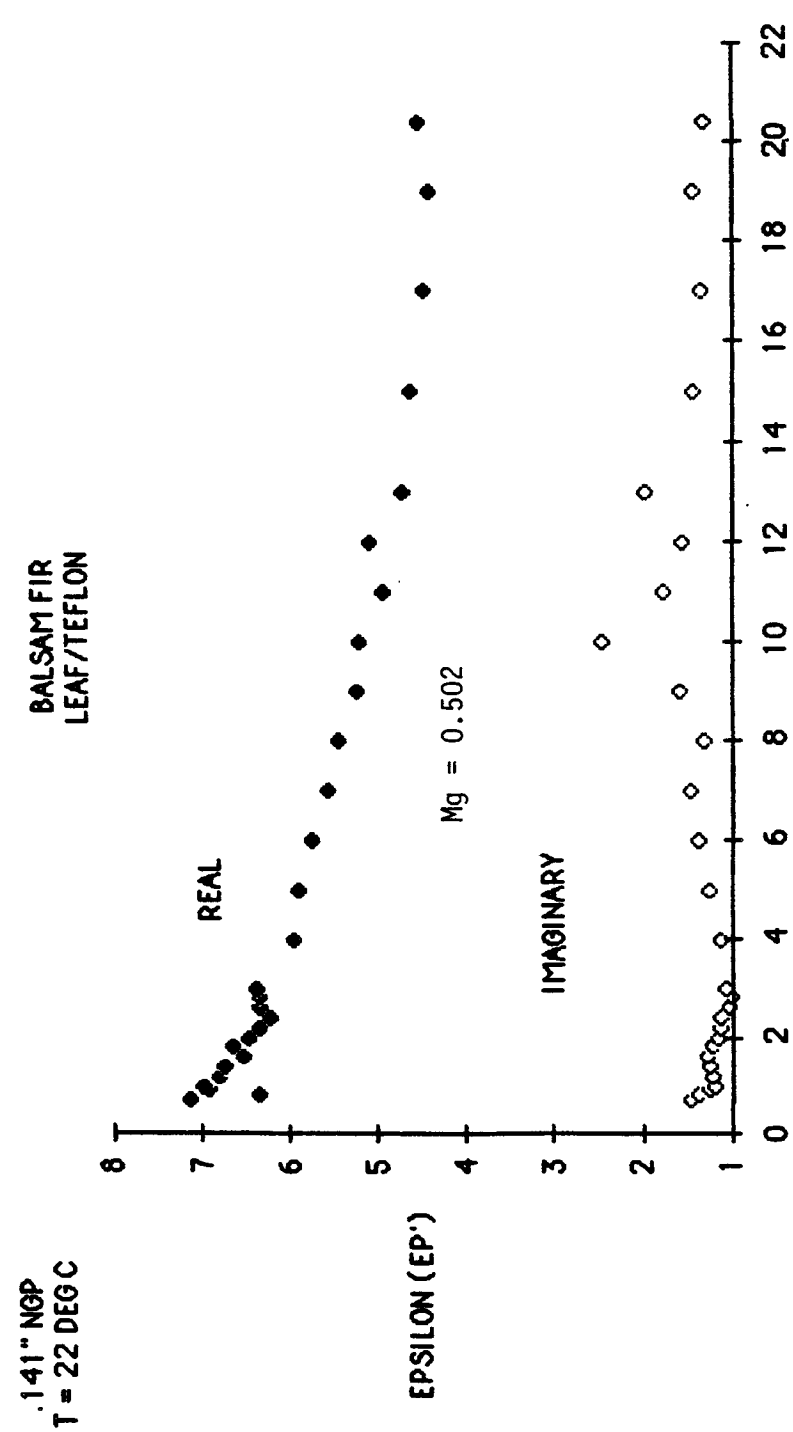
11/5/85
BALSAM FIR
LEAF/TEFLON
.141" NGP
T = 22 DEG C
REAL
IMAGINARY
Mg = 0.502
EPSILON (EP')
FREQUENCY (GHZ)
8
7
6
5
4
3
2
1
0
2
4
6
8
10
12
14
16
18
20
22

Figure A.43

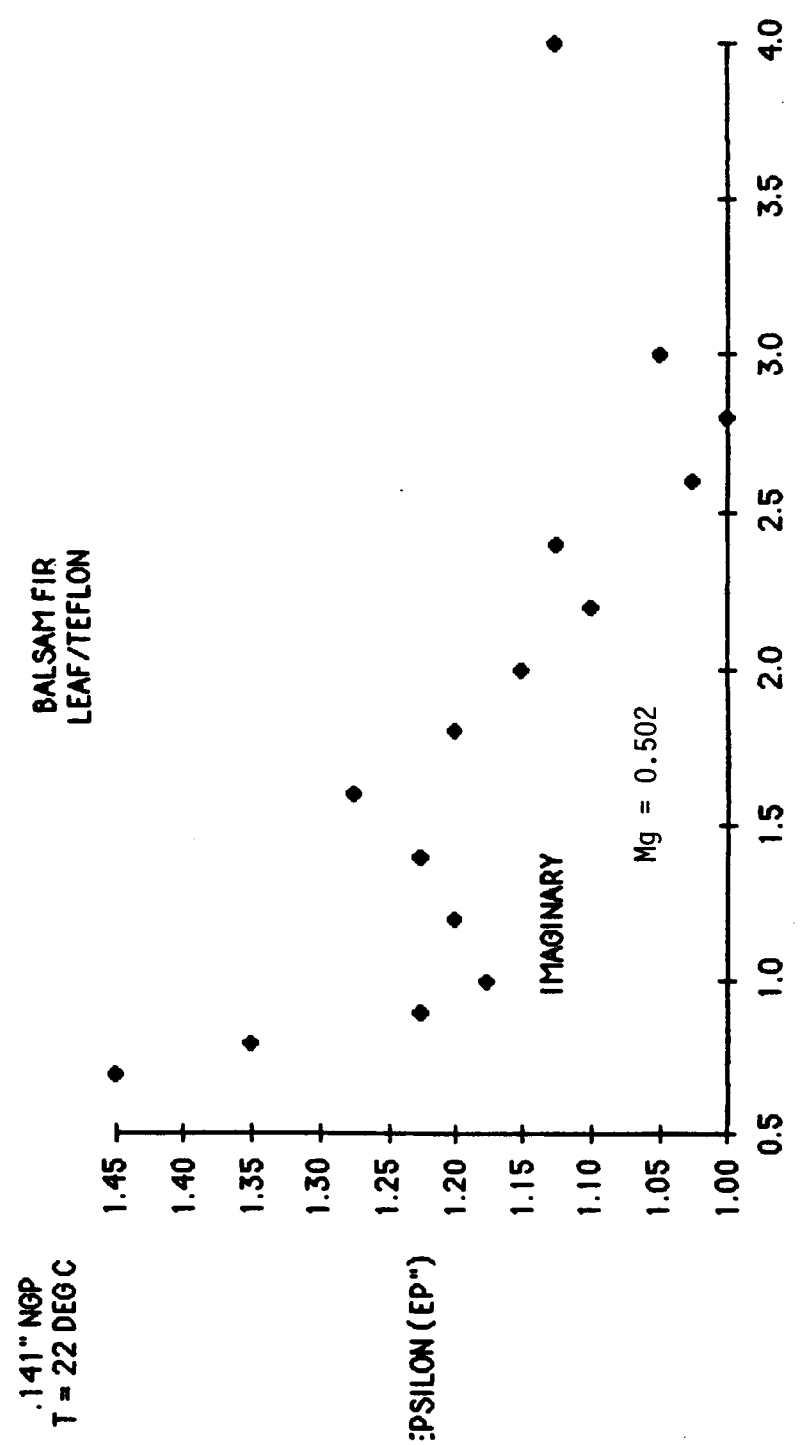
11/5/85
BALSAM FIR
LEAF/TEFLON
.141" NGP
T = 22 DEG C
:PSILON (EP")
IMAGINARY
Mg = 0.502
FREQUENCY (GHZ)
1.45
1.40
1.35
1.30
1.25
1.20
1.15
1.10
1.05
1.00
0.5
1.0
1.5
2.0
2.5
3.0
3.5
4.0

Figure A.44

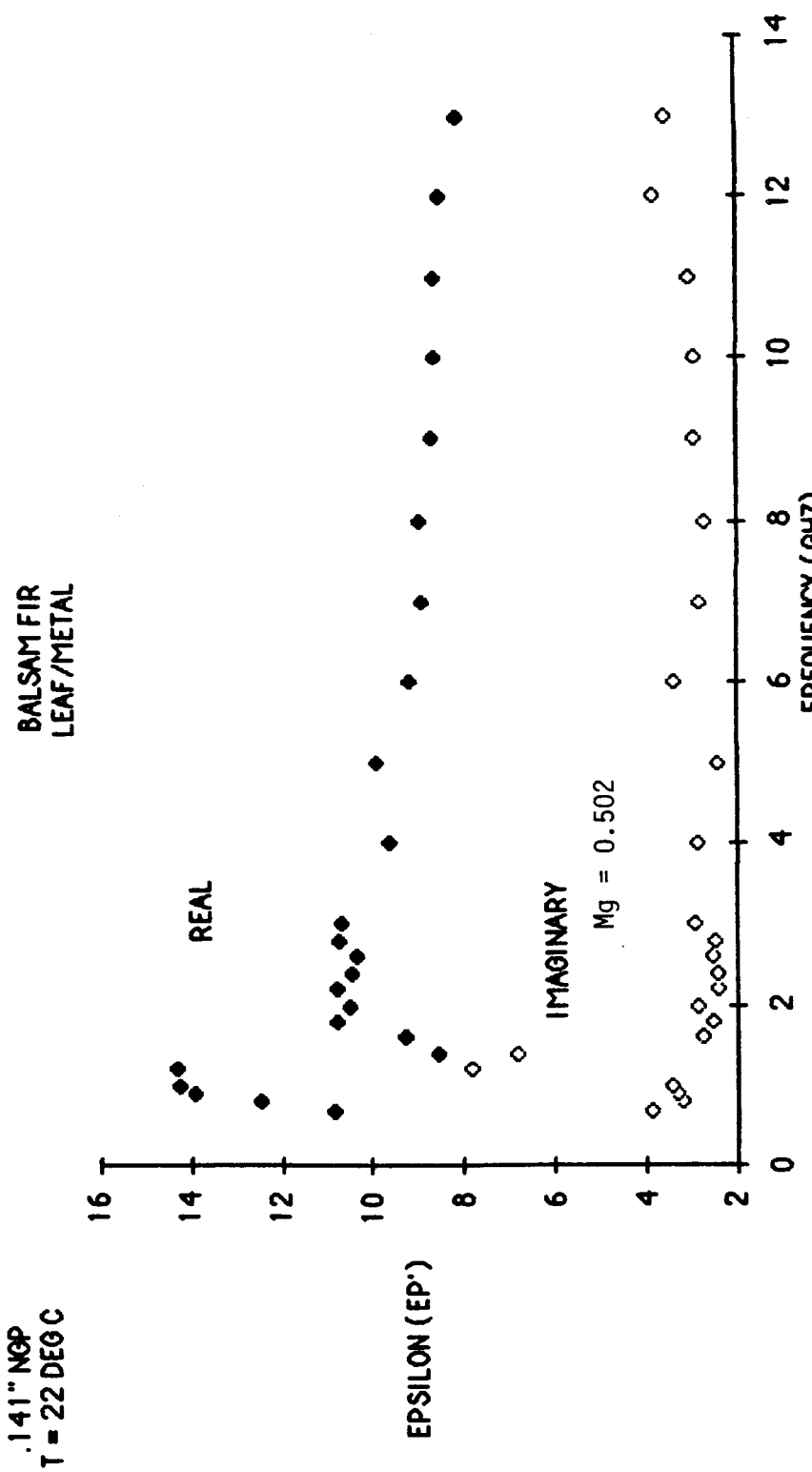
11/5/85
BALSAM FIR
LEAF/METAL
.141" NOP
T = 22 DEG C
REAL
IMAGINARY
Mg = 0.502
EPSILON (EP')
FREQUENCY (GHZ)
16
14
12
10
8
6
4
2
0
2
4
6
8
10
12
14

Figure A.45

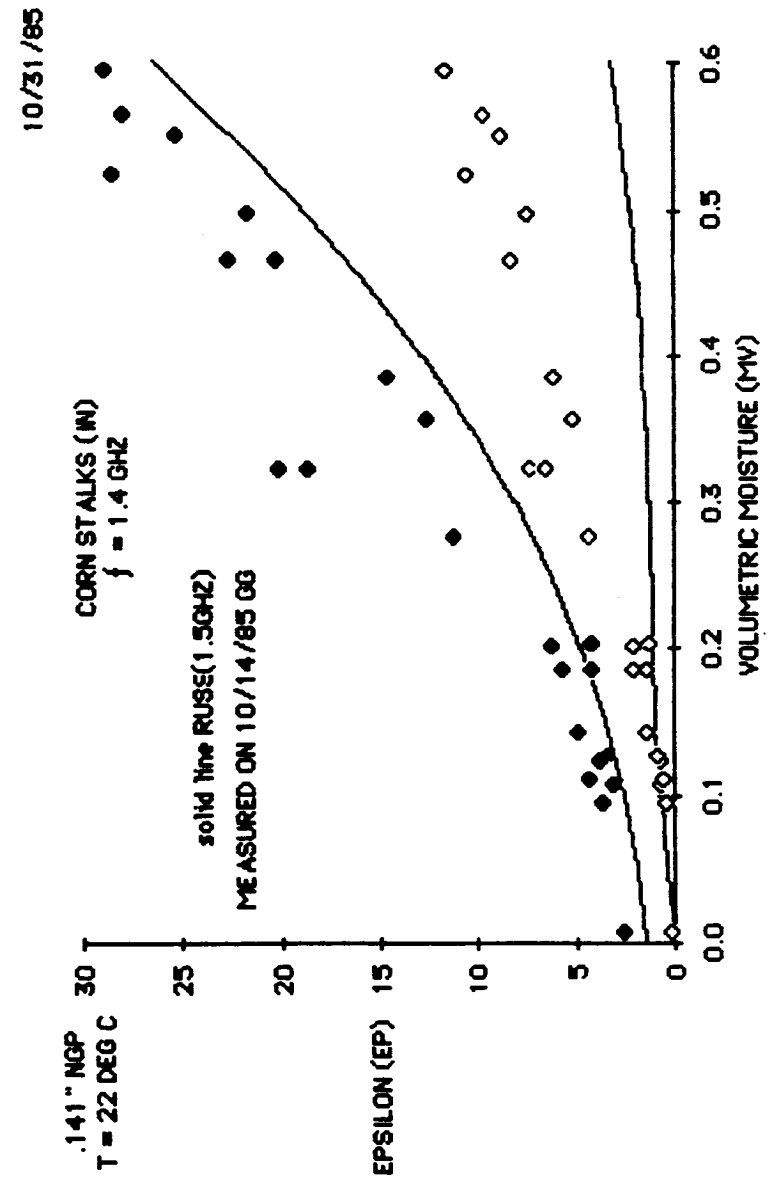
10/31/85
CORN STALKS (W)
f = 1.4 GHZ
solid line RUSE(1.5GHZ)
MEASURED ON 10/14/85 GG
.141" NGP
T = 22 DEG C
EPSILON (EP)
VOLUMETRIC MOISTURE (MV)
30
25
20
15
10
5
0
0.0
0.1
0.2
0.3
0.4
0.5
0.6

Figure A.46

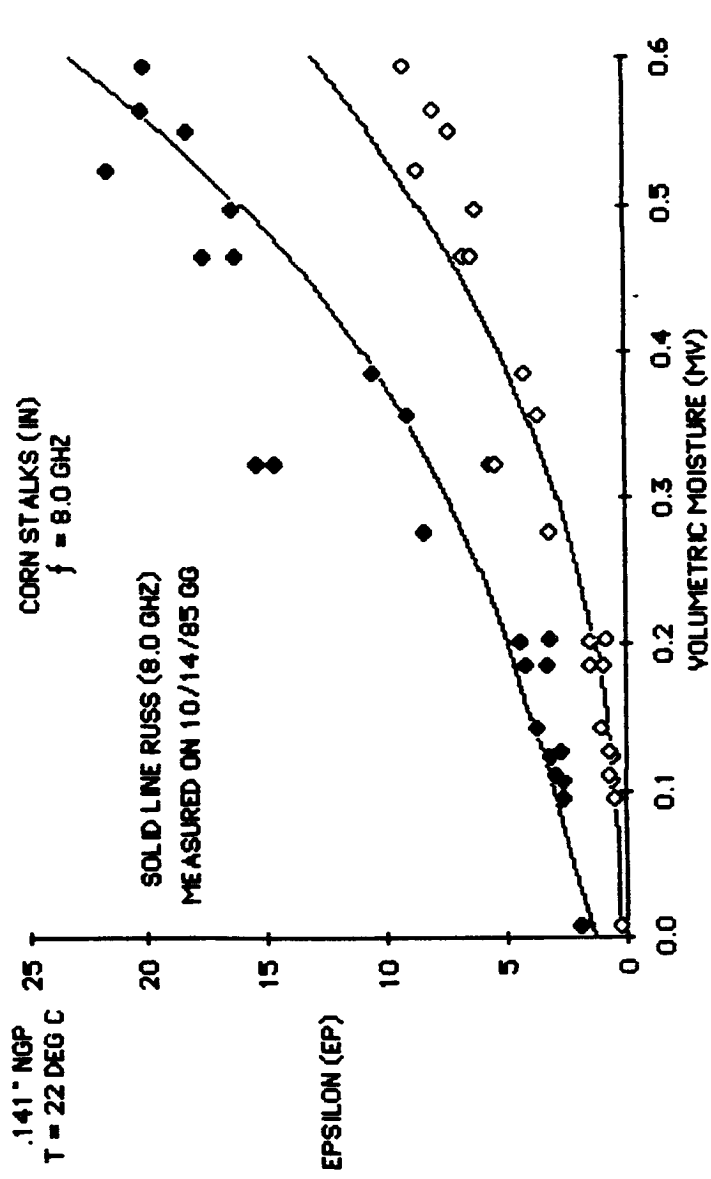
10/31/85
CORN STALKS (IN)
f = 8.0 GHZ
SOLID LINE RUSS (8.0 GHZ)
MEASURED ON 10/14/85 GG
.141" NGP
T = 22 DEG C
EPSILON (EP)
VOLUMETRIC MOISTURE (MV)
25
20
15
10
5
0
0.0
0.1
0.2
0.3
0.4
0.5
0.6

Figure A.47

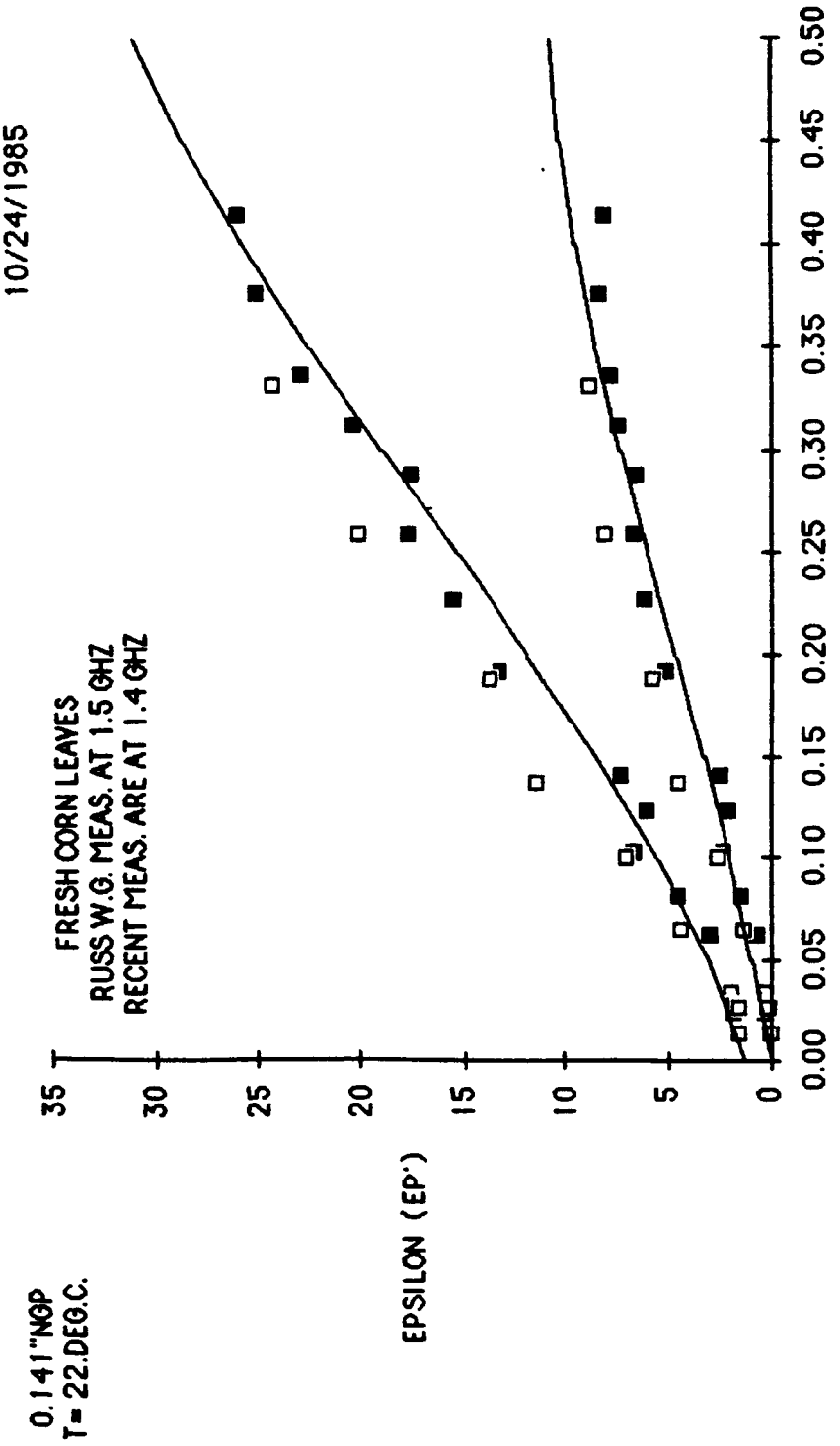
10/24/1985
FRESH CORN LEAVES
RUSS W.G. MEAS. AT 1.5 GHZ
RECENT MEAS. ARE AT 1.4 GHZ
0.141"NOP
T= 22.DEG.C.
EPSILON (EP')
VOLUMETRIC MOISTURE (MV)
35
30
25
20
15
10
5
0
0.00
0.05
0.10
0.15
0.20
0.25
0.30
0.35
0.40
0.45
0.50

Figure A.48

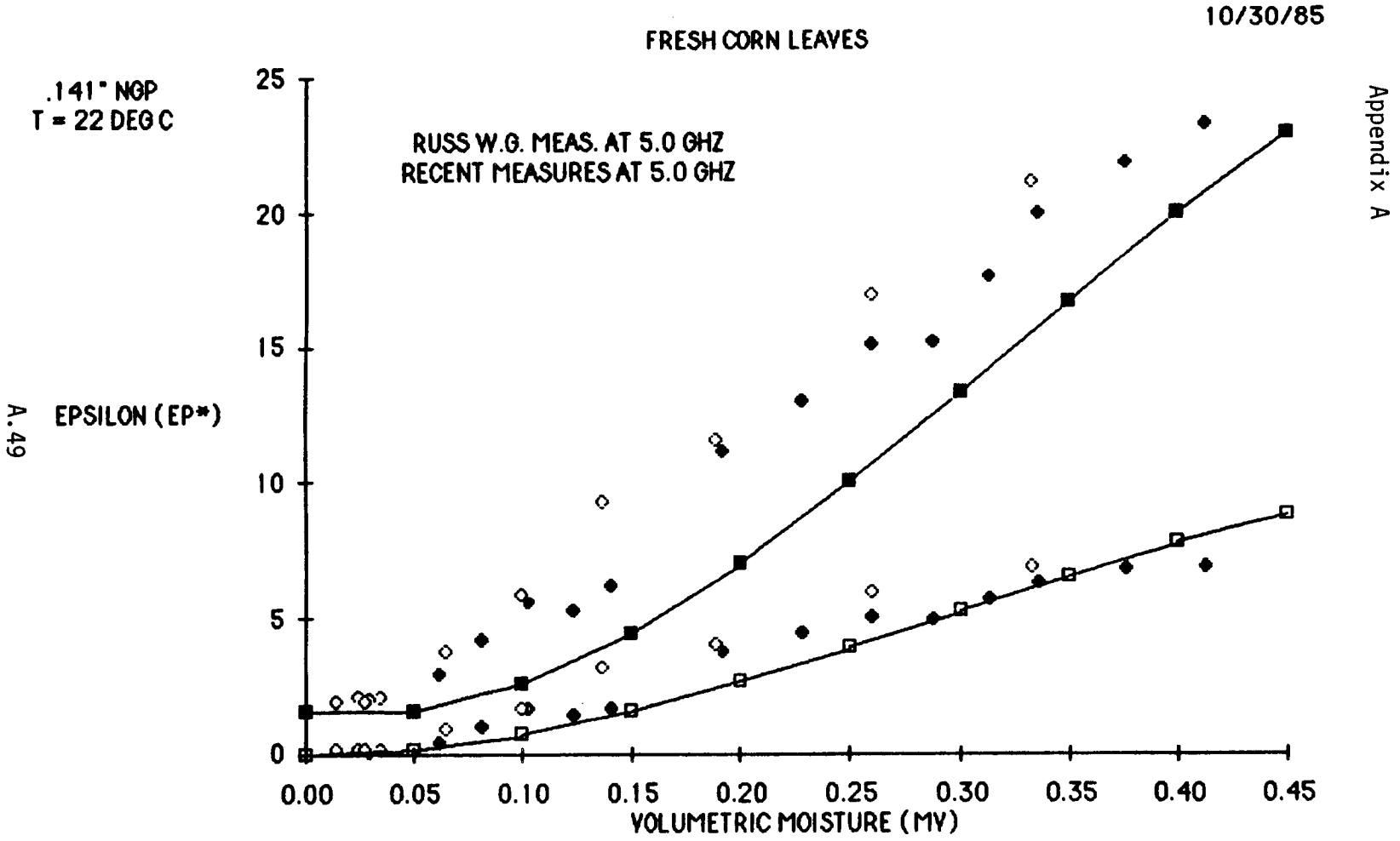
10/30/85
FRESH CORN LEAVES
.141" NGP
T = 22 DEG C
RUSS W.G. MEAS. AT 5.0 GHZ
RECENT MEASURES AT 5.0 GHZ
EPSILON (EP*)
25
20
15
10
5
0
0.00
0.05
0.10
0.15
0.20
0.25
0.30
0.35
0.40
0.45
VOLUMETRIC MOISTURE (MV)

Figure A.49

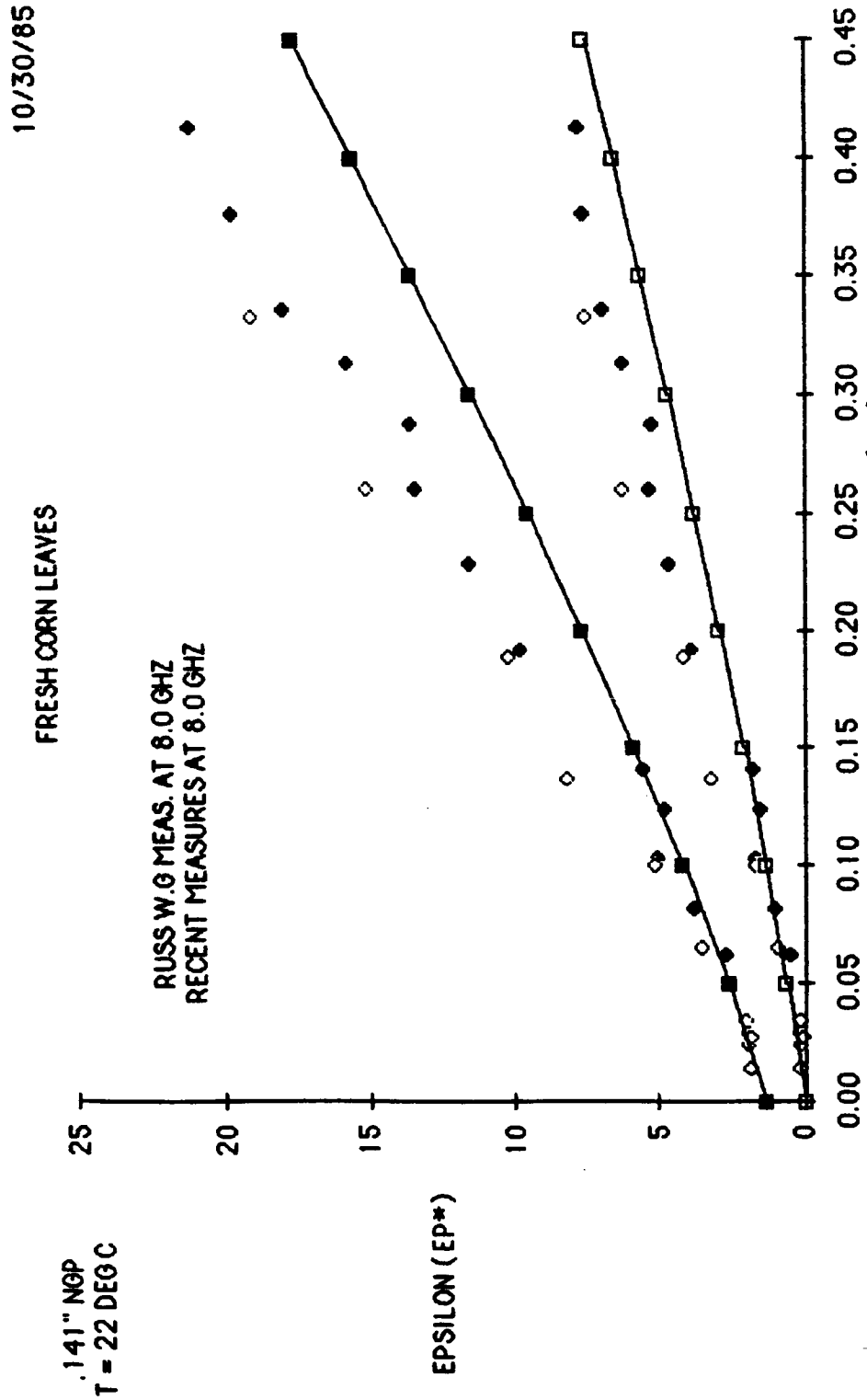
10/30/85
FRESH CORN LEAVES
RUSS W.G MEAS. AT 8.0 GHZ
RECENT MEASURES AT 8.0 GHZ
.141" NGP
T = 22 DEG C
EPSILON (EP*)
VOLUMETRIC MOISTURE (MV)
0
5
10
15
20
25
0.00
0.05
0.10
0.15
0.20
0.25
0.30
0.35
0.40
0.45

Figure A.50

APPENDIX B

Dielectric Data as a Function of Temperature

This appendix contains the temperature data collected during the course of this work. The set consists of four parts:

1. Fatshedera temperature measurement (experiment # 1 in Section 5.6). (B.1 - B.17)
2. Banana-like tropical tree temperature measurement (experiment # 2 in Section 5.6) (B.18 - B.23)
3. Fatshedera temperature measurement (experiment # 3 in Section 5.6). (B.24 - B.34)
4. Fresh corn leaves temperature measurement (experiment # 4 in Section 5.6). (B.35 - B.42)

Appendix B

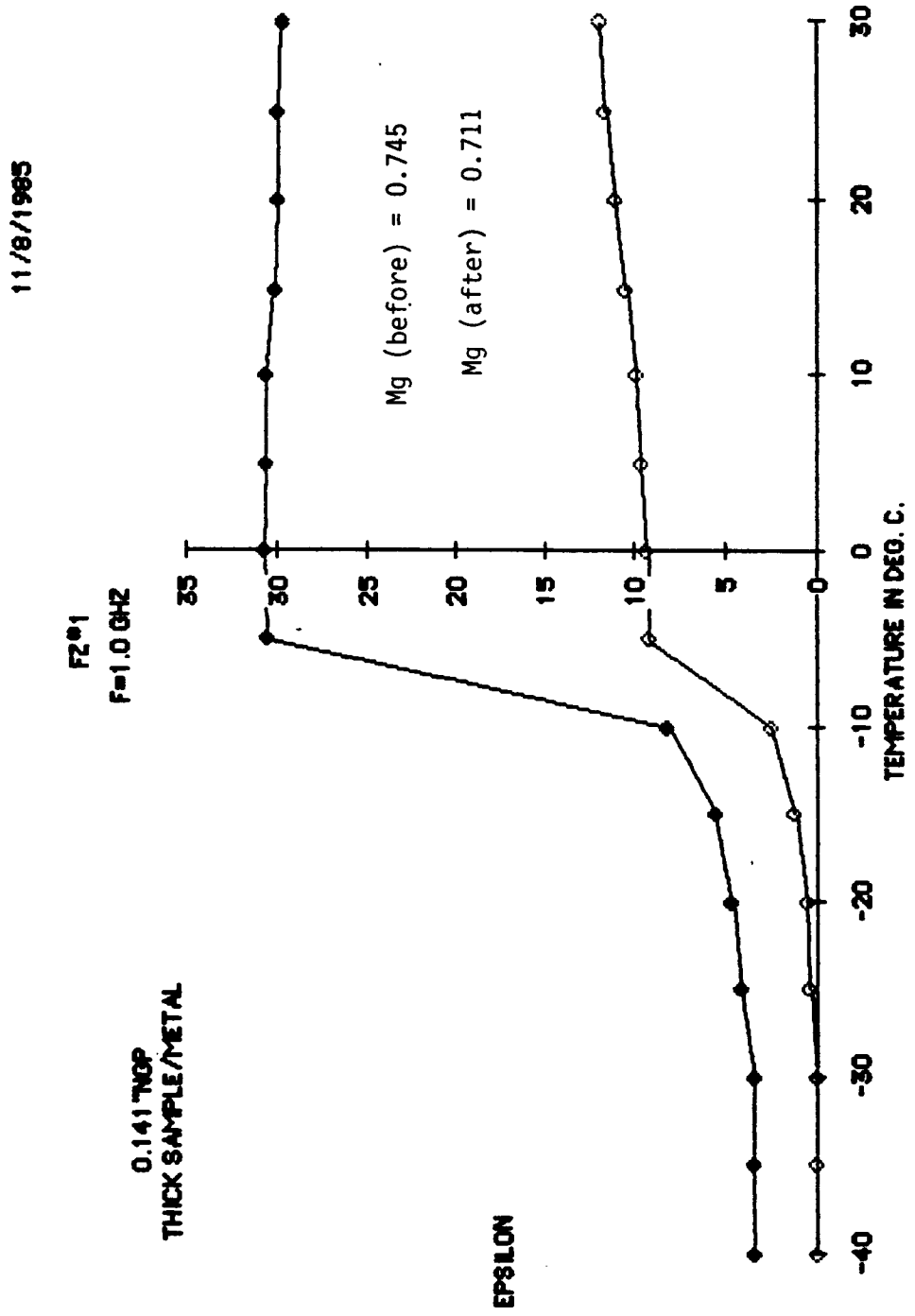

Figure B.1

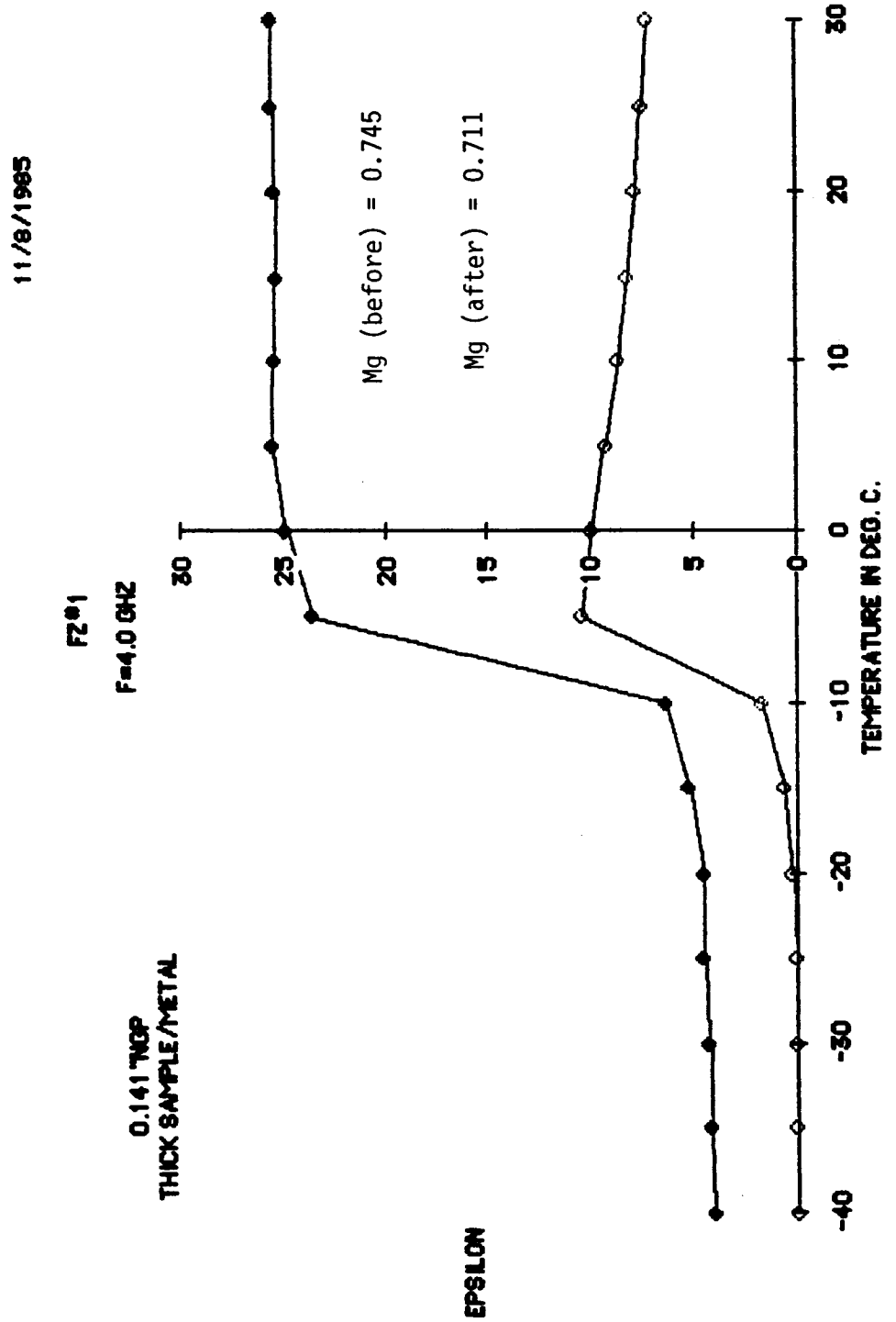
11/8/1985
FZ#1
F=4.0 GHZ
0.141"NOP
THICK SAMPLE/METAL
EPSILON
Mg (before) = 0.745
Mg (after) = 0.711
30
25
20
15
10
5
0
-10
-20
-30
-40
TEMPERATURE IN DEG. C.

Figure B.2

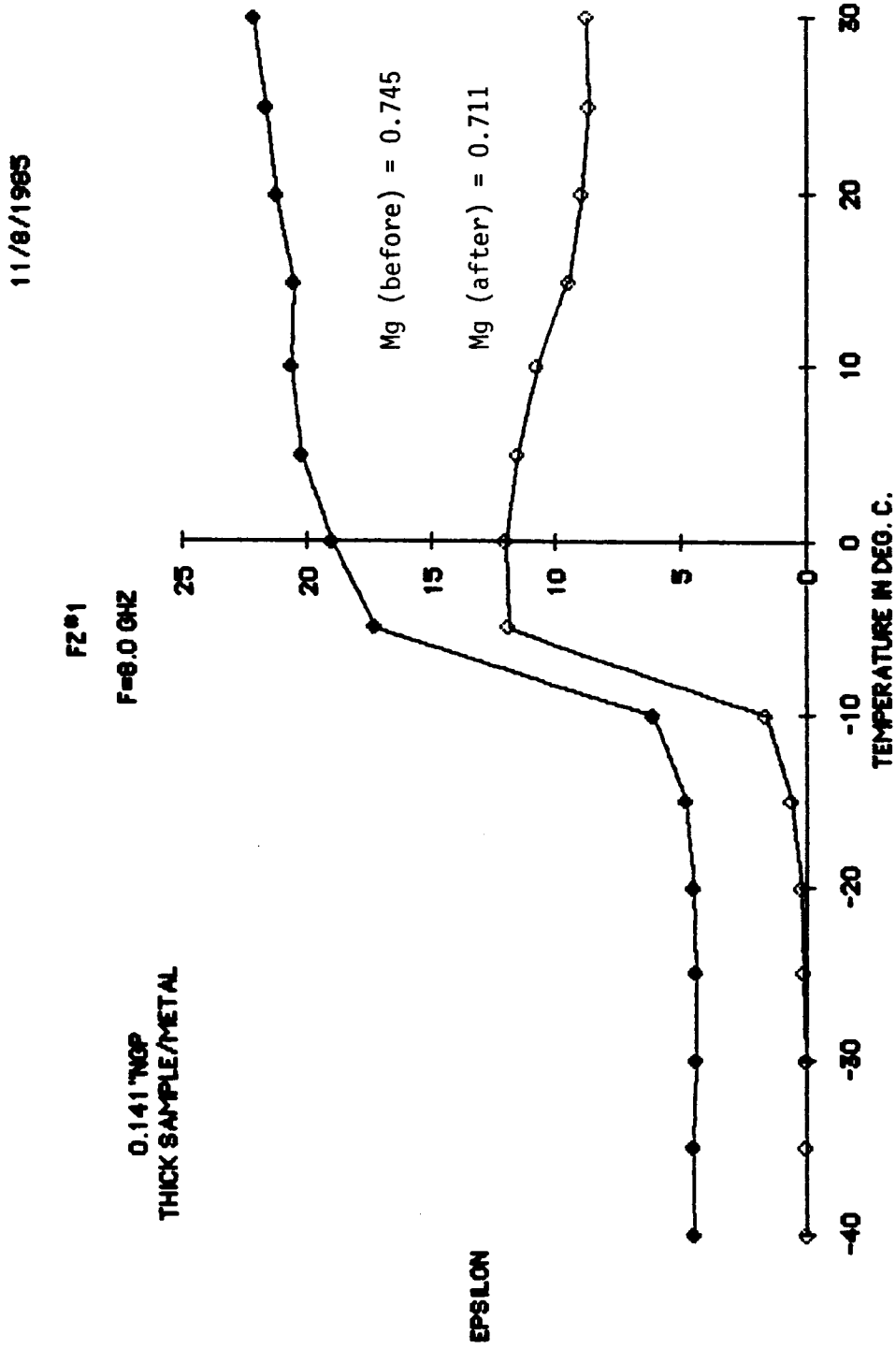
11/8/1985
F2*1
F=8.0 GHZ
0.141"NGP
THICK SAMPLE/METAL
Mg (before) = 0.745
Mg (after) = 0.711
EPSILON
TEMPERATURE IN DEG. C.
25
20
15
10
5
0
-40
-30
-20
-10
0
10
20
30

Figure B.3

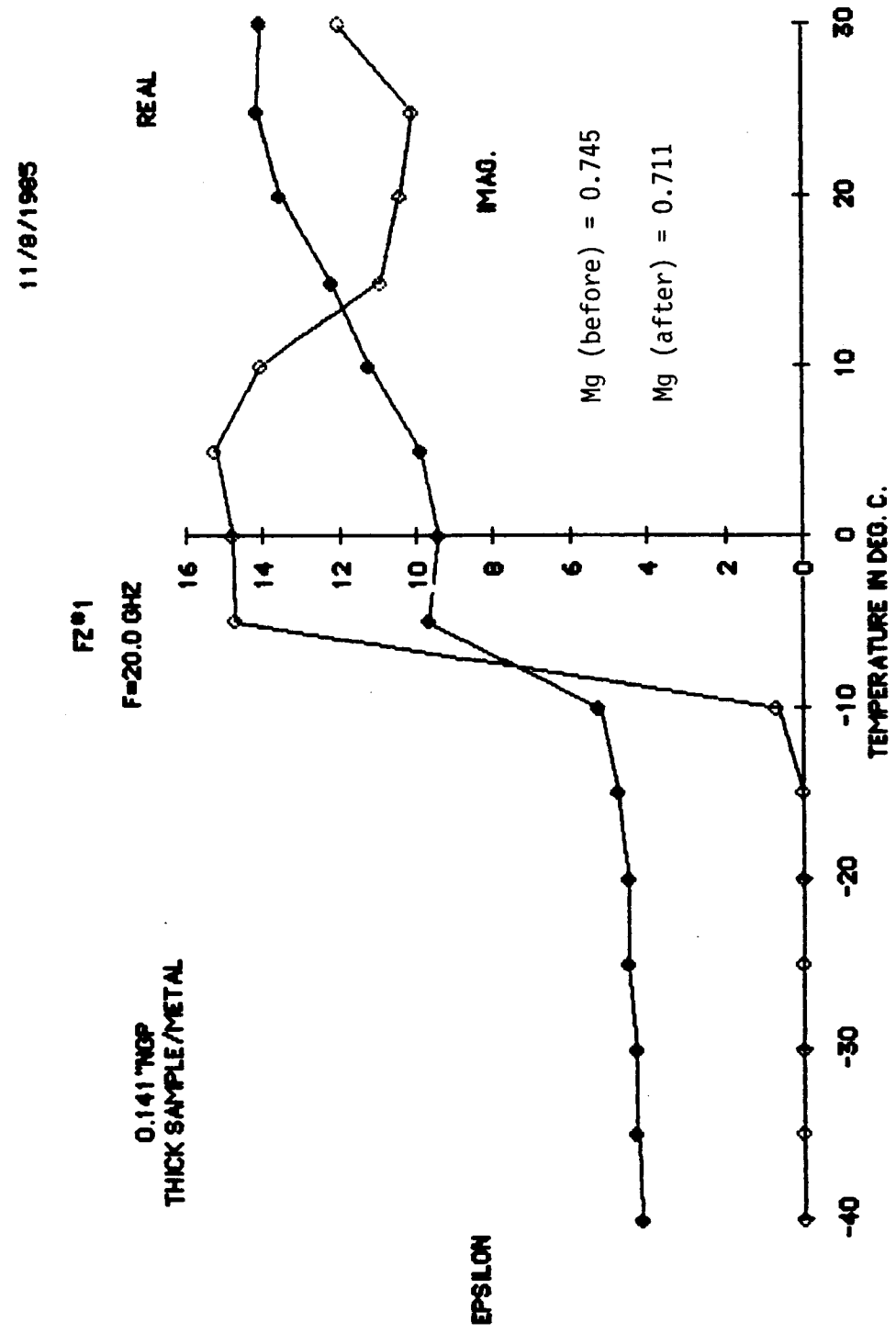
11/8/1985
REAL
IMAG.
FZ#1
F=20.0 GHZ
0.141"NOM
THICK SAMPLE/METAL
EPSILON
Mg (before) = 0.745
Mg (after) = 0.711
TEMPERATURE IN DEG. C.
16
14
12
10
8
6
4
2
0
30
20
10
0
-10
-20
-30
-40

Figure B.4

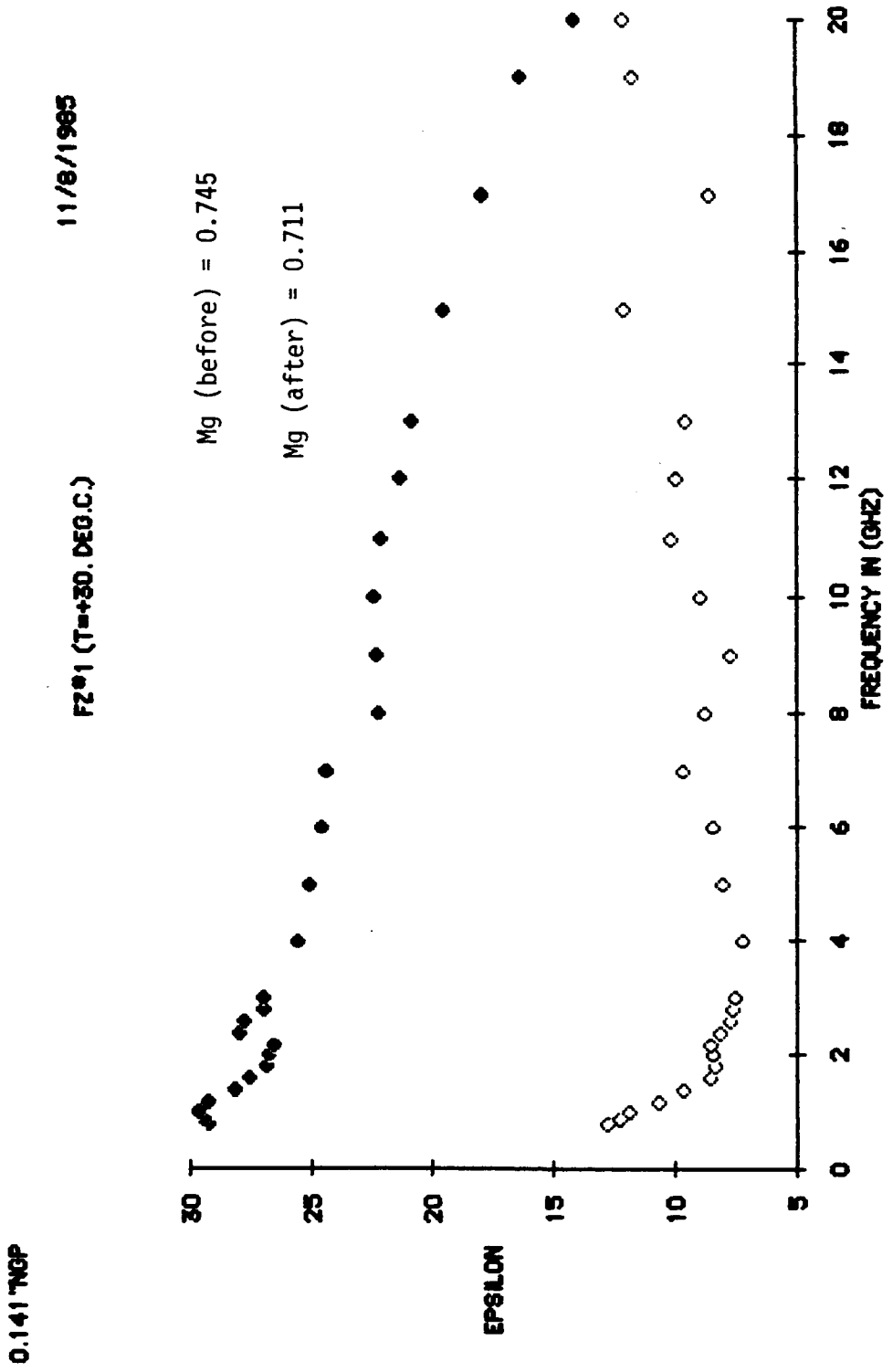
0.141"NGP
F2*1 (T=+30. DEG.C.)
11/8/1985
Mg (before) = 0.745
Mg (after) = 0.711
EPSILON
FREQUENCY IN (GHZ)
30
25
20
15
10
5
0
2
4
6
8
10
12
14
16
18
20

Figure B.5

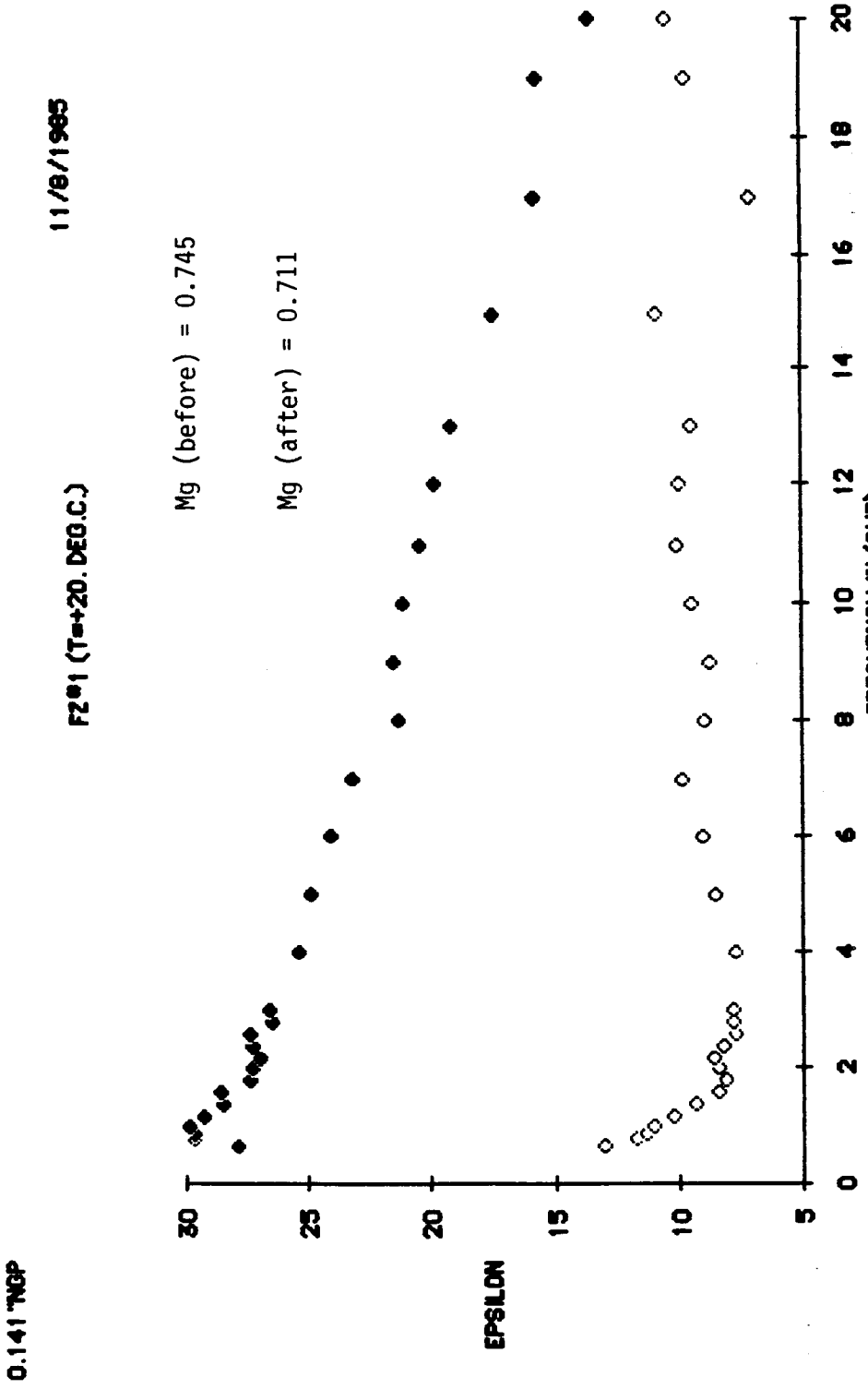
11/8/1985
F2#1 (T=+20. DEG.C.)
Mg (before) = 0.745
Mg (after) = 0.711
0.141"NGP
EPSILON
FREQUENCY IN (GHZ)
30
25
20
15
10
5
0
2
4
6
8
10
12
14
16
18
20

Figure B.6

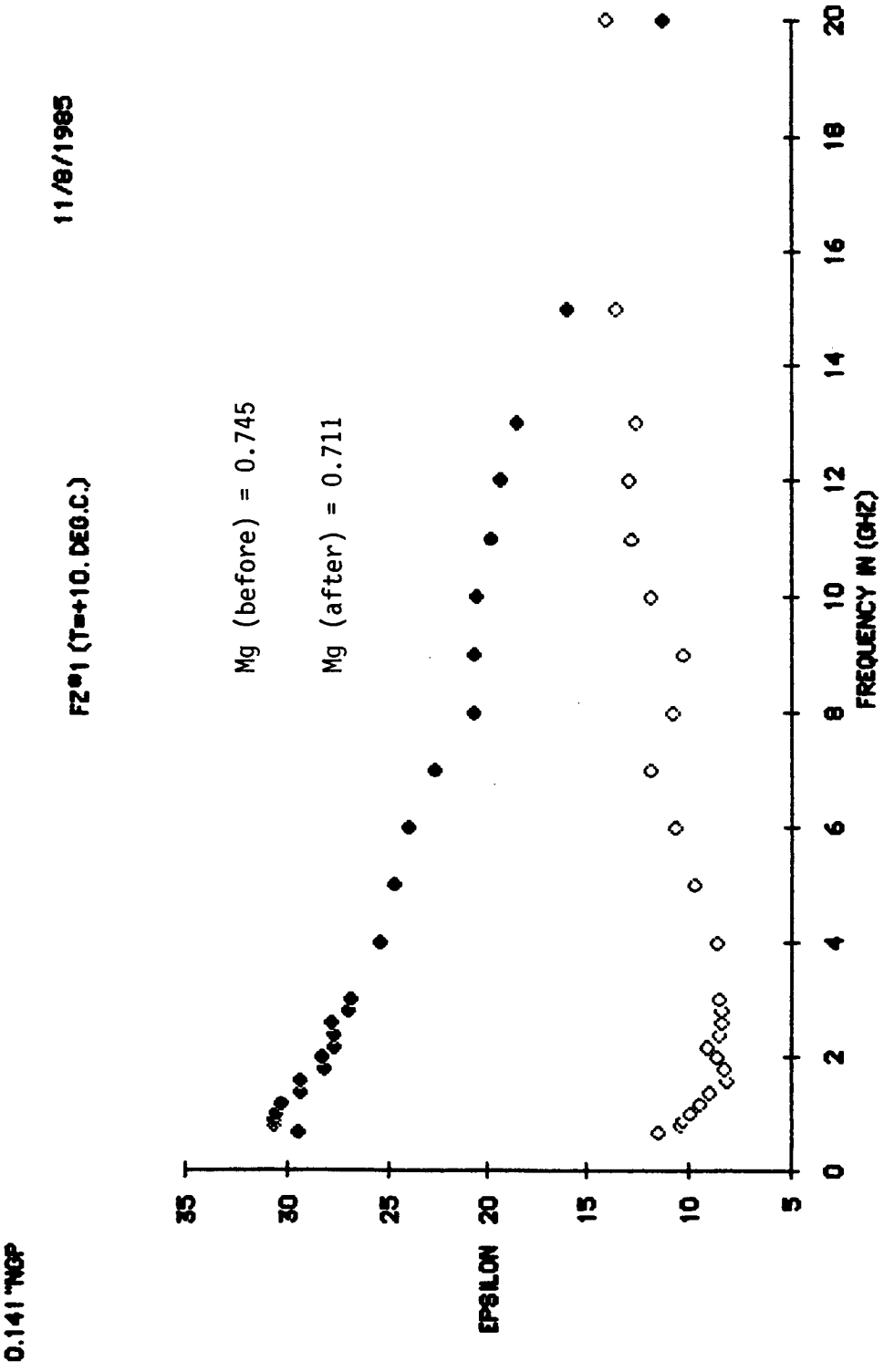
0.141"NGP
FZ#1 (T=+10.DEG.C.)
11/8/1985
Mg (before) = 0.745
Mg (after) = 0.711
EPSILON
FREQUENCY IN (GHZ)
35
30
25
20
15
10
5
0
2
4
6
8
10
12
14
16
18
20

Figure B.7

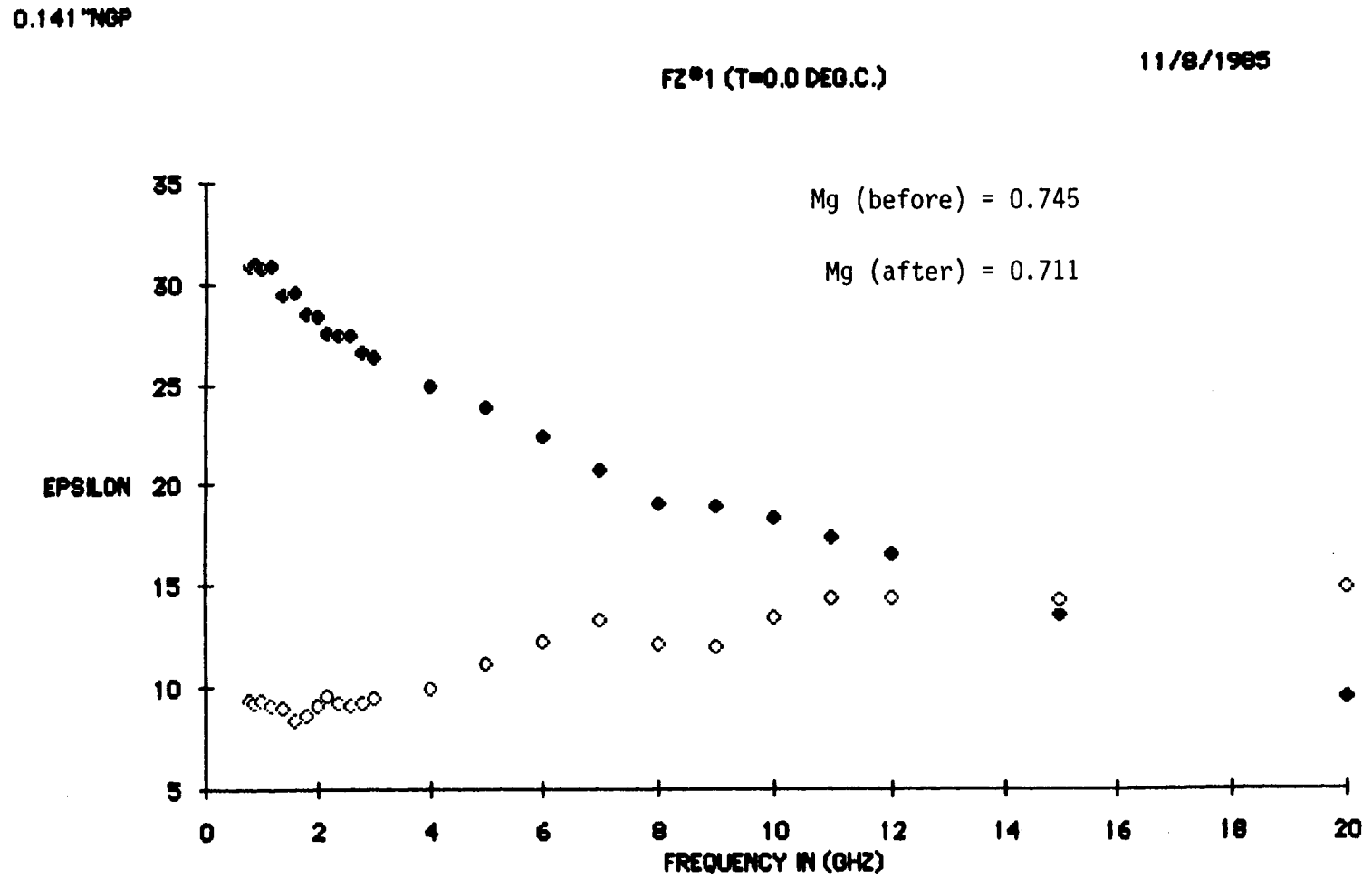
0.141"NGP
FZ#1 (T=0.0 DEG.C.)
11/8/1985
Mg (before) = 0.745
Mg (after) = 0.711
EPSILON
35
30
25
20
15
10
5
0
2
4
6
8
10
12
14
16
18
20
FREQUENCY IN (GHZ)

Figure B.8

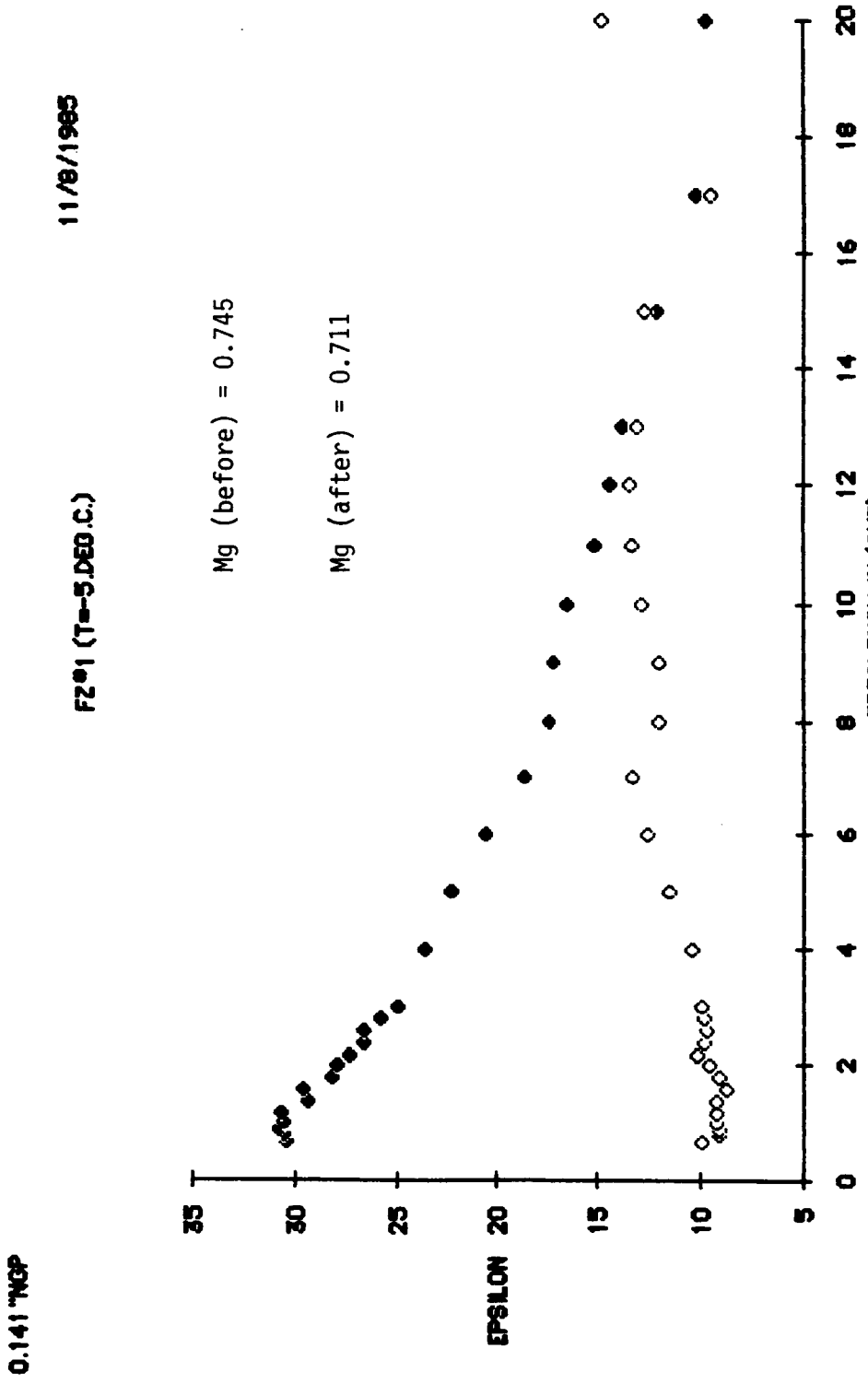
0.141"WGP
FZ#1 (T=-5.DEG.C.)
11/8/1985
Mg (before) = 0.745
Mg (after) = 0.711
EPSILON
FREQUENCY IN (GHZ)
35
30
25
20
15
10
5
0
2
4
6
8
10
12
14
16
18
20

Figure B.9

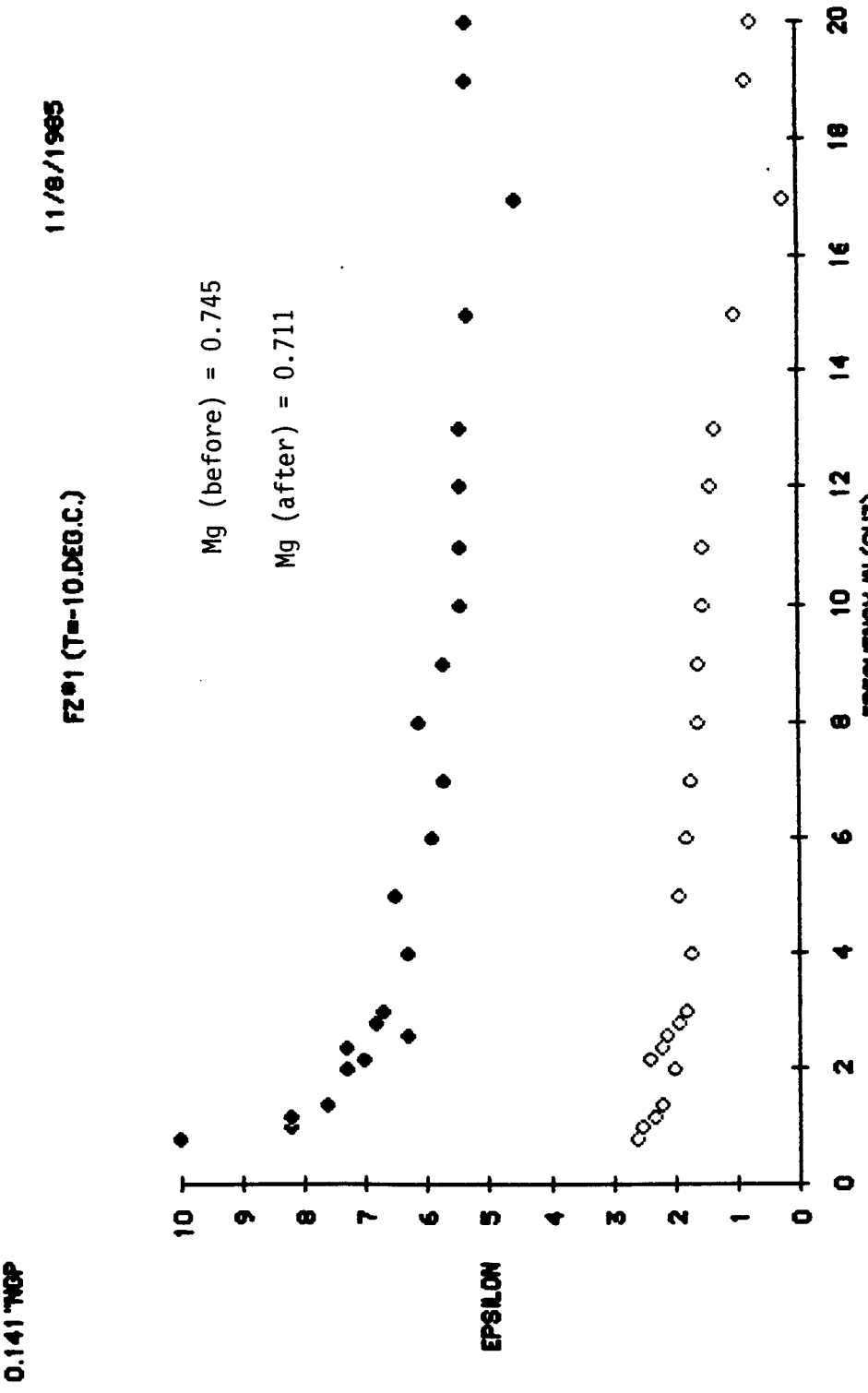
11/8/1985
FZ#1 (T=-10.DEG.C.)
Mg (before) = 0.745
Mg (after) = 0.711
EPSILON
FREQUENCY IN (GHZ)
0
1
2
3
4
5
6
7
8
9
10
0
2
4
6
8
10
12
14
16
18
20

Figure B.10

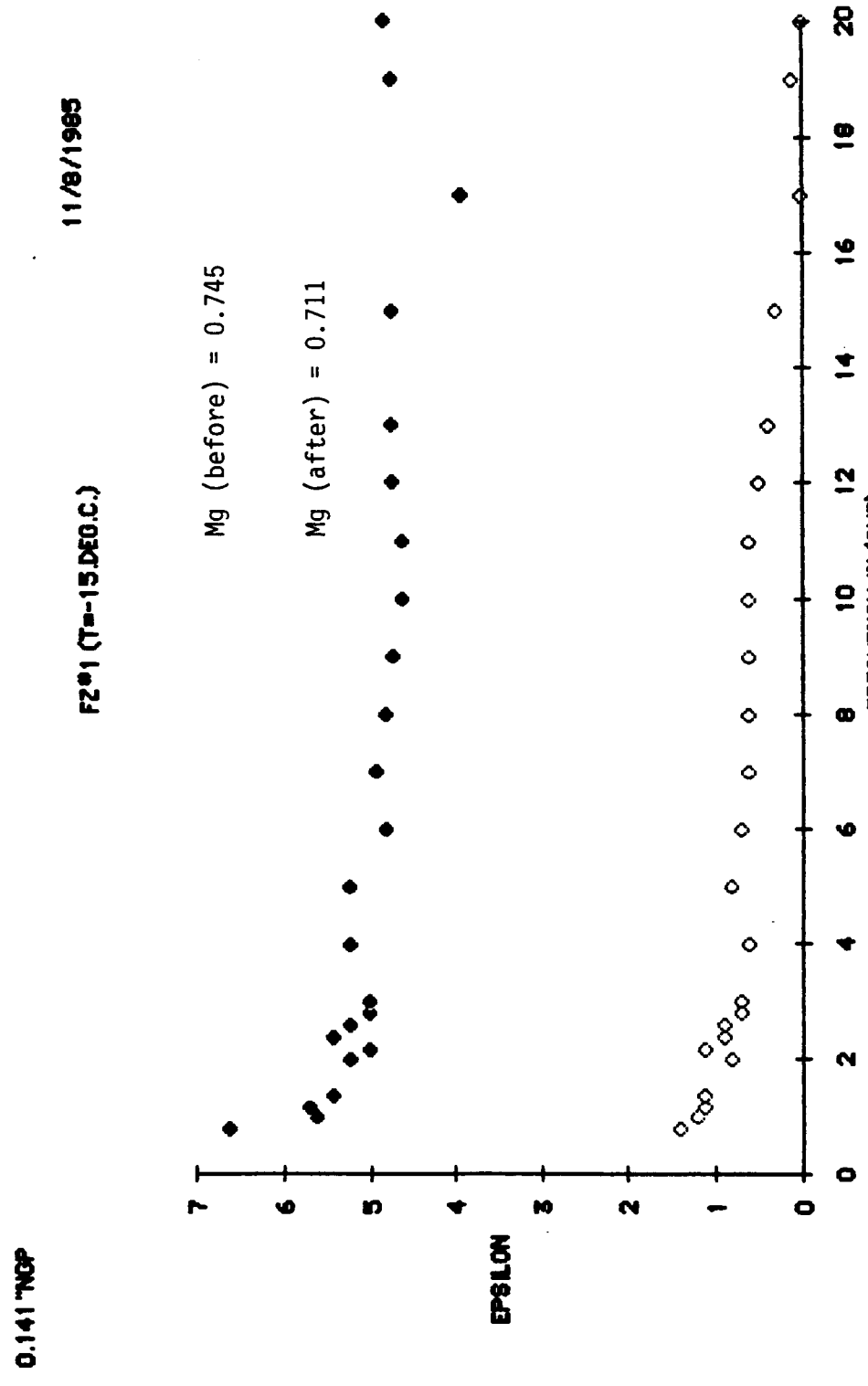
0.141 "NGP
F2*1 (T=-15.DEG.C.)
11/8/1985
Mg (before) = 0.745
Mg (after) = 0.711
EPSILON
FREQUENCY IN (GHZ)
0
1
2
3
4
5
6
7
0
2
4
6
8
10
12
14
16
18
20

Figure B.11

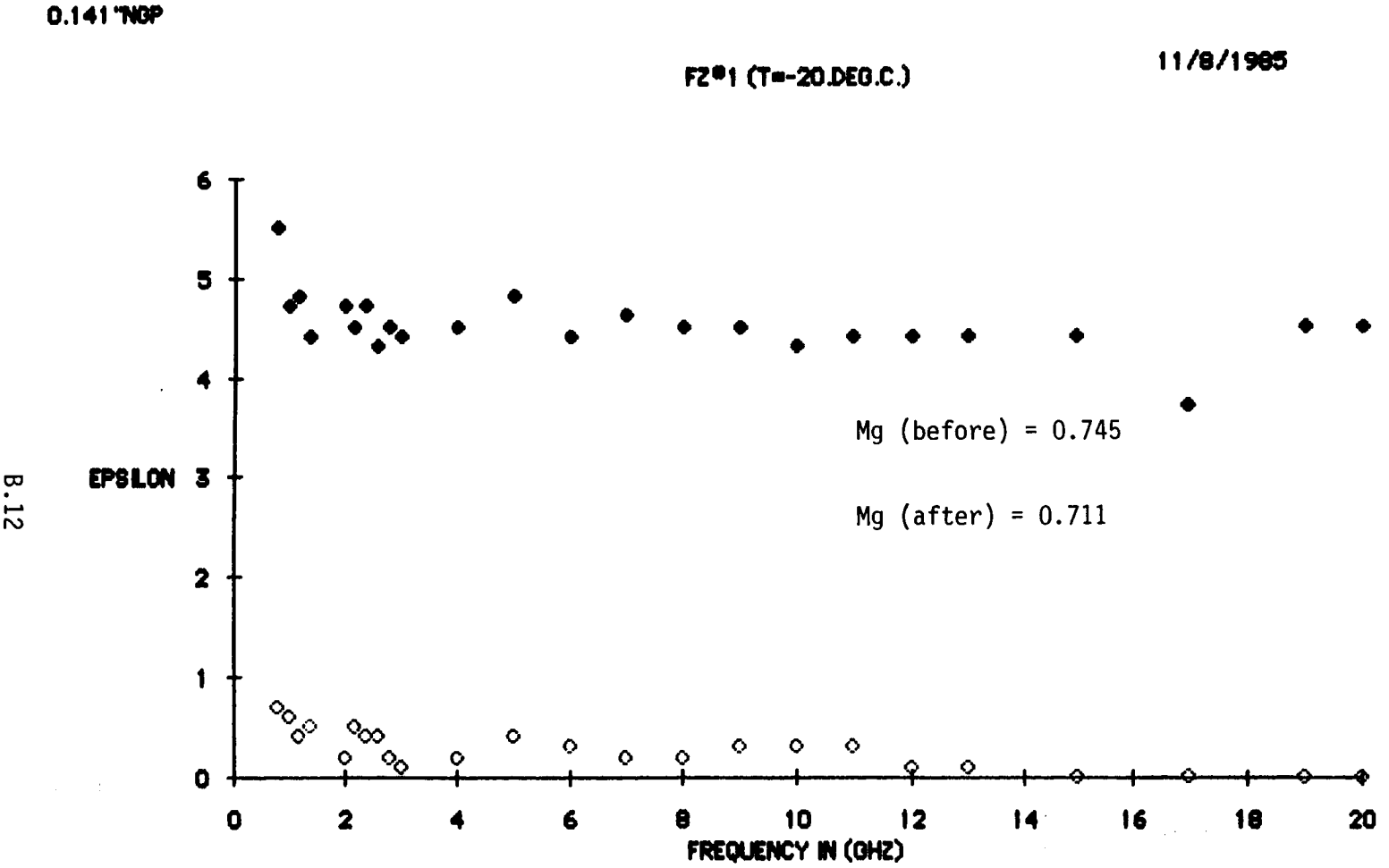
0.141"NGP
FZ#1 (T=-20.DEG.C.)
11/8/1985
EPSILON
FREQUENCY IN (GHZ)
Mg (before) = 0.745
Mg (after) = 0.711
0
1
2
3
4
5
6
0
2
4
6
8
10
12
14
16
18
20

Figure B.12

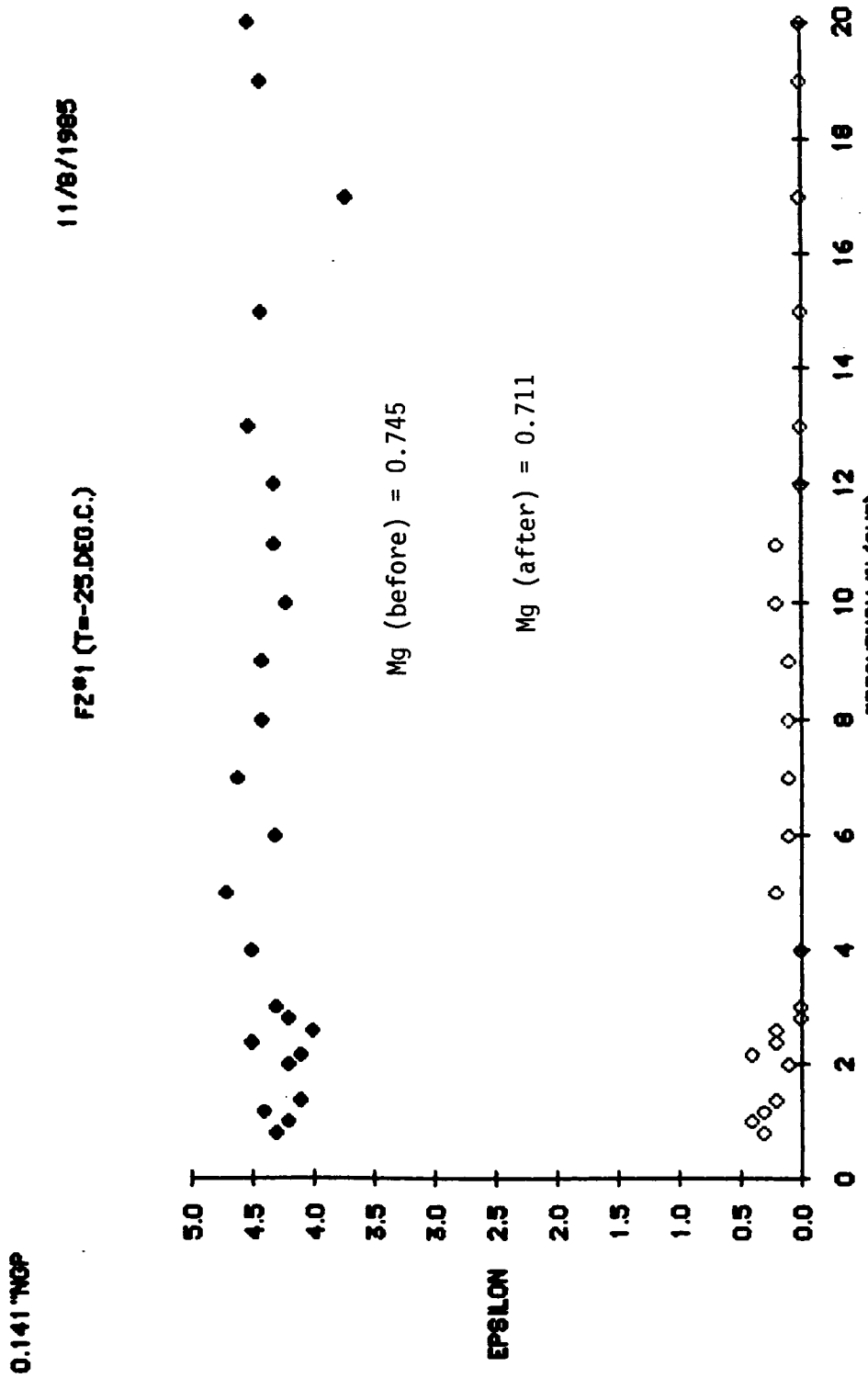
11/8/1985
F2*1 (T=-25.DEG.C.)
Mg (before) = 0.745
Mg (after) = 0.711
EPSILON
FREQUENCY IN (GHZ)
0.141 "NGP
5.0
4.5
4.0
3.5
3.0
2.5
2.0
1.5
1.0
0.5
0.0
0
2
4
6
8
10
12
14
16
18
20

Figure B.13

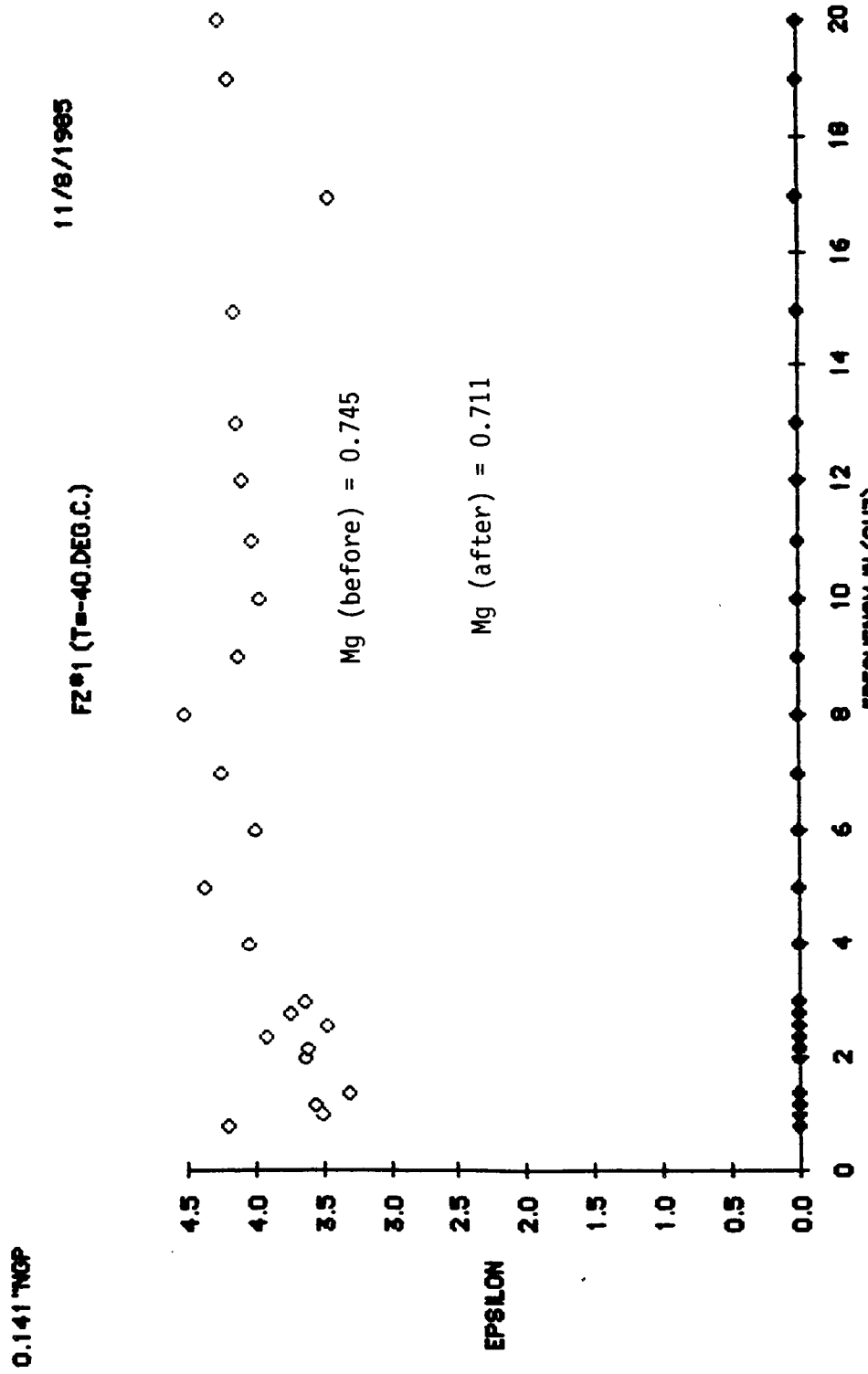
11/8/1985
FZ#1 (T=-40.DEG.C.)
Mg (before) = 0.745
Mg (after) = 0.711
0.141"NOP
EPSILON
FREQUENCY IN (GHZ)
4.5
4.0
3.5
3.0
2.5
2.0
1.5
1.0
0.5
0.0
0
2
4
6
8
10
12
14
16
18
20

Figure B.14

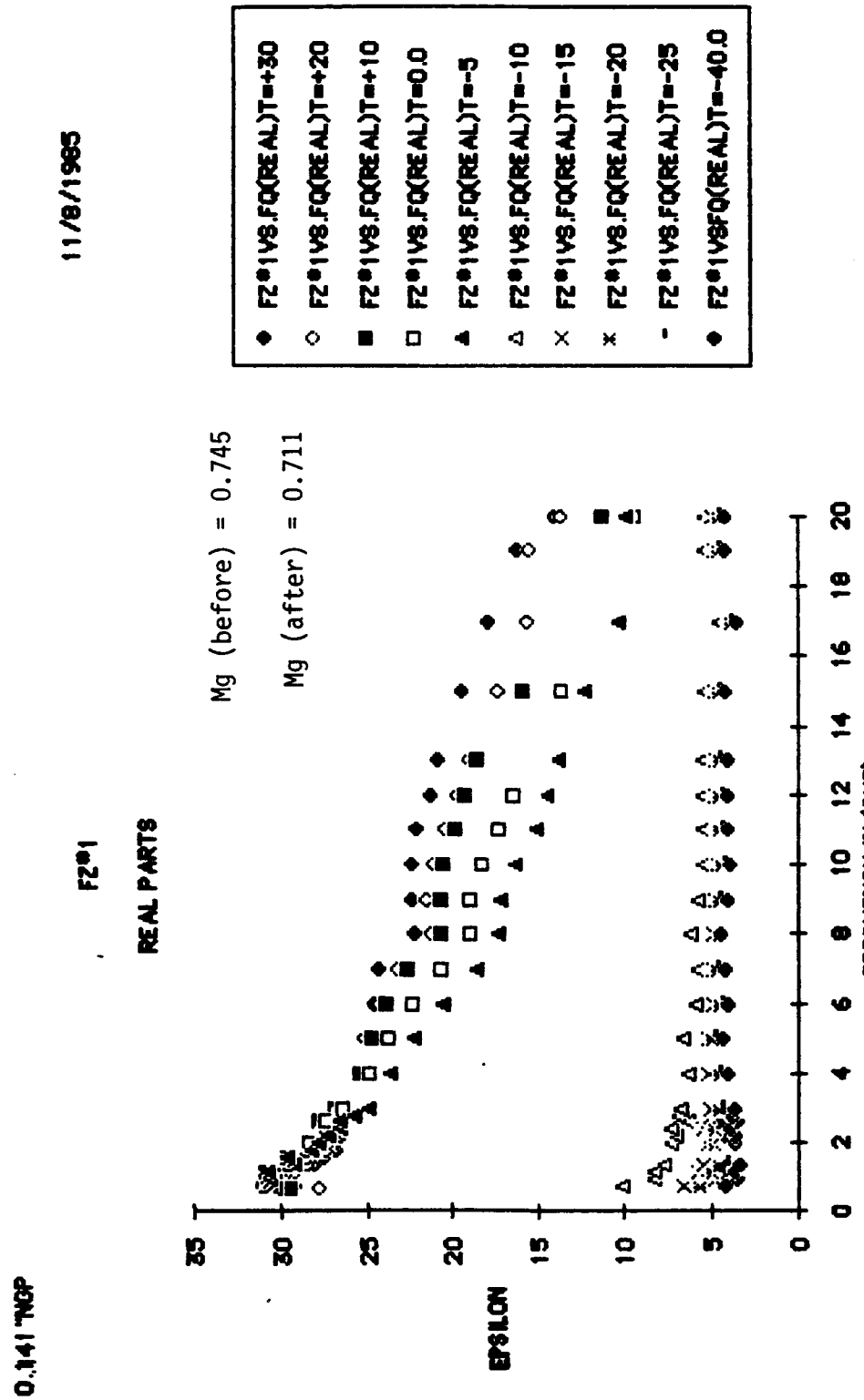
11/8/1985
FZ*1V8.FQ(REAL)T=+30
FZ*1V8.FQ(REAL)T=+20
FZ*1V8.FQ(REAL)T=+10
FZ*1V8.FQ(REAL)T=0.0
FZ*1V8.FQ(REAL)T=-5
FZ*1V8.FQ(REAL)T=-10
FZ*1V8.FQ(REAL)T=-15
FZ*1V8.FQ(REAL)T=-20
FZ*1V8.FQ(REAL)T=-25
FZ*1V8FQ(REAL)T=-40.0
Mg (before) = 0.745
Mg (after) = 0.711
FZ*1
REAL PARTS
EPSILON
FREQUENCY IN (GHZ)
0 5 10 15 20 25 30 35
0 2 4 6 8 10 12 14 16 18 20
0.141 "NOP

Figure B.15

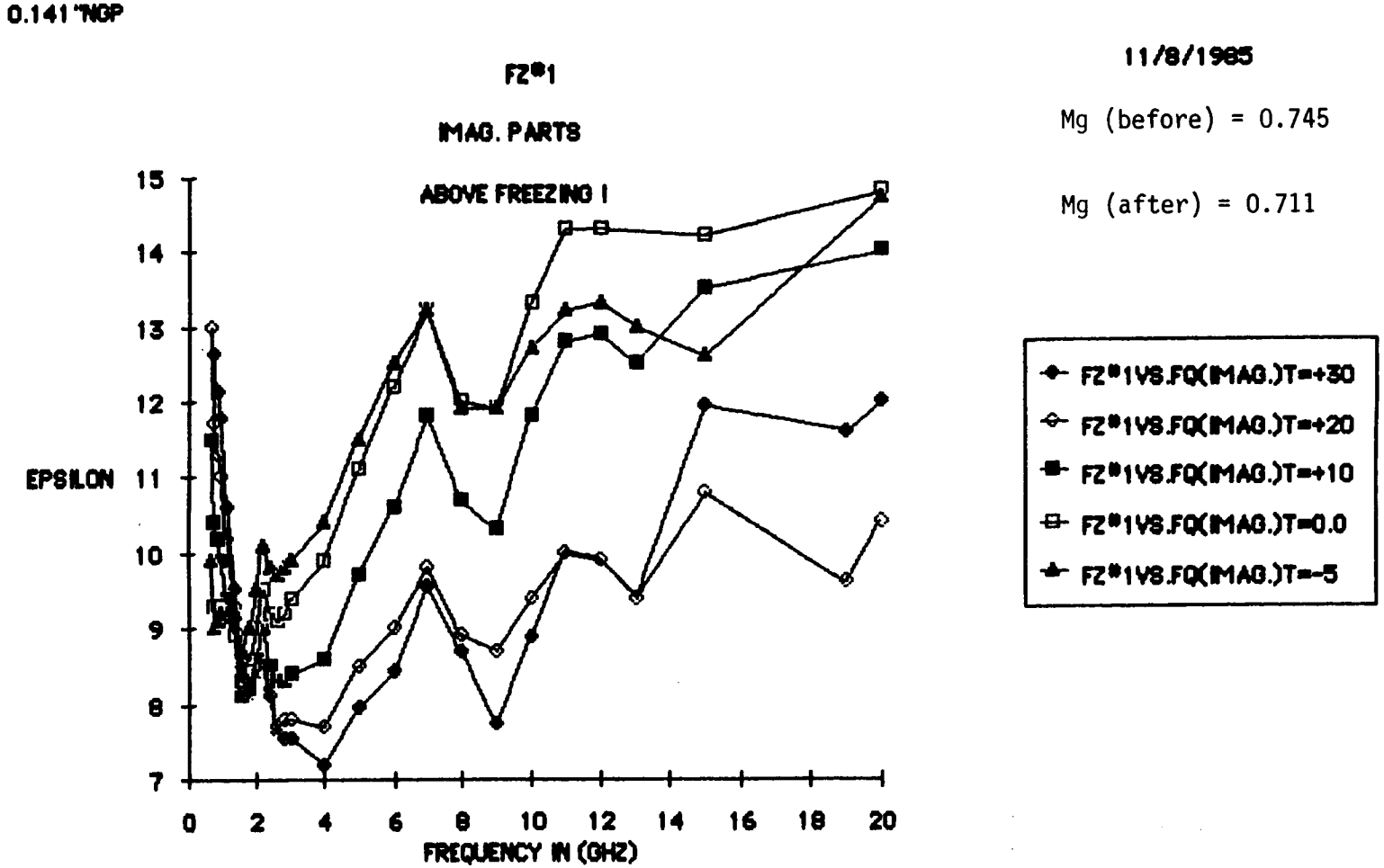
0.141 "NGP
FZ*1
IMAG. PARTS
ABOVE FREEZING !
11/8/1985
Mg (before) = 0.745
Mg (after) = 0.711
EPSILON
FREQUENCY IN (GHZ)
FZ*1VS.FQ(IMAG.)T=+30
FZ*1VS.FQ(IMAG.)T=+20
FZ*1VS.FQ(IMAG.)T=+10
FZ*1VS.FQ(IMAG.)T=0.0
FZ*1VS.FQ(IMAG.)T=-5

Figure B.16

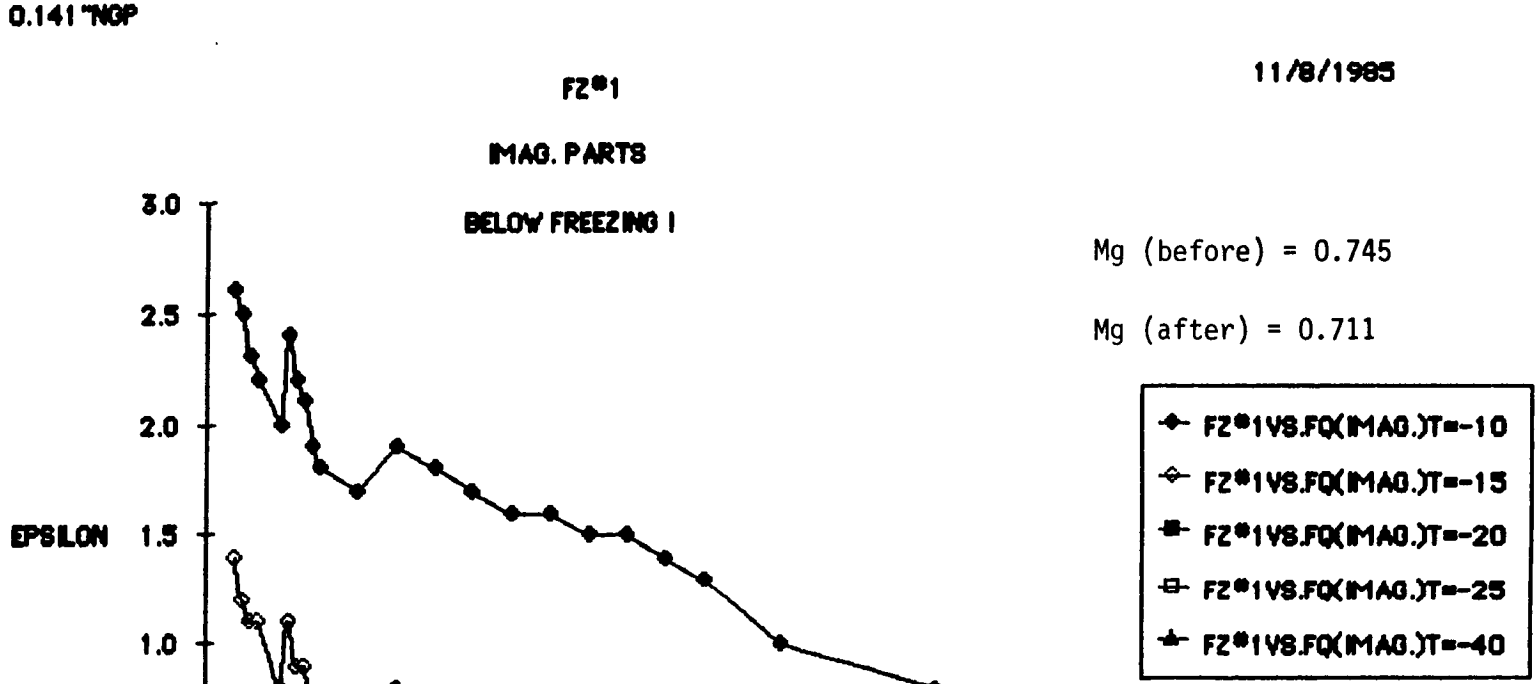
0.141 "NGP
FZ*1
IMAG. PARTS
BELOW FREEZING I
11/8/1985
EPSILON
3.0
2.5
2.0
1.5
1.0
0.5
0.0
0
2
4
6
8
10
12
14
16
18
20
FREQUENCY IN (GHZ)
Mg (before) = 0.745
Mg (after) = 0.711
FZ*1VS.FQ(IMAG.)T=-10
FZ*1VS.FQ(IMAG.)T=-15
FZ*1VS.FQ(IMAG.)T=-20
FZ*1VS.FQ(IMAG.)T=-25
FZ*1VS.FQ(IMAG.)T=-40

Figure B.17

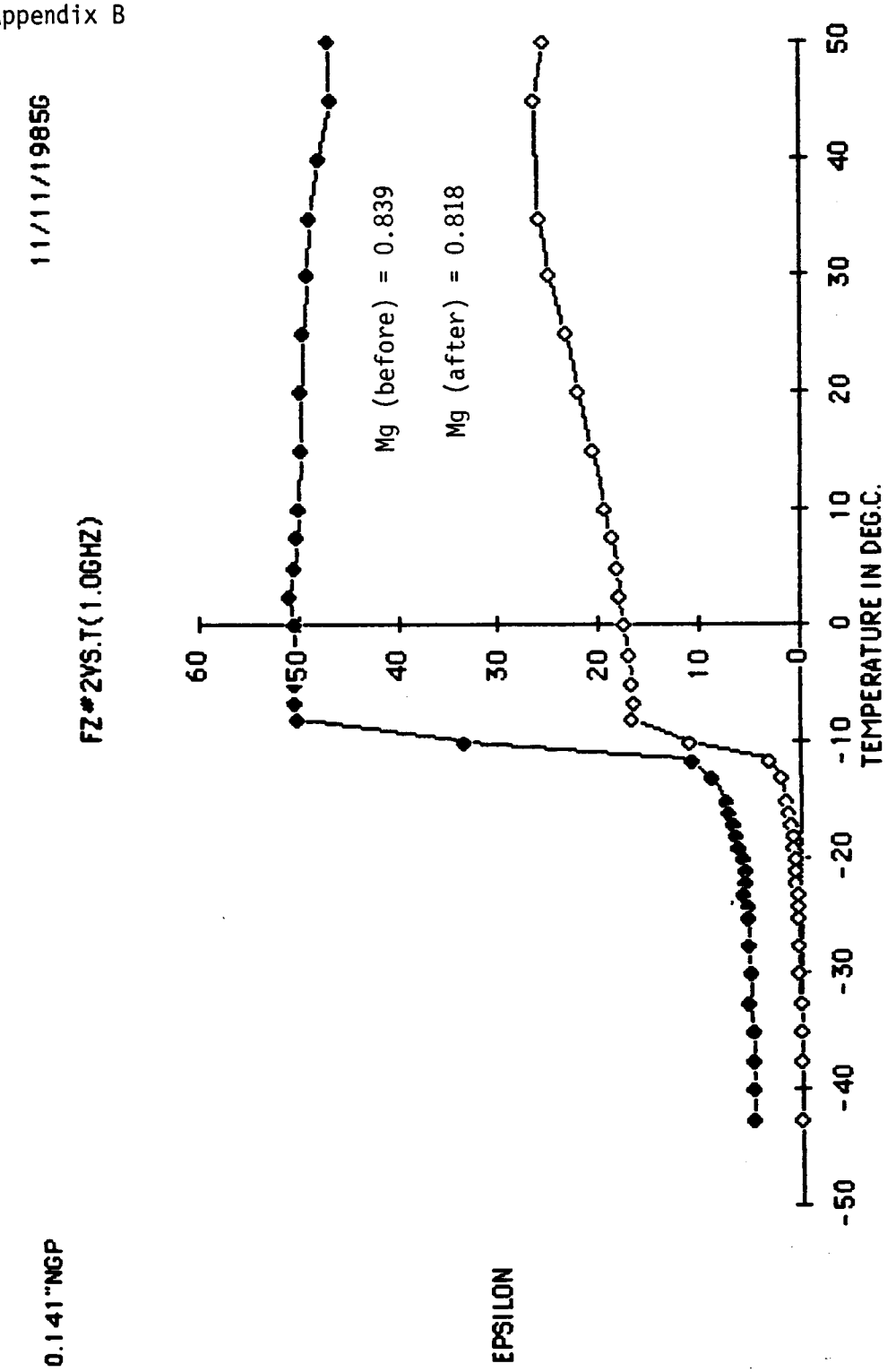
11/11/1985G
FZ*2YS.T(1.0GHZ)
0.141"NGP
Mg (before) = 0.839
Mg (after) = 0.818
EPSILON
TEMPERATURE IN DEG.C.
60
50
40
30
20
10
0
-50
-40
-30
-20
-10
0
10
20
30
40
50

Figure B.18

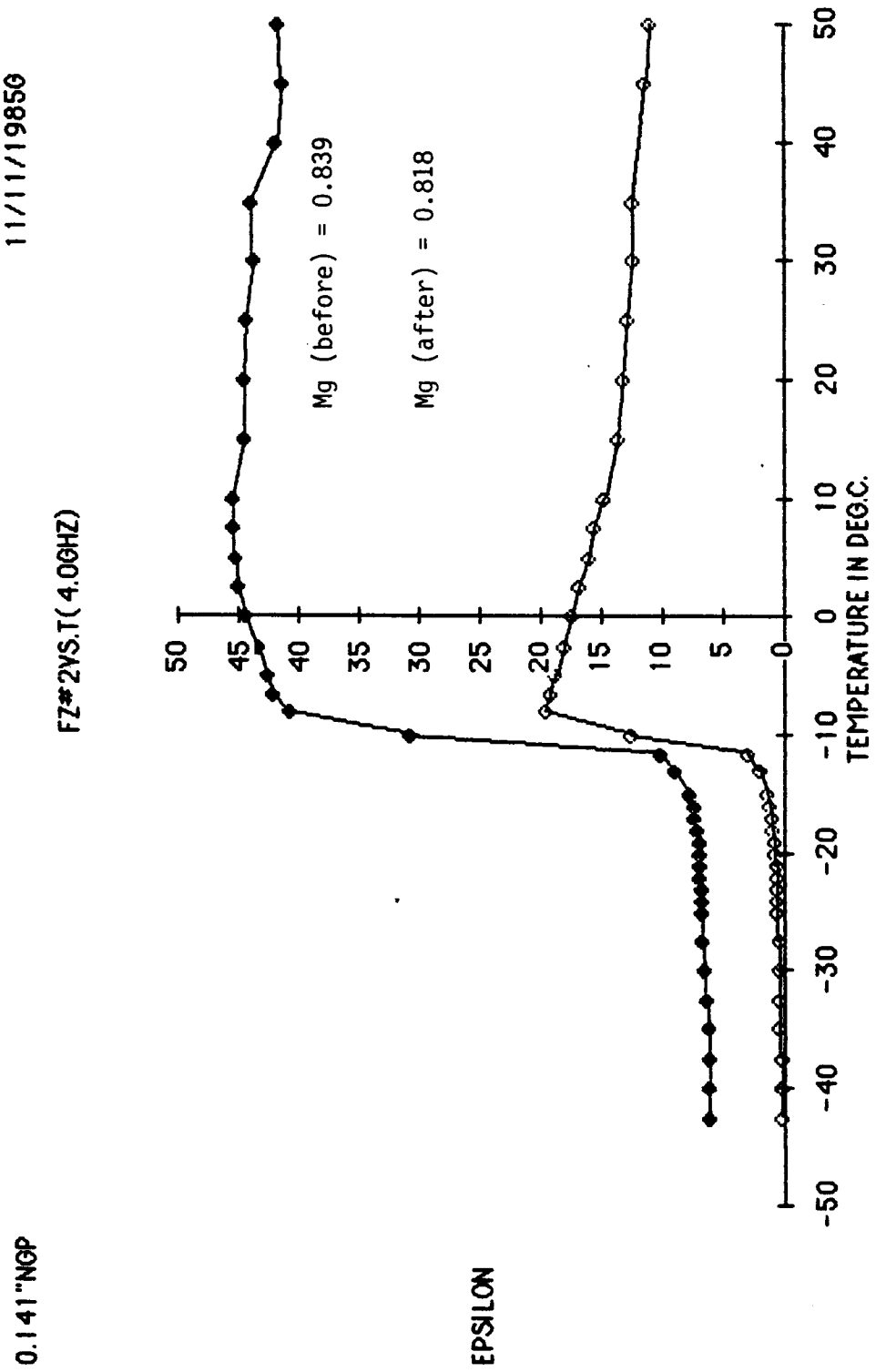
11/11/19850
FZ*2YS.T(4.0GHZ)
0.141"NGP
Mg (before) = 0.839
Mg (after) = 0.818
EPSILON
TEMPERATURE IN DEG.C.
50
45
40
35
30
25
20
15
10
5
0
-50
-40
-30
-20
-10
0
10
20
30
40
50

Figure B.19

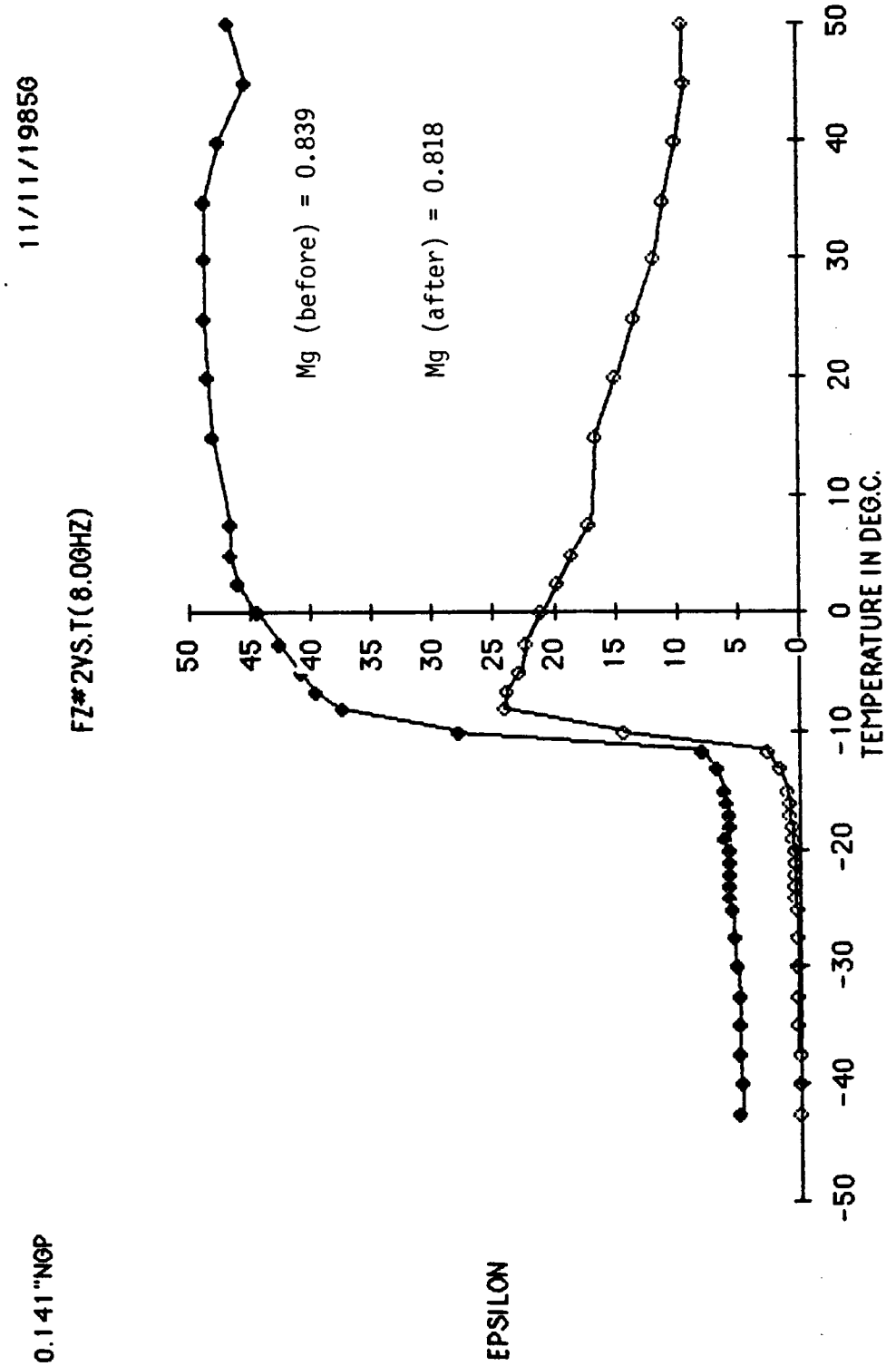
11/11/1985G
FZ#2VS.T(8.0GHZ)
Mg (before) = 0.839
Mg (after) = 0.818
0.141"NGP
EPSILON
TEMPERATURE IN DEG.C.
50
45
40
35
30
25
20
15
10
5
0
-50
-40
-30
-20
-10
0
10
20
30
40
50

Figure B.20

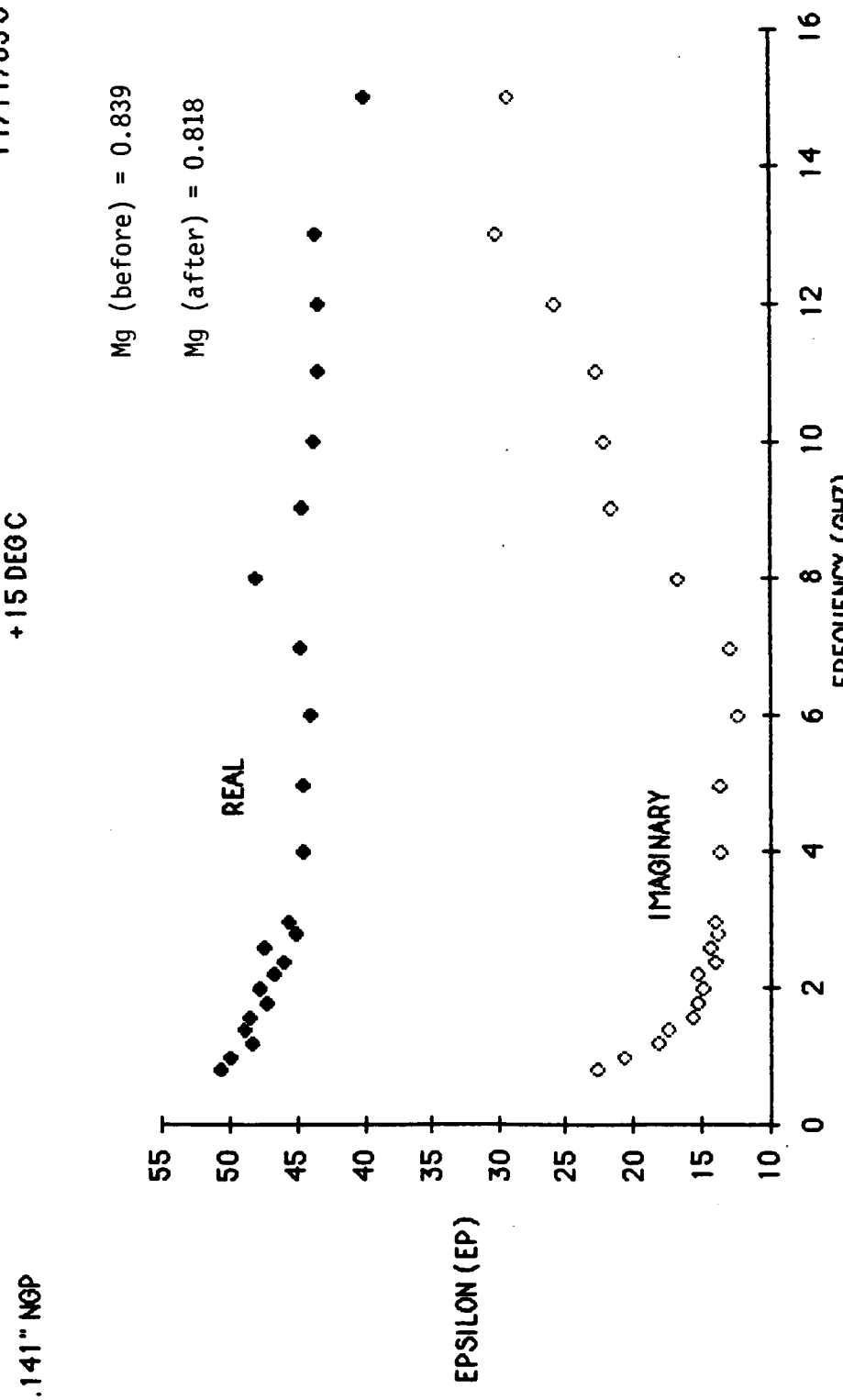
11/11/85 0
+15 DEG C
.141" NGP
Mg (before) = 0.839
Mg (after) = 0.818
REAL
IMAGINARY
EPSILON (EP)
FREQUENCY (GHZ)
55
50
45
40
35
30
25
20
15
10
0
2
4
6
8
10
12
14
16

Figure B.21

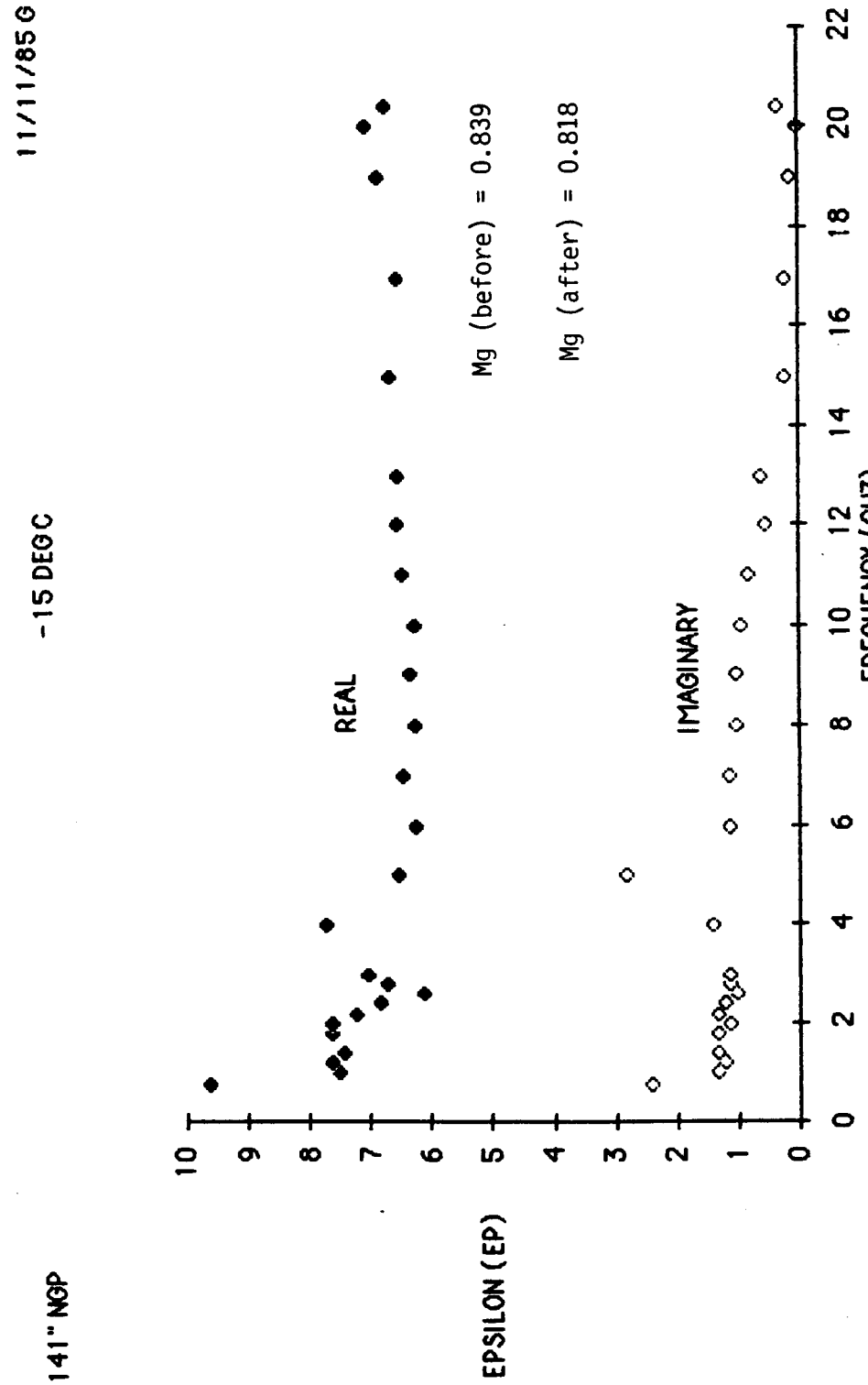
11/11/85 G
-15 DEGC
.141" NGP
REAL
IMAGINARY
Mg (before) = 0.839
Mg (after) = 0.818
EPSILON (EP)
FREQUENCY (GHZ)
0
1
2
3
4
5
6
7
8
9
10
0
2
4
6
8
10
12
14
16
18
20
22

Figure B.22

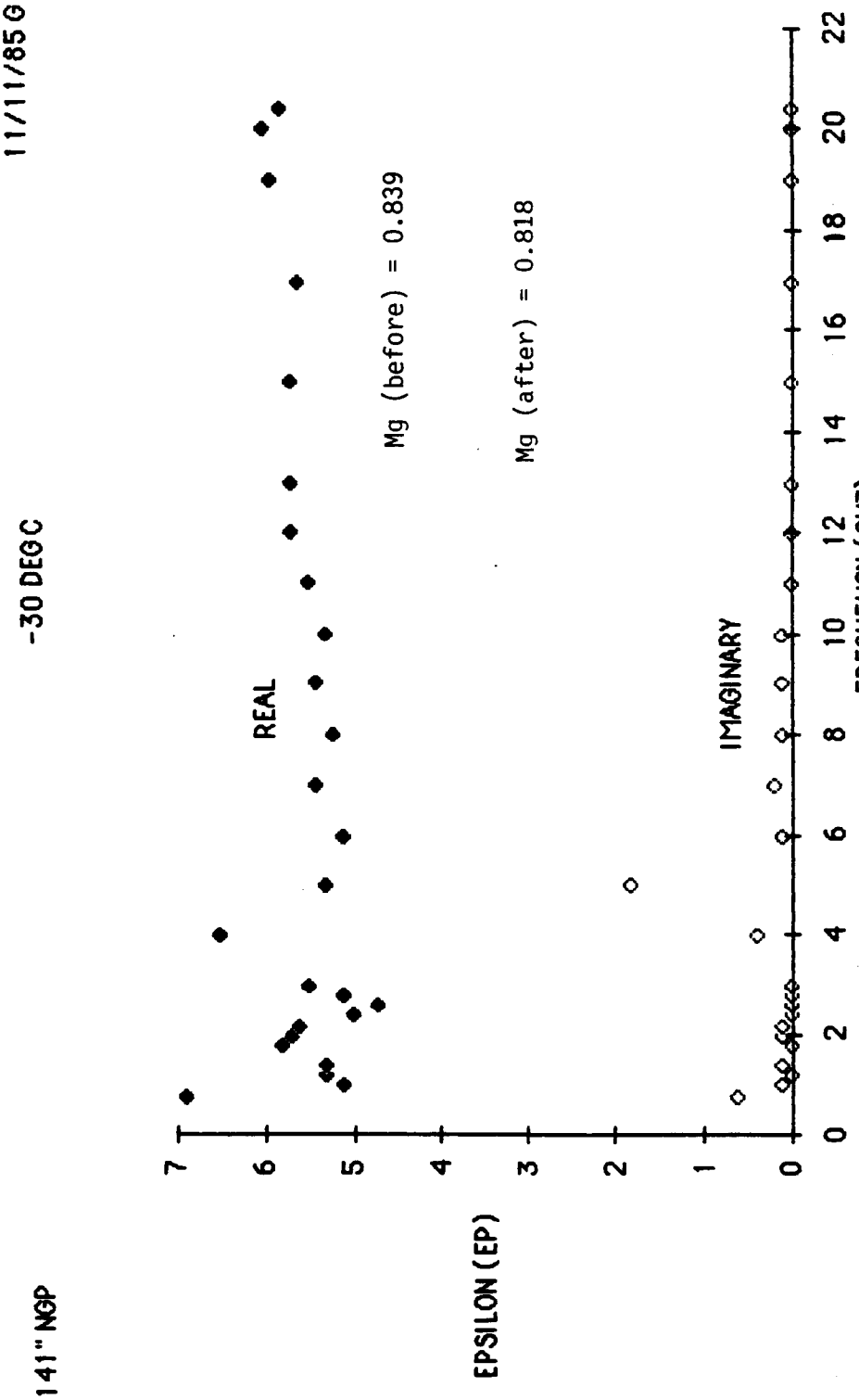
11/11/85 G
-30 DEG C
.141" NGP
REAL
IMAGINARY
EPSILON (EP)
FREQUENCY (GHZ)
Mg (before) = 0.839
Mg (after) = 0.818
0
1
2
3
4
5
6
7
0
2
4
6
8
10
12
14
16
18
20
22

Figure B.23

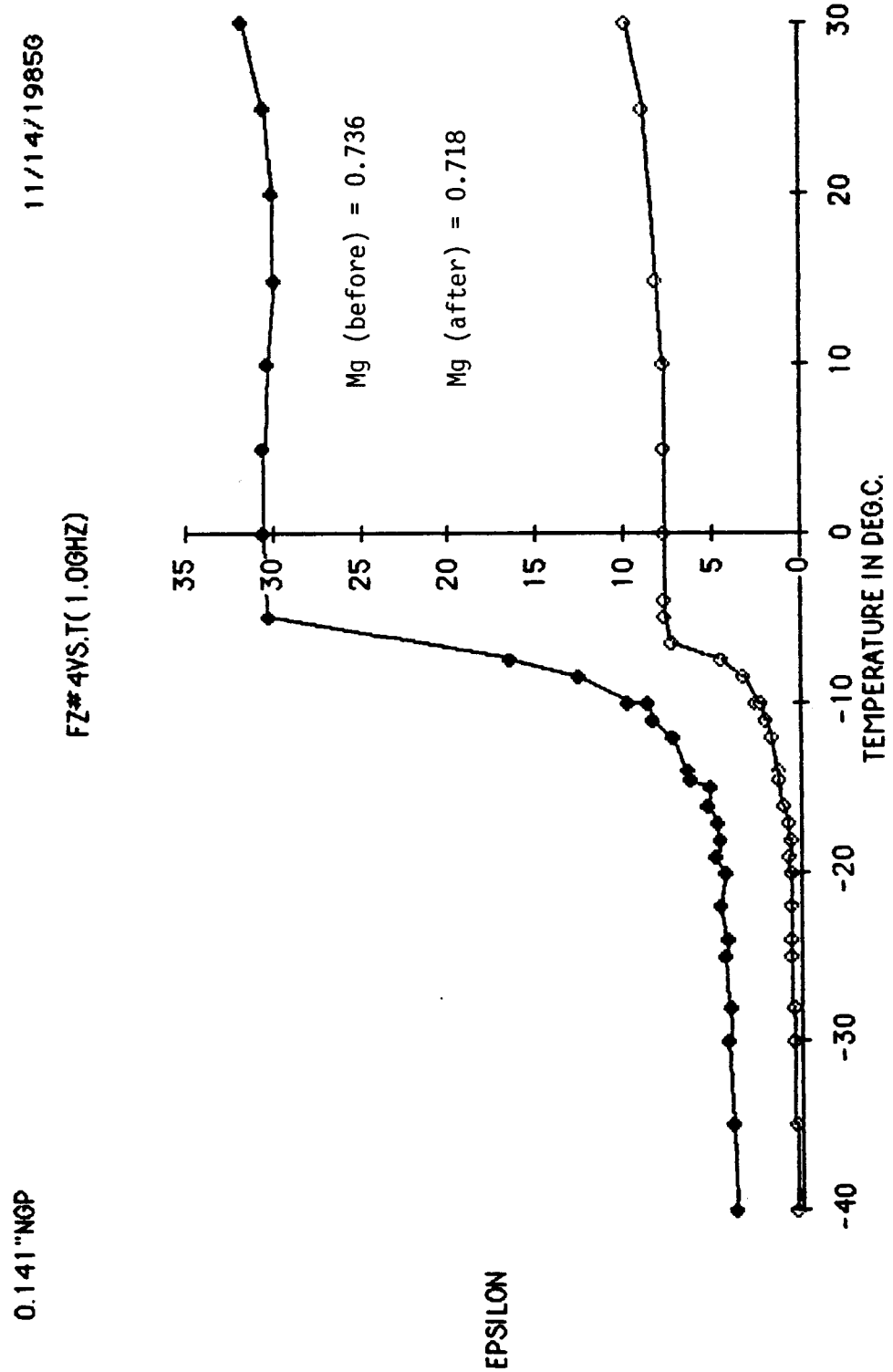
11/14/19850
FZ*4VS.T(1.0GHZ)
0.141"NGP
Mg (before) = 0.736
Mg (after) = 0.718
EPSILON
TEMPERATURE IN DEG.C.
35
30
25
20
15
10
5
0
30
20
10
0
-10
-20
-30
-40

Figure B.24

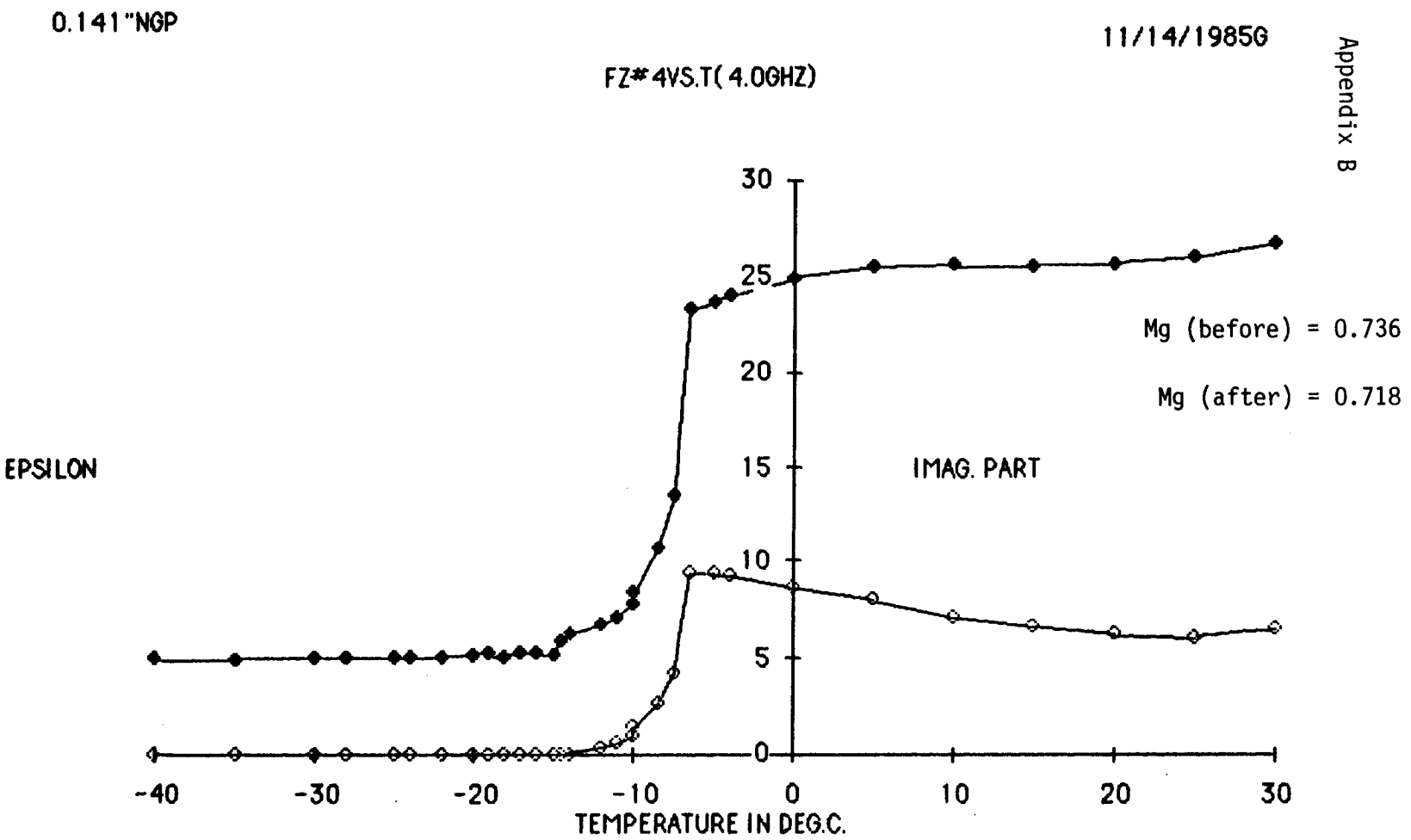
0.141"NGP
11/14/1985G
FZ*4VS.T(4.0GHZ)
EPSILON
IMAG. PART
Mg (before) = 0.736
Mg (after) = 0.718
30
25
20
15
10
5
0
-40
-30
-20
-10
0
10
20
30
TEMPERATURE IN DEG.C.

Figure B.25

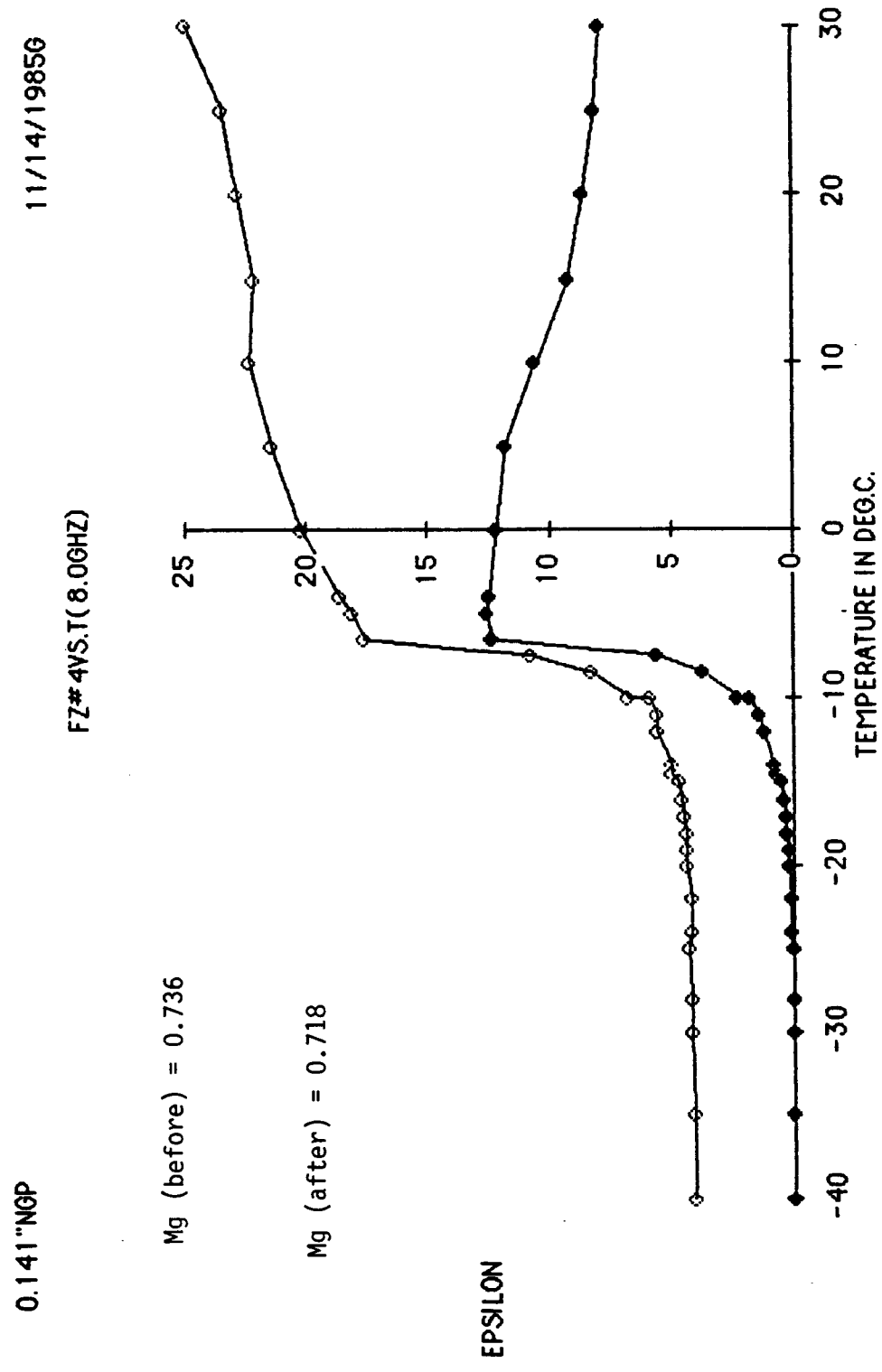
0.141"NGP
11/14/1985G
FZ#4VS.T(8.0GHZ)
Mg (before) = 0.736
Mg (after) = 0.718
EPSILON
25
20
15
10
5
0
30
20
10
0
-10
-20
-30
-40
TEMPERATURE IN DEG.C.

Figure B.26

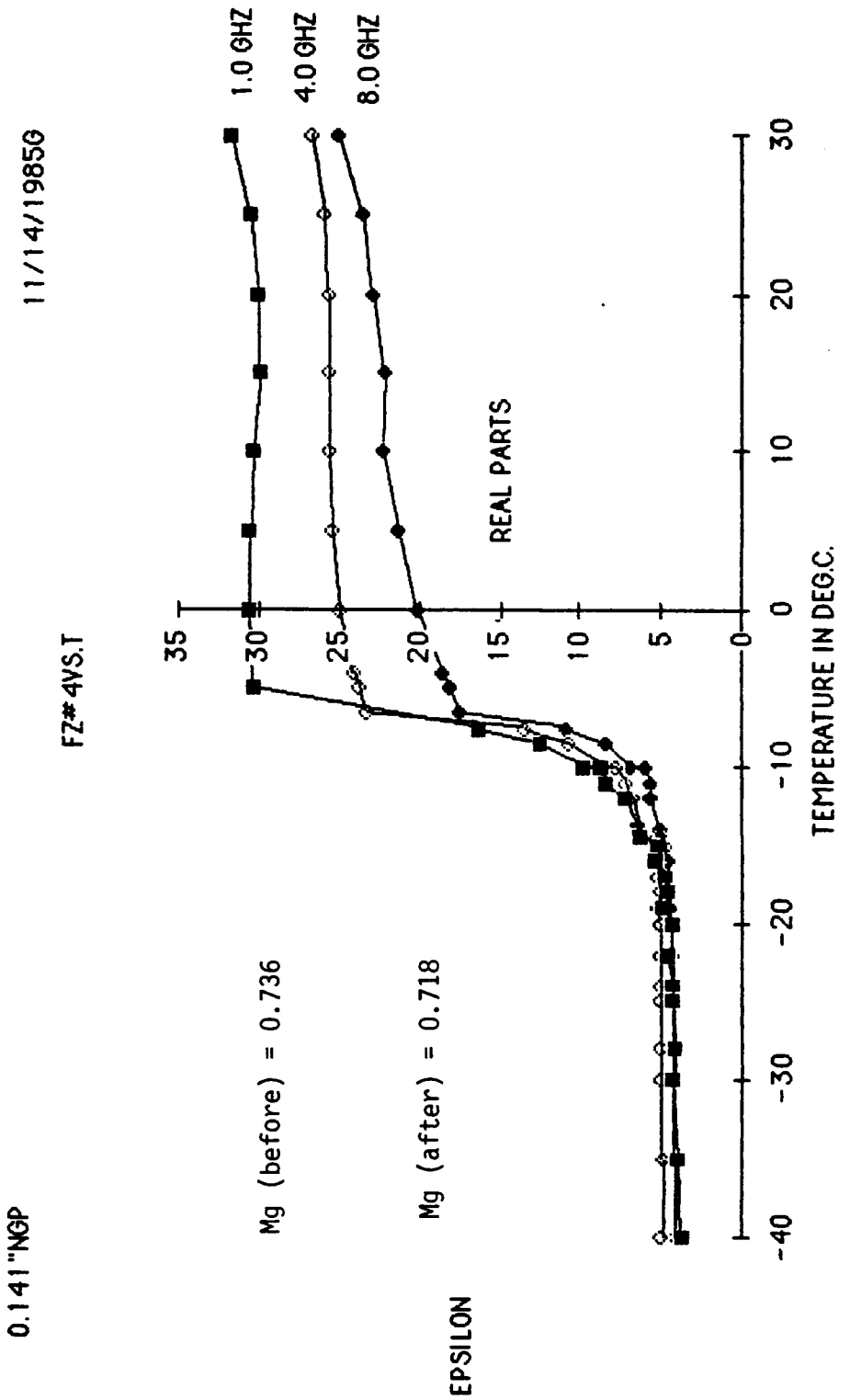
0.141"NGP
11/14/1985G
FZ# 4VS.T
1.0 GHZ
4.0 GHZ
8.0 GHZ
REAL PARTS
EPSILON
Mg (before) = 0.736
Mg (after) = 0.718
TEMPERATURE IN DEG.C.
35
30
25
20
15
10
5
0
30
20
10
0
-10
-20
-30
-40

Figure B.27

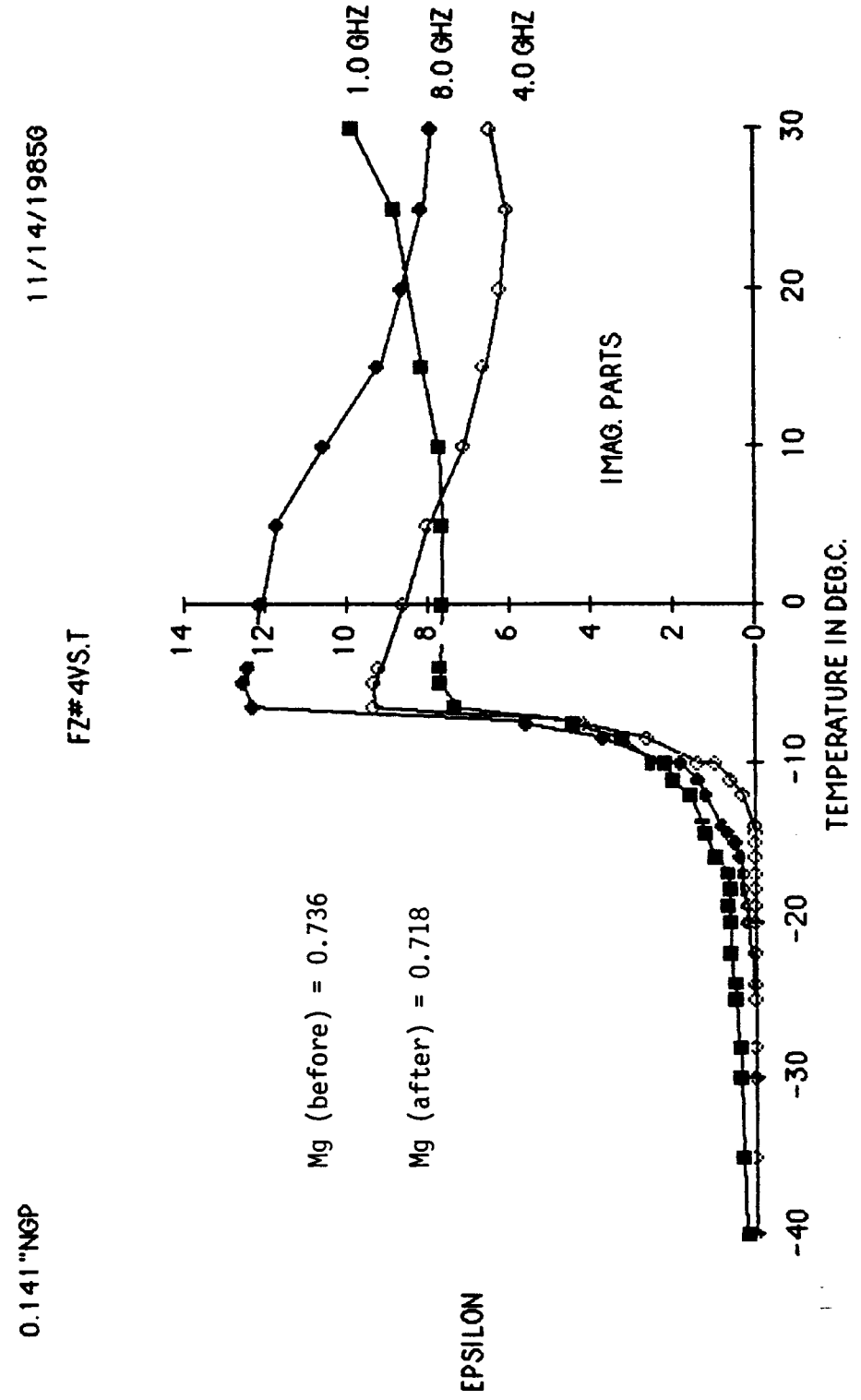
0.141"NGP
11/14/1985@
FZ#4VS.T
1.0 GHZ
8.0 GHZ
4.0 GHZ
IMAG. PARTS
Mg (before) = 0.736
Mg (after) = 0.718
EPSILON
TEMPERATURE IN DEG.C.
14
12
10
8
6
4
2
0
30
20
10
0
-10
-20
-30
-40

Figure B.28

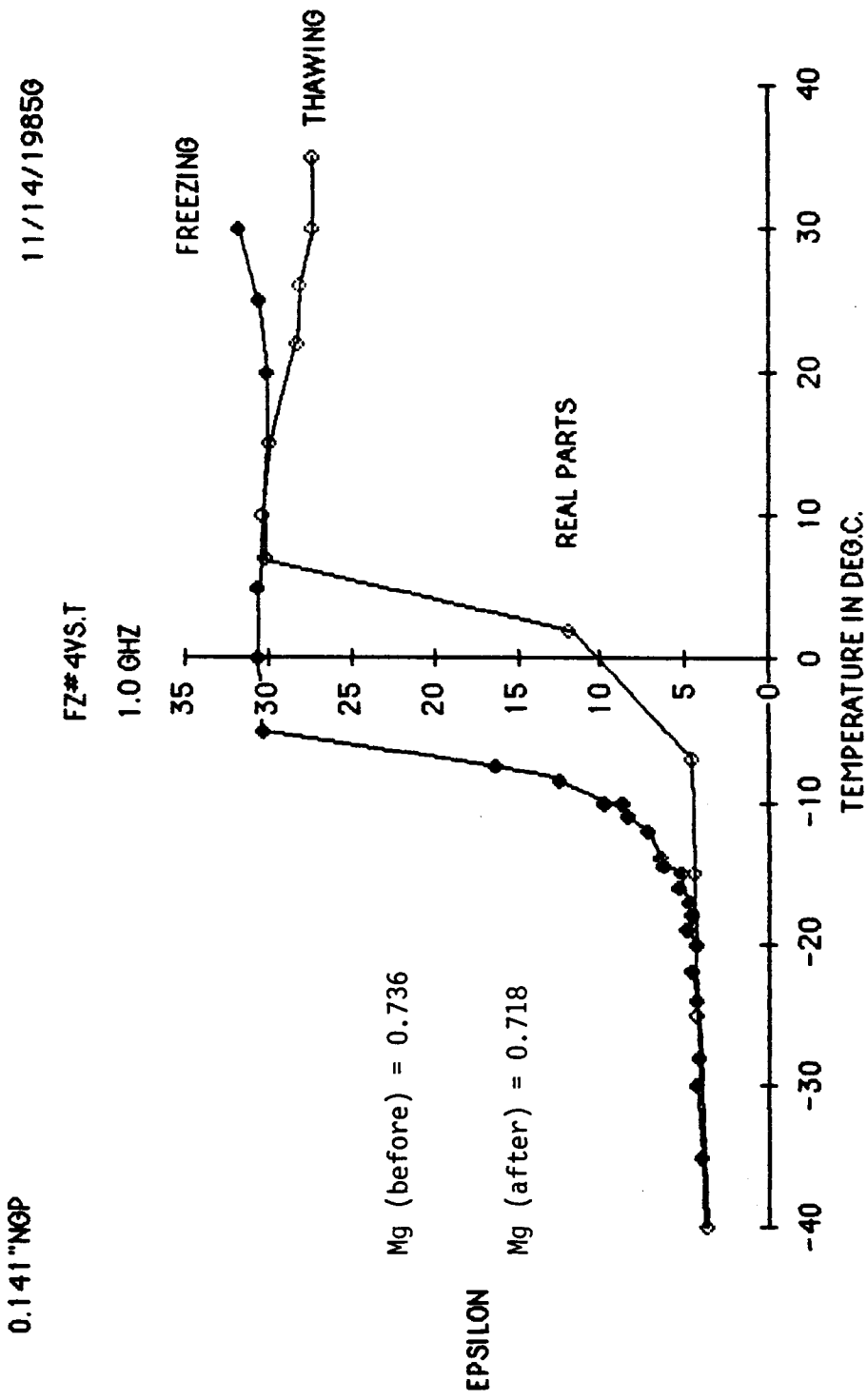
0.141"NGP
11/14/19850
FZ*4VS.T
1.0 GHZ
FREEZING
THAWING
REAL PARTS
EPSILON
Mg (before) = 0.736
Mg (after) = 0.718
35
30
25
20
15
10
5
0
40
30
20
10
0
-10
-20
-30
-40
TEMPERATURE IN DEG.C.

Figure B.29

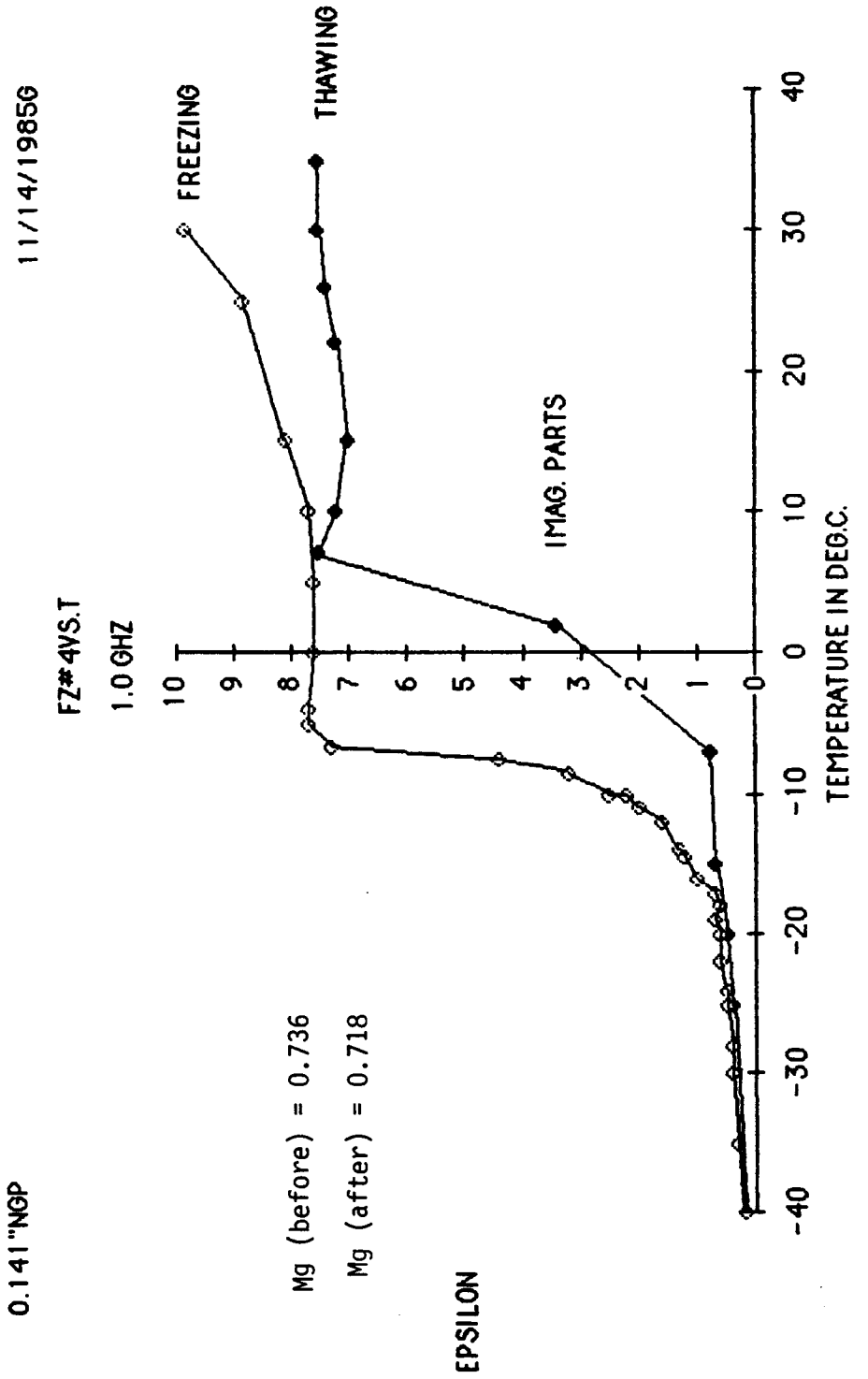
0.141"NGP
11/14/1985G
FZ#4VS.T
1.0 GHZ
FREEZING
THAWING
IMAG. PARTS
EPSILON
Mg (before) = 0.736
Mg (after) = 0.718
TEMPERATURE IN DEG.C.
10
9
8
7
6
5
4
3
2
1
0
40
30
20
10
0
-10
-20
-30
-40

Figure B.30

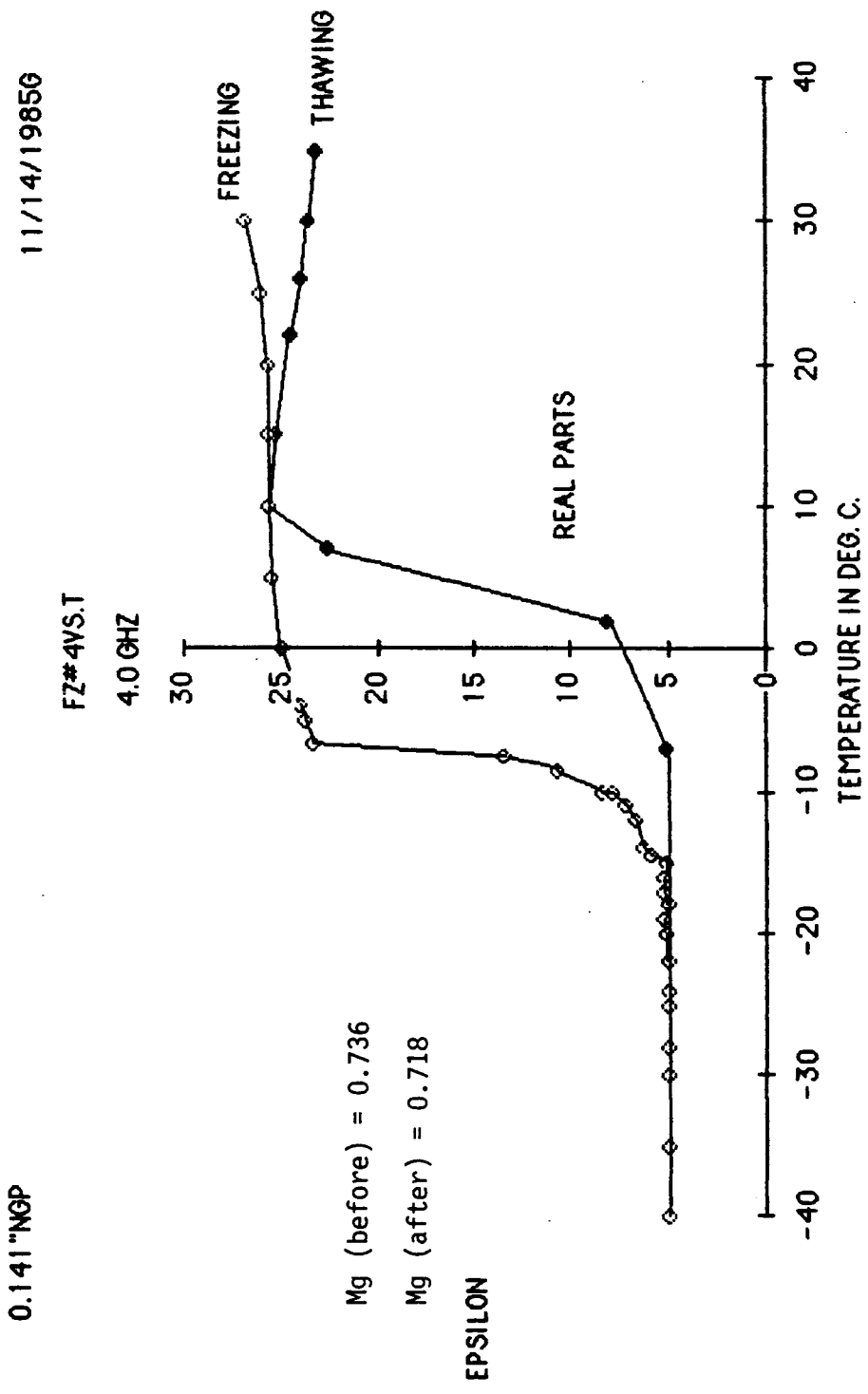
11/14/1985G
FZ#4VS.T
4.0 GHZ
FREEZING
THAWING
REAL PARTS
EPSILON
Mg (before) = 0.736
Mg (after) = 0.718
0.141"NGP
30
25
20
15
10
5
0
40
30
20
10
0
-10
-20
-30
-40
TEMPERATURE IN DEG. C.

Figure B.31

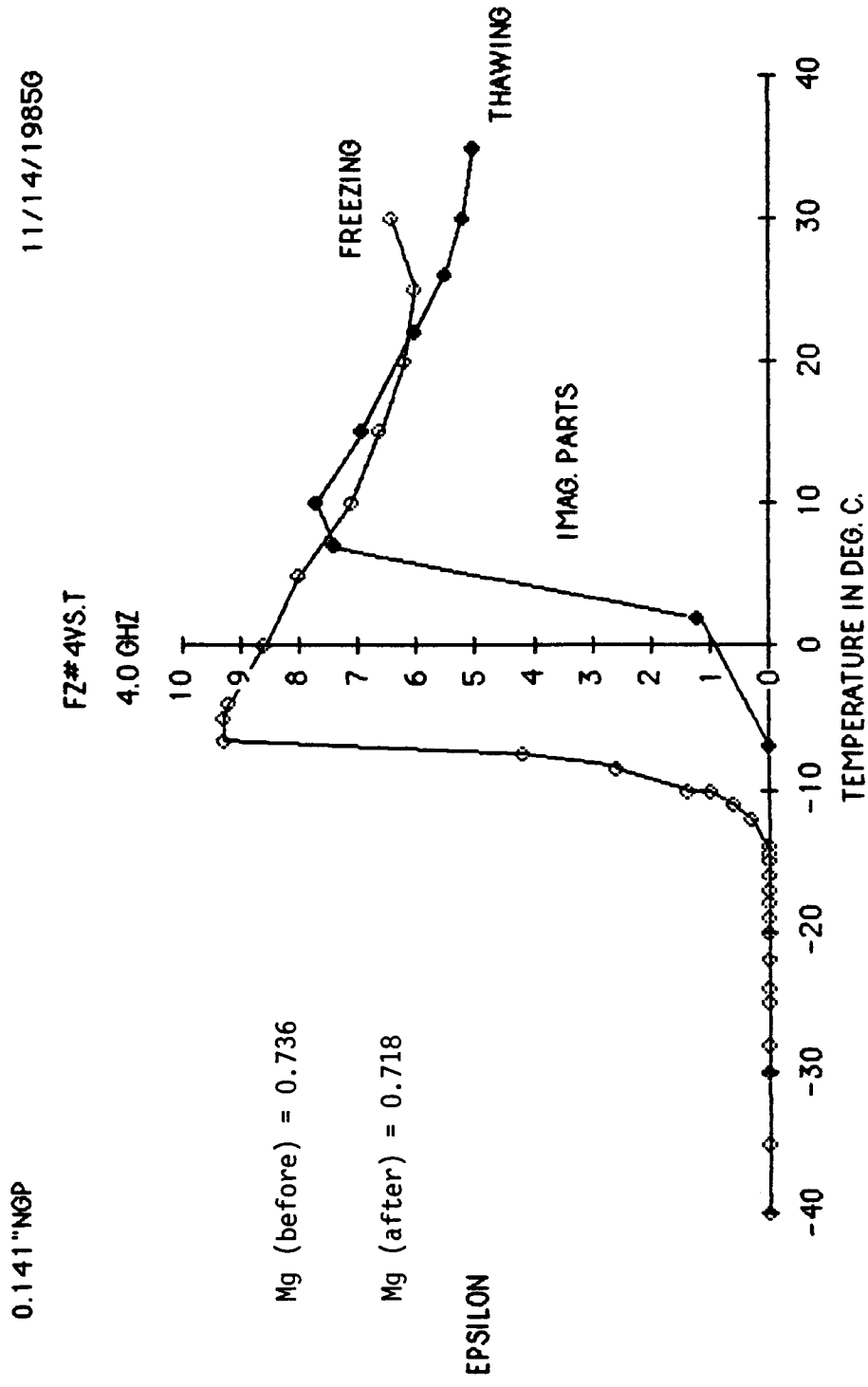
11/14/1985G
F2#4VS.T
4.0 GHZ
FREEZING
THAWING
IMAG. PARTS
TEMPERATURE IN DEG. C.
10
9
8
7
6
5
4
3
2
1
0
40
30
20
10
0
-10
-20
-30
-40
0.141"NGP
Mg (before) = 0.736
Mg (after) = 0.718
EPSILON

Figure B.32

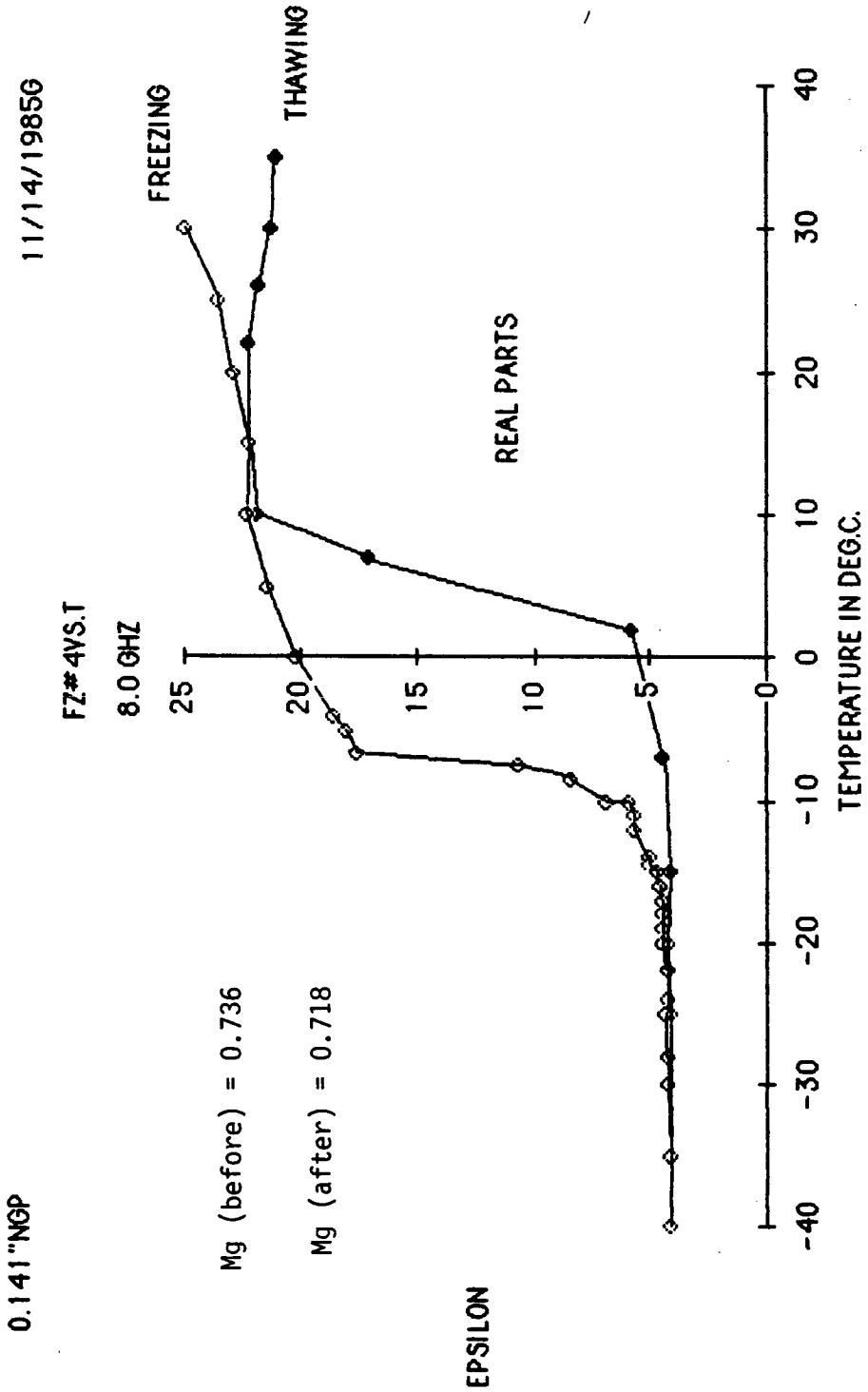
11/14/1985G
FREEZING
THAWING
FZ#4VS.T
8.0 GHZ
REAL PARTS
25
20
15
10
5
0
40
30
20
10
0
-10
-20
-30
-40
TEMPERATURE IN DEG.C.
0.141"NGP
Mg (before) = 0.736
Mg (after) = 0.718
EPSILON

Figure B.33

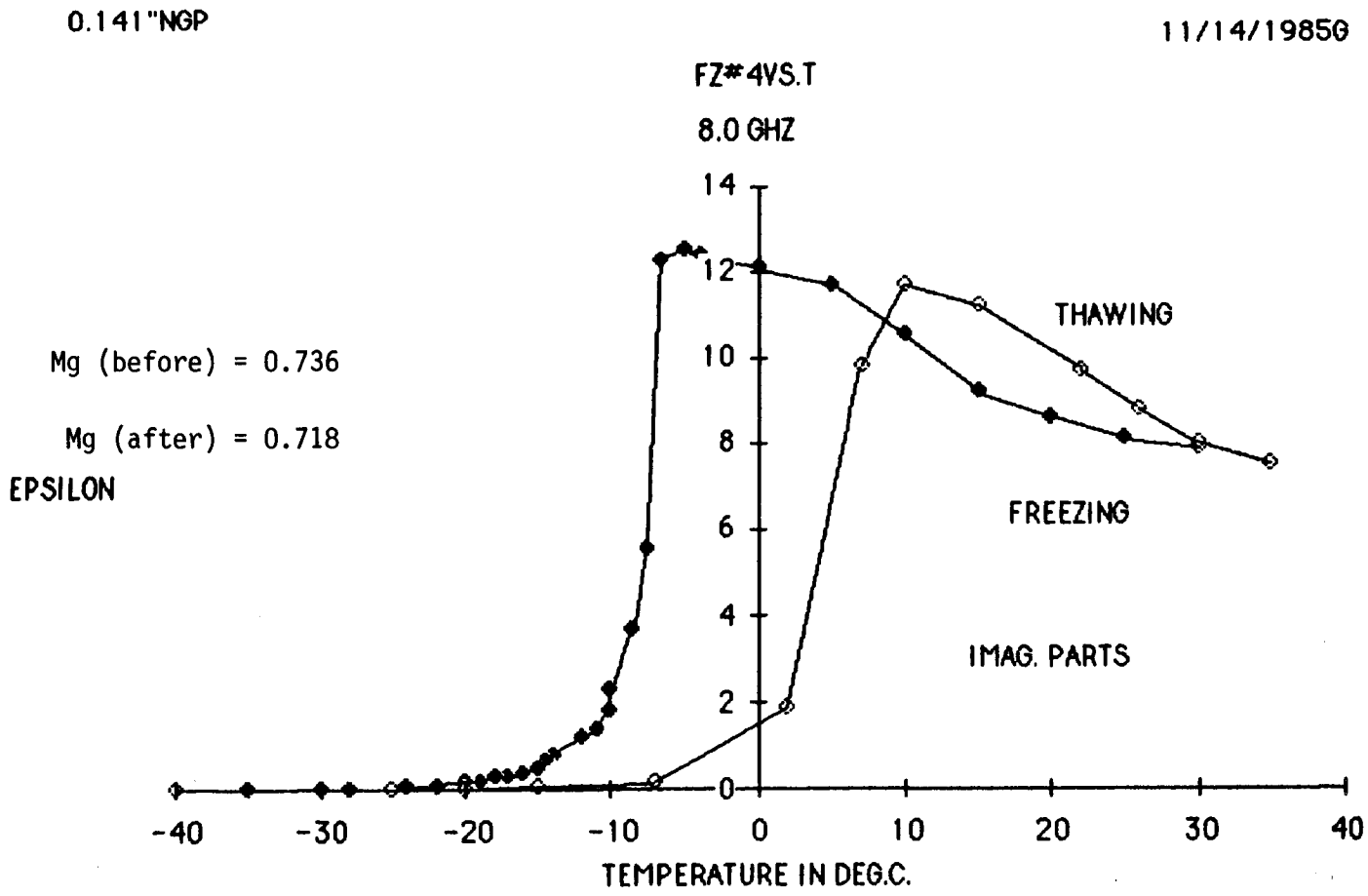
0.141"NGP
11/14/1985G
FZ#4VS.T
8.0 GHZ
Mg (before) = 0.736
Mg (after) = 0.718
EPSILON
THAWING
FREEZING
IMAG. PARTS
14
12
10
8
6
4
2
0
-40
-30
-20
-10
0
10
20
30
40
TEMPERATURE IN DEG.C.

Figure B.34

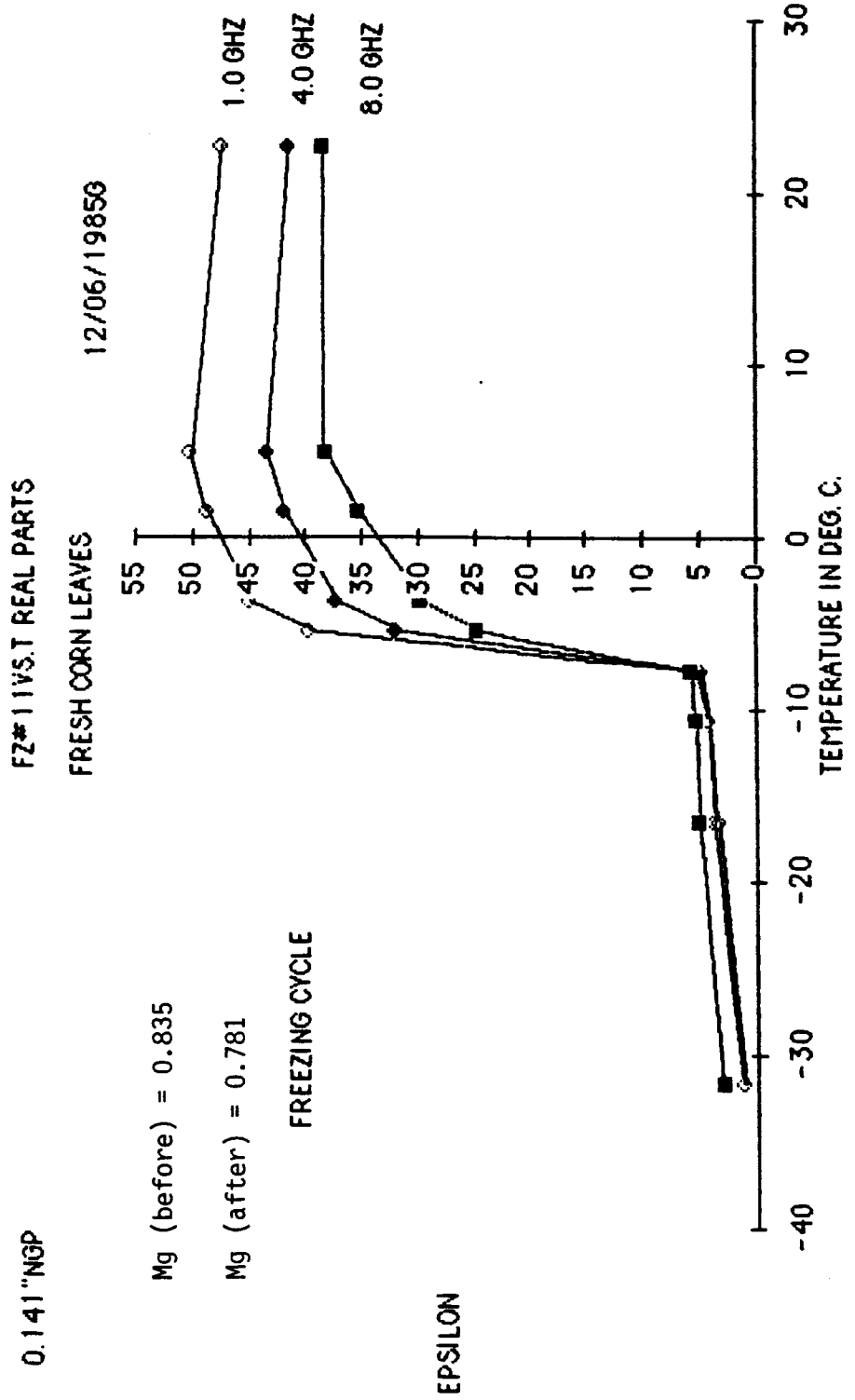
F7* 11VS.T REAL PARTS
FRESH CORN LEAVES
12/06/19850
1.0 GHZ
4.0 GHZ
8.0 GHZ
0.141"NGP
Mg (before) = 0.835
Mg (after) = 0.781
FREEZING CYCLE
EPSILON
55
50
45
40
35
30
25
20
15
10
5
0
-40
-30
-20
-10
0
10
20
30
TEMPERATURE IN DEG. C.

Figure B.35

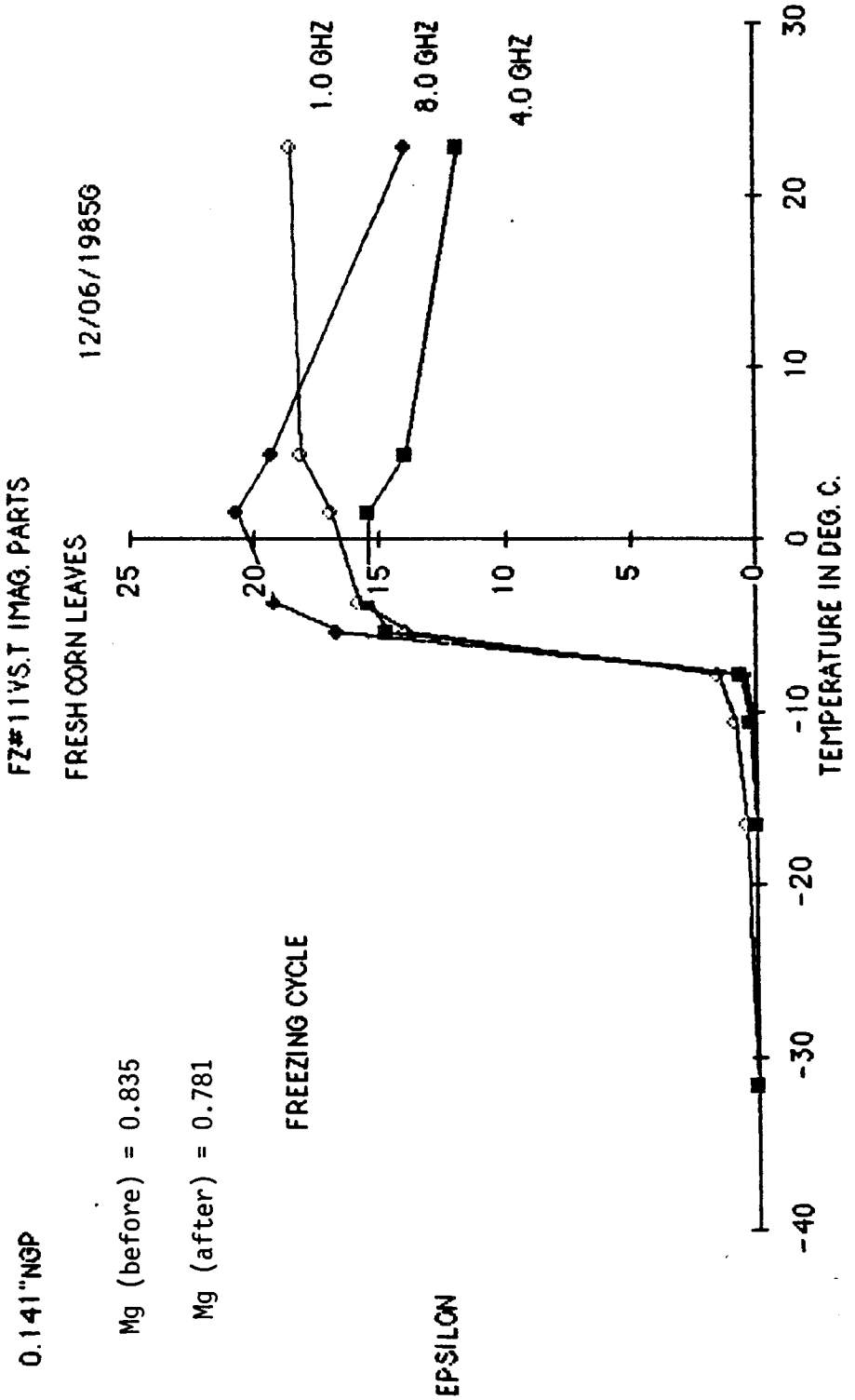
FZ#11VS.T IMAG. PARTS
FRESH CORN LEAVES
12/06/1985G
1.0 GHZ
8.0 GHZ
4.0 GHZ
0.141"NGP
Mg (before) = 0.835
Mg (after) = 0.781
FREEZING CYCLE
EPSILON
25
20
15
10
5
0
30
20
10
0
-10
-20
-30
-40
TEMPERATURE IN DEG. C.

Figure B.36

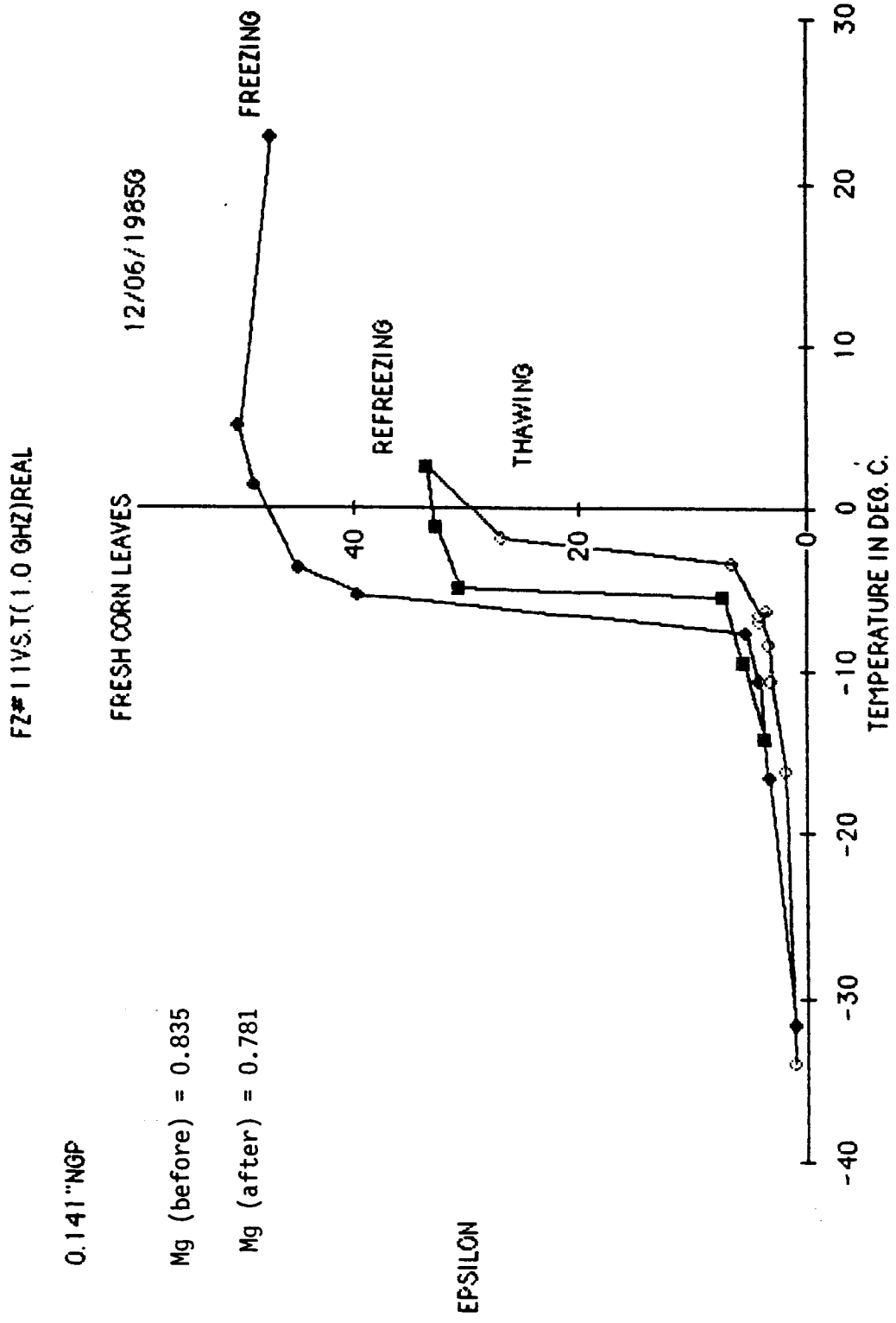
FZ* 11VS.T(1.0 GHZ)REAL
12/06/19858
FRESH CORN LEAVES
FREEZING
REFREEZING
THAWING
0.141"NGP
Mg (before) = 0.835
Mg (after) = 0.781
EPSILON
40
20
0
-40
-30
-20
-10
0
10
20
30
TEMPERATURE IN DEG. C.

Figure B.37

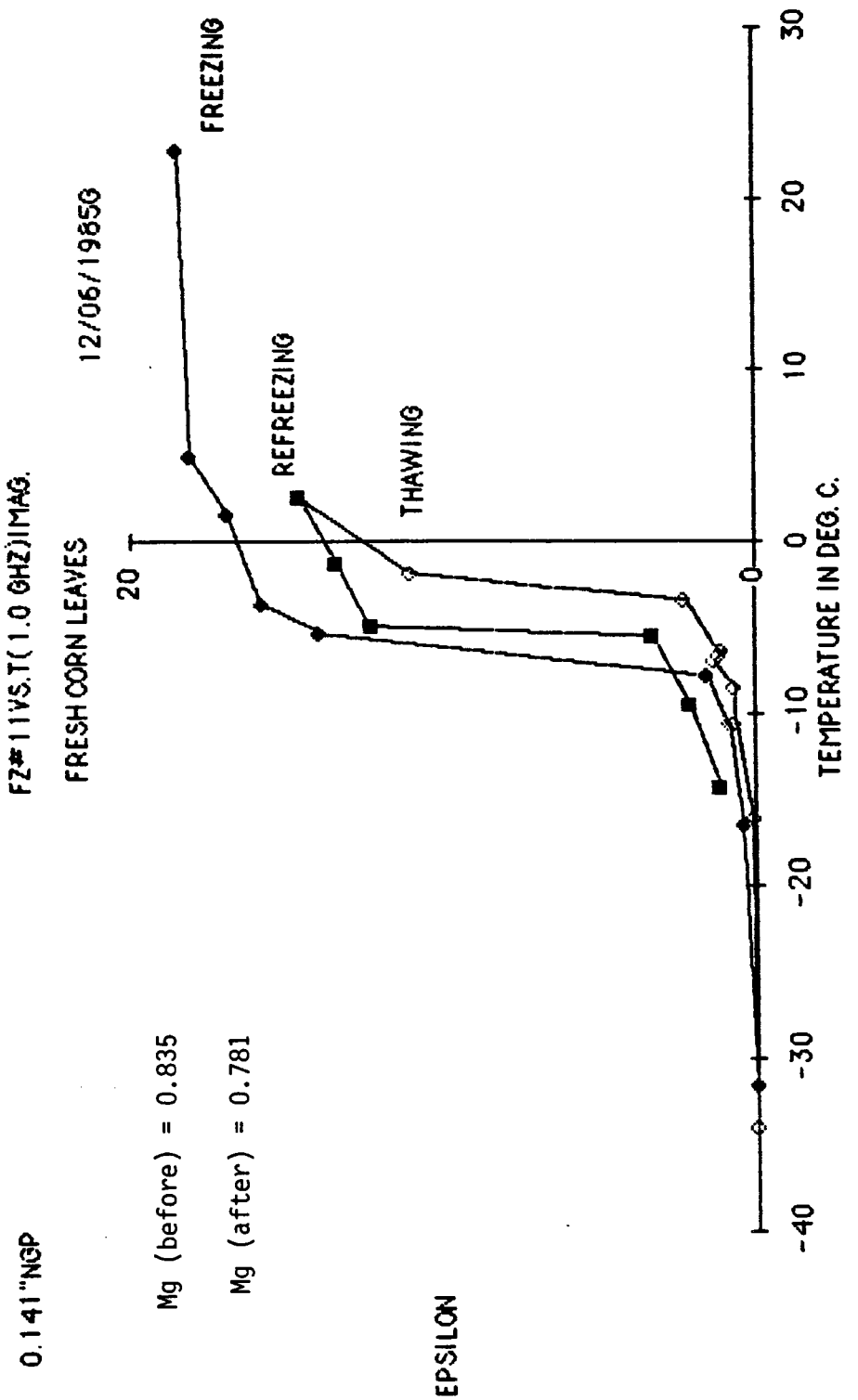
FZ#11VS.T(1.0 GHZ)IMAG.
FRESH CORN LEAVES
12/06/1985G
FREEZING
REFREEZING
THAWING
20
0
-10
-20
-30
-40
10
20
30
TEMPERATURE IN DEG. C.
0.141"NGP
Mg (before) = 0.835
Mg (after) = 0.781
EPSILON

Figure B.38

Appendix B

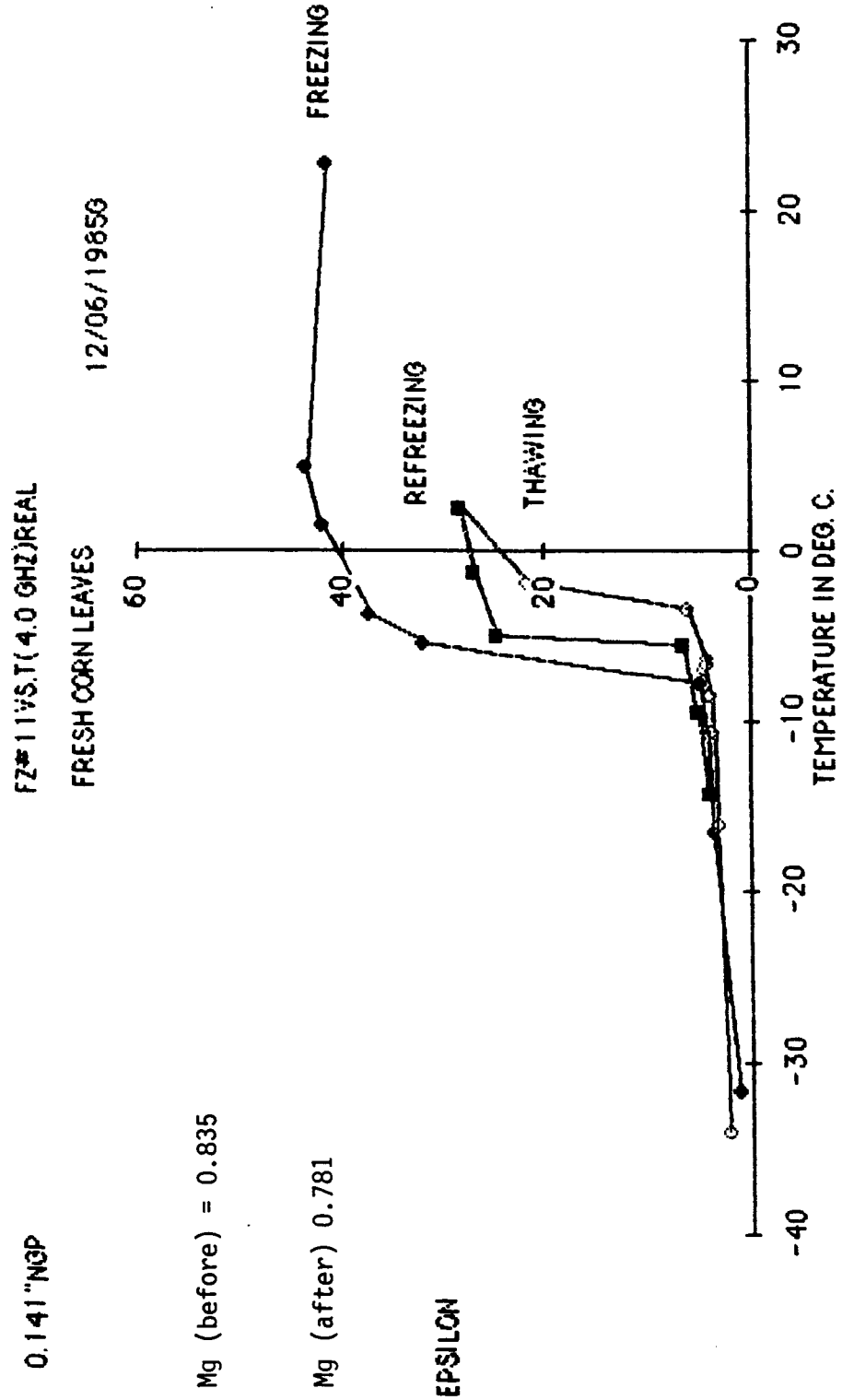

Figure B.39

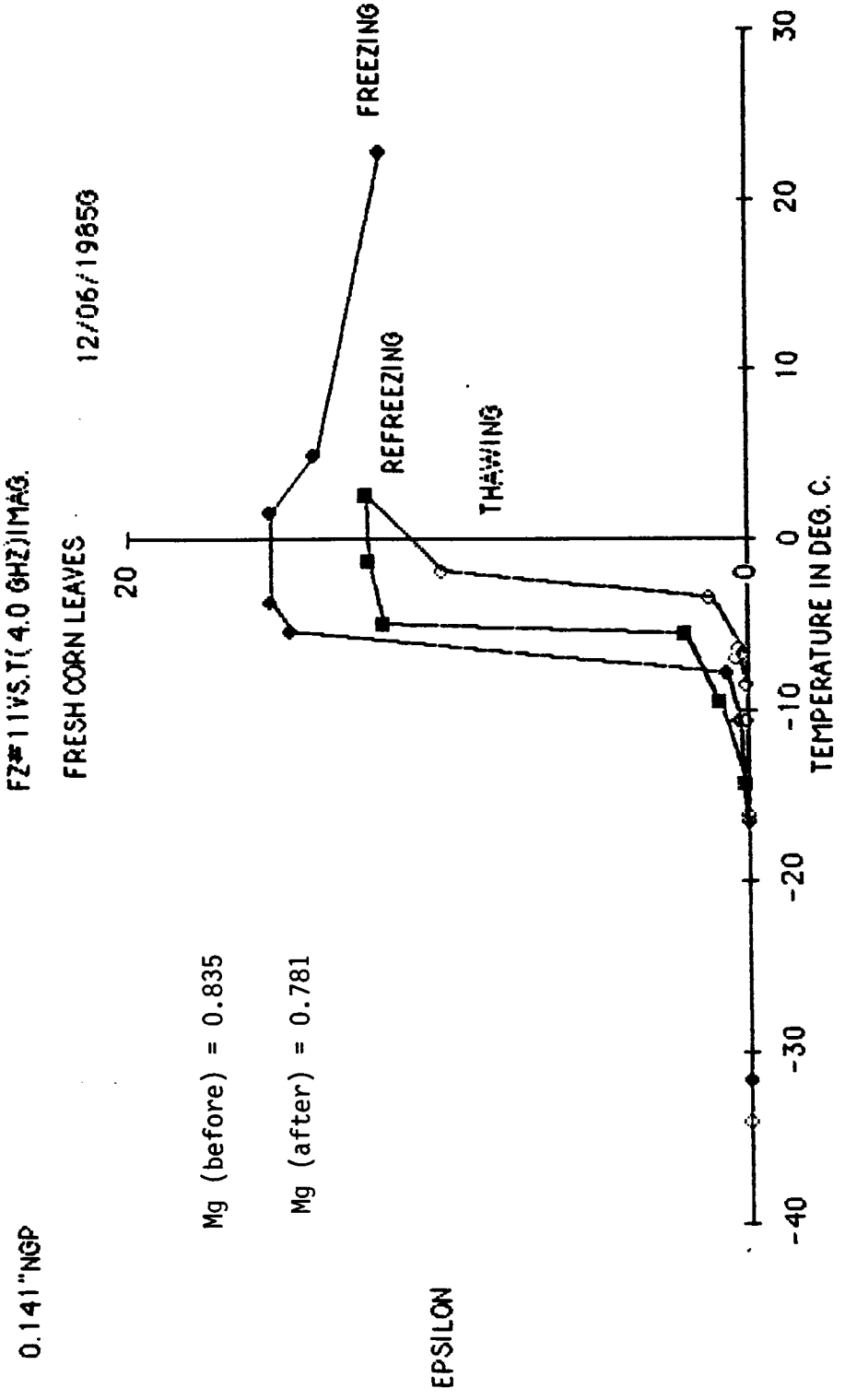
FREEZING
REFREEZING
THAWING
12/06/1985G
FRESH CORN LEAVES
F2=11VS.T(4.0 GHZ)IMAG.
0.141"NGP
Mg (before) = 0.835
Mg (after) = 0.781
EPSILON
TEMPERATURE IN DEG. C.
30
20
10
0
-10
-20
-30
-40
20

Figure B.40

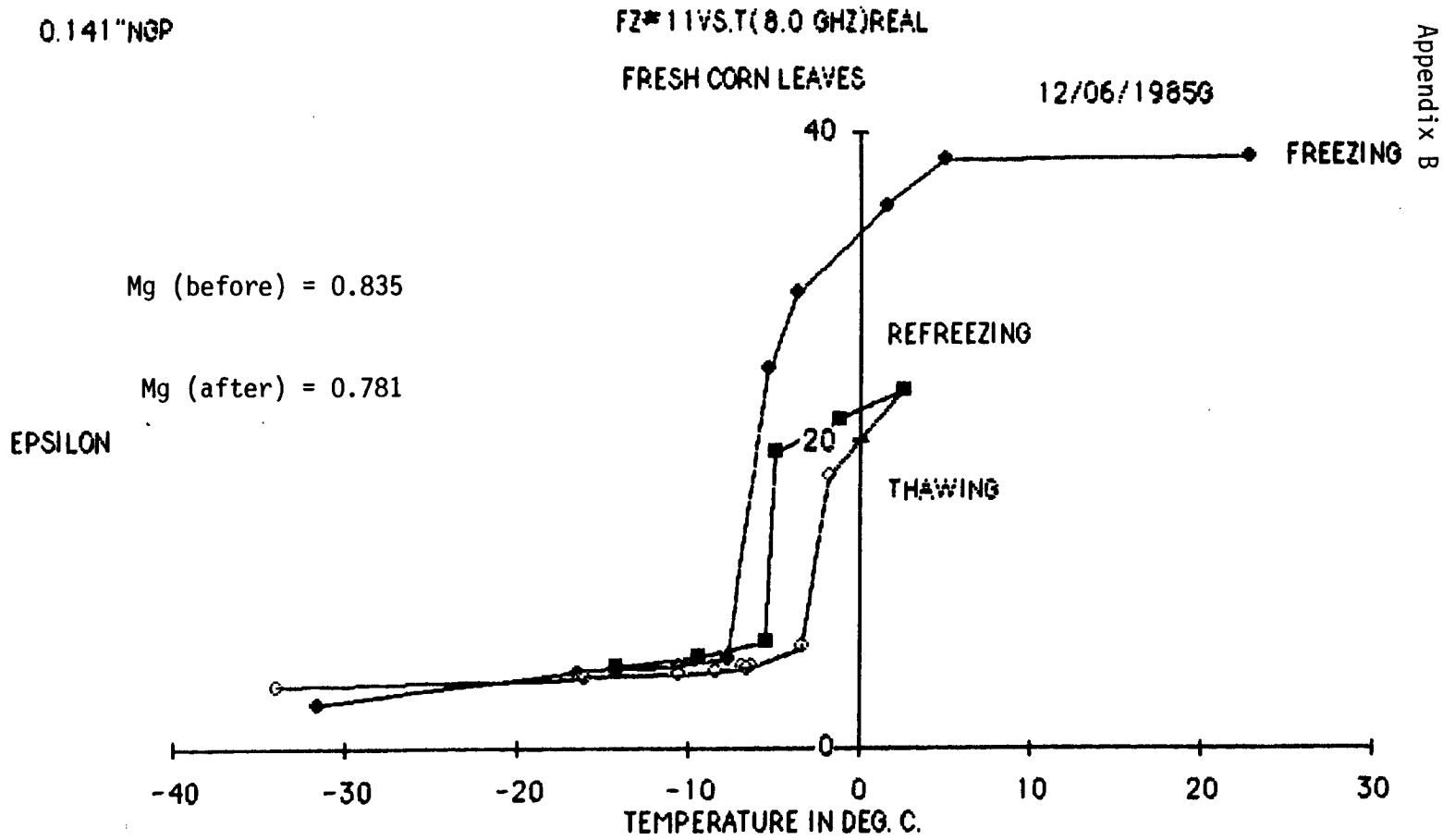
0.141"NGP
FZ*11VS.T(8.0 GHZ)REAL
FRESH CORN LEAVES
12/06/1985G
FREEZING
REFREEZING
THAWING
Mg (before) = 0.835
Mg (after) = 0.781
EPSILON
40
20
0
-40
-30
-20
-10
0
10
20
30
TEMPERATURE IN DEG. C.

Figure B.41

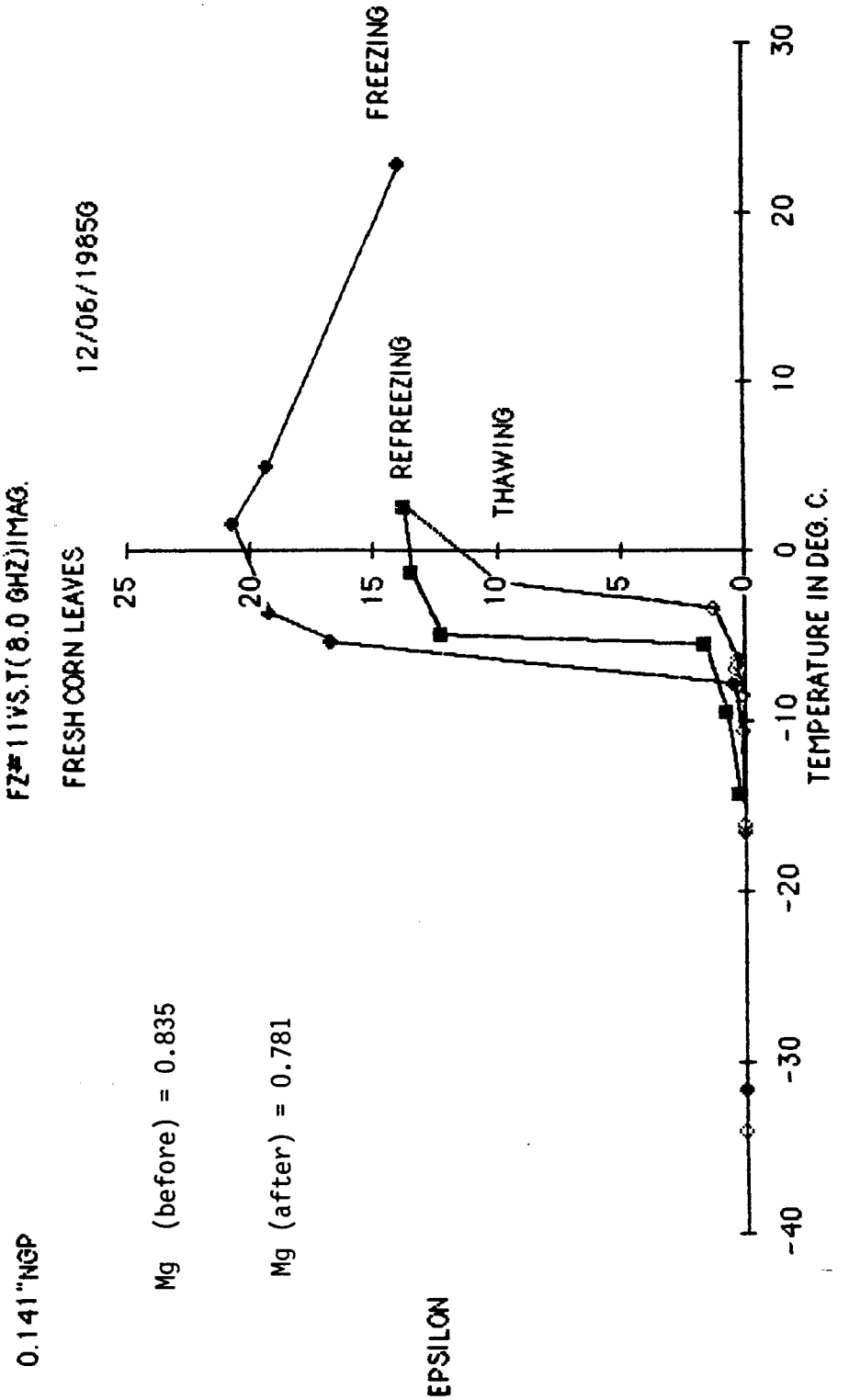
FZ#11'S.T(8.0 GHZ)IMAG.
FRESH CORN LEAVES
12/06/1985G
0.141"NGP
Mg (before) = 0.835
Mg (after) = 0.781
EPSILON
FREEZING
REFREEZING
THAWING
25
20
15
10
5
0
30
20
10
0
-10
-20
-30
-40
TEMPERATURE IN DEG. C.

Figure B.42

APPENDIX C

Probe Modeling Program Listing

Appendix C

```
C
C       PROGRAM TO CALIBRATE PROBE SYSTEM
C       O.C,S.C,S11,D.W.,METH.,AND UNKNOWN MATERIAL
C       REFLECTION COEFFICIENTS ARE KNOWN    .
C       ON 5/23/1984  BY M.A.EL-RAYES  .
C
        COMPLEX Z,RS,RO,RW,RM,S11,ROP,RSP,ROSP,EM,Z1,Z2,ECW
        COMPLEX S22,RCW,RCM,S121,ROA,S121P,ZOC,ZW,ZM,EMM,EMW
        COMPLEX ECB,RB,RCB,ZB,EMB,RCO,ZWC,RWA,S111,S1111
        PI=4.*ATAN(1.)
        Z=(0.0,1.0)
        Z0=50.0
        T=22.0
        S=0.0

C       O P E N     T H E     I/P     A N D     O/P     F I L E S    .

        OPEN(1,ERR=99,FILE='*PLEASE ENTER INPUT FILE NAME :  ')
        OPEN(2,ERR=99,FILE='*PLEASE ENTER OUTPUT FILE NAME : ')
 1      READ(01,*,END=99)F,AO,PO,AS,PS,AW,PW,AB,PB
        READ(01,*,END=99)XS11,YS11,AM,PM
        IF(S.LE.0.0)CALL WATER(F,T,ECW)
        IF(S.GT.0.0)CALL SWAT(F,T,S,ECW)
        IF(S.GT.20.0)CALL SWATH(F,T,S,ECW)
        CALL METH(F,T,ECB)
        PRINT *,'D.W. CALC. = ',ECW
        PRINT *,'METH. CALC.= ',ECB
        WRITE(02,111)ECW
        WRITE(02,112)ECB
 111    FORMAT(1X,'D.W.  CALC. = ',2(1X,F9.3))
 112    FORMAT(1X,'METH. CALC. = ',2(1X,F9.3))
        CF1=0.006E-12
        C01=0.028E-12
        B1=0.0
        A1=0.5E-12
        W=2.E9*PI*F
        WA=2.*PI*F
        AS=10.**(-(25.-AS)/20.)
        AO=10.**(-(25.-AO)/20.)
        AW=10.**(-(25.-AW)/20.)
        AB=10.**(-(25.-AB)/20.)
        AM=10.**(-(25.-AM)/20.)
        PS=PS*PI/180.
        PO=PO*PI/180.
        PW=PW*PI/180.
        PB=PB*PI/180.0
        PM=PM*PI/180.
        RS=AS*CEXP(Z*PS)
        RO=AO*CEXP(Z*PO)
        RW=AW*CEXP(Z*PW)
        RB=AB*CEXP(Z*PB)
        RM=AM*CEXP(Z*PM)
        S11=CMPLX(XS11,YS11)
        ROP=RO-S11
        RSP=RS-S11
        ROSP=ROP/RSP
        PRINT *,' FREQUENCY IN (GHZ) =  ',F
        WRITE(02,73)F
 73     FORMAT(1X,' FREQUENCY IN (GHZ) = ',F7.3)
```

```
      PRINT *,'----------------------'
      WRITE(02,74)
 74   FORMAT(1X,'----------------------')
      II=0
 2    CONTINUE
      II=II+1
      CF=CF1
      C0=C01
      B=B1
      A=A1
      ZOC=1./(A*(WA**4)+Z*W*(CF+C0+B*(WA**2)))
      ROA=(ZOC-Z0)/(ZOC+Z0)
      S22=(ROSP+ROA)/(ROA*(ROSP-1.))
      S121=ROP*(1.-S22*ROA)/ROA
      S121P=-RSP*(1.+S22)
      PRINT *,S121,S121P
      WRITE(02,75)S121,S121P
 75   FORMAT(1X,'S121,S121P= ',4(1X,F12.5))
C
C     CORRECTIONS  .
C
      RCW=(RW-S11)/(S121+(RW-S11)*S22)
      ZW=Z0*(1.+RCW)/(1.-RCW)
      RCB=(RB-S11)/(S121+(RB-S11)*S22)
      ZB=Z0*(1.+RCB)/(1.-RCB)
      RCM=(RM-S11)/(S121+(RM-S11)*S22)
      ZM=Z0*(1.+RCM)/(1.-RCM)
C
C    EVALUATION OF EQUIVALENT CIRCUIT PARAMETERS  .
C
      CALL FEQUIV(RCW,RCB,ECW,ECB,CF1,C01,B1,A1,W,WA,Z0)
      IF(II.GT.20)GO TO 9
      IF(ABS(CF1-CF).GE.1.E-15.OR.ABS(C01-C0).GE.1.E-15.
     +  OR.ABS(B1-B).GE.1.E-20.OR.ABS(A1-A).GE.1.E-15)GO TO 2
 9    CALL ITER(ZM,CF,C0,B,A,W,WA,EM,DM)
      CALL ITER(ZW,CF,C0,B,A,W,WA,EMW,DW)
      CALL ITER(ZB,CF,C0,B,A,W,WA,EMB,DB)
      PRINT *,' CALIBRATION USING O.C.,S.C.,AND S11  :'
      WRITE(02,76)
 76   FORMAT(1X,' CALIBRATION USING O.C.,S.C.,AND S11 :')
      PRINT *,'--------------------'
      WRITE(02,77)
 77   FORMAT(1X,'--------------------------------')
      PRINT *,' # OF ITERATION =  ',II
      WRITE(02,78)II
 78   FORMAT(1X,' # OF ITERATION = ',I3)
      II=0
      PRINT *,'D.W. = ',EMW
      WRITE(02,79)EMW
 79   FORMAT(1X,' D.W. = ',2(1X,F12.3))
      PRINT *,'METH.= ',EMB
      WRITE(02,80)EMB
 80   FORMAT(1X,' METH. = ',2(1X,F12.3))
      PRINT *,'MATERIAL EPS = ',EM,DM
      WRITE(02,81)EM,DM
 81   FORMAT(1X,' MATERIAL EPS = ',3(1X,F12.3))
      EMR=REAL(EM)
      EMI=-AIMAG(EM)
      PRINT *,'CF,C0,B,AND A  =  '
```

```
      WRITE(02,82)
82    FORMAT(1X,' CF,C0,B,AND A = ')
      PRINT *,CF,C0,B,A
      WRITE(02,83)CF,C0,B,A
83    FORMAT(4(1X,E12.5))
      PRINT *,'-------------------------------------------------
     + -------------------'
      WRITE(02,84)
84    FORMAT(1X,'-----------------------------------------')
700   CONTINUE
      GO TO 1
99    PRINT *,'ERROR IN WRITING TO OR READING FROM A FILE  '
      WRITE(02,91)
91    FORMAT(1X,' ERROR IN READING FROM OR WRITING TO A FILE')
      STOP
      END
C
C     SUBROUTINE TO SOLVE THE INVERSE PROBLEM (GIVEN
c     REFLECTION COEFFICIENT CALCULATE THE UNKNOWN DIELECTRIC
c     CONSTANT OF THE MEDIUM) USING AN ITERATION ALGORITHM AS
C     OPPOSED TO SOLVING A 5TH ORDER EQUATION (ACCURACY IN
c     THIS CASE IS XX.XX).
C
      SUBROUTINE ITER(ZM,CF,C0,B,A,W,WA,EMM,D1)
C
C     THIS PROGRAM SOLVE THE EQUATION IN ZM
C     TO GET EM BY ITERATION  .
C     BY M.A.EL-RAYES  ON 5/25/1984  .
C
      COMPLEX ZM,EM,Z,EM1,EMM
      Z=(0.0,1.0)
C
C
C     FIRST ITERATION  .
C
      N=11
      M=11
      EPI=1.0
      EDI=0.0
      IF(EPI.LE.1.0)EPI=1.0
      IF(EDI.LE.0.0)EDI=0.0
      D1=1.E9
      DO 100 I=1,N
      EP=EPI+(I-1.)*10.
      DO 100 J=1,M
      ED=EDI+(J-1.)*10.
      EM1=CMPLX(EP,-ED)
      D=CABS(ZM-(1./(Z*W*(CF+C0*EM1+B*(WA**2)*
     + (EM1**2))+A*(WA**4)*(EM1**2.5))))
      IF(D.LE.D1)EM=EM1
      IF(D.LE.D1)D1=D
100   CONTINUE
C
C     SECOND ITERATION  .
C
      EP=REAL(EM)
      ED=AIMAG(-EM)
      N=22
      M=22
```

```
      EPI=EP-10.
      EDI=ED-10.
      IF(EPI.LE.1.0)EPI=1.0
      IF(EDI.LE.0.0)EDI=0.0
      D1=1.E9
      DO 201 I=1,N
      EP=EPI+I
      DO 201 J=1,M
      ED=EDI+J
      EM1=CMPLX(EP,-ED)
      D=CABS(ZM-(1./(Z*W*(CF+C0*EM1+B*(WA**2)*
     + (EM1**2))+A*(WA**4)*(EM1**2.5))))
      IF(D.LE.D1)EM=EM1
      IF(D.LE.D1)D1=D
 201  CONTINUE
C
C     THIRD ITERATION  .
C
      EP=REAL(EM)
      ED=AIMAG(-EM)
      N=22
      M=22
      EPI=EP-1.0
      EDI=ED-1.0
      IF(EPI.LE.1.0)EPI=1.0
      IF(EDI.LE.0.0)EDI=0.0
      D1=1.E5
      DO 200 I=1,N
      EP=EPI+I*0.1
      DO 200 J=1,M
      ED=EDI+J*0.1
      EM1=CMPLX(EP,-ED)
      D=CABS(ZM-(1./(Z*W*(CF+C0*EM1+B*(WA**2)*
     + (EM1**2))+A*(WA**4)*(EM1**2.5))))
      IF(D.LE.D1)EM=EM1
      IF(D.LE.D1)D1=D
 200  CONTINUE
C
C     FOURTH ITERATION   .
C
      EP=REAL(EM)
      ED=AIMAG(-EM)
      N=22
      M=22
      EPI=EP-0.1
      EDI=ED-0.1
      IF(EPI.LE.1.0)EPI=1.0
      IF(EDI.LE.0.0)EDI=0.0
      D1=1.E5
      DO 300 I=1,N
      EP=EPI+I*0.01
      DO 300 J=1,M
      ED=EDI+J*0.01
      EM1=CMPLX(EP,-ED)
      D=CABS(ZM-(1./(Z*W*(CF+C0*EM1+B*(WA**2)*
     + (EM1**2))+A*(WA**4)*(EM1**2.5))))
      IF(D.LE.D1)EM=EM1
      IF(D.LE.D1)D1=D
 300  CONTINUE
```

```
      EMM=EM
      RETURN
      END
C
C       SUBROUTINE TO SOLVE 4 EQUATIONS IN 4 UNKNOWNS,
C       FOR THE COMPLETE EQUIVALENT CIRCUIT (CF, C0, B, AND A).
C
      SUBROUTINE FEQUIV(RCW,RCB,ECW,ECB,CF1,C01,B1,A1,W,WA,Z0)
C
C     SUB. TO ESTIMATE EQUIVALENT CIRCUIT PARAMETERS  .
C
      COMPLEX Z,RCW,RCB,ECW,ECB,RHW,RHB
      DIMENSION A(4,5),B(4,5)
      Z=(0.0,1.0)
      RHW=(1.-RCW)/(1.+RCW)/Z0
      RHB=(1.-RCB)/(1.+RCB)/Z0
      A(1,5)=AIMAG(RHW)
      A(2,5)=AIMAG(RHB)
      A(3,5)=REAL(RHW)
      A(4,5)=REAL(RHB)
      A(1,1)=WA
      A(2,1)=WA
      A(3,1)=0.0
      A(4,1)=0.0
      A(1,2)=WA*REAL(ECW)
      A(2,2)=WA*REAL(ECB)
      A(3,2)=WA*AIMAG(-ECW)
      A(4,2)=WA*AIMAG(-ECB)
      A(1,3)=(WA**3)*REAL(ECW**2)
      A(2,3)=(WA**3)*REAL(ECB**2)
      A(3,3)=(WA**3)*AIMAG(-(ECW**2))
      A(4,3)=(WA**3)*AIMAG(-(ECB**2))
      A(1,4)=(WA**4)*AIMAG(ECW**2.5)
      A(2,4)=(WA**4)*AIMAG(ECB**2.5)
      A(3,4)=(WA**4)*REAL(ECW**2.5)
      A(4,4)=(WA**4)*REAL(ECB**2.5)
C
C     PROCESS THE MATRIX USING DIAGONAL METHOD  .
C
      DO 111 I=1,4
      DO 111 J=1,5
      B(I,J)=A(I,J)
 111  CONTINUE
C
C     PROCESS THE MATRIX USING DIAGONAL METHOD  .
C
      DO 10 I=1,4
      IF(ABS(A(I,I)).LE.1.E-37)GO TO 20
 10   CONTINUE
C
C     CHANGE DIAGONAL ELEMENTS TO UNITY .
C
      DO 100 J=1,4
      X=A(J,J)
      DO 200 L=1,5
      A(J,L)=A(J,L)/X
 200  CONTINUE
      DO 100 I=1,4
      IF(I.EQ.J)GO TO 100
```

```
      X=A(I,J)
      DO 300 K=1,5
      A(I,K)=A(I,K)-X*A(J,K)
300   CONTINUE
100   CONTINUE
      CF1=A(1,5)*1.E-9
      C01=A(2,5)*1.E-9
      B1=A(3,5)*1.E-9
      A1=A(4,5)
      DO 700 I=1,4
      D=B(I,5)
      DO 701 J=1,4
      D=D-B(I,J)*A(J,5)
701   CONTINUE
700   CONTINUE
      GO TO 30
20    PRINT *,'DIAGONAL ELEMENT/S WITH ZERO !!!!'
      WRITE(02,87)
87    FORMAT(1X,'DIGONAL ELEMENT/S WITH ZERO !!!!!')
30    RETURN
      END
C
C       SUBROUTINE TO SOLVE 2 EQUATIONS IN 2 UNKNOWNS,
        FOR THE SIMPLE EQUIVALENT CIRCUIT (ONLY C0 AND A).
C
      SUBROUTINE EQ(RC,EC,AK,C0,A,W,WA,Z0)
C
      COMPLEX Z,RC,EC,Y
C
      Z=(0.0,1.0)
      Y=(1.-RC)/(1.+RC)/Z0
      CF=AK*C0
      XK1=REAL(Y)
      XK2=AIMAG(Y)
      A11=-W*AIMAG(EC)
      A12=(WA**4)*REAL(EC**2.5)
      A21=W*AK+W*REAL(EC)
      A22=(WA**4)*AIMAG(EC**2.5)
      C0=(XK1/A12-XK2/A22)/(A11/A12-A21/A22)
      A=(XK1-A11*C0)/A12
      AP=(XK2-A21*C0)/A22
      RETURN
      END
C
C       DIELECTRIC CONSTANT OF DISTILLED WATER ( S = 0.0 PPT).
C
      SUBROUTINE WATER(F,T,EDW)
C     THIS IS A PROGRAM TO CALCULATE THE COMPLEX DIELECTRIC
C     CONSTANT OF FRESH WATER. .
C     BY M.A. EL-RAYES .
C     OCT.15,1981 .
      COMPLEX EDW
      PI=4.*ATAN(1.0)
      EPSWI=4.9
      TAW=(1.1109E-10-3.824E-12*T+6.938E-14*(T**2)
     + -5.096E-16*(T**3))
      TAW=TAW/(2*PI)
      EPSWZ = 88.045-0.4147*T + 6.295E-4*(T**2)
     + +1.0735E-5 *(T**3)
```

```
      EPSWP=EPSWI+((EPSWZ-EPSWI)/(1+((2*PI*F*1E9*TAW)**2)))
      EPSWD=(2*PI*F*1E9*TAW*(EPSWZ-EPSWI)
     + /(1+((2*PI*F*1E9*TAW)**2)))
      EDW=CMPLX(EPSWP,-EPSWD)
      PRINT *,'EPS.D.W. =  ',F,EDW
      RETURN
      END
C
C       DIELECTRIC CONSTANT OF SALINE WATER WITH LOW SALINITIES
C       ( S < 20 PPT ).
C
      SUBROUTINE SWAT(F,T,S,ESW)
C     A PROGRAM TO CALCULATE SALINE WATER DIELECTRIC
C     CONSTANT AS A FUNCTION OF FREQUENCY , TEMPERATURE ,
C     AND SALINITY .
C     ON 4/22/1982 .
C     BY M.A.EL-RAYES .
C
      COMPLEX ESW
      PI=4.*ATAN(1.0)
      ESWI=4.9
      ESW0=87.134-1.949E-1*T-1.276E-2*(T**2)+2.491E-4*(T**3)
      A=1.0+1.613E-5*T*S-3.656E-3*S+3.21E-5*(S**2)-4.232E
     + -7*(S**3)
      ESW0S=ESW0*A
      TAW0=(1./(2.*PI))*(1.1109E-10-3.824E-12*T+6.938E
     + -14*(T**2)-5.016*(T**3))
      B=1.0+2.282E-5*T*S-7.638E-4*S-7.76E-6*(S**2)
     + +1.105E-8*(S**3)
      TAWS=TAW0*B
      DELT=25.0-T
      PHI=DELT*(2.033E-2+1.266E-4*DELT+2.464E-6*(DELT**2)-
     + S*(1.849E-5-2.551E-7*DELT+2.551E-8*(DELT**2)))
      SIG25=S*(0.18252-1.4619E-3*S+2.093E-5*(S**2)-1.282E
     + -7*(S**3))
      SIG=SIG25*EXP(-PHI)
      EPS0=(1.E-9)/(36.*PI)
      ESWP=ESWI+((ESW0S-ESWI)/(1.+((2.*PI*F*1.E9*TAWS)**2)))
      ESWD=2.*PI*F*1.E9*TAWS*(ESW0S-ESWI)
     + /(1.+((2.*PI*F*1.E9*TAWS)
     + **2))+SIG/(2.*PI*EPS0*F*1.E9)
      ESW=CMPLX(ESWP,-ESWD)
      PRINT *,'EPS.S.W. =  ',F,ESW
      RETURN
      END
C
C       DIELECTRIC CONSTANT OF SALINE WATER WITH HIGH SALINITIES
C       ( S > 20 PPT ).
C
      SUBROUTINE SWATH(F,T,S,ESW)
C     A PROGRAM TO CALCULATE SALINE WATER DIELECTRIC
C     CONSTANT AS A FUNCTION OF FREQUENCY , TEMPERATURE ,
C     AND SALINITY .
C     ON 4/22/1982 .
C     BY M.A.EL-RAYES .
C
      COMPLEX ESW
      REAL N
      AA=1.0
```

Appendix C

```
      PI=4.*ATAN(1.0)
      N=AA*(1.707E-2+1.205E-5*S+4.058E-9*S**2)*S
      D=25.-T
      C1=1.-1.96E-2*D+8.08E-5*D**2-N*D*(3.02E-5+3.92E-5*D
     + +N*(1.72E-5-6.58E-6*D))
      SB=N*(10.39-2.378*N+0.683*N**2-0.135*N**3+1.01E-2*N**4)
      B1=1.+0.146E-2*T*N-4.89E-2*N-2.97E-2*N**2+5.64E-3*N**3
      TB=1.1109E-10-3.824E-12*T+6.938E-14*T**2-5.096E-16*T**3
      TB=TB/(2.*PI)
      A1=1.-0.255*N+5.15E-2*N**2-6.89E-3*N**3
      EW0=88.045-0.4147*T+6.295E-4*T**2+1.075E-5*T**3
      SB=SB*C1
      TB=TB*B1
      EW0=EW0*A1
      EWI=4.9
      E0=(1.E-9)/(36.*PI)
      EFP=EWI+(EW0-EWI)/(1.+(2.*PI*F*1.E9*TB)**2)
      EFD=(2.*PI*F*1.E9*TB)*(EW0-EWI)/(1.+(2.*PI*F*1.E9*TB)**2)
      EFD=EFD+SB/(2.*PI*E0*F*1.E9)
      ESW=CMPLX(EFP,-EFD)
      PRINT *,'EPS.S.W. =  ',F,ESW
      RETURN
      END
C
C       DIELECTRIC CONSTANT OF METHANOL.
C
C
      SUBROUTINE METH(F,T,EMETH)
C
      COMPLEX  Z,EMETH
C
      PI=4.*ATAN(1.0)
      Z=(0.0,1.0)
      W=2.E9*PI*F
      IF(T.LT.10..OR.T.GT.40.)GO TO 111
      ES=39.2-0.22*T
      IF(T.LE.20..AND.T.GE.10.)EI=4.9-0.02*T
      IF(T.LE.30..AND.T.GE.20.)EI=4.7-0.01*T
      IF(T.LE.40..AND.T.GE.30.)EI=5.6-0.04*T
      IF(T.LE.20..AND.T.GE.10.)TAU=84.-1.4*T
      IF(T.LE.30..AND.T.GE.20.)TAU=80.-1.2*T
      IF(T.LE.40..AND.T.GE.30.)TAU=71.-0.9*T
      TAU=TAU*1.E-12
      IF(T.LE.20..AND.T.GE.10.)ALP=0.026+0.0009*T
      IF(T.LE.30..AND.T.GE.20.)ALP=0.052-0.0004*T
      IF(T.LE.40..AND.T.GE.30.)ALP=0.082-0.0014*T
      EMETH=EI+(ES-EI)/(1.+(Z*W*TAU)**(1.-ALP))
      PRINT *,'F,T,EPS  =  ',F,T,EMETH
      RETURN
111   PRINT *,'TEMP. SELECTED BEYOND LIMITS !!!!! '
      WRITE(02,89)
89    FORMAT(1X,' TEMP. SELECTED BEYOND LIMITS !!!!!')
      RETURN
      END
```